Kjell Karlsrud

Prediction of load-displacement behaviour and capacity of axially loaded piles in clay based on analyses and interpretation of pile load test results

Kjell Karlsrud

Doctoral thesis

NTNU – Trondheim
Norwegian University of
Science and Technology

NTNU – Trondheim
Norwegian University of
Science and Technology

◙ NTNU

Kjell Karlsrud

Prediction of load-displacement behaviour and capacity of axially loaded piles in clay based on analyses and interpretation of pile load test results

NTNU – Trondheim
Norwegian University of
Science and Technology

ABSTRACT

The main objective of the work presented herein was to develop new semi-empirical design procedures for determination of bearing capacity and load-displacement response of axially loaded piles in clay. Hereunder also prediction of how the capacity will build up with time following the pile installation, primarily as a result of consolidation.

A main basis for developing new procedures was the collection, detailed review and assessment of results from a series test programs carried out over the past 30 years on well instrumented piles. The data collected and reviewed include the pile installation, re-consolidation, and loading phases. The pile instrumentation includes measurement of the distribution of loads or shaft friction, pore pressure and earth pressure along the pile shafts. The soil conditions range from soft NC clays with undrained shear strength down to about 15 kPa, to very stiff and high OCR clays with undrained shear strength up to about 500 kPa. The plasticity index of the clays mostly lies in range 10 to 60 %. The test piles range from small scale model piles with diameter down to 36 mm and length down to 1- 2 m, to large scale piles with diameter up to 800 mm and length up 71 m. In addition to these fully instrumented pile tests, some recent large scale tests on non-instrumented piles are also reviewed and included as basis for developing the new proposed design procedures.

Two new procedures for predicting ultimate shaft friction are proposed, respectively a so-called α- and β approach. They tie the local ultimate shaft friction along a pile to the "true" undisturbed in-situ undrained strength of the clay as determined from Direct Simple Shear Tests, the in-situ vertical effective stress, the overconsolidation ratio, and the plasticity index of the clay.

No clear evidence is found of effects of pile diameter, length or stiffness on the local ultimate shaft friction, or whether the pile is open-or closed- ended. A moderate effect of pile length or flexibility on the total ultimate pile capacity will still come out of the proposed t-z curves, which include some post-peak reduction.

A brief review and summary is also given of measured effects of cyclic loads on the axial capacity and pile head displacements of piles. It is concluded that this issue can be well accounted for by analytical or numerical procedures already in existence.

A semi – empirical analytical procedure, based on linear radial consolidation theory, is proposed for predicting the time required for re-consolidation and "set-up" of the ultimate shaft friction. The main input parameters are the in-situ permeability and virgin modulus number (or virgin compression index) of the undisturbed clay. The same basic formula and correlations were found applicable to both open- and closed- ended or partially plugging piles. For design purposes it is very important to recognise that the time for full set-up can easily be a factor of 10 longer for a closed– ended pile than for an ideal non-plugging open- ended pile.

It was also an objective to study how well the measured pile response during installation, re-consolidation and pile loading could be predicted from analytical and numerical models. Although such procedures can give very valuable insight, there is still a way to go before they can correctly capture all relevant elements of the pile response. The greatest need for improvement is to establish a better understanding of how the severe disturbance and strains induced by the pile installation affects the basic stress-strain, strength-, and volumetric compressibility- characteristics of the clay, depending on the level of induced shear strains as function of radial distance from the pile wall.

ACKNOWLEDGEMENTS

Content

1 BACKGROUND AND SCOPE OF WORK

1.1 Background

The static axial bearing capacity of piles in clay has traditionally been determined by use of semi-empirical methods. Such methods have commonly been linked either to the state of effective stress in the ground, or to the undrained shear strength of the clay. The impact of stress history of the clay deposit, plasticity index, peak and residual effective friction angle have over the past 10-30 years also been considered in semi-empirical correlations. The same applies to possible effects of pile length or flexibility, pile diameter, mode of penetration (e.g. open versus closed penetration), type of pile material and mode of loading (e.g. tension versus compression).

The early empirical correlations were developed on the basis of load tests on piles where only the load and displacement at the pile top were measured. In these early studies the determination of the in-situ stress-strain and strength characteristics of the clays was often based on what we today may classify as rather rudimentary tests on samples of poor quality, which in itself introduces significant uncertainties in the empirical correlations proposed.

Over the past 30 years a large number of model and large scale load tests have been carried out on piles which were instrumented to measure earth- and pore pressures and local shaft friction along the piles during the pile installation, re-consolidation and loading phases. The author has been involved with a number of such instrumented load testing programs, as summarised in later section 1.5. These fully instrumented load testing programs have generally been combined with more elaborate in-situ and laboratory testing to determines both the "true" in-situ stress-strain- and strength characteristics of the clay deposit, and the impact that the pile installation may have on these properties. There have also been significant developments of analytical and numerical models over the past 30 years, in particular for predicting the rather complex stress and strain changes imposed in the clay surrounding a pile during the pile installation and re-consolidation phases. Different "schools of thought" have come out of such past studies, as will be reviewed and elaborated upon in this work.

1.2 Scope and objectives of the present study

It is a main objective of the work presented herein to establish a coherent understanding of what factors that primarily govern the ultimate shaft friction along piles in clay, and develop new semi-empirical design methods that best reflect and capture key aspects of the observed behaviour. The main elements of the study are:

- Determine the earth and pore pressures generated against the pile shaft during the installation and re-consolidation and loading phases, including the time required for reconsolidation.
- How the ultimate shaft friction may be related to general soil characteristics, the state of in-situ effective stresses, stress history and the "true" in-situ undrained shear strength prior to pile installation, as well as the state of effective stress against the pile shaft at onset of pile loading.

- How the stresses and strains induced by the pile installation in the surrounding clay as a result of the installation and re-consolidation process may alter the physical properties of the clay, and thereby affect the pile performance.

The work is primarily based on observations and data collected in connection with "fully instrumented" pile testing programs that the author has been responsible for or become involved with, or that have been found in the literature. The dimensions of the fully instrumented test piles range from what may be called small (model) scale piles (down to about 100 mm diameter and 5 m length) to large full scale piles (up to 800 mm diameter and 71 m length). A special category is what may be called "pile probe tests" with probes of diameter 36 to 76 mm and length around 1-2 m.

The most relevant results from the various fully instrumented pile testing programs are summarized, including both soils data and load test results. In this connection the actual data have been carefully scrutinized and re-interpreted. Data that have been considered ambiguous or questionable have been identified and left out of the subsequent data interpretation.

In relation to soils data, special emphasis has been put on establishing the best possible assessment of the "true" in-situ undrained strength characteristics and apparent over consolidation ratio of the clay deposits in question. In this respect the author has chosen to use undrained strength according to Direct Simple Shear (DSS) mode of failure as reference strength throughout the study. For some tests on well instrumented piles found in the literature, the pile test results were not included due to insufficient information about soils data.

In addition to results from fully instrumented test piles, this study also incorporates assessment of some recent large scale pile test on non-instrumented piles. These are tests that have not been included in past common data bases. It is also limited to cases where it was considered that sufficient information about relevant soils data were available.

This study primarily uses the results from the first initial load test carried out on the individual piles after full re-consolidation or "set-up" was reached. In many of the load testing programs dealt with herein the piles were subsequently subjected to one or more load tests after the first initial test was carried out. Because repeated loading to failure of the same pile usually will alter the ultimate shaft friction, the results of such subsequent repeated testing are not included in this study.

The study of effects of cyclic loading on pile response has been part of several of the load testing programs dealt with herein. Cyclic loading effects can be an important aspect, for instance in design of piles for offshore structures and wind turbines, and to some extent in relation effects of earthquake loading effects. The impact of cyclic loading on the axial pile bearing capacity and pile head displacements will be summarized. Analytical and numerical methods for dealing with this aspect will also be reviewed.

This study limits itself to defining the ultimate shaft friction for classical undrained loading conditions, e.g. loading rates that are considered sufficiently rapid to ensure that little or no drainage occur in the clay surrounding the pile during loading to failure.

It should also be mentioned that although end-bearing contributes to the total bearing capacity of piles, it is not made a direct part of this study. The reason for not doing so is firstly that the author believes end-bearing is well understood and can be reliably calculated by conventional bearing capacity theory. Furthermore, for most friction piles in actual use the length to diameter ratio is relatively large, mostly in the range 50 to 100, which will imply that the end bearing only contributes to 5 to 20 % of the total pile capacity. The theoretical end bearing is still accounted for when calculating the load carried by the shaft for the pile load tests dealt with in this study.

1.3 Outline of work undertaken

Chapter 2 presents a summary of the results from "fully instrumented" pile testing programs, site by site. For each site a summary is first given of the test program, followed by an assessment of key soil parameters and main load test results. Chapter 3 presents a similar case –by-case presentation of non-instrumented pile tests included in this study.

The main result and observations made from the pile installation phase are summarised and assessed in Chapter 4, the re-consolidation phase in Chapter 5 and the axial load testing phase in Chapter 6. The load-displacement response is assessed in Chapter 7, and cyclic loading effects in Chapter 8. In each of these chapters the main results are compared to existing analytical or numerical solutions and design methods, and new semi-empirical procedures are proposed as seen needed.

Chapter 9 presents the main conclusions drawn from this study and give recommendations for how these results can be used in future design of axially loaded piles in clay.

In approaching this study, all relevant data were first collected and summarized and interpreted site by site as presented in Chapters 2 and 3. This was done prior to onset of the subsequent studies of the overall results, and how they may be correlated and used to establish semi-empirical design procedures as described in Chapters 4 to 8. As will be shown, assessing relevant soil parameters and pile test results include some element of personal judgement. It is therefore emphasized that no attempts have been made to adjust the soil parameters and pile test results after they first had been assessed in Chapters 2 and 3.

The following two sub-sections give first a very brief overview of some historic developments up until about 1980 when the author first became involved with research on the topic, followed by a brief review of the authors past work on the subject at hand. A more comprehensive general review of past work relating to ultimate shaft friction for piles in clay is included in the first section of chapter 5 dealing with ultimate shaft friction. Other relevant literature is directly referred to within the text of the respective chapters.

Appendix 1 (installation and reconsolidation phase) and 2 (loading phase) present summary tables with all main test results from the instrumented pile tests, including assumed key soil parameters. Appendix 3 presents summary tables with test results from the non-instruments pile tests.

Key symbols and abbreviations used in this study are defined after the List of Content. In some cases, where a formulae or expression is taken from other sources, the symbols and abbreviations may differ from what is given in this list, but are then defined directly within the text.

1.4 Brief historic overview

Many researchers or research groups have even as far back as the early 1900 collected pile load test results on which various semi-empirical design procedures have been proposed. Methods that have been in common use after around 1950 and up until around 1980 can broadly be grouped in three categories as summarised in the following:

1) Alfa methods in which the ultimate shaft friction is primarily correlated to the (assumed) undisturbed absolute or normalised undrained shear strength, i.e.:

   $\tau_{us} = \alpha \cdot s_u$,where

   $\alpha = f(s_u \text{ or } s_u / \sigma'_{v0}$, pile length and/or other parameters)

2) Beta methods in which the ultimate shaft friction is primarily related to in-situ vertical effective stress, i.e.:

   $\tau_{us} = \beta \cdot \sigma'_{v0}$,where

   $\beta = f(\varphi, K_0$ and/or OCR), pile length and/or other parameters)

3) λ- methods in which both the undrained strength and vertical effective stress enters , i.e.:

   $\tau_s = \lambda \cdot (\sigma'_{v0m} + 2s_u)$,where

   $\lambda = f($pile length or other parameters)

In the late 1950's it was recognized that the driving of a pile into a clay deposit significantly disturbs the clay and lead to a change in soil strength characteristics and state of total and effective stresses around the pile. Evidence of the effect on soil characteristics was also collected and documented by digging ditches or taking samples close to piles that had been in the ground for some time, and compare that to properties of the assumed undisturbed in-situ clay material.

In 1950 an analytical solution was presented to determine the stress changes caused by driving a pile into the ground. The solution was based on plasticity theory and expansion of an ideal cylinder in the ground (named the Cavity Expansion Method, CEM).

In the late 1970's the offshore piling industry and a number of university research groups started to extend the CEM theory and introduced more advanced non-linear total and effective stress soil models in the analysis. This was also accompanied by the use of numerical (FEM) methods to model the stress changes imposed by pile installation, and the subsequent reconsolidation phase. To support these theories, a number of instrumented miniature pile tests were carried out in the laboratory. Some instrumented small scale model pile tests were also carried out in the field in the late 1970's and early 1980's. Such small scale tests have later been followed by more large scale test programs as dealt with in detail in this study.

Use of numerical models in combination with results of instrumented pile load test have over the past 30 years lead to development of more theoretically well- founded analytical methods that attempt to account for pile installation effects on the stress field and stress-strain and strength characteristics of the clay surrounding a pile. Present and commonly applied design methods are however, still of a semi-empirical nature.

1.5 A brief summary of relevant past work by the author

The following gives a brief summary of relevant past pile research work undertaken by the author at the Norwegian Geotechnical Institute (NGI).

It all started in 1980 when the author was asked by Kaare Høeg, NGI's director at the time, to be responsible for planning and execution of an extensive pile load testing program which had as primary focus to address the impact of cyclic loading on the axial and lateral bearing capacity of piles in clay. The selected test site was at Haga in Norway. The clay at the site was medium plastic and moderately overconsolidated due to removal of overburden. The test piles used were mainly closed- ended, had a length of 5.15 m and diameter of 153 mm and were heavily instrumented with strain gages and earth and pore pressure sensors along the shaft. A total of 28 different piles were installed and tested to get a comprehensive picture of how different combination of static and cyclic loads affected the pile capacity. To fully understand the effects of cyclic loading it was vital, as a reference, to also establish a good understanding of the pile behaviour during static monotonic loading. This research project therefore also included assessments of stress changes around a pile during the installation and re-consolidation phases. As part of that, trenching and testing of soil next to the pile was undertaken, and a series of laboratory tests were carried out to study the impact of severe remoulding on the properties of the clay close to the pile wall. On that basis the author proposed a new approach to determine the limiting shaft friction for piles in clay. A procedure was also developed for predicting load-displacement response and the impact of any type of cyclic loading on the axial capacity and pile displacements.

Following the Haga test program (1980-84) the author took the initiative to, and was responsible for, a series of larger scale instrumented pile load tests in three soft clay deposits (1986-1988). The test sites were located at Lierstranda and Onsøy in Norway and at Pentre in the UK. The clay at Onsøy and Lierstranda were respectively medium plastic and low plastic normally consolidated deposits. The clay deposit at Pentre was somewhat overconsolidated and of medium to low plasticity. Three types of instrumented test piles were used. The type-A test piles installed at each site were closed-ended 219 mm steel pipe piles driven through casings to depths ranging from 15 to 37.5 m at each site. The casings extended to 10 m above the pile tip. Pile type B, only tested at Lierstranda and Onsøy, was an open ended pile with diameter 812 mm and driven to depth of 15 m. The purpose of pile B was to get a direct comparison between open and closed-ended piles. Pile type C was of the same dimension as the type A piles, but was driven without any casing to a depth of 35 m. It was only installed and tested at the Onsøy site. The purpose of pile C was to see if there was an effect of pile length on the pile performance. A striking feature of these pile test results was that they revealed extremely low shaft friction in the low-plastic silty clay deposits found at Lierstranda and partly at Pentre. The author therefore proposed that the plasticity index was an important factor impacting the ultimate shaft friction, a finding which was also supported by some older load tests on wooden piles in Norway. The data also showed that the low shaft friction in silty clay was related to very low measured effective earth pressures against the piles at onset of pile loading. Analytical models for predicting earth and pore pressures during installation and re-consolidation were proposed for both open and closed-ended piles. Cyclic testing was also part of the load testing program on these piles, and a numerical model that could capture effects of pile flexibility on pile displacements in addition to local cyclic degradation effects were refined and verified.

In 1983-85 Conoco Norway financed a large axial pile load testing program in a high plastic normally consolidated clay deposit in the West Delta area of the Gulf of Mexico. The Earth Technology Corporation with support of DNV was contracted to plan and execute the test

program, but NGI and with the author as project manager was sub-contracted to review the test program and to undertake some laboratory tests on the clay. Furthermore, in 1988 NGI, with the author as project manager, got a separate assignment to independently review, assess and in detail analyse all test results. The West Delta test program included load tests on a large scale fully instrumented 762 mm pipe pile driven to a depth of 71 m, and a series of tests on small model pile segments, with diameter of respectively 76 mm and 44 mm. The large scale pile was loaded statically and cyclically to failure 116 days and 500 days after the pile was installed. The model piles were load tested at various times after installation to study the increase in pile capacity with degree of consolidation.

In 1988-1991 NGI, again with the author as project manager was contracted to undertake pile tests in a very stiff clay deposit at Tilbrook Grange in the UK. The clay had undrained shear strength typically in the range 400 to 700 kPa. NGI's test program included static and cyclic testing on three instrumented closed-ended piles of the same type as used in previous tests at Onsøy, Lierstranda and Pentre. The piles were driven to tip penetration of 12.5 to 27.5 m. A non-instrumented 273 mm open-ended pile that had served as casing for the deepest of the closed-ended piles was also load tested. Previous to NGI's tests at the Tilbrook Grange site, load tests had been carried out on two large open ended piles with a diameter of 762 mm driven to a depth of 30 and 32 m. It also became part of NGI's scope of work to compare NGI's own pile tests to these large diameter pile tests, and to review and recommend design methods for piles installed in stiff and very stiff clay deposits.

Most results of the aforementioned projects were published by 1992. The author then let the subject lie for some years but kept track of new investigations by others. In connection with an invited lecture at the Lymon Reese Symposium in 1999 the author made a fresh and critical review of NGI's and other published fully instrumented pile load test results that had become available by that time, but that work was never published. That was partly the reason for embarking upon the work presented herein.

C.J. Frimann Clausen (private consultant for the past 30 years), started around 1995 to put together a new data base on pile load test results for both piles in clay and sand. He was engaged to work with NGI to develop the database further and on that basis evaluate existing design procedures or propose new or modified procedures for axially loaded piles. The test data base contained all well documented load tests that could be accessed in international journals and other geotechnical literature. The author got involved in this work, and in the process also studied the results of some new large scale pile load tests that had been undertaken in Norway and abroad. The work resulted in a new proposed semi-empirical design procedure.

In 2007 the author took the initiative to a new pile load testing program to primarily study the effects of aging on the axial bearing capacity of piles both in sands and clays. The test program includes a series of load tests at six different test sites on steel pipe piles of diameter around 400 mm driven to depths of 15 to 25 m. Six test piles are installed at each site, and they will be load tested over time period ranging from about 2 months to 2 years after the piles were installed. The results of the first static reference tests on the piles installed at the four clay sites are incorporated in the present study.

2 OBSERVATIONS FROM INDIVIDUAL INSTRUMENTED LOAD TESTS

2.1 General approach

This chapter summarises the most important factual results from the instrumented pile load tests covered in this study, including overall ground conditions and soil parameters used for assessing the results, testing arrangements, and key test results. In this way it is hoped that the data will be more easily accessible to others, and that the interpretations made by the author are possible to check or verify.

With respect to soil conditions the author has focused on identifying two key parameters in a consistent and transparent manner, namely a representative undisturbed in-situ undrained shear strength, and the stress history as represented by the apparent preconsolidation pressure, p'_c, and corresponding overconsolidation ratio, OCR. The use of "apparent" in this context is because OCR, always being greater than 1.0, can be due to ageing or secondary creep effects (e.g. Bjerrum, 1973), true overloading (physical larger overburden or lower pore pressures in the past than at present), or chemical weathering or "cementation" effects. Although the reason for OCR>1 in principle may have an impact on the general stress-strain-and strength characteristics of a clay deposit, it has been chosen in this study not to make any such distinctions.

The pre-consolidation pressure has traditionally been determined by incremental (IL) type oedometer tests with 24 hr load steps. In more recent years the constant rate of stain (CRS) oedometer test is also widely used. The pre-consolidation pressure depends on the rate of loading (e.g. Bjerrum, 1973). CRS testing reported by Sällfors (1975) and Leroueil et al (1983) also clearly documented that the apparent pre-consolidation pressure from CRS tests depends on the rate of strain applied. At NGI a CRS test is typically run at a rate of 0.6 % pr. hour (Sandbækken et al, 1985). Compared to a standard type IL test run with 24 hr increments, it has commonly been observed that the CRS test gives 10-15 % larger preconsolidation pressure (Berre, 2011, personal communication). The "standard" CRS test is used as basis for estimating the preconsolidation pressure in this study. When only IL tests have been available, the p'_c-values interpreted from these tests were upgraded by 10 %.

Most data bases on piles in clay established in the past, have used a variety of undrained shear strength values as basis for back-calculating apparent mobilised α-values, for instance UC strength, fall cone strength, miniature lab vane strength, UU strength and in-situ vane shear strength. The undrained strength derived from such different tests can vary within wide limits, easily by a factor of 2, see for instance Flaate (1965) and Chen and Kulhawy (1993). The lab strengths were also often determined on driven or pushed samples that we today would expect to give very poor quality for most clay deposits.

It has been well recognised for more than 40 years (e.g. Bjerrum, 1973 and Ladd et al 1977) that anisotropically consolidated triaxial compression (CAUC) and extension (CAUE) tests, combined with direct simple shear tests (DSS) are needed to get a reasonably complete picture of the anisotropic nature of the in-situ undrained shear strength characteristics of clays. The mode of shearing a soil element along a pile will experiences during axial loading, most closely resembles the DSS strength, s_{ud}. It has therefore been chosen in this study to consistently use s_{ud} as the reference undrained shear strength for back-calculating apparent mobilized α-values.

Even with proper tests, the results can be significantly influenced by sample disturbance. The impact of sample disturbance on the stress strain and strength characteristics of clays has been dealt with by for instance Lunne et al (2006[a]) and Lunne et al (2006[b]). A new block sampler developed by Lefebvre and Poulin (1979) has been shown to greatly improve sample quality in soft clays, and has been used fairly extensively by NGI at different test sites. Anticipated strength and pre-consolidation pressure from such high-quality samples are used as basis in this study. Such data on high quality block samples only exist for a limited number of the test sites considered in this study. Karlsrud and Hernandez (2011) have however, summarised volumetric compressibility and undrained shear strength relationships on basis of a large number of oedometer tests, CAUC, CAUE and DSS tests that have been carried out on such high quality samples. The data base covers a wide variety of clays (mostly from Norway), with water content ranging from about 25 to 75 %, OCR from 1.1 to 6.7, and undrained CAUC type strength ranging from about 15 to 200 kPa. This work also involved establishing SHANSEP type correlations (e.g. Ladd and Foott, 1974, Ladd and DeGroot, 2003) for these clays. Furthermore, Karlsrud et al (2005) presented correlations between CPTU cone factors and undrained strength and OCR determined on such high quality block samples.

When there has been a lack of sufficiently and relevant oedometer and DSS tests on high-quality (block) samples, the empirical correlations presented in the aforementioned studies, including the CPTU correlations, have been used to arrive at reference values of s_{ud} and OCR. The actual correlations used will be shown, where relevant, later in this Chapter.

In some cases the load tests dealt with were carried out at a time when the degree of consolidation, U, (taken as the degree of excess pore pressure dissipation at the pile shaft) had not fully reached 100 % (in some cases only 85 %). In such cases the effective stresses against the pile shafts and the ultimate shaft friction have been extrapolated to represent 100 % consolidation. The procedure used to do that is described, where relevant, in the subsequent sections.

2.2 Haga

2.2.1 General overview of test site and load tests

The Haga test site lies about 60 km NE of Oslo. The marine clay at the site is leached but not very sensitive, and is overconsolidated, primarily as a result of removal of overburden. The test site is located in an area where the original ground surface sloped at about 1:20 down towards the river Glomma. The original ground surface in the test area was on average at Elev. +99.0, but clay had been excavated down to about Elev. +96.5 for tile production in the mid 1970's. As part of a plate load testing program undertaken by NGI (Andersen and Stenhammer, 1982) the ground surface was lowered further down to Elev. +94.5 on the outside of the reaction ring beam where most of the pile tests were carried out, and to Elev. + 93.7 inside this ring beam, Figure 2.2.1 and 2.2.2.
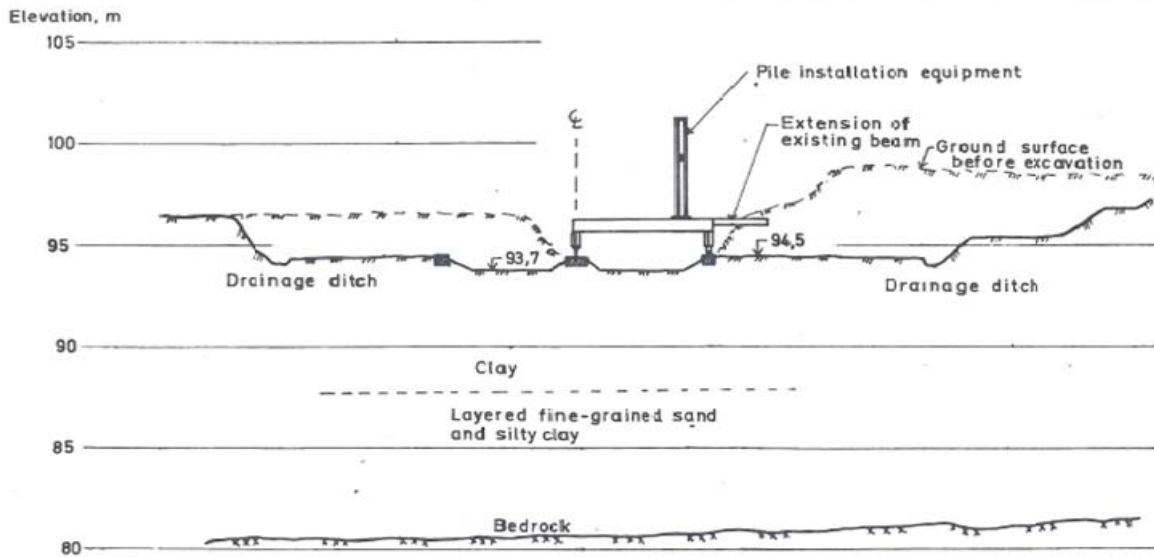
Figure 2.2.1- Typical cross section through the test site at Haga (from Karlsrud and Haugen, 1984)

A total of 28 individual axial pile load tests were carried out at the site. Figure 2.2.2 shows the location of the individual pile tests. All test piles had a length of 5.15 m, outer diameter of 153 mm and wall thickness 4.5 mm. The piles were jacked into the ground from a special installation tower mounted on a reaction beam that could rotate around the precast foundation ring beam, ref. Figure 2.2.1 and the picture in Figure 2.2.3.
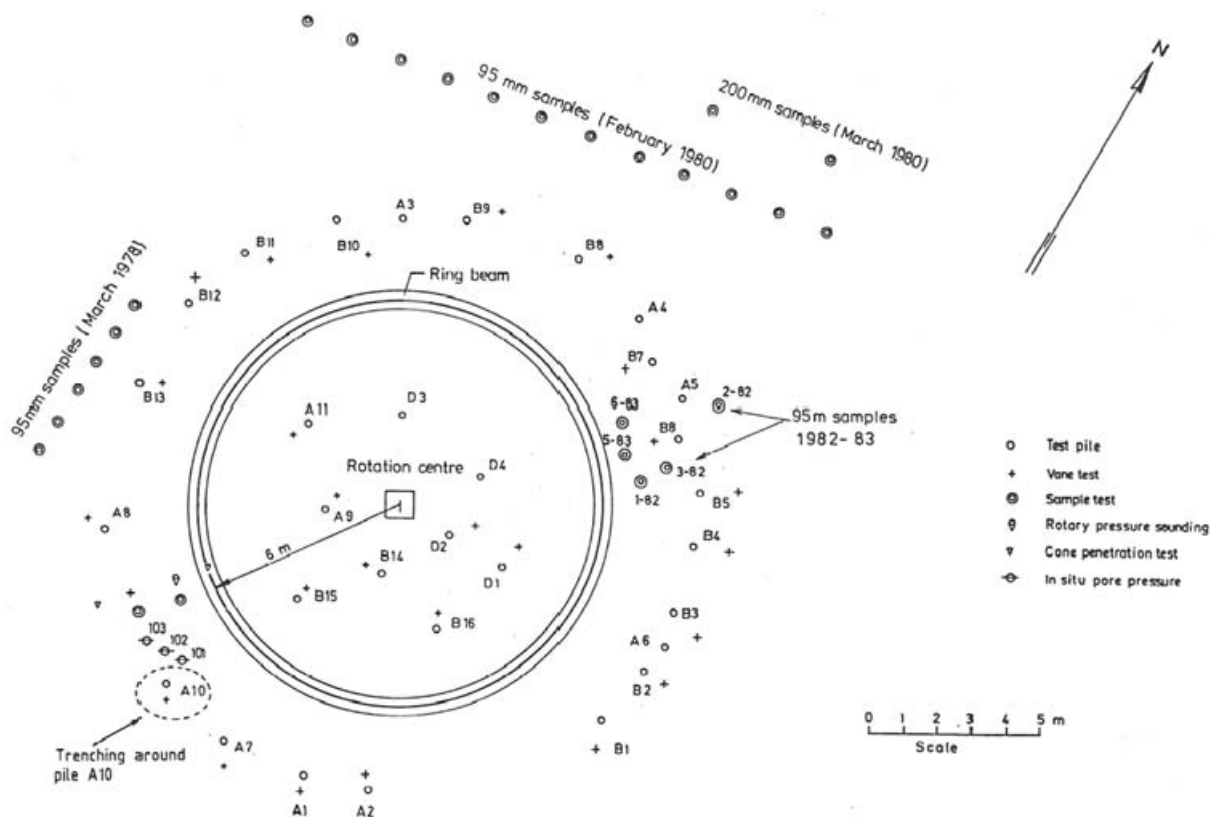
Figure 2.2.2- Layout of test site, Haga (from Karlsrud and Haugen, 1983)
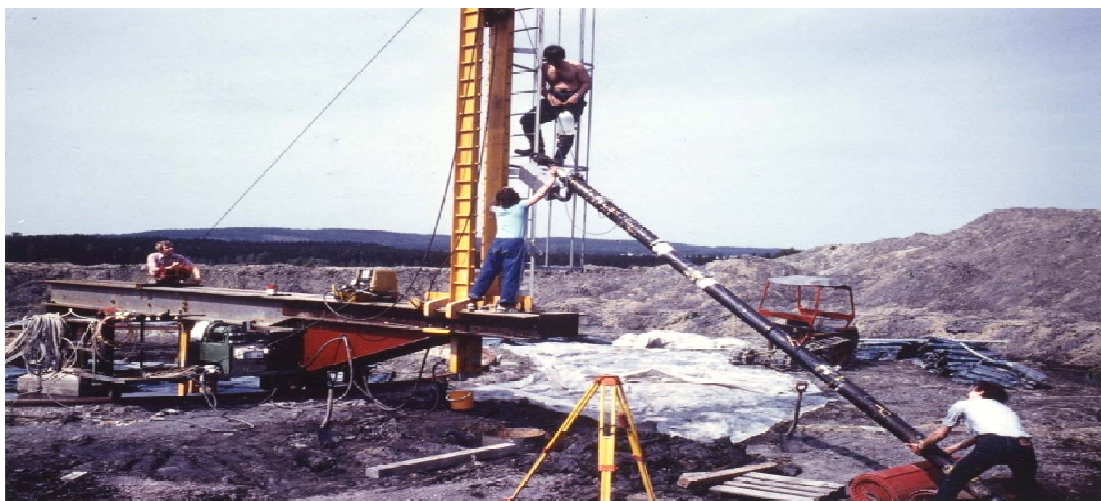
Figure 2.2.3- Picture from installation of test pile, Haga (from Karlsrud and Haugen, 1983)

The individual piles tested had the following characteristics.

- Pile A1- Open-ended without instrumentation.
- Pile A2- Closed-ended with earth and pore pressure cells mounted at 4 levels, and strain gages near the top and bottom of the pile. As shown in Figure 2.2.4, 6 free-field piezometers, P1 to P6 were installed in the ground between piles A1 and A2 prior to their installation. The purpose was to study the radial extent of pore pressures generated by the pile installation.
- Piles A3 to A11- Closed-ended without instrumentation. The same pile was used for all these tests by extracting the pile at re-installing it after the end of a test.
- Piles B1 to B16- Closed-ended pile fully instrumented with earth and pore pressure cells mounted at 4 levels, and strain gages at 6 levels, Figure 2.2.5. The same pile was used for all these tests by extracting the pile and re-installing it after the end of a test.

Membrane type vibrating wire gauges, with a membrane diameter of 20 mm, were used to measure earth (EP) and pore pressures (PP) against the pile wall on the A2 and B-piles. The EP membranes were curved to fit the pile diameter and mounted flush with the pile surface. The PP gages were mounted with a high-air entry filter in front. The PP filters were saturated under vacuum and protected with a rubber gasket prior to installation. The gasket was ripped off just before the PP gages entered into the clay.

A small local hole was dug around each pile so that the pile top on average was located 0.45 m below surrounding ground (range 0.15 to 0.65 m). This hole was kept filled with water during pile installation to allow the protective membrane covering the piezometers on the pile to be taken off under water.

Note that there were pairs of 2 diametrically mounted EP and PP gages and 4 strain gages at each instrumentation level. In addition to the strain gages, there was a vibrating wire (VW) load cell mounted at the pile head. Pile-head displacements were monitored by both an LVDT transducer (Linear Variance Displacement Transducer) and a manual dial gage. They were mounted on a reference beam supported on earth screws placed 1.25 m to each side of the test piles.

Figure 2.2.4- Instrumentation in connection with test piles A1 and A2, Haga (from Karlsrud and Haugen, 1983)
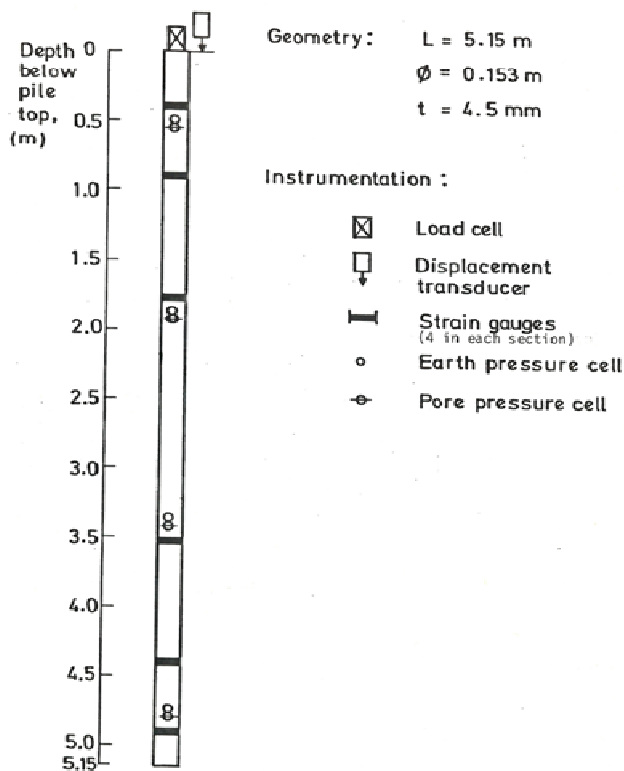
Figure 2.2.5- Instrumentation test pile B, Haga (from Karlsrud and Haugen, 1983)

All but one the 27 individual test piles were subjected to a first static load test to failure (or near failure), carried out between 7 and 36 days after the piles were installed. 24 piles were loaded in tension and 2 in compression. All piles were after a waiting period of typically 1 day subjected to cyclic loading. The cyclic load amplitudes covered a wide range, from symmetric two-way loading to pure one-way loading, immediately followed by a new static test to failure. After some resting time, generally varying from one to two weeks, most test piles were then subjected to a similar series of static and cyclic testing, and in some cases also a third series of load testing.

The load tests were carried out in a stepwise and load-controlled manner. The magnitude and duration of the load steps generally decreased towards failure, with the first steps being 10 kN lasting for 3 minutes, and the last steps 2.5 kN lasting 3/4 minute.

Herein it is primarily the first static load test carried out on the individual piles that will be dealt with. As mentioned in Section 1.2, effects of cyclic loading are presented and discussed in Chapter 7.

The results of the Haga tests have been extensively documented, analyzed and interpreted in a series of reports prepared by NGI, reference for instance the two summary reports by Karlsrud and Haugen (1983 and 1984). Karlsrud (1986) took the overall interpretation of the static and cyclic load test results a step further, including modelling of the installation phase, ultimate shaft friction, load-displacement response and effects of cyclic loading on the performance of the test piles. The results and interpretation have also been highlighted in a series of papers by Karlsrud and Haugen (1985[a,b]), Karlsrud et al (1986) and Karlsrud and Nadim (1990). Most of the following data and results are taken directly from these publications. The only major new revision is that the reference undrained strength used for calculating α- values have been slightly modified.

2.2.2 Key soil parameters

Figure 2.2.6 shows that the clay at the Haga site is very homogeneous to a depth of about 4.5 m with a water content of typically of w=38 %, a plasticity index of I_p=15 %, and a clay content of 40-60 %. Note that the depth scale in this figure for convenience refers to zero at the top of the 5.15 m long test pile. From 4.5 to 5.5 m there is a more plastic clay layer with water content reaching up 55 % and I_p reaching 30 %. Below 5.5 m the clay gradually becomes siltier. At a depth of about 8 m, there is a transition to layered fine grained sands with some inter-bedded silty clay layers reaching down to bedrock at a depth of about 13 m, Figure 2.2.1. The total unit weight of the upper clay layer is on average around γ_t =18.5 kN/m^3, and γ_t= 17.5 kN/m^3 for the most plastic layer.
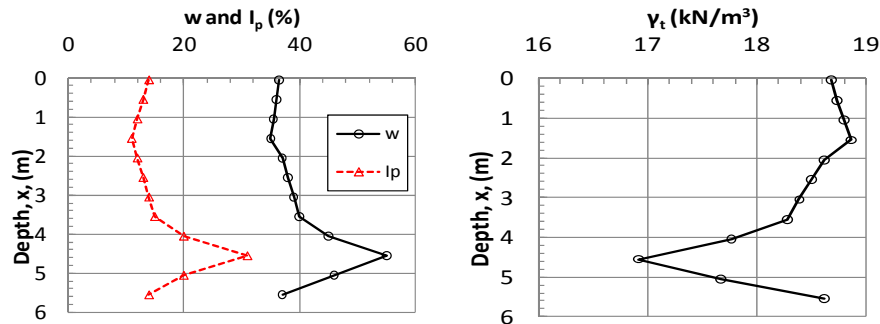
Figure 2.2.6- Summary of index data, Haga

Due to leaching, the salt content of the clay is low, less than 1g/l. Probably due to chemical weathering, the sensitivity is still moderate and in the range S_t =4-6 according to fall cone tests and in-situ vane borings.

The in-situ pore pressure conditions at the Haga site are somewhat special. The sandy layers below the clay (Figure 2.2.1) drain rather freely laterally out to the slope going down to the river Glomma. This implies an under drainage that has lead to very low pore pressures throughout the clay profile as shown by Figure 2.2.7. The data in this figure is based on monitoring of free field pore piezometers as well as the equilibrium pore pressures measured along the various B-pile tests. The pore pressure data cover variations observed over a 2 year period (1981-82) when most pile testing took place. The extreme low values were observed during a very dry period in late August 1981. In-spite of the low in-situ pore pressures, all laboratory tests show that the clay is fully saturated. In this connection it can be mentioned that the test site formed a low point or pit compared to the surrounding ground surface. Some water (up to about 0.5 m) was allowed to impound in the pit during rainy periods and when no testing was going on. This has contributed to maintaining a fully saturated condition through the clay profile.
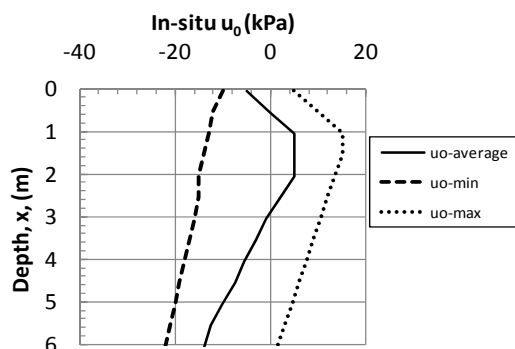
Figure 2.2.7- In-situ pore pressures, Haga

Figure 2.2.8 shows that the pre-consolidation pressure defined by Karlsrud (1986) from standard CRS and IL oedometer tests, p_c', is considerably larger than the present vertical effective stress. This is probably a combined effect of unloading and chemical weathering. The apparent over consolidation ratio, OCR, decreases considerably with depth, from OCR=15-20 near the top to OCR=3-4 near the bottom of the pile, Figure 2.2.8. A series of oedometer tests were also carried out on specimens cut vertically from the tube sample to try to determine the apparent horizontal pre-consolidation pressure, p_{ch}', in the ground. As seen in Figure 2.2.8, p_{ch}' corresponds typically to 2/3 of the vertical preconsolidation pressure.
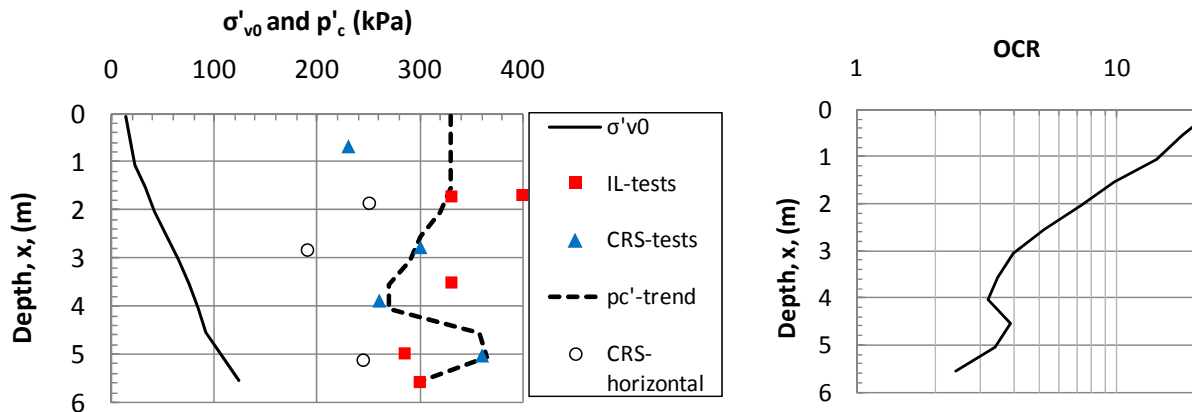
Figure 2.2.8- In-situ vertical effective stress, preconsolidation pressure and OCR, Haga

Figure 2.2.9 summarizes values for the virgin compressibility determined from the oedometer tests in terms of modulus number, m_0, as defined by Janbu (1963). The M-p' curve for virgin loading was in this case defined with $p_r' = 0$, which implies that the classical virgin compression index, $C_c/(1+e_0)$ is the same at all stress levels and correlated to m_0 through the relationship:

$$C_c/(1+e_0) = \ln(10)/m_0 \qquad\qquad (2.2.1)$$
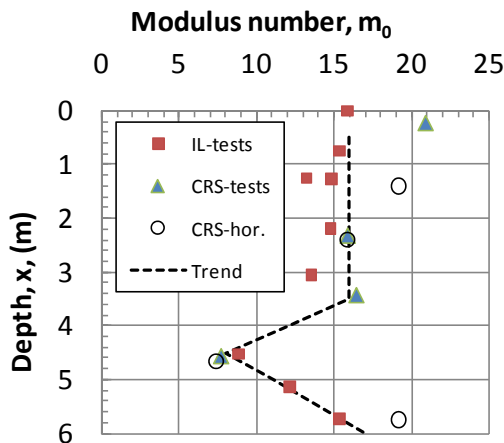
Figure 2.2.9- Modulus number, m_0, as defined from oedometer tests, Haga

Figure 2.2.10 presents values for the coefficient of consolidation, c_v, defined at a stress level corresponding to $p' = 1.5 \cdot p_c'$. The values typically lie around $c_v = 8$ m^2/yr, apart from the plastic clay layer where it drops to about 2 m^2/yr.
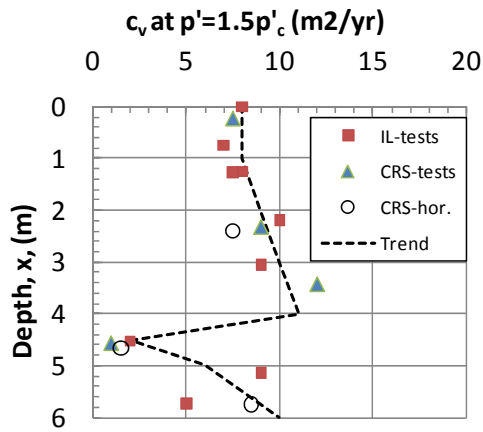
Figure 2.2.10- Coefficient of consolidation, c_v at p'=1.5p'$_c$ from oedometer tests, Haga

The permeability of the clay has not been directly measured, but values have been back-calculated from the c_v-values determined for each load increment using the expression:

$$k = c_v \cdot \gamma_w / M \tag{2.2.2}$$

To establish the in-situ vertical permeability, k_0, the k-values as function of volumetric strain from the oedometer tests have been extrapolated back to zero volumetric strain. (The procedure is described in later section 2.3.2). When drawing the trend line in Figure 2.2.11 most weight was placed on the CRS test results, where at least one direct test of permeability was normally made to check values that are automatically calculated as part of a CRS test (e.g. Sandbækken et al, 1985).
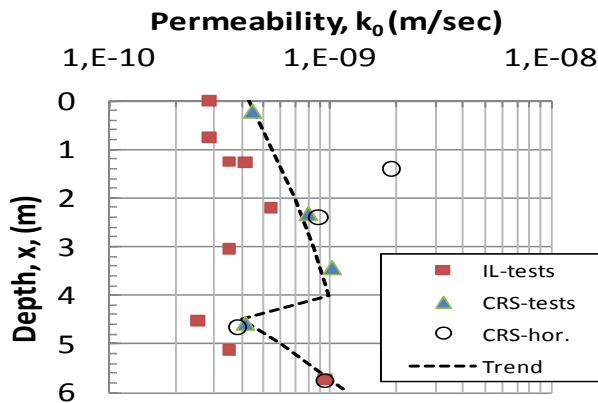
Figure 2.2.11- In-situ permeability, k_0, derived from oedometer tests, Haga

In-situ remote vane borings were carried out close to essentially all test piles at Haga. Figure 2.2.12 shows that there are some but small variations across the site, with an average s_{uv} generally around 40 kPa in the low-plastic clay and 55 kPa in the medium plastic clay layer. Karlsrud (1986) showed that there was a general tendency for lower vane strengths inside the ring beam than outside, especially in the top part. This may partly have to do with the 0.8 m deeper excavation on the inside. Otherwise there were no specific trends in the deviations from the average vane strength profile, with the exception of boring B1.
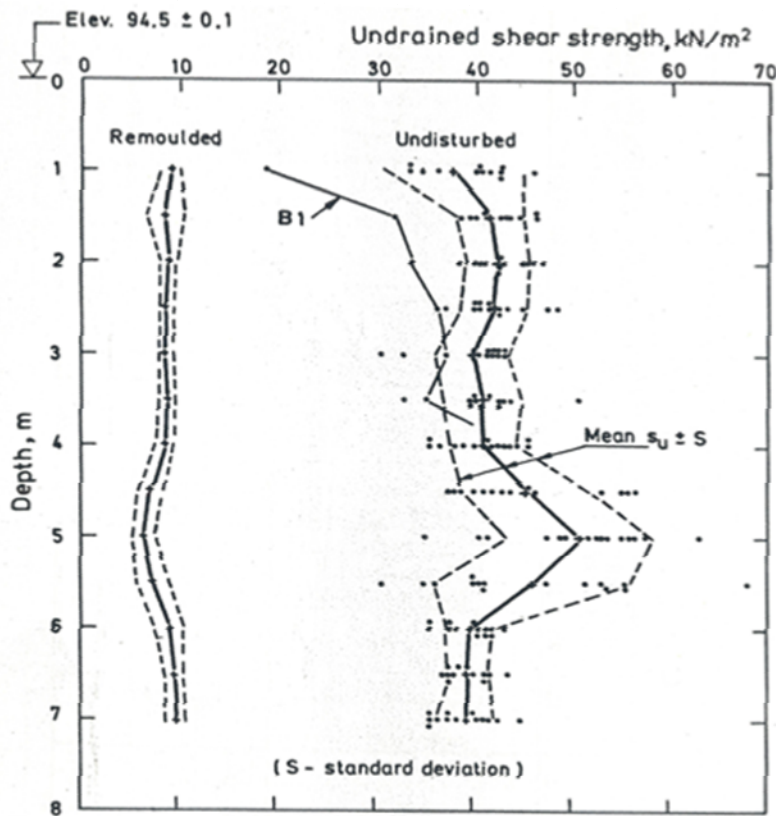
Figure 2.2.12- Summary of in-situ vane strength values (after Karlsrud & Haugen, 1984)

Figure 2.2.13 presents undrained shear strengths as determined by CAUC and CAUE triaxial tests as compared to the average in-situ vane strength. The triaxial test results were taken from Lacasse (1979) and Andresen and Stenhammer (1982). The tests were made on 95 mm piston samples of normal good quality. The anisotropy ratio of s_{ue}/s_{uc} appears to be rather constant and equal to 0.39. The in-situ vane strength is just about equal to the average of the triaxial compression and extension values at all levels.

As part of the pile testing program a series of direct simple shear (DSS) tests were carried out on the Haga clay to study more fundamental aspects of the undrained shear strength and how it depends on specimen orientation and consolidation procedures, e.g. Karlsrud and Haugen (1984). In terms of consolidation procedures some samples were consolidated directly to σ'_{v0}, and others were first consolidated up to the assumed pre-consolidation pressure, p'_c, and then unloaded back to σ'_{v0} prior to undrained shearing. Figure 2.2.14 clearly shows that the $p'_c \rightarrow \sigma'_{v0}$ procedure gives much higher strength (up to factor of about 2) than when consolidating directly to σ'_{v0}. Karlsrud (1986) suggested that the reason for the much lower shear strength when samples are consolidated directly to σ'_{v0} rather than $p'_c \rightarrow \sigma'_{v0}$, is that the test will then start off with much too low radial effective stress, causing much more stress rotation and degradation of the clay skeleton during shearing than for $p'_c \rightarrow \sigma'_{v0}$ consolidated specimens.

Figure 2.2.14 also presents results from tests carried out on the vertically trimmed specimens. The vertically trimmed specimens gave essentially the same strength as the standard horizontally trimmed specimens provided that they were also pre-consolidated. The apparent horizontal pre-consolidation pressure shown in figure 2.2.8 was used when pre-consolidating the vertically trimmed specimens.
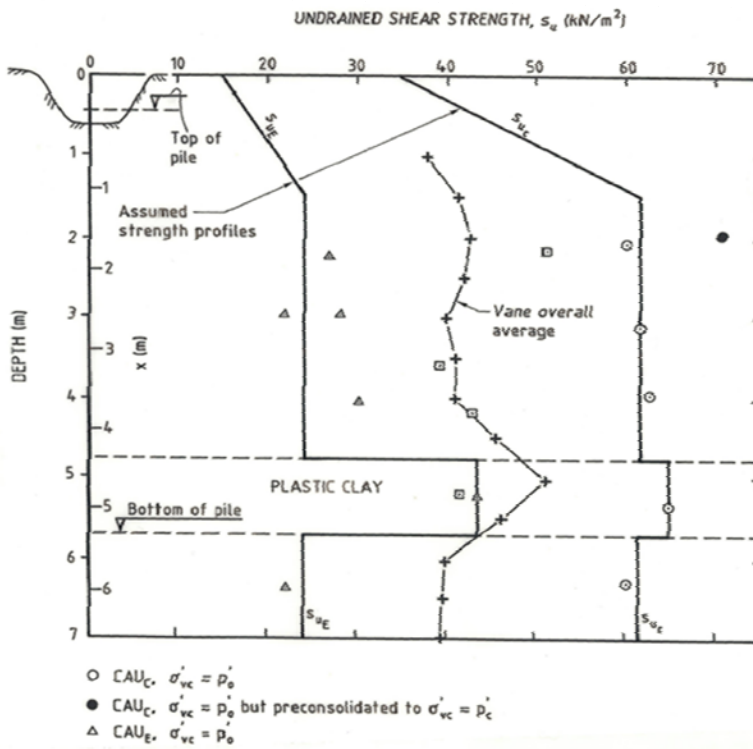
Figure 2.2.13- Strengths form triaxial CAUC and CAUE tests, Haga (from Karlsrud and Haugen, 1984)
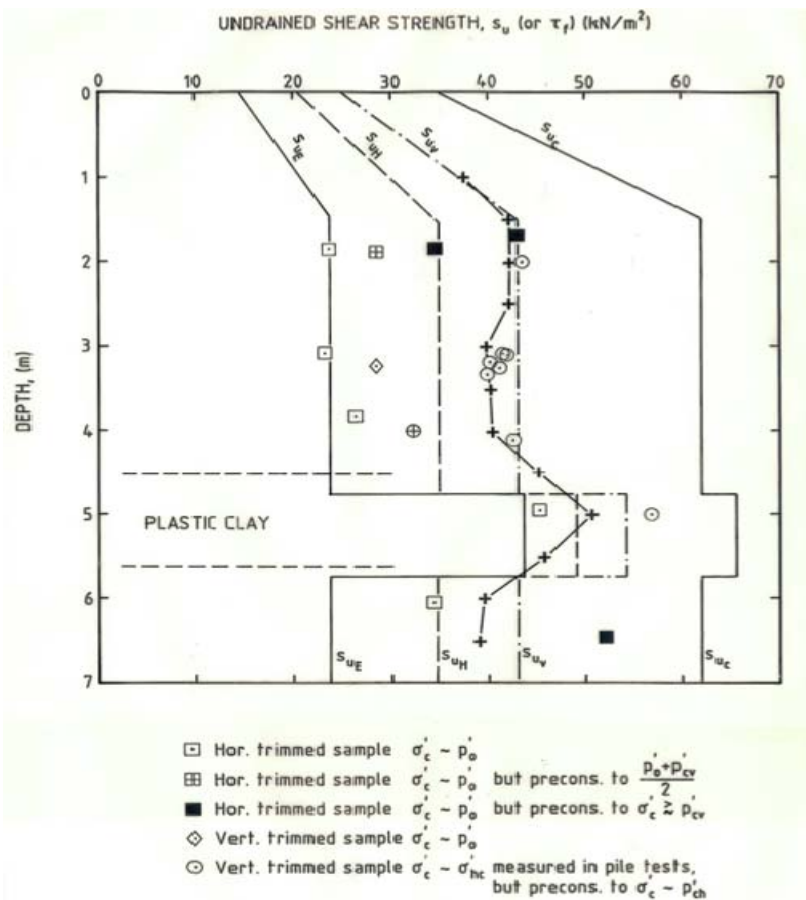
Figure 2.2.14-Results of DSS tests on intact vertically and horizontally trimmed specimen, Haga (after Karlsrud, 1986)

 The DSS strengths for the $p'_c \rightarrow \sigma'_{v0}$ consolidated specimens agree very closely with the in situ vane strength profile. The s_{ud} profile actually chosen for comparison against the measured shaft friction is therefore in this study taken as equal to the average s_{uv} vane strength profile in Figure 2.2.14.

Both the triaxial and DSS tests show normalised strengths that are closely linked to the overconsolidation ratio. According to Karlsrud (1986) the following average correlations applies:

$s_{uc}/ \sigma'_{v0} = 0.28 \cdot OCR^{0.8}$

$s_{ue}/ \sigma'_{v0} = 0.12 \cdot OCR^{0.8}$

$s_{ud}/ \sigma'_{v0} = 0.20 \cdot OCR^{0.8}$

The undrained tests show that also the undrained modulus relates closely to the OCR value, Figure 2.2.15, with G_{50}/s_u decreasing from 200-300 at OCR around 2 to 25-75 at OCR of 10.
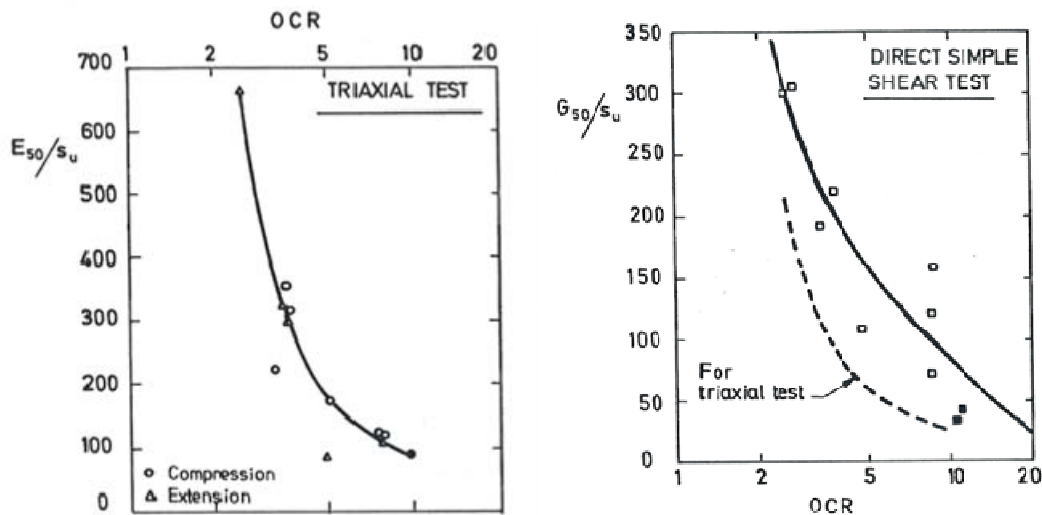
Figure 2.2.15- Normalised secant modulus values from triaxial and DSS tests, Haga (after Karlsrud, 1986)

The triaxial tests on the Haga clay defines a consistent effective friction angle of $\varphi' = 34.5^0$ and with no cohesion intercept. The apparent mobilised friction on the horizontal shear plane in the DSS tests corresponds on average to $\tan\delta = 0.6$ or $\delta = 30.9^0$. As discussed by Karlsrud (1986), the horizontal plane is in general not the critical shear plane at failure in a DSS test. If the horizontal (radial) effective stress is equal to the axial effective stress at failure, which often has been observed to be the case (e.g. Dyvik et al 1981), then $\tan\delta = \sin \varphi' = 0.566$, which is close to what was measured.

A special investigation was made at the Haga site to study the change in properties of the clay close to the wall of pile A10 after all testing on that pile was completed. A trench was excavated down to a depth of 2.2 m along the pile and then another 20-30 cm was carefully excavated by hand in a wedge shaped zone. Finally, by use of a knife and wire- saw several 10 cm thick blocks of clay were carefully cut out from the zone within 30 cm distance from the pile surface. Figure 2.2.16 shows a photograph from this operation.

Figure 2.2.16- Picture from trenching and block sampling next to Pile A10, Haga (after Karlsrud and Haugen, 1984)

During excavation and cutting of the blocks of clay, it was noted that the clay slipped easily off the pile surface. In contrast, when the pile was later pulled out, a 4-5 cm thick layer of clay adhered to the lower 1-1.5 m of the pile, Figure 2.2.17. This suggests that failure took place at the pile wall along the upper 3.5-4 m of the pile, and at 4-5 cm distance from the pile wall along the lower part, partly being located in the more plastic clay zone. The implications of this observation will be discussed further in Chapter 6.

Figure 2.2.17- Picture from extraction of pile A10 out of the ground, Haga (after Karlsrud and Haugen, 1984).

Figure 2.2.18 presents water content and fall cone strength determined on the block samples in relation to distance from the pile wall. For the clay closest to the pile wall the data shows a pronounced reduction (about 10 %) in the water content, and increase in fall cone strength of about 40 kPa. This is followed by a gradual transition to original undisturbed values at a distance of about 20 cm from the pile surface.
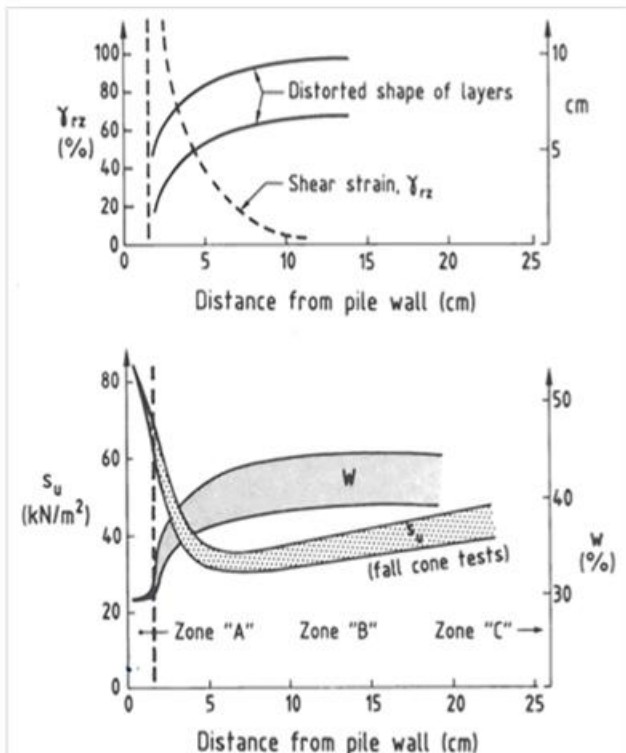
Figure 2.2.18 – Measured shear distortions, water content and fall cone strength as function of distance from pile wall, Haga (after Karlsrud and Haugen, 1985).
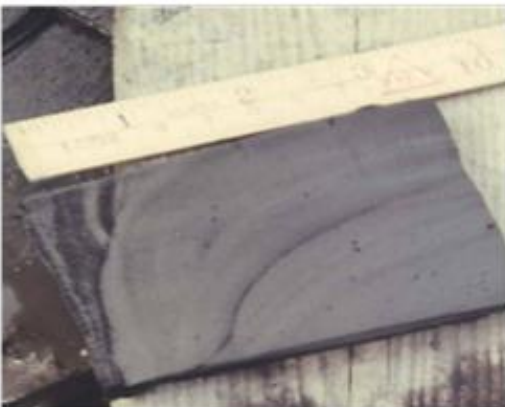
Figure 2.2.19- Picture of trimmed block samples taken next to the pile wall, Haga (after Karlsrud, 1986)

Based on the picture of a cut block sample in Figure 2.2.19, and x-ray photography on specimens taken at various distances from the pile wall, Karlsrud and Haugen (1984, 1985[a]), defined three distinct zones next to the pile wall, Figure 2.2.20:

- Zone A (RR-clay): An inner about 1.5 cm thick zone that has been very severely remoulded and has lost all traces of its original fabric. As a result of the reconsolidation phase the clay in this zone A has undergone a reduction in water content of about 13 %, corresponding to a volume change of 16-17 %. This reduction in water content is accompanied with a doubling of the fall cone strength from about 40 to 80 kPa.
- Zone B (Disturbed clay): This zone appears to have been subjected to more uniform shear distortions. The vertical shear strain, γ_{rz}, have actually been calculated from the distorted shape of the layers seen in Figure 2.2.18, and decrease asymptotically from

more than 100% in the transition to Zone A, to essentially zero around 12 cm from the pile wall. The water content gradually increases back to close to the original through this zone. The fall cone strength shows however a minimum value around 5 cm from the pile wall, and is first back to the original around 20 cm from the pile wall, Figure 2.2.18. The x-ray photographs show that the clay fabric has a preferred orientation which corresponds well with the vertical deformation pattern.

- Zone C (Intact clay): This zone, staring around 20 cm from the pile surface, corresponding to about 3.6 times the pile radius, shows no apparent influence of the pile.

In relation to these data it may be recalled that pile A10 was closed-ended.
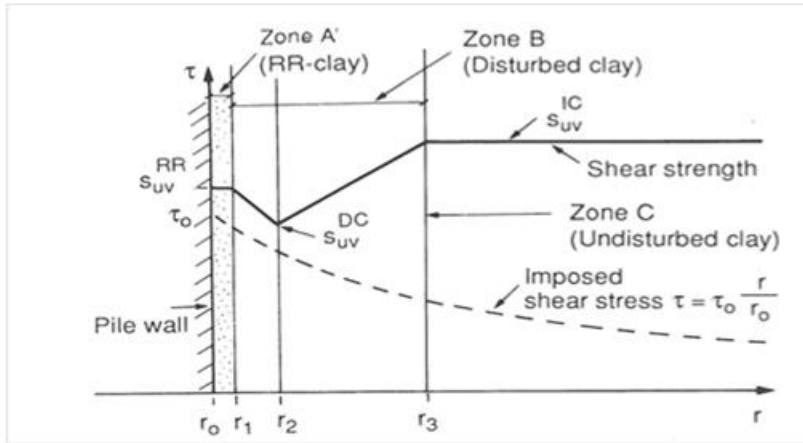
Figure 2.2.20- Schematic variation in impact of pile installation on clay properties, (after Karlsrud and Nadim, 1990)

To try to better understand the fundamental properties of the clay in the RR-zone, a fairly comprehensive program of DSS and direct shear box (DSB) tests were carried out on specimens that were severely remoulded in the laboratory and consolidated to a range of stress levels prior to undrained shearing. The remoulding procedure was to first knead the clay by hand and then smear it out on a glass plate with a spatula. The clay was then scraped off the glass plate and patched into a 16 mm high 10x 10 cm square shear box. The DSB had a filter to allow for consolidation at the top, and a standard steel grade bottom part. The DSB specimens were then consolidated and sheared. Specimens used for DSS tests were first consolidated in the DSB box and then taken out and trimmed to fit into the standard DSS apparatus.

When failure was reached, the samples were allowed to consolidate again under the same axial stress for 1 to 6 days, and then sheared a 2nd time. Figure 2.2.21 shows that the results of both the DSB and DSS tests gave quite similar strength when correlated to the axial consolidation stress, and as defined by:

$\tau_f = 0.31 \cdot \sigma'_{ac}$ for 1st time loading and

$\tau_f = 0.48 \cdot \sigma'_{ac}$ for 2nd time loading

At failure the DSS tests on the RR clay gave the following apparent mobilised friction angles, δ, as follows:

$\tau_f = \tan\delta \cdot \sigma'_{af} = 0.50 \cdot \sigma'_{af}$ ($\delta = 26.6^0$) for 1st time loading and

$\tau_f = \tan\delta \cdot \sigma'_{af} = 0.55 \cdot \sigma'_{af}$ ($\delta = 28.8^0$) for 2nd time loading
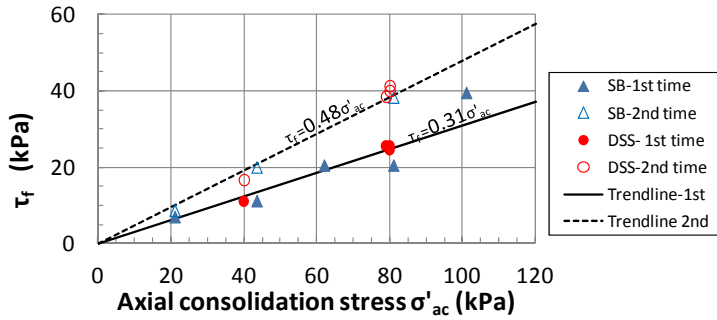
Figure 2.2.21-Results of DSS and SB tests on RR clay, Haga

Figure 2.2.22 summarize observed volume change in the laboratory tests on the RR clay as compared to that of tests on piston samples and the block sample taken 15 cm from the pile surface. The vertical effective stress at about 2.5 m depth is 46 kPa where the block sample was taken. According to Figure 2.2.22 that should correspond to a volume change of about 9.0 % This is less than the volume change of 16-17 % measured on the block sample next to the pile wall. This may partly be due to a difference in mean effective stress. Along the pile the horizontal (radial) effective stress was a factor of 1.39 larger than the vertical, leading to a mean effective stress of about 1.13 σ'_{v0}. In the oedometer, assuming a K_0 value of 0.5, the mean effective stress is $0.667 \cdot \sigma'_{v0}$. By correcting the volume change for this difference in mean effective stress, the volume change becomes $9 \cdot 1.13/0.667 = 15.2$ %, which is close to what was actually measured on the block sample.

Fall cone tests were also carried out on RR clay in the laboratory. As shown by Karlsrud (1986), for a volume change of the RR clay of 15 %, the fall cone strength was found to be typically 120 kPa, which is close to the value of 100 kPa measured on the block samples (Figure 2.2.18). Thus, most aspects of the observed properties of the clay in the RR zone closest to the pile wall were reproduced in the laboratory tests.
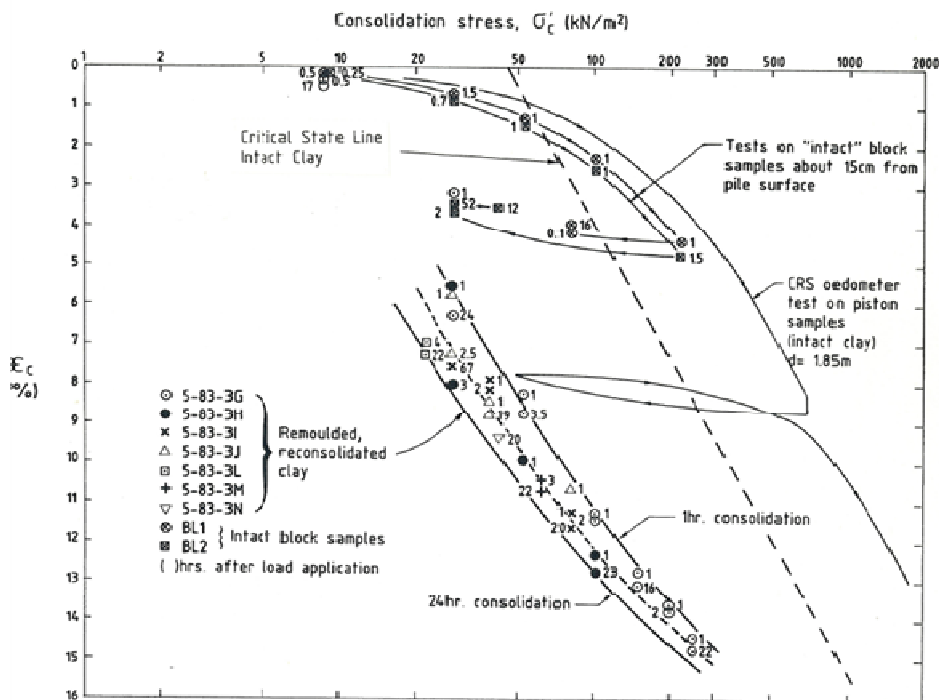
Figure 2.2.22-Consolidation data for RR clay compared to intact clay, Haga (after Karlsrud and Haugen, 1984)

2.2.3 Load test results

Figure 2.2.23 summarizes trajectories of pore pressure that were observed against all 16 instrumented B-piles as the piles penetrated into the ground. Only pressures for the sensors BPP3 and BPP4, located respectively 1.75 m and 0.4 m above the pile tip, are shown. The pore pressures generated by BPP4 near the tip were typically a factor of 1.5 larger than for the sensor above. This difference is reflects most likely a tip or end effect. Figure 2.2.23 also shows the average pore pressure measured at end of penetration at all instrumentation levels for all the tests. At the level of the BBP2, 1.9 m below the top or 3.25 above the tip, the end of installation pore pressures where about 85 % of what was measured when BBP3 passed the same level, which may be an effect of dissipation during pile installation. The final installation pore pressure at the very top level, 0.55 m below the pile top, was relatively speaking even lower, more like 60 % of the BBP3 values. Surface effects may be of some importance at that level.
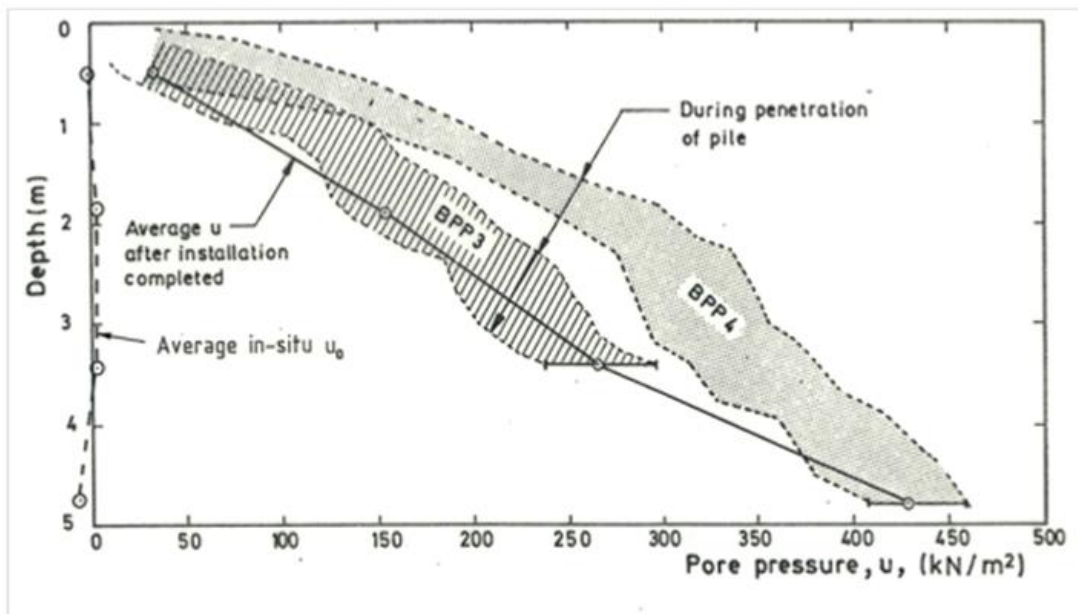
Figure 2.2.23- Summary of trajectories of measured pore pressure during pile penetration, Haga (after Karlsrud and Haugen, 1983)

Figure 2.2.24 presents normalised values of excess pore pressures at the end of pile installation. The normalised excess pore pressures generally increase with depth. As will be shown later this is primarily an effect of decreasing OCR with depth.
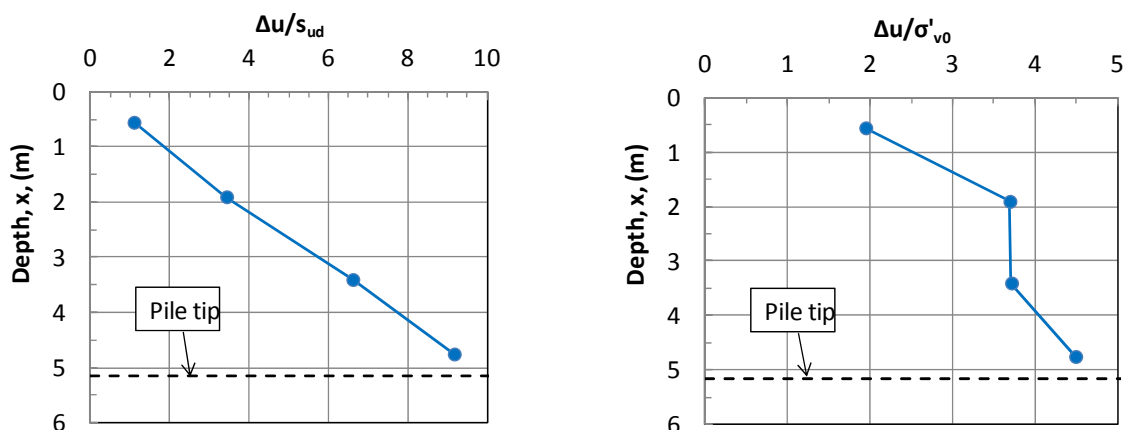
Figure 2.2.24- Normalised excess pore pressures at end of pile penetration, Haga

During and at the end of pile installation the measured total horizontal earth pressures were essentially identical to the pore pressure. The only exception was for the sensors closest to the pile tip, which showed total earth pressures that were about 15 kPa or 3 % smaller than the pore pressure.

Free field pore pressures were measured during installation of piles A1 and A2, Figure 2.2.25. The data suggest a delayed response in pore pressures at all locations but one (P4), probably due to incomplete saturation of the piezometer filters. Reasonable pore pressures were first observed after some hours had elapsed, Figure 2.2.25. For the closed-ended pile A2, which also had piezometers on the pile surface, an attempt has been made to estimate how the initial excess pore pressure tapers of with distance from the pile surface. The results presented in Figure 2.2.26 suggest that the initial excess pore pressure field extended to a distance corresponding to r_p/r_0 =15 to 20. The data for the open ended pile A1 penetration is even more uncertain in the initial phases, Figure 2.2.26, but may also suggest r_p/r_0 =15 to 20. After 1 day, the excess pore pressures around pile A1 were only about 40 % of those for the closed-ended pile A2.
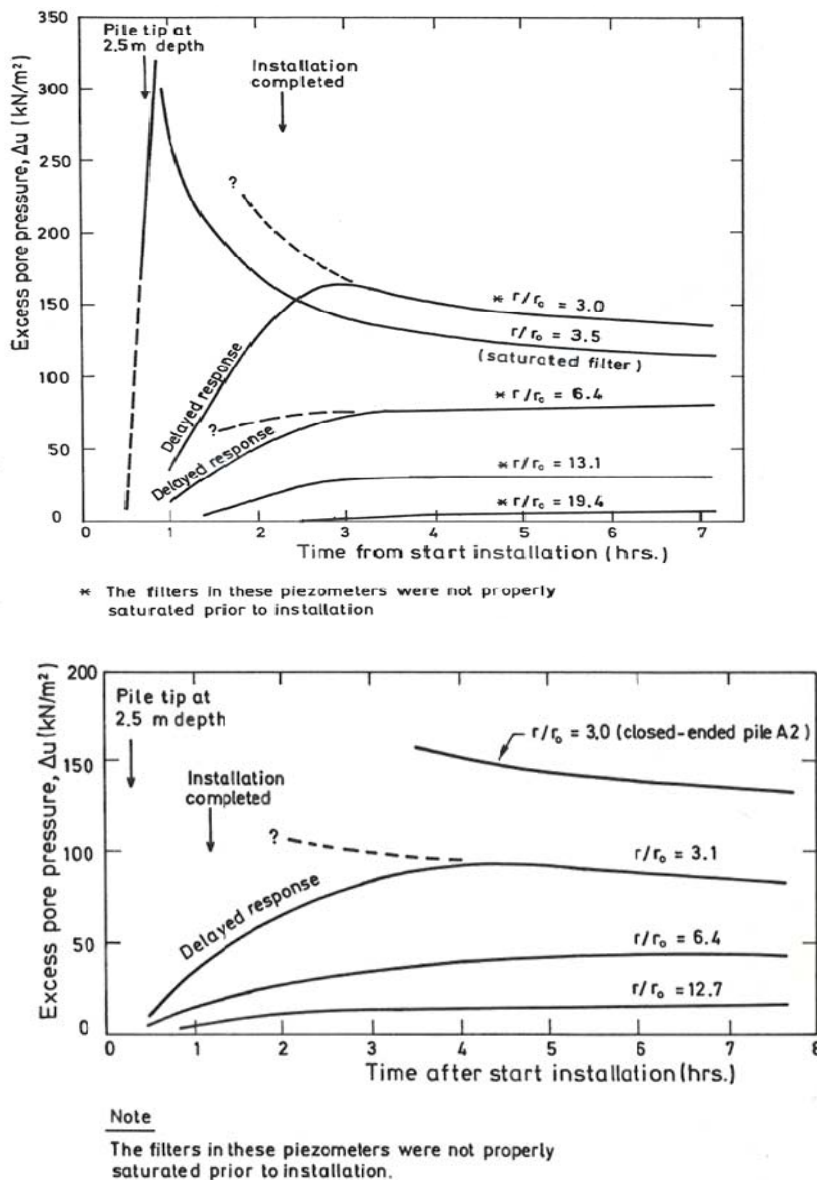
Figure 2.2.25 - Free-field pore pressures during installation of piles A1 and A2 Haga (after Karlsrud, and Haugen, 1983)
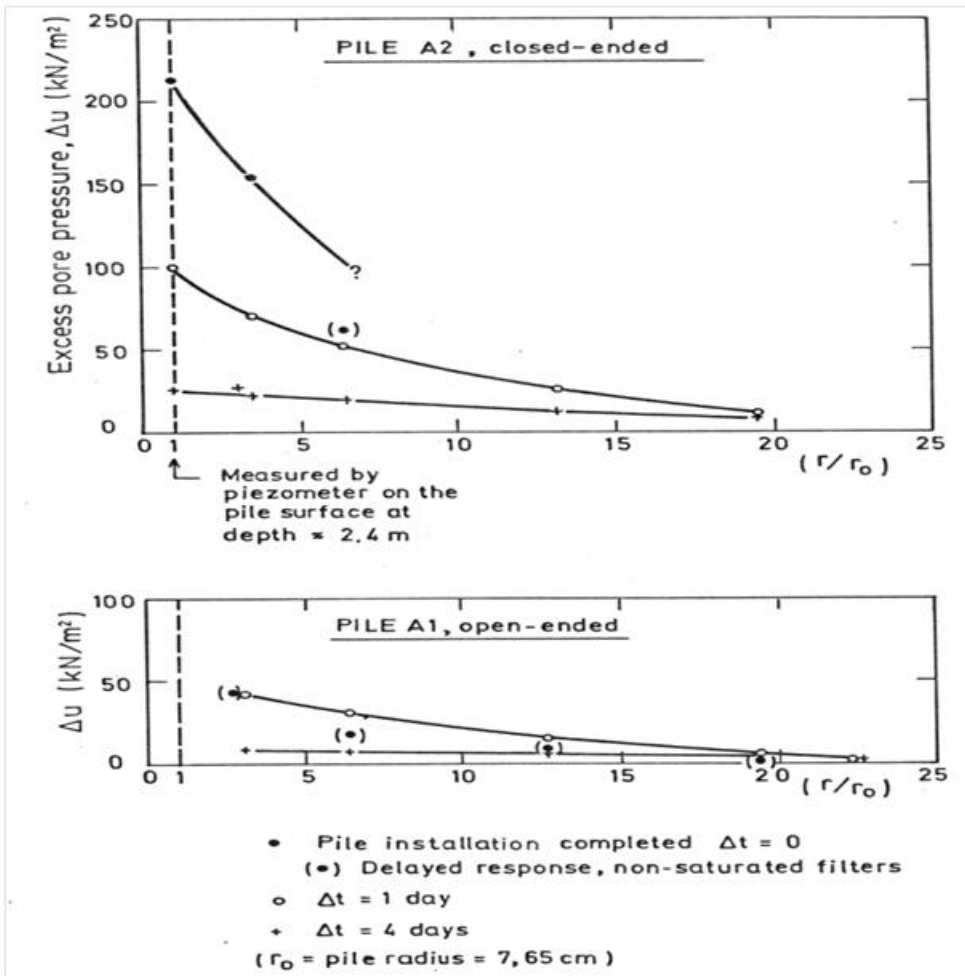
Figure 2.2.26- Pore pressures as function of radial distance, piles A1 and A2, Haga (after Karlsrud, 1986)

During jacking of piles A1 and A2 into the ground, the vertical ground movements around the pile were monitored. The heave developed proportionally to the pile volume in the ground, and was as presented in Figure 2.2.27 at the end of installation. By extrapolating the heave curve for pile A2 to about 40 mm at $r/r_0=1$ the total heave volume was calculated to correspond to about 52 % of the pile volume. That could suggest some volume reduction in the ground around the pile during pile installation. If it is assumed that all the missing volume comes from volume change in the clay, the average required volume change
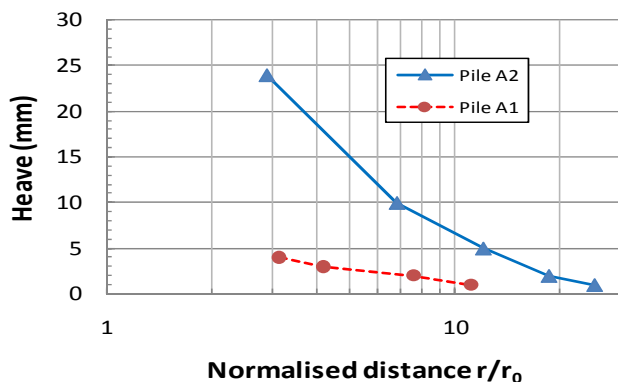
Figure 2.2.27 - Observed heave of the ground surface at the end of installation Piles A1 and A2, Haga

During jacking of the pile into the ground, the force applied was recorded. As presented by Karlsrud (1986) the installation force gave a back-calculated average shaft friction during installation in the range 6.2 to 7.7 kPa, which is almost identical to average measured remoulded in-situ vane shear strength along the piles, which ranged from 7.2 to 8.9 kPa, Figure 2.2.12.

During the re-consolidation phase, both the total earth pressure and the excess pore pressure reduced more or less in parallel. Figure 2.2.28 shows a typical example of this. Both the pore pressure and effective stress level off after 5-6 days, but there are no significant gain in effective stress before the degree of pore pressure dissipation exceeds about 40 %.
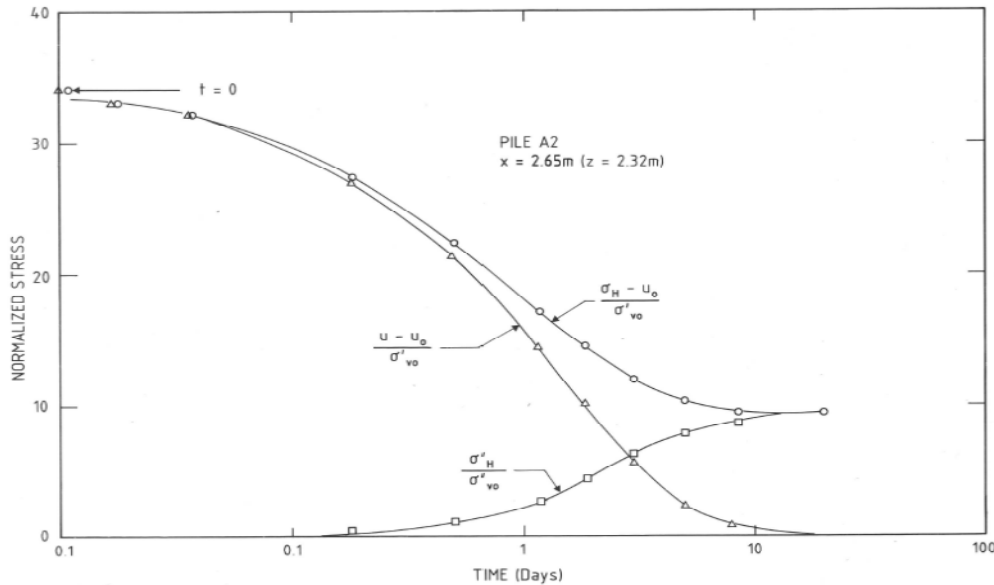
Figure 2.2.28- Example of evolution of normalised earth and pore pressure after completion of pile installation, Pile A2, Haga- after Karlsrud (1986).

Figure 2.2.29 shows the degree of pore pressure dissipation, U, versus time for selected tests. The times to reach 50 and 90% degree of pore pressure dissipation for piles A2, B6 and B7 are summarised in Table 2.2.1, and correspond to typically 12-20 hrs for t_{50} and 80-120 hrs for t_{90}. The proximity of the lowest sensors to the pile tip may have lead to slightly faster dissipation at these levels than higher up.
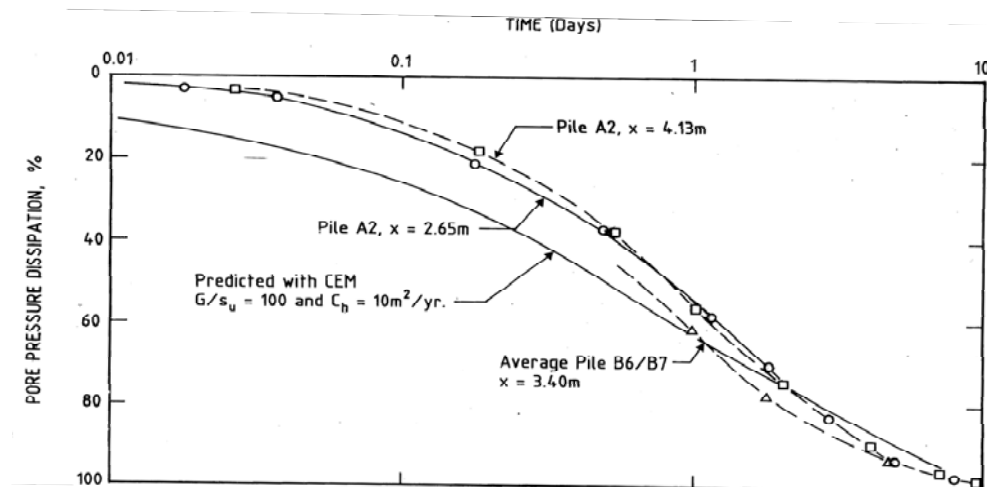
Figure 2.2.29- Degree of pore pressure dissipation (consolidation) versus time, Haga (after Karlsrud and Haugen, 1985)

Table 2.2.1 - Summary of pore pressure dissipation data, Haga

Pile	Depth below pile top x, (m)	Pile top relative to ground (m)	Depth below ground z(m)	t50 (hrs)	t90 (hrs)
A2	2,65	0,15	2,5	22	120
A2	4,15	0,15	4	21	120
B6	3,4	-0,45	3,85	13	84
B6	4,75	-0,45	5,2	11	72
B7	3,4	-0,54	3,94	20	84
B7	4,75	-0,54	5,29	16	79

95% consolidation was reached after a little less than 6 days. Pile load testing was generally carried out minimum 7 days after pile installation, but for some up to 36 days. This means that the degree of consolidation exceeded 96 %.

Figure 2.2.30 presents the measured horizontal (radial) effective stress measured against the pile shaft at commencement of the first static load tests on the instrumented test piles. The data are generally consistent. The average trend values have been used as basis for subsequent interpretations of the test results. As seen from Figure 2.2.31, the inferred horizontal effective stress ratio, k'_c, is significantly larger than the estimated in-situ K_0 values below a depth of about 2 m. The in-situ K_0 was estimated using the correlation to OCR and plasticity index proposed by Andresen et al (1979), which represents a slight modification of the original Brooker and Ireland (1965) version.
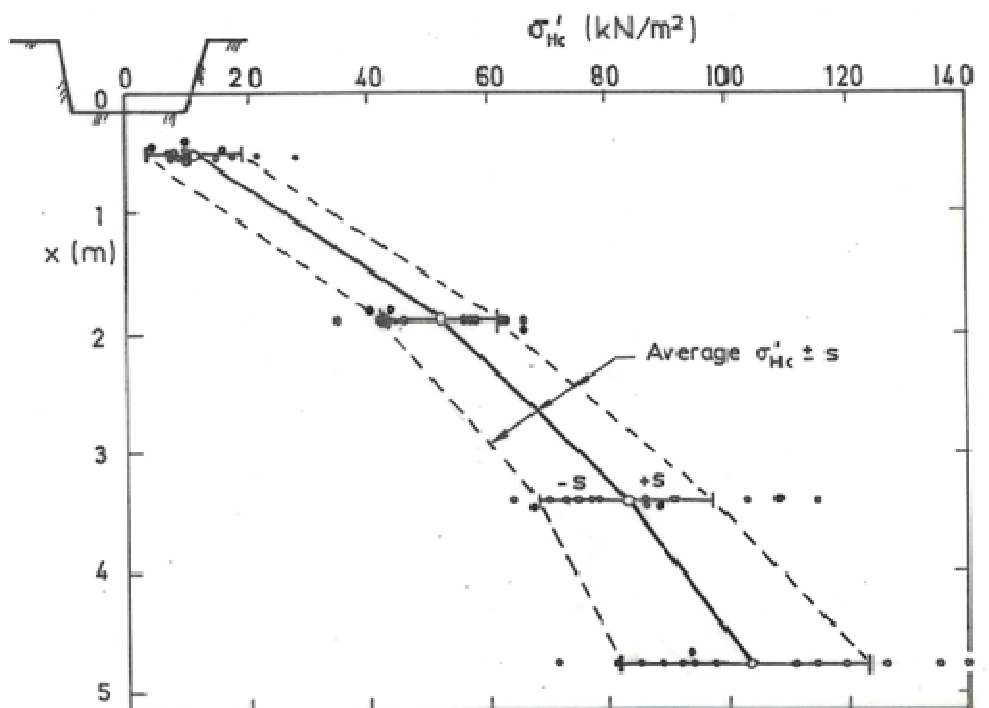
Figure 2.2.30- Measured effective horizontal earth pressures against the piles at onset of pile loading, all tests Haga (after Karlsrud, 1986)
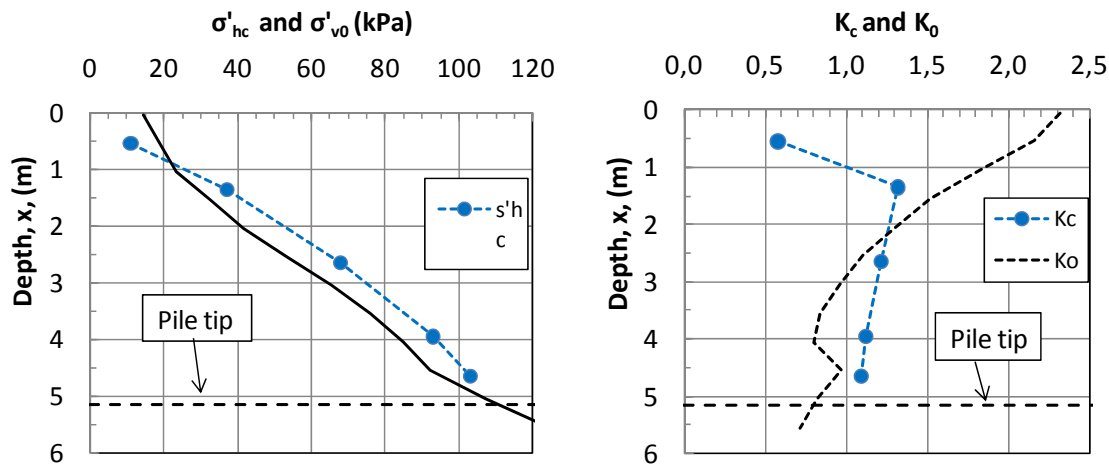
Figure 2.2.31- Average measured horizontal effective stress and k'$_c$ compared to in-situ K$_0$, Haga

The Haga piles were loaded incrementally to failure in a load controlled manner as illustrated in Figure 2.2.32. Loading to failure took typically around 20 minutes. Displacements were monitored continuously so that the creep rate under the period of constant load at each step could be determined. The load-displacement curve in Figure 2.3.32 is quite typical of all the pile tests, with a displacement at failure of 3 to 5 mm. Large creep deformations were recorded at the last load step in some of the tests. To make a consistent definition of failure for such tests Karlsrud (1986) made a study of the development of creep rate with normalised load as shown by the examples in Figure 2.2.33. It was on that basis concluded that failure could be most consistently defined as when the creep rate exceeded about 1 mm/min, which typically occurred at a pile top displacement of 3.0 mm.

Karlsrud (1986), and Karlsrud and Nadim (1990), recognised that the failure was depending on the rate of loading. A creep failure was actually shown to eventually take place when the load exceeded about 95 % of the failure loads as defined above, and/or when the creep rate the first minutes or so after load application was constant with log(time) and exceeded about 0.1 mm/min. Then the creep rate would after some time accelerate and failure would occur.
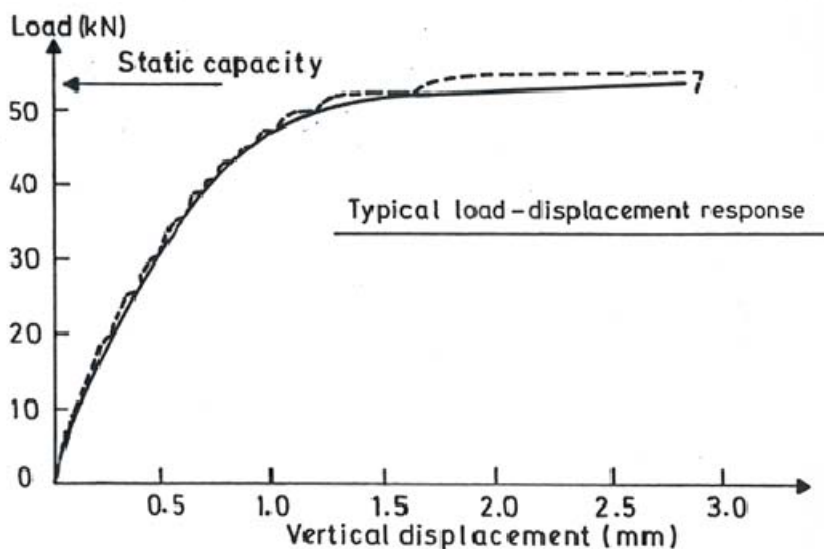
Figure 2.2.32 - Typical load displacement curve, Haga (after Karlsrud & Haugen, 1985)
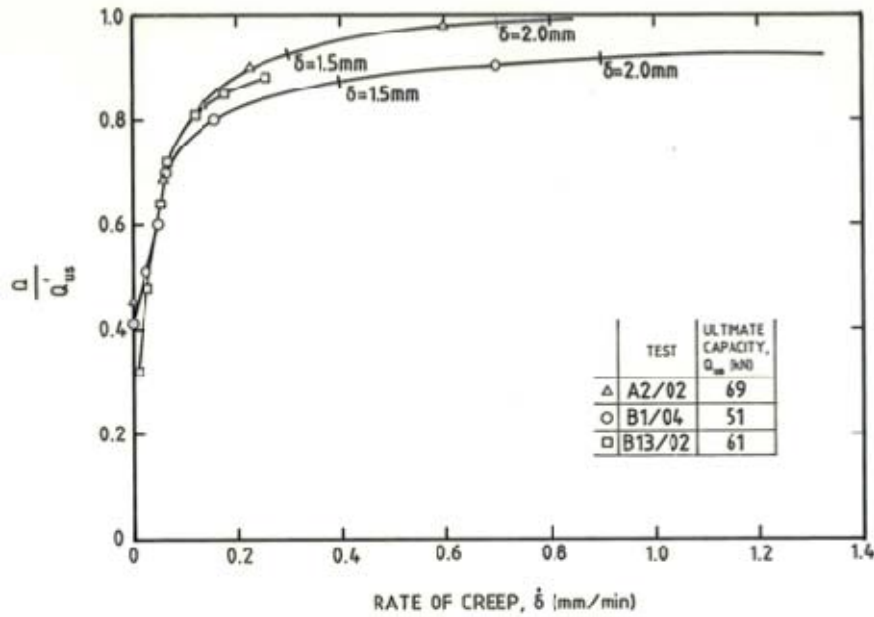
Figure 2.2.33- Rate of creep versus normalised load for selected tests, Haga (after Karlsrud, 1986)

Figure 2.2.34 shows the defined failure loads from all the initial static tests in relation to the time of loading after pile installation. It appears that there is a tendency for increase in capacity with time, even after the time of 100 % consolidation was reached, which was typically 7-10 days. The results also suggest no significant difference in capacity for the two piles loaded in compression as compared to all the other piles loaded in tension.
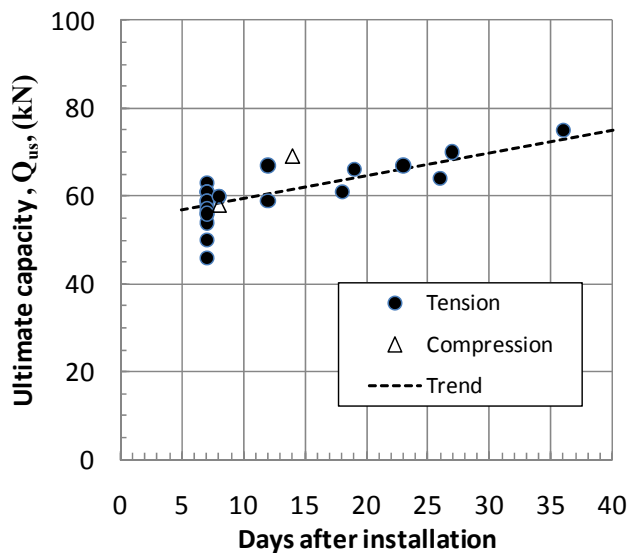
Figure 2.2.34- Measured ultimate capacity for all initial static tests in relation to time after pile installation, Haga (based on Karlsrud and Haugen, 1984)

Ten of the Haga test piles were subjected to several series of static and cyclic loading with some period of consolidation in between. As presented by Karlsrud (1986), all piles showed a significant gain in capacity in the static tests that were carried out after such previous loading and reconsolidation. The average gain in capacity was 28 % (range 16-43 %). Piles A3 and A9 were subjected to also a 3rd and 4th test series, which apparently enhanced the capacity even

further to up to 63 % beyond the 1ˢᵗ test, Figure 2.2.35. This effect of past loading to failure followed by reconsolidation is later referred to as "preshearing effect".
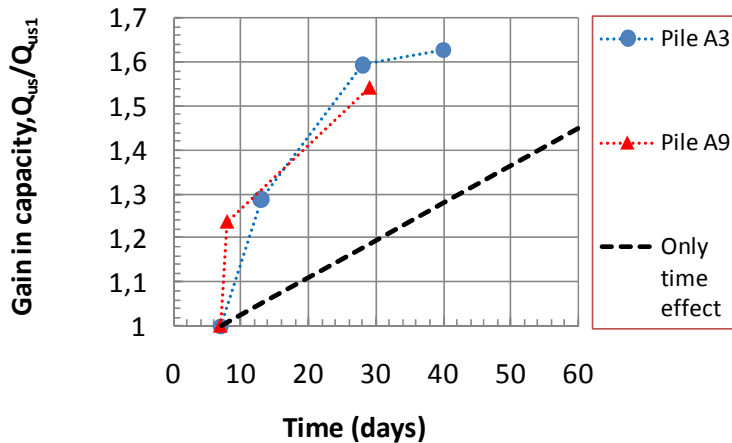
Figure 2.2.35 – Gain in capacity due to repeated loading on the same pile, piles A3 and A9, Haga

Figure 2.2.36 presents the ultimate shaft friction values deduced for the loads measured at the strain gauged sections (Figure 2.2.5) for all the tests. The local shaft friction values were arrived at by dividing the difference in load at two sections by the pile surface area, and taking this as the shaft friction value at the average depth. There is some variability, but the results are fairly consistent for all the tension tests. The two compression tests tend to show somewhat different distributions from the tension tests.
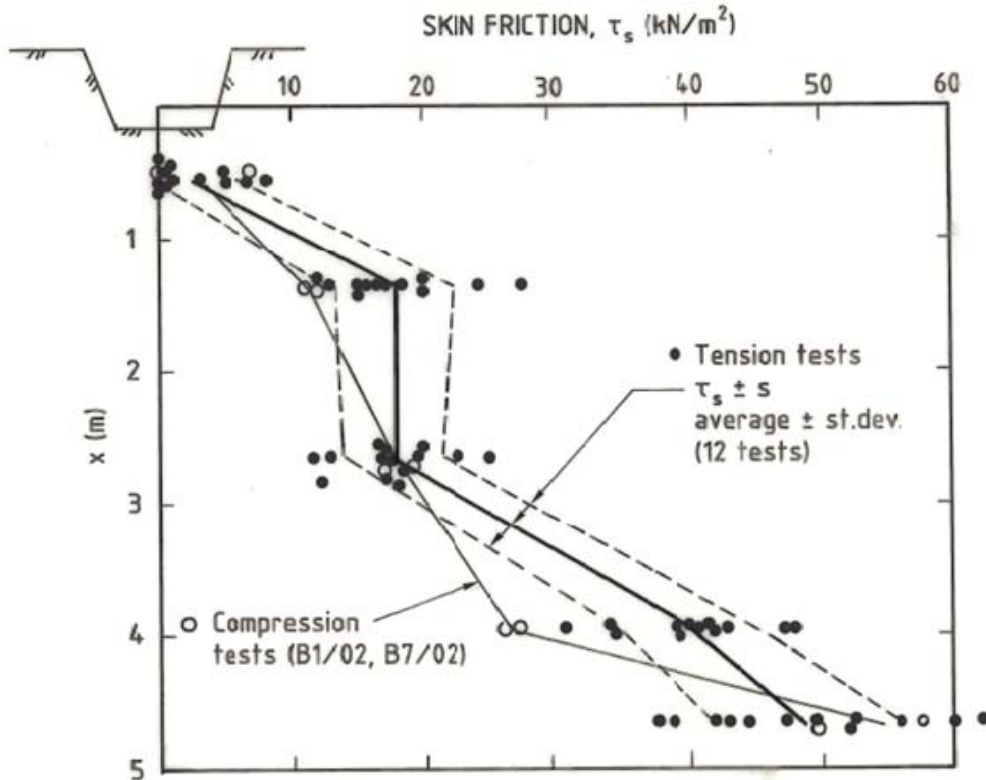
Figure 2.2.36 - Distribution of ultimate shaft friction with depth deduced from measured loads along the piles, Haga (after Karlsrud, 1986)

Figure 2.2.37 shows the average shaft friction compared to the assumed in-situ s_{ud} profile. The α- and β- values deduced from the average shaft friction are presented in Figure 2.2.38. It appears that the α- values increase almost linearly with depth, whereas the β- values are more constant with depth.
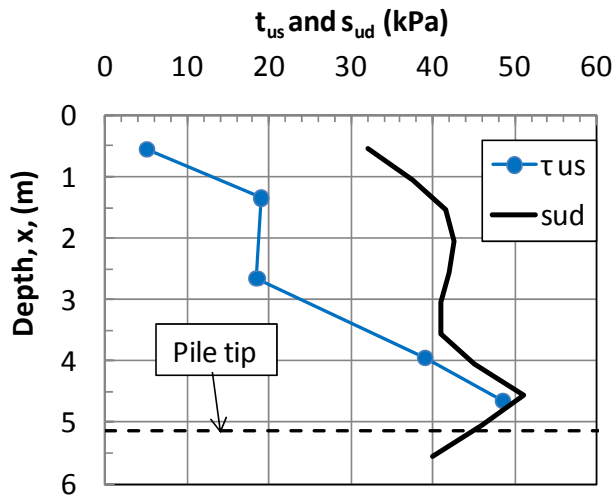
Figure 2.2.37- Average ultimate shaft friction compared to in-situ s_{ud} strength profile, Haga
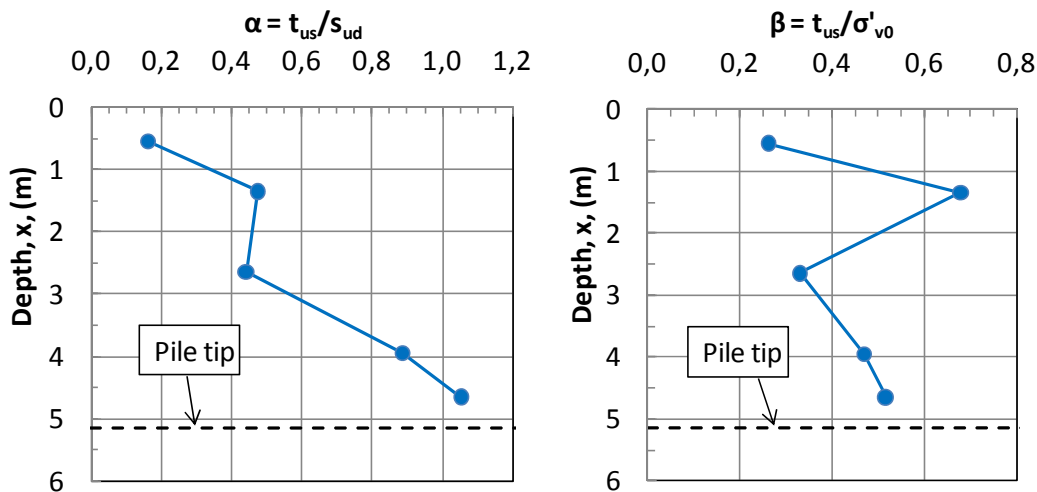
Figure 2.2.38 - Average α-and β-values for all piles, Haga

Figure 2.2.39 presents the average shaft friction against the measured average horizontal effective stress against the pile surface at onset of pile loading. There is a clear trend that the shaft friction increases more or less linearly with σ'_{hc}, and typically corresponds to:

$$\tau_{us} = 0.39 \cdot \sigma'_{hc}$$

For comparison the DSS and SB tests on RR-clay also show a linear increase in strength with axial (normal) consolidation stress, but at a lower rate of $\tau_f = 0.31 \cdot \sigma'_{ac}$ (Figure 2.2.21). This may still suggest that for the Haga case there is a link between the strength determined on RR-clay and shaft friction. This issue will be discussed in more detail in Chapter 6.
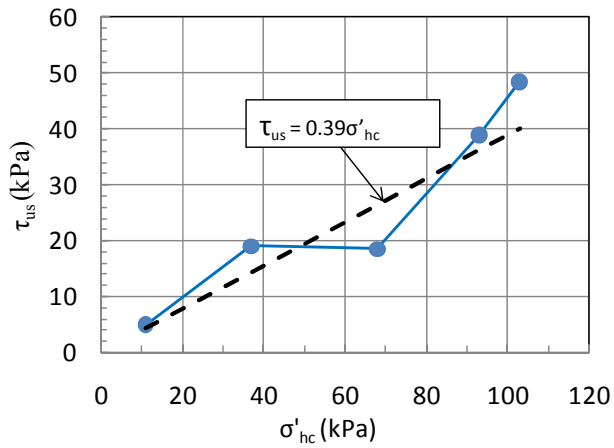
Figure 2.2.39 - Measured ultimate shaft friction in relation to horizontal effective stress at onset of pile loading, Haga.

Figure 2.2.40 shows range of normalised t-z curves for all the pile tests. At failure the local displacement corresponds to 1-2 % of the pile radius.
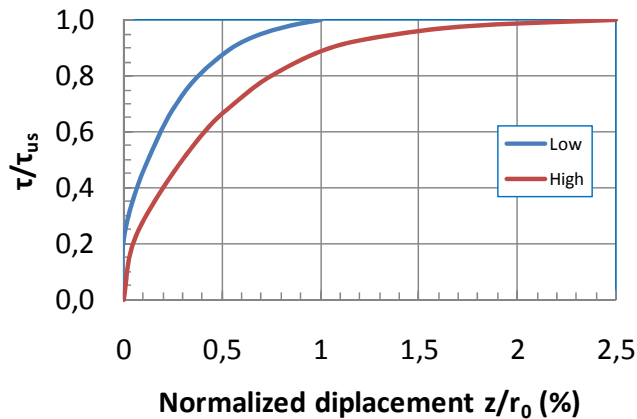
Figure 2.2.40- Measured normalised τ-z curves, Haga
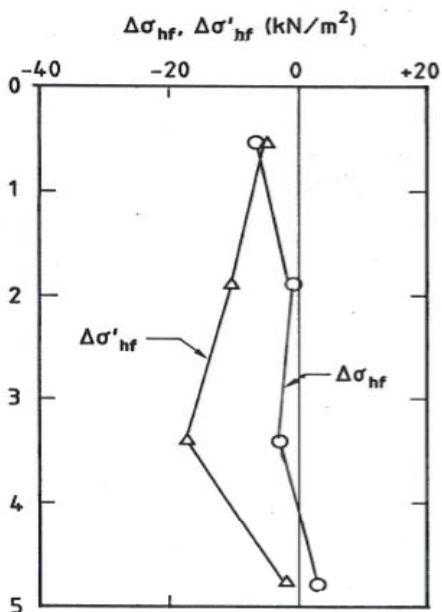
Figure 2.2.41- Measured change in horizontal effective stress at failure, Haga (after Karlsrud, 1986)

During pile loading the measured total earth pressure remained more or less constant (change of 5kPa up or down), whereas the pore pressure on the pile surface showed a tendency for increase, Figure 2.2.41.This effective stress reduction gives a relationship with between shaft friction and horizontal effective stress at failure as given in Figure 2.2.43, and on average represented by:

$$\tau_{us} = 0.46 \cdot \sigma'_{hf}$$

Again for comparison, failure in the DSS and SB tests on RR clay gave $\tau_f = 0.50 \cdot \sigma'_{af}$, resembling closely the relationship between shaft friction and normal (horizontal) effective stress at failure in the these pile tests.
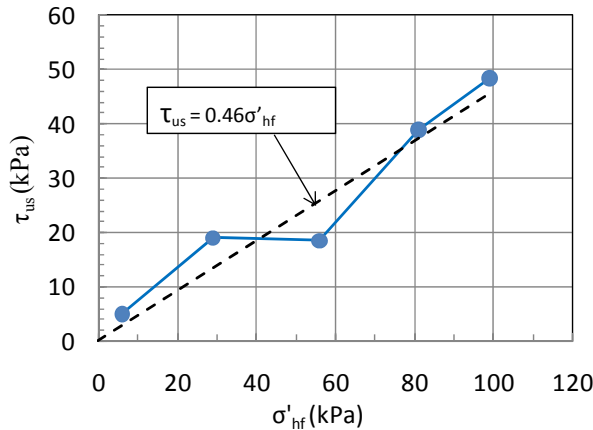
Figure 2.2.42- Measured ultimate shaft friction in relation to measured horizontal effective stress at failure, Haga

2.3 West Delta

2.3.1 General overview of the test site and load tests
The West Delta site lies in the Gulf of Mexico. Testing was carried out from a decommissioned jacket platform D-58A located 15-20 miles southwest of Venice, Louisiana where the water depth was about 16 m. This is an area with deep sediments of soft clays and fairly high sedimentation rates arising from the Mississippi river outlet.

Conoco Norway fully financed the test program, but involved a number of organisations in the planning and implementation of the test program and assessment of the test results, including Veritec (part of DNV Norway at the time), The Earth Technology Corporation (Ertec), McClelland Engineers and NGI, ref. Chan and Birrell (1998).

The West Delta test program included several load tests on a large scale fully instrumented 762 mm pipe pile with wall thickness of 19.1 mm driven to a depth of 71.3 m below seabed, and a series of tests on small scale model pile segments (probes), with diameter of respectively 3" (76 mm) and 1.72" (44 mm).

The detailed testing arrangements and results have been described in a series of papers to the OTC conference in 1998 by Matlock and Chan (1998), Bogard and Matlock (1998[a,b,c]), Audibert and Hamilton (1998). Factual data on soil conditions test arrangements and results have also been reported in a series of detailed project reports by Ertec (1982, 1985, 1986[a,b,c,]), Veritec

(1984) and NGI(1989[a,b,c,d]). This past documentation will only be referred to directly when it is considered relevant for documenting where data presented herein have been taken from.

Figure 2.3.1 shows the instrumentation of the large diameter pile. It included total earth and pore pressure gauges at 6 levels with two gauges placed diametrically at each level, and a combination of strain modules, extensometers and tell-tale rods for determination of the load distribution along the pile (Matlock and Chan, 1998). Loads and displacements were also measured at the pile top. Both earth pressure and pore pressure gauges were fitted with a curved shape flush with the pile surface.

The large diameter pile was driven open ended. It was made of 6 segments that were welded up during the installation process. The installation process took 5 days and was completed on 8 December 1984.

The large scale pile was load tested several times. A compression and tension test was first carried out immediately after driving, a static tension test and various cyclic load testing was then carried out 116 days, 498 days, and finally 2.5 years after the pile installation was completed.

As described by Matlock and Bogard (1998), the 3" probe had a total length of 4.28 m (14 ft), whereof the lower half (7 ft) was a cutting shoe to model an open-end pile penetration. As shown in Figure 2.3.2 the probe was driven in from the end of a cased borehole. For 12 of the 16 tests carried out, the model pile was driven to a depth of 4.28 m below the bottom of the cased borehole so that the soil in the vicinity of the upper instrumented part would experience displacements corresponding to an open-ended pile penetration. For the other 4 tests the model pile was driven at least 2.14 m (7 ft) deeper below the cased borehole. This way they should model a full displacement pile penetration of the instrumented section. The 3" probe was instrumented with miniature earth and pore pressure gauges placed at the middle of the upper part, corresponding to about 1.22 m or 16 diameters below the bottom of the borehole for the open-end cases. The lower cookie cutter had a slip joint to the upper instrumented part and acted as anchor point for measuring displacement. The loads were measured by load cells placed at about 0.76 m spacing, Figure 2.3.2.

Each probe was first load tested in tension, and then subjected to large-displacement cyclic loading. The load tests were carried out at various times after installation to look at increase in capacity with degree of consolidation. The load tests were carried out at depths of 17.7, 45.1, 54.3 and 63.4 m below seabed.

The 44 mm closed-ended so called x-probe was also instrumented with miniature earth and pore pressure gages, displacement transducers and load cells to determine shaft friction. (Details for this probe are missing). The x-probe was also driven in from the end of a cased borehole. Only two tests were carried out with the x-probe, at depths of respectively 45.1 and 54.3 m. Both an initial static tension test followed by cyclic testing was carried out.
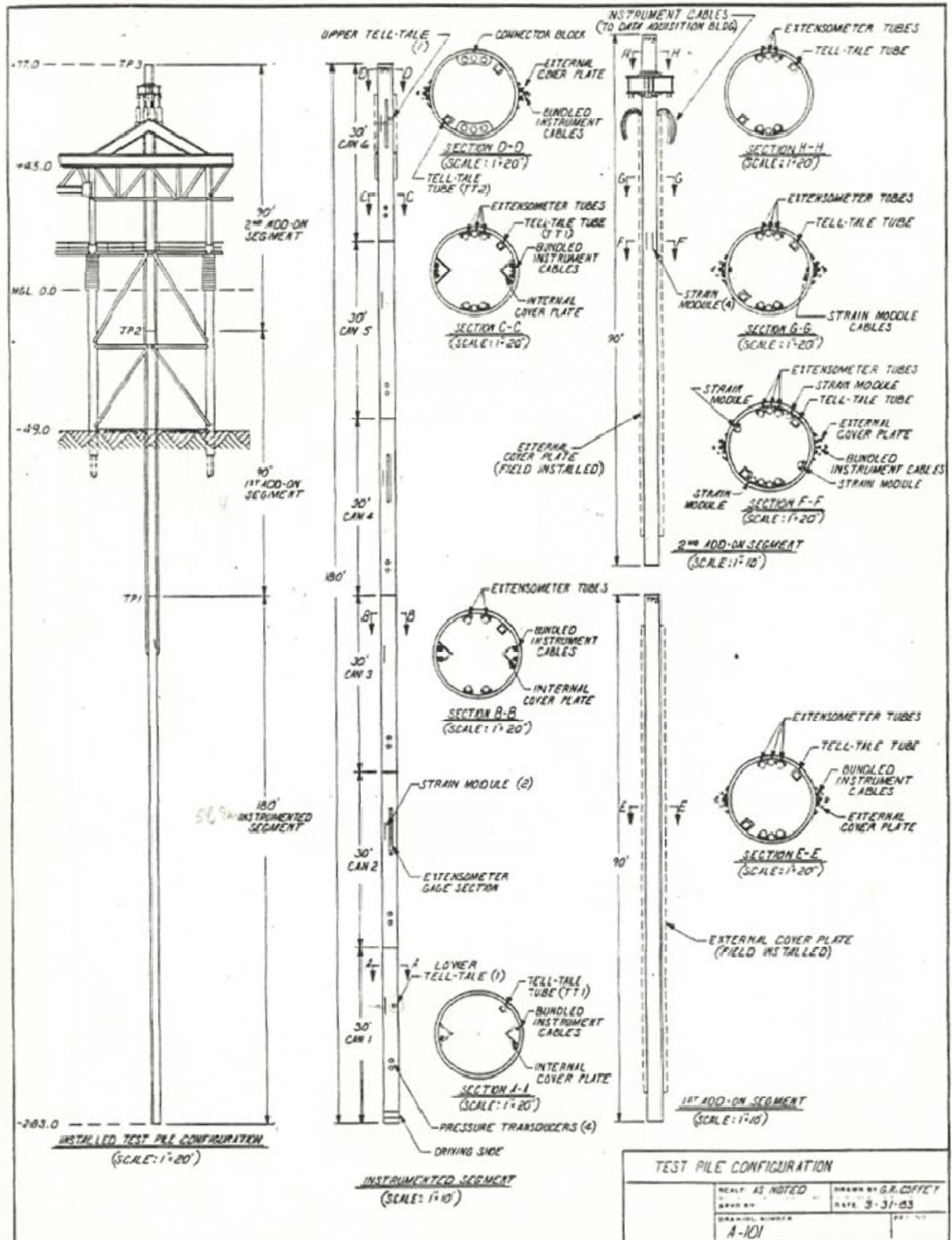
Figure 2.3.1- Layout of testing arrangements and instrumentation of LD-pile test, West Delta (after Ertec, 1985)
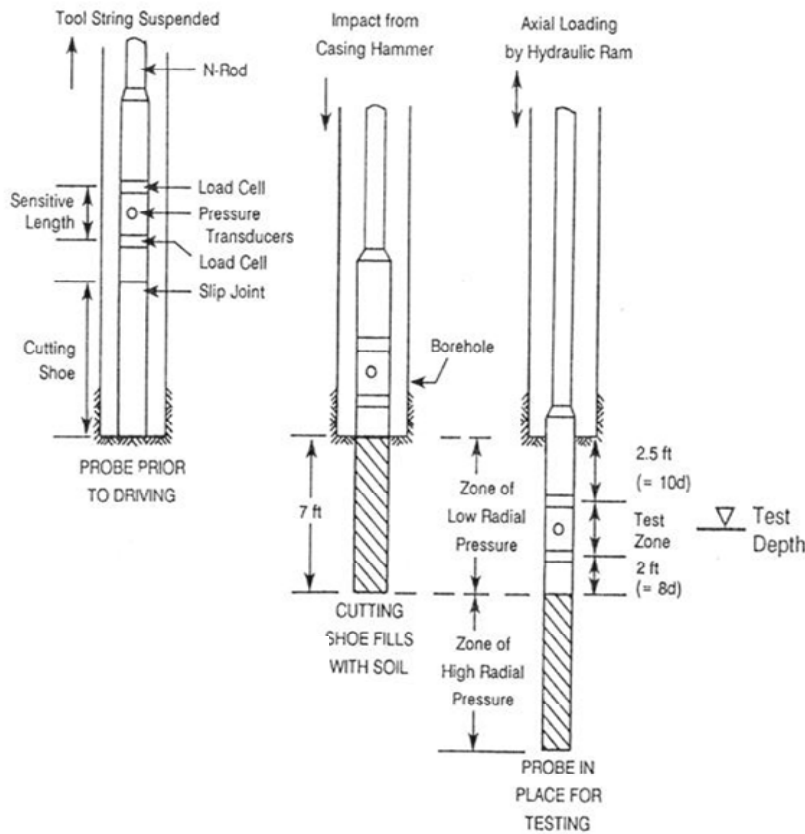
Figure 2.3.2- Testing arrangement for the 3" (76 mm) probe, West Delta (after Bogard and Matlock, 1990)

2.3.2 Key soil parameters

The general soil characteristics at the test site have been presented by Audibert and Hamilton (1998), but NGI (1989[c]) have made an independent assessment of the basic properties and did also carry out some special laboratory tests to look at the strength of remoulded reconsolidated clay. The following highlights data taken from these two sources.

In terms of index parameters the various sampling campaigns and laboratory tests give a fairly consistent picture of the key clay properties. Figure 2.3.3 shows the typical distribution of water content, plasticity index and total unit weights with depth.
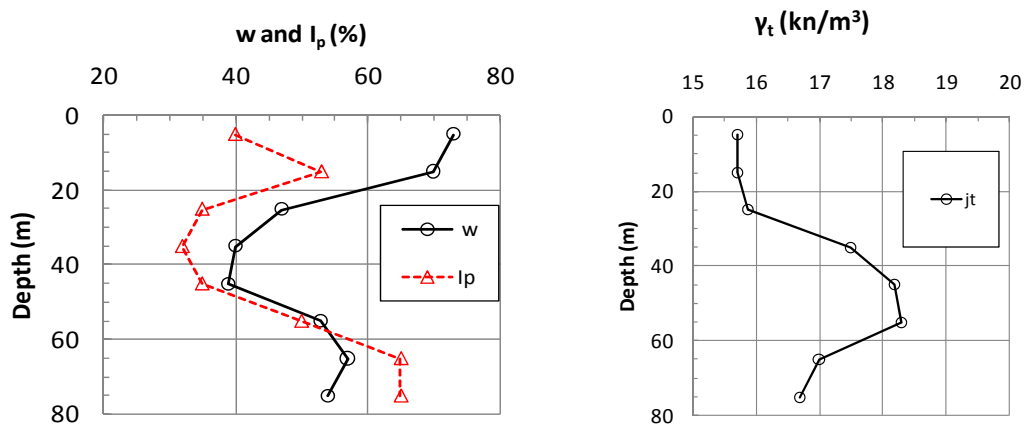
Figure 2.3.3- Summary of index data, West Delta

It appears that clay is more plastic in the top and bottom part than in the middle part, and the water content shows a similar trend. A special note should be made regarding the total unit weight. These have been computed by the author from the water contents using the equation for saturated soils:

$$\gamma_t = G \cdot (1+w) \cdot \gamma_w / (1+G \cdot w) \tag{2.3.1}$$

The specific gravity was based on some measurements by NGI (1989[a]), which suggested a typical value of G=2.72. The unit weight of the saline pore water was taken as γ_w = 9.97 kN/m^3.

Direct measurements of unit weight on samples retrieved suggested values that were typically 10 % lower than the values in Figure 2.3.3. NGI (1989[a]) suggested that the primary reason was that the clay contained saturated gas, which expanded the volume when the samples were subjected to atmospheric pressure.

Data on grain size distribution show clay content of 30-38 % at 34 m depth and 55-63 % at 68 m depth (NGI, 1989[c]). The difference in clay content agrees with the corresponding difference in plasticity index.

A special feature of the WD site is that three piezometers installed at depths of 30.3, 57.1 and 68.7 m showed a considerable artesian pressure with depth, Figure 2.3.4. For the deepest piezometer the artesian excess pressure was as large as about 200 kPa. Combined with the relatively low unit weights, this implies that the effective stresses are very low as compared to a case of hydrostatic pore pressures, by almost a factor of two below 60 m depth. This aspect was accounted for in NGI's (1989[a,b,c,d]) reports, but does not seem to have been dealt with in other publications relating to the WD tests.
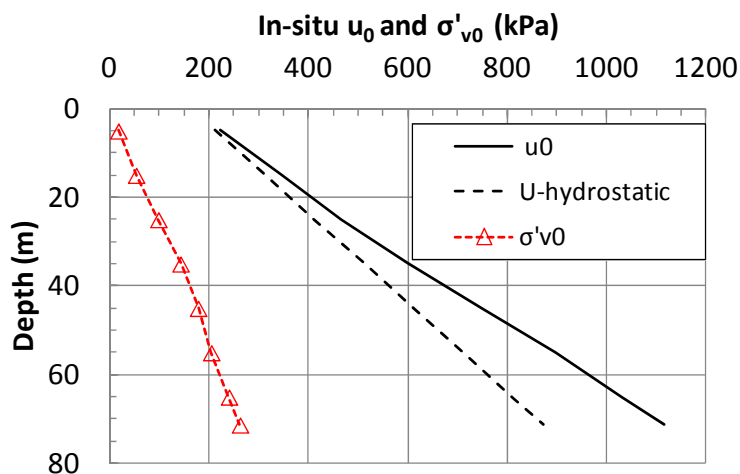
Figure 2.3.4 - In-situ pore pressure and vertical effective stress, West Delta

Due to the excess pore pressure condition it is assumed that the clay deposit has apparent overconsolidation ratio close to 1.0, but if some volumetric creep has accompanied the primary consolidation process, it may still show an apparent overconsolidation ratio of maybe OCR=1.1 to 1.2. The sample quality has not been sufficiently good to verify this OCR from the oedometer tests carried out.

Figure 2.3.5 presents values for the volumetric compressibility as represented by the modulus number, m_0, determined by incremental (IL) and constant rate of strain (CRS) oedometer tests. There is as expected a tendency for the modulus number to be highest at 30-45 m depth where the clay has the lowest water content, with the lowest values in the top and bottom where the water content is highest.
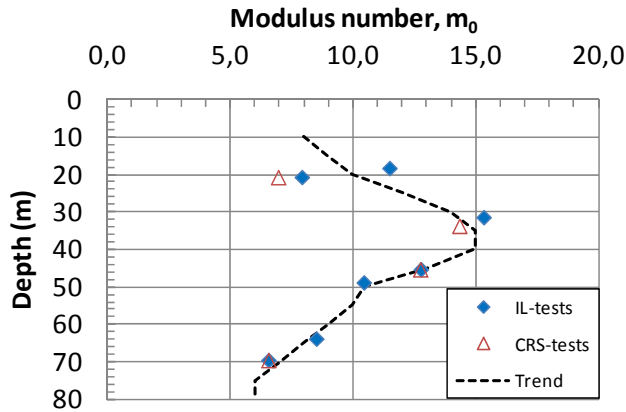
Figure 2.3.5 - Modulus number, m_0, determined from oedometer tests, West Delta.

Figure 2.3.6 shows values for the coefficient of consolidation, c_v, determined for the oedometer tests in the virgin compression region at a stress level corresponding to $1.5 \cdot \sigma'_{v0}$. The CRS tests are probably the most reliable and suggest values ranging from about 0.4 to 1.8 m^2/yr.
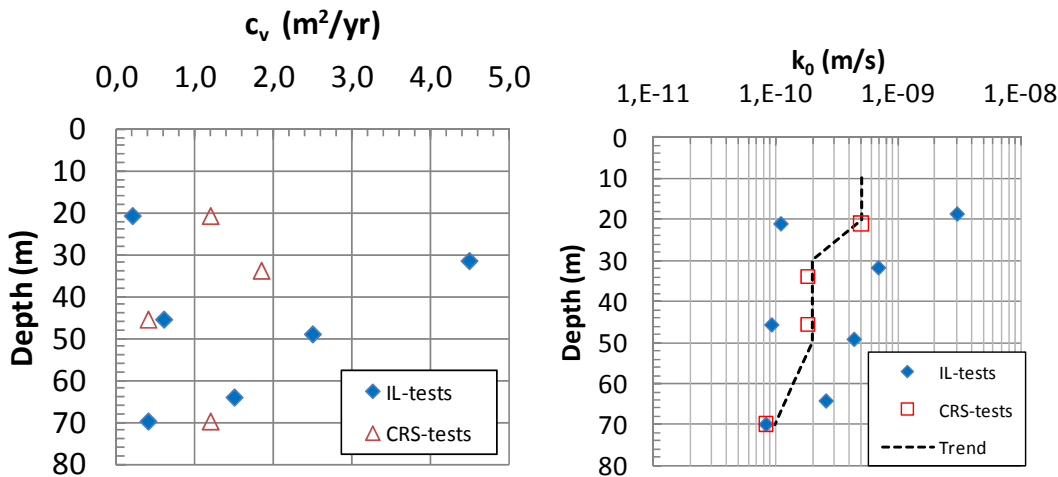
Figure 2.3.6 - Coefficient of consolidation, c_v, from oedometer tests at stress level corresponding to $1.5 \cdot \sigma'_{v0}$, and calculated permeability, k_0, West Delta

The permeability of the clay has not been directly measured, but values have been back-calculated from the c_v-values using eq. (2.2.2), and with modulus $M = m_0 \cdot 1.5 \sigma'_{v0}$. This gave a permeability ranging typically from $k = 1 \cdot 10^{-10}$ to $1.7 \cdot 10^{-9}$ m/s, with an average of $3.01 \cdot 10^{-10}$ m/s. To establish the in-situ vertical permeability, k_0, these k-values were corrected for the volumetric strain that had occurred at the stress level of $1.5 \sigma'_{v0}$, which typically was in the range of 6-8 %. The applied correction was based on the following expression generally applicable to clays:

$$k_0 = 10^{\,(\log k - \varepsilon \cdot \beta_k)} \qquad \text{where} \qquad (2.3.2)$$

ε = absolute vertical strain, here taken at stress $p' = 1.5 \cdot \sigma'_{v0}$

β_k = permeability change index

NGI have carried out testing of very high quality block samples from 22 different sites in Norway and one abroad, e.g. NGI (2011) and Karlsrud and Hernandez (2011). Data on permeability change index are presented in Figure 2.3.7, on which basis it was selected a value of β_k=3.0 for the West Delta clays.

Figure 2.3.6 shows that the derived values of in-situ vertical permeability tend to decrease with depth. The average value is about k_0=0.5·10^{-9} m/s, which is considered quite reasonable for this type of clay. The assumed trend line gives however, most weight to the CRS tests.
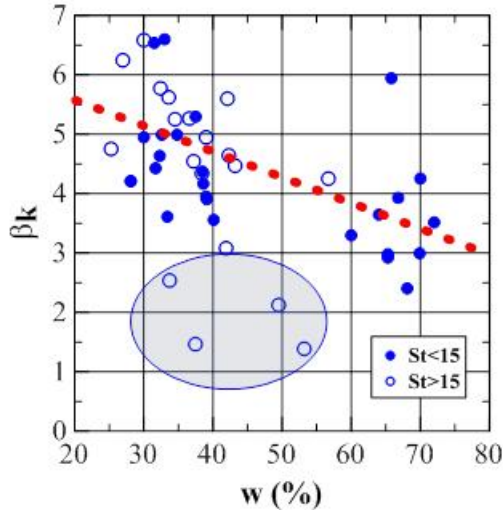
Figure 2.3.7 – Permeability change index, β_k, determined from CRS oedometer tests on block samples (after Karlsrud and Hernandez, 2011)

A range of different types of tests have been carried out to determine the in-situ undrained shear strength of the clay, including UU tests, in-situ remote vane tests, DSS tests and triaxial tests. Figure 2.3.8 presents the most relevant undrained shear strength profiles based on these data.
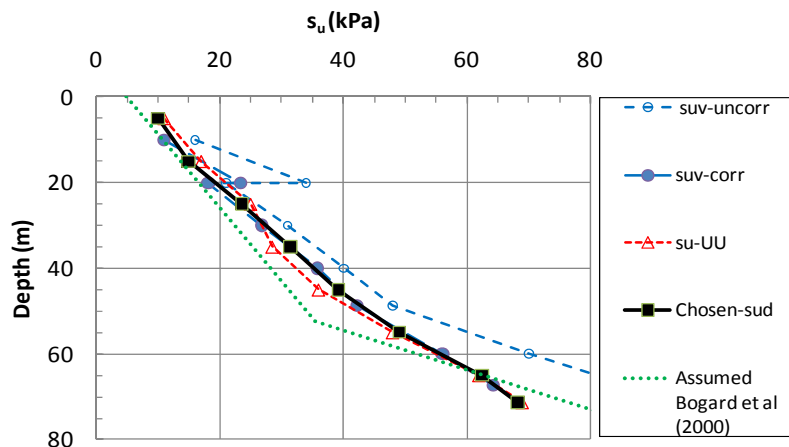
Figure 2.3.8 - Undrained shear strength profiles, West Delta

Some comments can be given to these shear strength profiles:

- The s_{u-UU} strength profile is taken from the paper by Audibert and Hamilton (1998).
- The s_{uv} profile comes from in-situ remote vane tests and was taken from NGI (1989^c). It was based on 22 individual vane readings relatively uniformly distributed between 10

and 75 m depth. The corrected vane values were established using the correction factors proposed by Aas et al (1985).

- The s_{ud} profile chosen was established on basis of DSS tests presented in NGI (1989[c]). Altogether 13 DSS tests were carried out by Ertec, McClelland and NGI. All samples were consolidated well beyond the in-situ vertical effective stress prior to undrained loading. They gave a normalised strength ratio, s_{ud}/σ'_{ac}, mostly in the range 0.23-0.28, but with two isolated values of 0.215 and 0.32. Table 2.3.1 shows the normalised values actually assumed herein. The variation with depth was partly assumed on basis of expected lower values for low plastic clay than for higher plastic clay, which also to some extent was supported by the test data. The normalised strengths were multiplied by the in-situ vertical effective stress to produce the chosen s_{ud} profile.

Table 2.3.1 - Strengths derived from UU and DSS tests, West Delta

Depth	σ'_{v0}	$s_{u\text{-}UU}$	DSS	s_{ud}
(m)	(kPa)	(kPa)	s_{ud}/σ'_{ac}	(kPa)
0	0	5	0,28	8,0
5	18	11	0,28	10,0
15	53	17	0,28	14,9
25	98	25	0,24	23,5
35	143	28,5	0,22	31,4
45	178	36	0,22	39,2
55	204	48	0,24	49,1
65	240	62	0,26	62,4
75	277	69	0,26	68,2

The three types of undrained strength tests in Figure 2.3.8 gave for this case give quite similar values. The chosen s_{ud} profile deviates however, from the undrained shear strength profile assumed by Bogard et al (2000) as basis for their interpretation of the pile test results. This difference will impact the interpreted normalised shaft friction in terms of α-values.

A series of 21 CIU and CAUC undrained triaxial tests were also undertaken on the West Delta clay. All samples were consolidated well beyond the vertical effective stress prior to undrained shearing. As shown in NGI (1989[c]), the normalised strength ratio, s_{uc}/σ'_{ac}, varies from as low as 0.24 to a high of 0.37, with no clear difference between CIU and CAUC, and no clear variation with depth. The effective friction angle interpreted from the triaxial tests, and assuming effective cohesion c'=0, lies in the range φ=29[0] to 33[0].

Various tests to determine the remoulded shear strength suggested that the sensitivity of the clay is low and in the range of S_t= 1.5 to 2.0.

NGI carried out 4 DSS tests to determine the undrained strength of completely remoulded and reconsolidated clay. The procedure was the same as described in section 2.2.2 for the Haga clay. The samples were taken from depths of about 34 and 68 m. The normalised undrained strength from these tests lie in the range s_{ud}^{RR}/σ'_{ac}=0.27 to 0.34, or on average 17% larger than the normalised DSS strength of intact samples consolidated well beyond the preconsolidation pressure.

2.3.3 Load test results

Figure 2.3.9 presents measured normalised excess pore pressure values for both the probe tests and the LD pile, and Figure 2.3.10 the installation effective stresses derived by subtracting the pore pressure from the measured total earth pressure. In NGI (1989[a]) the reliability of the data from at least some of the probe tests were questioned when it comes to measured earth and pore pressures during installation. Only probe data classified to have medium to high reliability are included in Figures 2.3.9 and 2.3.10.

For the open LD-pile the normalised excess pore pressure is higher along the upper and lower part of the pile, located in the zones with highest plasticity index, than along the middle part located within the leaner clay. The installation effective stress ratio, K_i, tends to decrease with depth.

The open 3" probe showed generally lower installation effective pressures than the LD-pile. The closed-ended 3" probe and the x-probes, agree more with the LD-pile results.
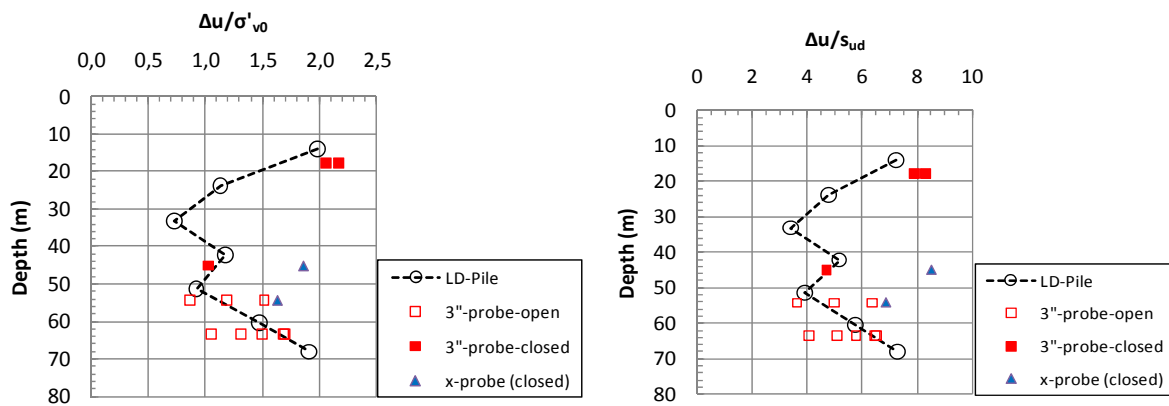
Figure 2.3.9 - Normalised excess installation pore pressures
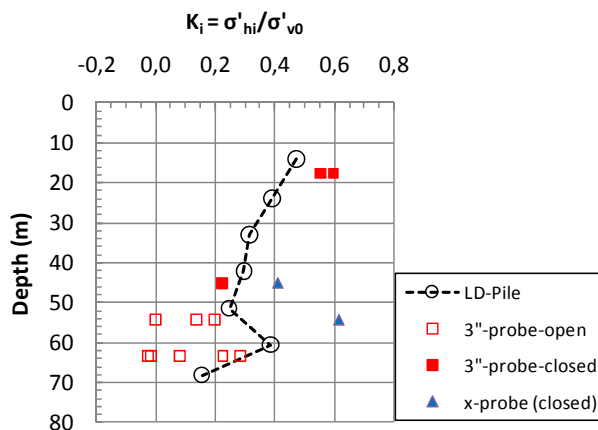
Figure 2.3.10 - Normalised installation effective earth pressure, West Delta

Both the LD-pile and the probes were subjected to an initial static tension test just after completion of installation. Figure 2.3.11 shows that the normalised shaft friction, t_{si}/s_{ud}, from these initial tests mostly part lies in the range of 0.2 to 0.35. The inverse of this ratio, i.e. the ratio s_{ud}/t_{si}, should reflect the sensitivity of the clay, which gives values of sensitivity in the range 2.85-5.0. This apparent sensitivity is a factor of about 2 larger than the sensitivity derived from remoulded strength measured in the laboratory.
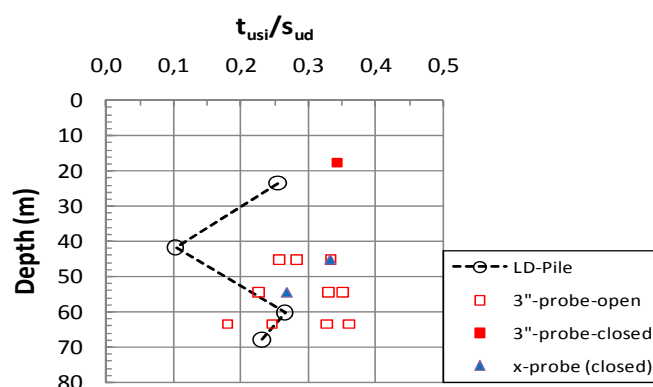
Figure 2.3.11 - Normalised shaft friction immediately after pile installation, West Delta

Table 2.3.2 presents times to reach 50 and 90 % pore pressure dissipation for both the LD-pile and the probe tests. For the load test on the LD-pile carried out at t=116 days after installation the t_{90} data are based on some extrapolation of pore pressure data beyond that time. Most of the load tests on the probes were carried out well before t_{90} was reached. That is why such data are missing for these tests. Note that for the probe tests, only an average value for the tests considered most reliable at a given depth is given.

Table 2.3.3 shows the measured stress conditions for the LD-pile just prior to onset of the tension load test at t=116 days. As shown, there still remained some excess pore pressures at the onset of the test, and the degree of pore pressure dissipation or consolidation, U, compared to the end of installation pore pressures range from about 74 to 86 %.

Table 2.3.2 - Measured times to reach 50 and 90 % pore pressure dissipation, West Delta

	Depth	t_{50}	t_{90}
Pile	(m)	(days)	(days)
LD-pile	24,1	19	x
LD-pile	33,2	40	180
LD-pile	42,4	18,5	150
LD-pile	51,5	24	145
LD-pile	60,7	14,5	260
LD-pile	68,3	11	265
3" probe-open	54,3	0,25	x
3" probe-open	63,4	0,69	ca.7
3" probe closed	17,7	1,18	x
1.72"-x-probe	45,1	0,15	x
1.72"-x-probe	54,3	0,26	x

Table 2.3.3 - Stress conditions at onset of the LD-pile load test at t=116 days, West Delta

Depth	σ'_{v0}	u_0	u	σ_{hc}	σ'_{hc}	$K_c=$	Δu	Degree cons
(m)	(kPa)	(kPa)	(kPa)	(kPa)	(kPa)	$\sigma'_{hc}/\sigma'_{v0}$	(kPa)	U
24,1	97	455	484	531	47	0,485	29	0,74
33,2	138	585	611	655	44	0,319	26	0,74
42,4	169	710	737	814	77	0,456	27	0,86
51,5	195	835	871	964	93	0,477	36	0,80
60,7	223	975	1032	1190	158	0,709	57	0,83
68,3	252	1080	1163	1371	208	0,825	83	0,83

Figure 2.3.12 shows that the degree of pore pressure dissipation or consolidation, U, at onset of pile loading was in general much lower for the various probe tests compared to the LD-pile.
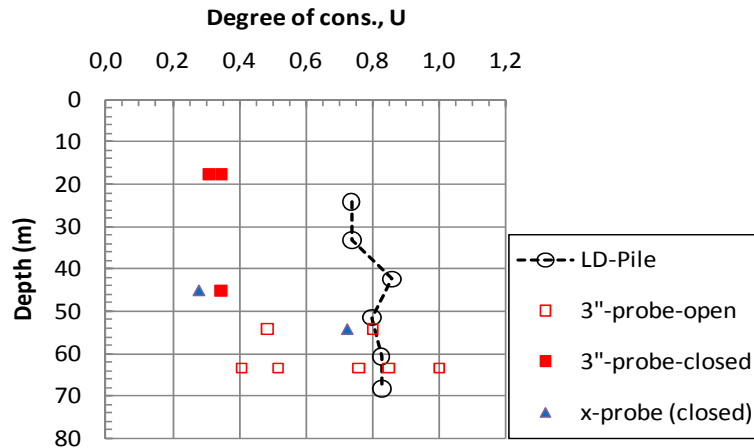
Figure 2.3.12 - Degree of pore consolidation at onset of t= 116 day static load tests, West Delta

Figure 2.3.13 shows the measured horizontal effective stresses against the pile surface for the LD pile at t= 116 and t=500 days just prior to onset of pile loading. It can be observed that the effective stresses have increased over this time. This is mostly due to reduced pore pressures, and to a lesser extent some increase in measured total stresses.
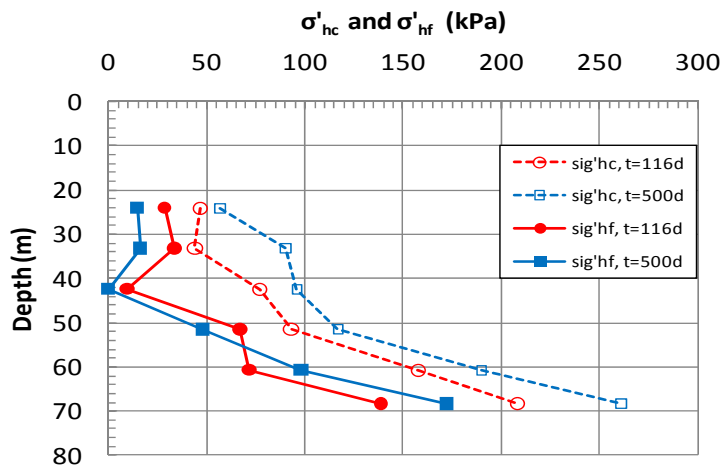
Figure 2.3.13 - Measured horizontal effective stress against the LD pile at onset of loading and at failure, t = 116 and 500 days, West Delta

In spite of the quite varying degree of consolidation, the measured horizontal effective stress ratios at onset of pile loading, K_c, were surprisingly similar for the LD pile and the probes, Figure 2.3.14. For the LD-pile there is a clear tendency for K_c to increase with depth and approach or even exceed the assumed K_0 values.

Figure 2.3.15 still suggests that there is some correlation between degree of consolidation and K_c, but the effective stress level does not seem to increase significantly before about 60% consolidation is reached. The same seem to apply to the shaft friction measured in the probe tests, Figure 2.3.16, which increased relatively little beyond the initial (t=0) values before about 50 % consolidation was passed.
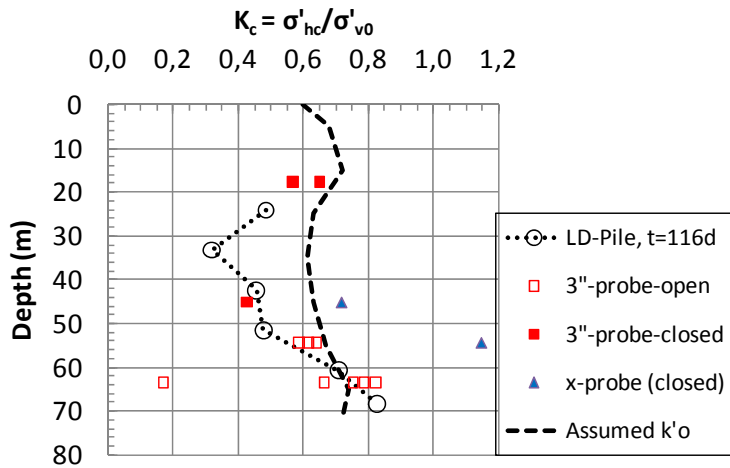
Figure 2.3.14 - Measured normalised horizontal effective stress at onset of pile loading, West Delta.
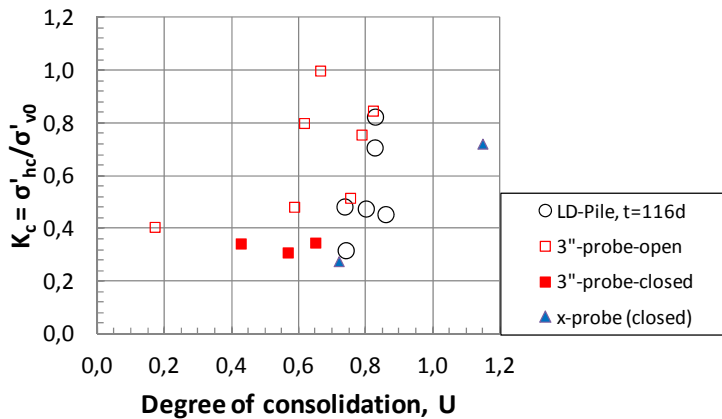
Figure 2.3.15 - Horizontal effective stress ratio in relation to degree of consolidation at onset of pile loading, West Delta
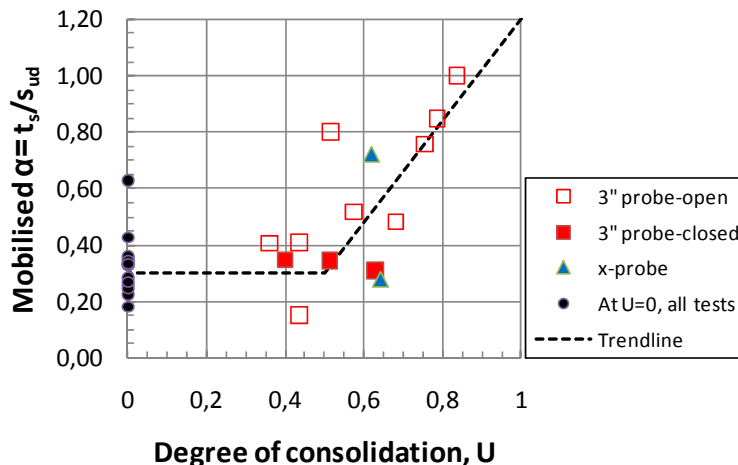
Figure 2.3.16 - Mobilised α-values for probe tests in relation to degree of consolidation at time of loading, West Delta

The LD pile was load tested immediately after installation as well after 116 days, 500 days and 2.5 years after installation. Each test series consisted of first a load test to failure in tension, followed by compression, one-way cyclic loading and/or sustained (creep) load testing. Only the

results of the first tension tests at each time of load testing will be dealt with herein. Figure 2.3.17 shows a selected example of load- displacement response for the t=116 day test, taken directly from the Ertec (1985) report. The loads herein are as measured at the strain-gauged sections. Note that the axial displacement refers to the displacement at mud line, and not the local axial displacement at a given level.

The load-displacement curves in Figure 2.3.17 show a clear tendency for strain softening when the peak load is exceeded, corresponding to a drop of about 9 % at the Pile Head. As a comment to the load measurements neither Ertec (1985) nor any of the published papers (e.g Bogard& Matlock, 1998; Bogard et al, 2000), define what Pile Head means in this respect, but it is assumed to mean the top of the instrumented pile. Notice also that Figure 2.3.1 suggests that the instrumented pile was sleeved down to somewhat below the level of the top of the instrumented pile segment, which is located at (234'-180') = 54'=16.45 m below mud line. However, no description has been given of such an assumed pile sleeve in the reports and papers referred to.
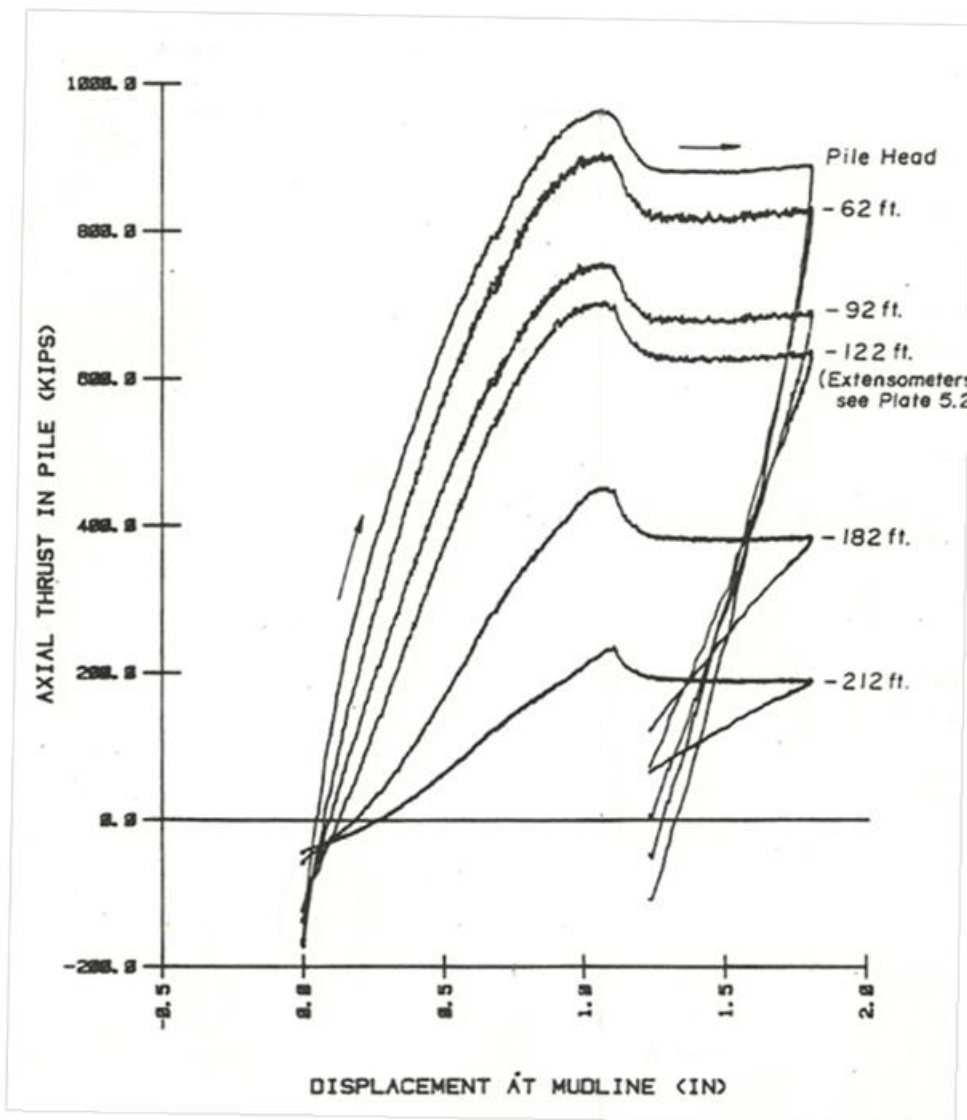
Figure 2.3.17- Examples of load-displacement curves for the LD-pile at t=115 days, West Delta (after Ertec, 1985)

For the LD-pile, the load test results have been re-interpreted to arrive at the distribution of shaft friction. One reason for doing that, is that it was not clear if the weight of the pile and soil plug

had been accounted for in past work presented by Ertec (1985), and which also formed the basis for the shaft friction assumed by NGI (1989[a,d]). Table 2.3.4 presents the actually measured loads along the pile for the t=116d test for both the strain gauged sections (SG) and the values based on the LVDT displacement transducers.

To arrive at the load actually carried by the external shaft, the full theoretical weight of the pile and the weight of the soil plug have been subtracted from the total load measured at each level. The reason for including the full weight of the plug is that the internal shaft friction is considerably larger than the weight of the plug. The actual weight of the steel pile and soil plug are given in Table 2.3.4, and correspond to 18 % reduction in shaft capacity, which is quite significant. The only uncertainty in this calculation is actually how high up into the pile the actual soil plug went. It has not been possible to find such information in the Ertec reports or published papers. Herein it has been assumed that the plug went up to mud line.

Across the steel area of the very pile tip, there will act some upward pressure. If the full tip resistance due to uplift is fully mobilised this upward acting pressure can be calculated from the classical bottom heave bearing capacity formula as:

$$q_{tip} = \sigma_{v0} - 9 \cdot s_{ud} \text{ for tensile loading} \qquad (2.3.3 \text{ a})$$

$$q_{tip} = \sigma_{v0} + 9 \cdot s_{ud} \text{ for compressive loading} \qquad (2.3.3 \text{ b})$$

For tensile loading of the LD-pile this leads to: $q_{tip} = (1378 - 9 \cdot 68.2)$ kPa = 764 (kPa).

The steel area at the tip is 0.045 m^2, which gives a force of Q_{tip} = 34 kN. It may be argued that the displacement required to mobilise the full tip resistance is larger than what it takes to mobilise full shaft friction. If no shear strength is mobilised at all, the local tip resistance will correspond to the total vertical stress, which gives a load of Q_{tip} = 62 kN. As an approximate assumption the upward acting tip force was selected as Q_{tip} = 50 kN.

Table 2.3.4 -Summary of measured loads in tension test at t=116 days, LD-pile West Delta

Depth	Depth		Total Load	Total Load	Correction plug+weight	Shaft load
(ft)	(m)	Type	(kips)	(kN)	(kN)	(kN)
0	0,0	SG	965	4293	784	3559
62	18,9	SG	900	4003	576	3477
92	28,0	SG	752	3345	476	2919
122	37,2	SG	701	3118	375	2793
182	55,5	SG	448	1993	174	1869
212	64,6	SG	263	1170	74	1146
62	18,9	LVDT	907	4035	576	3508
122	37,2	LVDT	705	3136	375	2811
182	55,5	LVDT	484	2153	174	2029
234	71,3		Qt-assumed	-50	0	0

Figure 2.3.18 presents the actual load values measured as function of depth for both the immediate tension test and the tests at t=116 and 500 days. The assumed idealised ultimate load distributions, which form the basis for the calculated shaft friction values presented in Tables

2.3.5 and 2.3.6, are also shown. Notice that as the pile is assumed sleeved at the top, only the shaft friction below a depth of 18.9 m is considered relevant.
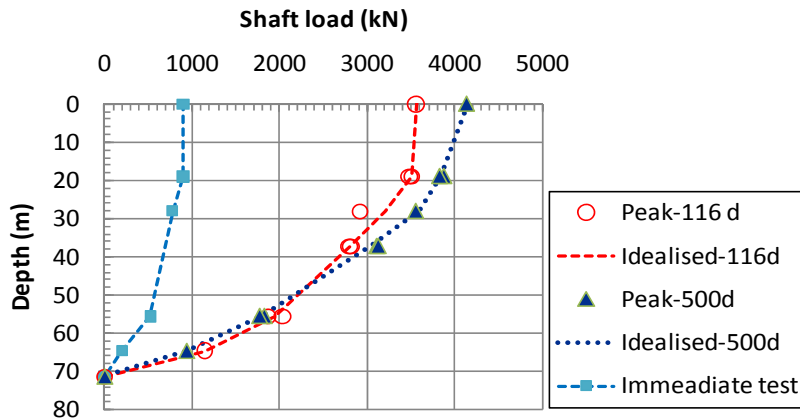
Figure 2.3.18 – Load distributions at failure, LD tension pile tests, West Delta

Table 2.3.5 - Calculated average shaft friction, LD-pile, t= 116 days, West Delta

Depth	Measured shaft load	Average depth	Average t_{us}	σ_{v0}'	s_{ud}	α	β
(m)	(kN)	(m)	(kPa)	(kPa)	(kPa)	t_{us}/s_{ud}	t_{us}/σ_{v0}'
0	3559	9,5	1,3	x	x	x	x
18,9	3500	23,5	13,8	92	19	0,725	0,150
28	3200	32,6	18,2	132	32	0,568	0,138
37,2	2800	46,4	19,4	183	43,5	0,446	0,106
55,5	1950	60,1	37,2	222	57	0,653	0,168
64,6	1140	68,0	71,1	252	65,5	1,086	0,282
71,3	0						

Table 2.3.6 - Calculated average shaft friction, LD-pile, t= 500 days, West Delta

Depth	Measured shaft load	Average depth	Average t_{us}	σ_{v0}'	s_{ud}	α	β
(m)	(kN)	(m)	(kPa)	(kPa)	(kPa)	t_{us}/s_{ud}	t_{us}/σ_{v0}'
0	4137	9,5	6,3	x	x	x	x
18,9	3850	23,5	11,5	92	18,5	0,621	0,125
28	3600	32,6	25,0	132	26	0,961	0,189
37,2	3050	46,4	28,5	183	33	0,865	0,156
55,5	1800	60,1	39,5	222	51	0,774	0,178
64,6	940	68,0	58,6	252	62	0,946	0,233
71,3	0						

Table 2.3.7 compares the measured total ultimate shaft loads to a shaft load corresponding to full mobilisation of the undrained strength, s_{ud} along the same length of pile. The data in Table 2.3.7 suggest that the shaft friction capacity has increased by 10 % from the test at 116 days to the test at 500 days, but that it dropped again by 7 % from the 500 day test to the 2.5 year test.

Table 2.3.7 - Summary of measured ultimate tension capacity and apparent average mobilised α-values, LD-pile West Delta

Time of load test	Measured from 18.9 to 71.3 m Q_{usm} (kN)	Calculated assuming t_{us} = sud (α = 1.0) Q_{uscal} (kN)	Apparent average mobilised α-value Q_{usm}/ Q_{uscal}
115 days	3500	5183	0.675
500 days	3850	5183	0.742
2.5 years	3600	5183	0.695

Figure 2.3.19 shows the distribution of shaft friction for both the 116 and 500 day tests. In addition to actual data, the shaft friction values have also been corrected to what would correspond to U=100%. These corrected values were calculated assuming that the gain in capacity is linear in relation to the degree of consolidation as presented in Figure 2.3.16. Along the middle part of the pile, the data suggests a gain in shaft friction of about 20 % from t=116 to t=500 days, but essentially no change, even reduction along the upper and lower part. It is quite possible that these relative changes reflect uncertainties in the data, rather than reality.
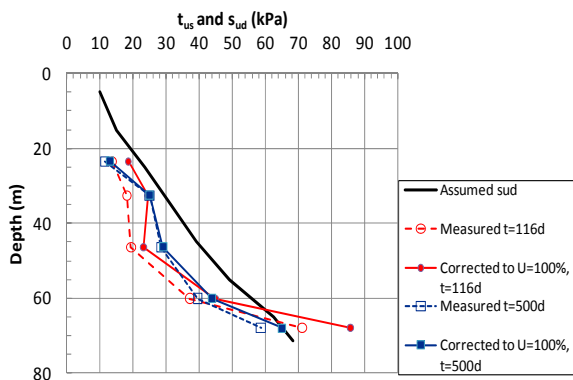
Figure 2.3.19 - Measured shaft friction at peak pile head load for tension tests LD-pile, West Delta

Figure 2.3.20 presents the mobilised normalised shaft friction values represented by α and β values for the tests at t=116 and 500 days. The lowest normalised shaft friction values are found at a depth of about 47 m, which may be related to the fact that the water content and plasticity are lowest around this level (Figure 2.3.3). Strain softening effects may also to some extent explain why the normalised values are highest at the bottom. When the peak pile load is reached the displacement is significantly larger along the upper at part of the pile than what it is at the bottom.
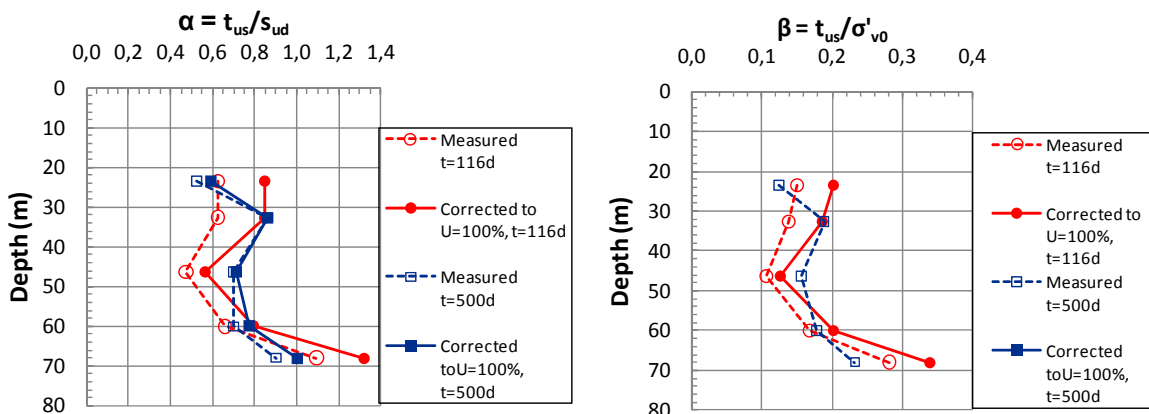
Figure 2.3.20 - Measured α-and β-values at peak pile head load for LD-pile, West Delta

The report by Ertec (1985) presents deduced values of mobilised shaft friction in relation to the local pile displacement. Figure 2.3.21 shows an example of such a curve. Table 2.3.8 summarizes local displacements when the peak shaft friction was reached, and the ratio of post-peak to peak shaft friction. Neglecting the data at 32.6 m which are "out of line", the results are consistent and shows that the peak shaft friction typically occurred at a peak displacement of 8.1 mm, corresponding to 1.0 % of the pile diameter, and that the post-peak strength is typically 88 % of the peak. For comparison, the ratio between post-peak and peak axial load as measured at the 18.9 m depth level is 0.95, ref. Figure 2.3.19, and the peak load occurred at a displacement of 27 mm at the pile head.
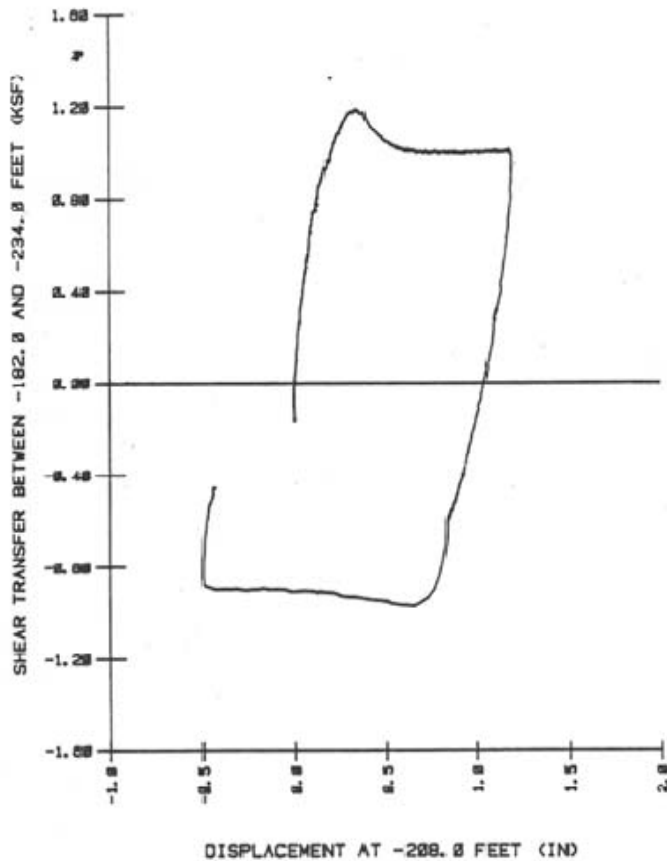
Figure 2.3.21 – Example of measured local t-z response along LD-pile, West Delta (after Ertec, 1985)

Table 2.3.8 - Local displacement at peak shear transfer and reduction in post-peak shaft friction (based on data presented by Ertec, 1985)

Average depth (m)	Type of data	Disp. at peak (mm)	Ratio Postpeak/ Peak
23,45	SG	10,1	0,92
32,6	SG	4,5	0,65
46,35	SG	8,3	0,9
60,05	SG	8	0,85
67,95	SG	8,9	0,81
23,45	LVDT	6,1	0,96
46,35	LVDT	7	0,88
67,95	LVDT	8,3	0,85
	Average	7,7	0,85
	Average	8,1	0,88

The additional local displacement to reach a stable post-peak shaft friction was typically 5 mm in addition to the displacement at peak, e.g. typically at 13 mm of total displacement. Figure 2.3.22 presents the distribution of axial displacements calculated from peak load on the pile top for the t=116d test using the load distribution in Figure 2.3.18, and assuming that 8.1 mm displacement is required to mobilise the full shaft friction near the tip. The calculated pile top displacement of 27 mm agrees extremely well with what was actually measured.
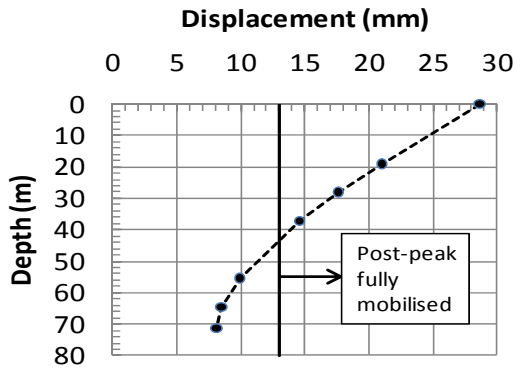
Figure 2.3.22 - Calculated axial displacement along pile at peak load, t=116 day test, LD-pile, West Delta

Figures 2.3.23 and 2.3.24 present the estimated peak shaft friction along the pile. This was arrived at by using the corrected U=100% shaft friction values in Figure 2.3.19, combined with the average post peak reduction ratio of 0.88 according to the Table 2.3.8 down to a depth of 44 m, and a gradual transition to a reduction ratio of 1.0 at the pile tip. The results suggest an average α-value around 0.9 for the entire pile, with α ≈ 0.9 in the top, decreasing to about 0.7 in the middle part and increasing to 1.15 near the tip of the pile. The β-values show a corresponding variation, with an average around β = 0.20 at the top, decreasing to β ≈ 0.15 at the middle and increasing to β ≈ 0.30 near the tip.
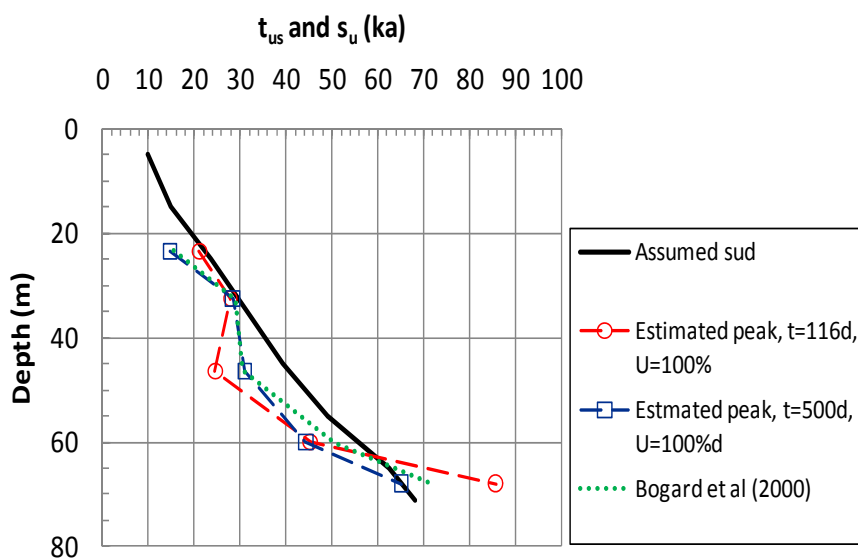
Figure 2.3.23 - Estimated peak shaft friction at U= 100 %, LD-pile, West Delta
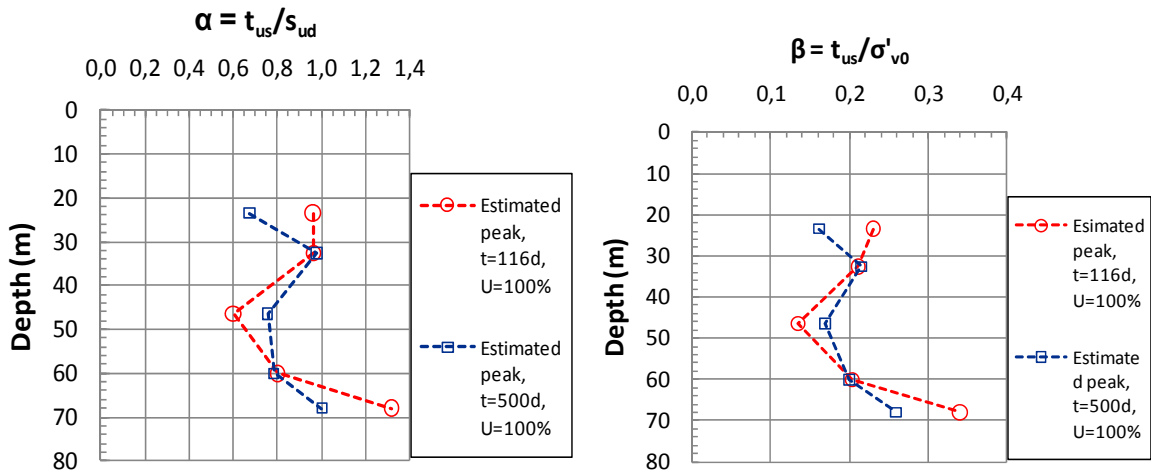
Figure 2.3.24 - Estimated peak α-and β-values for LD-pile, West Delta

Using the peak shaft friction values in Figure 2.3.23, the ultimate capacity (for an infinitely stiff pile) becomes about 5 % larger than the actually measured peak pile head load.

The peak shaft friction values arrived at in Figure 2.3.23 agree reasonably well with what was interpreted by Bogard et al (2000), but as presented in Figure 2.3.8 they used a generally lower in-situ undrained shear strength profile as basis for comparison to the shaft friction, and thus, obtained correspondingly higher α–values, close to unity along the entire pile.

Figure 2.3.25 shows that the ultimate shaft friction generally increases with the measured horizontal effective stress at onset of pile loading. Although there is scatter in the data, a typical average relationship may be taken as:

$$\tau_{us} = 0.25 \cdot \sigma'_{hc}$$
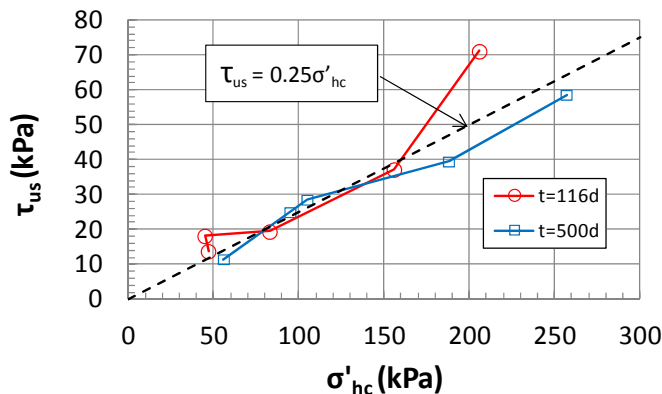
Figure 2.3.25 - Measured ultimate shaft friction in relation to horizontal effective stress at onset of pile loading, West Delta

For the LD pile the measured earth pressures at failure were generally somewhat lower than at start of loading, and the pore pressures were higher. As was shown in Figure 2.3.13 this lead to effective stresses at failure that were considerably lower than at onset of loading. Figure 2.3.26 shows that for the 116 day test the ultimate shaft friction in relation to the horizontal effective stress at failure can typically be represented by:

$$\tau_{us} = 0.52 \cdot \sigma'_{hf}$$

This disregards the very low effective stress measured at a depth of 42.6 m. At 500 days the data show far more scatter and a unique failure envelope is hard to define. In this context it may be recalled that failure does not necessarily occur at the pile surface. Bogard and Matlock (1998[a]) actually reported that a layer of clay about 3" (76 mm) thick was sticking onto the LD pile when it was pulled out of the ground 2.5 years after installation. This is very similar to the Haga experience (Figure 2.2.17).
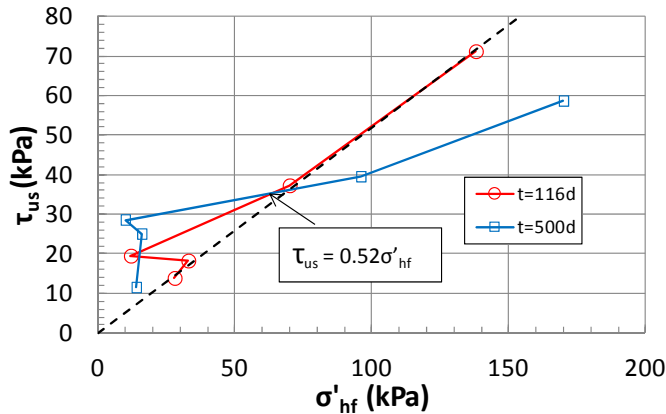
Figure 2.3.26 – Measured shaft friction at peak load in relation to horizontal effective stress at failure, West Delta

Bogard and Matlock (1998[a]) presented Scanning Electron Microscopic x-ray studies of the clay that adhered to the pile when it was pulled out, and could define three distinct zones as follows:

- An inner about 0.5" thick Zone 1, where the clay platelets where strongly oriented parallel with the pile surface, and appeared slicken-sided at the transition to Zone 2, where failure was assumed to occur during the first 116 day test. Furthermore the clay in this zone was found to be rich from iron oxide stemming from chemical reaction with the steel.
- Zone 2 extending from 0.5" to 1.4" the clay platelets also showed high degree of parallelism with the pile surface and contained a large number of shear bands and shear band formation, especially in the outer 0.2" thick zone where failure was assumed to have occurred during the 500 day test.
- Zone 3, extending from 1.4" to 3". Failure was assumed to have occurred at the edge of this zone during the last load test 2.5 years after pile installation.

2.4 Onsøy

2.4.1 General overview of test site and load tests

The Onsøy test site lies about 3 km NW of the City of Fredrikstad, Norway. At the site there is a 45 m deep deposit of normally consolidated medium to highly plastic marine clay. The area had previously been used as a test site by NGI for a large scale test embankment (1972-74) and various in-situ testing (1979-85), including piezocone, pressure meter, dilatometer and in-situ vane testing.

The pile testing program at Onsøy was part of Joint Industry Project (JIP) initiated by NGI and named: "Design of offshore piles in clay- field tests and computational modelling". This project also included testing at the Lierstranda and Pentre test sites described in subsequent sections. The project started in 1985 and was completed in 1989. Testing at the Onsøy site took place in 1985-

86. Cyclic response of flexible piles was the main focus in this JIP project, but the static behaviour formed an important basis for understanding the cyclic response.

The testing arrangements and results have been fully documented in reports by NGI (1987[b], 1988[b and c]) and have also been summarized by Karlsrud et al (1992[a,b]). As part of this study all results have been checked and re-interpreted, and will therefore in some respects appear slightly different from what was presented in the aforementioned publications.

Three types of piles were tested at Onsøy, Lierstranda and Pentre as illustrated in Figure 2.4.1:

- Pile type A: Closed-ended fully instrumented pile with diameter of 219 mm, wall thickness of 8.2 mm and embedded length of 10 m. These test pile were driven through cased boreholes to reach a tip penetration ranging from 15 to 37.5 m.
- Pile type B: Open-ended fully instrumented pile with diameter of 809 mm and wall thickness of 9.5 mm driven through a 5 m deep casing to a tip penetration of 15 m (only Onsøy and Lierstranda).
- Pile type C: Closed-ended pile of the same dimensions as pile A but driven through a 5 m deep casing to tip penetration of 35.0 m. Test pile C1 was fully instrumented and actually put together of the instrumented segments used for piles A1 to A4, whereas pile C2 was without any instrumentation. These piles were only installed at Onsøy.

For test piles A1-A4 and C1 special instrumentation units were manufactured, Figure 2.4.2. Each unit contained 2 vibrating wire (VW) type strain gauges for measuring axial loads, 2 pairs of diametrically positioned earth and pore pressure gauges of the membrane VW type, and a temperature sensor. Test piles A1-A4 contained three of these instrumentation units placed at a distance of 2.5 m, 5.0 m and 7.5 m from the pile tip. Test pile C1 had 5 such instrumentation units placed at 5.0 m intervals along the pile, Figure 2.4.1. The earth pressure gauges had a 20 mm diameter flat membrane, but was equipped with a curved rubber front to make it flush with the curved pile surface. The pore pressure sensors had a porous ceramic filter in front that was vacuum- saturated in the laboratory and protected with a water filled gasket until the sensors entered into the ground.

The open-ended test pile B was instrumented at 3 levels, respectively 2.5, 5.0 and 7.5 m above the pile tip, Figure 2.4.1. At each level there were two pairs of membrane type VW earth and pore pressure sensors and 8 VW strain gauges. The strain gauges were placed 0.5 m above the level of the earth -and pore pressure gauges. The earth pressure gauges were specially made with a curved 68 mm diameter steel membrane that was installed such that it became flush with the pile surface. The pore pressure sensor had a vacuum saturated ceramic filter in front as for the A-piles, and was also protected with a water filled gasket prior to entering the ground.

In addition to the above, loads were measured at ground surface using a specially made VW type load cell. Displacements were measured by two analogue transducer mounted to an independent reference beam founded on soil anchors placed about 2 m to each side of the test piles.
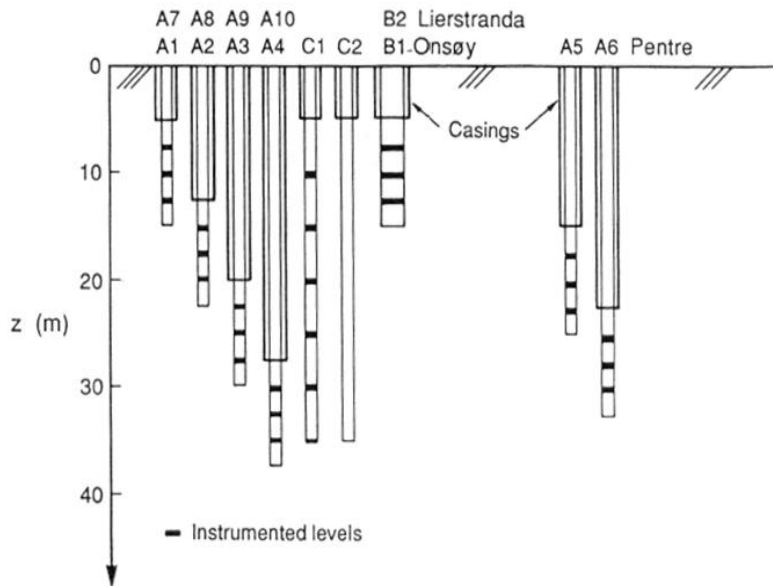
Figure 2.4.1-Test piles used at Onsøy, Lierstranda and Pentre test sites
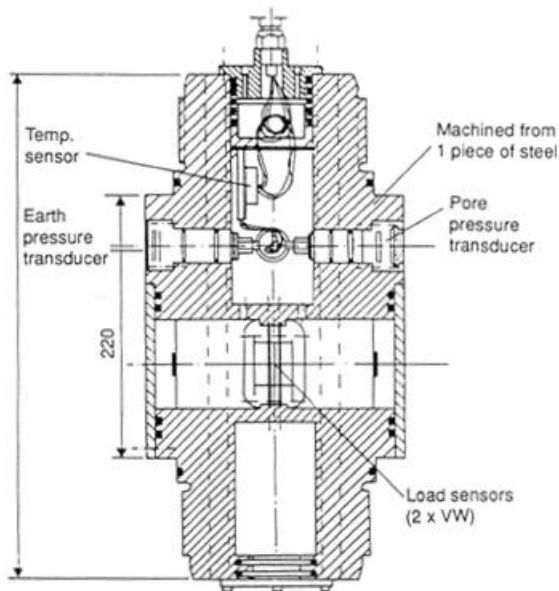
Figure 2.4.2-Special instrumentation unit used on type test piles A1 to A4 and C1, Onsøy

All instrumentation units were carefully calibrated in the laboratory prior to installation, and also tested for impact loading (apart for the strain gauges on the B1-pile). Zero readings were taken just prior to installation and just after retrieval of the piles out of the ground. The change in zero readings from installation to retrieval were generally small and acceptable in relation to the pressure gauges (generally less than 10 kPa in pressure up or down).The strain gauges in the A-segment piles showed a change in frequency mostly corresponding to 10-20 kN in load. For the B-pile the change was larger, corresponding to load of 50 to 100 kN. It was in all data treatment relied mostly on zero frequencies after pull-out, as it was considered that driving stresses affected the zero frequencies more than the non-dynamic pull-out of the piles. The load cell at the top was of course also calibrated and checked, and showed very high resolution and accuracy.

All test piles were driven into the ground by use of 1 to 3 ton drop hammer. All sensors were continuously logged during these operations.

Loads were applied by hydraulic jacks through a special actuator capable of controlling both static and cyclic load levels as desired. The load testing program on each of the test piles included on all piles a first initial static tension test to failure. This was carried out from 26 to 80 days after pile installation when excess pore pressures generated against the pile surface during installation were essentially fully dissipated. As shown in Table 2.4.1, the initial static test was in general immediately followed by cyclic loading. After a resting period of 1 to 7 weeks, most piles (apart from C2) were subjected to a second and in one case (A2) also a third test series. Although the main focus herein will be on the initial static tension results, some reference will also be made to the later static tests when it is seen relevant. No reference will be made to the cyclic test results, which as described earlier is outside the scope of this study.

In the initial static tests load was applied in a load-controlled stepwise mode, with typically 5 steps corresponding to 10 % of the estimated failure load first, followed by steps of 5 %. Each load step lasted 3 minutes.

Table 2.4.1- Load testing program, Onsøy

Test pile	Test no.	Date installed	Type of test	Days after installation
A1	02	06.09.1985	Initial static tension	26
	03		Rapid static tension	26
	04		Static tension	35
	05		Rapid static tension	35
	06		One-way cyclic	35
	07		Static tension	35
A2	02	25.10.1985	Initial static tension	27
	03		One-way cyclic	27
	04		Static tension	34
	05		One-way cyclic	34
	06		Static compression	46
	07		Two-way cyclic	46
A3	02	16.05.1986	Initial static tension	55
	03		One-way cyclic	55
	04		Static tension	70
	05		Two-way cyclic	70
A4	02	20.06.1986	Initial static tension	35
	03		One-way cyclic	35
	04		Static creep in tension	74
B1	02	27.10.1986	Initial static tension	80
	03		One-way cyclic	80
	04		Static tension	97
	05		One-way cyclic	97
C1	02	17/18.09.1986	Initial static tension	37
	03		One-way cyclic	37
	04		Static tension	88
	05		One-way cyclic	88
C2	02	17.09.1986	Initial static tension	51
	03		One-way cyclic	51

2.4.2 Key soil parameters

At the site there is a 1-1.5 m thick desiccated crust at the top, followed by soft plastic clay that contains some black spots of iron oxide (especially in the top part), and some traces of organic matter and shell fragments. Figure 2.4.3 shows that the water content ranges from about 50 to 70 %, with the highest value around 10 m depth and a clear decreasing tendency with depth below that level. The plasticity index lies in the range 35 to 50% with the largest values between 15 and 25 m. The clay content varies from 40 to 60 %. The salt content increases from 8% at 2m to 30 % from 8 m and onward. With a specific gravity around 2.7 the total unit weight typically lies in the range 16 to 17 kN/m3. It should be noted that that the deepest sample comes from a depth of 32.5 m. Data beyond that level were extrapolated. As shown in Figure 2.4.4 there is a slight artesian pore pressure condition at the site, corresponding to about 11.3 % above hydrostatic values.
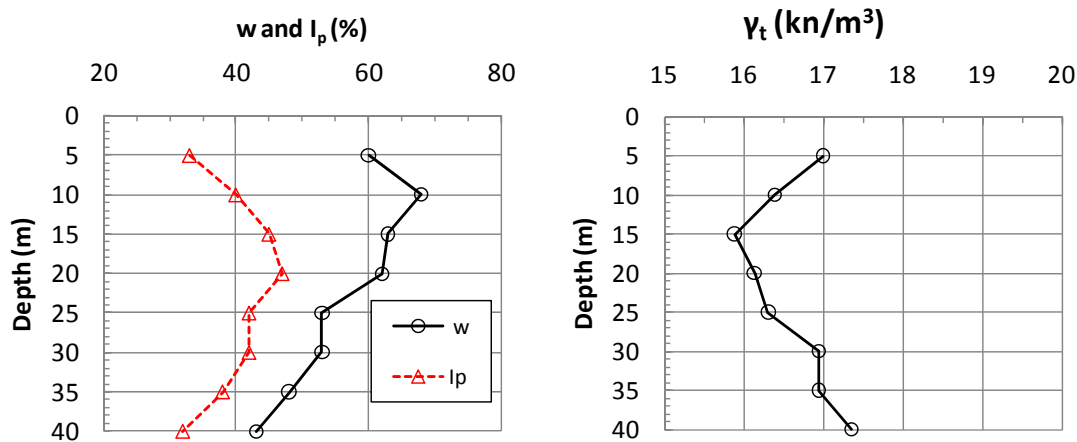
Figure 2.4.3- Summary of index data, Onsøy

A large number of IL and CRS type oedometer tests have been carried out on 95 mm piston samples taken in the "in-situ test" area about 100 m west of the pile teat area (NGI, 1985[c]), as well as on 95 mm piston samples from the test fill area 30-50 m away (NGI (1973[a,b,c,d]). Oedometer tests were also carried out on samples taken with a special block sampler, Lacasse et al (1985). These results were also reported in NGI (1985[c]). For this reason only three new oedometer tests were carried out on samples of intact clay from the pile test area, NGI (1986[a]). The oedometer tests show that the deposit in geologic terms is normally consolidated. It is still assumed to have an apparent pre-consolidation pressure due to creep or ageing effects (e.g. Bjerrum, 1973) corresponding at depth to OCR =1.3, Figure 2.4.4. That is considered a conservative (low) estimate. The very top part down to about 5 m depth shows higher pre-consolidation pressures and OCR values due to effects of desiccation and chemical weathering.
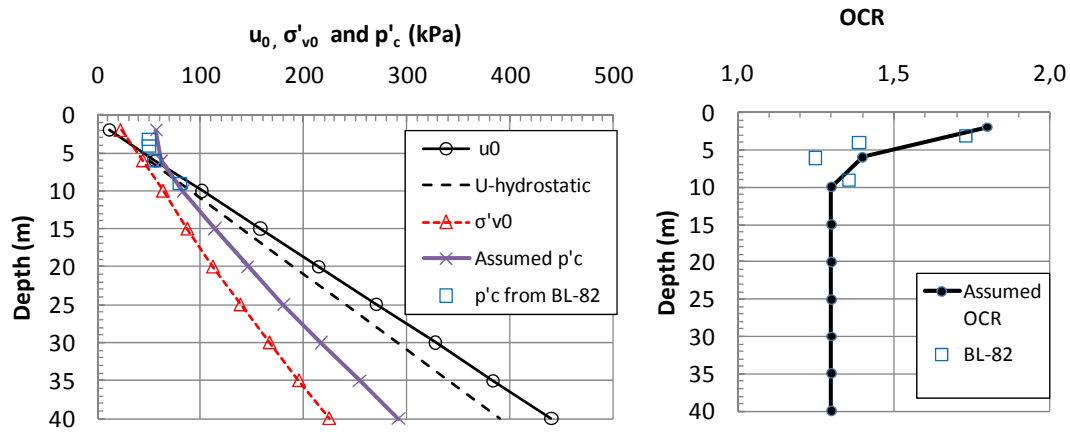
Figure 2.4.4 - In-situ stresses and pre-consolidation pressure, Onsøy

The oedometer data shows that the virgin compressibility index $C_c/(1+e_0)$ varies with stress level. This means that the virgin M-σ modulus curve as defined by Janbu (1963) shows a positive intercept, p'_r, at M =0. By selecting modulus values in the virgin region at a stress level about 50-100 kPa in excess of p'_c, and taking $p'_r=0$, gives modulus numbers, m_0 as shown in Figure 2.4.5. It can be observed that m_0 typically lies in the range 6 to 9, and as expected is lowest at 10 m depth where the water content is highest.
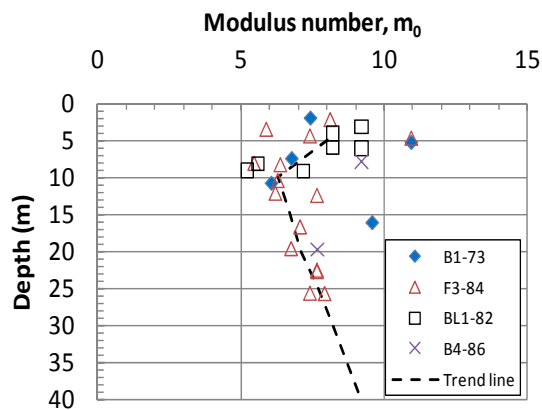
Figure 2.4.5 - Modulus number from oedometer tests, Onsøy

The in-situ vertical permeability at zero volumetric strain, k_0, was determined from the oedometer tests in a similar manner as described in Section 2.3.2 for West Delta, and decrease from about $3 \cdot E^{-9}$ m/s at 5 m to about $0.6 \cdot E^{-9}$ m/s at 25 m, Figure 2.4.6.
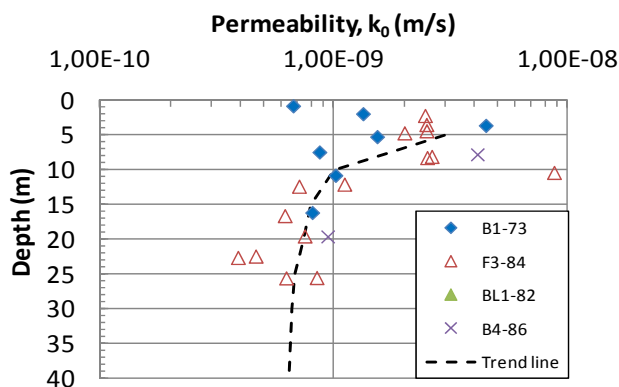
Figure 2.4.6 – Permeability derived from oedometer tests, Onsøy

Figure 2.4.7 shows typical average undrained shear strength profiles derived from a large number of triaxial compression, extension and DSS tests (at least 15 of each) carried out on samples from the various test areas at Onsøy. This is based on data summarized in NGI (1988[a]). It can be mentioned that the CAUC tests on the four high quality block samples taken at Onsøy gave strengths that were 5-20 % higher than for the comparable 95 mm piston samples, but there were no significant difference between block samples and 95 mm piston samples for DSS and CAUE tests. Normalised strength values are presented in Figure 2.4.8. The anisotropy ratios typically correspond to $s_{ud}/s_{uc} = 0.725$ and $s_{ue}/s_{uc} = 0.45$, which are in line with the anisotropy ratios determined from testing of numerous high quality block samples as presented inFigure 2.4.9 from Karlsrud et al (2005).
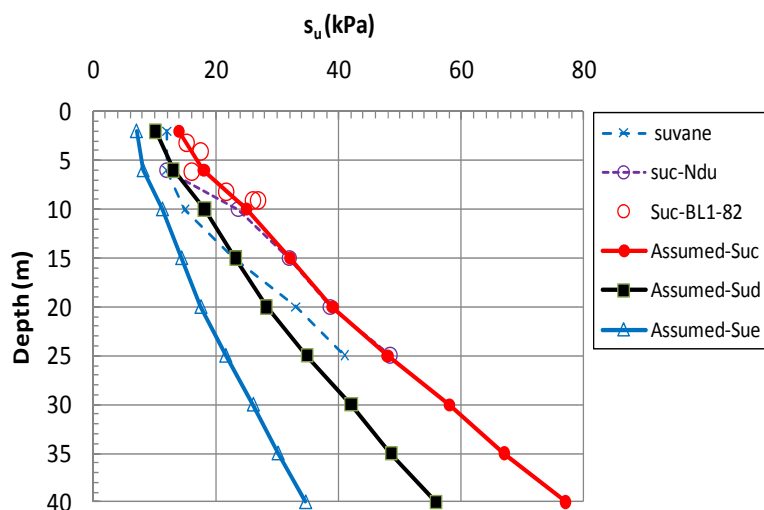
Figure 2.4.7 - Undrained shear strength profiles, Onsøy
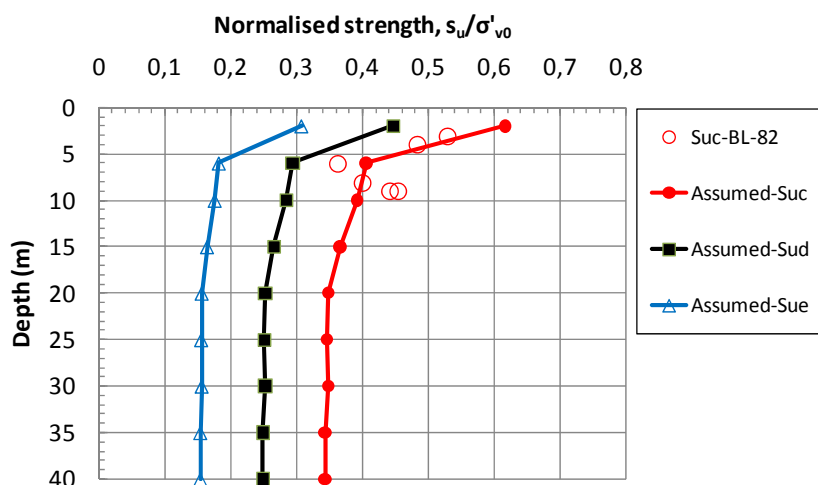
Figure 2.4.8 – Assumed normalised undrained strength profiles, Onsøy

Figure 2.4.7 also shows a typical un-corrected average in-situ vane shear strength profile, which in this case agrees reasonably well with the DSS profile. Below the upper weathered zone, the normalised strength s_{ud}/σ'_{v0} tend to decrease somewhat with depth from 0.31 at 10 m, 0.27 at 15 m and 0.25 at 25 m, Figure 2.4.7. This is also in line with the somewhat decreasing plasticity index with depth. Below 25 m, the normalised strength is assumed constant.
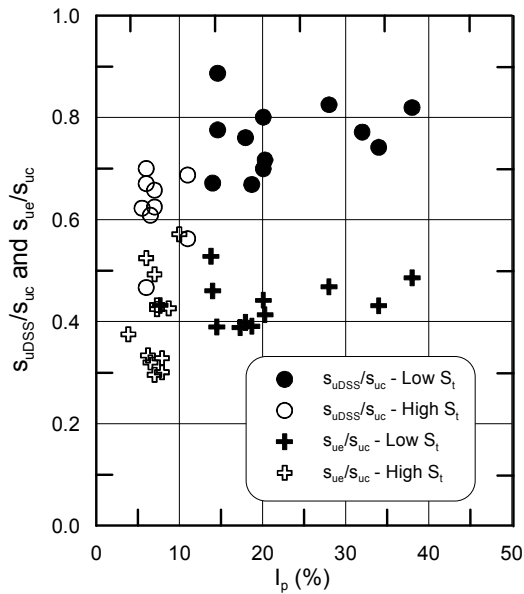
Figure 2.4.9 - Measured anisotropic strength ratios sue/suc and sud/suc from tests on high quality block samples (after Karlsrud et al, 2005)

A large number of piezocone tests have also been carried out at this site, ref. NGI (1985[b]) and Lunne et al (1989). Using the u_2 pore pressure measured just beyond the neck of the cone, the undrained triaxial compression strength has been interpreted using the procedures and correlations between s_{uc} and the cone factor $N_{\Delta u}$ proposed by Karlsrud et al (2005) in Figure 2.4.10 and the following expression for low sensitive clays (St<15):

$$N_{\Delta u}= 6.9 - 4.0 \cdot logOCR+0.07(Ip) \qquad Ip \text{ in } \% \tag{2.4.1}$$

As seen in Figure 2.4.7 these CPTU derived s_{uc} strengths agree reasonably well with the results from the triaxial tests. For the purpose of this study, the s_{ud} profile shown in Figure 2.4.7 has been used as basis. It is very close to the average of the s_{uc} and s_{ue} strengths.
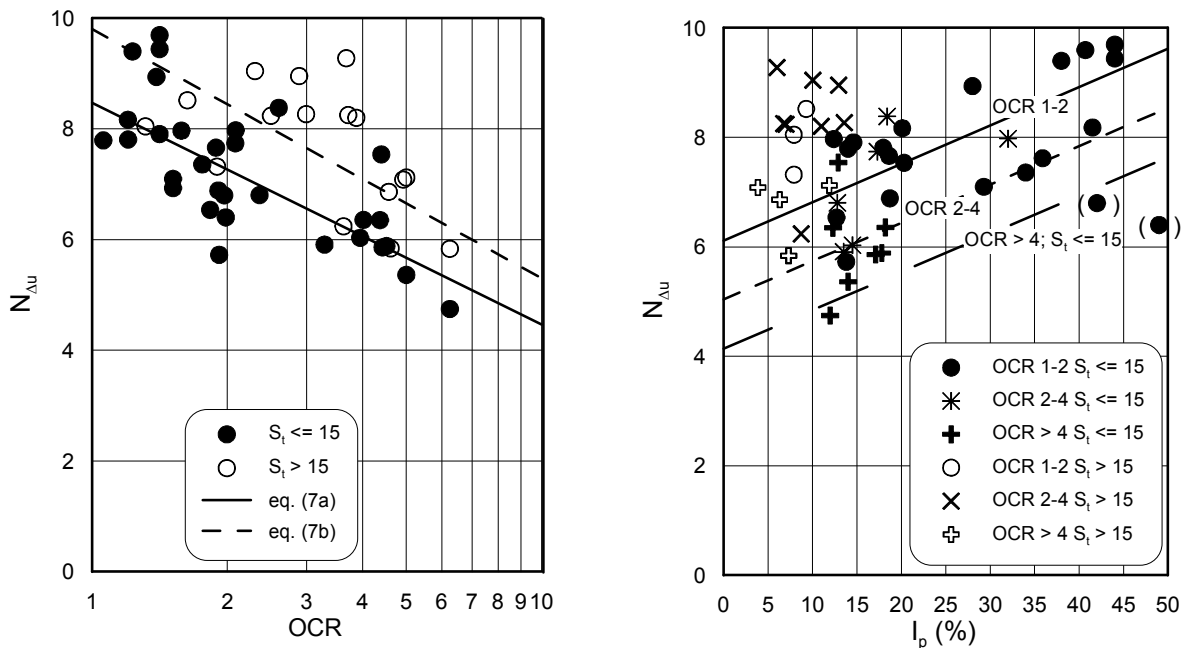
Figure 2.4.10- Relationship between $N_{\Delta u}$, OCR and I_p (from Karlsrud et al, 2005)

The triaxial tests show that the effective strength failure envelope for Onsøy clay can be typically defined by $\varphi' = 29.5^0$ and attraction intercept a=5-10 kPa. By setting a= 0 the best fit to the failure envelopes gives $\varphi' = 34^0$.

Undrained shear modulus values from both triaxial and DSS tests lie in lie the range G_{50}/s_u =100-200.

As part of the pile testing program a total of 9 DSS and 3 DSB tests were carried out on RR clay samples taken from the depth range 12 to 27 m. The DSS tests showed a normalised strength corresponding to $(s_{ud}/ \sigma'_{ac})^{RR} = 0.24$ (range 0.21-0.27). After some cyclic testing and one day of reconsolidation, the normalised strength had increased by about 35 % to $(s_{ud}/ \sigma'_{ac})^{RR} = 0.325$.

The DSB tests on RR clay gave higher strength than the DSS tests, with $(s_{uDSB}/ \sigma'_{ac})^{RR} = 0.29$ after first shearing. These samples were loaded statically to failure 3 times, with a reconsolidation period of 1 to 5 days in between. Figure 2.4.11 suggests that the relative increase in strength after a 1st load test increases with time, and that it gains even more when a third test is carried out on the same specimen.
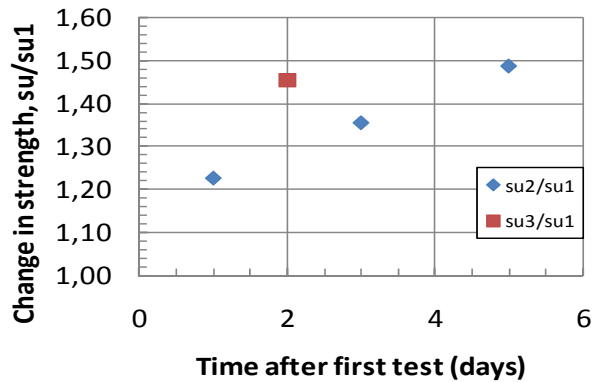
Figure 2.4.11 – Change in strength from repeated testing to failure with reconsolidation in between each test, based on DSB tests on RR clay, Onsøy

As part of the pile testing program at Onsøy, a series of DSS tests were also carried out on specimens cut vertically (at 90^0 angle) in the sample cylinder, as was also done on Haga clay (Section 2.2.2). These samples, taken from depths of 7.2 to 32.8 m, were prior to undrained shearing consolidated to a stress corresponding to the estimated in-situ horizontal effective stress assuming K_0=0.6. First time shearing gave a typical normalised strength value of s_{udv}/σ'_{ac}= 0.34. Normalised with respect to the in-situ vertical effective stress the strength ratio becomes of s_{udv}/σ'_{v0}= 0.204, which is nearly the same as observed for the standard horizontally trimmed specimens. Following one day of reconsolidation, the s_{udv} strength typically increased by 25 % (ref. NGI, 1988[a]). This is about the same strength increase as was observed for the DSS and DSB tests on RR clay.

Figure 2.4.12 compares the results of oedometer tests on Intact Clay (IC) and remoulded reconsolidated (RR) clay. As was observed for Haga clay (Figure 2.2.23), the effect of the severe remoulding is to increase the volumetric strain at in-situ stress level by 8 to 12 %, but the virgin compression index is lower for RR clay than for intact (IC) clay. In relation to Figure 2.4.12 it may be noted that the tests on intact clay samples to some extent were affected by sample disturbance, and especially so for the deepest sample from 32.9 m depth.
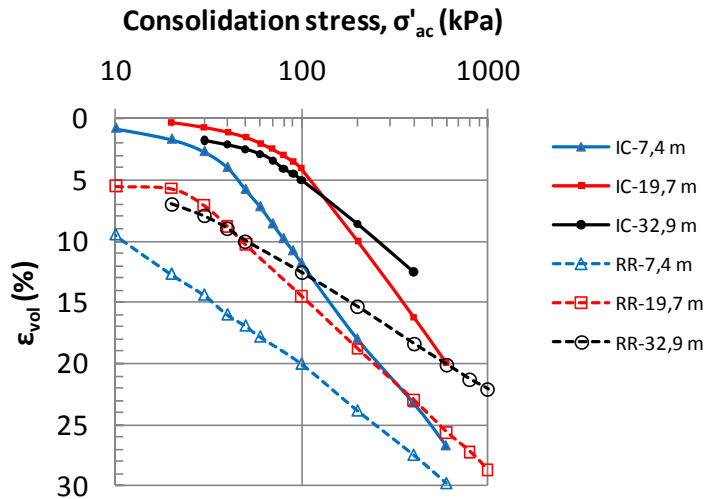
Figure 2.4.12 - Comparison between oedometer tests on Intact and RR clay, Onsøy

2.4.3 Load test results

Figure 2.4.13 presents normalised excess pore pressures at the end of installation for all the piles. For the A-segment piles it may be observed that the lowest sensor shows the highest excess pore pressures. The likely explanation is that some pore pressure dissipation occurs even during penetration of the pile, and that the lowest sensors on each A-pile represent most closely the pressures generated for perfect undrained penetration. In the depth range 30-35 m the long C1-pile generated excess pore pressures that perfectly match the A4 pile. The C1 pile values also generally agree closely with the lowest values observed for the A-segment piles from 5 to 15 m. From 15 to 25 m the end of installation pressures for the C1 pile are up to 15-20 % smaller than for the comparable A-segment piles. The explanation for this difference is probably that the installation of pile C1 went over 2 days, which will have caused more pore pressure dissipation along the pile by the time the installation was completed. In comparison to the closed-ended A1 pile, the open-ended B1-pile generated excess pore pressures that were 25 to 50 % lower. For comparison, such difference between closed and open pile penetration was not observed in the tests at West Delta.
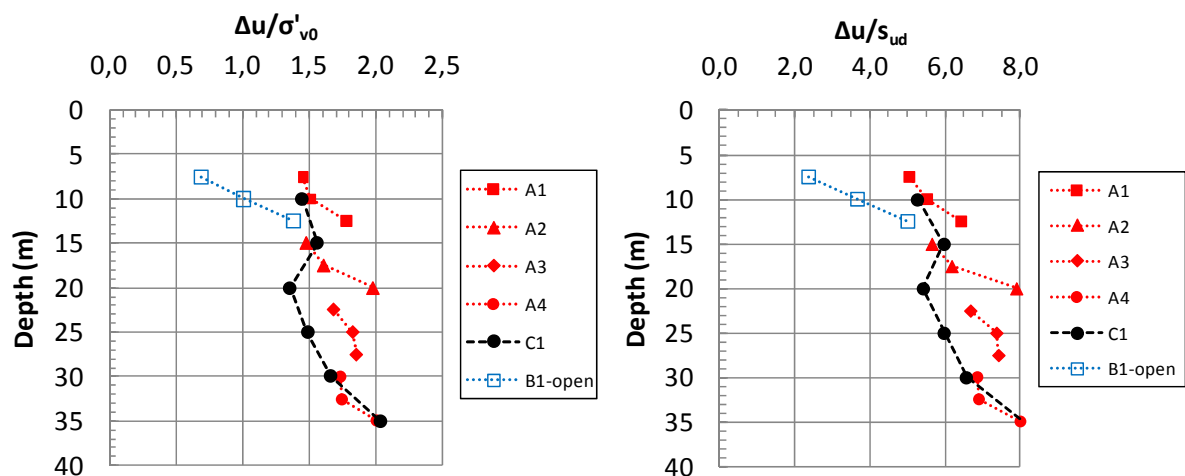
Figure 2.4.13 – Normalised excess pore pressure at end of pile installation, Onsøy

At the end of pile installation, the measured total earth pressures were in general lower than the measured pore pressures, leading to negative effective stress, Figure 2.4.14. This strongly

suggests that the measured total pressures are too low. As a consequence of such a possible error in the measured total earth pressure a correction of these values has been introduced. It is firstly assumed that the effective earth pressure should at least be equal to zero at end of pile installation. At later stages during the re-consolidation and loading phase it is assumed that the error in total earth pressure is linear to the absolute value of the pressure measured, which gives a corrected earth pressure at any stage corresponding to:

$$(\sigma_h)_{corrected} = \sigma_h - (\sigma_h / \sigma_{hi}) \cdot \sigma'_{hi} , \text{ where} \tag{2.4.2}$$

σ_h = Measured total earth pressure at any stage

σ_{hi} = Measured total earth pressure at end of pile installation

σ'_{hi}= Measured effective stress at end of pile installation (only negative values apply,

no correction if $\sigma'_{hi} > 0$)
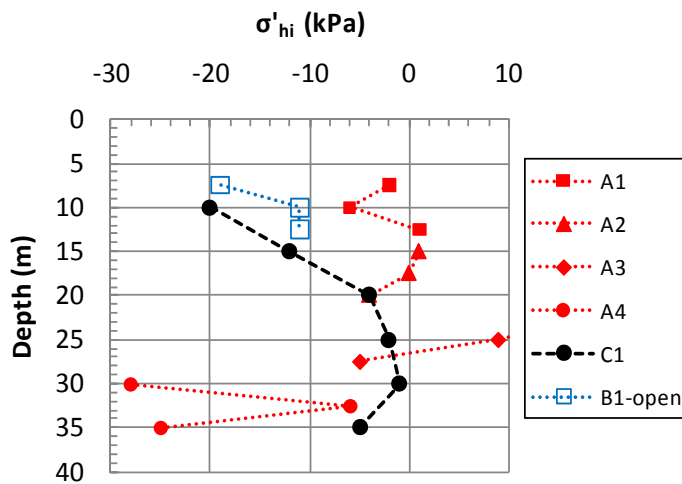
Figure 2.4.14 - Measured effective stress against the pile at end of pile installation, Onsøy

Figure 2.4.15 shows typical examples of earth- and pore pressure changes during the reconsolidation phase. At Onsøy the effective stress started to increase when the degree of consolidation, U, surpassed about 10 % for the A-segment piles and the upper part of the C1 pile, but not before U exceeded 15-35 % for the lower part of the C1-pile. For the B1-pile the gain in effective stress started almost immediately after pile installation. In contrast, at West Delta no significant gain in effective stress was observed before U ≥ 50 %.
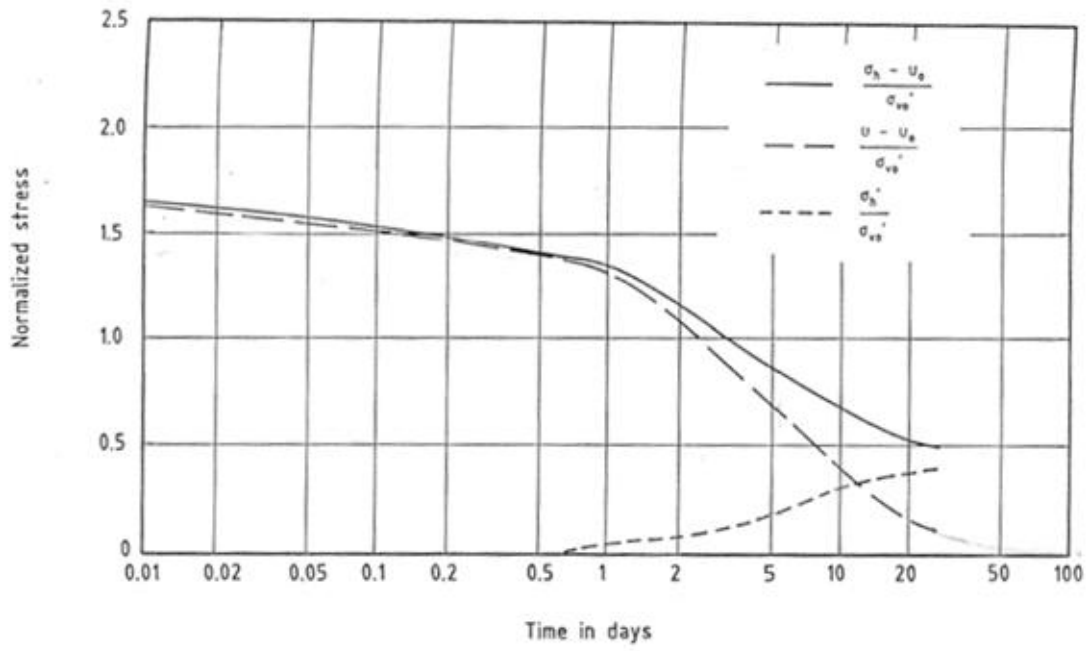
a) *Pile A2, z=17,5 m*
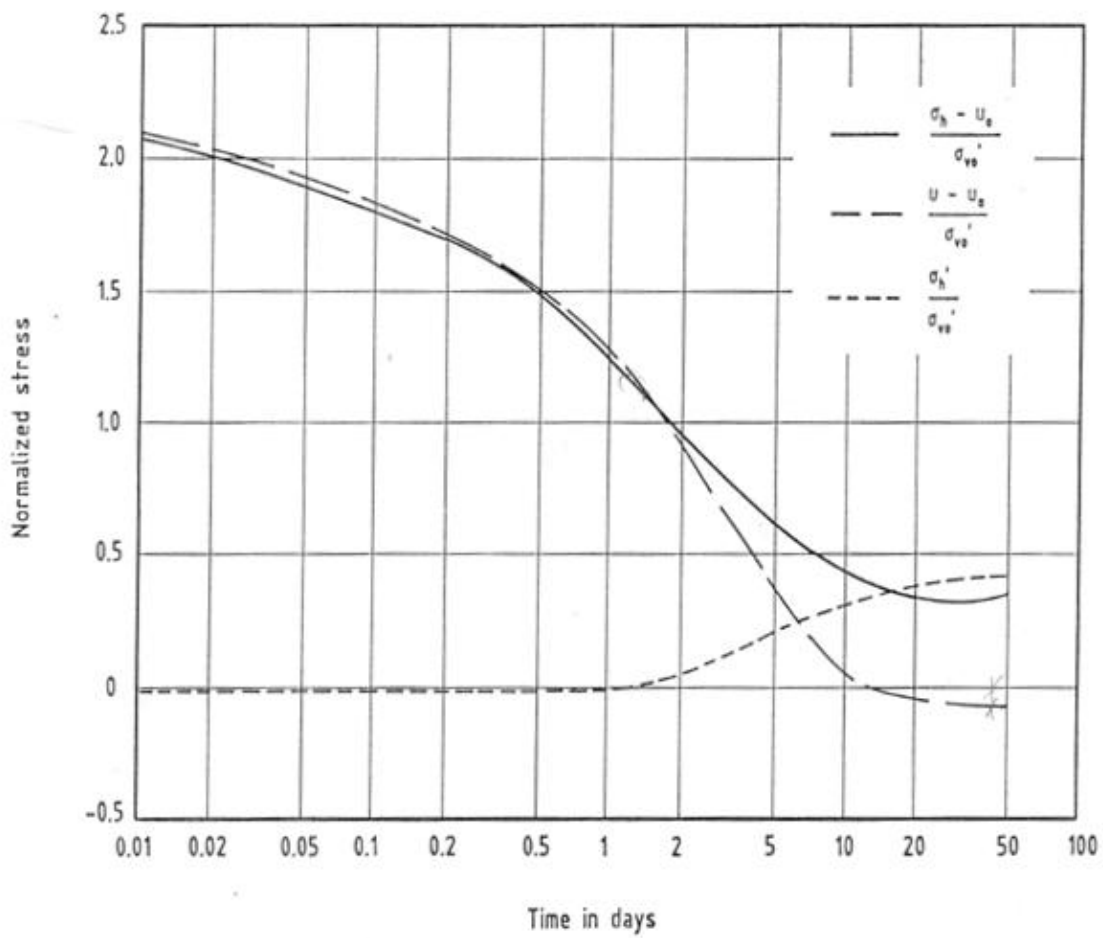
b) *Pile C1, z=35.0 m*
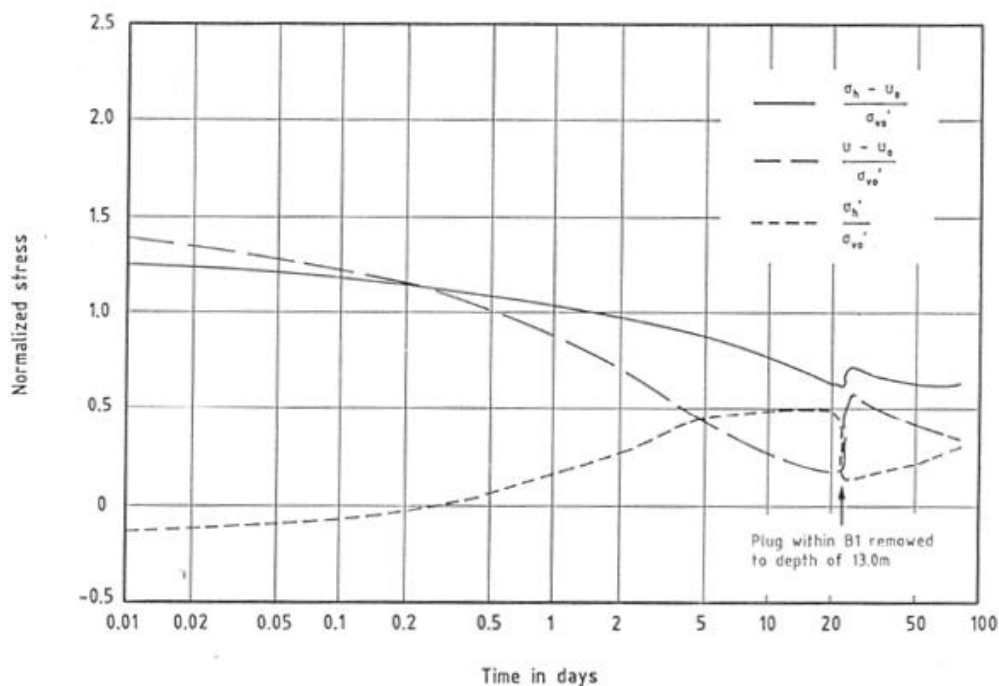
c) Pile B1 at 12.5 m

Figure 2.4.15 - Example of changes in normalised earth and pore pressures during the re-consolidation phase, Onsøy, a) Pile A2, at 17.5m, b) Pile C at 35m, c) Pile B1 at 12.5 m

Figure 2.4.16 summarizes data on times to reach 50 and 90 % consolidation. It may be noted that the consolidation process was considerably slower for the upper part of the C1 pile as compared to the A-segment piles at the same level. The re-consolidation was apparently faster for pile A1 than the deeper A-segment piles, which at least partly may be due to the higher permeability in the top (Figure 2.4.6).

At time of onset of the first load test, the degree of consolidation was only about 75 % for the upper part of the C1-pile and for the B1-pile, Figure 2.4.17.
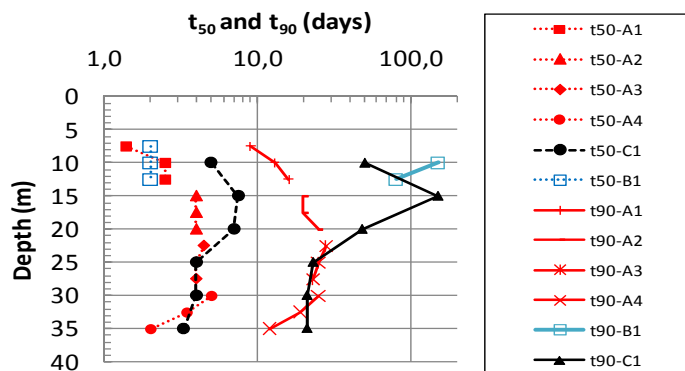
Figure 2.4.16 - Observed times to reach 50 and 90 % consolidation, Onsøy

A special comment should be made regarding the B1-pile. 22 days after installation the clay plug within the pile was removed. The purpose was to avoid any uncertainty with respect to what extent the clay plug would contribute to loads in the pile. During this plug removal there was a significant and sudden increase in pore pressure at all instrument levels, most so (about 20 %

increase) at the bottom level, Figure 2.4.15 c). Total earth pressures showed less response. Although no displacements could be visually observed at ground level, it is fair to assume that the plug removal caused a tendency for bottom heave up into the pile, leading to generation of shear stresses and pore pressure around the pile. After this temporary increase, the pore pressures decreased gradually back towards the "pre-event" level, but had not quite reached that level when the load test was carried out at t= 80 days. For this reason the results of test B1 must be taken with some caution, and the t_{90} data are particularly misleading for this case.
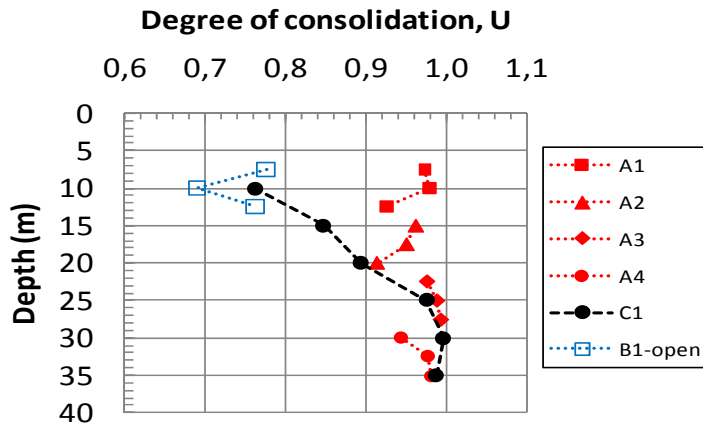
Figure 2.4.17 - Degree of consolidation at onset of pile loading, Onsøy

In the subsequent presentation of load test results the ultimate capacity and shaft friction as well as the corrected horizontal stress have been extrapolated to U=100%, assuming as for West Delta, that both σ'_{hc} and τ_{us} increase linearly in proportion to the degree of consolidation (i.e. they are upgraded by multiplying with the ratio of 1/U). It is only for the upper part of the C1-pile and the B1- pile that this correction is significant (Figure 2.4.17).

Figures 2.4.18 presents the horizontal effective stress at onset of pile loading and Figure 2.4.19 the corresponding horizontal effective stress ratio, K_c, compared to the assumed in-situ K_0 values. Note that the actual measured earth pressure data were first corrected as described above (eq. 2.4.2).
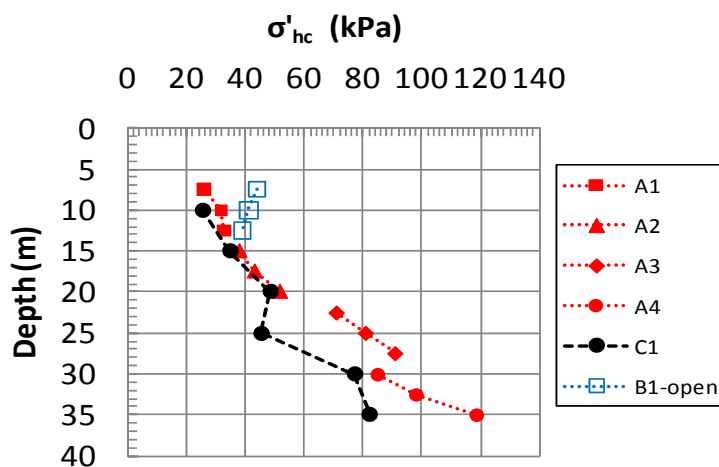
Figure 2.4.18 - Measured horizontal effective stress at U=100%, Onsøy
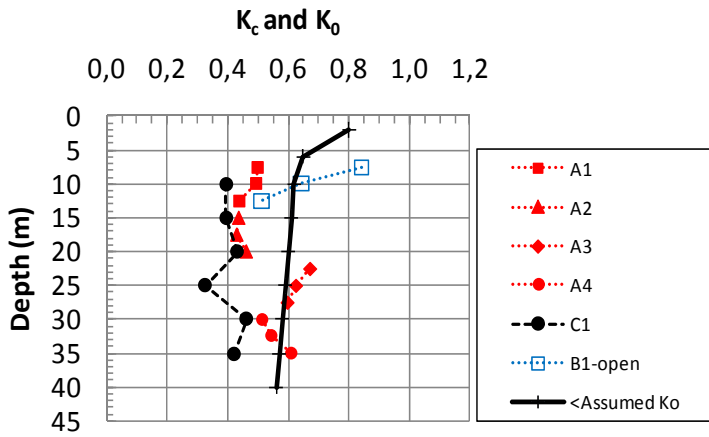
Figure 2.4.19- Measured horizontal effective stress ratio at U=100 %, Onsøy
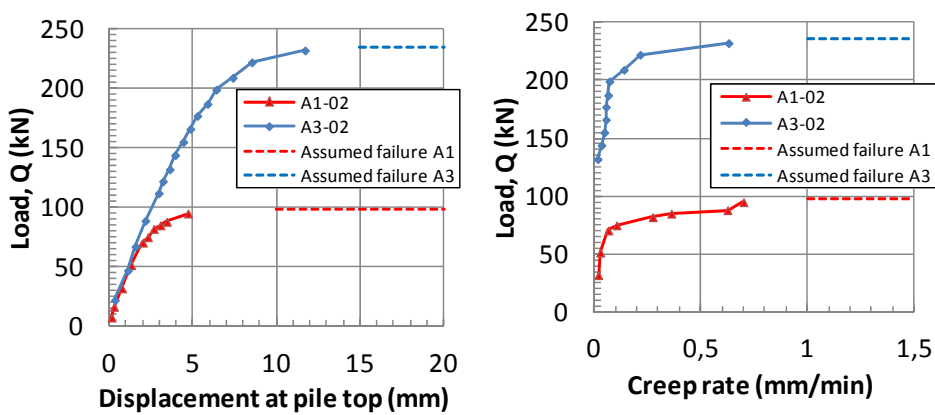
a) Piles A1 and A3
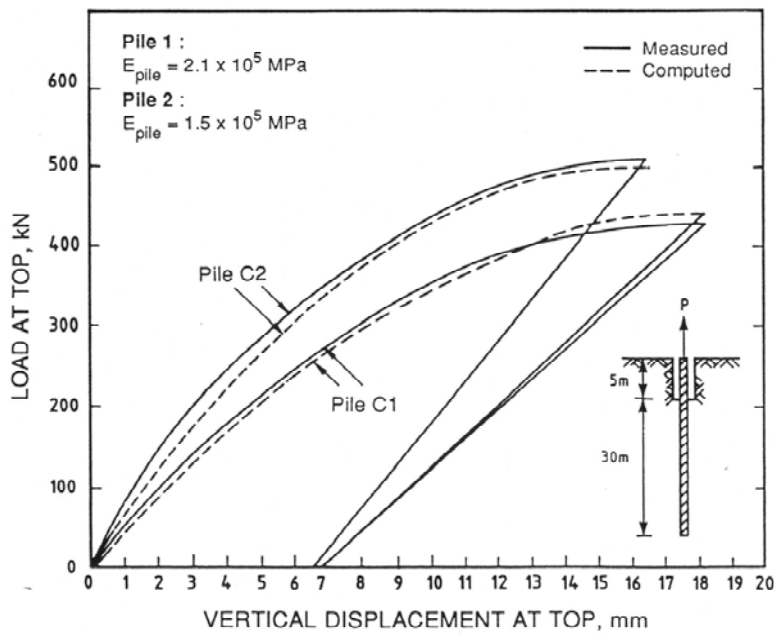
b) Piles C1 and C2,

Figure 2.4.20 – Examples of load- displacement curves from 1st static tests, Onsøy (after Karlsrud, et al, 1992)

Figure 2.4.20a) presents examples of load displacement curves for the 1st static test on piles A1 and A3. Note that the displacements here refer to what was measured at ground level. The elastic displacements along the cased portions have not been deducted. This is a main reason for the apparently larger displacement of pile A3 compared to A1. Figure 2.4.20b) compares the load-displacement curves for piles C1 and C2. The explanation for the apparent much larger displacements for the instrumented pile C1 compared to the non-instrumented pile C2 is believed to be that the threaded joints at each end of the six instrument units along pile C1 introduced extra flexibility.

Table 2.4.2 presents the defined ultimate failure loads for all the initial static pile tests. Failure was in general defined, as for the Haga tests, as when the creep rate at the pile top exceeded about 1 mm/min as was done for the Haga tests, ref. Section 2.2.3 and figures 2.2.32 and 2.2.33 . The figure at the right hand side of Figure 2.4.20a) shows the actual creep rates for the two tests A1 and A3 and the interpreted failiure loads. In relation to pile A2 it should be noted that this pile was unintentionally loaded very fast when the load was increased from about 80 kN until failure occurred (at 164 kN). This increase took place within 12 seconds, which gives a loading rate of 420 kN/min, about 140 times faster than the average loading rate for the other piles (about 3 kN/min). Assuming a rate of loading effect corresponding to what was observed for the Haga piles (Karlsrud and Haugen, 1984), means that the ultimate capacity of pile A2 should be scaled down by 21.5 %. This correction has been introduced in the following comparisons of ultimate shaft friction values.

Table 2.4.3 presents the static capacities reached in the 2nd series of load tests carried out after some period of rest after the 1st test series. Note in this connection that after the initial static test in the 1st test series, the piles were immediately subjected to various cyclic and static testing (ref. Table 2.4.1). For all piles, the second tests gave from 4 to 19 % larger capacity than the initial tests. This is also illustrated by Figure 2.4.21. It may be recalled that the DSS tests on IC and RR clay samples showed similar but larger (typically 25-35 %) gain from one test to a next with consolidation in between.

Table 2.4.2 - Measured ultimate static capacity (extrapolated to U =100%), 1st test series, Onsøy

Pile	Time after installation (days)	Total measured ultimate capacity Q_{ut} (kN)	Correction for weight of pile+estimated tip resistance (kN)	Ultimate shaft capacity Q_{us} (kN)
A1	26	98	5	91
A2	27	164[1] (136)	8	156[1] (128)
A3	55	235	10	225
A4	34	262	12	250
B1 (open-ended)	80	455	30	425
C1	37	440	11	429
C2	51	535	11	524

1)   Pile A2 was unintentionally loaded to failure in 12 seconds when the load was increased beyond 80 kN. Loads corrected for an estimated rate effect are shown in parenthesis.

Table 2.4.3 – Static capacity from 2nd test series, Onsøy

Pile	Time after installation (days)	Time after 1st test series (days)	Total measured ultimate capacity Q_{ut2} (kN)	Correction for weight of pile+estimated tip resistance (kN)	Ultimate shaft capacity Q_{us2} (kN)	Change relative 1st test Q_{us2}/Q_{us1}
A1	35	9	112	5	107	1.15
A2	34	7	140	7	133	1,04
A3	70	15	245	10	235	1,04
A4	34	-	-	-	-	-
B1 (open-ended)	97	17	480	30	450	1,07
C1	88	51	520	11	509	1,19

Pile A1 was loaded very rapidly to failure in 5 seconds 10 minutes after the 1st and 2nd initial static tests were carried out. This gave a capacity of 150 kN, which is 34% larger than the previous standard test where time to failure was reached in about 1 hour. This apparent rate effect is also quite similar to what was observed for the Haga piles (Karlsrud and Haugen, 1985[a]).
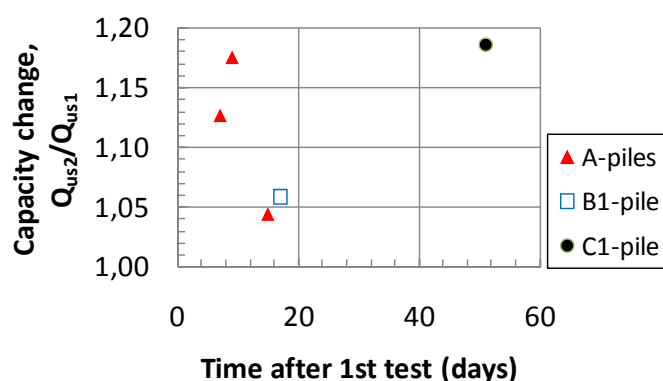
Figure 2.4.21 - Gain in static capacity from 1st to 2nd test series, Onsøy

Figure 2.4.22 shows the local shaft friction values derived between the different instrument units for each pile. In this connection the following should be noted:

- The load measured at ground level was assumed to act at the top of the test piles (i.e. no friction through the casing.
- The weight of the pile below a given instrument level was deducted from the total load measured.
- For the A-piles it was assumed a load at the pile tip corresponding to full mobilization of theoretical tip resistance. This was based on eq. (2.3.3). In reality this theoretical net tip resistance is very small, only about 1.5 % of the total load at failure.
- For pile B1, where the plug was removed prior to testing, the net tip resistance was taken as zero.

- For pile C1, there was a load cell mounted at the very tip of the pile. At failure the measured net tip resistance was 15 kN acting downward as a tensile force on the pile. For comparison, the theoretical net tip resistance at this level is 4 kN acting upwards. To give a theoretical net tip resistance of 15 kN as measured, the undrained shear strength must be taken as 123 kPa, which is considered unrealistic compared to the actual $s_{ud} = 54$ KPa at this level. This suggests that the measured tip load is not quite correct. For this reason the theoretical tip resistance (eq. 2.3.3) was used as basis for calculating the shaft load and shaft friction also for piles C1 and C2.

The very high apparent shaft friction near the bottom of pile B1 may be due to the local disturbance caused by the plug removal. The relatively large shaft friction at the top of Pile A3 is most likely due to some friction taken in the casing (probably not quite successful emptying of the casing). The same may be the case at the upper level of Pile A4.

Figure 2.4.23 shows the average shaft friction computed for each A-segment pile and the B1 pile as compared to the C1 pile. Two sets of average shaft friction are shown for the segments, one based on the difference in measured load between instrument units L1 and L3 5 m apart, and one based on the average shaft friction along the entire segments. The latter is based on the load measured at the pile top but deducted the weight of the pile and he theoretical tip resistance. Apart from segment A3, these two sets of values match completely. The shaft friction based on the (L1-L3) loads forms the basis for the corresponding deduced α and β-values presented in Figure 2.4.24.

It is apparent that the shaft friction for the long pile C1 is lower than for the corresponding A-segment piles, and the difference is largest, up to 33 %, along the lower part of the C1- pile. If the ultimat capacity of pile C1 is calculated from the shaft friction deduced for the A-segment piles it becomes $Q_{us} = 499$ kN, which is 22 % larger than the measured value for pile C1 of $Q_{us} = 410$ kN.
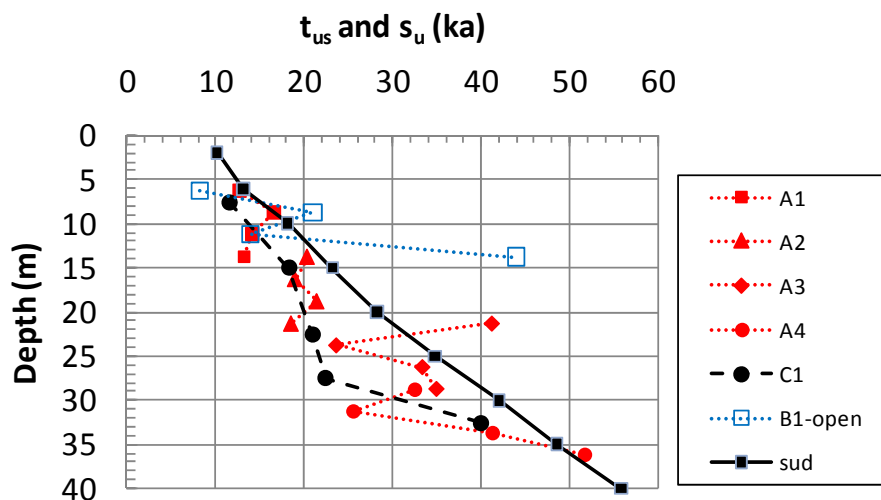
Figure 2.4.22- Ultimate shaft friction based on all instrument units, Onsøy (Shaft friction extrapolated to U=100 %)
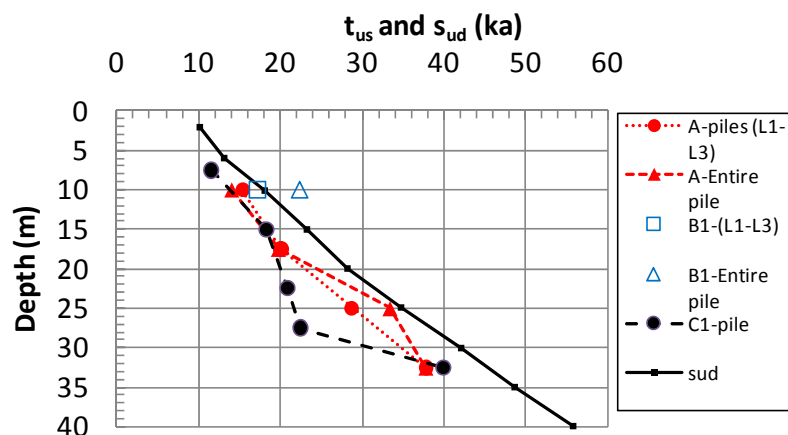
Figure 2.4.23 - Average shaft friction values for the A1 to A4 and B1 piles compared to the C1 pile, Onsøy (Shaft friction extrapolated to U= 100%)
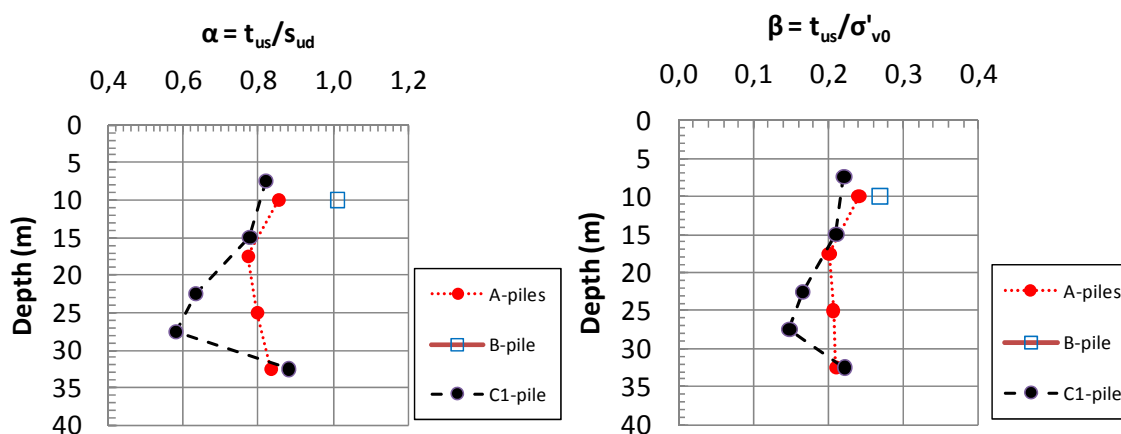
Figure 2.4.24- Measured α- and β- values for all piles, Onsøy (extrapolated to U=100%)

For the non-instrumented pile C2 the degree of consolidation is not known, but based on the A-pile results it is assumed to be U=95%, which at 100 % consolidation gives Q_{us} = 524 kN for pile C2. This is 28 % larger than what was measured for the instrumented C1-pile and closer (only 5 % larger) than what was calculated from the shaft friction for the A-segment piles. This strongly suggests that the relatively low shaft friction along the lower part of the C1-pile is anomalous. A tentative explanation could be that the threaded instrumented sections along the pile enhance the lateral flexibility of the pile and that it may be more exposed to "whipping" effects during driving, tending to "block out" the clay around the pile. This also ties in with the fact that the measured horizontal effective stresses are lower along the lower part of the C1 pile than for the A-segment piles, Figure 2.4.18. As was shown in Figure 2.4.20, the C1 pile showed 40 % larger axial displacements than the C2 pile for the same load, confirming that the threaded joints reduced the pile stiffness.

As seen from Figure 2.4.23 and 2.4.24 the load test on the open-ended pile B1 suggests a shaft capacity that is about 10 % larger than for the A1-pile.

Piles A1and B1 apparently show somewhat larger α-and β-values than the deeper piles. Neglecting Pile C1, and focusing on A2, A3 and C2, the average values are typically α ≈ 0.8 and β ≈ 0.2.

Figure 2.4.25 presents selected local normalised t-z curves as established from the test data. It appears that the A- piles generally show somewhat softer normalised response than the B1-pile. For the B1-pile the local displacement at ultimate failure of about 1 % of the pile diameter is practically identical to what was observed for the LDP-pile at West Delta.
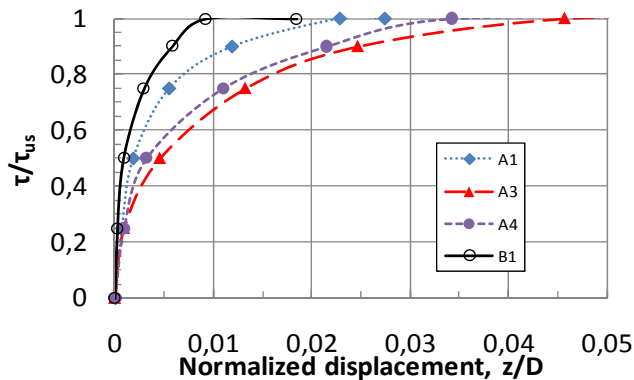
Figure 2.4.25 - Observed t-z curves, Onsøy

Figure 2.4.26 shows that there is a fairly good correlation between the horizontal effective stress at onset of pile loading and the ultimate shaft friction, as typically given by:

$$\tau_{us} = 0.44 \cdot \sigma'_{hc}$$
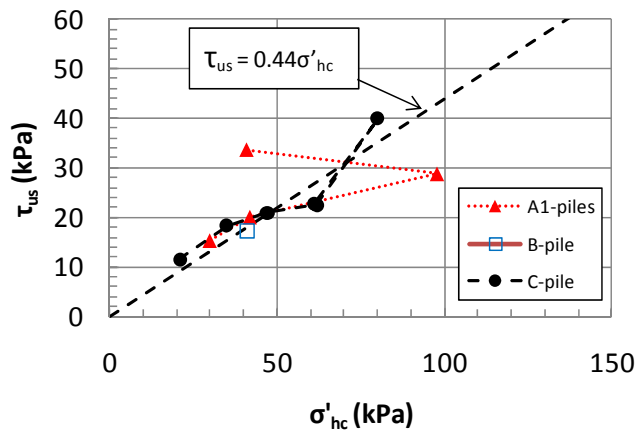
Figure 2.4.26 - Ultimate shaft friction in relation to horizontal effective stress at onset of pile loading, Onsøy

During pile loading there were no significant or systematic changes in total earth pressure (ref. NGI, 1988[a]), but the pore pressures increased somewhat, especially at the deepest levels. The net effect in terms of change in horizontal effective stress during pile loading is presented in Figure 2.4.27 and shows a general trend of increasing effective stress reduction with depth. Note that for the A2 pile, which was loaded very rapidly, the pore pressure increase and the effective stress reduction would probably have been larger if it had been loaded at the same rate as the other piles.
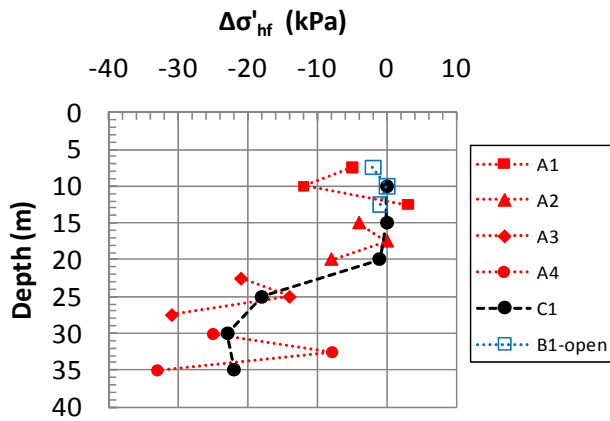
Figure 2.4.27 - Change in horizontal effective stress during pile loading, Onsøy

Figure 2.4.28 suggests a reasonably linear correlation between ultimate shaft friction and the measured horizontal effective stress at pile failure, typically given by:

$$\tau_{us} = 0.52 \cdot \sigma'_{hf}$$

The two points that deviate the most from this failure envelope are from the lowest level along the C1 pile (30-35 m depth), pile A4, and to some extent pile B1.
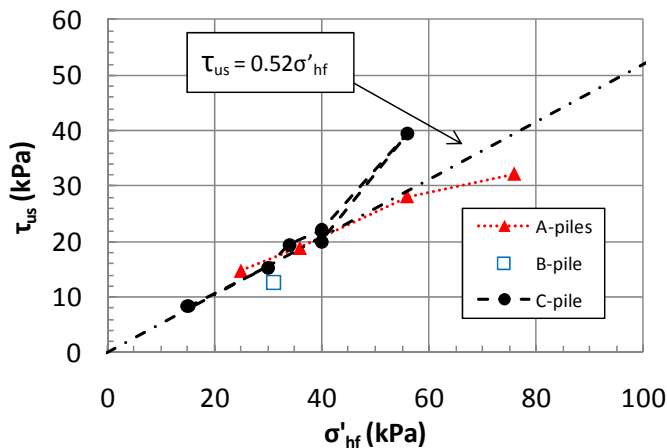
Figure 2.4.28 - Ultimate shaft friction in relation to horizontal effective stress at pile failure, Onsøy

Some important observations that can be made from the Onsøy pile tests are:

- Even in this normally consolidated high plastic clay deposit, the ultimate shaft friction is generally lower than the in-situ undrained strength.
- Comparing Pile C1 and C2 to the A-segment pile tests, and accounting for the anomalous results probably introduced by the numerous instrumentation joints in the C1 pile, there seems to be no effect of pile length or flexibility on the ultimate shaft friction and capacity. This is supported by the fact that deduced t-z curves show no tendency for strain softening effects, which is in contrast to what was indicated by the West Delta LDP tests presented in Section 2.3.
- The ultimate shaft friction for the open-ended pile B1 agrees closely with the corresponding closed-ended pile A1 (10% higher for the B1-pile).

- There is a fairly good linear correlation between ultimate shaft friction and measured effective stress against the pile surface.
- The pile capacity increases as a result of repeated load testing with time for consolidation in between, but not to the same extent as was suggested by the tests at Haga.

2.5 Lierstranda

2.5.1 General overview of test site and load tests

The Lierstranda test site lies near the shoreline of Drammensfjorden about 1.2 km east of the outlet of the Drammen river and 1.5 km west of the outlet of the Lier river. At the site there is a more than 50 m deep layer of normally consolidated clay. The ground level at the test site was raised from about Elev. +0.5 to + 3.0 in the early 1970's, or about 15 years prior to the pile testing described herein, which took place in 1987. Land reclamation had also been carried out another 300-500 m further south from the test site. The reclaimed area was essentially a tidal flat with water depths less than 3 m.

The piles tested at Lierstranda were shown in Figure 2.4.1, and included testing of 4 A-segment piles (A7, A8, A9 and A10) and one open-ended B-pile (B2). The test piles, pile tip penetration, casing levels and pile instrumentation were the same as for the Onsøy tests carried out a year earlier (Figure 2.4.1), and will therefore not be further described in this section.

The load testing program which the piles were subjected to is summarised in Table 2.5.1. It was a similar but less elaborate test program than what the Onsøy piles were subjected to.

Table 2.5.1- Load testing program, Lierstranda

Test pile	Test no.	Date installed	Type of test	Days after installation
A7	02	17.07.1987	Initial static tension	29
	03		One-way cyclic	29
	04		Static tension	29
	05	20.07.1987	Static tension	32
	06		Two-way cyclic	32
A8	02	20.07.1987	Initial static tension	32
	03		One-way cyclic	32
A9	02	03.09.1987	Initial static tension	31
	03		One-way cyclic	31
	04	08.09.1087	Static tension	36
	05		One-way cyclic	36
A10	02	04.08.1987	Initial static tension	30
	03		One-way cyclic	30
B2	02	24.09.1987	Initial static tension	51
	03		One-way cyclic	51
	04		Static tension	57
	05		One-way cyclic	57

2.5.2 Key soil parameters

A fair amount of site investigations had been carried out across the land reclamation area 300-500 m south of the test site. This included 10 boreholes with 54 mm piston sampling to up to 40 m depth, and 11 in-situ vane borings. In addition to oedometer tests and classification tests both CAUC and CAUE undrained triaxial tests were carried out on some of the retrieved samples. The results of these past investigations were summarized by NGI (1988[a]).

As part of the pile testing program, one borehole with 54 mm sampling, 2 in-situ vane borings and 2 CPT tests were undertaken. Due to the pre-existing knowledge about the general soil conditions in the area, samples were only taken from about every 7.5 m.

During the period 1988-1996 the pile test site was used for other research purposes, including testing and comparison between various in-situ testing devices (BAT-probe, dilatometer, cone, pressuremeter, triple CPTU probes), see for instance NGI (1996[a]). Comparative laboratory testing was also carried out on 54 mm, 75 mm and high quality block samples. The factual data from these laboratory tests were presented by NGI (1996[b]). These new site investigations have formed a basis for re-interpreting the in-situ soil conditions as compared to what was assumed in earlier interpretation of the pile test results at Lierstranda (e.g. NGI, 1988[a] and Karlsrud et al, 1992).

Below an upper 1.5 to 2 m thick layer of recent fill there is clay to large depth. Figure 2.5.1 shows that below the fill there is an upper layer of medium plastic clay that extends to a depth of about 12 m and has a water content of w= 40-42 % and plasticity index I_p =20-25 %. This layer is followed by a gradual transition to a rather silty low-plastic clay layer with water content decreasing from 34 % at 15 m to 27 % at 40 m. The plasticity index correspondingly decreases from 15 to 12 %. The total unit weight increases with decreasing water content from a minimum of γ_t= 17.8 kN/m^3 at 10 m to γ_t= 19.6 kN/m^3 at 40 m.
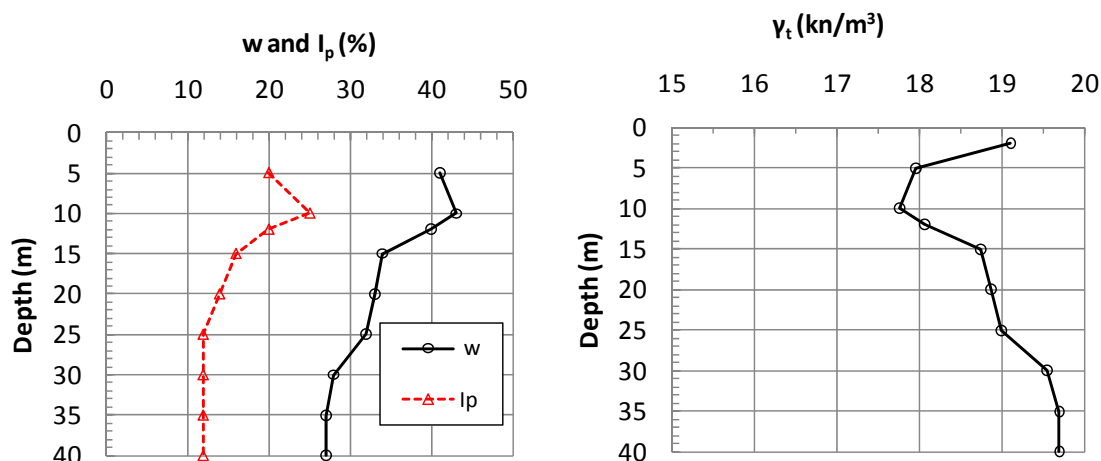
Figure 2.5.1 – Summary of index data, Lierstranda

The clay content has been determined to lie around 32-38 % in the upper plastic layer and decreasing to around 20 % at 32.5 m depth in low-plastic layer. The salt content lies around 32 g/l, close to that of natural sea water, i.e. the clay has not been leached. The organic content is low throughout. The sensitivity of the clay as defined from the in-situ vane borings is typically S_t=3.5 (range 3-6) throughout the profile, but around S_t=11 (range 7-14) according to fall cone tests.

Three piezometers were installed at depths of 8, 22 and 25.8 m. They revealed that also at this site there was an artesian pore pressure that increase essentially linearly with depth, Figure 2.5.2. The oedometer tests on 54 and 75 mm samples were in general too much influenced by sample disturbance to make it possible to determine the pre-consolidation pressure. The data in Figure 2.5.2 have therefore exclusively been established from the tests on the B1/95 block samples.
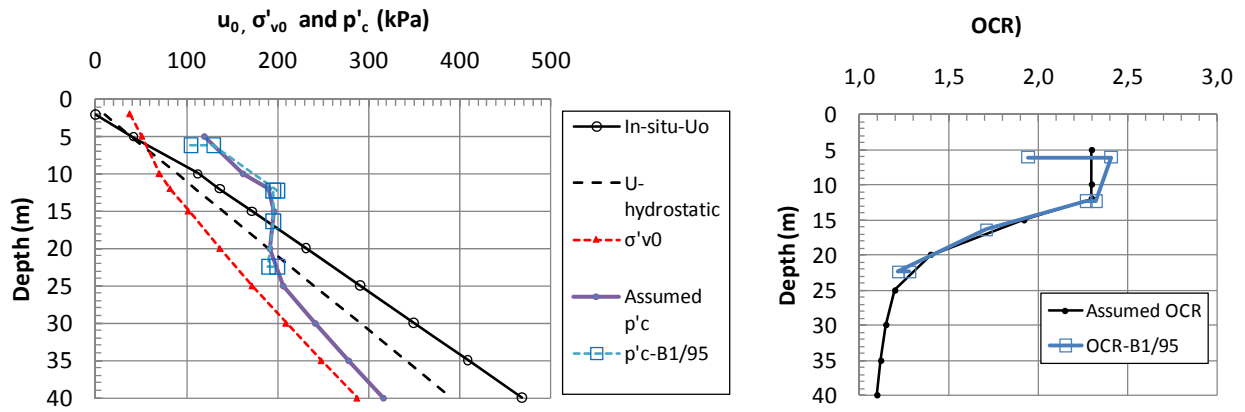
Figure 2.5.2 – In-situ stresses, pre-consolidation pressure, and OCR, Lierstranda

From a geologic point of view it may be difficult to fully explain the reason for the significantly larger values of (p_c'-σ'$_{v0}$) and OCR (up to 2.4) in the upper medium plastic clay compared to the lower low-plastic clay. It may partly be an effect of a higher effective stress level in the past than compared to the present, and partly be associated with long-term creep effects, which according to Bjerrum (1973) should lead to an OCR that increase with I_p. The assumed trend-line in Figure 2.5.2 is, however, somewhat speculative below the level of the deepest block sample (22.4 m).

Figure 2.5.3 shows, as expected, that the modulus number, m_0, as defined earlier, tends to be lower in the upper plastic clay that in the low-plastic clay. The in-situ vertical permeability, k_0, determined from the oedometer tests at zero volumetric strain, varies from about 1.5 to 3.5·10^{-9} m/s. Due to limited data, the assumed trend line is a bit speculative below 20 m depth.
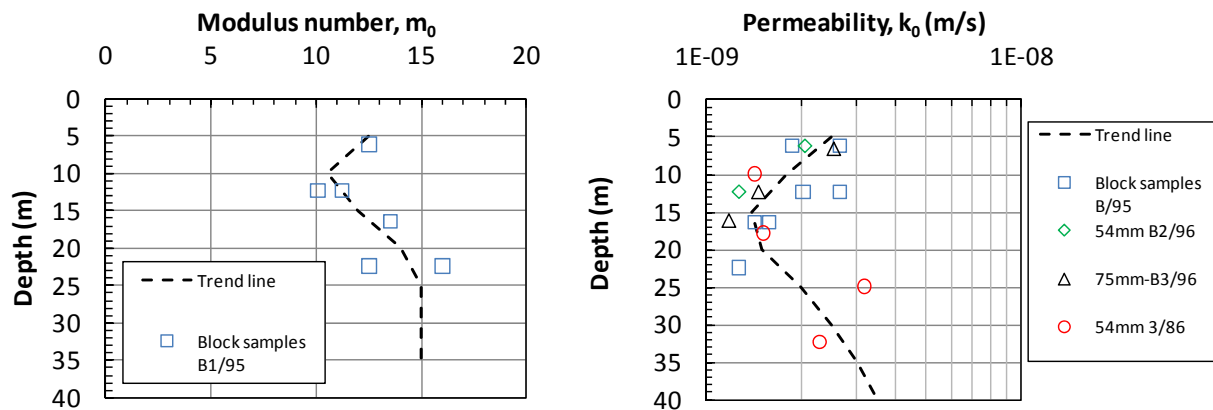
Figure 2.5.3 - Modulus number and in-situ vertical permeability, Lierstranda

Figure 2.5.4 compares undrained shear strength values, s_{uc}, determined from the CAUC tests on the high quality block samples with values derived from the CPTU tests using the $N_{\Delta u}$ correlation proposed by Karlsrud et al (2005). Strengths from the two in-situ vane borings are also shown for comparison. The block samples and the CPTU data agree closely, and form the basis for the proposed s_{uc} trend line. One CAUE test was carried out on the block sample from 6.1 m depth, which showed a ratio of s_{ue}/s_{uc} =0.40. On that basis, and the general anisotropy correlation presented in Figure 2.4.9, it is throughout the profile assumed s_{ue}/s_{uc}=0.40 and s_{ud}/s_{uc}= 0.70.
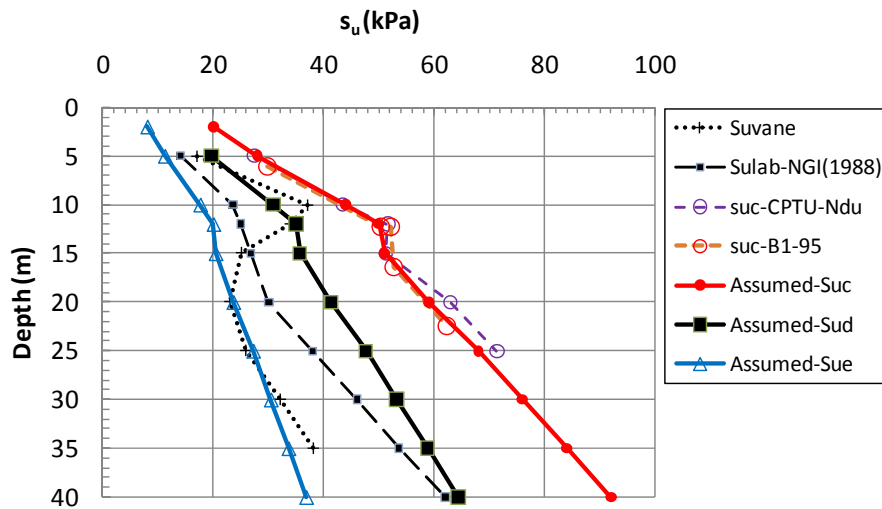
Figure 2.5.4 - Undrained shear strength profiles, Lierstranda

In relation to Figure 2.5.4 it may be noted that the s_{ud} strengths assumed herein are up to 40 % higher than the s_{ulab} profile used in past interpretations of the Lierstranda pile results by NGI (1988[b]) and Karlsrud et al (1992[a]). The relatively low in-situ vane shear strength values in the low plastic clay layer, as compared to the assumed the s_{ud} strength profile, may be noticed. The vane strength is actually close to the s_{ue} strength profile in this zone. Such relatively low in-situ vane strengths have in the authors experience often been observed in low plastic Norwegian clays, and even to a larger extent if the clay also is highly sensitive or quick. For that reason, back-analyses of failures using vane strengths gives also often far too low safety factors in such cases, e.g. Aas et al (1986).

The undrained strength of clays is closely related to the overconsolidation ratio, OCR. Ladd and Foott (1974) suggested a relationship, based on what was called the SHANSEP procedure, as follows:

$$s_u / \sigma_{v0}' = S \cdot OCR^m \qquad \text{where,} \qquad (2.5.1)$$

$S = s_u / \sigma_{v0}'$ for OCR=1.0 is the normalised strength for a sample consolidated well beyond the pre-consoldation pressure, p'_c

m= power

The value of S for OCR =1.0 would correspond to a young truly normally consolidated clay which has not had the opportunity to develop any apparent pre-consolidation pressures due to secondary (creep) consolidation ,e.g. Bjerrum (1973).

Based on samples that were artificially consolidated in the laboratory, Ladd and Foott (1974) suggested typical values of S=0.28 and m=0.85 for triaxial compression.

Figure 2.5.6 shows normalised strength derived from triaxial tests on very high quality block samples taken from Karlsrud et al (2005). From Figure 2.5.6 it is apparent that natural clays do not show such a unique relationship between undrained strength and OCR as has been indicated by testing clays that have been artificially pre-consolidated in the laboratory (e.g. Ladd and Foott, 1974). The reason may be that soil structure and possible local chemical bonding or cementation effects play a role in-situ, which is lost when a sample is artificially pre-

consolidated in the laboratory. The normalised values of s_{uc}/σ'_{v0} shown in Figure 2.5.5, combined with the assumed OCR profile in Figure 2.5.2, would fall right in the middle of the trend curves in Figure 2.5.6.
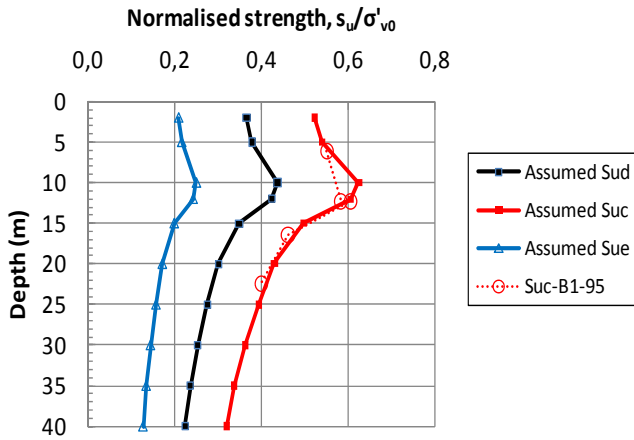
Figure 2.5.5 - Assumed normalised undrained strength values, Lierstranda
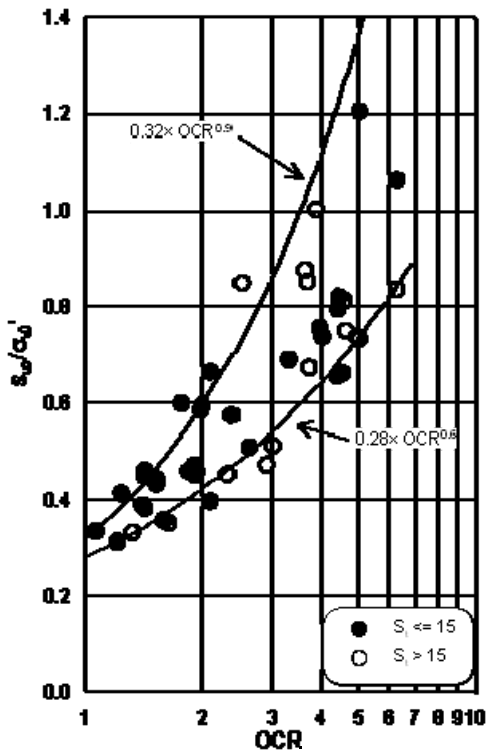
Figure 2.5.6 - Normalised CAUC strength values, s_{uc}/σ_{v0}', from tests on high quality block samples in relation to OCR (from Karlsrud et al, 2005)

At large strains the CAUC triaxial tests define an effective friction angle of $\varphi'=34$ to 36^0 when the effective cohesion or attraction is set to zero. The normalised undrained modulus from the block samples lie in the range $G_{50}/s_{uc} = 60$ to 170.

Both oedometer tests and DSS tests were carried out on remoulded and re-consolidated (RR) clay. For the Lierstranda RR tests, a special consolidation box of size 200x200 mm was used to first consolidate the remoulded clay up to a stress level of about 40 kPa. Test specimens were then cut out from this box to fit into the oedometer and DSS apparatus. Only two oedometer tests were carried out on RR clay. Figure 2.5.7 shows a comparison of the RR tests to two oedometer

tests on high quality block samples (hole B1) as well as the volume change inferred from the end of the consolidation for the DSS tests. It should be noted that the in the factual data report presenting the laboratory tests on RR clay (NGI,1987[a]), the initial water content was erroneously taken as the water content when the samples were built into the DSS test apparatus after they has first been consolidated to 40 kPa in the box, and not the actual in-situ water content. This error has been corrected for as part of this study by assuming that the respective samples had an in-situ water content and corresponding voids ratio according to Figure 2.5.2. The volume changes presented for RR clay in Figure 2.5.7 are therefore correctly given relative to the in-situ water content and void ratio. At the in-situ stress level, the RR clay shows a volume change that is 10-15 % larger than the intact clay specimens, who is quite significant and on the high side of what was observed for the Haga and Onsøy clays.
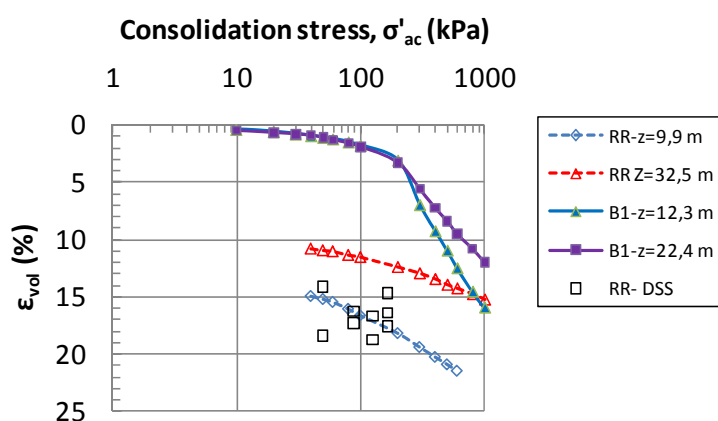
Figure 2.5.7- Comparison of volume change during consolidation of RR and Intact clay, Lierstranda

The DSS tests on RR clay showed for some specimens a tendency for dilation at large strain without reaching a clear peak. This dilation was most pronounced for the most low-plastic silty clay samples. For this reason Figure 2.5.8 shows two sets of normalised strength values:

- "Failure" when that was defined by a clear peak, otherwise taken as the shear stress at a shear strain of 6 %, at which level the effective stress paths typically started to bend up along the effective stress failure envelope.
- "Maximum" as defined by the shear stress at the end of the test (up to 18 % strain).

The DSS samples were consolidated to stresses ranging from about 50 to 165 kPa, but the normalised strength values could not be seen to depend on that.
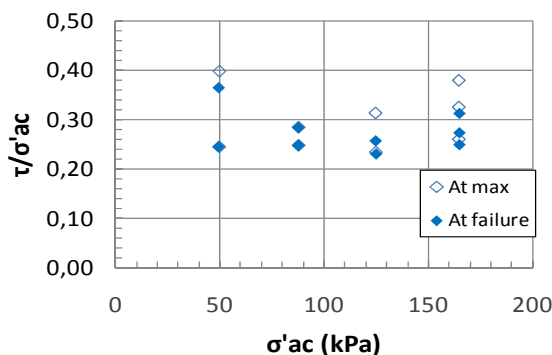
Figure 2.5.8 - Normalised strength from DSS tests on RR clay, Lierstranda

Following an initial static test to failure, the DSS specimens were subjected to various types of cyclic loading. After a reconsolidation period of one day, a new static test was carried out. As shown in Figure 2.5.9 both the Intact and RR clay samples tested showed a pronounced increase in DSS strength as a result of this pre-shearing and re-consolidation sequence. The effect seems to increase with depth or stress level applied.
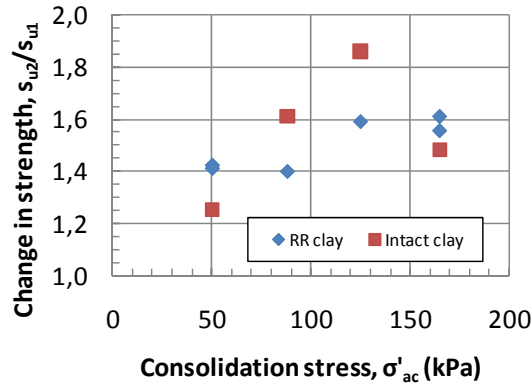
Figure 2.5.9 - Change in DSS strength between 1ˢᵗ and 2ⁿᵈ static loading to failure, Lierstranda (cyclic loading and 1 day re-consolidation between static tests)

2.5.3 Load test results

At Lierstranda the earth and pore pressures were monitored during penetration. Figure 2.5.10 shows the maximum normalised excess pore pressures generated during pile installation. The A segment tests gave quite similar values of $\Delta u/s_u \approx 6$, but $\Delta u/\sigma'_{v0}$ shows a decreasing tendency with depth. The open ended B2 pile generated pore pressures that were about 2/3 of the closed ended A7 segment pile. This is quite in line with the Onsøy tests.
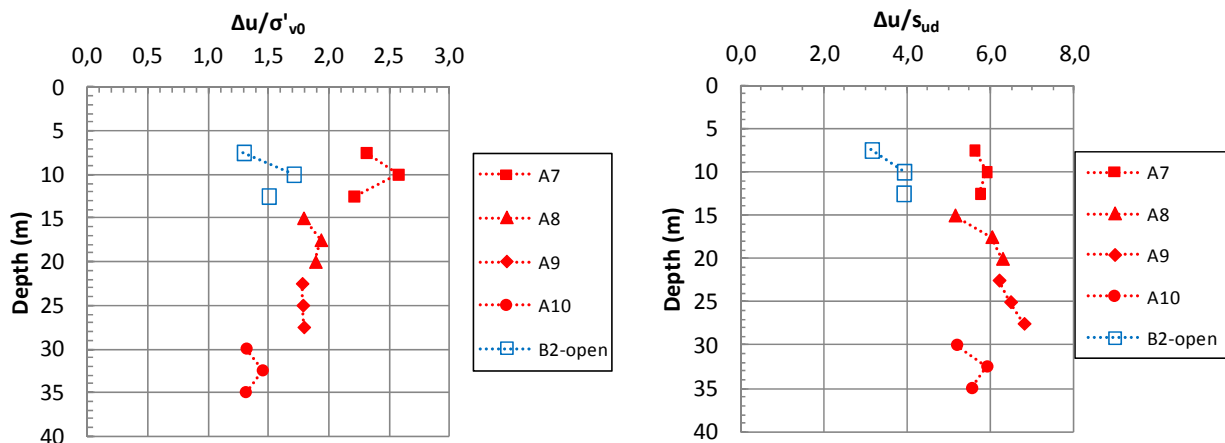
Figure 2.5.10 - Normalised excess pore pressures generated during pile installation, Lierstranda

Figure 2.5.11 shows that for the A-segment piles the effective stress measured against the pile surface at the end of pile installation was negative below 15 m depth. As at Onsøy, this suggests that the measured total earth pressures are too low. A correction factor was therefore introduced to the measured total earth pressures using the same procedure as described for the Onsøy tests in Section 2.4. 3

σ'hi (kPa)
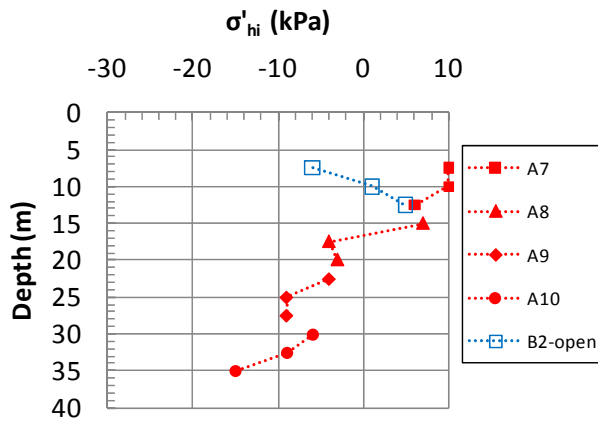
Figure 2.5.11- Measured effective stress against the pile at end of pile installation, Lierstranda

Figure 2.5.12 presents a typical example of earth-and pore pressures changes during the reconsolidation period for pile A8. As seen, the total horizontal stress decreased dramatically during the reconsolidation phase, and even more so than observed at Haga and Onsøy. No build up of effective stresses occurred before the degree of consolidation had passed about 50 % for both the A- segment piles and the B2 pile. This is similar to what was observed at the West Delta site, but rather different from the Onsøy site where effective stresses started to increase already when the degree of consolidation exceeded 10 to 35 % (Figure 2.4.15).
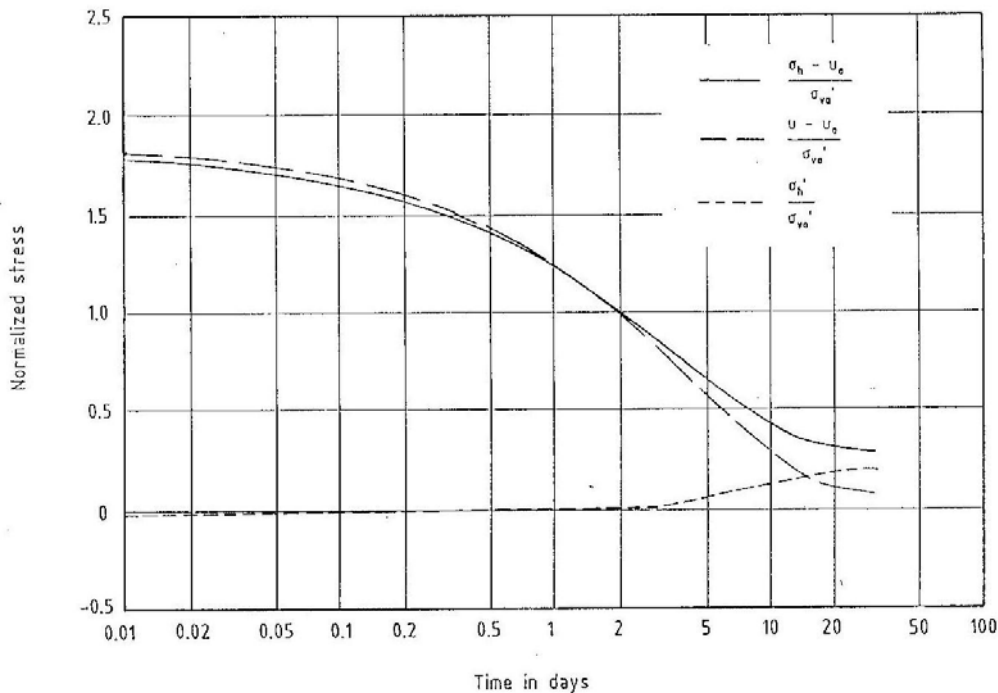
Figure 2.5.12- Example of measured earth-and pore pressures during re-consolidation, pile A8, Lierstranda

Figure 2.5.13 presents the observed times to reach 50 and 90 % pore pressure dissipation. For the A-segment piles the consolidation times decrease considerably with depth, which is probably partly related to the lower plasticity index and higher permeability in the lower half of the deposit (Figure 2.5.1 and 2.5.3). At the time of pile testing the degree of consolidation ranged from 96 to 100 %, Figure 2.5.14.
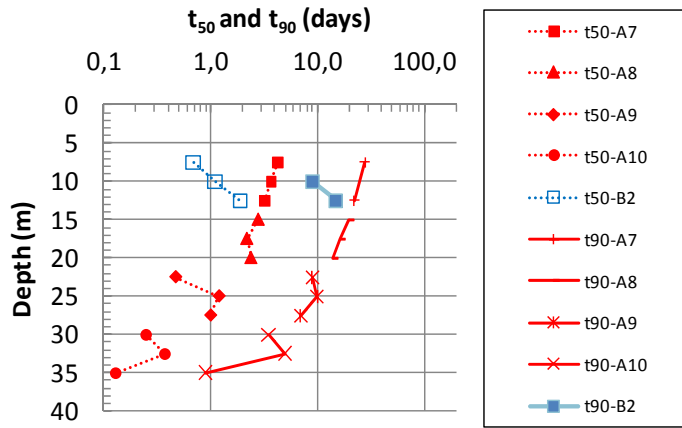
Figure 2.5.13- Observed times to reach 50 and 90 % consolidation, Lierstranda
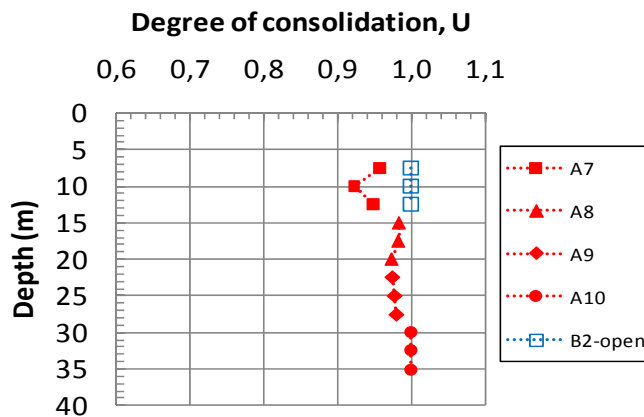
Figure 2.5.14 - Degree of consolidation at onset of pile loading, Lierstranda

Figure 2.5.15 shows that the horizontal effective stress at onset of pile loading was almost constant with depth. For the A-segment piles the corresponding horizontal effective stress ratio, K_c, shown in Figure 2.5.16 therefore decreases with depth, from around $K_c = 0.5$ in the plastic clay layer at 10 m depth to about $K_c = 0.15$ in the leanest clay at 30-35 m depth. The B2 pile showed lower effective stress than the comparable A1 pile. This is an opposite trend compared to what was observed at Onsøy (Figure 2.4.19). These effective stress ratios are at all levels significantly lower than the assumed in-situ K_0 condition, estimated based on the modified Brooker and Ireland (1965) approach discussed earlier.
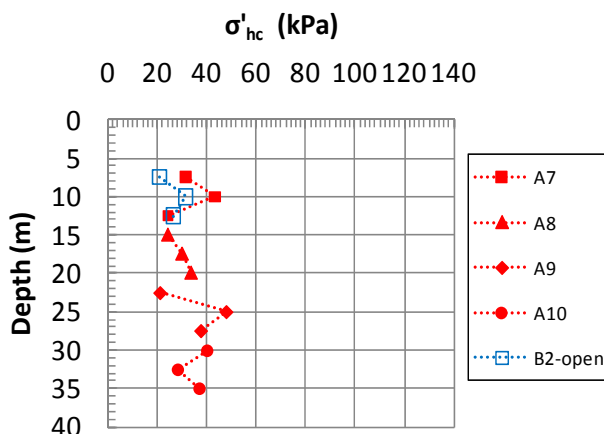
Figure 2.5.15 - Measured horizontal effective stress at U=100%, Lierstranda
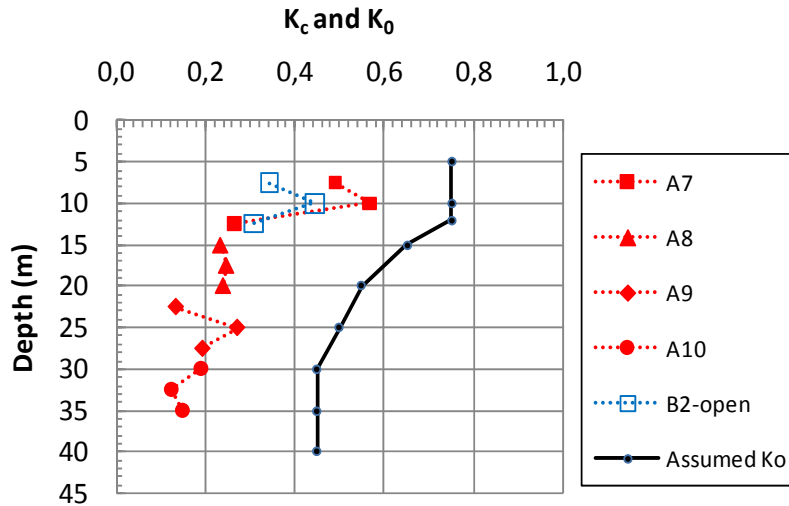
Figure 2.5.16 - Measured horizontal effective stress ratio at U=100 %, Lierstranda

The Lierstranda piles were loaded to failure by the same stepwise procedure as used for the Onsøy piles. The shape of load-displacement curves, as shown by two typical examples in Figure 2.5.17 a) and b) were also quite similar to the Onsøy piles (Figure 2.4.20). The load-displacement curves for the Lierstranda piles showed however, less well defined failure, and at relatively large displacements. The ultimate failure load was as for the Onsøy piles defined as when the rate of pile top displacement exceeded 1 mm/min. The rate hand sides of Figures 2.517 a) and b) shows the creep rates and defined failure loads. This required in some cases an extrapolation of the data beyond the level when loading was stopped. Table 2.5.2 summarise the defined total failure load and ultimate shaft capacities. As at Onsøy the shaft capacities for the closed-ended piles were deduced assuming mobilisation of full end bearing.
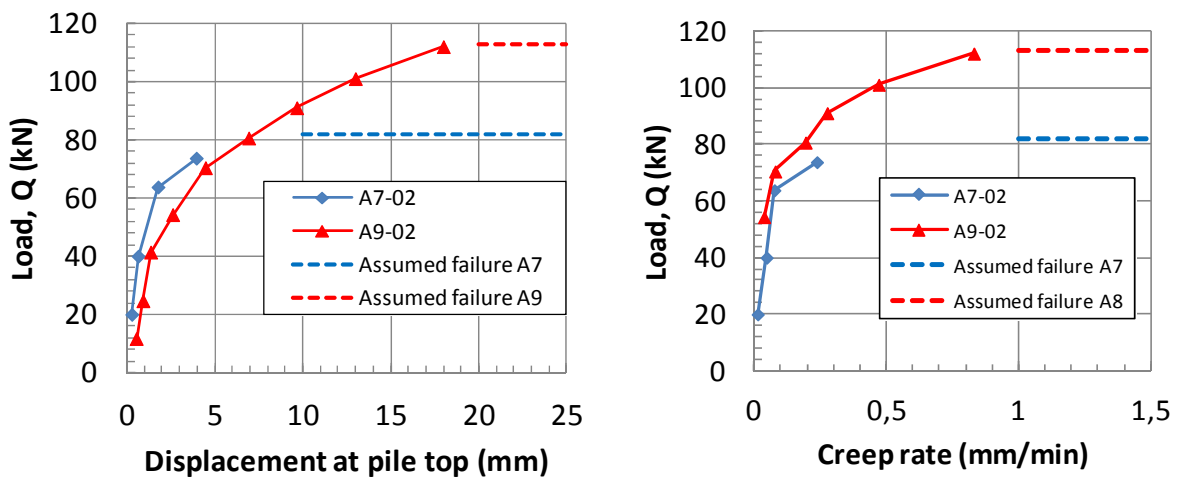
a) Piles A7 and A9
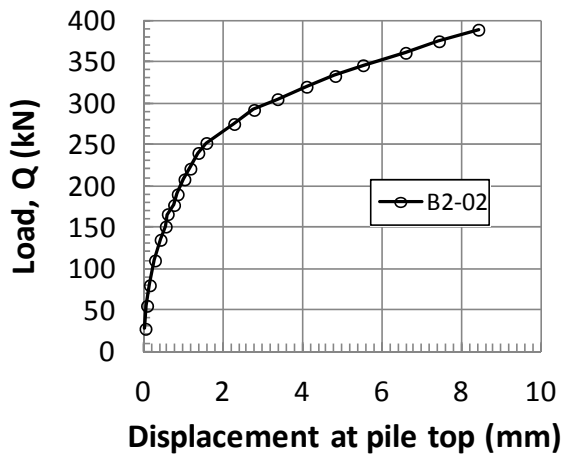
b) Pile B2

Figure 2.5.17 – Examples of load-displacement curves, Lierstranda

Due to the experiences with tendencies for bottom failure during plug removal for pile B1 at Onsøy, the plug was not removed for the B2 pile. To limit the internal shaft friction a wash boring equipment was instead used to drill out an annulus of soil along the inside face of the pile. By pushing sounding rods through this annulus it was estimated that the remaining remoulded slurry had shear strength of about 2 kPa, ref. NGI (1988[a]).

This assumed interior shaft friction of 2 kPa was deducted for the measured loads to determine the exterior ultimate shaft capacities presented in Table 2.5.2.

Table 2.5.2- Measured ultimate static capacity (extrapolated to U =100%), 1ˢᵗ test series, Lierstranda

Pile	Time after installation (days)	Total measured ultimate capacity Q_{ut} (kN)	Correction for weight of pile+estimated tip resistance (kN)	Ultimate shaft capacity Q_{us} (kN)
A7	26	82	7	75
A8	27	88	10	78
A9	55	113	13	100
A10	34	95	16	79
B2 (open-ended)	80	400	110	290

Piles A7, A9 and B2 were subjected to a second static test after the first test series and some days for re-consolidation (Table 2.5.1). Figure 2.5.17 shows 15 to 38 % gain in capacity due to this pre-loading or "pre-shearing" history. That is less than the strength increase of 25 to 85 % observed due to "pre-shearing" in the DSS tests (Figure 2.5.9).
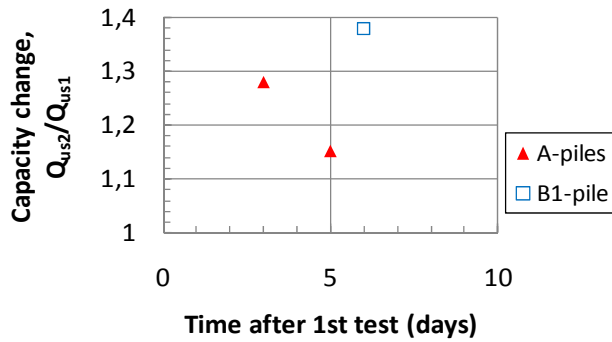
Figure 2.5.17- Gain in capacity I from 1st to 2nd tests, Lierstranda

Figure 2.5.18 presents the distribution of shaft friction determined for all the Lierstranda piles. The shaft friction was computed in the same manner as previously described for the Onsøy piles.
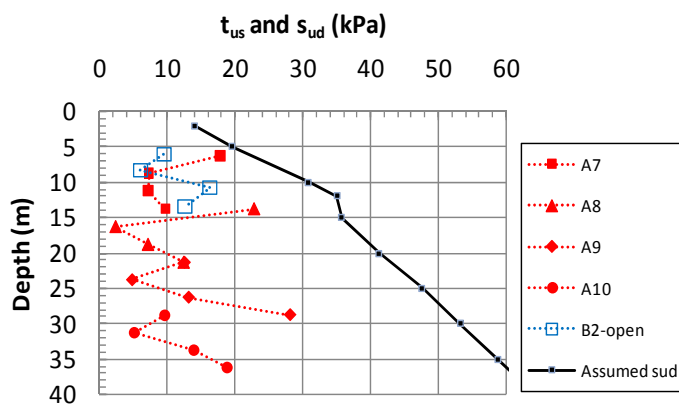
Figure 2.5.18 - Ultimate shaft friction based on all instrument units, Lierstranda (Shaft friction extrapolated to U=100 %)

Figure 2.5.19 shows the average shaft friction computed for each A-segment pile and the B1 pile. For pile A7 to A9 the average shaft friction is considerably lower when computed from the load cells L1 and L3, that are 5 m apart, than when it is computed for the entire 10 m pile length. The latter was calculated based on an assumed tip resistance, and no friction through the casing. In Appendix 2 and Chapter 6 the average of these two sets of shaft friction distributions has been used as basis.
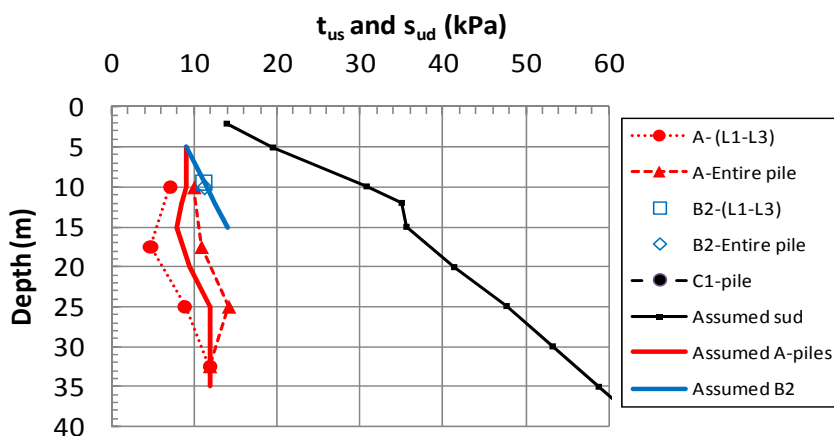
Figure 2.5.19 - Average shaft friction values for the A7-A10 and B2 piles, Lierstranda (Shaft friction extrapolated to U= 100%)

The shaft friction values can in general be characterised as extremely low, which is further emphasised by Figure 2.5.20 showing α-values as low as 0.22 and β-values down to about 0.05.
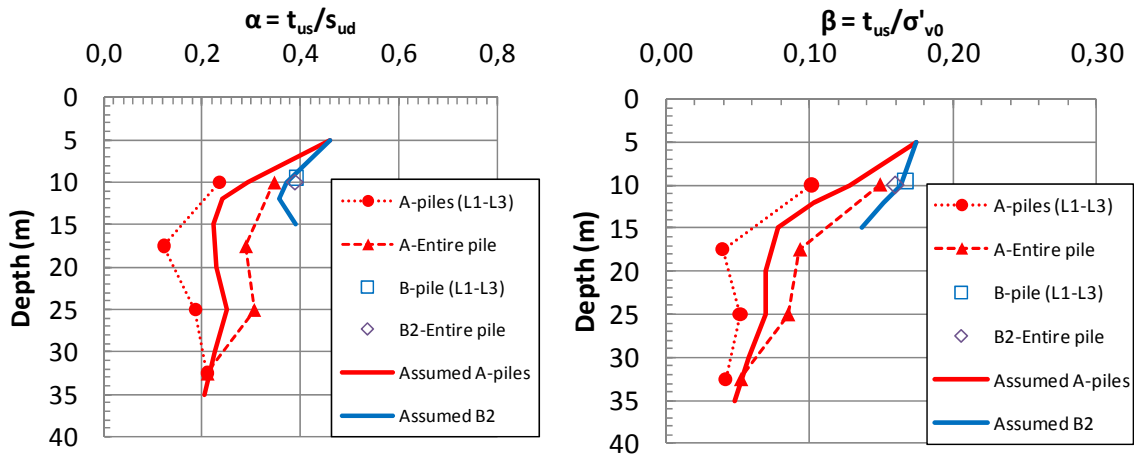
Figure 2.5.20 - Measured α- and β- values all piles, Lierstranda (extrapolated to U=100%)

That such low shaft friction is not uncommon in low-plastic silty Norwegian clays will be demonstrated by some recent non-instrumented pile tests presented in Chapter 3.

Figure 2.5.21 shows that the ultimate (peak) shaft friction is mobilised at a displacement corresponding to about 2 % of the pile diameter. The open-ended pile B2 shows somewhat stiffer response than the A-segment piles.

As seen from Figure 2.5.22 the average shaft friction in relation to the horizontal effective stress at onset of pile loading typically corresponds to: $\tau_{us} = 0.40 \cdot \sigma'_{hc}$

During pile loading the total horizontal stress remained essentially constant, but pore pressure increased, leading to an effective stress reduction of 20 kPa for pile A7, decreasing to about 5 kPa for pile A10, Figure 2.5.23. This is of the same order that was observed for the Onsøy piles, but in that case the effective stress reduction was largest for the deepest piles. For pile B2 the sensors failed before onset of pile loading.
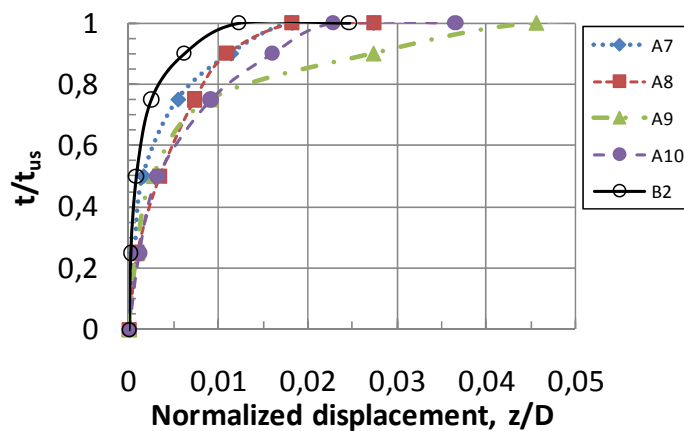
Figure 2.5.21- Observed normalised t-z curves, Lierstranda
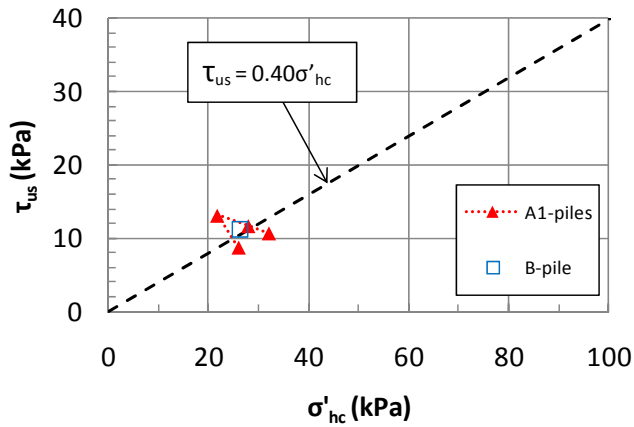
Figure 2.5.22 - Ultimate shaft friction in relation to horizontal effective stress at onset of pile loading, Lierstranda
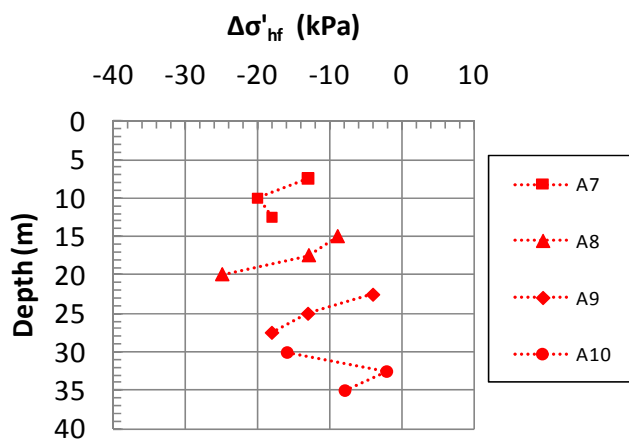
Figure 2.5.23 - Change in horizontal effective stress during pile loading, Lierstranda

Figure 2.5.24 suggests that the relationship between shaft friction and effective stress at failure is much the same as for Onsøy and given by: $\tau_{us} = 0.50 \cdot \sigma'_{hf}$
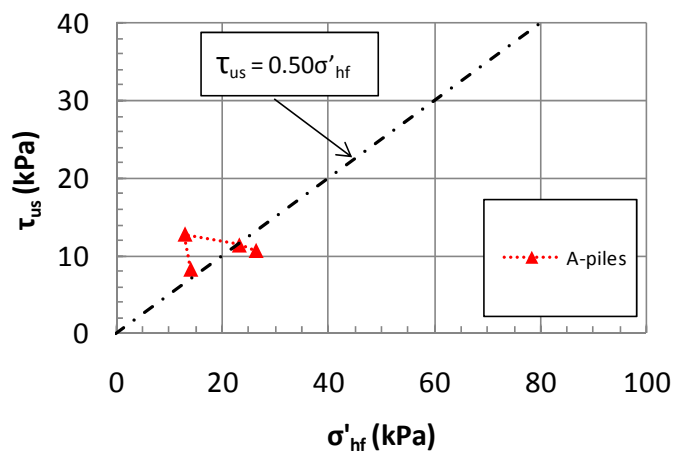
Figure 2.5.24 - Ultimate shaft friction in relation to horizontal effective stress at pile failure, Lierstranda

The following main observations can be made from the Lierstranda tests:

- First of all the ultimate shaft friction is extremely low and in particular in the low plastic clay below 15-20 m depth. This low shaft friction is clearly related to very low measured effective stresses against the pile shaft.
- The relationship between shaft friction and effective stress against the pile surface is otherwise quite similar to the Onsøy piles.
- The open-ended B2 pile showed shaft friction that is about 25% larger than for the corresponding A7 closed-ended pile.

2.6 Pentre (UK)

2.6.1 General overview of the test site and load tests

The Pentre test site lays SE of Liverpool, UK. At the site there is a more than 60 m thick deep deposit of moderately overconsolidated mostly clayey SILT, with some inclusions of silty CLAY.   The site was selected for the Large Diameter Pile (LDP) test program run in the UK and organised by British Petroleum (Mullis, 1993).

The LDP test pile had a diameter of 762 mm and wall thickness of 15 mm. A casing was first installed to a depth of 15 m and emptied by auguring. The test pile was then driven open ended to a tip penetration of 55.0 m using a hydraulic hammer. It has been reported that there was no tendency for plugging during driving. As shown in Figure 2.6.1, the test pile was heavily instrumented with strain gauges at 11 sections (4 gages at 90 degrees each section) and total earth pressure and pore pressure cells at 4 sections (2 diametrically placed cells at each level), ref. Solomon et al (1993) and Cox et al (1993). The pile was loaded in compression at a constant rate of displacement of 1 mm/min, and failure was reached in about 35 minutes. Following the static test, creep load testing and some cyclic testing was carried out.

NGI carried out two closed- ended segment pile tests A5 and A6 at the Pentre site, with piles identical to those used previously at the Lierstranda and Onsøy test sites, ref. Karlsrud et al (1992[a]). The 10 m long test sections were installed from the bottom of slurry-filled casings extending to respectively 15 m and 22.5 m, see earlier Figure 2.4.1. The pile testing program carried out on these piles are summarised in Table 2.6.1. In the static tests the loads were applied incrementally until failure was reached as previously described for the Onsøy and Lierstranda tests. Failure was reached after 1-2 hours.

Table 2.6.1- Load testing program, NGI piles Pentre

Test pile	Test no.	Date installed	Type of test	Days after installation
A5	02	31.03.87.	Initial static tension	30
	03		One-way cyclic	30
	04		Static tension	31
A6	02	30.03.1987	Initial static tension	31
	03		One-way cyclic	31
	04		Static tension	32
	05		One-way cyclic	32
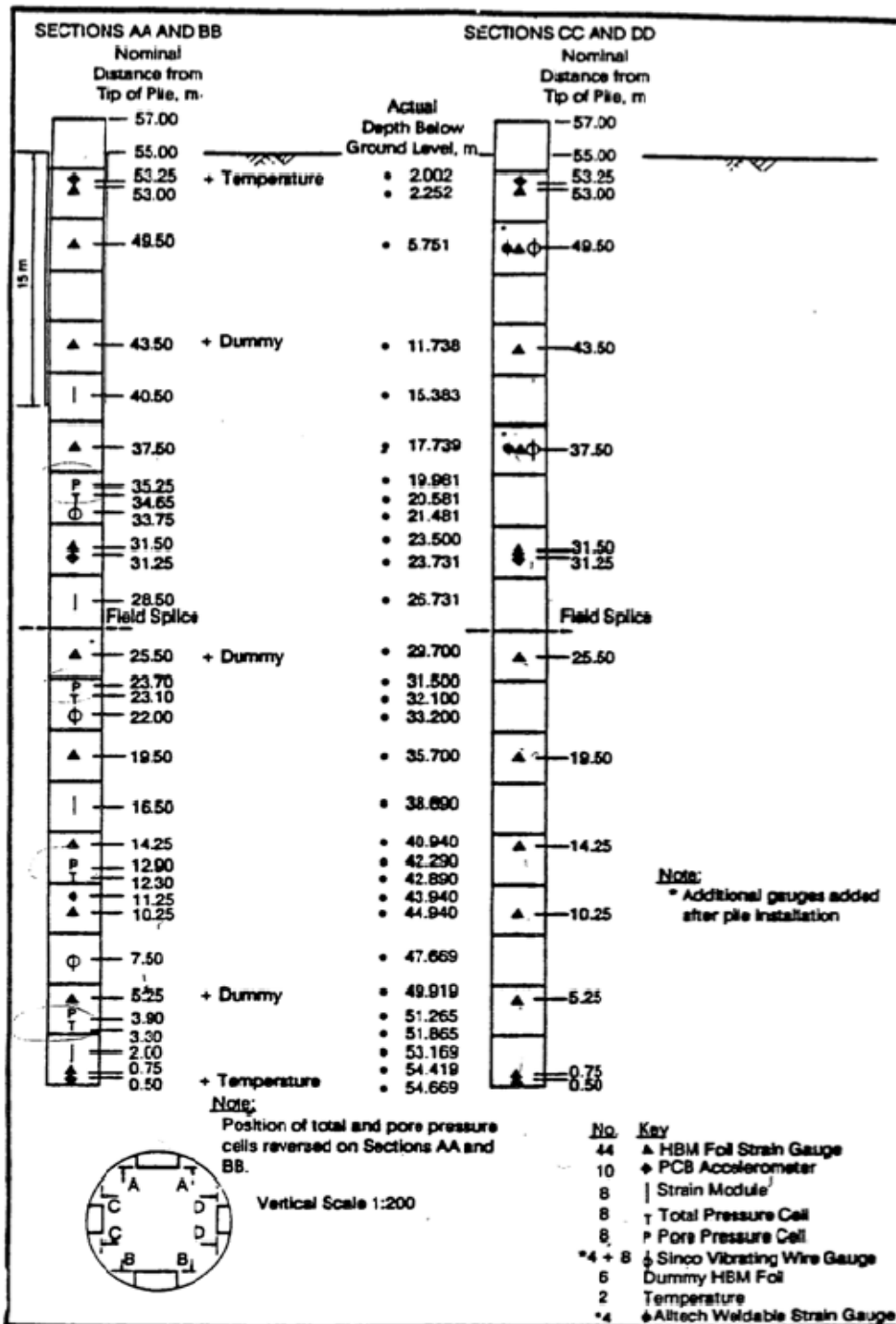
Figure 2.6.1- Layout of instrumentation of the LDP-pile, Pentre (after Cox et al 1993)

Imperial College has developed a closed ended model pile (called the ICP pile) that has been used at four different test sites, including the Pentre site, ref. Chow (1996). As shown in Figure 2.6.2 the model pile used at Pentre has a diameter of 101.6 mm and contained 4 instrumentation clusters. It can be mentioned that the first versions of the ICP pile used at the Canons Park site in London only had 3 instrumentation clusters, ref. Jardine (1985). The instrumentation systems were also completely modified and improved by Bond (1989). Each cluster contained an axial load cell, 2 pore pressure probes, a special total radial earth pressure transducer, and a temperature sensor. The following description of the test program undertaken at Pentre is taken from Chow (1996).

The ICP model pile was jacked into the ground through 4 different pre-installed casings extending to depths ranging from 7 to 10 m. Three of the piles were re-jacked to a larger depth after a first test series at a higher level. The piles were jacked down in about 7 steps, with a waiting period in between each stroke. The jacking rate was fast, typically around 0.5 m per minute, but the waiting period between each stroke varied considerably from a few minutes to more than an hour. Thus the total installation time ranged from about 4 to 6 hours.

Figure 2.6.3 shows the depth of casings and pile tip when the piles were tested. The tip penetration ranged from 14.0 to 19.0 m. The first time load testing on the piles was carried out less than a day after installation. At that time excess pore pressures set up during pile penetration were fully dissipated. The static loads were applied displacement controlled at a very slow rate of generally 0.01 mm/min (Pile 6 and 7 at 0.04 mm/min), corresponding to a time to failure of about 6-7 hours. The deliberate intension was to ensure **fully drained** conditions during pile loading. One pile was, however, subjected to a second rather rapid test at a rate of to 1.2 mm/min, giving a time to failure of about 4 minutes. One pile was loaded cyclically after the first static test, and another was reloaded after a 2.5 months resting period.
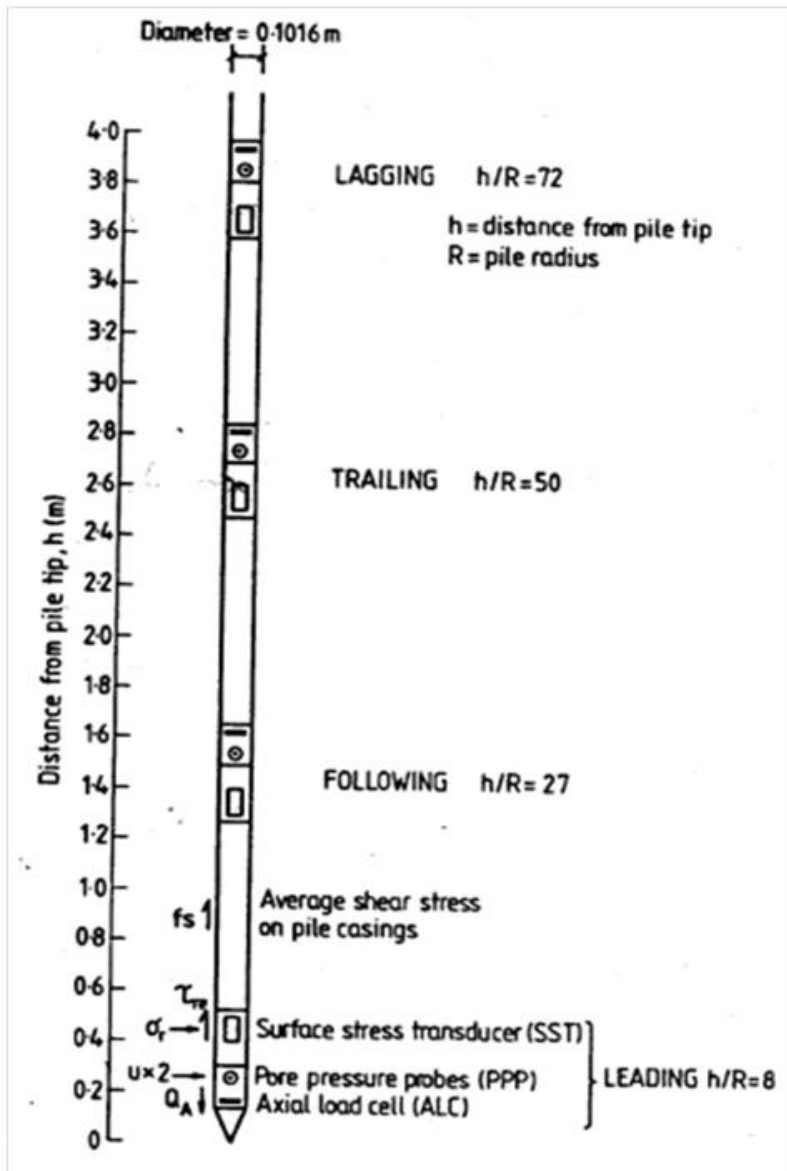
Figure 2.6.2- The ICP model pile (after Chow, 1996)
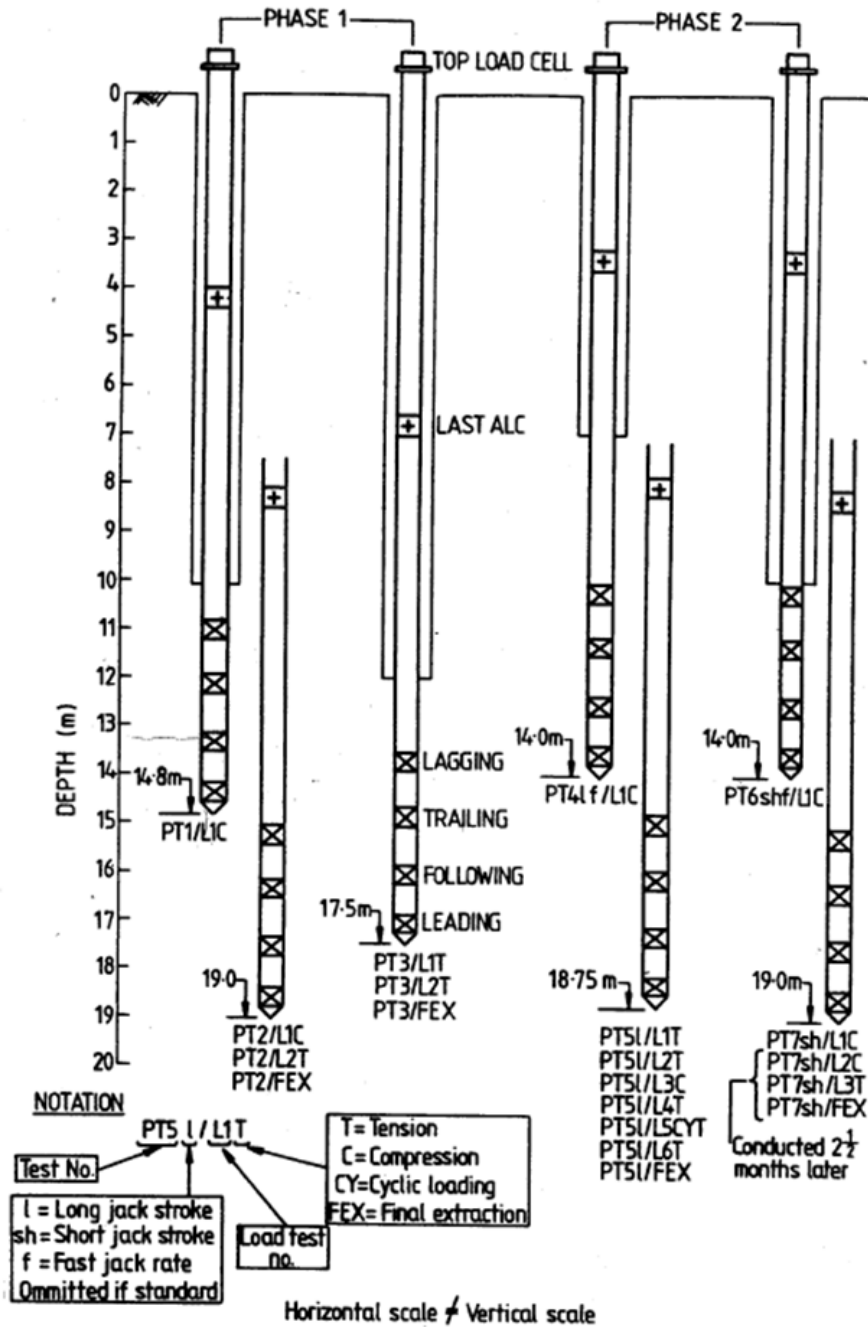
Figure 2.6.3- Schematic overview of ICP pile tests, Pentre (after Chow, 1996)

2.6.2 Key soil parameters

A very comprehensive site investigation program was carried out at the Pentre test site, both in terms of laboratory testing and in-situ testing. The test programs and results were summarised by Lambson et al (1993). NGI also undertook some laboratory testing on selected samples, (NGI, 1988[b]). A supplementary site investigation and soil testing program was later undertaken by Imperial College (IC), ref. Chow (1996).

The drilling and sampling for the LDP test program at Pentre was deliberately carried out using procedures typical of offshore site investigations. Sampling was undertaken sequentially at 1 m intervals from the bottom of the cased boreholes, mostly using a hydraulic 76 mm thin-walled

piston sampler, but some push-in samples were also taken in harder strata. The following presents soil parameters considered of most relevance to the assessment of the pile test results.

The soils at Pentre are of quaternary origin and were deposited in a glacial fresh water lake. For that reason it was found to have an oriented fabric, and not a flocculated structure as is typical for marine clay deposits.

The deposit is dominated by silt size particles. Sand size particles constitute 0-10 %, and clay size particles 0-20 %. Although Lambson et al (1993) on basis of plasticity data generally classify the soil as silty CLAY, the author would on basis of the grain size data rather classify it as clayey SILT. It is apparent that the deposit in general is strongly laminated or stratified, and has seams or layers with varying clay content. Completely disoriented "Marbel" type structures are also found, which have been contributed to slide events during deposition. Based on mineralogical studies it has been suggested (Chow, 1996) that the clay size particle fraction is underestimated in the sieving due to clay particles forming aggregates.

According to Figure 2.6.4 the natural water content shows a slight tendency to decrease with depth, from w =26-32 % in the upper 10-20 m to w = 22-28 % at 50-60 m. The exception is a layer of more silty CLAY around 42 to 47 m depth with w= 30-32 %. The total unit weight varies as expected with the water content, from typically 19.3 kN/m^3 in the upper part to 19.5 kN/m^3 in the lower part. The plasticity index typically lies in the range I_p=10-20 %, but with values up to about 30 % in the more silty CLAY layer around 42-47 m depth. The plasticity index is larger than what would be expected from the clay size fraction, which may be due to the clay aggregates being broken down during this type of testing.
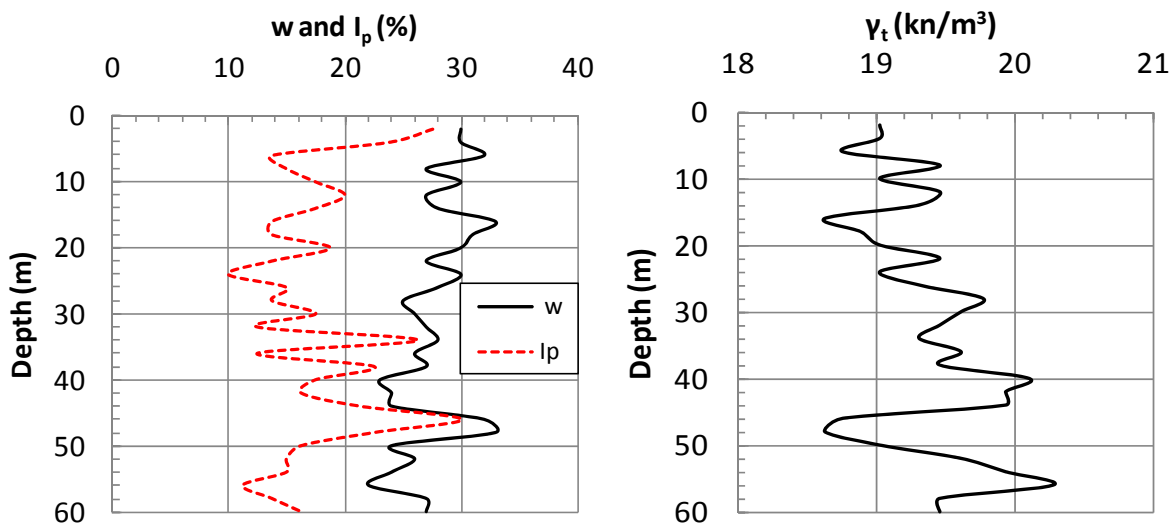
Figure 2.6.4 – Summary of index data, hole 101, Pentre

The in-situ pore pressure distribution at Pentre is reported to be slightly artesian below an upper ground water table at a depth of 1 m, Figure 2.6.5.

The data from oedometer tests, as well as undrained strength tests, suggest that these test results were significantly affected by sample disturbance, which is quite a common problem for clayey silts.

Figure 2.6.5 presents OCR values interpreted byLambson et al (1992). These OCR values were interpreted using the Casagrande (1936) method. The interpretation of OCR from what appears to be rather disturbed specimens is associated with great uncertainty. From the two oedometer tests run by NGI (NGI, 1988[a]), it was actually impossible to define any preconsolidation pressure, p'_c, from linear scale ε- σ or M-σ plots. As pointed out by Janbu (1963), if the ε- σ and M-σ curves appear as a more or less straight line, no preconsolidation pressure can be defined. But one may be misled from an ε -log(σ) plot, which even for a truly linear case will tend to curve downwards with increasing stress. Due to the difficulty in interpreting p'_c from the oedometer tests, it has been attempted to back-calculate p'_c from the assumed normalised undrained strength profile as discussed later in this section.
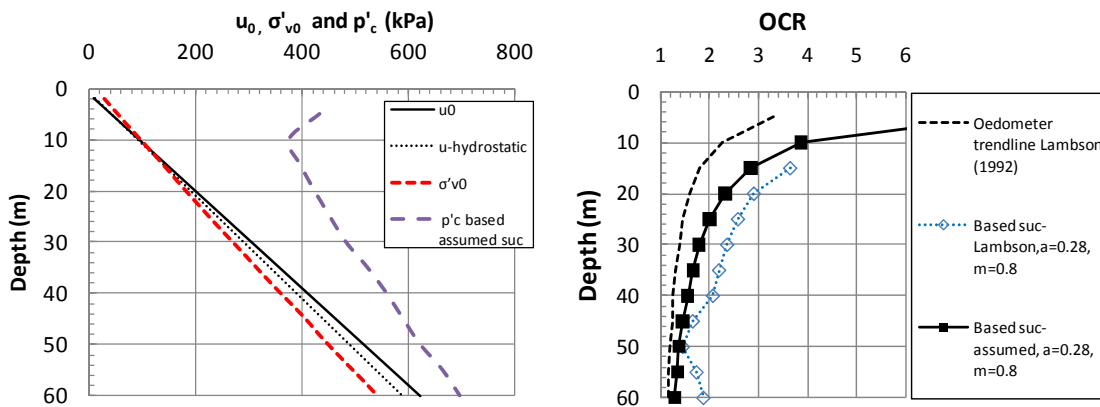
Figure 2.6.5 – In-situ stresses, Pentre

Another observation from the oedometer tests on Pentre clayey silt is that the modulus, M, do not increase linearly with stress level for stresses well above p'_c, as is typical for clays, but increase to a power less than one, which is more typical of SILTS and SANDS, e.g. Janbu (1963).

Table 2.6.2 summarises ranges of compression index values (determined at large stresses) based on the data presented by Lambson et al (1993), together with coefficients of consolidation taken at the in-situ stress level. The compression index values are considered typical of clayey SILT and silty CLAYS.

Table 2.6.2 - Summary consolidation properties and permeability, Pentre

Depth range z, (m)	Water content w(%)	Plasticity index I_p (%)	Compression index $C_c/1+e_0$	Vertical coefficient of consolidation [1] c_v (m²/yr)	Horizontal coefficient of consolidation [1] c_h (m²/yr)	Vertical permeability k_v (m/s)
5-42	22-32	10-23	0.12- 0.18 (0.22)	30-300	100-300	$4 \cdot 10^{-10}$-$1 \cdot 10^{-7}$
42-47	30-32	25-35	0.20-0.22	10-100	100-300	$4 \cdot 10^{-10}$-$1 \cdot 10^{-7}$
47-60	22-28	13-22	0.18-0.22	30-300	100-300	$4 \cdot 10^{-10}$-$1 \cdot 10^{-7}$

    1)   Taken from oedometer tests at in-situ stress level

The variation by a factor of 10 in coefficient of consolidation probably reflects the layered nature of this deposit. The layered nature becomes even more apparent when considering the results of the 19 permeability tests run in the traxial apparatus. As presented by Lambson et al (1993) and summarized in Table 2.6.2, the permeability varies by a factor of more than 100. The lowest

permeability of $4 \cdot 10^{-10}$ m/s is typical of silty CLAY, and the highest of 10^{-7} m/s is typical of sandy SILT or silty SAND. The permeability values measured by NGI (1988[a]) in the two CRS oedometer tests carried out on samples from 21.0 and 30.5 m depth, were $k_0= 0.95$ and $1.4 \cdot 10^{-7}$ m/s, and lie at the high end of the data presented in Table 2.6.2.

The re-consolidation phase following pile installation is a radial consolidation problem which will be governed by the horizontal permeability and coefficient of consolidation. It is reasonable to assume that these horizontal values lie in the upper range of the vertical values given in Table 2.6.2. Interpretation by Lambson et al (1993) of pore pressure dissipation from some t-z probe tests, self boring pressure meter tests and cone penetration tests, suggested c_h-values mostly in the range 70-5000 m^2/yr, which is generally larger than the vertical coefficient of consolidation from the oedometer tests in Table 2.6.2.

The implications of such relatively large horizontal permeability and coefficient of consolidation is that the reconsolidation around the test piles would be expected to occur very rapidly and also during pile installation. More importantly, significant drainage would be expected to take place during pile loading. These issues can have important consequences for the interpretation of the pile tests at Pentre, as will be discussed in Chapters 4 to 6.

Figure 2.6.6 shows a typical average trend line of undrained triaxial compression strength values, s_{uc}, determined from a total of 72 CIUC, CAUC and CAK_0UC type tests. This line is based on data presented by Lambson et al (1993). The data showed no systematic difference between the different types of triaxial tests. Figure 2.6.6 also shows a trend line for $s_{u(UU)}$ values from the 150 UU triaxial tests carried out. The $s_{u(UU)}$ strengths correspond typically to $(0.4$ to $0.5) \cdot s_{uc}$ in the top, and increasing to $(0.7$ to $1.0) \cdot s_{uc}$ at the bottom.
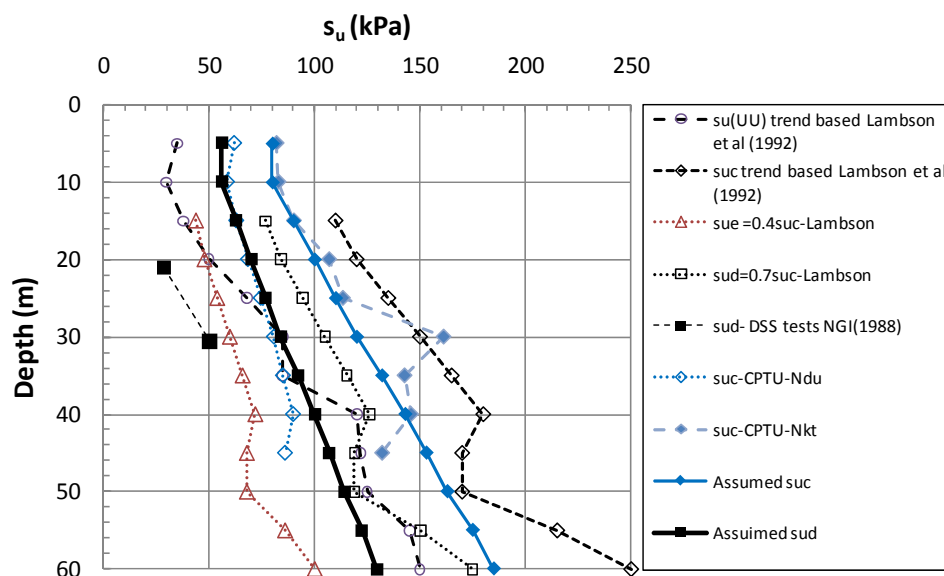
Figure 2.6.6 - Summary of undrained strength data, Pentre

Figure 2.4.9 suggests that for Pentre type silt/clay the anisotropy ratios may typically correspond to $s_{ue}/s_{uc} = 0.4$ and $s_{ud}/s_{uc} = 0.7$. These undrained strength profiles are also shown in Figure 2.6.6. Two DSS tests were actually carried out by NGI on Pentre clayey silt specimens. The undrained strength determined on these two samples is very low in comparison to what was estimated from the empirical correlation to the s_{uc} strength in Figure 2.6.6.

In-situ vane tests at Pentre gave strengths that were typically 15-20 % higher than the s_{uc} trend line. As suggested by Karlsrud et al (1992[a]), the explanation may be drainage effects during shearing caused by the high horizontal permeability. Strengths interpreted from Self Boring Pressure meter tests gave similar values as the in-situ vane tests, which Lambson et al (1992) also contributed to drainage effects. Results from both of these in-situ test types are therefore neglected.

Chow (1996) presented typical results from some piezocone penetrometer tests (CPTU) that were carried out at the site by the British Research Establishment (BRE) in 1994. Using typical average values for the reported tip resistance, q_c, and pore pressure , u, the undrained triaxial compression strength has been calculated from the CPTU-correlations proposed by Karlsrud et al (2005) (i.e. eq. 2.4.1). Figure 2.6.6 shows that the strength based on tip resistance (s_{uc}-N_{kt}) corresponds to about 80% of the values given by the triaxial test trend line, whereas the s_{uc}-N_{du} pore pressure based values are only about 50% of the trend values from the triaxial tests. That the pore pressure based values are low may well be explained by the generally high permeability of the deposit, causing some dissipation effects also during cone penetration. Dissipation during penetration would on the other hand normally lead to too high tip resistance, and strength derived from that.

The effective stress paths from the CAUC traxial tests generally show a strong tendency for dilation at large strains, (e.g. figure 23 in Lambson et al, 1992). Such dilation may partly be due to overconsolidation but could also mainly be a result of sample disturbance. That sample disturbance can lead to strong tendencies for dilation and too high strength is well established (e.g. Lunne et al, 2006 and Hight et al, 1992). The effect of dilation is generally most pronounced in low-plastic silty clays.

From Figure 2.6.6 and the discussion above it is concluded that there is significant uncertainty with respect to what is the true undrained strength characteristics of the Pentre clayey SILT deposit. Weighing the uncertainties, the author chose to use the "assumed" s_{uc} and s_{ud} values presented in Figure 2.6.6 as basis in this study.

Figure 2.6.5 presents OCR values calculated from the SHANSEP eq. (2.5.1) using both the "Lambson" s_{uc} profile and the "assumed" s_{uc} profile, and using typical average values of m=0.8 and S=0.28. They both give OCR values well above the oedometer results, which as stated earlier may be affected by sample disturbance. The "assumed" OCR and s_{uc} profiles, and the corresponding OCR values, are however, consistent through the assumed SHANSEP relationship based on eq. (2.5.1).

Lambson et al (1993) summarized friction angles from all types of test carried out on the Pentre soils, including all undrained triaxial tests, undrained or constant volume DSS tests, drained direct shear (shear box) tests (DS), and drained ring shear tests (RS). The DSS tests were carried out on both vertically and horizontally trimmed specimens. The drained DS and ring RS tests were carried out to determine both the apparent peak and residual (large displacement) soil/soil and soil/steel friction angle. The DS tests were carried out on both undisturbed and remoulded clay. The undisturbed DS specimens were oriented vertically and sheared under an axial stress corresponding to the estimated horizontal effective stress. Table 2.6.2 presents the main test results in terms of apparent mobilised effective friction angles, φ, from the triaxial tests, and

apparent mobilized interface friction angles soil/soil (δ) and soil/steel (δ_{ss}) from the DS and RS tests. Only the typical average values summarised by Lambson et al (1993) are presented in Table 2.6.3.

Table 2.6.3- Summary of apparent friction angles determined from triaxial, direct shear (DS) and ring shear (RS) tests, Pentre

Test type	Shear stress	Low plastic clay layers ($I_p<22$)		Plastic clay layers ($I_p>22$)	
		Soil/soil, φ or δ	Soil/steel, δ_{ss}	Soil/soil, φ or δ	Soil/steel, δ_{ss}
Triaxial	At peak	30	-	26	-
DSS-Vert.-Undist	At peak	29.5	-	25?	-
DSS-Hor.-Undist	At peak	25	-	21	-
DS-Undist.	At peak	28	25	25	25
DS-Undist.	Residual	23.5	19	13	15
DS-Remoulded	At peak	26.5	24	25	19
DS-Remoulded	Residual	17	18	11	14
RS-Remoulded	Residual	27	16.5	13	11

In addition to the 2 DSS tests on undisturbed clay, 8 DSS tests were carried out by NGI on remoulded and reconsolidated (RR) clay, e.g. NGI (1988[a]). Some samples were also subjected to cyclic loading after the first static test, and then allowed to consolidate before a second static test to failure was carried out. Figure 2.6.7 summarizes these results in the form of axial consolidation stress versus shear stress at failure or peak as defined earlier. In most of these tests, the specimens first contracted and built up positive pore pressures, but started to dilate and build up negative pore pressures after reaching a shear strain of 3 to 6 %. Failure has been defined when the tendency for strong dilation starts. There appears to be no systematic difference in strength between"undisturbed" and RR specimens. Undrained failure is typically given by the following:

At defined failure: $\tau_f = 0.275 \cdot \sigma'_{ac}$

At peak: $\tau_{peak} = 0.34 \cdot \sigma'_{ac}$

Five DSS specimens were after the 1st static test and some cyclic testing allowed to reconsolidate for one day and then sheared again to failure. As shown in Figure 2.6.8, a gain in both "failure" and "peak" strength was observed, and most so for the one test on undisturbed clay. The average gain in strength is about a factor of 1.35.
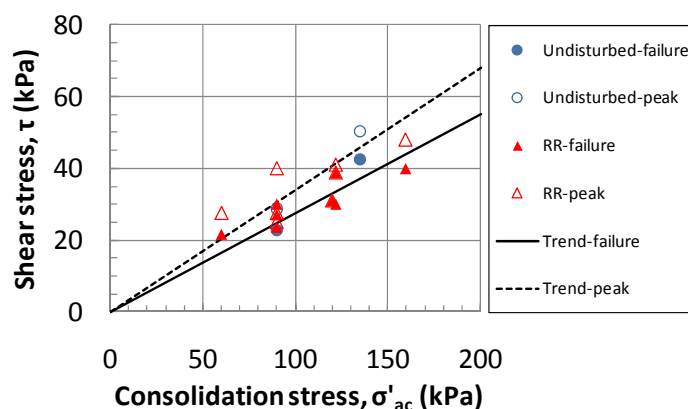
Figure 2.6.7 – Shear strength versus consolidation stress from DSS tests carried out by NGI, Pentre
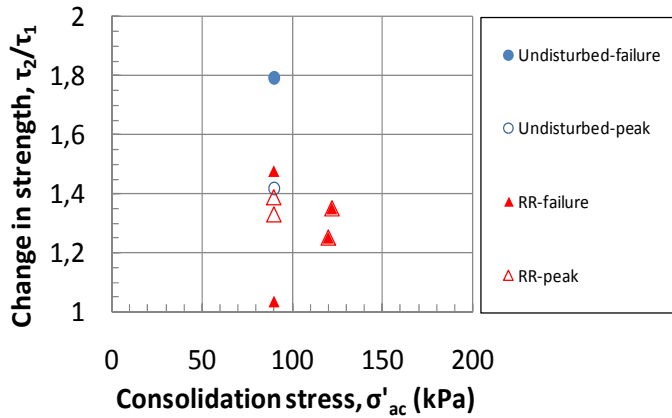
Figure 2.6.8 – Gain in strength from 1ˢᵗ to 2ⁿᵈ DSS test, Pentre

Chow (1996) reported additional RS tests carried out by Imperial College, and compared the results to the LDP tests and typical North Sea clay data as shown in Figure 2.6.9. The LDP-data for the residual friction angle in Figure 2.6.9 suggest for the low plastic layers δ= arctan(0.32) = 17.7^0. That does not match the δ =27^0 suggested by Lambson (1992) and given in Table 2.6.3.
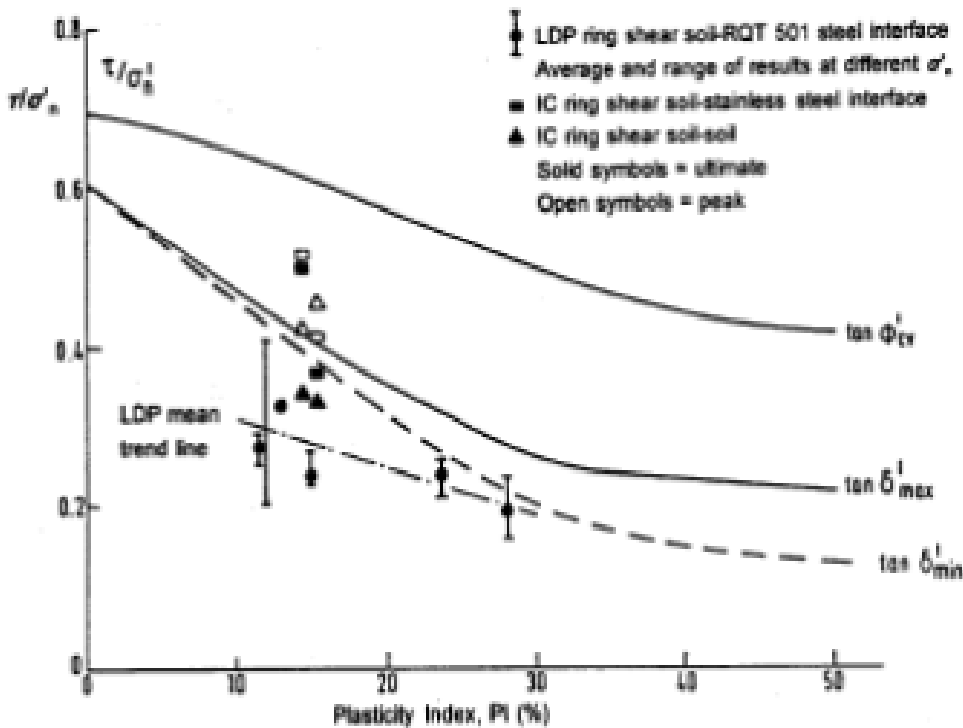
Figure 2.6.9 – Summary of friction mobilised in ring shear tests, Pentre (from Chow, 1996)

2.6.3 Load test results

During installation of all test piles at Pentre it was apparent that the stresses set up during pile installation were affected by dissipation of pore pressures generated during the installation process. This was most clearly seen in the IC pile tests, in which complete pore pressure dissipation in general occurred between each jacking stroke. Figure 2.6.10 (taken from Chow, 1996) shows as an example installation pressures for the "following" instruments along test pile PT4lf.

The variation in recorded total earth and pore pressures during pile penetration in Figure 2.6.10 confirms the laminated nature of the Pentre silts. Whatever excess pore pressures that were

generated during a stroke in most cases went back to about in-situ level before the start of the next stroke. The exception was for this pile the pressures recorded during penetration from 11 to 12.6 m where pore pressures at the end of penetration were larger than the in-situ level.

Figure 2.6.11 summarises measured normalised excess pore pressures against the pile shaft at the end of each pile installation. For the IC-pile only pile PT4lf is included as a typical example. The negative values observed at shallow depth for the IC-pile may be erroneous. The lowest piezometer along the IC-pile is located only 8 pile radii behind the pile tip, and is therefore probably more affected by tip effects than the others. The results otherwise suggest a general increase in excess pore pressure with depth, and that the excess pore pressures are larger for the closed-ended NGI and IC piles, than for the open- ended LDP pile.
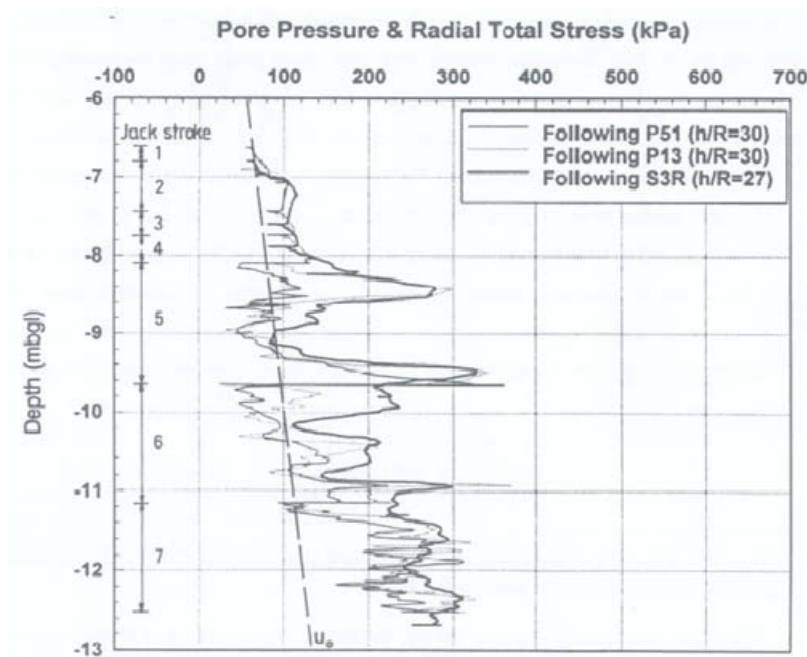
Figure 2.6.10 – Example of recorded pressures during pile jacking for "following" instruments along IC pile PT4lf, Pentre (from Chow, 1996).
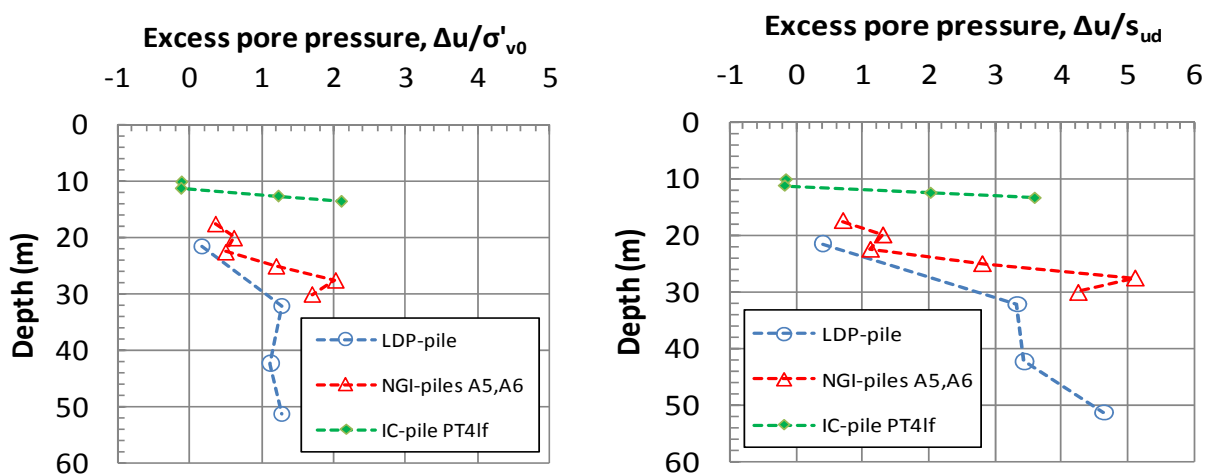
Figure 2.6.11 - Normalised excess pore pressures at end of pile installation, Pentre

Figure 2.6.12 presents measured normalised effective stresses at the end of the installation process. Note in this respect that the earth pressures registered on the LDP-pile during pile penetration in general were significantly lower than the pore pressures, suggesting that the earth pressure cells gave erroneously low values.
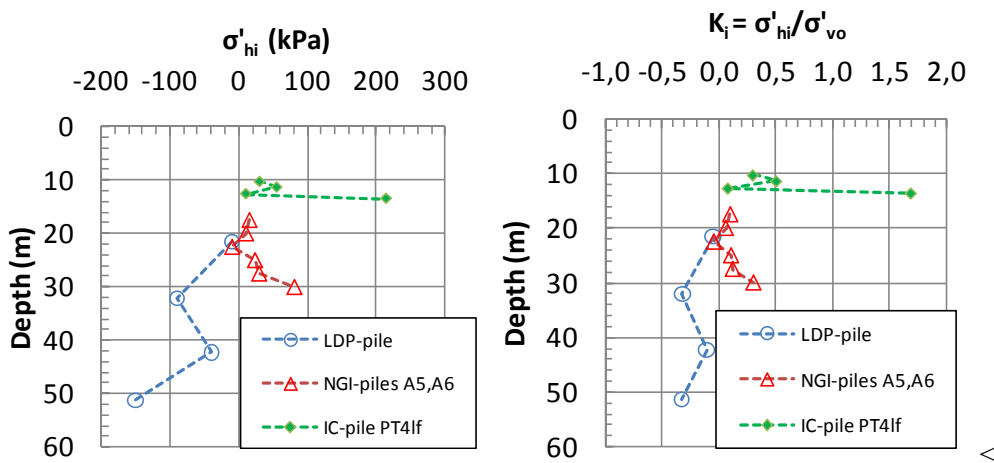
Figure 2.6.12 - Normalised radial effective stress at end of pile installation, Pentre

Figure 2.6.13 shows examples of pore pressure dissipation curves as measured by the lowest instrument units on NGI piles A5 and A6.
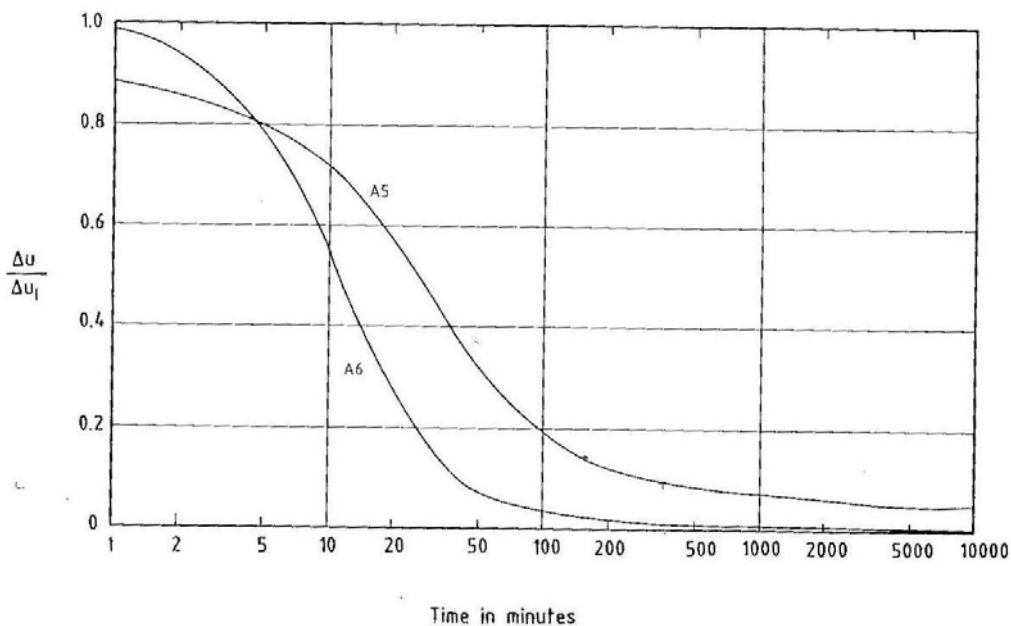
Figure 2.6.13 – Example of observed pore pressure dissipation for NGI-piles A5 and A6-middle sensor level, Pentre (after NGI, 1988)

Figure 2.6.14 shows that the time to reach 90% pore pressure dissipation varies greatly for each pile type and with depth. This confirms the very variable nature of the Pentre deposit when it comes to permeability and coefficient of consolidation, ref. Table 2.6.2. In relation to the data presented in Figure 2.6.14 it should be noted that these refer to changes that occurred after the end of pile installation. Due to the high permeability, significant dissipation already occurred during the installation phase, but it is difficult to quantify how much.
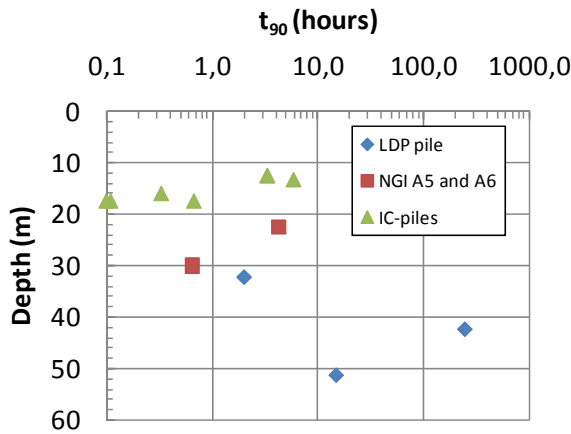
Figure 2.6.14 – Observed times to reach 90 % consolidation, Pentre

Cox et al (1993) related the relatively speaking long reconsolidation time for the LDP pile at 42.3 m depth to that at this depth there is silty CLAY rather than clayey SILT, as also evidenced by the tendency for higher water content and plasticity index around this depth, ref. Figure 2.6.4.

During the equalisation period following the end of pile installation, all piles showed a reduction in total earth pressure with time, but there were considerable variations in how much it reduced. The reduction was generally larger for the sensors closest to the pile tip, both for the NGI piles and the IC piles. Overall the reduction ranged from 0 to 50 %.

Figure 2.6.15 presents the fully equalised horizontal (radial) effective stress against the pile surface in comparison to the assumed in-situ horizontal effective stress. Figure 2.6.16 shows the corresponding effective stress ratio, K_c, compared to the estimated K_0 values. Considering the low-plastic nature of the Pentre silt the K_0 values were in this case calculated from the empirical expression proposed by Mayne and Kulhawy (1982):

$$K_0 = (1-\sin\varphi)\cdot OCR^{\sin\varphi} \tag{2.6.1}$$

Based on Table 2.6.3 the value of the friction angle was taken as $\varphi=30.0$. OCR-values were taken from Figure 2.6.5.
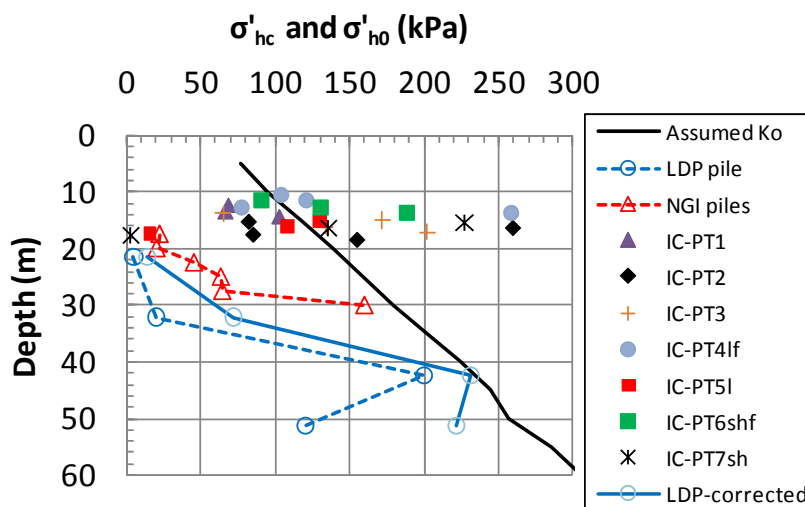
Figure 2.6.15 – Measured horizontal effective stress at U=100%, Pentre
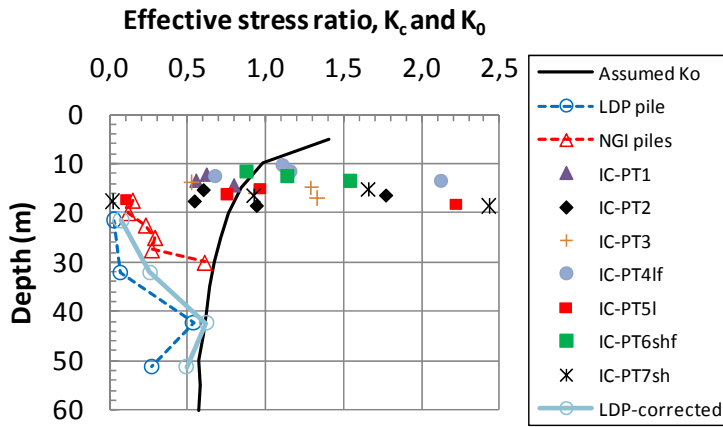
Figure 2.6.16 - Measured horizontal effective stress ratio at U=100%, Pentre

There is considerable variation in effective stress level measured along the different piles as well as with depth. The IC-piles show in general higher K_c values than the other piles. Note in this connection that the lowest data point for each IC-pile test is data from the leading instrument unit most affected by tip effects. Neglecting data from the leading instrument unit, the K_c values for the IC piles are on average close to the assumed K_0 values, but the scatter is still large. Chow (1996) showed that IC- piles that were jacked with many short strokes and dissipation in between attained the lowest Kc values, Figure 2.6.17. The numbers on the data points in Figure 2.6.17 represent the h/R ratio at the different sensor levels, where h is the distance of the sensor from the pile tip and R the pile radius. The h/R effect is considered in more detail in Figure 2.6.18.
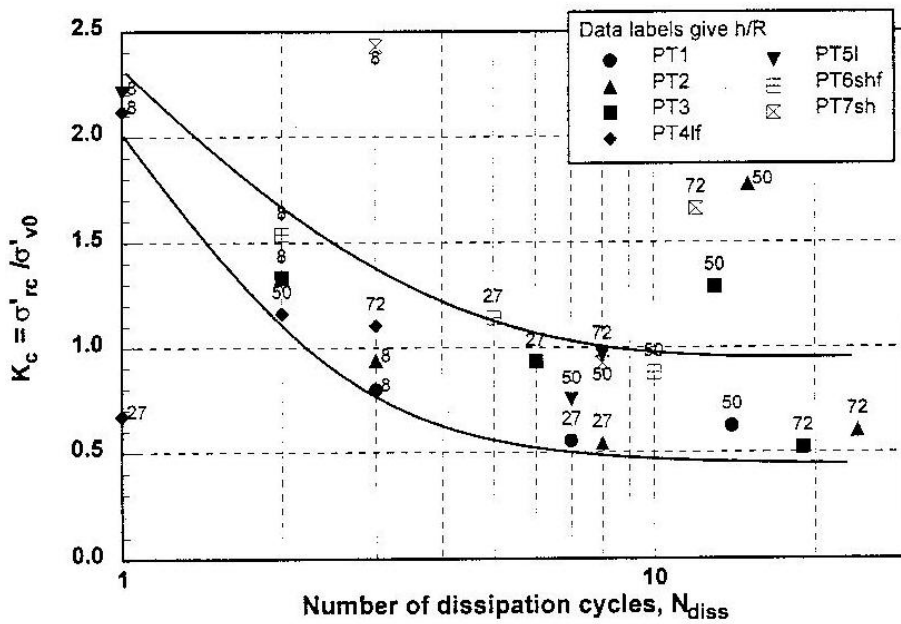
Figure 2.6.17 – Impact of installation dissipation cycles on K_c for IC piles, Pentre

The IC pile data suggest that the h/R effect in this case is limited to the first sensor level at h/R≈8. Due to the larger testing depth and difference in soil characteristics with depth, the NGI data are not considered directly comparable to the IC pile data, but do not suggest any significant h/R effect. The LDP pile was driven open ended and for that reason may not be relevant to compare against. The lowest sensor level at h/R= 9.7, showed however lower stresses than measured at the level above, Figure 2.6.16.
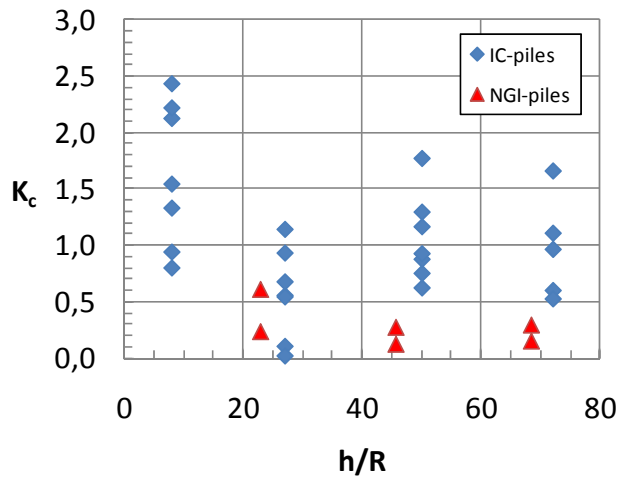
Figure 2.6.18 – Measured K_c values against h/R, IC and NGI piles, Pentre

Chow (1996) have suggested that membrane type earth pressure cells, as used on the NGI and LDP piles, are more flexible than the pedestal type earth pressure measurement system used on the IC piles, and that this could have led to some arching effects and too low measured total earth pressures for the NGI and LDP piles.

The negative installation effective stresses measured along the LDP pile (Figure 2.6.12) indeed suggest that the K_c values for this pile could also be too low. For the LDP pile, Figure 2.6.15 and 2.6.16 therefore also show effective stresses corrected for the negative values measured at the end of pile installation. The correction applied was calculated as follows:

- It was assumed that the total horizontal pressure at end of pile installation should at least be equal to the pore pressure, i.e. $(\sigma_{hi})_{corr} = u_0$. This correction corresponds to the measured negative installation stress, i.e. to $\Delta p = -\sigma'_{hi}$.

- The corrected total horizontal pressure at the end of the reconsolidation phase is assumed such that the error is proportional to the absolute value of total stress, i.e.

    $(\sigma_{hc})_{corr} = (1 + \Delta p/u_0) \cdot (\sigma_{hc})_{measured.}$

These corrected K_c values are still lower than K_0, and still seem to fall low compared to the trend in the NGI data, and even more so when compared to the IC data.

It can of course be argued that the effective stress at end of installation could have been larger than zero. If as an example, it is assumed that the installation effective stress ratio should have been for instance $K_i = 0.2$ rather than zero, the corrected K_c values for the LDP pile would increase to values of 0.26, 0.37, 0.77 and 0.62 respectively from the upper to the lower sensor level. If so, the data would fall more in line with the NGI data, but as a whole still lower than the IC data.

The relatively high K_c value for the LDP pile around 42 m may well be explained by the higher plasticity at this level. The same may apply to the relatively high value for the NGI-pile A6 at 30 m depth. The lowest K_c values for the NGI and LDP piles tend to confirm the observations from Lierstranda (Figure 2.5.16) that piles installed in low plastic clays may attain very low effective stresses against the pile shaft.

The LDP pile was loaded to failure in compression at a constant rate of displacement of about 1 mm/min. As seen from Figure 2.6.17, the peak load of 6.031 MN was reached at a displacement of about 36 mm. The load had dropped by about 10 % when the displacement reached 100 mm.
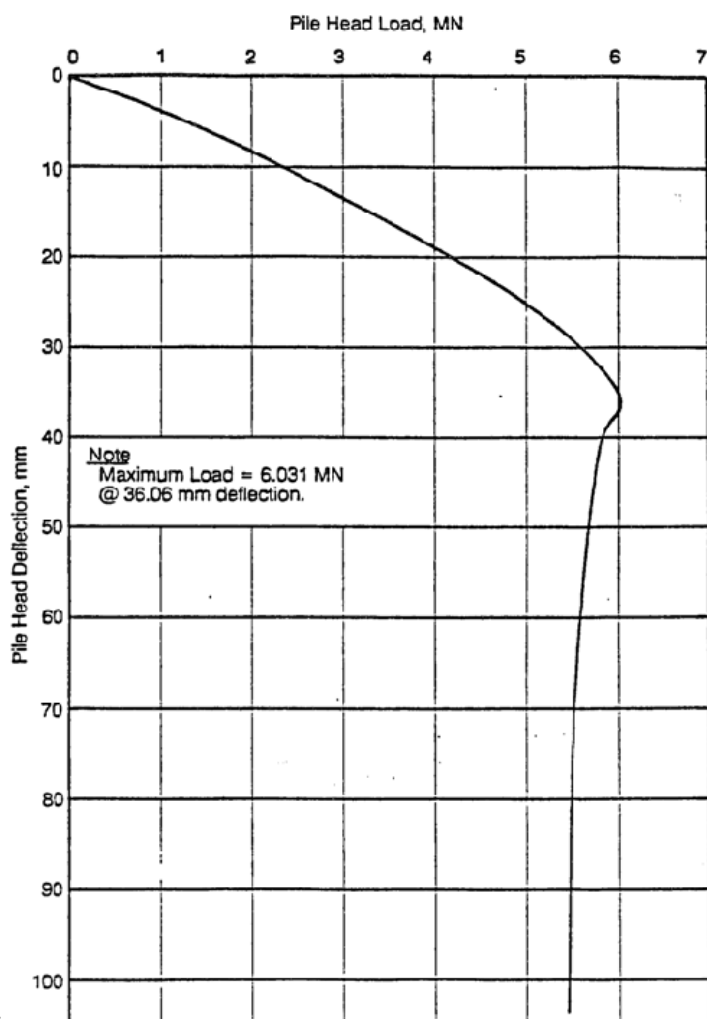
Figure 2.6.19- Measured load-displacement curve LDP pile, Pentre (from Cox et al, 1993)

The NGI piles were loaded incrementally in the same manner as the tests at Onsøy and Lierstranda. Failure was reached at a pile top displacement og about 16 mm for pile A5 and 22 mm for pile A6. Table 2.6.4 presents the ultimate total pile capacity defined from the 1st and 2nd static tests on the NGI-piles. The failure load was defined as the load at which the displacement rate exceeded 1 mm/min. The ultimate capacities generally agree with what was defined in NGI (1988[a]), apart for the first test on pile A5 which has been reduced from 190 to 180 kN.

Table 2.6.4- Measured ultimate capacities, NGI tests, Pentre

Pile	Time after installation (days)	Total ultimate capacity, Q_{ut} (kN)	Correction for weight of pile and tip resistance (kN)	Ultimate shaft capacity, Q_{us} (kN)	Change from 1st to 2nd test Q_{us}^2/Q_{us}^1
A5	27	180	20	160	1.09
A6	28	460	21	439	0.87

The 2nd static tests on NGI-piles A5 and A6 were carried out one day after the 1st test. As shown in Table 2.6.4, pile A5 gained 9 % in capacity from the first to the second test, whereas pile A6 lost 13 %. All NGI pile test at Haga, Onsøy and Lierstranda showed a gain in capacity from the 1st to the 2nd test, so the loss observed for pile A6 was a new experience. Comparing piles A5 and A6, it may be noted that the one-way cyclic tests carried out immediately following the 1st static tests, were stopped at an accumulated displacement of respectively 30 mm for pile A5 and 48 mm for pile A6. As a tentative explanation, the larger accumulated cyclic displacement for pile A6 than for pile A5 could have contributed to the lower re-gained capacity.

For the IC –piles, only the deduced average shaft friction values will be dealt with herein, but Chow (1996) give also the locally measured values.

Figure 2.6.20 presents a summary of ultimate shaft friction for all the different tests compared to the assumed in-situ s_{ud} and UU strength profiles (from Figure 2.6.6). Figure 2.6.21 shows the corresponding normalised α- and β values. The NGI-piles are here presented by the shaft friction observed along the part from the top to the tip, as well as a weighted average value. The shaft friction was calculated assuming a tip resistance according to eq (2.3.3). As noted in NGI (1988[b]), the shaft friction deduced from the load cells L1 and L3 was considered to be low when compared to the total load measured at the pile top. This could be due to friction through some remaining remoulded soil in the casings. For the long LDP pile the local distribution of shaft friction is based on the load distribution curve presented by Gibbs et al (1992). The IC data were taken from Chow (1996).
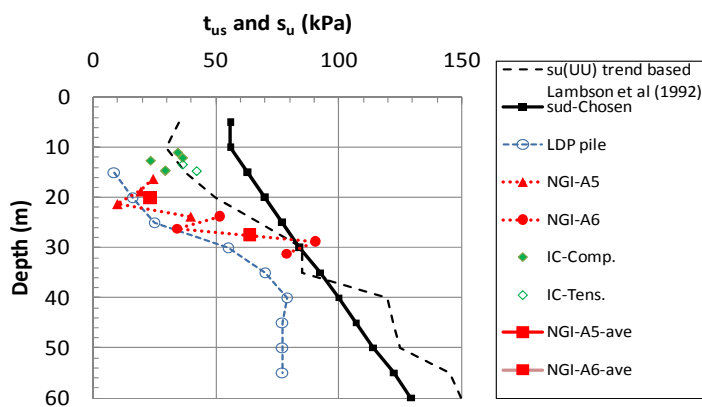
Figure 2.6.20 - Ultimate shaft friction, Pentre
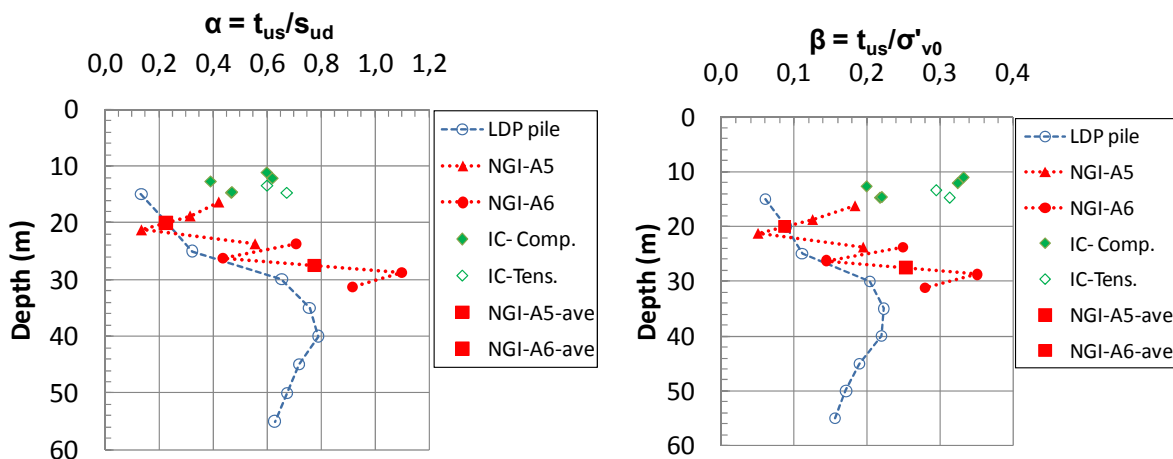
Figure 2.6.21 - Mobilised α and ß -values, Pentre

In relation to the IC and LDP results, past interpretations by Chow (1996) were based on the UU strength profile in Figure 2.6.20, which leads to different α-values compared to the present study.

For all piles tested at Pentre, the failure was well defined, with the local shear stress reaching a clear peak or ultimate plateau level. For the displacement-controlled LDP and IC tests, a post-peak reduction wa observed at some levels. As shown by Figure 2.6.22 (after Gibbs et al, 1993), a post-peak reduction was observed at all levels below about 30 m depth along the LDP-pile, and amounted to up to 25 % of the peak value.
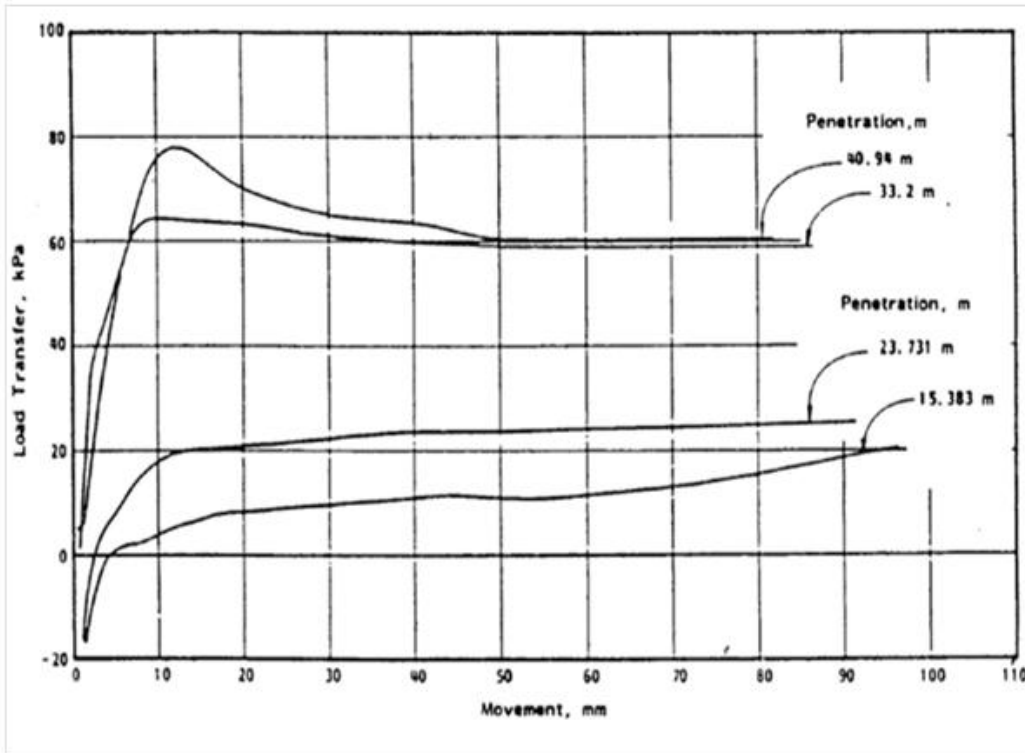
Figure 2.6.22 – Example of t-z curves along LDP pile, Pentre (after Gibbs et al, 1993)

Figure 2.6.23 summarizes displacement at failure for all the different tests. The displacement at peak ranges from about 1.5 to 7.5% of the pile diameter. There are no apparent difference between the different pile types and between compression and tension, but the data suggest that the normalised peak displacement tend to decrease with depth.
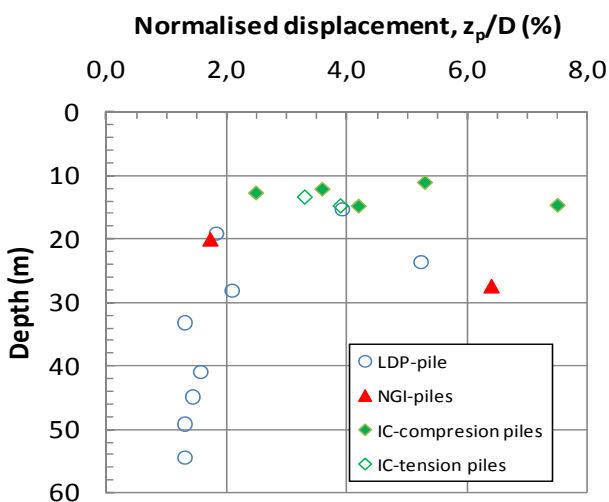
Figure 2.6.23 – Normalised displacement at failure versus depth, Pentre

Figure 2.6.24 shows the relation between measured shaft friction and horizontal effective stress at onset of loading. For the LDP-pile both actually measured and corrected values of σ'_{hc} are given. Even after that correction, the data suggest rather large scatter. The IC-piles clearly show the lowest shaft friction in relation to effective stress.
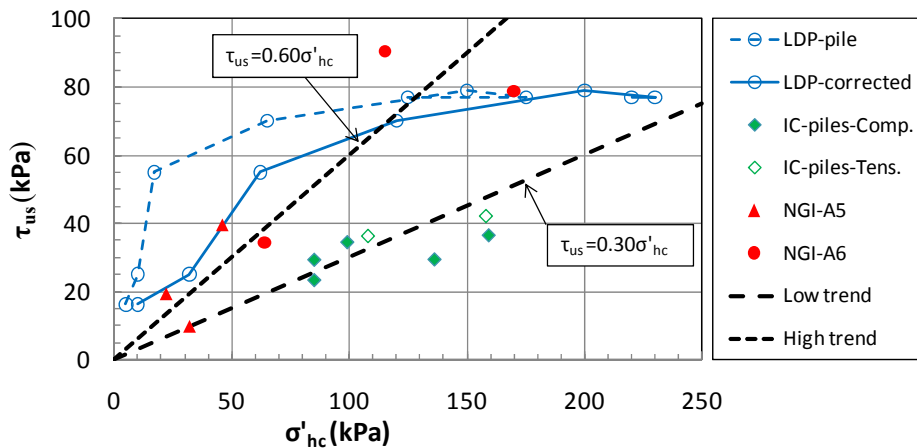
Figure 2.6.24 - Measured ultimate shaft friction in relation to horizontal effective stress at onset of pile loading, Pentre

The upper and lower trend lines shown in Figure 2.6.24 are represented by:

$\tau_{us} = 0.6 \cdot \sigma'_{hc}$ which may be typical for the LDP and NGI piles

$\tau_{us} = 0.30 \cdot \sigma'_{hc}$ which is typical for the IC-piles

It is hard to see any good explanation for this large difference or scatter between the IC-piles on one hand and the LDP and NGI piles on the other hand. That the LDP- data tend to approach the IC data at large stresses is mainly due to the deduced shaft friction being constant with depth along the lower part of that pile (Figure 2.6.20), whereas the effective stress at onset of pile loading increases in the same depth range (Figure 2.6.15). At the same depth levels, the NGI data and LDP data are in reasonable agreement.

Figure 2.6.25 shows that the net effective stress changes at failure were generally small for all the piles. For the NGI A5 pile there were no changes in pore pressure during pile loading, and a slight reduction (0 to 6 kPa) in total pressure. For NGI pile A6 the pore pressure increased by 9 to 27 kPa, and the total pressures increased by 3 to 10 kPa, giving a slight net reduction in effective stress at all levels. For the LDP-pile Gibbs et al (1992) have only reported data for the gauges at 42.3 m depth. At this level the pore pressure increased to failure by about 90 kPa and the total earth pressure increased by 60 kPa, giving a net effective stress reduction of 30 kPa. For the IC-piles, the data presented by Chow (1996) only give the net effective stress changes (no split between total earth pressure and pore pressure change). It can still be assumed that due to the very slow loading rate no pore pressure change took place. All IC-piles but one showed on average some decrease in effective stress. There is no clear explanation why an increase in effective stress was observed only for pile IC-PT3.
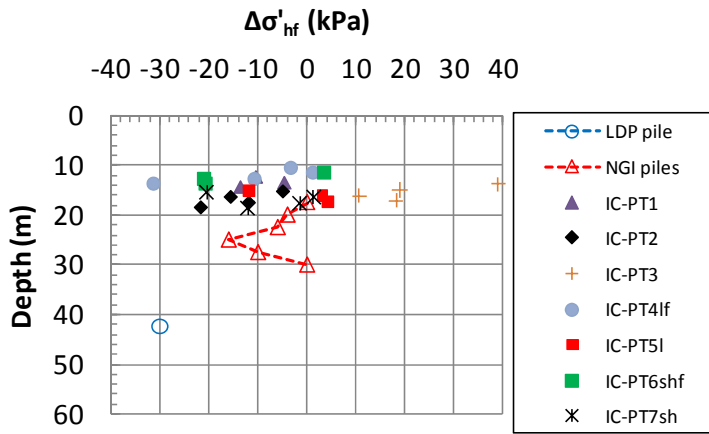
Figure 2.6.25 - Change in horizontal effective stress during pile loading, Pentre

The apparent relationship between effective stress at failure and ultimate shaft friction is presented in Figure 2.6.26. Note that for the LDP-pile only estimated data from 40 to 45 m depth range is included (due to lack of other reported data). A large scatter in the data is also in this case apparent. Typical upper and lower trend lines are given by:

$\tau_{us} = 0.7 \cdot \sigma'_{hf}$ (typical for the NGI piles), implying an apparent mobilised friction angle of $\delta = 35.0^0$

$\tau_{us} = 0.32 \cdot \sigma'_{hf}$ (typical for the IC-piles), implying an apparent mobilised friction angle of $\delta = 17.7^0$

The upper trend line fall somewhat outside the maximum apparent peak friction angle determined in DSS tests on the Pentre soils of 29.5^0 (see Table 2.6.3). The lower trend line lie within the range of measured residual friction angles in DS and RS tests. The data are as a whole still considered ambiguous, and could reflect errors in the measured earth pressures (maybe too low for NGI and LDP piles or too high for IC piles).
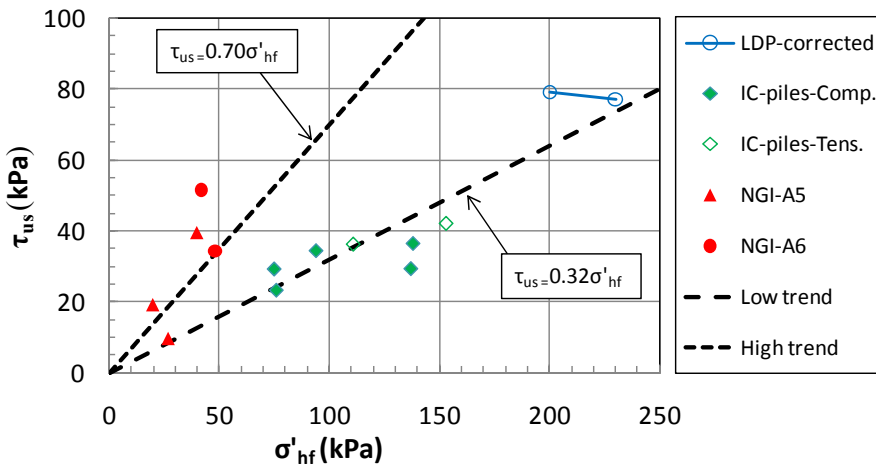
Figure 2.6.26 - Ultimate shaft friction in relation to horizontal effective stress at pile failure, Pentre

The following main observations are made from the pile tests at Pentre:

- Owing to the apparent very stratified nature of the Pentre deposit and large horizontal permeability in general, significant pore pressure dissipation occurred during pile installation and the time for full reconsolidation after pile installation was much faster than for other pile tests included in this study
- The equalised horizontal (radial) effective stress at onset of pile loading as expressed by Kc, shows large variation with depth and between the different piles, the IC-piles in general giving the highest values. The differences could reflect errors in the measured effective stresses.
- The shaft friction for the IC-piles seems at first glance to be relatively speaking higher than for the other piles, which to some extent ties in with the higher K_c – values for these piles. It should in this connection be recalled that the IC-piles were deliberately loaded very slowly to achieve **fully drained** conditions during pile loading. This as well as the stepwise jacking procedure used during pile installation could have had an impact on the shaft friction and radial effective stresses observed for the IC piles.
- The normalised shaft friction values for the IC-piles at about 11 to 14 m depth are however, in line with the maximum values observed in the 30-40 m depth range for the NGI and LDP piles. Thus the IC-values could reflect on the variability in soil conditions with depth.
- The NGI and LDP piles tend to confirm each other with respect to variation in ultimate shaft friction with depth, but the open-ended LDP piles suggest up to 25 % lower shaft friction as compared to the closed-ended NGI piles.
- The normalised shaft friction values from 15 to about 25 m can in general be characterised as very low, considering that the deposit is assumed to be only moderately overconsolidated. This seems to coincide with the depths where the plasticity index is lowest, ref. Figure 2.6.4.
- The IC-piles suggest in general some "friction fatigue effects" as expressed by a tendency for some reduction in installation effective stress with normalised distance, h/R, from the pile tip, but the data are not all that consistent. In any case the effect seems limited to a distance of h/R< 20.
- The LDP and the NGI-piles give no clear indication of any h/R effect. The variation in normalised shaft friction with depth for these piles is most likely rather a reflection of the variability in soil characteristics with depth.
- The LDP-pile and 5 of the IC-piles were loaded in compression, whereas the NGI- piles and two of the IC-piles were loaded in tension. The direct comparison between compression and tension for the IC-piles suggests that there is no significant difference in shaft friction for compression and tension. The LDP-pile compared to the NGI- piles could actually suggest that compression gives lower shaft friction, but this difference could also be an effect of open versus closed penetration, or alternatively a scale effect.
- The relationship between measured horizontal effective stress against the pile and ultimate shaft friction shows large scatter, primarily owing to large variation in the measured effective stresses. The IC-piles tend to show the largest measured effective stresses and consequently, the lowest apparent mobilised interface friction angle.

2.7 Tilbrook Grange (UK)

2.7.1 General overview of test site and load tests

The Tilbrook Grange (TG) test site lies near Bedford in Cambridgeshire in the middle of UK, about 80 km north of London. The site was selected for pile testing as part of the Large Diameter Pile Test (LDPT) research program managed by BP, which also included the Pentre LDPT program described in Section 2.6 (Mullis, 1993). The TG site was selected because the clay at the site is highly overconsolidated and very stiff, resembling conditions often met in the parts of the North Sea that have been overlain by glaciers.

As part of the LDPT program, two large diameter piles were installed and tested in 1987 and 1988, ref. Figure 2.7.1, and the following description.

The LDPT-McClelland compression pile. This test pile, herein referred to as LDPTC, had an outer diameter D= 762 mm and wall thickness decreasing from 40 mm for the upper part to 32 mm for the lower part, Figure 2.7.1. It was driven open ended to a tip penetration of 30.0 m using a 40 t BSP HA40 hydraulic hammer with a rated energy of 470 kNm. Factual data from this test were presented in a report by McClelland (1988[b]). Data and analyses of the driving record were presented by Poskitt et al (1993). The pile experienced partial plugging during driving. At the end of driving the top of the clay plug inside the pile was located at a depth of 16.9 m. Note that Figure 2.7.1 incorrectly shows the depth of the plug at 13.1 m and not 16.9 m. The LDPTC pile was instrumented with strain gauges at 12 levels prior to driving, using 4 resistance type foil gauges at each level. In addition there were two sets of diametrically positioned earth-and pore pressure gauges at 4 levels. The selection and testing of the instrumentation systems were described by Solomon et al (1993), and were much the same as for the LDPT pile at Pentre.

The LDPT- Arup tension pile. This pile, herein referred to as the LDPTT (tension) pile test, also had D=762 mm, but a constant wall thickness of 34 mm throughout. Factual data from this test were presented by Ove Arup & Partners (1988). As also described by Clark et al (1993), this pile was driven non-instrumented as a trial pile prior to the LDPTC pile. The original purpose was to get a feeling for driving resistance. The pile was driven using the same equipment as for the LDPTC-pile. It was first driven 16-19 January 1987 to a tip penetration of 30.5 m. This pile also partially plugged during driving, and at end of driving the depth to the top of the plug was 11.1 m. The pile was re-driven another 0.5 m to 31.0 m penetration on 5 October 1987 to study set-up. Before load testing on 28 September 1988, about 11 months after the re-driving, the plug was augered out to 2.5 m above the pile tip and instrumented with foil strain gauges at 11 levels, Figure 2.7.1.   This post-driving instrumentation means that the residual stresses in the pile after driving is not captured, which must be considered when interpreting the test results. This pile was load tested in tension.

 In addition to the LDP pile tests, NGI undertook in 1988 a series of additional pile tests at the site as outlined in Figure 2.7.1. The test piles were partly the same as had been used at Onsøy, Lierstranda and Pentre, but with some specially designed instrumentation, as described in the following, ref. also Karlsrud et al (1993) and NGI (1991).

NGI pile A. This pile had basically the same dimensions and instrumentation systems as the Onsøy, Lierstranda and Pentre A-segment piles, and contained 4 levels of instrumentation units.

Due to the much stiffer clay, the various sensors were designed for much higher loads than in these previous tests. Furthermore, whereas at the other sites each instrument unit was equipped with 2 gauges for measuring total earth pressure and 2 for measuring pore pressure, this was reduced to 1 of each at Tilbrook. The eliminated total earth and pore pressure gauges were in each unit instead replaced by 2 gauges to measure directly the effective earth pressure against the pile shaft. This was achieved by allowing the pore pressure to enter through a porous filter to the backside of the earth pressure membrane, Figure 2.7.2. The pile wall thickness was 16 mm apart from the lowest section which was reduced to 8 mm. The pile was driven through a 3 m deep casing to a tip penetration of 12.85 m.

NGI pile B. This was similar to pile A but the lowest instrumentation unit was replaced with a 2m long telescopic section. The purpose was to eliminate end effects and tip resistance during the load testing in tension. This pile was driven through a 17.5 m deep casing (test pile D) to a tip penetration of 27.61 m, including the telescopic section. The wall thickness was 16 mm apart from the top 5 m which was 25 mm.

NGI pile C. This pile had only one full instrumentation unit (at 5.11 m) but was also instrumented with strain gauges at 9.76 m depth. It was driven through a 3 m deep casing to a tip penetration of 19.47 m. It had like pile B a 2 m long telescopic section at the end, Figure 2.7.1. The wall thickness was 25 mm down to the load cell at 9.76 m, and 16 mm further down to the tip.

NGI pile D. This was the casing for pile B, and was driven to a tip penetration of 17.5 m. The pile had a diameter of 273 mm and wall thickness of 32 mm along the upper 5 m and 16 mm below that. To avoid plugging it was equipped with a 290 mm long driving shoe with internal clearing of 7.5 mm. This worked well and essentially no plugging occurred. The pile was emptied prior to driving of pile B.

Table 2.7.1 summarizes the load testing program on the different piles. The LDPT-piles were first load tested statically respectively 134 days (LDPTC-compression pile) and 350 days (LDPTT-tension pile) after installation. The LPDT load tests were displacement controlled, with a constant rate of load application of about 1 mm/min in the static tests. Failure was reached in about 30 minutes in the compression test and 50 minutes in the tension test. After failure was reached, both piles were subjected to sustained (creep) loading to relatively large displacements. A cyclic load test was also carried out on the compression pile.

The NGI-piles were subjected to two series of load testing with a waiting period of 3 days in between. The test programs were quite similar to those carried out on the test piles at Onsøy and Lierstranda. Both test series started with an initial static incremental loading test, followed by a one-way cyclic and post-cyclic static test. The only exception was pile NGI-A, which in the 2nd series, rather than a cyclic test, was subjected to large displacement static testing. In the incremental static tests failure was typically reached in 30-40 minutes.
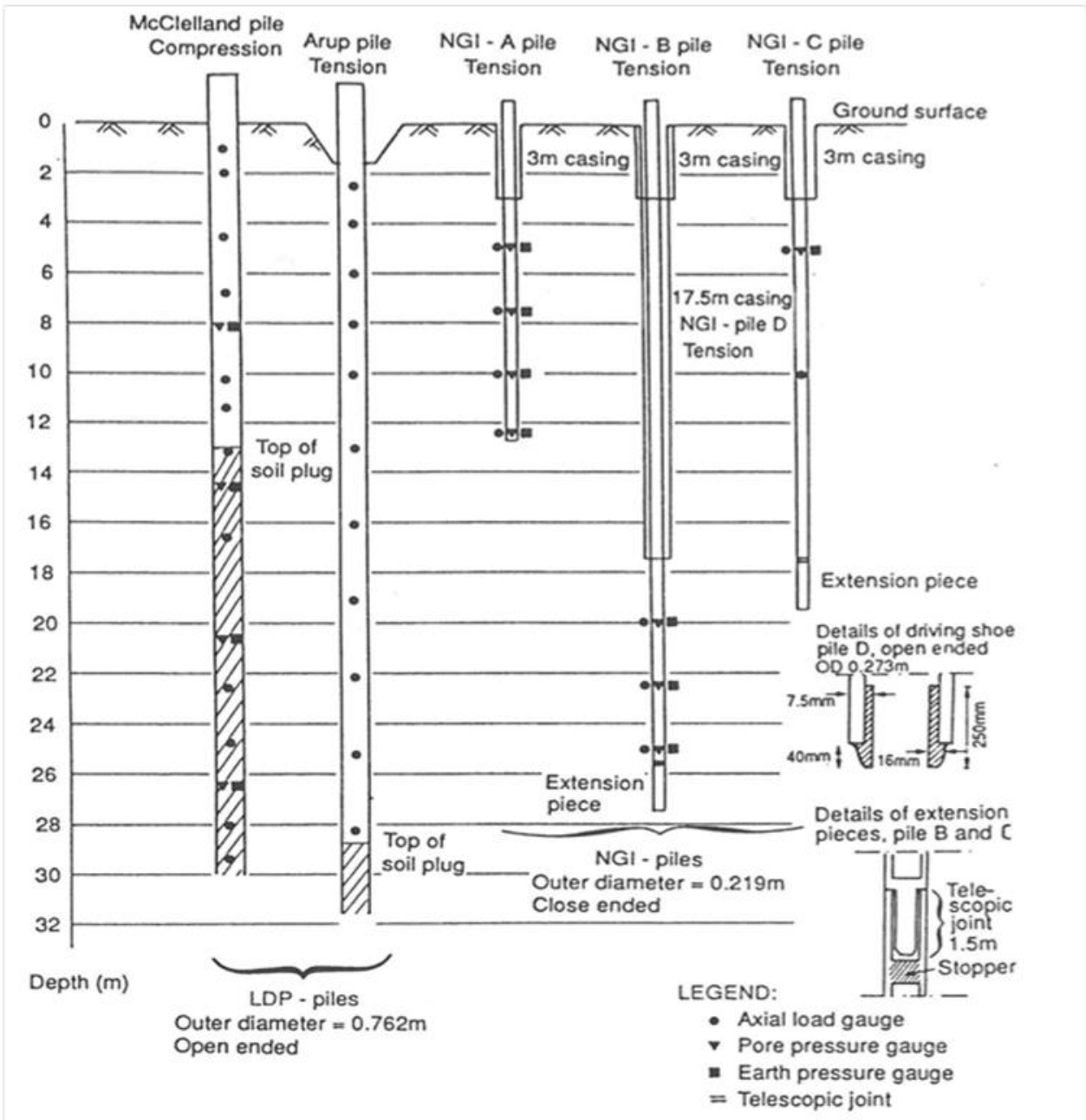
Figure 2.7.1- Overview of all pile tests, Tilbrook (from Nowacki et al, 1993)
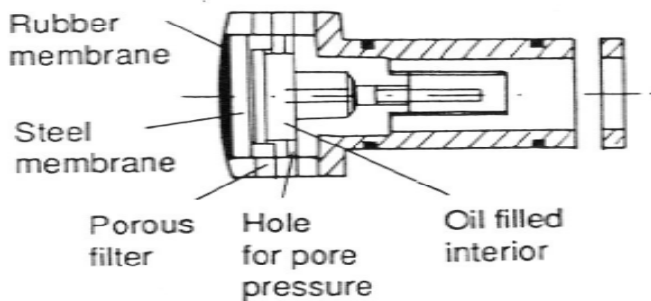
Figure 2.7.2- Gauge used to measure directly effective earth pressure against the pile shaft of NGI-piles, Tilbrook

Table 2.7.1- Load testing program, Tilbrook

Pile test	Test no.	Date installed	Type of test	Days after installation
McClelland – Comp.	LDPTC1	05.10.1987	Static-compression	134
	LDPTC2		Creep test	135-136
	LDPTC3		Rapid static test	137
	LDPTC4		One-way cyclic test	137
Arup-Tension	LDPTT1	05.10.1987[1]	Static –tension	350
	LDPTT2		Creep test	351
NGI-A	A1	08.02.1989	1st static -tension	61
	A2		One-way cyclic	61
	A3		Post cyclic static	61
	A4		2nd static- tension	64
	A5		Large displacement	64
NGI-B	B1	08.02.1989	1st static -tension	59
	B2		One-way cyclic	59
	B3		Post cyclic static	59
	B4		2nd static- tension	62
	B5		One-way cyclic	62
	B6		Post cyclic static	62
NGI-C	C1	09.02.1989	1st static -tension	60
	C2		One-way cyclic	60
	C3		Post cyclic static	60
	C4		2nd static- tension	63
	C5		One-way cyclic	63
	C6		Post cyclic static	63
NGI-D	D1	02.02.1989	1st static -tension	68
	D2		One-way cyclic	68
	D3		Post cyclic static	68
	D4		2nd static- tension	71
	D5		One-way cyclic	71
	D6		Post cyclic static	71

1)   Time when the pile was re-driven from 30.5 to 31.0 m depth.

2.7.2 Soil parameters

A very comprehensive soil investigation program was undertaken at the TG site. The investigations have been documented in a factual report by McClelland (1988 a) and an interpretive report by McClelland (1988 b). Lambson et al (1993) have summarised the derived soil parameters which were used by Gibbs et al (1993) as basis for the interpretation of test results. The soil data have however, also been independently assessed by NGI (1991), as also presented by Nowacki et al (1993). The author has re-visited and to some extent re-interpreted some of the soil parameters as found relevant for this study.

The clay deposit at TG consists of two geologic units .The upper unit extending to about 17.1-18.6 m depth is called Lowstoft Till, which is described in McClelland(1988b) as very stiff grey clay with scattered sand to gravel size fragments of flint, chalk and mudstone within the clay matrix. The lower unit extending further on to bedrock at around 40 m depth is defined as Middle Oxford clay, described as very stiff dark grey fissured clay with scattered silt and sand pockets or partings.

Figure 2.7.3 shows that the water content is lowest, and mostly around w=14-16 %, in the Lowstoft Till, increasing to 17-19 % in the Oxford clay. The total unit weight lies in the range of γ_t = 21 to 22 kN/m^3, Figure 2.7.3. These unit weights are as can be expected for the given water content and a specific gravity in the range G_s= 2.68-2.70.

The plasticity index is lowest in the till, typically I_p = 25 % as compared to I_p = 35 % in the Oxford clay. This difference in w and I_p is reflected in the mineralogy and clay content. The clay content typically lies in the range of 35-50 % in the Lowstoft till and 45-60 % in the Oxford clay. The mineralogy is dominated by illite (Lowstoft till) and/or illite-smectite (Oxford clay).

In-situ pore pressures have been measured by two stand-pipe piezometers at depths of 12.1 and 35.8 m. They suggested hydrostatic conditions below a ground water table at 2 m in the upper part, but an under pressure in the lower part, Figure 2.7.4. It should be mentioned that, Lambson et al (1993) reported that it took 5 months after the piezometers were installed for the pore pressures to come to an equilibrium level. This long equilibration period was assumed due to the very low permeability of the clay.
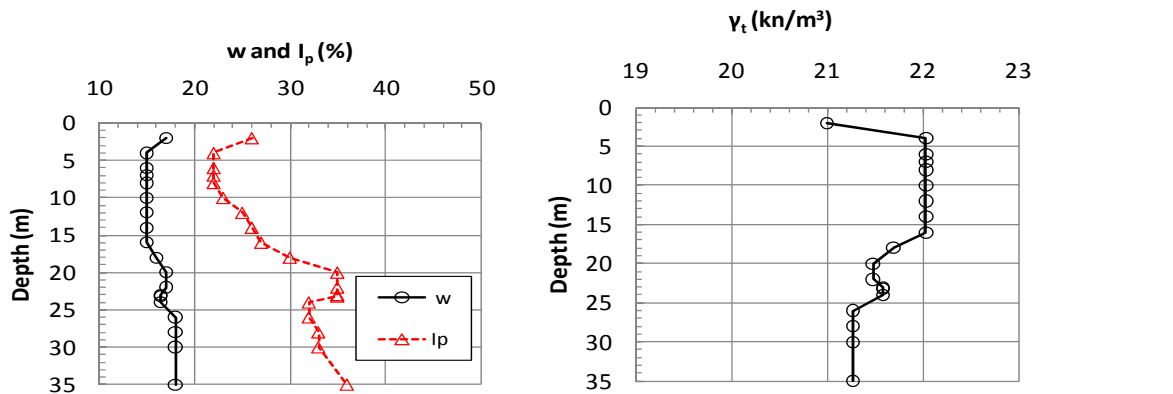
Figure 2.7.3- Summary of index data, Tilbrook
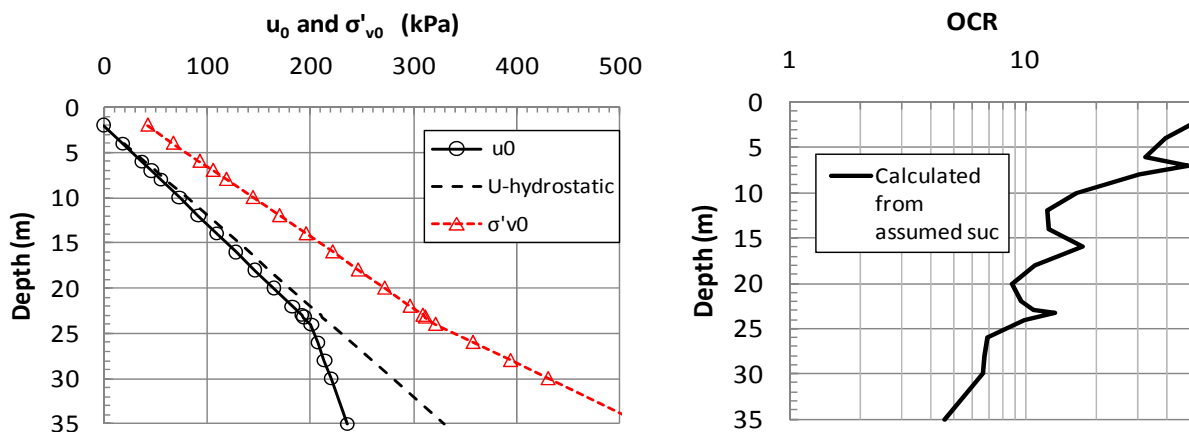
Figure 2.7.4- In-situ stresses and assumed OCR, Tilbrook

The in-situ effective stress ratio, K_0, have been estimated on basis of the assumed OCR profile in Figure 2.7.5 (discussed later in this section) and the Ip-values in Figure 2.7.3, using the modified Brooker and Ireland (1965) correlations proposed by Andresen et al (1979). McClelland (1988a) also carried out and reported a series of K_0-consolidation tests in the triaxial apparatus. As seen in Figure 2.7.5, the measured and estimated values are generally in good

agreement. The dashed assumed trend line is used as basis for later interpretations of the pile test results. The slight jump in assumed K_0 at 18m depth reflects the approximate transition between the Lowstoft till and the Middle Oxford clay.
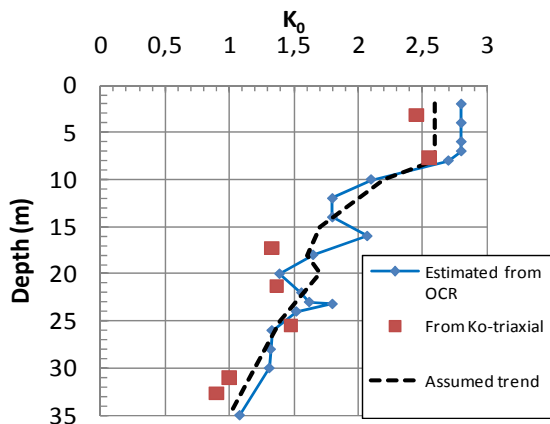
Figure 2.7.5- Measured and estimated in- situ K_0 values, Tilbrook

A total of 27 incremental oedometer tests have been reported in McClelland (1988[a]). Unfortunately, it is not possible from these tests to define the pre-consolidation pressure, p'_c, and hence OCR. Figure 2.7.6 shows an example of a typical test on one of the samples that seemingly looked best, plotted in both logarithmic and linear scales. Using the Casagrande method (Casagrande, 1936) on the log-plot one could possibly define p'_c to be around 300-600 kPa. The linear plot to the right shows, however, no evidence of any p'_c value at all, which would appear as a downward bend or kink of the ε-p' curve. All tests were subjected to unloading and reloading. It is not even from the re-loading curve possible to define the maximum pressure (i.e. pre-consolidation pressure) to which the sample was subjected. This feature applies to all oedometer tests carried out on these clays. Thus, definition of p'_c from oedometer tests seems simply not possible for this type of very stiff clays. The OCR values shown in Figure 2.7.4 were therefore back-calculated from the assumed undrained strength as will be discussed later in this section.

It is also a general feature of these oedometer tests that the compression index is not constant, but tends to increase more or less continuously with stress level. Figure 2.7.7 shows tangent modulus versus stress level as used with the Janbu (1963) method. Even at high stress level the re-loading branch does not match up with the 1st-time loading branch, which is unusual. Thus it seems not possible to define any unique combination of p'_r and modulus number, m, for the virgin compression curve.
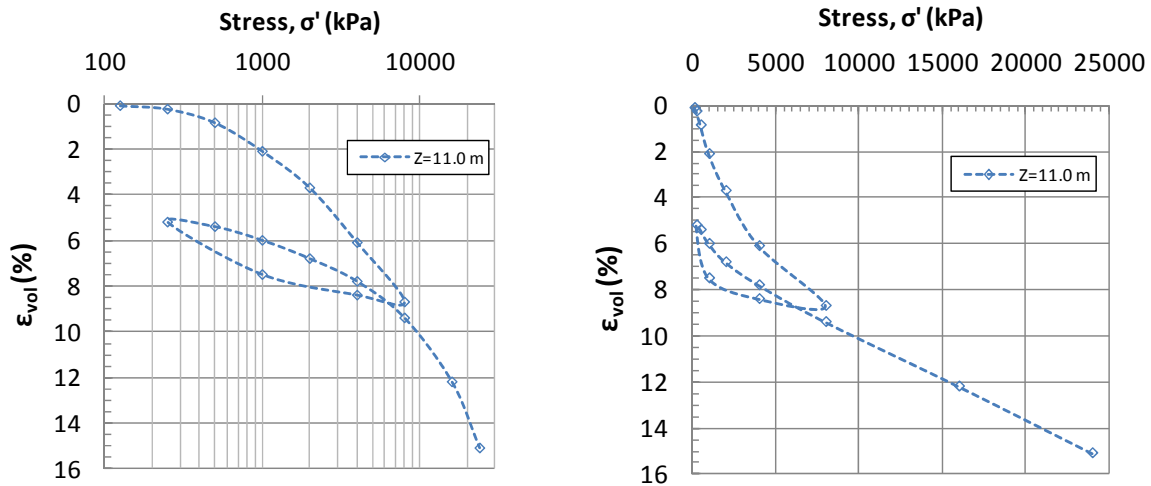
Figure 2.7.6- Example of oedometer curve for test on sample from z=11.0 m, Tilbrook
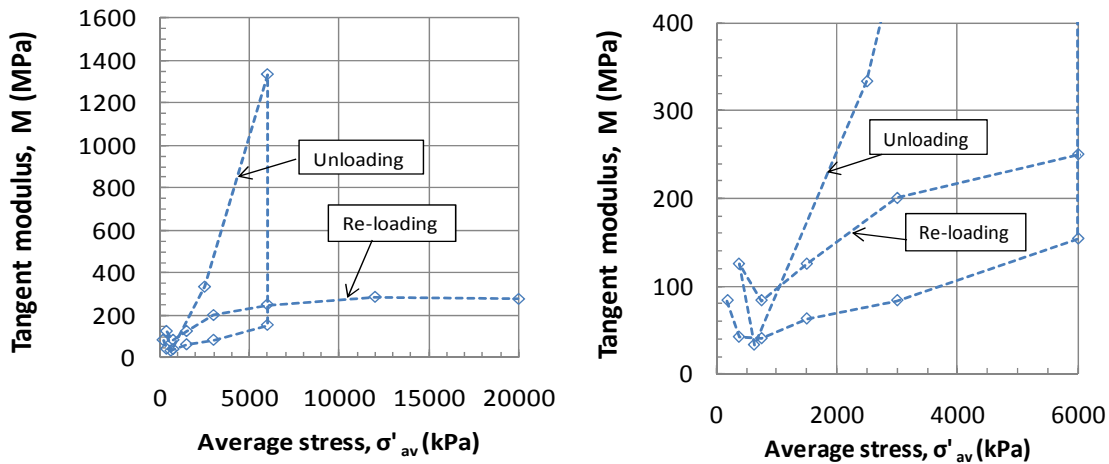
Figure 2.7.7- Example of modulus curves from oedometer tests z=11.0m, Tilbrook

Figure 2.7.8 presents values for the modulus number, m_0, assuming $p'_r=0$. This is based on modulus values taken along the 1st time loading curve at a stress corresponding to 6 MPa, or typically about 2.5 times the estimated pre-consolidation pressure. This modulus number is seen to be fairly constant with depth.

Figure 2.7.8 also shows in-situ vertical permeability of the clay, k_0, as back-calculated from the c_v-values reported from the oedometer tests (using the same procedure as described earlier for other sites). Figure 2.7.8 also shows 4 direct measurements of vertical permeability in the triaxial apparatus. In the Lowstoft till the directly measured values agree well with the permeability values deduced from the oedometer tests, but are a factor of 1.5 to 3.0 lower in the Oxford clay. The proposed trend line gives most weight to the oedometer tests. It may be noted that the permeability of this clay deposit is quite low, and about a factor of 15-20 lower than what is the case for the other sites (apart from Pentre with very high permeability).
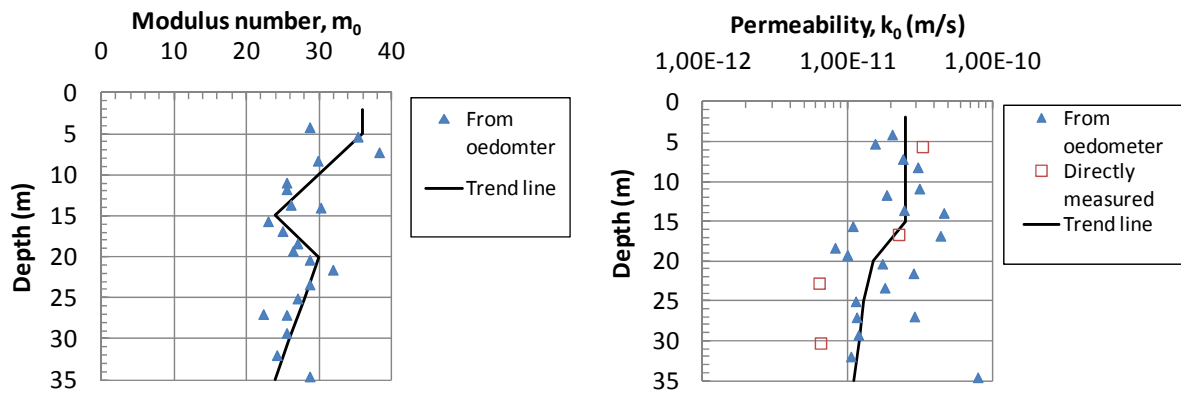
Figure 2.7.8 - Modulus number and in-situ vertical permeability, Tilbrook

A large number of UU (104 tests) and CIUC/CAUC (43 tests) have been carried out on the TG clays. For simplicity Figure 2.7.9 only presents the average trend lines from these tests, which are quite similar to what was assumed by NGI (1991). A striking and unexpected feature of these results is that the UU strengths are consistently larger than the CIU/CAU strengths, by as much as a factor of 1.35 to 2.27. Checking on the general description of testing procedures applied, it seems that in the CIUC/CAUC tests the cell pressure and back pressure were increased incrementally until a B-value of at least 0.95 was achieved. What is not clear from the test descriptions is if dry or wet filter stones were used during this consolidation procedure. If wet filter stones were used from the very start, the clay can suck water from the filter stones, and thus swell and possibly loose strength. For such stiff and high OCR clays it would be appropriate to first apply the in-situ stresses and then circulate de-aired water though the filter stones prior to undrained shearing.

One downhole CPTU test was carried out at the TG site. Figure 2.7.9 shows the s_{uc} strength profile derived from the tip resistance. The values of N_{kt} were based on the correlation proposed by Karlsrud et al (2005), although that data base does not cover such stiff and high OCR clays. The assumed N_{kt} values typically decrease from about 14 near the top to 11.5 near the bottom of the profile. It may be mentioned that the measured q_c values typically was about 5 MPa in the top 5m increasing to around 10 MPa below 15 m depth, but with some local high peaks and troughs. Pore pressure measurements seemed unsuccessful in the top 10-12 m part, but the measured u_2 pressure was increasingly negative below that level , with $u_2 = -0.5$ MPa at 12 m and $u_2 = -2.0$ MPa at 35 m.

Only three DSS test were carried out as part of the McClelland investigations, where off two were carried out on vertically trimmed specimens and one on a horizontally trimmed specimen. The detailed testing procedure was not described. As discussed for the Haga tests in Section 2.2.2, to give correct strength for high OCR clays, the DSS specimens must be pre-loaded to an axial stress approaching the pre-consolidation pressure and then unloaded again to σ'_{v0} prior to undrained shearing. It has not been possible to establish if this in was done in the current case. If not, these DSS shear strengths can be too low. The DSS strengths are on the other hand about equal to the laboratory determined s_{uc} strengths. The opposite is generally the case, which lends support to the possibility that the triaxial CIU/CAU s_{uc} strengths are in error and too low.
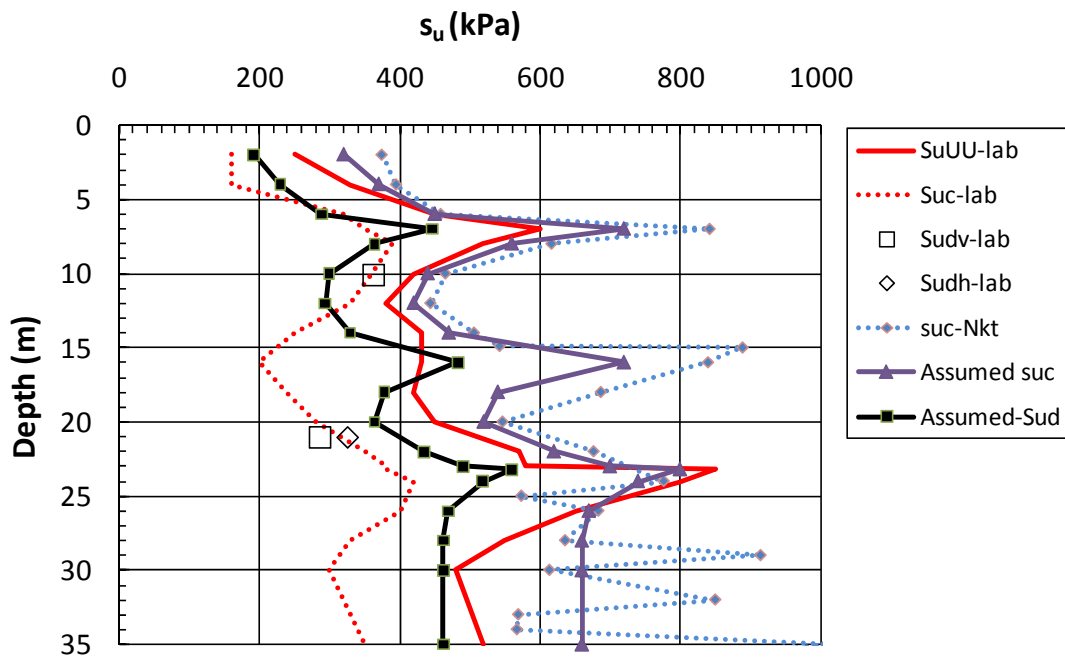
Figure 2.7.9- Undrained shear strength values, Tilbrook

Little data have been found in available literature on the anisotropy of the undrained strength of such stiff and high OCR clays as at the TG site. Some tests have been run on samples of Drammen clay (Andersen, 2004) and Haga clays (Lacasse, 1979) that were artificially preconsolidated to OCRs up to 40 prior to undrained shearing. The results suggest typical values of $s_{ud}/s_{uc}= 0.70$ for OCR <10 but with a tendency to decrease to about of $s_{ud}/s_{uc}= 0.60$ at OCR =40. Figure 2.4.9, which is based on tests on natural clays with OCR<7, suggests $s_{ud}/s_{uc} \approx 0.70$ and independent of OCR.

On basis of the preceding assessments, the following conclusions have been drawn with respect to the reference in-situ undrained strength at the TG site, reference also Figure 2.7.9:

- The assumed s_{uc} strength profile is taken as a reasonable weighted average of the s_{uUU} and the s_{uc}-N_{kt} based values.
- The assumed reference DSS strength is assumed to increase from $s_{ud} = 0.6 \cdot s_{uc}$ at the top to $s_{ud} = 0.7 \cdot s_{uc}$ below a depth of 16 m.

The OCR-profile in Figure 2.7.4 was derived from the assumed s_{uc}-profile and the SHANSHEP expression, eq. (2.5.1), using factors S=0.3 and m=0.795.

The effective stress paths from the CIU and CAU triaxial tests show quite a large scatter when it comes to maximum mobilised friction and attraction (or effective cohesion). This is illustrated in Figure 2.7.10. Assuming zero attraction or cohesion, the peak effective friction angle lies in the range of $\varphi = 23$ to 35 degrees with an average of $\varphi = 29$ degrees. Some tests on the lower Oxford lay suggest a loss in effective friction angle at large strain down towards $\varphi = 18$ degrees.
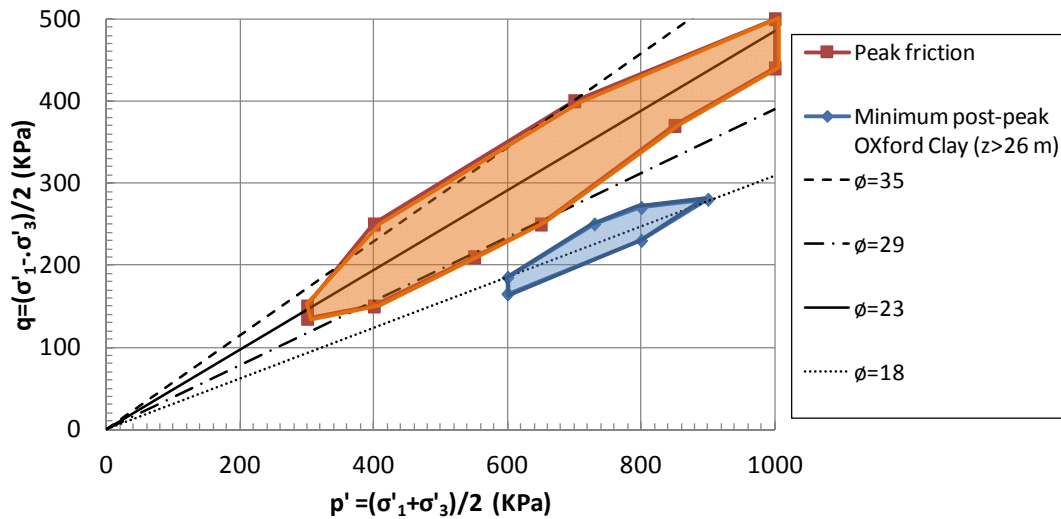
Figure 2.7.10- Summary of effective stress conditions at maximum mobilised friction and at post-peak from CAUC and CIU triaxial tests, Tilbrook.

Both drained direct shear box tests (DS) and ring shear tests (RS) were carried out to determine the apparent peak and residual (large displacement) soil/soil and soil/steel friction angle. The shear box tests were carried out on both undisturbed and remoulded clay. The undisturbed specimens were oriented vertically and sheared under an axial stress corresponding to the estimated horizontal effective stress. Table 2.7.2 presents the test results in terms of apparent mobilised friction angles, δ and δ_{ss} on the assumed horizontal (radial) failure plane, as they were summarised by Lambson et al (199).

Table 2.7.2- Summary of apparent friction angles determined from direct shear (DS) and ring shear (RS) tests

Test type	Shear stress	Lowestoft Till		Oxford Clay	
		Soil/soil, δ	Soil/steel, δ_{ss}	Soil/soil, δ	Soil/steel, δ_{ss}
DS-Undist.	At peak	27.5	26.0	25.5	25.5
DS-Undist.	Residual	23.5	17.5	12.5	11.5
DS-Remoulded	At peak	25.0	22.0	22.0	20.5
DS-Remoulded	Residual	23.5	17.0	13.5	11.5
RS-Remoulded	Residual	27.5	16.0	13.5	11.0

The following observations can be made from these results:

- The apparent peak friction angle is 2-3 degrees lower for the Oxford Clay than for the Lowestoft Till.
- The residual friction angles are on the other hand as much as 10 degrees lower for the Oxford Clay than for the Lowestoft Till.
- The apparent peak interface soil/steel friction angles are 0 to 3 degrees lower than soil/soil values.
- For Oxford clay there is little impact of interface type on the residual apparent friction angle, but more so for the Lowestoft Till where a steel interface reduced the apparent friction angle by about 6 degrees.
- The ring shear tests gave essentially the same residual friction angle as direct shear tests.

The peak interface friction angles from the DS and RS tests of 25.5 to 27.5 degrees are as expected somewhat smaller than the average peak friction angle of 29 degrees derived from the triaxial tests.

2.7.3 Load test results

The results presented in the following have, unless otherwise stated, been extracted from the factual data reports by NGI (1989), McClelland (1988[b]) (LPDTC-test) and Ove Arup & Partners (1988) (LDPTT –test).

Figure 2.7.11 presents the normalised excess pore pressures of $\Delta u/\sigma'_{v0}$ and $\Delta u/s_{ud}$ as measured at the end of pile installation for all the piles. The excess pressures appear to be rather variable, but the trend is increasing normalised pressures with depth. Some points may be noted in relation to the pore pressure data:

- The lowest gauge at 12.61 m depth along the NGI-A pile is located very close to the pile tip. The relatively large excess pore pressure at this level, compared to the levels above, is most likely a 3D tip effect.
- An extreme low pore pressure was measured at end of installation for the gauge at 20 m depth along the LDPTC pile. As shown in Figure 2.7.12, the pore pressure increased substantially during the first 15 days after installation, and reached an average peak for the two sensors of 465 kPa. That pressure is very close to the values measured with the two free-field piezometers installed at 1 and 2 m distance from the pile surface at nearly the same depth (21m). By extrapolating back to time t=0, using a similar slope as the free field piezometers, the t=0 pressures at the pile wall is estimated to be around 700-800 kPa, corresponding to $\Delta u/\sigma'_{v0} = 1,86$-$2,21$. That is more in line with the other data in Figure 2.7.11.
- The low pore pressure at 20 m depth, and the subsequent increase in pore pressure with time, is most likely due to poor saturation of the piezometer filter. Coop and Wroth (1989) made similar observations in some small scale model pile tests in an OC clay deposit at Madingley. They suggested however, that in stiff clays the maximum excess pore pressure may occur at some distance from the pile wall, and that this will cause a tendency for increasing pore pressure at the pile wall during the reconsolidation phase. It is still hard to see why this was not observed at all levels at Tilbrook.
- For the NGI pile C, showing the lowest pressure at the 5m level, there seems to have been a sensor problem as the pore pressures were essentially constant throughout installation and testing, which is considered unreasonable.

The assumed trend lines for $\Delta u/\sigma'_{v0}$ and $\Delta u/s_{ud}$ in Figure 2.7.11 were selected such that they are mutually consistent with the assumed values of s_{ud}/σ'_{v0}. The trend lines suggest larger installation pressures for the LDPTC pile than for the NGI-piles. This is surprising considering that the upper part of the LDPTC pile penetrated in an open mode.

The measured total and effective earth pressures along the test piles also showed large variations. It may be noted that along the LDPTC pile, two of eight EP-gauges sensors were lost. For the NGI-piles A, B, and C a total of 3 of 16 effective EP gauges were lost and 2 of 10 total EP gauges. This means that at each level there may be 1, 2 or 3 sets of effective earth pressure data available along the different piles.
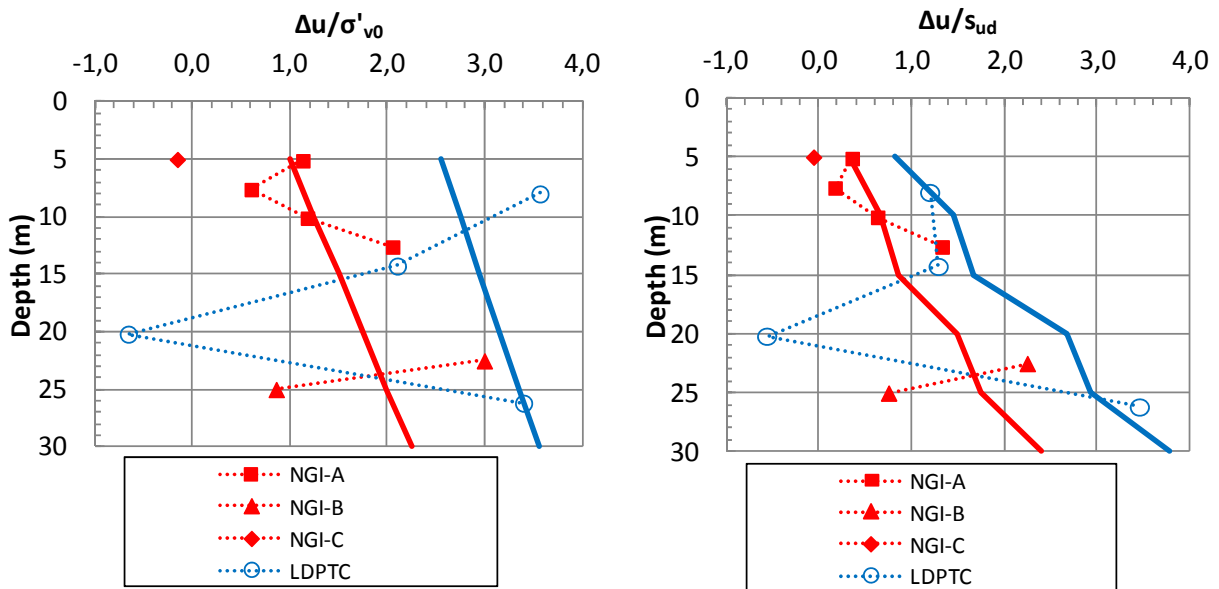
Figure 2.7.11- Normalised excess pore pressures at end of pile installation, Tilbrook
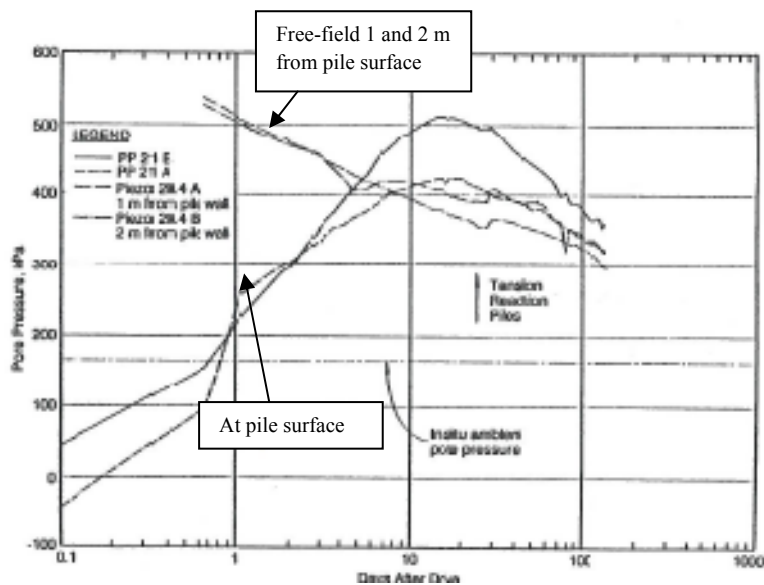
Figure 2.7.12- Measured pore pressures at 20m depth- LDPTC pile, Tilbrook (from Cox et al, 1993)

Figure 2.7.13 shows effective earth pressures, σ'_{hi} and effective stress ratio, K_i at end of pile installation. For the NGI piles the data marked NGI-A etc come from taking the difference between measured total earth pressure and pore pressure, and those marked NGI-dir are based on averaging the data from the two effective stress gauges at each level (if both were in operation). For the LDPT-C pile the data from the two total EP gauges and PP gauges were averaged.

Some of the effective earth pressures are apparently unreasonable due to unreasonable pore pressure. If for instance, the pore pressure at 20 m for the LDPTC pile is corrected by an assumed error in pore pressure of about 750 kPa, the effective pressure will fall more in line with the NGI-B data. It is apparent, however, that the LDPTC measurements of total earth pressure are too low at the upper two levels, leading to negative effective stress. As discussed earlier for the Onsøy and Lierstranda case, membrane arching effects may lead to measured pressures being too low.

After extraction of the NGI-piles it was for some effective earth pressure gauges observed a considerable drift in zero reading before and after pile extraction, corresponding to a pressure difference of 400-500 kPa (ref. NGI, 1989). In those cases the pressure based on an average of the before and after zero reading was assumed.

As discussed by Karlsrud et al (1993), the Tilbrook clays contain some fragments or pebbles of rock (chalk and flint) which could have caused local point loads and too large deduced earth pressures on some gauges, especially for the small diameter earth pressure membranes (20 mm) used on the NGI piles. The NGI-piles are also relatively slender. Any tendency for bending of the pile as a result of the rather heavy driving resistance could also cause uneven pressures around the pile. Where both effective earth pressure cells functioned, it was actually in most cases observed a substantial difference between pressures measured on the diametrically opposite cells. As an overall observation, there remains significant uncertainty in the observed earth pressure data.
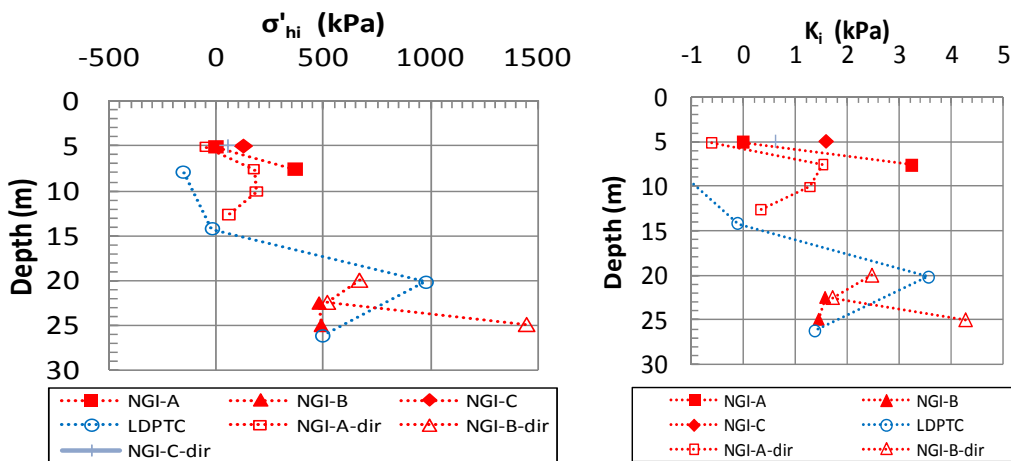
Figure 2.7.13- Measured effective earth pressures at end of pile installation, Tilbrook

Figure 2.7.14 shows curves of normalised pore pressure dissipation for the LDPTC-pile, and Figure 2.7.15 selected examples for the NGI A- and B-piles.
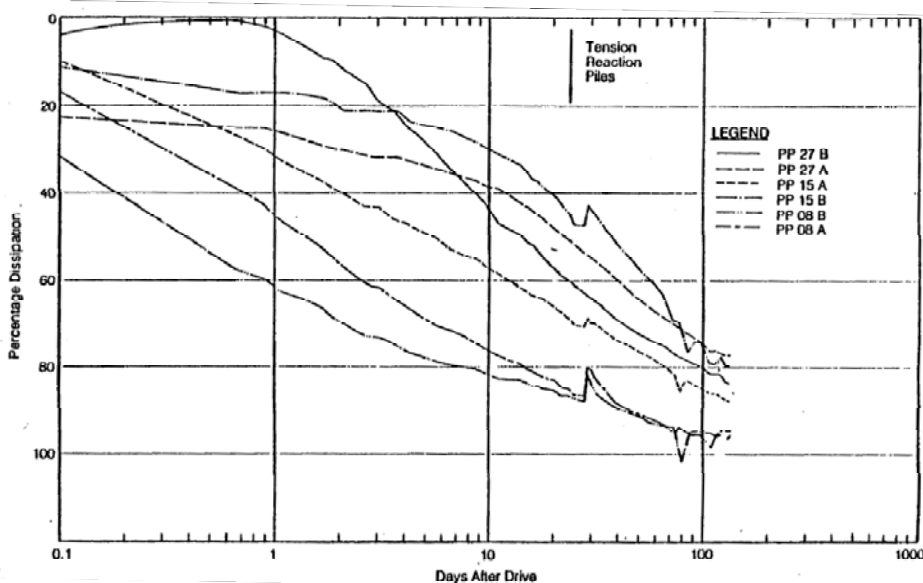
Figure 2.7.14- Pore pressure dissipation curves for LDPTC-pile, Tilbrook (after Cox et al, 1993)
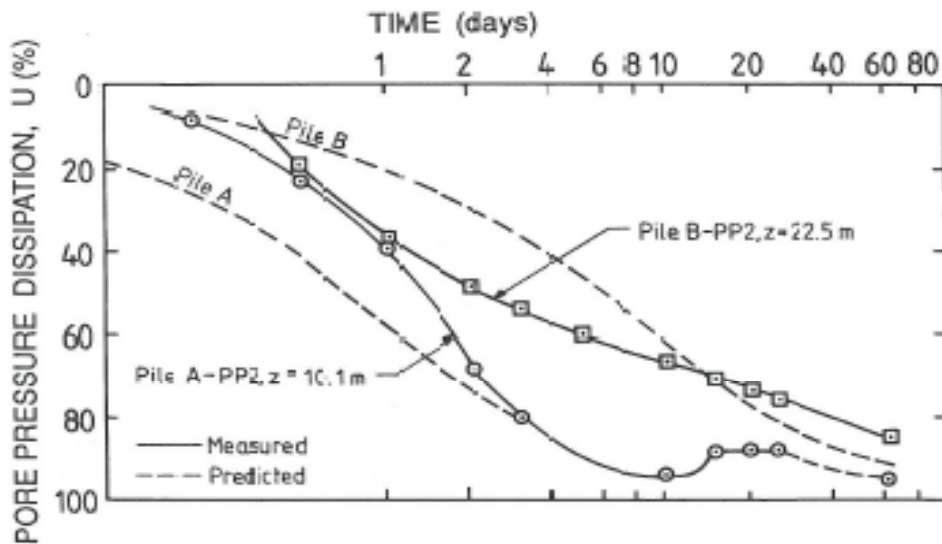
Figure 2.7.15- Example of observed pore pressure dissipation for NGI-piles, Tilbrook (after Karlsrud et al, 1993)

Figure 2.7.16 presents data for times to reach 50 and 90 % pore pressure dissipation. The t_{90} values were in most cases extrapolated from the trend in the dissipation curves (Figures 2.7.14 and 2.7.15). The reason for limited data for the NGI piles is uncertainty in the measured initial excess pore pressures (low or negative values and/or increasing pressure with time during the early phase). The same applies to the data from 20.4m for the LDPTC-pile. It should also be kept in mind that the data for the NGI-B pile at 12.6 m may to some extent be influenced by 3D tip effects.

At the time of pile loading the degree of consolidation lies in the range from 80 to 96 %, Figure 2.7.17. Only the data considered most reliable are presented here. Both Figure 2.7.16 and 2.7.17 suggest slower consolidation in the lower Oxford Clay than in the Upper Lowestoft Till.

During the reconsolidation phase it was observed both decrease and increase in total earth pressures, but on average there was relatively little change. The major changes occurred during the first few days after pile installation. This is in strong contrast to the pronounced reduction in total earth pressure which has been observed throughout the reconsolidation phase at the soft NC clay sites dealt with in Sections 2.2 to 2.6.
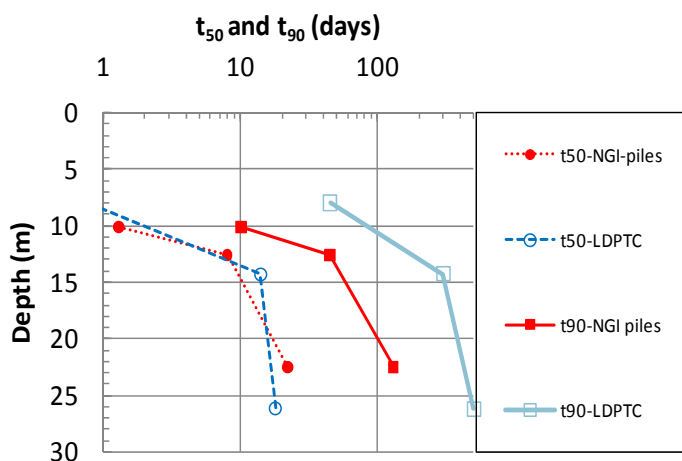
Figure 2.7.16- Observed times to reach 50 and 90 % consolidation, Tilbrook
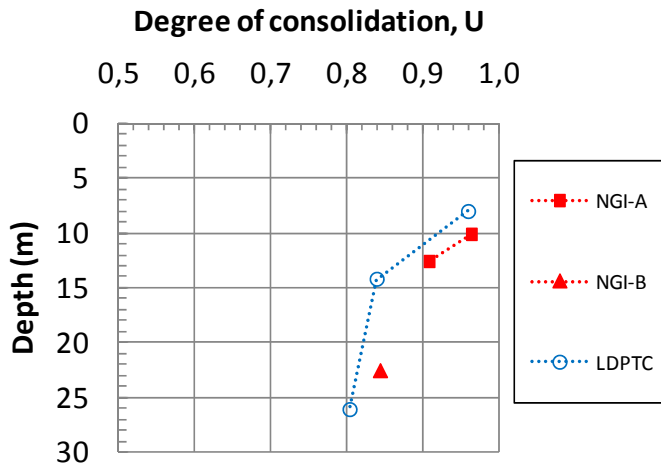
Figure 2.7.17- Degree of consolidation at onset of pile loading, Tilbrook.

Figure 2.7.18 presents the horizontal effective stresses measured at onset of the 1st load test on the different piles. Note that for the NGI-piles it is shown both directly measured effective stress values, as well as values obtained by taking the difference between measured total- and pore pressure. At levels where two effective stress EP gauges were intact, the average value for both of them was used.

The horizontal effective stress at U=100 % has at Tilbrook been estimated by simply assuming that the total horizontal stress would be the same as at the time of the load tests. Thus the increase in horizontal effective stress, from when the load test was carried out to U =100 %, corresponds to the remaining excess pore pressure at that time. This leads to effective stresses as presented in Figure 2.7.19. The corresponding measured or estimated horizontal effective stress ratios "At test" and "At U=100%" are for these two cases presented in Figure 2.7.20.
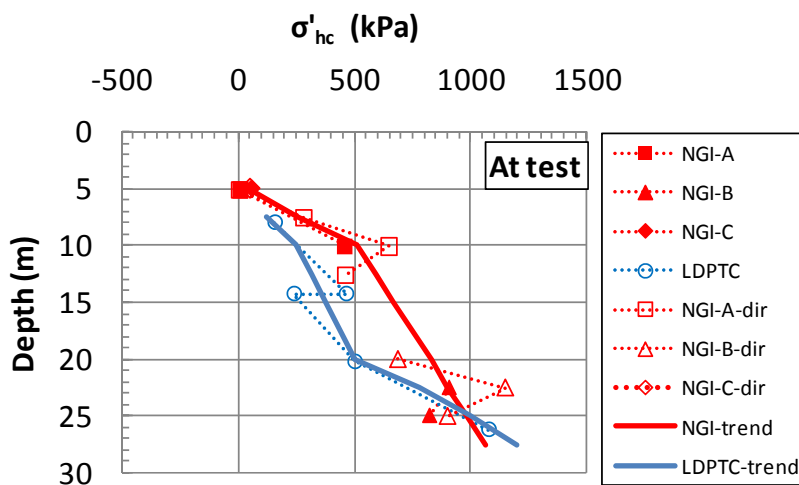
Figure 2.7.18- Measured effective stresses at onset of pile loading, Tilbrook.
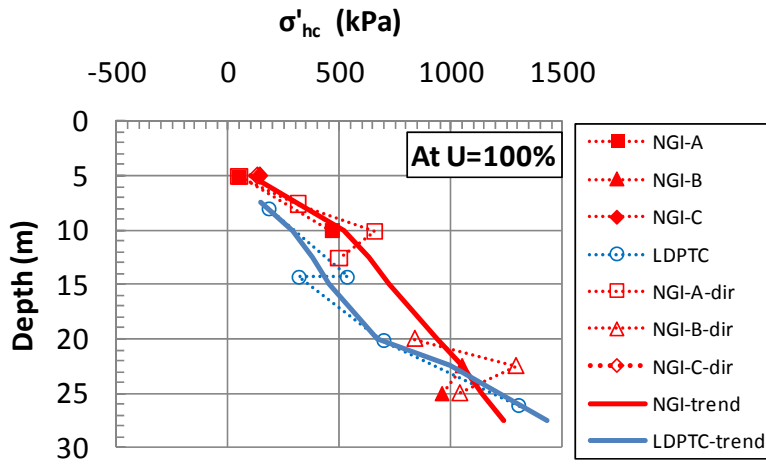
Figure 2.7.19- Estimated effective stresses at U=100%, Tilbrook

The data in Figure 2.7.20 suggest that, apart from the upper 7 m below ground, the closed ended NGI-piles gave K_c-values that are larger than the estimated in-situ K_0 and nearly constant with depth. A value of K_c around 3.0 may well reflect a limiting passive earth pressure coefficient. The main reason for the apparently lower K_c -values along the upper part of the LDPTC-pile is most likely that this penetrated in an essentially open mode. Along the lower part of the LDPTC-pile, which penetrated in a nearly fully plugged mode, the K_c -values agree well with the NGI-pile B.
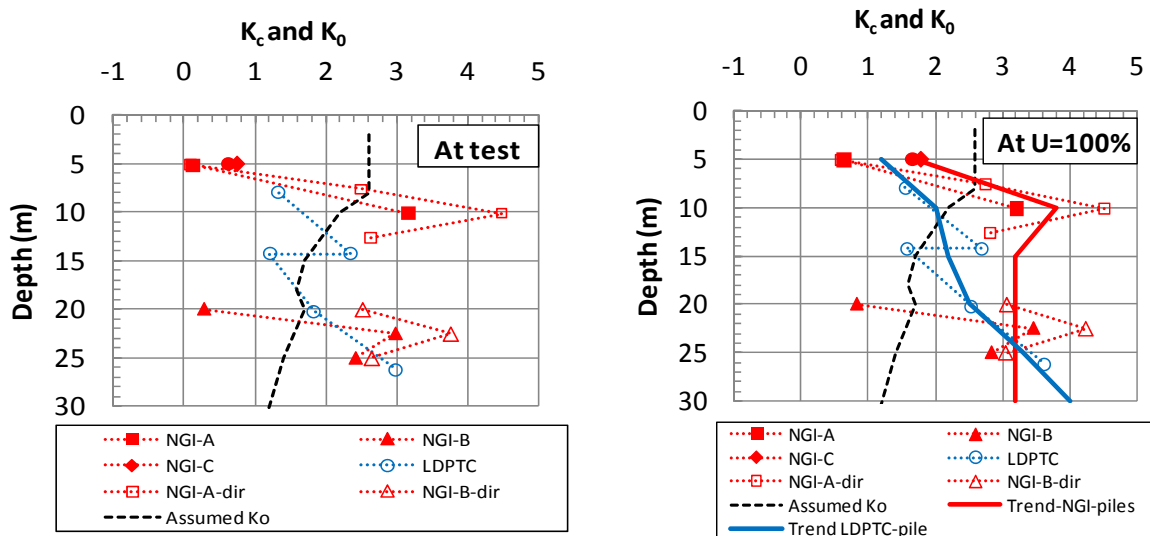
Figure 2.7.20 - Measured effective stress ratios, K_c , compared to in-situ K_0, Tilbrook

The LDPT piles were loaded to failure by application of a constant rate of displacement of approximately 1 mm/min. Figure 2.7.21 shows the measured load-displacement response for the LDPTC compression test carried out 134 days after pile installation. The peak load of 16.13 MN was reached at a displacement of about 28 mm. As the displacements were increased further, the load dropped and reached 14.21 MN at a displacement of about 120 mm.
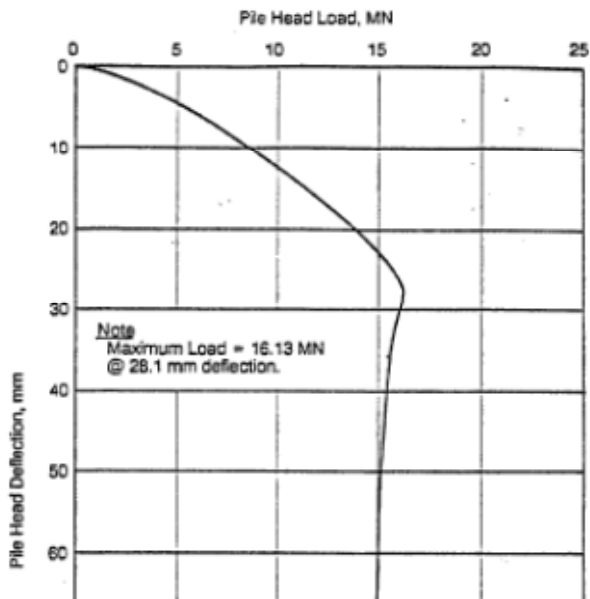
Figure 2.7.21- Measured load-displacement curve, LPTTC –pile, Tilbrook (after Cox et al. 1993).
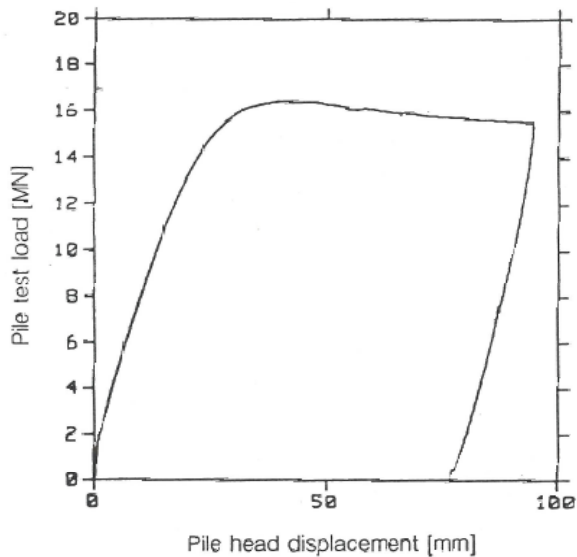
Figure 2.7.22- Measured load-displacement curve LDPTT (tension) test, Tilbrook (after Clarke et al 1993).

The LDPTT tension test was carried out 350 days after the pile was re-driven 0.5 m. The pile reached a peak load of 16.28 MN at a displacement of about 40 mm, which decreased to 15.92 MN at a displacement of 96 mm, Figure 2.7.22 .These loads are based on the uppermost strain gauge readings corrected for the weight of the reaction system of 0.38 MN as given by Arup (1988).

All the NGI-piles were load tested in an incremental load-controlled manner similar to the Onsøy, Lierstranda and Pentre tests. Figure 2.7.23 summarizes all the load-displacement curves based on the measured displacement at the end of each load increment, including the 2nd static load tests carried out 3 days after the first static and cyclic test series (see Table 2.7.1).
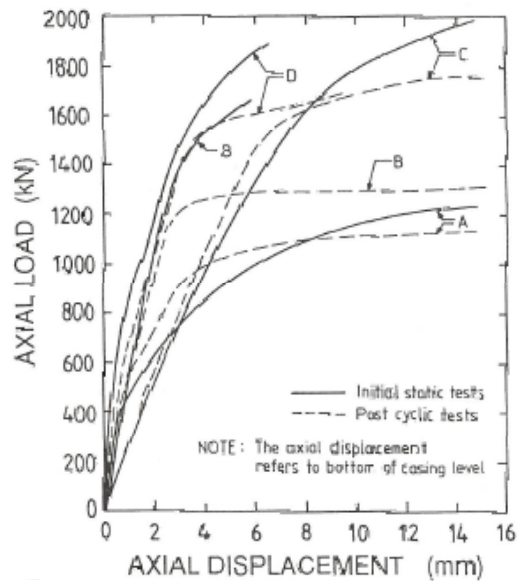
Figure 2.7.23- Load-displacement curves from static tests on NGI-piles, Tilbrook (after Karlsrud et al, 1993).

For the NGI-piles failure was defined the same way as for other NGI pile tests presented previously when the average rate of displacement during a load increment (lasting 2 minutes) exceeded 1 mm/min, giving ultimate failure loads as presented in Table 2.7.3. For test NGI-B, which was stopped slightly before that load level was reached, the failure load was extrapolated from the data. In contrast to pile test results from most other sites presented herein, the 2nd static test showed lower capacity than the first test. The reduction was largest for pile B located within in the plastic Oxford Clay. Thus in this case cyclic loading to failure followed by re-consolidation caused a permanent loss in ultimate static capacity. The second (post-cyclic) static tests showed on the other hand a stiffer response up to failure than the initial static tests. That is in general agreement with what has been observed at other test sites, e.g. NGI (1988).

Table 2.7.3 - Summary of defined total ultimate capacities for NGI-piles, Tilbrook (based on Karlsrud et al, 1992).

	Change in capacity after first test series					
	1st- Qus	Days after	2nd-Qus	Days after		Time diff
Pile	(kN)	inst	(kN)	inst	Ratio	(days)
NGI-A	1236	62	1143	65	0,92	3
NGI-B	1670	60	1382	63	0,83	3
NGI-C	1993	60	1950	63	0,98	3
NGI-D	1888	75	1656	78	0,88	3

To arrive at measured values of local shaft friction along the piles, the measured loads were corrected for the weight of the pile and the estimated tip resistance, as described previously for other sites. A few special aspects relating to how the shaft friction was determined in these specific cases should be mentioned:

- In the case of the LDPTC (compression) test there was a soil plug inside the lower 13.1 m of the pile. The interior shaft friction mobilised along this plug against the inside face

of the pile wall must be deducted from the measured pile forces to get the correct exterior shaft friction. This interior shaft friction is in the outset unknown, but is limited upwards by the tip resistance that can be mobilized at the bottom of the plug, subtracted the weight of the plug. It can then be shown that the average internal skin friction is limited upwards to a value of:

$$\tau_{is} = ((\sigma_{vtip} + 9 \cdot s_{udtip}) - \gamma_{plug} \cdot L) \cdot D_i / 4 \cdot L_P$$

σ_{vtip} = Total vertical stress at tip = 650 kPa

s_{udtip} = Undrained strength at tip = 462 kPa

γ_{plug} = Total unit weight of clay plug = 21,5 kN/m^3

D_i = internal pile diameter = 0.698 m

L_P = Plug length = 13.1 m

This leads to an average internal side friction of about τ_{is} = 60 kPa, which has been deducted from the measured total sum of internal and external shaft friction along the plugged part of this pile.

- The LDPTT tension pile was post-instrumented with strain gauges. Therefore, the residual loads along the pile after driving and later emptying are not known. Like in the Ove Arup (1988) report, and the papers by Clarke et al (1993) and Nowacki et al (1993), it was herein assumed that the residual load distribution was identical to that of the LDPTC-pile. The maximum residual load was actually about 1.6 MN at a depth of 12 m.
- In the case of both the LDPTC and LDPTT piles, the shaft friction was computed from the actually reported (measured) axial loads rather than using the deduced shaft friction values presented in the relevant reports and papers. Notice in this connection that McClelland (1988) stated that they slightly adjusted the measured loads to: "give a smooth curve that eliminates abrupt, and unrealistic, changes in the load curve".
- In the case of the LDPTT pile no such smoothing had been undertaken. The data from the strain gauges at 2.5 m depth showed however an unreasonably high load of 17.5 MN at peak load, or about 1.3 MN above the load measured by the load cell at the pile top. The strain gauges at 1.0 m depth also showed somewhat larger load (about 0. 3 MN) than the load cell on top. The data above from 2.5 m depth have therefore been neglected when computing the shaft friction.
- In the case of the NGI-A and C piles the telescopic joint at the end was assumed to give zero load at this level. The casing pile D was also assumed having no contribution from tip resistance.

Figure 2.7.24 presents the deduced ultimate shaft friction values for all the piles at the time of testing. For the LDPPT-pile both the shaft friction deduced herein (LDPTT-KK) and a curve (LDPTT-Ar) presented by Arup (1988) are shown. They agree well on average. The humps in the LDPT-KK curve seem to some extent to reflect the highs and lows in the assumed undrained strength profile.

Two curves are also presented for the NGI-D non-instrumented casing pile. One curve averaging the shaft friction over the entire pile length, the other assumes that the shaft friction distribution is increasing with depth similar to what is suggested from the NGI-A and C pile tests.
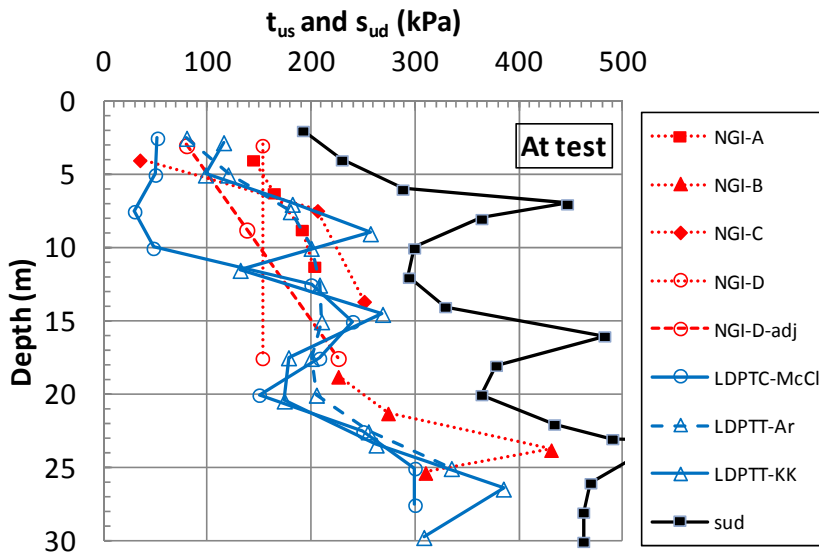
Figure 2.7.24- Measured ultimate shaft friction at time of loading for all pile tests, Tilbrook

The ultimate shaft friction at U=100 % have been estimated in a different manner compared to the direct correlation to the degree of consolidation used for the sites presented earlier. The procedure used was based on the assumed idealised relationship between τ_{us} and σ'_{hc} at the time of the test as presented in Figure 2.7.25, and that a subsequent increase in effective stress to U=100 % would give a shaft friction that increased in accordance with the same relationship. This means that the following expression was used to determine the τ_{us} value at U=100 %:

τ_{us} (at test) $= 0.18 \cdot (\sigma'_{hc}+600)$

τ_{us100} (at U=100%) $= \tau_{us} \cdot (\sigma'_{hc100}+600) / (\sigma'_{hc}+600)$
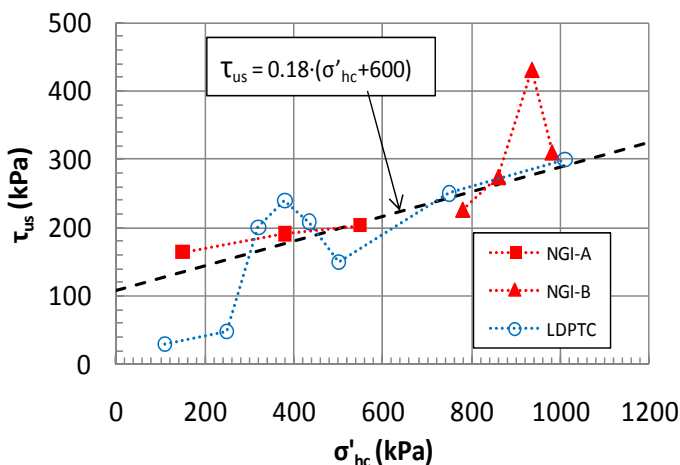
Figure 2.7.25- Ultimate shaft friction in relation to horizontal effective stress at onset of pile loading, Tilbrook

The correction factor typically corresponds to 2 % for the NGI-A and C piles, 8 % for the NGI-B pile, and 5 to 15 % for the LDPTC-pile. The deduced τ_{us} values at U =100 % are presented in

Figure 2.7.26 and the corresponding α and β-values in Figures 2.7.27 and 2.7.28 . For clarity, only the LDPTT-KK data are presented for the LDPTT-pile and only the NGI-D-adj for the NGI-D pile.
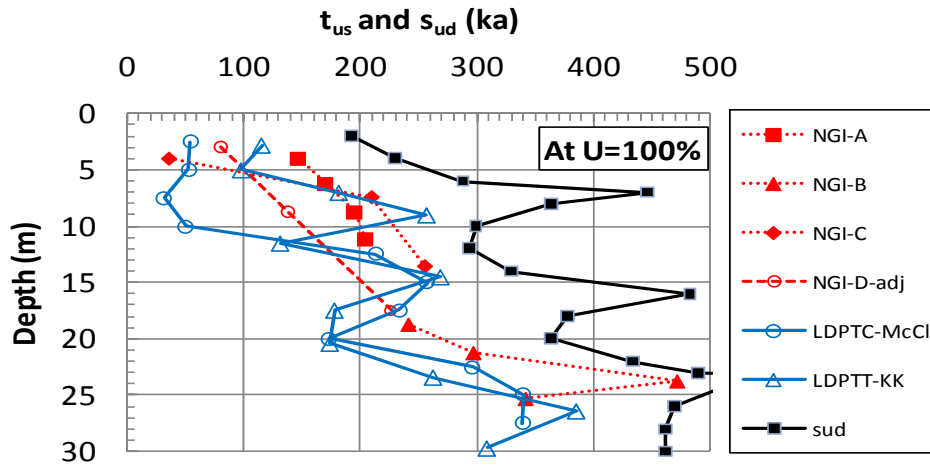
Figure 2.7.26- Ultimate shaft friction corrected to U=100 %, Tilbrook
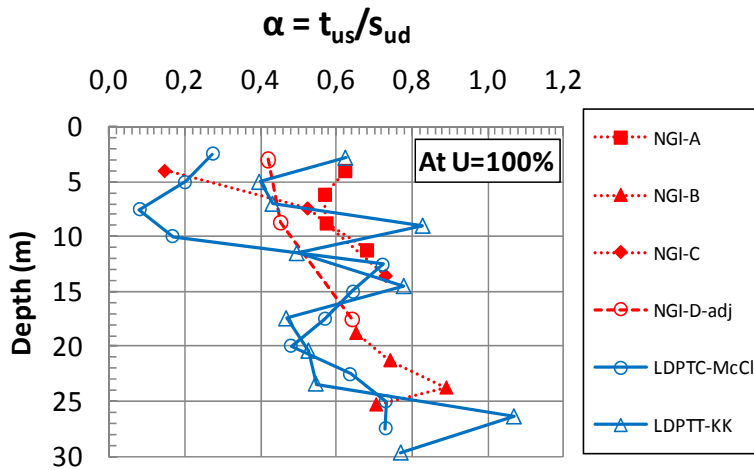
Figure 2.7.27- Measured α-values corrected to U=100%, Tilbrook
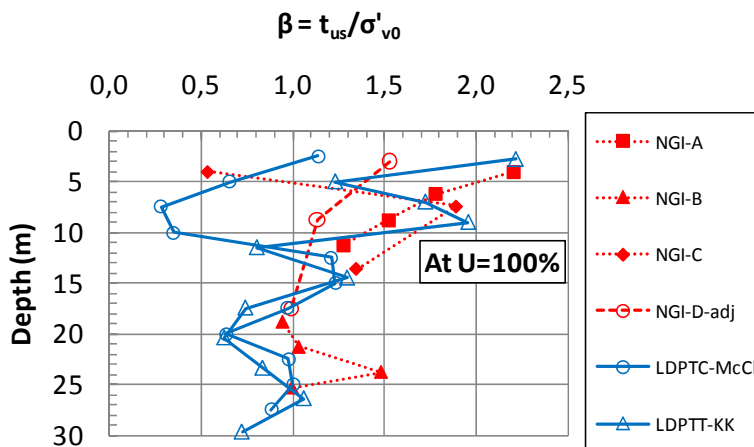
Figure 2.7.28- Measured β-values corrected to U=100%, Tilbrook

Table 2.7.4 compares the total shaft friction calculated assuming α=1.0 to what was measured. On that basis an average α-value has been calculated for each pile. Note that the measured failure loads given in Table 2.7.4 were computed from the total failure loads corrected for the weight of

the pile and plug, and for tip resistance as relevant for each case. The measured values have also been corrected to U=100%. When looking at the individual piles, the average α-values in Table 2.7.4 appear to be in good agreement with the average values in Figure 2.7.27 computed from the measured loads down along the piles.

Table 2.7.4 - Calculated total shaft friction, Q_{us}, and average α-values at U=100% for all piles, Tilbrook

Pile	Measured at test (kN)	Average correction factor	Estimated for U=100% (kN)	Calculated for α=1.0 (kN)	Av. α-value for U=100% (kN)
NGI-A	1185	1,02	1209	2058	0,587
NGI-B	1705	1,08	1841	2388	0,771
NGI-C	1990	1,05	2090	3757	0,556
NGI-D	1930	1,02	1969	4655	0,423
LDPTC	14370	1,1	15807	26544	0,596
LDPTT	15905	1	15905	27645	0,575

It should be specially noted that the α–values given herein are typically 10-25 % higher than those previously presented by Karlsrud et al (1992) and Nowacki et al (1992). This is mainly due to the lower undrained shear strength values assumed herein compared to these previous studies.

A few key observations regarding measured the shaft friction for the different piles may be noted:

- The shaft friction values fall more or less in the same range for all the piles. The only main exception is the upper 10-15 m of the LDPTC pile, suggesting much lower shaft friction than all other piles in this depth range.
- When comparing average α-values, the LDPTC pile and LDPTT pile agree on the other hand very closely. This could suggest that the low shaft friction along the top part of the LDPTC pile is not correct and due to measurement errors.
- The closed-ended NGI pile B located within the Middle Oxford clay suggests on average about 15 % higher shaft friction than the corresponding values for the LDPTC and LDPTT piles at the same level. As the LDPT-piles penetrated in a nearly fully plugged mode during pile penetration through the Middle Oxford clay, this apparent difference cannot be related to open (non-plugged) versus closed (or plugged) pile penetration.
- The NGI open-ended casing pile D shows the lowest average shaft friction and corresponding α-values of all the piles (Table 2.7.4). This may reflect a lower shaft friction due to the fully open mode of penetration of pile D as compared to the other piles. However, as suggested by Nowacki et al (1993), the relatively low shaft friction for pile D could also be caused by pile B "whipping" inside pile D during driving, causing lower horizontal stresses against the surface of pile D than for the other piles.
- The main purpose of NGI pile C was to see if there was any effect of length of pile driven beyond a point in the ground as compared to pile A. The average α-values found for pile C were very similar to pile A, and thus, suggest no pronounced length effect for this case.

Figure 2.7.29 summarizes normalised t-z curves for all the piles. As for previous cases, the local displacement was derived from the pile top displacement by correcting for the theoretical elastic

displacements of the piles down to the level of the measured local shaft friction. The normalised displacement to reach peak shaft friction mostly lie in the range 1 to 2 %.

During pile loading it was observed both increase and decrease in pore pressure up to failure, Figure 2.7.30, without any clear systematic trend. As seen in Figure 2.7.30 the change in horizontal effective stresses during pile loading were also fairly small compared to the level at start of testing (Figure 2.7.18). Figure 2.7.31 shows the absolute measured effective stresses at pile failure, and Figure 2.7.32 the measured shaft friction versus effective stress at failure using the trend lines for in Figure 2.7.31 as basis.
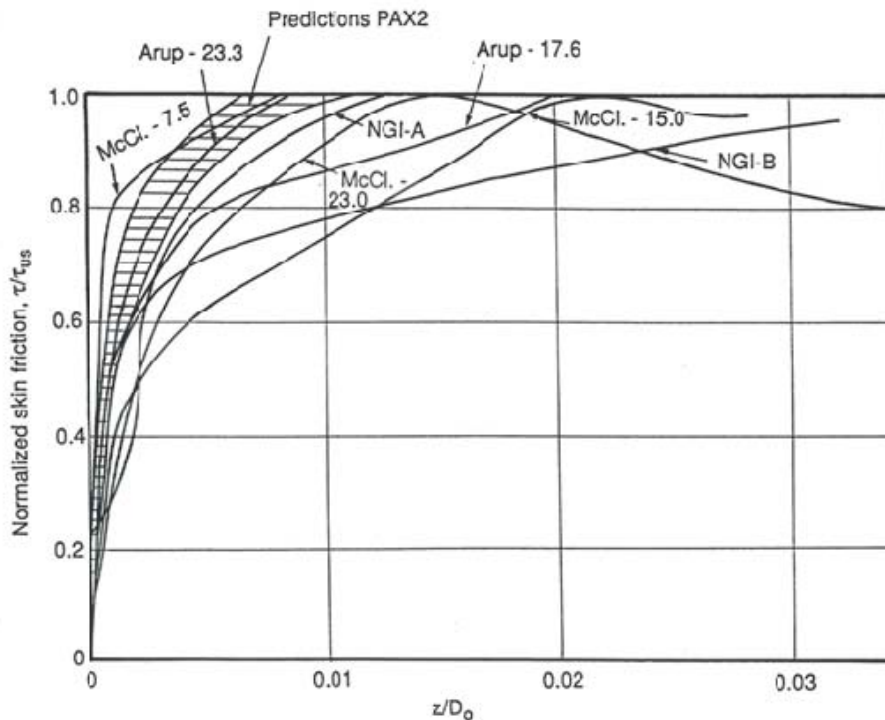
Figure 2.7.29 - Summary of normalised t-z curves for all piles, Tilbrook (after Nowacki et al, 1993)
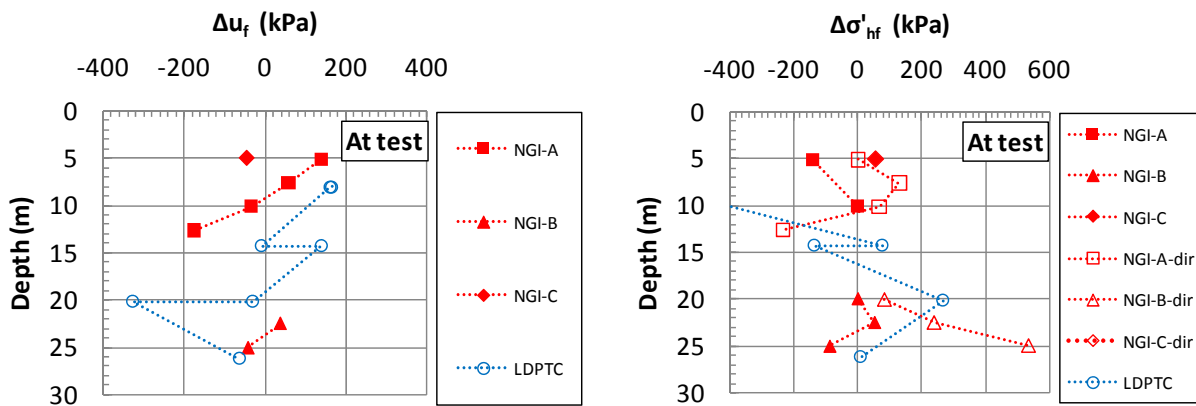
Figure 2.7.30- Changes in pore pressure and effective stress against the pile surface during pile loading, Tilbrook
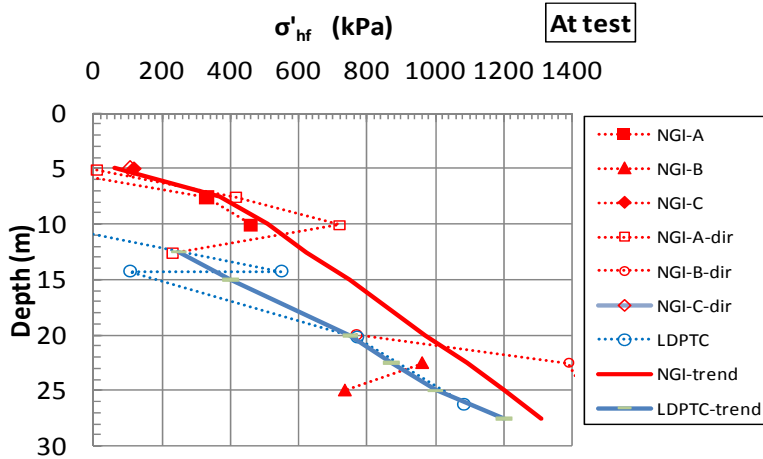
Figure 2.7.31- Measured horizontal effective stresses at pile failure, Tilbrook

It appears that the best fit between shaft friction and the effective stress at failure is much the same as against the effective stress at onset of pile loading (Figure 2.7.25.), and given by:

τ_{us} (at test) $= 0.18 \cdot (\sigma'_{hf} + 600)$

An alternative fit may be made assuming no "attraction" or cohesion intercept, and a different relationship for the upper Lowstoft till compared to the lower Middle Oxford clay. This gives the following typical values:

Lowestoft Till: τ_{us} (at test) $= 0.50 \cdot \sigma'_{hf}$, which implies apparent mobilised friction angle of $\delta = 26.6^0$

Oxford Clay: τ_{us} (at test) $= 0.27 \cdot \sigma'_{hf}$, which implies apparent mobilised friction angle of $\delta = 15.1^0$
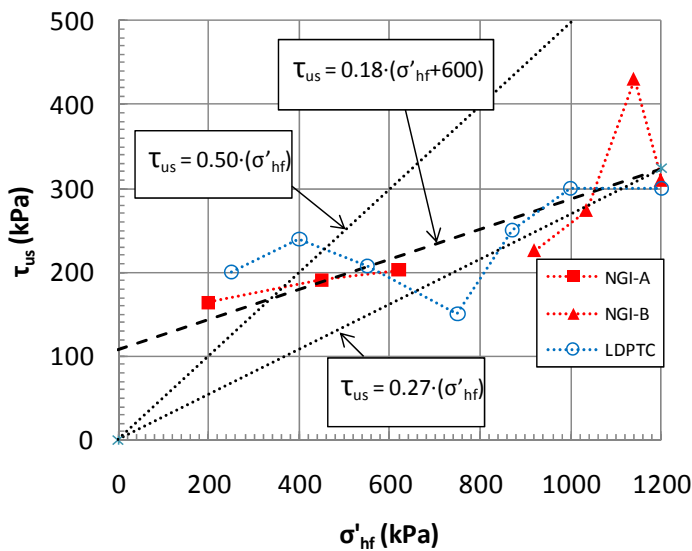
Figure 2.7.32 – Ultimate shaft friction in relation to horizontal effective stress at failure, Tilbrook

2.8 Hamilton Air Force base

As part of the ESACC Project (Effective Axial Capacity Cooperative) organized by Amoco Production Company, a pile test program was carried out in soft San Francisco Bay mud at the Hamilton Air Force base in California. The test program and detailed results were presented by Woodward-Clyde (1979), and summarized by Kraft et al (1980).

The ground level at the site is about 1.3 m below sea level, but protected by a dike against flooding. As seen from Figure 2.8.1, below an upper weathered crust extending to a depth of about 4 m, there is soft and essentially normally consolidated clay with water content of w=95-97 % and plasticity index of 55 %. The ground water table varies seasonally but was assumed at about 1.5 m depth during pile testing. Two piezometers installed at depths of 6.1 and 12.2 m showed somewhat artesian conditions below the assumed water table, Figure 2.8.2. Five incremental oedometer tests carried out on samples judged to be of good quality, suggested OCR = 1.4 below the upper crust. In this respect the author upgraded the p'_c - values from the standard IL tests by 10 % to correspond with CRS tests.

The oedometer tests showed a modulus number of m_0 =5.0 below the upper crust. The in-situ vertical permeability values given in Appendix 1 were typical average values back-calculated as part of this study. This was based on the reported coefficient of consolidation, c_v, at a stress level of about $(1.5-2) \cdot p'_c$, and correcting for the measured volume change, assuming a permeability change index of β_k=3.0.
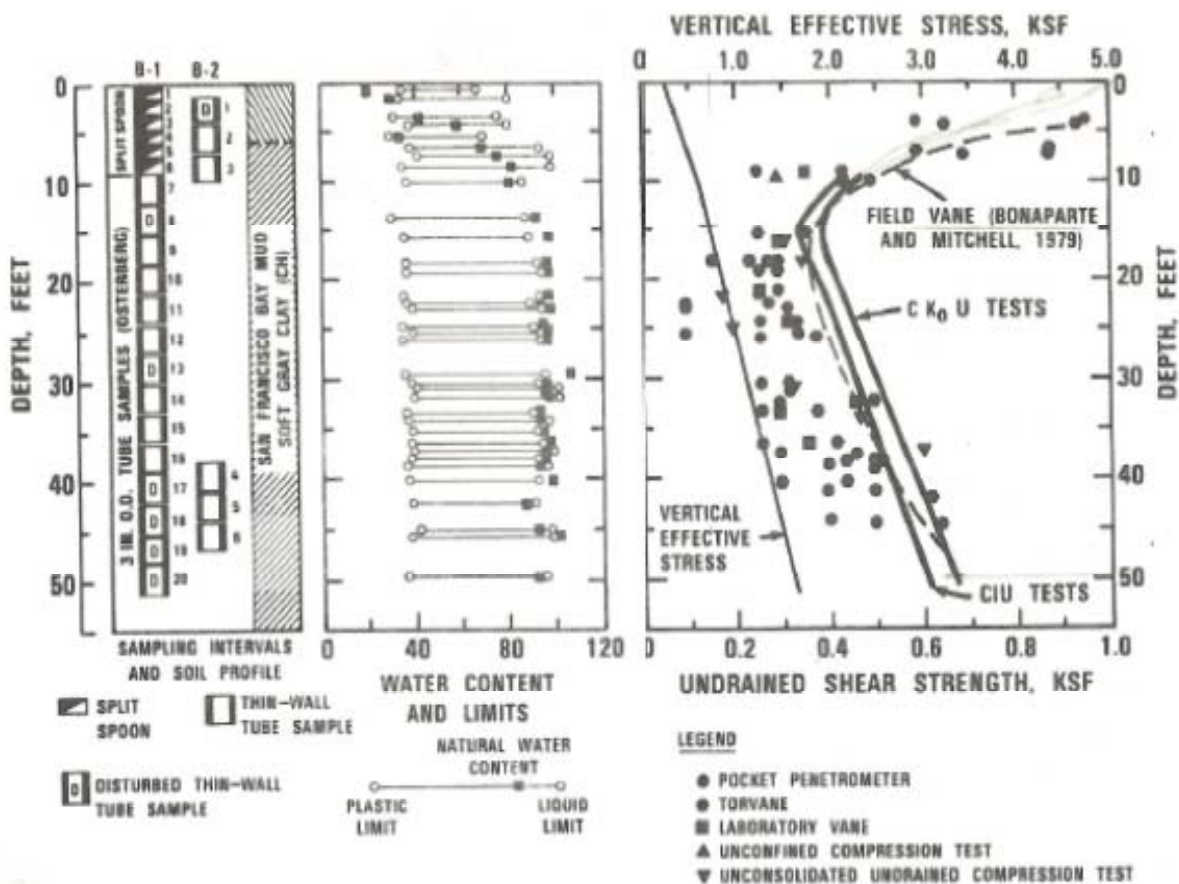
Figure 2.8.1- General soil profile, Hamilton (from Kraft et al, 1980)

A series of CAUC SHANSEP type consolidated undrained triaxial tests were carried out on the clay. The results suggested typical values of S=0.355 and m=0.86 for this clay. This was used in combination with the assumed OCR-profile to establish the assumed s_{uc} profile in Figure 2.8.3. It may be observed that the author's s_{uc} values are about 10-15 % higher than the corresponding strength profile presented by Kraft et al (1980), Figure 2.8.1. For this high plastic clay the author assumed $s_{ud} = 0.8s_{uc}$.
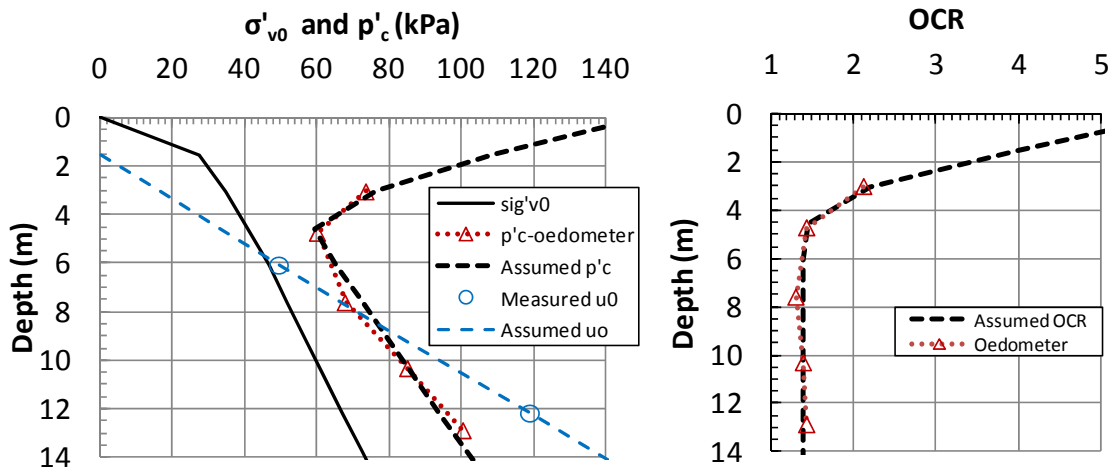
Figure 2.8.2- In-situ stress conditions, Hamilton
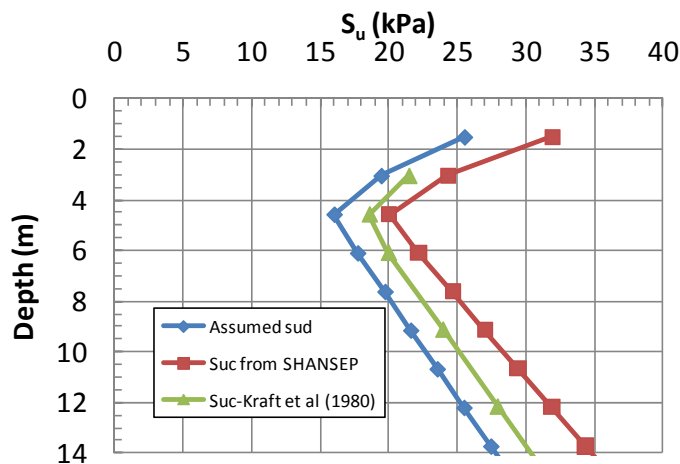
Figure 2.8.3- Assumed undrained strength profile, Hamilton

Four different test piles were installed at the Hamilton site, Table 2.8.1. They all had diameter of 111.9 mm and were installed to tip penetration of 12.19 m below ground. The two closed-ended instrumented piles had modules to measure axial loads at 7 levels, two diametrically positioned pore pressure gauges at 3 levels and earth pressure gauges at 2 levels, Figure 2.8.4. Kraft et al (1980) reported considerable drift in zero readings for measured vertical loads and total earth pressures upon retrieval of the piles, and therefore concluded that such data should be disregarded or treated with caution.

Table 2.8.1- Overview of pile tests and measured shaft friction, Hamilton

Test pile	Type	Installation	Instrumented	Q_{us} (kN)	Average τ_{us} (kPa)	Average α	Average β
TP1	Closed	Jacked	Yes	72,7	16,6	0,780	0,370
TP3	Closed	Driven	Yes	46	10,5	0,493	0,234
TP2	Open	Driven	No	43,8	10,0	0,470	0,223
TP4	Cookie- cutter	Driven	No	59,4	13,6	0,637	0,302

The "cookie-cutter" of pile TP4 a is just acutting edge at the front of the open which has slightly smaller diameter than the the rest of the pile, as illustrated in Figure 2.8.4.

The excess pore pressures generated against the pile shaft at end of installation – which are presented in Appendix 1 – exclude the sensor just behind the pile tip. The normalised values of $\Delta u_i/s_{ud}$ are on the low side of data from other soft clay sites. In this connection it may be noted that the pore pressures increased during the first 1-2 minutes after end of installation. This may suggest that the piezometer filters were not fully saturated, and therefore responded poorly during the initial phases.

Two free field piezometers were installed at normalised distances of r/r_0 of about 7.5 to 20 from the pile surface of the jacked and driven instrumented piles. They suggested a linear decrease in excess pore pressure with $\log(r/r_0)$, and becoming zero at about $r/r_0 = 20$ (jacked) and $r/r_0 = 30$ (driven).

The total horizontal stress at end of installation suggested a positive effective stress corresponding to $K_i = 0.30$ to 0.78, but if the excess pore pressures are too low, these normalised effective stress ratios would be too high.

The total earth pressure was reduced by a factor of about 2 during the re-consolidation phase, similar to what has been observed of other soft clay sites. In some cases the measured values became erratic and unstable towards the end of the re-consolidation phase, making it difficult to select precise values. It is possible that this reflects that some bending of these rather slender piles have occurred during pile installation. Where both sensors at opposite sides of the pile functioned, they tended to show quite different values towards the end of re-consolidation phase, especially for the driven pile. The K_c- values given in Appendix 1, ranging from 0.48 to 0.79 should therefore be considered more indicative for this case, but an average value corresponding to $K_c = 0.7$ may be considered more reliable.

The failure loads given in Table 2.8.1 refer to the first load test carried out after complete re-consolidation. All piles were first time loaded in compression. Only the shaft load is presented, which was arrived at by deducting an estimated net effect of pile weight and tip resistance of 2 kN from the total load at failure. The data show a very large difference in ultimate capacity for the different piles, the jacked pile giving the highest capacity and the open driven the lowest. Kraft et al (1980) observed that the capacity decreased with increasing energy used to get the different piles into the ground. Although the piles were driven through a form of pile guide, another explanation may be that these rather slender piles would be subjected to some "whipping" effects as also discussed in relation to some of the the Onsøy Tilbrook pile tests.
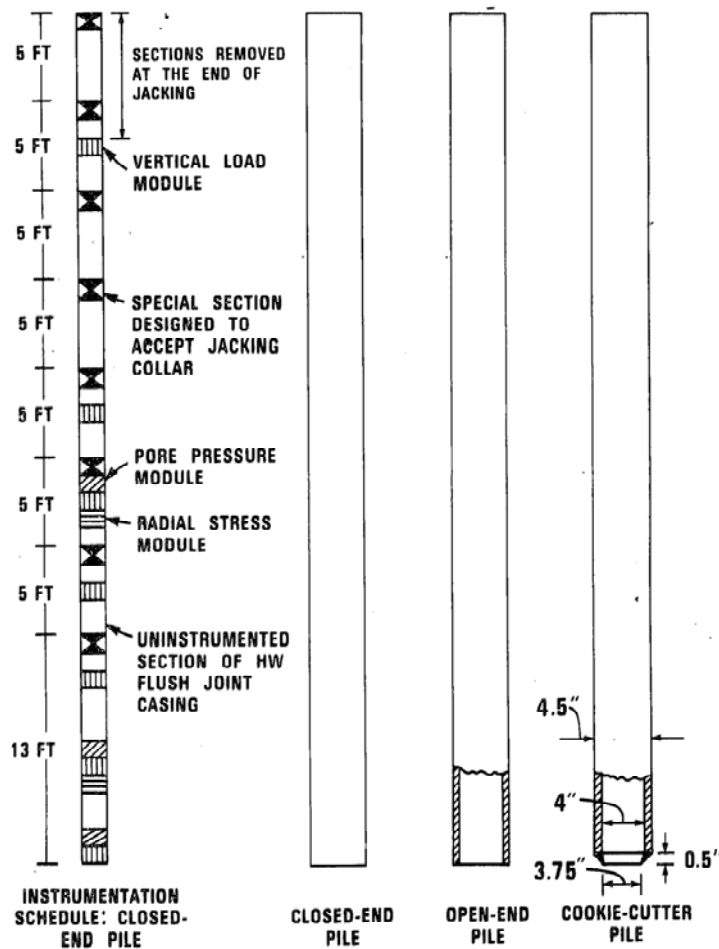
Figure 2.8.4 – Schematic layout of pile instrumentation, Hamilton

Only the average shaft friction values for the jacked and driven pile are included in Appendix 2. In this connection it should be mentioned that the relatively high strength and correspondingly high normalised strength and OCR values along the upper 1/3 of the pile, makes it somewhat difficult to calculate representative average values for the entire pile length. The basis for the values given in Appendix 2, was first to calculate actual average values along the entire pile length of the absolute strength, effective stress and apparent pre-consolidation pressures. The average normalised strength and OCR values were then calculated.

The ultimate load was reached at a pile top displacement of about 4 mm. For the loads in question the elastic compression of the pile would be around 1 mm, giving a typical local displacement at failure of 3 mm, corresponding to z_f/D =2.6 %. The piles showed some tendency for post-peak reduction in capacity, and were typically reduced by 10% at 25 mm displacement.

All test piles were after the first compression test at the end of re-consolidation, subjected to new compression and tension tests to failure. Although the capacity for all piles tended to reduce upon such repeated load testing, the results suggest little or no difference in capacity for loading in tension and compression. The non-instrumented pile, as well as the cookie-cutter pile, partially plugged during installation, and are therefore not conclusive with respect to impact of ideal open versus closed penetration at this site.

2.9 Other tests with the IC-model pile

2.9.1 Overview of IC-tests

The IC-model pile described in Section 2.6 (Pentre) has been used at three other clay sites in the UK, namely in overconsolidated London clay at Cannons Park (CP), in a glacial till clay at Cowden (CW), and in a more recent and softer marine clay deposit at Bothkennar (BK). As discussed by for instance Chow (1996), the instrumentation has over the years undergone some improvements, and the earliest version had only three instrumented sections.

A main focus of these various Imperial College load testing programs has been to study the relationship between shaft friction and effective stresses measured against the pile surface, and compare that to effective friction angles as measured in ring shear tests. Impact of installation procedure (jacked vs. driven and rate of jacking), compression versus tension loading, and impact of rate of loading, has also been studied at these sites. Detailed results from these test programs have been presented by Bond (1989) –CP, Lehane (1992) - CW and BK, and a series of papers and other publications, some of which will be referred to in the following.

Key soil parameters and pile load test results have been reviewed and to some extent reinterpreted as part of this study. The following gives only a short presentation of key results, and what interpretations that deviates the most from what have been published previously. Only first time testing of the different test piles are used in this study.

The selected parameters and test results are summarized in the tables in Appendix 1 (installation and re-consolidation phase) and Appendix 2(loading phase).

2.9.2 Cannons Park (CP)

Factual pile results and soils data were primarily selected from a report by Bond & Jardine (1990) and a later paper by Bond &Jardine (1995). At the test site there is so-called disturbed London clay to a depth of 4.1 m and Intact London clay below. The natural water content lies around 30 %, and the plasticity index is typically 60 % along the top part of the pile and 40 % along the bottom part.

Figure 2.9.1 presents the interpreted undrained shear strength profile and corresponding OCR. These were primarily arrived at by using the reported CPTU tip resistance as basis, and the CPTU correlations between q_t and s_{uc} proposed by Karlsrud et al (2005). The cone factor depends on OCR, which Bond & Jardine (1990) suggested could vary within wide limits. It was therefore chosen to back-calculate OCR from the assumed s_{uc} using the SHANSEP equation (2.5.1) with S=0.3 and m=0.85. Iterations were carried out until there was correspondence between calculated and assumed s_{uc} and OCR. Considering that this is a high plastic clay, it was assumed that $s_{ud} = =0.75s_{uc}$ throughout. The assumed s_{ud} values are 15-20 % larger than the peak undrained strength profile proposed in Bond & Jardine (1990, 1995). The OCR values are a factor of 2 or more lower.

The piles at CP were jacked through a 2 m deep pre-installed casing to a tip penetration of about 6 m depth for most of the 6 instrumented piles tested. Herein only the results of load testing of test piles CP2C (Compression) and CP4T (Tension) are used. They were load tested respectively 20 and 63 days after installation.
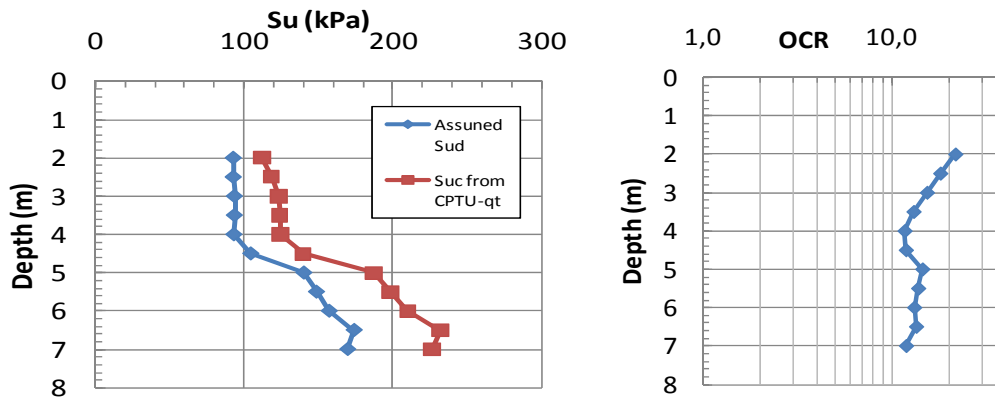
Figure 2.9.1– Interpreted undrained strength and OCR profiles, Cannons Park

During pile jacking it was generally recorded negative pore pressures for the following (F) and trailing (T) sensors, and rather large radial stresses and apparent shaft friction. The shaft friction during jacking that was reported to be of similar magnitude as during the later pile loading, but this can partly be contributed to rate of loading effects. The jacking rate was about 500 mm/min for the standard "fast jacked" piles whereas the pile loading rate was about 3 mm/min towards the end of the test when large creep displacements occurred.

During the re-consolidation phase the total radial stress only reduced by about 5-15 %. Prior to pile loading the radial effective stresses showed fairly large scatter. The typical values selected in Appendix 1 are therefore associated with a fair amount of uncertainty, but suggest K_c-values around 4.0. The average shaft friction at failure was quite similar for the compression and tension piles, and typically corresponds to $\alpha=0.71$ and $\beta=1.48$.

The peak shaft friction was observed at a local displacement of about 3 mm, but dropped rapidly off after peak, to a value about 30 % lower.

Following testing a trench was excavated next to one of the jacked and driven piles and block samples were cut out for detailed examinations. It was in this case observed a vertically oriented clay fabric close to the pile surface, with a tendency for forming a highly polished surface next the slow-jacked pile. The driven pile showed however, less evident vertical orientation than the slow-jacked pile. It could not be observed any pronounced variation in water content with radial distance for the pile surface, which is in strong contrast to what has been observed for soft clays.

2.9.3 Cowden

Cowden is a test site with glacial till that has been used as a research site by The Building Research Establishment (BRE) since the 1980's. The site conditions and pile test results were summarized by Lehane (1992), Jardine and Lehane (1993), and Lehane and Jardine (1994).

The glacial till clay has a water content of typically 16-18 % and plasticity index of about 20 %. The clay contains some fragments of chalk and flint within its matrix. Figure 2.9.2 presents interpreted undrained strength and OCR profiles for the site.
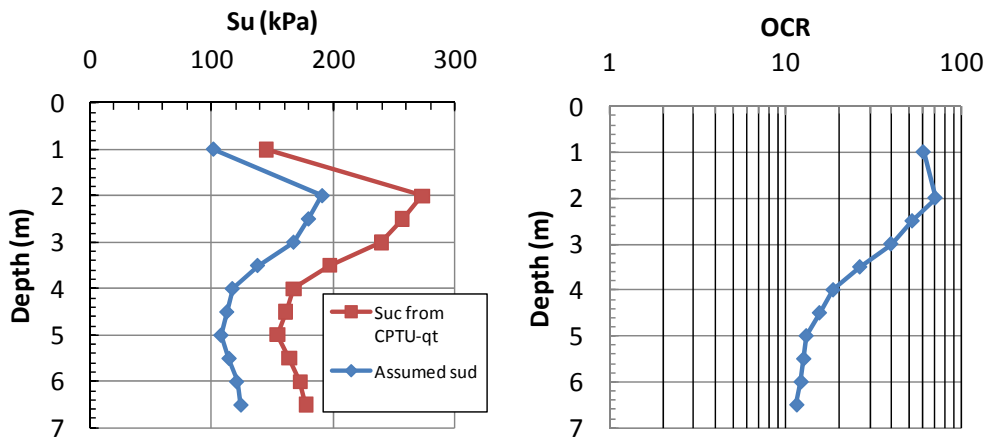
Figure 2.9.2 – Interpreted undrained strength and OCR profiles assumed for Cowden

The undrained strength and OCR values were also at this site interpreted on basis of CPTU data, using the same procedure as for the CP site. Due to the lower plasticity index the SHANSEP factors were in this case taken as S=0.28 and m_0 =0.8. The anisotropy ratio was taken as s_{ud} /s_{uc} =0.70.

Notice that at Cowden there is a rather stiff layer around a depth of 1.0 to 3.5 m. The selected s_{ud}- profile is quite close to the UU strength profile presented by Lehane and Jardine (1994), but the SHANSEP interpreted OCR values are higher than theirs below 3 m depth.

At CW the casing extended to about 2.5 m depth, and the test piles penetrated to depths of 5.95 to 6.35 m. Herein, only the results from testing of piles CW2C, CW4C and CW3T are used. During jacking it was in general observed a reduction in pore pressure, but within some minutes after end of jacking the pore pressures increased to well beyond in-situ level and then tapered off with time as expected. The excess pore pressures given in Appendix 1 refer to the maximum value observed after some minutes following pile installation. The measured total radial stresses reduced 10-20 % during the later parts of the re-consolidation phase, much like at CP. It was also in the case reported shaft friction during jacking that was of similar magnitude as during the later pile loading.

At the end of re-consolidation the radial effective stresses also in this case showed a fair amount of scatter, but neglecting the Leading instrument unit, it was typically observed $K_c \approx 3.9$, much like at CP. As presented in Appendix 2, the average shaft friction at failure for the compression piles typically corresponds to α=0.88 and β=1.77, but was about 26 % lower for the tension pile (α=0.58 and β=1.15).

The peak shaft friction was observed at a local displacement of about 2 mm, but dropped only slightly off after peak.

2.9.4 Botkennar (BK)

Factual pile results and soils data were primarily selected from a report by Jardine & Lehane (1993) and a later paper by Lehane and Jardine (1994). The clay at the Bothkennar (BK) test site is believed to have been deposited in a marine/estuarine environment. The natural water content increases gradually from about 40 % at 1 m depth to 73 % at 6 m depth. The plasticity index correspondingly increases from about 40 % to 70 %.

The Bothkennar test site is a national UK test site and has been very extensively investigated by means of in-situ testing and laboratory testing. Figure 2.9.3 presents the interpreted undrained shear strength profile and corresponding OCR. Both CAUC and CAUE triaxial tests and DSS tests have been carried out on samples of high quality taken with the 200 mm Laval piston sampler and the Sherbrook block sampler. Figure 2.9.3 shows undrained strengths based on the laboratory tests as summarized by Hight et al (1992), but including tests on block samples carried out at NGI, which fit well with the other data. Strengths have also been interpreted from the extensive series of CPTU tests presented by Jakobs and Coutts (1992), using both the tip resistance and u_2-pore pressure as basis and the correlations against triaxial compression strength proposed by Karlsrud et al (2005). As shown in Figure 2.9.3, the u_2- based strength came in this case out higher than all other strengths. The chosen s_{uc} and s_{ud} strength profiles are based on the Hight et al (1992) trend lines. They define an anisotropy ratio corresponding to $s_{ud}/s_{uc} = 0.80$, which is considered reasonable for such a high plastic clay.

The OCR profile selected is based on what was proposed by Nash et al (1992), and checks well with OCR back-calculated from the assumed s_{uc} profile and SHANSEP. In this case it was assumed S= 0.30 and m=0.85.
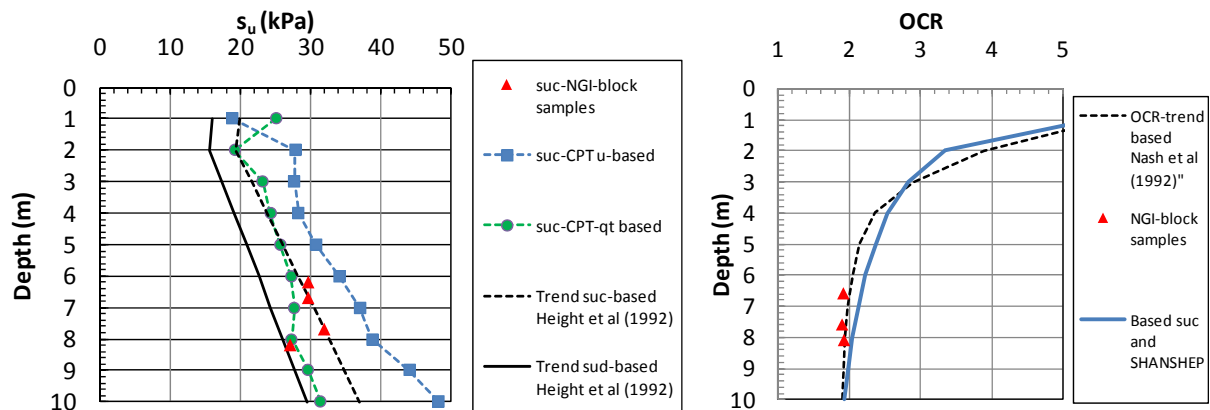
Figure 2.9.3 – Interpreted undrained strength and OCR profiles, Bothkennar

The 4 instrumented piles tested at BK were driven through a 1.2 m deep pre-installed casing to a tip penetration of about 6 m depth for. Herein mainly the results of first time load testing of test piles BK1T, BK2C and BK4C are dealt with. These piles were first time load tested after respectively 0.8, 2 and 4 days after installation.

During pile jacking it was generally recorded positive pore pressures during and at the end of pile installation. The radial effective stress at end of pile installation was close to zero, and then gradually increased with time following pore pressure dissipation. After 4 days the degree of pore pressure dissipation was about 85 %.

The total radial stress decreased significantly (by about 50 %) during the re-consolidation phase, as have been observed at other soft clay sites presented herein. As shown in Appendix 1, after 4 days the K_c-values were typically around 1.2.

Shaft friction observed during installation corresponds to about 30 % of the undrained strength. Figure 2.9.4 shows the relationship between average α-value and degree of consolidation. Herein is also included testing of some of the piles at 3.15 m penetration. The extrapolation to U=100%

suggests that both the tension and compression piles end up with α=1.0 and β=0.55, as given in Appendix 2.

The peak shaft friction was observed at a local displacement of about 4 mm with a tendency for some reduction after peak.
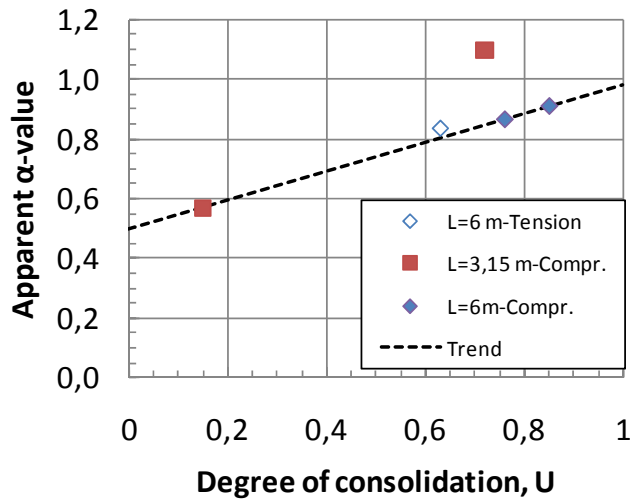
Figure 2.9.4- Apparent mobilized α-value in relation to degree of consolidation, Bothkennar

2.10 Tests with the MIT PLS probe

2.10.1 The PLS test probe and test carried out

The piezo-lateral stress (PLS) cell is a probe developed by the Massachusetts Institute of Technology (MIT), see for instance Morrison (1984) and Azzous & Lutz (1986). The probe has a diameter of 38 mm. The earth and pore pressures are measured at a distance of about 1.8 m above the tip of the probe. The load is measured at the top, about 2.06 m above the tip.

The PLS probe was first used in Boston Blue clay (BBC), ref. Morrison (1984), and later at the Empire (Em) site in Louisiana, ref. Azzouz and Lutz (1986). At the Em site there is a deposit soft somewhat overconsolidated clay with high plasticity, whereas the BBC clay deposit is lean and in geologic terms normally consolidated.

The data and test results presented in Appendix 1 and 2 for these tests have been taken directly from the referenced papers and reports, but with some reinterpretation when it comes to the soil conditions at the Empire test site.

2.10.2 Empire

The Empire test site was first established for undertaking a series of large scale load tests on 4 open-ended non-instrumented 14" piles, e.g. Cox et al (1979), which will be reviewed in Chapter 3. The 14" test piles were installed through casings to tip penetrations ranging from 35 to 111 m. The test with the MIT's PLS probe was made at a depth of 73.6 m.

The test site is located a few feet above normal sea level, with the ground water table close to the surface. Azzouz and Baligh (1984) give a very comprehensive review of soil data and geologic

history of the site, including past field and lab testing as well as results of a comprehensive supplementary laboratory testing program carried out by MIT.

The soil profile presented by Cox et al (1979) gives classification and index data. The data suggest fine sand with some clay layers and organic seams down to a depth of about 23 m. Below 23 m depth there is predominantly clay down to a depth of 135 m. Judging from CPT borings by Fugro, and a CPTU boring by MIT, below a depth of about 55 m there are fairly frequent seams or layers of silts and fine sands within the clay. In connection with interpretation of the 14" pile tests, Kraft et al (1981) divided this part of the soil profile into 4 Zones, which according to the boring log given by Cox et al (1979) have typical average characteristics as presented in Table 2.10.1. All layers show relatively high plasticity index. The natural water content is closer to the plastic limit than the liquid limit, and having a liquidity index, I_L, around 0.3.

Table 2.10.1- Clay units and classification data, Empire

Zone	Approximate Depth range (m)	w_n (%)	w_L (%)	w_P (%)	I_P (%)	Liquidity index I_L
1	35-50	46	90	27	63	0,3
2	63-78	36	75	22	53	0,26
3	82-95	36	70	20	50	0,32
4	99-111	38	78	21	57	0,30

Four free field piezometers were installed at the site in 1978, and suggested pore pressures somewhat above hydrostatic, Figure 2.10.1. MIT's CPTU tests suggested slightly higher in-situ pore pressures, and were used as basis herein.
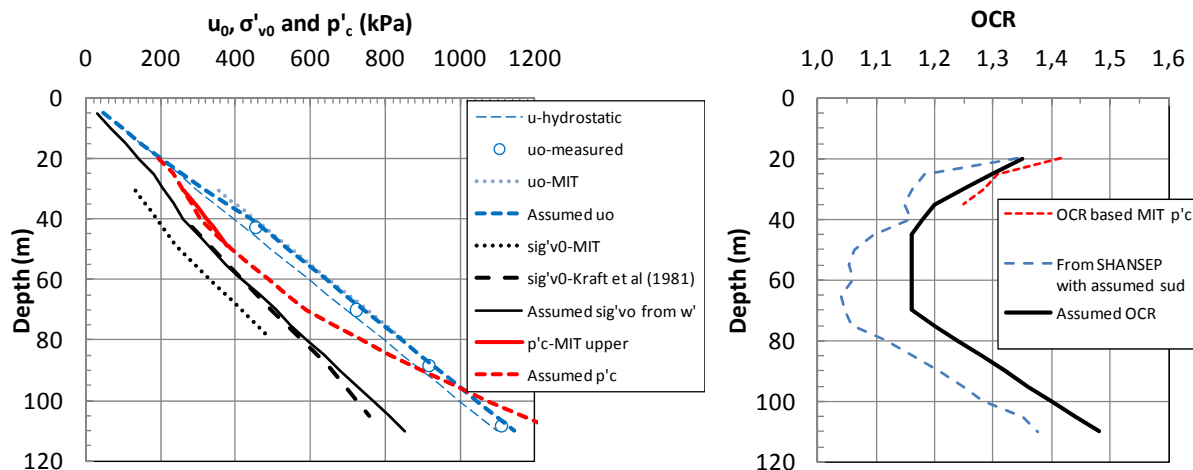
Figure 2.10.1 – In-situ stresses, Empire

The in-situ total vertical stress has been found to be of some uncertainty. Total unit weight data assumed by MIT are shown in Figure 2.10.2. The author has also calculated the total unit weight of the clay based on the water content data that were presented by Cox et al (1979), and assuming full saturation and a specific gravity of G=2.70. (MIT give values of Gs= 2.75 to 2.80 for 3 tests on clay samples, but in the author's experience that is on the high side). The unit weights calculated from the water content generally came out substantially higher than those

assumed by MIT. MIT used averaged measured total unit weights from several boreholes in the area. That was based on very few samples in the upper 20 m or so. They seem to have selected values from local layers with relatively high organic and water content, which does not seem representative based on the description given in the boring logs. The effect of such difference in total unit weight on total and effective vertical stresses is quite significant, Figure 2.10.1, amounting to a difference of about 80 kPa within the zones of interest. The σ'_{v0} values used herein match on the other hand quite well those presented by Kraft et al (1981), and has been used as basis in the following.
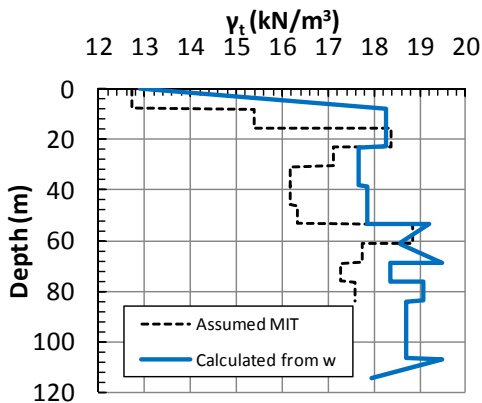
Figure 2.10.2 – Total unit weights, Empire

MIT carried out a comprehensive program of oedometer tests on the Zone 1 clay. Using MIT's "upper trend line" for depth range 30 to 50 m as basis, gives p'_c and OCR values as presented in Figure 2.10.1. This figure also shows the OCR values assumed by the author. This was based on a pragmatic choice, weighing the OCR–values arrived at on different basis, including back-calculation from the assumed undrained strength based on SHANSEP.

Whereas Kraft et al (1981) describes the clay as "underconsolidated" in light of the excess pore pressure condition that does not prohibit the clay from developing an apparent OCR due to creep or secondary consolidation. The low liquidity index might actually indicate that the clay some times in the past has been subjected to larger effective stresses than the present. OCR values well above 2 would not be unlikely for I_L=0.3. It is therefore possible that the OCR assumed herein could be too low. Alternatively, if MIT's σ'_{v0} profile is closer to the truth than the one assumed herein, the OCR values back-calculated would become significantly larger.

The in-situ K_0 values given in Appendix 1 were partly based on values measured in special oedometer tests on samples consolidated well beyond the apparent pre-consolidation pressure as reported by Azzouz and Baligh (1984), which gave K_{0NC}=0,605 at OCR =1. For other OCR's it was used the expression $K_0 = K_{0NC} \cdot OCR^{0.4}$ as was proposed by Azzouz and Baligh (1984).

The permeability of the clay was determined from constant head tests on both horizontally and vertically trimmed specimens, as well as values back-calculated from CRS and IL oedometer tests. All tests were carried out on samples from depths 35 to 50 m, within the Zone 1 clay defined in Table 2.10.1. Azzous and Baligh (1984) disregarded the IL oedometer tests as those gave permeability values a factor of 2 to 3 lower than the other tests. The other tests suggest that the inferred permeability at in-situ void ratio vary from about $0.6 \cdot 10^{-10}$ to $3.0 \cdot 10^{-10}$ m/s, with no

clear difference between vertical and horizontal permeability. In Appendix 1 it has been assumed a value $1.0 \cdot 10^{-10}$ m/s as a typical average.

MIT carried out a series of CAUC, DSS and CAUE tests on clay samples taken from Zone 1 (Table 2.10.1) on samples that were artificially pre-consolidated and run at OCR =1.0 and 1.6. Table 2.10.2 presents typical SHANSEP parameters defined by Azzouz and Baligh (1984) on that basis. As a comment to those, a value of S=0.24 for CAUC tests is considered very low, reference for instance Figure 2.5.6 based on tests on high quality undisturbed block samples, as well as data presented by Ladd and Foott (1974) and Ladd and DeGroot (2003). The explanation for this low undrained strength relationship was found in the very slow rate of straining of 0.07 %/hr that was adopted for these triaxial tests. MIT chose this rate to try to ensure uniform pore pressures in the sample during undrained shearing. This is not according to common practice at for instance NGI, where a rate of axial displacement of 0.6% pr. hour is used as a standard rate for all soft clays.

Table 2.10.2 – SHANSEP parameters S and m from artificially over consolidated samples, Empire (based on Azzouz and Baligh, 1984)

Type of test	Parameter, S	Parameter, m
CAUC	0,24	0,8
DSS	0,209	0,8
CAUE	0,18	0,8

The SHANSEP factors from the DSS tests are more in line with what could be expected. These tests were run at a shear strain rate of 4 % pr. hour, which also standard practice at NGI. If the undrained strength from the CAUC tests are corrected to a rate that is standard at NGI (0.6 % pr. hour), the correction factor would according to Figure 2.10.4 be typically 12 %, which would give S= 0.27 for CAUC loading. That is still on the low side, but more reasonable.
The anisotropy ratio s_{ud}/s_{uc} is typically 0.86 without correction for rate effect. After rate correction it reduces to sud/suc = 0.775, which falls more in line with empirical data in Figure 2.4.9.The triaxial tests show a peak friction angle of about $\varphi=23.6^0$.Within the Empire Zone 2 clay, no laboratory tests were carried out by MIT, but the same SHANSEP parameters was used also at these levels.
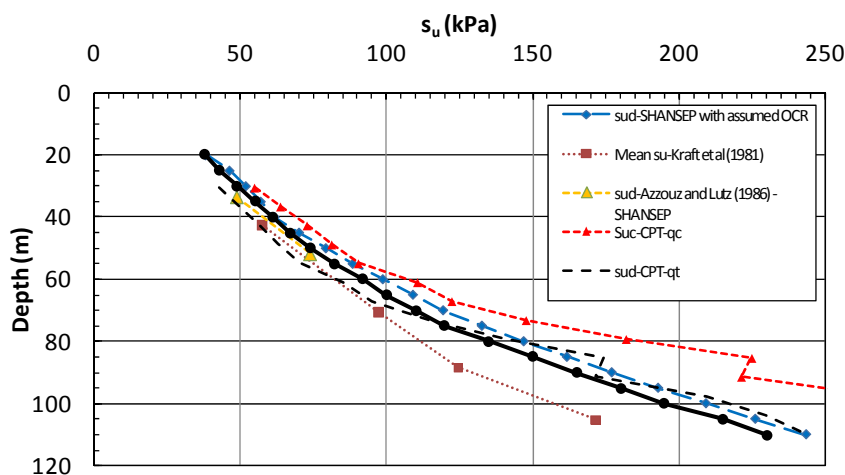
Figure 2.10.3 – Undrained strength profile, Empire

The test results for pile installation and loading given in Appendix 1 and 2 were taken from the actual data presented by Azzous & Baligh (1984), but using the authors interpreted in-situ stresses and undrained strength for normalization.

At end of installation it was measured a positive radial effective stress corresponding to $K_i \approx 0.3$ to 0.4. During the reconsolidation phase the effective stress started to build up when the degree of consolidation exceeded U=0.2. At U=1.0 the effective stress corresponded to $K_c=1.11$ in Zone 1 and $K_c=0.71$ in Zone 2.
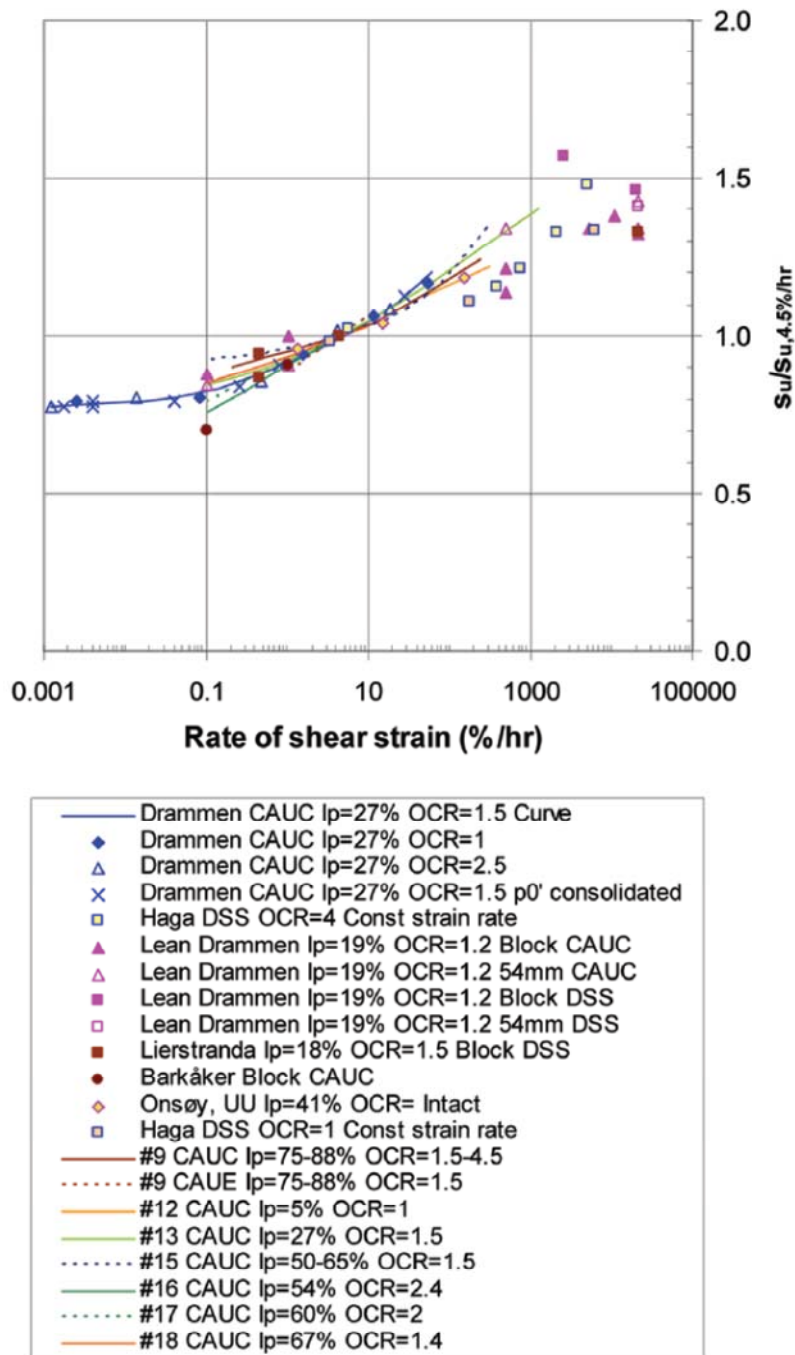
Figure 2.10.4 - Effect of rate of strain on undrained strength (from Lunne and Andersen, 2007)

The PLS probes were loaded in tension after all excess pore pressures set up by the probe installation were dissipated. It appears that the test in Zone 1 also gave higher normalised shaft

friction than in Zone 2, corresponding respectively to β= 0.30 and α=1.33 for Zone 1, and β= 0.22 and α=1.03 for Zone 2. Azzouz and Lutz (1986) suggested that the higher normalised capacity for the Zone 1 test could be contributed to a relatively high shear stress acting on the probe at the end of insertion. That application of a shear stress during consolidation enhances capacity is a well documented fact, e.g. Ladd and Edgers (1972) and Goulois et al (1985). It is still difficult to see why, as reported, a tension type shear stress should act on this probe during the re-consolidation phase (corresponding to mobilized β=-0.1), and a compression type shear stress (corresponding to mobilized β=0.04) on the probe tested in Zone 2. Upon second time testing the lower PLS probe gave essentially the same shaft friction in Zone 2, but dropped by 30 % in Zone 1. This may raise questions about the reliability of the results of the first test in Zone1.

2.10.3 Boston Blue Clay (BBC)

Morrison (1984) presented detailed results of a series of different PLS tests carried out in Boston Blue Clay (BBC). Most tests were carried out at the Saugus test site, but some also at the MIT campus.

BBC has a typical water content mostly in the range w=40-45 % and plasticity index I_P=19-26 %. Figure 2.10.5 shows a profile of in-situ stress conditions based on values given by Morrison (1984). The high OCR-values in the top part are assumed to primarily stem from chemical weathering. In the lower part of the deposit OCR=1.25 is assumed due to secondary consolidation (creep). The in-situ K_0 values proposed by Morrison (1984), and used herein (Appendix 1), were based on values proposed by Ladd et al (1979). The values check well with the modified Broker and Ireland (1965) used for other sites herein.

As seen from the data presented in Appendix 1, oedometer tests suggest that the modulus number decrease from about m_0 =18.5 in the upper weathered part of the deposit, to m_0 = 8.6 in the lower part. The in-situ vertical permeability of the deposit has been determined from CRS type oedometer tests and constant head permeability tests. There is a fair amount of scatter in the data at a given depth, especially within the lower clay (factor of about 1.5 up or down). The horizontal permeability has also been measured, and seems on average basis to be a factor of about 1.5 larger than the vertical.
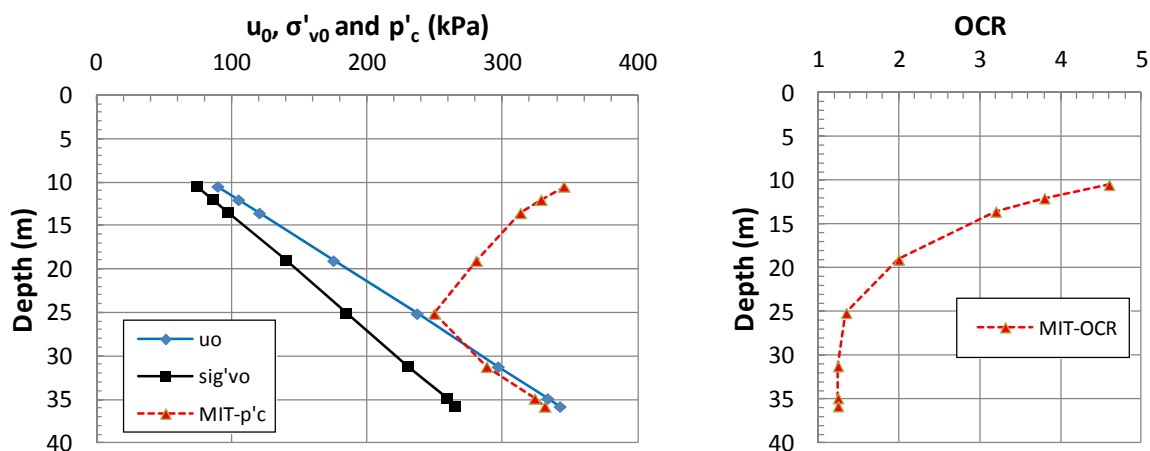
Figure 2.10.5 – In-situ stress conditions, BBC Saugus site

MIT has carried out DSS tests on SHANSEP type consolidated specimens. The best fit to the data presented by Morrison (1984) for the OCR range in question suggest S= 0.18 and m=0.8.

The assumed OCR and in-situ vertical stress conditions in Figure 2.10.5 leads to an undrained s_{ud} strength profile as shown in Figure 2.10.6. It may be mentioned that idealized relationship for BBC presented by Ladd and Foott (1974) suggest S=0.20 and m=0.8, which would lead to 11 % higher strengths. Different types of CPTU tests have also been carried out at the site. Attempts to use the Karlsrud et al (2005) correlations for N_{kt}, gave in this case s_{uc} strengths that were unreasonably low (about the same as or even lower than the s_{ud} strengths in Figure 2.10.6). The explanation may be the special design of the MIT CPTU probe, with an extended pore pressure tip at the end, which may affect the cone factor. These results were therefore not used.
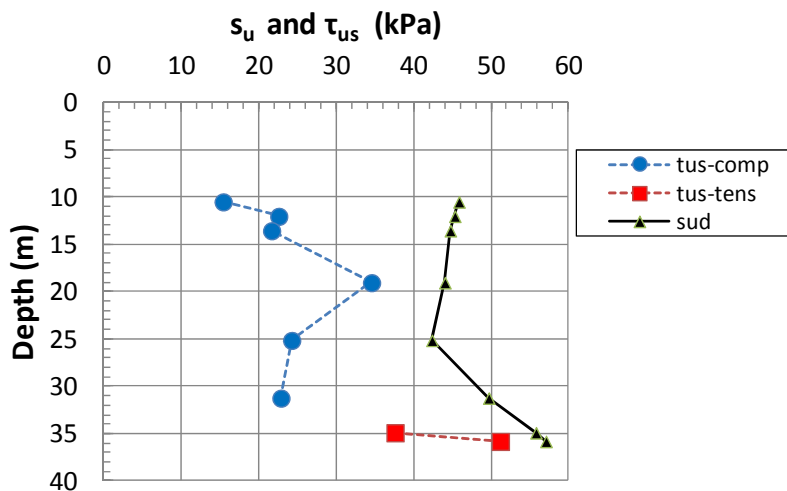
Figure 2.10.6 – Undrained strength and measured shaft friction, PLS-tests BBC

Extensive data on generated earth and pore pressures during penetration were collected from the various PLS tests. The results showed that stops in penetration and allowance for some dissipation, caused larger pressures during subsequent penetration as compared to steady penetration. In Appendix 1 only pressures form steady penetration are included, and only for the levels where full re-consolidation was achieved, and pile loading was undertaken. The normalised excess pore pressures $\Delta u_i/\sigma'_{v0}$ range from 1.4 to 2.5, but is fairly constant below the upper weathered zone (Appendix 1).

For steady penetration, the horizontal (radial) total stress was only marginally larger than the pore pressure. After correction for cross-sensitivity of the earth pressure sensors and axial load, Morrison (1984) showed K_i values typically in the range 0.1 to 0.2 in the lower part of the deposit (>22 m), but does not present similar interpreted values for the upper part. By checking Morrison's reported total radial stress and pore pressure values during steady penetration, the author found effective stresses about half of what Morrison reported. Morrison's values are still used herein.

Figure 2.10.7 shows a typical example of stress changes through the re-consolidation phase in the lower clay. The data confirm the large reduction in total horizontal stress that has been observed in other low OCR clay deposits. The effective stress ratio K_c ends in this case up around 0.6, close to the assumed in-situ K_0 value. In the upper weathered clay the effective stress ratio, K_c, was typically around 1.0 upon complete re-consolidation.

Most of the PLS probes were loaded in compression by applying the load through the drill rig used. This implied relatively poor load control at the level of the PLS probe, as there was a

continuous drill string without casing all the way up to the ground level. The loading was in principal stepwise, and in most cases loading to failure was reached within a few minutes. In the lower part of the deposit the load was (un-intentionally) applied more rapidly, and failure was reached in 5-20 seconds. Furthermore, due to insufficient capacity of the drill rig, loading was carried out in tension rather than compression for the two deepest tests.

At onset of loading most probes showed that a downdrag shaft load was acting on the probe, as also was observed in MIT's tests at Empire. The force (not presented for all cases), seemed to be limited to 10 % of the failure load, and would then be expected to have small impact on the measured capacities.
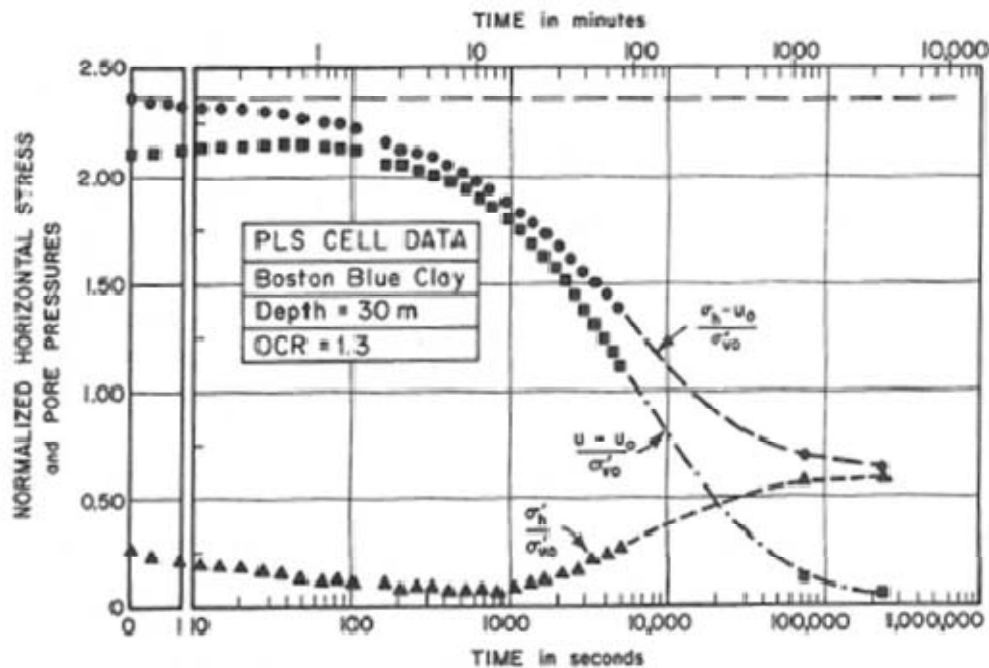
Figure 2.10.7- Example of measured stress changes during the re-consolidation phase in BBC with OCR=1.3 (after Azzouz et al, 1990).

The measured ultimate shaft friction values are presented in Figure 2.10.6. The data indicate that the tension tests in the lower part relatively speaking gave considerably higher shaft friction than the two compression tests above. Most other experiences suggest the shaft friction should be very much the same in compression and tension. This suggests that the shaft friction values below 20 m should be treated with some caution.

2.11 3" and x-probe tests at Empire

A series of tests with the 3" probe (open and closed mode) and with the 1.5 " closed x-probe, identical to those used at the West Delta site (ref. Section 2.3), have also been carried out at Empire. Some key results for probe tests carried out at a depth of about 120, 141 and 160' (36.6, 43.1 and 48.8 m) were reported by Bogard and Matlock (1990), Bogard et al (2000), and Bogard (2001). The results presented in Appendix 1 and 2 were interpreted using the same assumption regarding in-situ stresses and undrained strength as presented in Section 2.10.2 above (Figures 2.10.1 and 2.10.3).

For installation pore pressures, the reviewed papers do not include data for the 36.6 and 41.1 m levels, which are then missing in Appendix 1. The same applies to values for t_{50} and t_{90}. At 48.8 m, the open 3" probe induced about half of the excess pore pressures observed for the 3" closed and the x-probe.

Bogard (2001) showed that the pore pressure dissipation for all probes (open and closed), and at all levels, could be represented by an almost unique normalised dissipation relationship given by:

$$U = (t/t_{50})/(1+t/t_{50}) \tag{2.11.1}$$

The significance and general applicability of this expression will be discussed in Chapter 5.

Bogard (2001) also reports values for K_c extrapolated to U=100%, at all three levels. These value range from K_c= 0.77 to 1.83. As shown in Appendix 1, the closed 3" probe gave the highest K_c =1.8, and the 3" open probe the lowest, with the x-probe in between.

For the 48.8 m level, Bogard and Matlock (1990) present absolute measured shaft friction values and load-displacement curves. For the other two levels only the ultimate shaft friction was presented by Bogard et al (2000) and as normalised β values by Bogard (2011). As can be seen from Appendix 2 the mobilized normalised shaft friction values are lower than for the MIT's PLS probe test at 44.7 m.

Bogard (2001) could not find any clear correlation between ultimate shaft friction and measured K_c values for the 3" and x-probe tests . He showed, however, a close correlation between the degree of consolidation and build up of shaft friction.

The load-displacement curves presented by Bogard and Matlock (1990) show that peak shear transfer was reached at a displacement of typically 0.5 mm for the x-probe and 0.9 mm for the 3" probe, which in both cases would correspond to about 1.1 % of the pile diameter.

2.12 St. Alban-Quebec

Six closed-ended steel pipe piles were tested by Laval University in the Champlain Sea clay deposit at the St. Alban test site outside Quebec, Canada. All piles had D=219 mm, t=8 mm and were jacked into the clay deposit to a tip penetration of 7.6 m. The upper 1.5 m was pre-augured to a depth of about 1.5 m. The test piles were instrumented with 2 pairs of pore pressure sensors at 4 levels along the pile shaft and a load cell at the tip to measure tip resistance. Prior to the pile installation a total of 35 free-field piezometers were installed in the clay at various distances and depth to monitor the impact of pile installation.

The data and results presented herein were taken from published paper by Roy et al (1981), Roy and Lemiux (1986) and Konrad and Roy (1987).

Figure 2.12.1 presents a typical soil profile from the site. The clay deposit is a highly sensitive (S_t around 20), and structured clay deposit. The water content is as high as 100 % at 2 m depth, decreasing to typically 60 % below that level. Due to high sensitivity, the liquid limit is lower than normal, and consequently the plasticity index low compared to the water content. For that reason the plasticity index l_p gives a false impression of the characteristics of this clay deposit. As the clay in geologic terms is normally consolidated, if it was not so sensitive it would

probably have a liquid limit close to the water content. That would imply l_p decreasing from about 80 % at 2 m to 40 % below 4 m depth. These "corrected" l_p values are used as basis herein.

Figure 2.12.2 shows in-situ stress conditions and apparent pre-consolidation pressures as reported in the aforementioned papers. Regarding the in-situ vertical effective stress conditions, these values were computed on basis of reported total unit weights (also checked against water content) and in-situ pore pressures. This lead to 10-15 % higher vertical effective stress than represented by Roy et al (1980), and has been used as basis herein. Below the upper crust OCR=2.0.

Results of CIUC triaxial tests suggest typical s_{uc} values as presented in figure 2.12.3. The s_{ud} values were assumed to correspond to $s_{ud} = 0.8\ s_{uc.}$
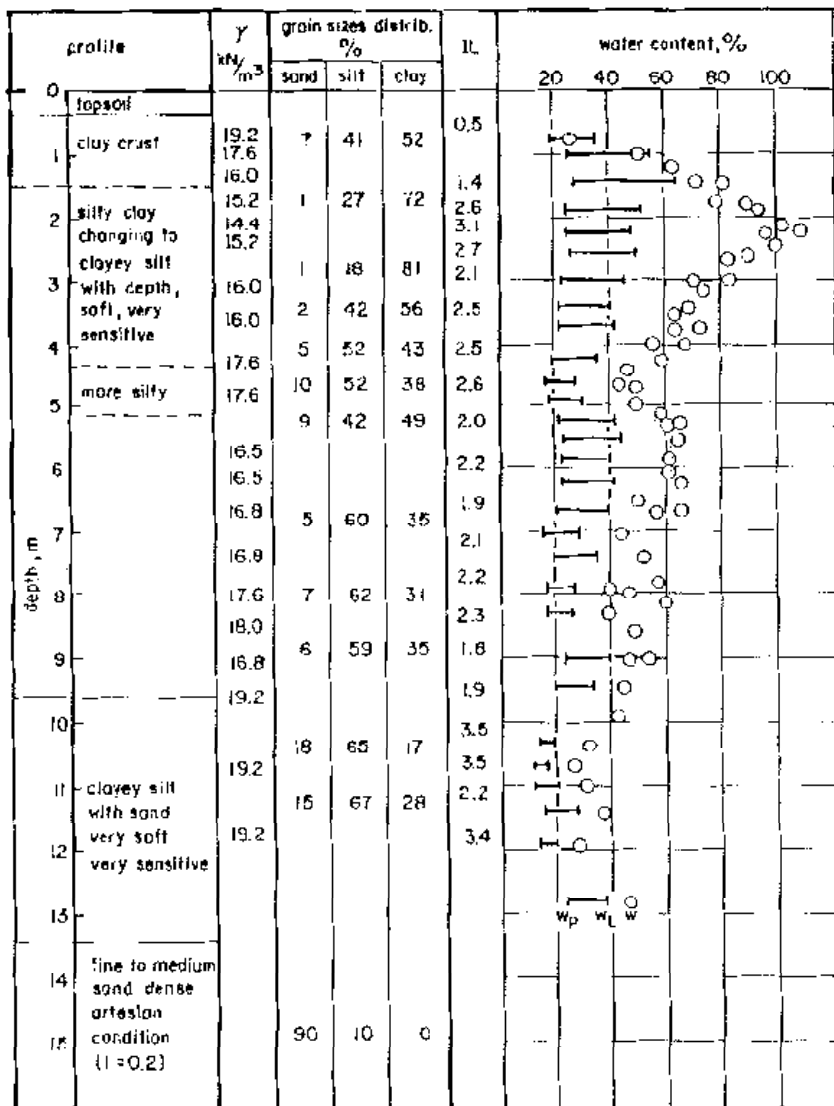
Figure 2.12.1- Soil profile St. Alban (after Roy et al, 1985)
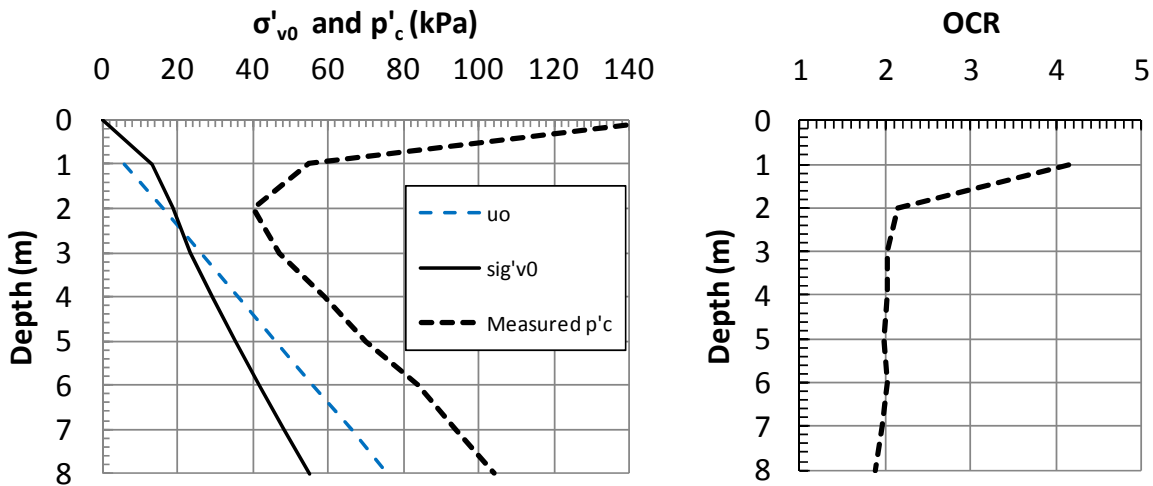
Figure 2.12.2 - In-situ stresses, St. Alban
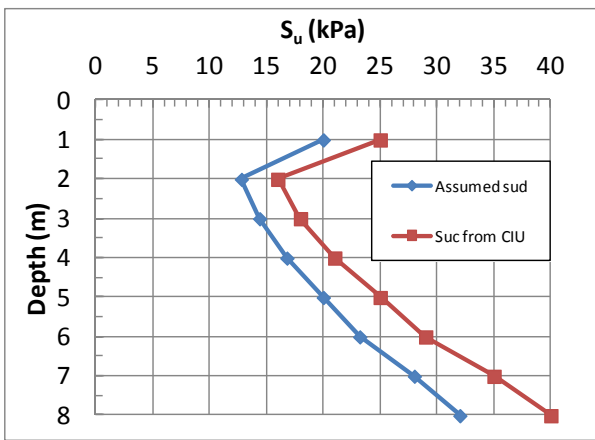
Figure 2.12.3 - Undrained shear strength profile, St. Alban

Pore pressures generated against the pile shaft showed a very consistent trend for all test piles after installation was completed. Only typical values at depths of 3 and 6 m are included in Appendix 1. Figure 2.12.4 shows data regarding free-field pore pressures at end of installation at levels above those influenced by the pile tip. These data were also quite consistent, and suggest that the excess pore pressures approached zero at a normalised distance of $r/r_o=12$. The Roy et al (1981) paper also includes very good data on pore pressures generated at and in the soils around the tip, but these data are not dealt with herein.
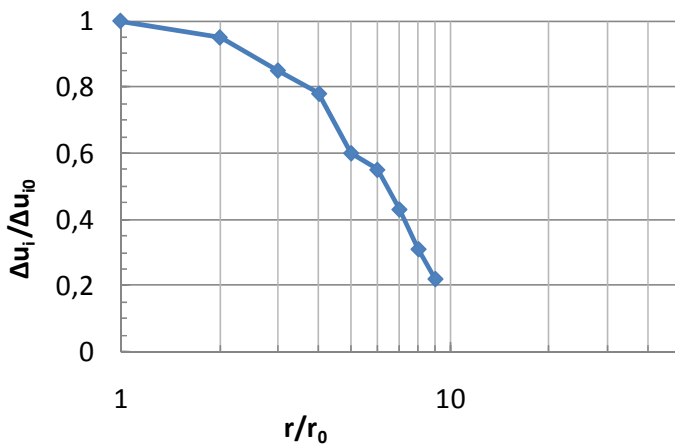
Figure 2.12.4 – Normalised excess pore pressure as function of radial distance, St. Alban

Pore pressures dissipation following pile installation was quite in line with what has been observed at other soft clay sites herein. Values of t_{50} and t_{90} are given in Appendix 1. The data suggest 100 % re-consolidation was reached in about 20-30 days.

All test piles were loaded to failure in compression. Most piles were loaded several times, from about 1 hour to 33 days after installation. One pile was, however, only loaded once after 2 years. The data in Konrad and Roy (1987) suggest that the bearing capacity built up more or less in proportion to the degree of consolidation as have been observed at several of the other sites in soft clays dealt with herein. To avoid any speculation on the effects of repeated loading to failure of the same pile, the 2 year test has been used as basis herein. The total ultimate capacity was for that test 87 kN. By subtracting measured tip resistance of 10.3 kN and adding the weight of the pile, the ultimate load carried by shaft friction becomes 80 kN. Since a 2 year test may be somewhat affected by ageing effects, the shaft friction was corrected for that based on the procedure proposed by Karlsrud et al (2005). This reduces the shaft friction to Q_{us} = 73.5 kN. That value was used in Appendix 2, and results in average values of α=0.90 an β=0.54.

2.13 University of Houston Campus site (UHHC)

A comprehensive pile testing test program was carried out at the University of Houston campus test site (UHHC). Although testing focused on a 3x3 pile group, two reference piles at sufficient distance from the group to be influenced by that, were also installed and tested. It is data from the reference pile tests that are dealt with herein. All piles had D= 273 mm and t= 9.2 mm. The piles were driven to a tip penetration of 13.1 m below ground surface. The piles were instrumented with earth- and pore pressure cells at 4 levels, and both strain gauges and extensometers to monitor axial loads along the pile in 11 sections along its length. The data and test results presented herein were extracted from O'Neill et al (1982 [a, b]) and Heydinger and O'Neill (1986).

Table 2.13.1 summarizes main soil units and their average and range of properties based on data presented by O'Neill et al (1982[a]). An important feature of this site is the transition from highly plastic stiff clay in units A and B, to low plastic stiff clay in units C and D. The water content is close to the plastic limit, with LI values in the range 0.1 to 0.3, which is typical of overconsolidated clays. O'Neill et al (1982[a]) suggests that the overconsolidation stems from desiccation.

Table 2.13.1 – Average soil properties, UHHC

Unit	Depth (m)	w (%)	I_p (%)	$S_{u(UU)}$ (kPa)	CPT-q_c (kPa)
A	0-2.6	20 (19-21)	30 (20-35)	115	1680
B	2.6-7.9	27 (22-38)	50 (30-55)	86	2680
C	7.9-9.2	17 (16-22)	8 (5-17)	38	2110
D	9.2-14.3	18 (15-23)	17 (12-28)	158	3490

Figure 2.13.1 shows interpreted in-situ stress condition. The apparent pre-consolidation pressure was back-calculated from undrained strength as described in the following.

Figure 2.13.2 shows undrained strength calculated from reported CPT tip resistance data using the Karlsrud et al (2005) correlations. It was in this case assumed that the s_{ud} strength increased from $0.6s_{uc}$ at shallow depth with the highest OCR, to $0.65s_{uc}$ below 2.5 m depth. The somewhat idealized UU strength profile lies on the average about 25 % lower than the calculated s_{ud} values, and are only about half of the s_{uc} values calculated from the CPT tip resistance. That may suggest that the calculated values are significantly on the high side. Nevertheless they have been used as they have been calculated. The OCR values in Figure 2.13.1 were computed from the calculated s_{uc} strengths using assumed SHANSEP parameters of S=0.3 and m=0.85.

Due to improper saturation of piezometer filters, no reliable data for pore pressures generated against the shaft of the reference pile have been reported in the referred papers. Therefore values of t_{50} and t_{90} are missing for this case. Unfortunately, there were also apparent problems with the lateral stress measurements. Although such data from piles within the 3*3 pile group seem to be consistent and reliable, they could be influenced by group effects. For these reasons only the values of ultimate shaft friction are presented in Appendix 2. The average ultimate shaft friction values within the upper plastic clay layer (3.3-7.9 m), and within the lower lean clay (7.9-13.1 m), are given separately. The normalised values correspond to β= 0.37 and α=0.78 in the upper plastic clay, and β= 0.23 and α=0.49 in the lower lean clay.
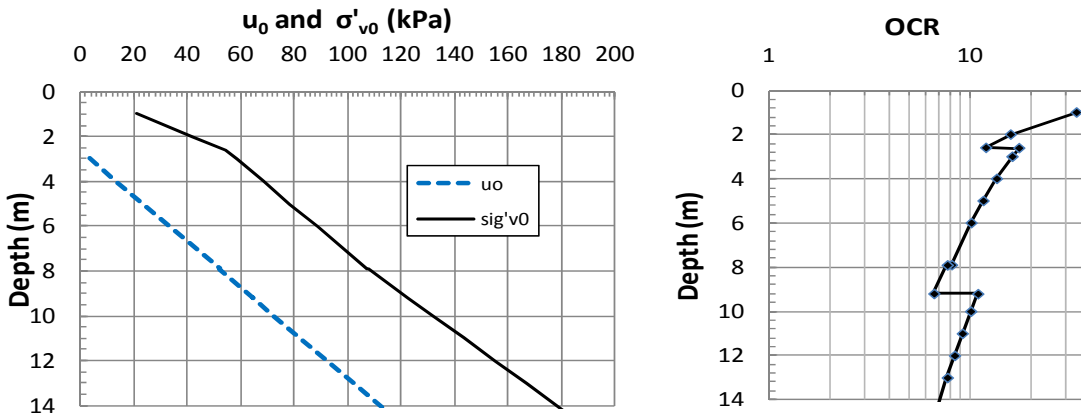
Figure 2.13.1 – In-situ stress conditions, UHCC
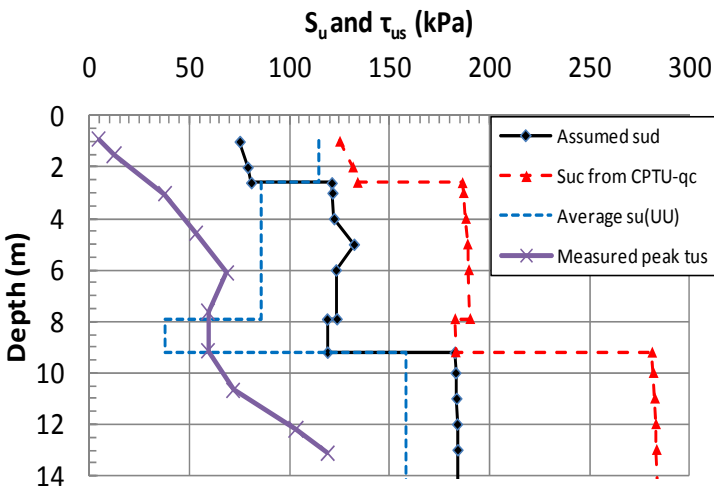
Figure 2.13.2 – Assumed undrained strength profile, UHCC

The reference piles reached failure at a pile top displacement of about 6 mm. Correction for pile flexibility, would give local displacement at failure of about 3 mm, corresponding to about 1.1 % of the pile diameter. After the peak load was reached, the load reduced by about 10 % at a displacement of about 15-20 mm.

2.14 Instrumented probe and small scale tests reviewed but not included

At Cambridge University it was also developed what they called an in-situ model pile (IMP). It had a diameter of 80 mm and length of 1.135 m. It was instrumented with pore pressure gauges at 3 levels, had total radial stress cells at 2 levels and axial load was measured at 3 levels.

Coop and Wroth (1989) presented test results from two sites:

- In stiff overconsolidated clay at Madingley near Cambridge
- In a soft recent clay deposit at Huntspill

The results from these tests show similar behaviour in terms of earth and pore pressure response as observed at other test sites with stiff and soft clays, but it was chosen not to include these data directly in this study. The main reason for not doing so are: 1) The IMP pile has very small L/D ratio of 14 which makes it prone to significant end effects; 2) The paper does not give sufficient detailed information on all soil parameters that are relevant for this study; 3) Load test data presented only cover steady penetration of the probe into the ground, and not testing after full set-up.

Testing has been carried out with the 3" probe and x-probe at several other sites in addition to West Delta and Empire as included herein. Bogard and Matlock (1990) mention tests at a total of 6 different sites. One was at Harvey Louisiana. The Harvey site seems quite similar to Empire, and the observed behaviour was reported by Bogard and Matlock (1990) to be much like at Empire. This site is still not included in this study due to lack of detailed soils data from this site.

3 REVIEW OF SELECTED NON-INSTRUMENTED PILE TESTS

3.1 Selection criteria

There exists a rather vast amount of data on pile load tests in clay that over the past 50 years or so have been used for developing various empirical design procedures, as will be reviewed later in Chapter 6. The main limitation in using such past test data is that the type of soils data the author has focused on in this study are missing or incomplete.

The limited number of non-instrumented pile tests included in this study, were selected mainly on basis of the following criteria:

- The soil parameters most relevant for this study (in-situ stresses, s_{ud} and OCR) could be established with reasonable reliability.
- Original soil data and pile test results were fairly easily accessible for checking and assessments.
- All tests are fairly large scale tests, i.e. pile length larger than 10 m and pile diameter larger than 25 cm.

In practice this meant that pile tests included were carried out within the past 10-15 years or so, and that NGI had been involved in many of them.

The results of all tests are summarized in Appendix 3 in terms of average soil characteristics and average ultimate shaft friction values. The following describes each case, and special features or results that are of special interest to notice.

3.2 Empire

The pile testing at Empire played a key role in the ESACC Program referred to in Section 2.8 and 2.10.2. Relevant interpreted soil parameters are the same as presented in Section 2.10.2.

As described by Cox et al (1979), the four test piles installed at this site all had diameter of 356 mm. No data on wall thickness has been found. The piles were driven open ended through pre-installed casings to depths ranging from 50.3 to 109.4 m. The test pile length varied from about 15.3 m for the shallowest tests and 12.2 m for the deepest, Table 3.2.1. No documentation has been found regarding plugging behaviour during driving. On basis of the type of clay, pile lengths and diameters in question, it seems fair to assume that none of the piles plugged.

The piles were instrumented with strain gauges at 4 levels, but only the average shaft friction is dealt with herein.

Table 3.2.1 – Pile testing levels, 14 "piles, Empire

Pile No	Depth casing (m)	Depth of pile tip (m)	Average depth (m)	Embedded pile length (m)
1	35.0	50.3	42.7	15.3
2	62.5	77.8	70.6	15.3
3	82.3	94.5	88.4	12.2
4	97.2	109.4	103.3	12.2

All piles were subject to a first "short term" testing sequence to failure in both compression and tension, and in two cases also a second compression test. These "short term" tests were carried out from 4 to 10 days after the piles were installed. After a resting period of about 300 days, the piles were subjected to a second testing sequence in tension and compression. Table 3.2.2 presents the average shaft friction values reported by Cox et al Kraft (1979) from the first tests in each test sequence. Except for pile 1, the ultimate shaft friction was lower in the 2nd test series, suggesting that the piles have experienced a permanent loss in capacity as a result of the 1st test series.

Table 3.2.2- Average shaft friction observed in first tests in each testing sequence, 14" pile tests, Empire

Pile	Time after inst. (days)	Type loading	Average τ_{us} (kPa)
1	7	Compr.	**53,1**
	323	Tens.	66,1
2	9	Compr.	**102,9**
	319	Tens.	96,2
3	10	Compr.	**138,9**
	313	Tens.	109,2
4	4	Compr.	**154,7**
	327	Compr.	113,5

In the first testing sequence the piles were loaded incrementally to failure at a rather slow rate, giving a time to failure in the range 4 to 9 hours. If this lead to partly drained conditions during pile loading, the ultimate capacities could be on the high side. If undrained response was achieved, the ultimate capacities could, due to rate effects, be somewhat on the low side when compared to time to failure in other tests dealt with herein. Another element of uncertainty in relation to the 1st testing sequence is the degree of pore pressure dissipation at the time of loading. An estimate of this was made by using the procedure proposed later in Chapter 5. With the assumed permeability of typically $1 \cdot 10^{-10}$ m/s (ref. Section 2.10.2), this gave U=0.78 for t = 4 days, U=0.87 for t=7 days, and U= 0.92 for t= 10 days. That could correspondingly mean that the ultimate shaft friction at U= 100 % is from 22% to 8% larger than given by these tests.

For the 2nd testing sequence, a constant rate of loading was applied, but the author has not been able to find any documentation on the rate of load application or the time to failure in these tests.

From the brief discussion above, it is apparent that there are some uncertainties regarding what should be taken as the most relevant ultimate shaft friction for these cases. The "long-term" tests are most likely on the low side. The "short term" tests could possibly be either on the somewhat low or somewhat high side. In Appendix 3 it was decided to use the "short term" tests at face value as the most relevant, as shown by the bold letters in Table 3.2.2.As seen from Appendix 3, this gives α=0.8 to 0.9 and β= 0.19 to 0.21.

The various compression and tension tests carried out during each testing sequence suggest, when the impact of repeated loading on the same pile is accounted for, that the capacity in compression and tension are about the same.

3.3 Børsa

In connection with design of foundations for a bridge for the new E39 across the river Børsa in Sør-Trøndelag, Norway, two test piles were installed. The piles were steel pipe piles with diameter 406 mm and wall thickness 12.5 mm. They were driven open ended into the ground to a depth of 50 m. Pile test results were reported by Aas-Jakobsen AS (2003a). Data regarding soil conditions were retrieved from project files at NGI (Project 20031160).

The river Børsa has cut into an old more or less flat marine seabed that has been exposed as a result of the post-glacial uplift of the area. The old seabed level is found at approximately Elev. +26. The load tests were carried out from a small terrace at Elev. +7, about 2/3 down the river slope.

Soil borings along the bridge included a number of rotary pressure (RP) soundings and CPTU tests.   Unfortunately, soil sampling was limited to about 15 m below ground level. The sampling shows clay with water content that below a 1-2 m upper weathered crust decreases from about 37 % at 3 m to 32 % at 8 m. Below that level, the water content further down to about 15 m depth is typically 30 % (range 28-32%). The plasticity index of the clay has been measured on just a few samples. It was 15 % at 3 m depth. A nearby sample of clay with w=31 % showed I_p= 13 %. Laboratory fall cone tests show sensitivity with S_t in the range 6 to 10. The CPTU and RP soundings suggest that the clay further down to 50 m depth is mainly of the same character as above, but the water content will probably reduce slightly with depth. The same applies to the plasticity index, which typically could be around 12 % for w=30 %, but could drop towards 10 % at large depth.

In-situ pore pressures were measured at various locations and depths along the bridge, and show a consistent picture of a somewhat artesian condition at this level in the slope, Figure 3.3.1.
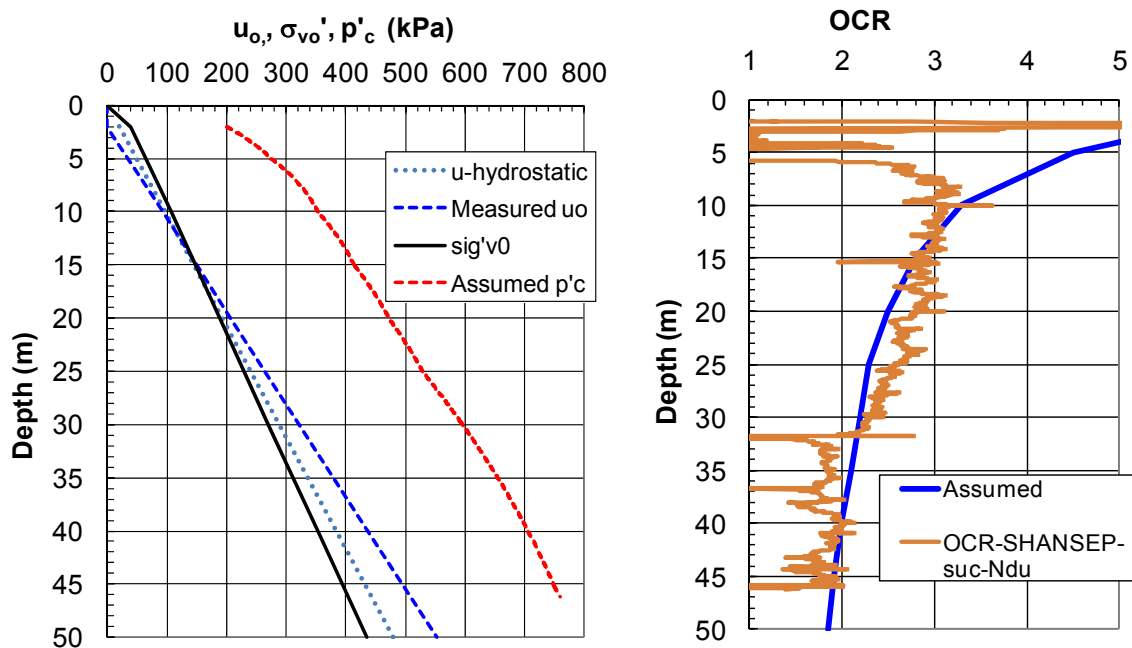
Figure 3.3.1 – Assumed in-situ stress conditions, Børsa

The assumed pre-consolidation pressure and OCR-profiles shown in Figure 3.3.1 were computed assuming that the maximum past vertical effective stress is given by the vertical effective stress

prior to erosion, which was calculated based on a submerged unit weight of typically 9.7 kN/m$^{3.}$. Furthermore, that the clay under the old sea bottom (pre-erosion) had built up an apparent pre-consolidation pressure due to secondary consolidation corresponding 1.25 times the past maximum vertical effective stress.

Figure 3.3.2 show the s_{uc} undrained strength profile derived from a CPTU test next to the test piles (Boring 136) using the CPTU cone factors proposed by Karlsrud et al (2005). Values calculated from both excess pore pressure and tip resistance are given. The OCR values assumed in this connection were as presented in Figure 3.3.1, and it was assumed I_p =12 % below 15 m depth. In this case there is generally good agreement between the strength derived from pore pressure and tip resistance. A few comments may be given to the actually assumed s_{uc} profile:

- In the top part (down to about 6-8 m depth) the pore pressure response seems to have been poor and lead to too low strengths. This is also confirmed by the low OCR-values back-calculated from SHANSEP using the $N_{\Delta u}$ derived strengths, and assuming S=0.30 and m=0.85, Figure 3.3.1. For this reason, the assumed strengths in the upper part were calculated using SHANSEP and the assumed OCR values based on the assumed pre-erosion ground level.
- At depths larger than 6-8 m most reliance was given to the $N_{\Delta u}$ derived strengths. This is in accordance with the general recommendations given by Karlsrud et al (2005).
- From a depth of 43 m to the end of the test at 46.3 m, it was apparent from the CPTU data that the silty clay within this zone contained some seams of silt or fine sand.
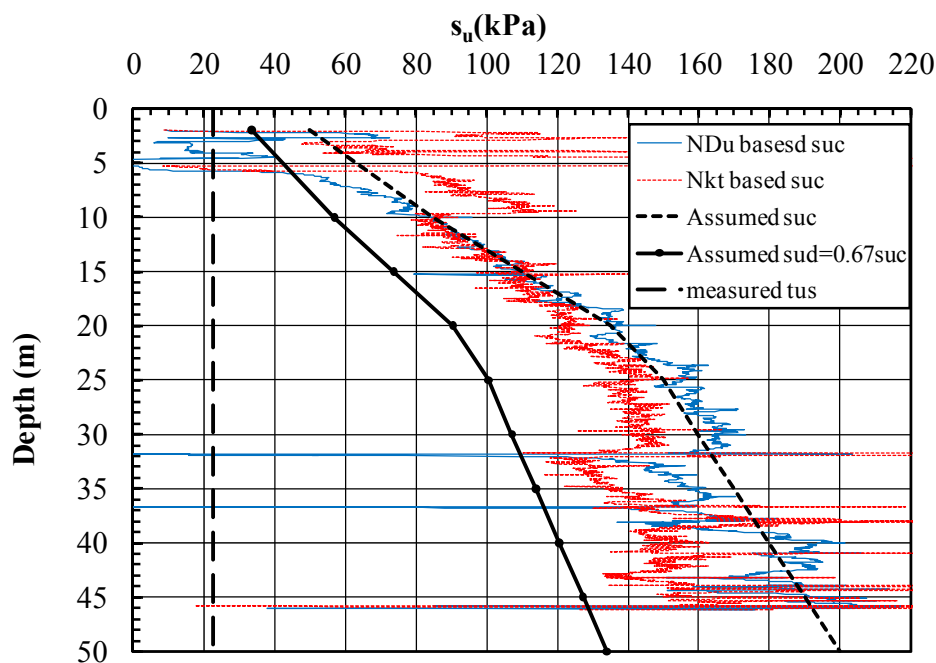
Figure 3.3.2 – Assumed undrained strength profile derived from CPTU, Børsa

The test piles were driven with a 6 t hydraulic hammer. The piles did not show any tendency for plugging during driving. Table 3.3.1 presents results of load tests on the piles. Both piles were loaded in tension by an incremental load-controlled procedure. They were actually intended to be loaded to failure on the same day, but as some problems arose during first time testing of Pile 1,

the test on Pile 2 was postponed until the problem was rectified. Pile 1 was re-tested at the same time.

Failure was in first time testing reached at a pile top displacement of about 40 mm. Loading to failure took about 1 hour. During un-loading the pile top relaxed about 10-15 mm. Loading of Pile 2 apparently stopped somewhat short of ultimate peak load, but the ultimate load could be reasonably well estimated based on comparison against the load-displacement curve for Pile 1. The net ultimate shaft friction values were calculated by subtracting the weight of pile and soil plug and net theoretical tip resistance from the total load measured at the pile top. This amounted to 150 kN. In Appendix 3 only the average shaft friction for the two piles from first time testing is given, and is also shown in Figure 3.3.2.

The shaft friction must for this case be characterized as extremely low when compared to the in-situ undrained strength, giving an average $\alpha=0.25$ and $\beta= 0.099$.

Table 3.3.1 – Summary of measured pile capacities, Børsa

Test No.	Time after inst (days)	Ultimate total Load Q_{ut} (kN)	Estimated ultimate shaft load Q_{us} (kN)	Average shaft friction τ_{us} (kN)
1-1	63	1920	1770	24.3
1-2	72	2020	1870	25.9
2-1	72	1720[1)]	1570	21.2

   1)   Loading was stopped slightly short of ultimate (at 1620 kN). This value is extrapolated.

3.4 Vigda

Two test piles were also installed and load tested in connection with design of foundations for another bridge for the new E39, this across the river Vigda in Sør-Trøndelag, Norway. The piles were steel pipe piles with diameter 457 mm and wall thickness 12.5 mm. They were driven open ended into the ground to a depth of respectively 26.7 m (Pile A) and 52.9 m (Pile B). Pile test results were reported by Aas-Jakobsen AS (2003b). Data regarding soil conditions were retrieved from project files at NGI (Project 20031160).

The river Vigda has also cut into an old more or less flat marine seabed that has been exposed as a result of the post-glacial uplift of the area. The old seabed level in this area is found at approximately Elev. +35. The load tests were carried out from a small terrace at Elev. +7 about 6 m above river bottom.

Soil borings along this bridge primarily included a number of rotary pressure (RP) soundings and CPTU tests and some soil sampling. Figure 3.4.1 shows the results of CPTU-112 next to the pile tests. This was stopped at a depth of 32 m due to lack of penetration capacity for the drill rig used. It is apparent that parts of the clay profile contain some distinct seams or layers of sandy or clayey silt interbedded within the silty clay deposit. The silty sand/sandy silt seams or layers appear as zones with high q_c and somewhat low pore pressure response (but not so low as to represent zero excess pore pressure indicative of sand or coarser materials). As seen from Figure 3.4.1 such zones are most apparent from about 7-7.5 m, 16.3-17.3 m, 22-24 m, and 27-32 m. The right hand side of Figure 3.4.1 gives as an example a more detailed look at data from 20 to 25 m depth. This shows that the seams or layers of sandy or clayey silt have a thickness of about 10 to

20 cm, and make out about 15-20 % of the soil profile from 21-25 m. Over the total length of test Pile A (from 0 to 26.7 m) seams of sandy or clayey silt makes out in total about 10 % of the profile.

Figure 3.4.2 shows the results from CPTU-111 carried out 3.6 m down slope from the test pile area. This CPTU test first stopped at 31 m due to too high resistance for the rig (as CPTU- 112), but a casing was installed to 35 m depth and augured out to allow further CPTU testing, which eventually gave stop at about 50 m penetration. It is apparent from this boring that seams or layers become even more dominating below a depth of about 25 m. From 25-30 m the total thickness of such layers actually amounts to 21 % of the total thickness. This introduces more uncertainty into assessment of results of test Pile B, than test Pile A. For that reason, it is herein focused on test Pile A.

Soil sampling at Vigda was limited to about 23 m below ground level at the test site. The samples showed that the water content decreased gradually with depth from on average of 31 % (range 28-34 %) around 5m depth to about 26 % (range 24-28) in the lowest part. The plasticity index was measured to I_p=15 % in the silty clay at depth of 5.5 m. Based on other data and water content values it may assumed that I_p for the silty clay gradually reduces with depth to maybe around 10 % below 25 m.

In-situ pore pressures were measured at various locations and depths along the bridge, and show a consistent picture of a fairly significant artesian condition at this level in the slope, 30 % above hydrostatic from a ground water table at about 3 m depth, Figure 3.4.3. The assumed pre-consolidation pressure and OCR-profiles shown in Figure 3.4.3 were computed assuming the maximum past effective stress was given by the vertical effective stress prior to erosion assuming a submerged unit weight of typically 10 kN/m^3, and that the clay under the old sea bottom (pre-erosion) had built up an apparent pre-consolidation pressure due to secondary consolidation corresponding 1.25 times the original effective stress.
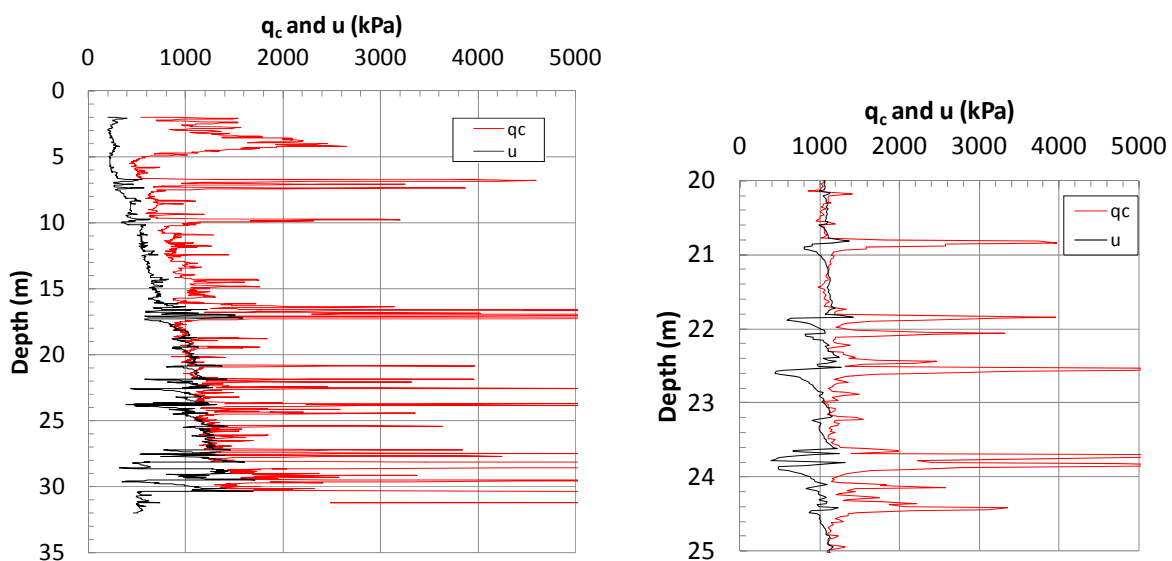
Figure 3.4.1 –Results from CPTU boring112 (Elev. 6.7) next to pile tests, Vigda
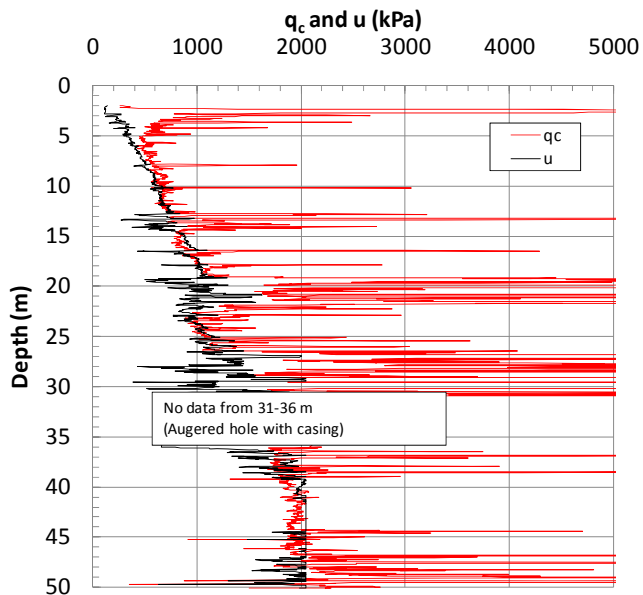
Figure 3.4.2 – Results from CPTU boring 111 (Elev. 3.1), Vigda
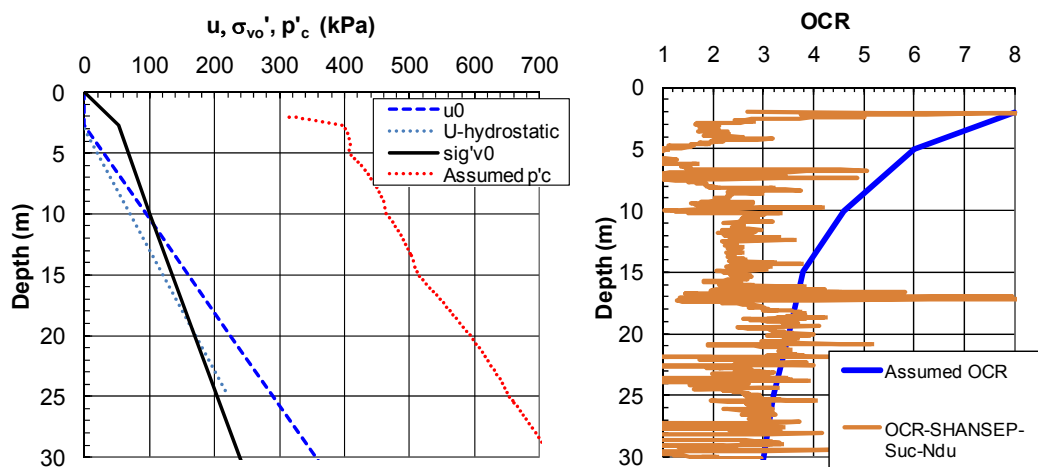
Figure 3.4.3 – Assumed in-situ stress conditions, Vigda

Figure 3.4.4 show the s_{uc} undrained strength profile derived from the CPTU test (boring 112) in Figure 3.4.1, using the same procedure as described for Børsa in Section 3.3. In this case there is larger difference between the strength derived from pore pressure and tip resistance. A few comments may be given to the actually assumed s_{uc} profile:

- The upper 5 m is dominated by a rather stiff weathered layer. The pore pressures response in boring CPTU-112 was apparently poor through this layer, leading to too low deduced strength.
- From 5-17 m the assumed s_{uc} profile tries to approximately match the largest values calculated from the measured pore pressure response, or the lower range of values calculated from the tip resistance.
- From 17-25 m most weight is given to values calculated from the pore pressure response.
- The criteria used to select the "assumed" s_{uc} profile was also to represent a reasonable match with OCR estimated from the assumed past overburden, and what could be back-calculated with the SHANSEP procedure from the assumed strength profile.

The test piles were driven with a 6 t hydraulic hammer. They showed no tendency for plugging during driving. Both piles were loaded to failure in tension by an incremental load-controlled procedure. The loading took place 58 days after pile installation, which based on other experiences on similar piles in similar clays (e.g. open-ended piles at Onsøy and Lierstranda described in Section 2.4 and 2.5) should ensure essentially 100 % consolidation.
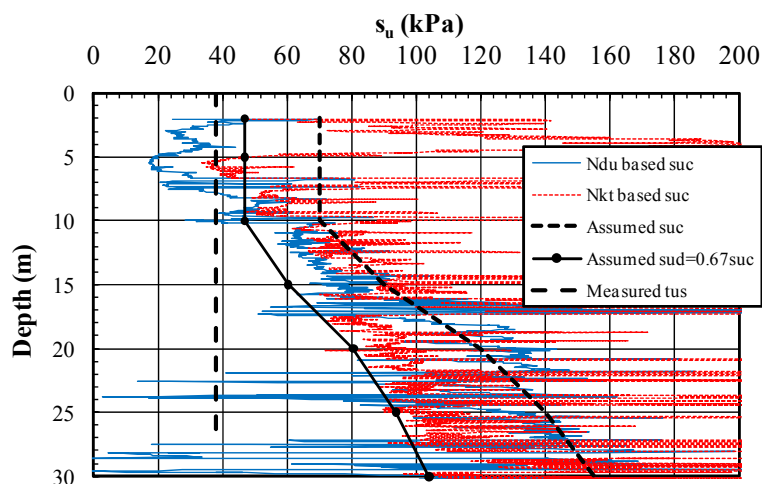
Figure 3.4.4 – Assumed undrained strength profile derived from CPTU, Vigda

Table 3.4.1 presents results of load tests on the piles. Failure was reached at a pile top displacement of 13 mm for Pile A and 52 mm for Pile B. Loading to failure took about 1 hour for Pile A and 1/2 hour for Pile B. The net ultimate shaft friction values were calculated by subtracting the weight of pile and soil plug and net theoretical tip resistance from the total load measured at the pile top. This amounted to 207 kN for Pile A and 410 kN for Pile B.

The average shaft friction for Pile A given in Appendix 3 implies average values of $\alpha=0.61$ and $\beta= 0.34$. The average shaft friction for Pile B was even lower than for Pile A, and gives average values of $\alpha=0.33$ and $\beta= 0.135$.

Table 3.4.1 – Summary of measured pile capacities, Vigda

Test No.	Time after inst (days)	Ultimate total load Q_{ut} (kN)	Estimated ultimate shaft load Q_{us} (kN)	Average shaft friction τ_{us} (kN)
Pile A	58	1670	1463	38.1
Pile B	58	2580	2170	28.6

3.5 Onsøy 2

Testing of piles at the Onsøy 2 test site is part of the ongoing Multi-industry research program "Time effects piles" mentioned in Section 1.3. A series of pile tests were here carried out on steel pipe piles with diameter of 508 mm and wall thickness of 6.3 mm driven open ended to a tip penetration of 19.1 m. The piles were driven through a 1.4 m deep augured casing.

The Onsøy 2 test site is located about 1 km away from the test site used earlier (Section 2.4), but the clay characteristics are very much the same. As shown in Figure 3.5.1, this normally consolidated clay deposit has w= 47-70% and I_p= 24-40 %. All data regarding the site conditions

and load tests were retrieved from NGI-files (Project No.20061251). The results have not yet been formally reported or published.

The site investigations consisted of continuous 72 mm piston sampling and CPTU test. Testing of the samples has, in addition to routine type classification tests, included CRS oedometer tests, undrained CAUC triaxial tests and DSS tests.
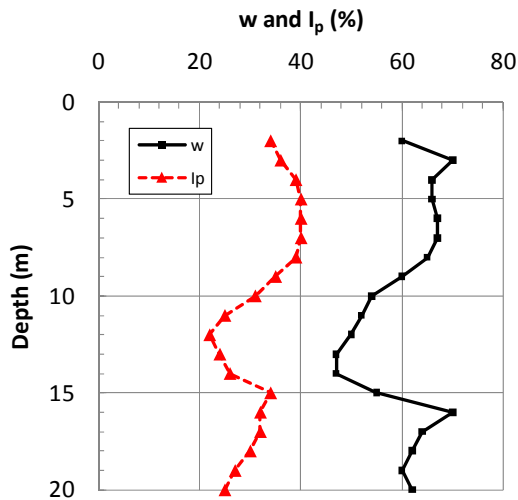
Figure 3.5.1 – Water content and plasticity index, Onsøy 2

Figure 3.5.2 show in-situ stress conditions derived from the soils data. The measured pore pressures show a slight artesian condition as compared to the hydrostatic, with measured ground water table at a depth of 0.8 m. The pre-consolidation pressures derived from oedometer tests were judged to be on the low side due to some apparent effects of sample disturbance. The selected OCR profile in Figure 3.5.2 was therefore primarily based on values back-calculated with SHANSEP from the CPTU- based s_{uc} values, assuming S=0.28 and m=0.85 for this clay.
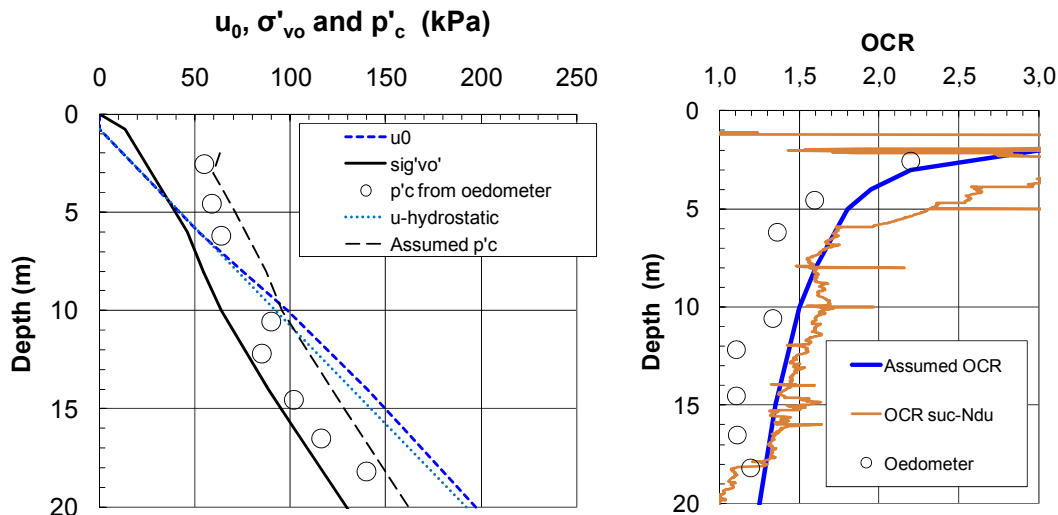
Figure 3.5.2 – Assumed in- situ stress conditions, Onsøy 2

Figure 3.5.3 shows undrained shear strengths from the CAUC and DSS tests carried out on samples from 3 levels, compared to the s_{uc} strength   derived from the pore pressure response in

the CPTU tests using the Karlsrud et al (2005) correlations. These CPTU derived s_{uc} strengths are on the high side of the strengths from the triaxial tests. The triaxial tests were, as the oedometer tests, to some extent influenced by sample disturbance as compared to high quality block samples, which the CPTU correlations are based upon. For that reason the selected s_{ud} profile also lies somewhat higher than the DSS test results. As a comment, due to the impact of stress rotation during DSS tests, the strength in DSS test is normally less influenced by sample disturbance effects than CAUC tests.
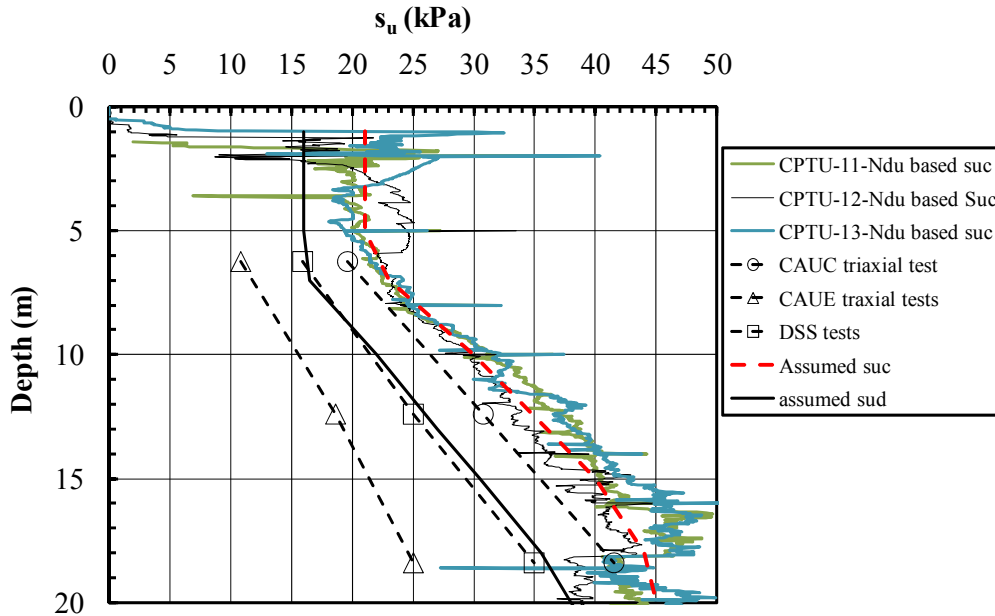
Figure 3.5.3 – Assumed undrained shear strength profile, Onsøy 2

The Onsøy piles were loaded incrementally to failure. The piles developed failure at a pile top displacement of 15 mm, ref. Figure 3.5.4. After unloading there was a permanent displacement of about 10 mm. The stepwise loading to failure took about 1 hour.
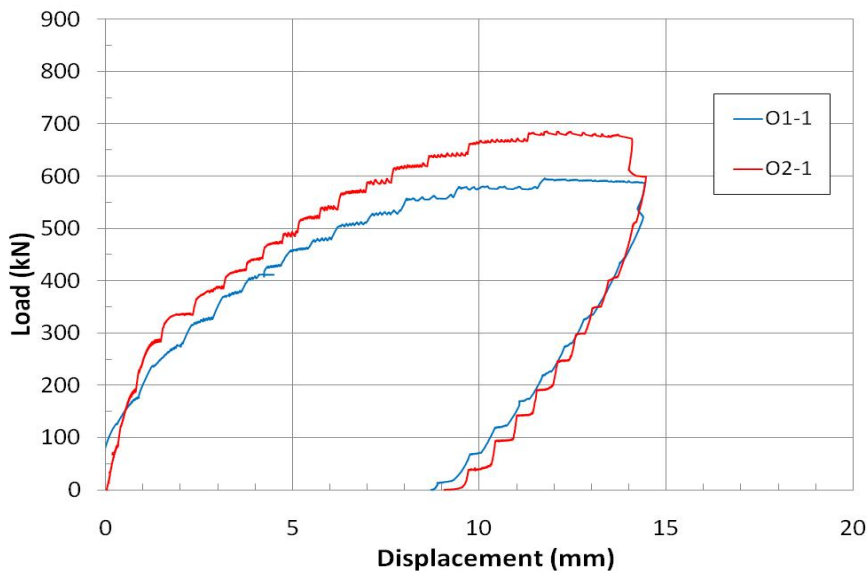
Figure 3.5.4 –Load-displacement response, Onsøy

Table 3.5.1 gives the measured capacities for the first time testing of pile 1 and 2 tested respectively 3 months and 6 months after pile installation. A net effect of weight of pile and soil plug and tip resistance, amounting to 46 kN, was deducted from the total failure load to arrive at the ultimate shaft friction. Pile 1 may not have reached quite 100 % consolidation at the time of loading, whereas Pile 2 may be impacted by some ageing effect. The chosen value of τ_{us} to represent 100 % consolidation was taken as 21.3 kPa, closest to the Pile 2 result. As seen from Appendix 3, it represents an average $\alpha=0.91$ and $\beta= 0.31$. These values are pretty much in line with the results from earlier tests at Onsøy, ref. Section 2.4. As the earlier A and C piles at Onsøy were closed- ended, this test verifies that open and closed piles in such clay show essentially the same ultimate shaft friction.

Table 3.5.1 – Summary of measured pile capacities, Onsøy

Test No.	Time after inst (days)	Ultimate total Load Q_{ut} (kN)	Estimated ultimate shaft load Q_{us} (kN)	Average shaft friction τ_{us} (kN)
Pile O1-1	78	595	549	19.4
Pile O2-1	164	680	634	22.4
Assumed for U=100%		650	604	21.3

3. 6 Stjørdal

Pile testing at the Stjørdal site is also part of the ongoing Multi-industry research program "Time effect piles". The test pile dimensions were the same as at Onsøy 2 (diameter of 508 mm and wall thickness of 6.3 mm), and they were driven open ended through a 1m deep casing to a tip penetration of 23.6 m.

This test site is located about 50 km north of Trondheim next to E6 and close to the Værnes airport. All data regarding the site conditions and load tests were retrieved from NGI-files (Project No. 20061251). The results have not yet been formally reported or published.

The site investigations consisted of more or less continuous 72 mm piston sampling and CPTU test. Testing of the samples has, in addition to routine type classification tests, included CRS oedometer tests, undrained CAUC triaxial tests and DSS tests.

Below an upper fine sand deposit extending to a depth of 3 m, there is a very uniform silty clay deposit. Figure 3.6.1 shows that the water content lies in the range w =28 to 32 %, and the plasticity index range from $I_p=12$ to 15 %.

Figure 3.6.2 show in-situ stress conditions derived from the soils data. The measured in-situ pore pressure is hydrostatic below the ground water table at depth of 2.0 m. The pre-consolidation pressures derived from oedometer tests were judged to be on the low side due to some effects of sample disturbance. The selected OCR profile in Figure 3.6.2 was therefore primarily based on values back-calculated with SHANSEP from the CPTU- based s_{uc} values, assuming S=0.28 and m=0.85 for this clay (se following).

Figure 3.6.3 presents undrained shear strengths from the CAUC and DSS tests carried out on samples from 3 levels, as well as the s_{uc} strength profile derived from the tip resistance in CPTU

tests using the Karlsrud et al (2005) correlation. It may be noted that the pore pressure response in the CPTU tests for some reason was very poor (most likely sensor trouble) and had to be disregarded as basis for determination of undrained strength. (Tests may be repeated later as part of the ongoing research program).The CPTU derived s_{uc} strengths agree very closely with the triaxial tests, which appeared to be of good quality. The same applies to the DSS tests which show a strength typically corresponding to $s_{ud} = 0.67 s_{uc}$ (range 0.62-0.71). The selected s_{ud} tries to reflect the variations in the CPTU derived values, but neglects the tendency for local high values from 22.5 to 26 m depth. (That is of little importance as the pile tip is at 23.6 m)
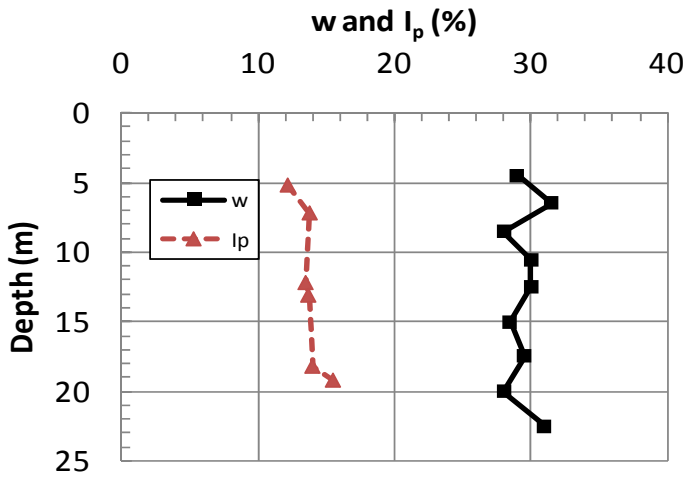
Figure 3.6.1 – Water content and plasticity index, Stjørdal
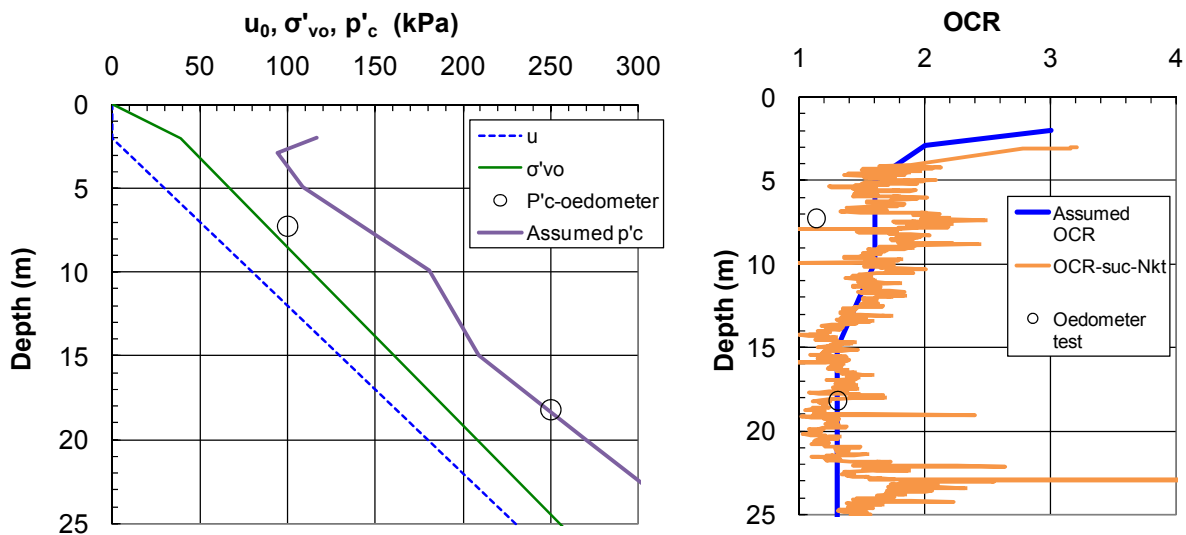
*Figure 3.6.2 – Assumed in- situ stress conditions, Stjørdal*
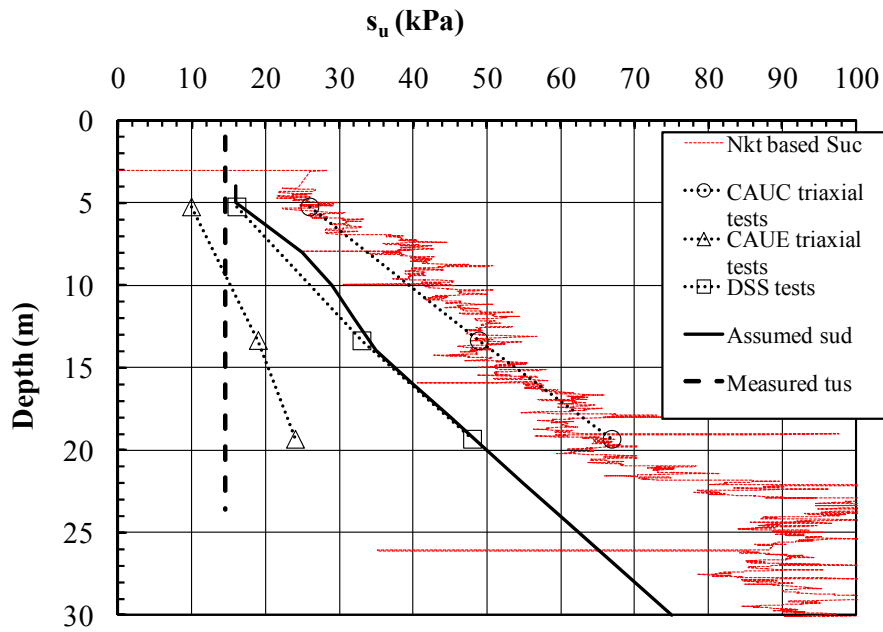
Figure 3.6.3 – Assumed undrained shear strength profile, Stjørdal

The Stjørdal piles were loaded incrementally to failure. The piles developed failure at a pile top displacement of about 30 mm (twice that of the directly comparable Onsøy 2 piles), Figure 3.6.4. After unloading there was a permanent displacement of about 20 mm. The stepwise loading to failure took about 1 hour.
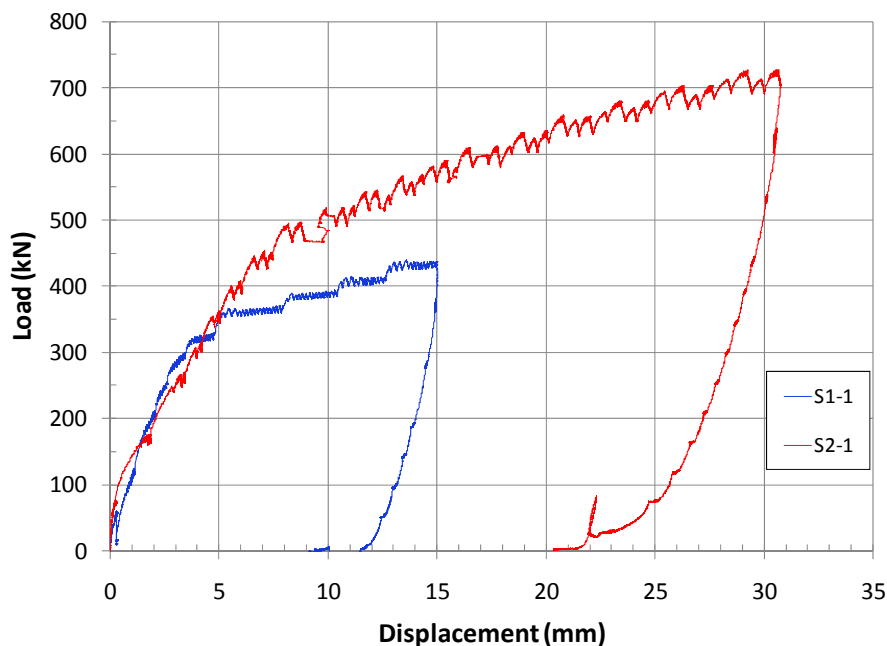

Figure 3.6.4 –Load-displacement response, Stjørdal

Table 3.6.1 gives the measured capacities for the first time testing of Pile 1 and 2. A net effect of weight of pile and soil plug and tip resistance amounting to 79 kN is deducted from the total failure load to arrive at the ultimate shaft friction. Pile S1-1 may not have quite reached 100 % consolidation at the time of loading and loading was stopped prematurely. Interpreted failure load for this pile is 480 kN. Pile S2-1 may be impacted by some ageing effect. The chosen value to represent 100 % consolidation was close to the average of the two test result, and is used in

Appendix 3. It represents an average value of α=0.45 and β= 0.11. These results confirm previously presented tests that low plastic lightly over-consolidated clays show relatively speaking low shaft friction, in this case only ½ the values for the very comparable Onsøy 2 tests.

Table 3.6.1 – Summary of measured pile capacities, Stjørdal

Test No.	Time after inst (days)	Ultimate total load Q_{ut} (kN)	Estimated ultimate shaft load Q_{us} (kN)	Average shaft friction τ_{us} (kN)
Pile S1-1	50	480	402	11.2
Pile S2-1	111	700	622	17.3
Assumed for U=100%		600	522	14.6

3.7 Cowden

These tests are also part of the ongoing Multi-industry research program "Time effect piles". The test site area lies fairly close to where the IC tests reported in Section 2.9.3 were made. The test pile dimensions were diameter of 457 mm and wall thickness of 12.5 mm, and they were driven open ended through a 1m deep casing to a tip penetration of 10.0 m. The piles partially plugged during driving. At end of driving the distance from the ground surface to the top of the plug was 2 m.

The Cowden site has been extensively used as a research site by the Building Research Establishment (BRE) in the UK. The soil characteristics described in the following were based on a comprehensive presentation of soils data given by Powell and Butcher (2003). On contract from NGI, BRE also implemented these new pile tests. The data, which are not formally reported as yet, were extracted from NGI files (Project 20061251).

Figure 3.7.1 shows that within the pile testing depth the Cowden till has a rather uniform water content and plasticity index. The plastic limit lies very close to the water content, as is typical of heavily over-consolidated clays.
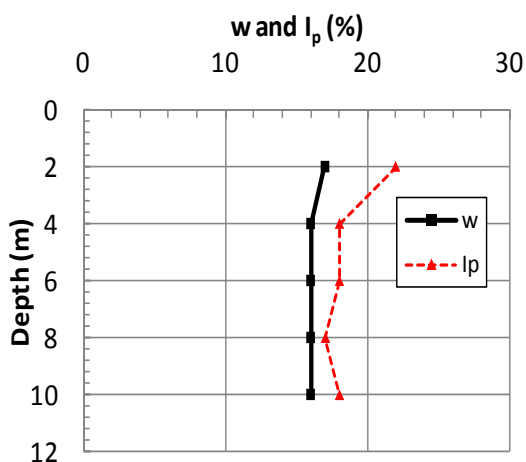
Figure 3.7.1 - Water content and plasticity index, Cowden

Figure 3.7.2 show in-situ stress conditions derived from the soils data. The measured in-situ pore pressure is hydrostatic below the ground water table at depth of 0.8 m. The selected OCR profile

in Figure 3.7.2 was based on values back-calculated with SHANSEP from the CPTU based s_{uc} values (Figure 3.7.3), assuming S=0.28 and m=0.80 for this clay (se following). It agrees well with the range of OCR-values given by Powell and Butcher (2003) based on oedometer tests and in-situ tests.

Figure 3.7.3 shows the undrained shear strength profile arrived at from the CPTU test. For the highest OCR clay in the top, it was assumed $s_{ud}=0.65s_{uc}$, and below 5m depth it was taken as $s_{ud}=0.70s_{uc}$.
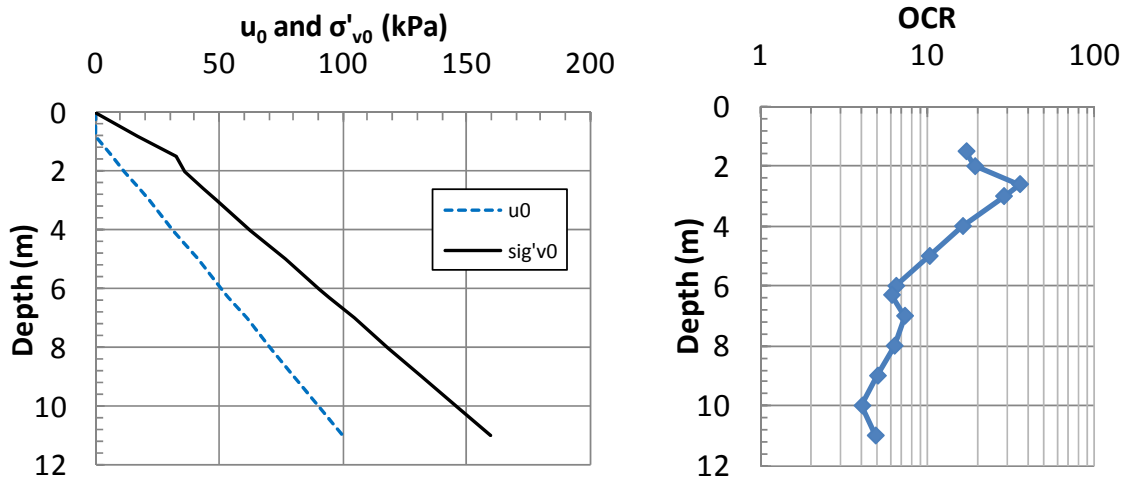
Figure 3.7.2 – Assumed in- situ stress conditions, Cowden
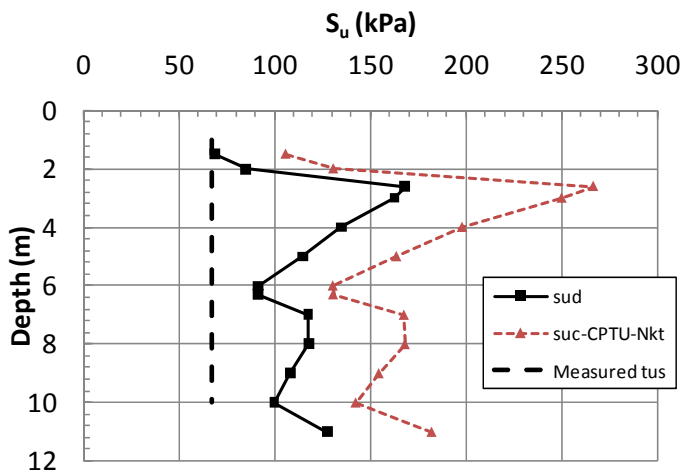
Figure 3.7.3 – Undrained shear strength profile, Cowden

The Cowden piles were also loaded incrementally to failure in tension. The piles developed failure at a pile top displacement of about 32 mm, Figure 3.7.4. After unloading there was a permanent displacement of about 28 mm. The stepwise loading to failure took about 1 hour.
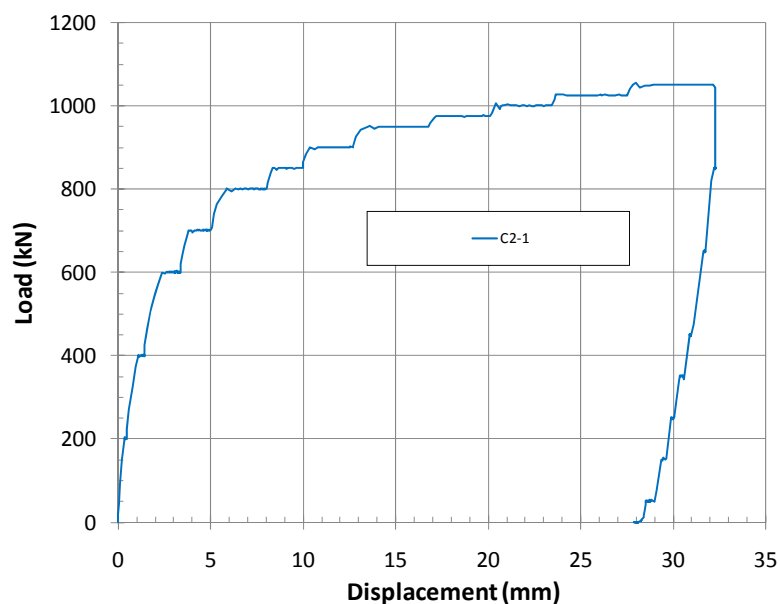
Figure 3.7.4 – Typical load displacement curve, Pile C2-1, Cowden

Table 3.7.1 gives the measured capacities for the first time testing of Pile C1 and C2. A net effect of weight of pile and soil plug and tip resistance amounting to 147 kN is deducted from the total failure load to arrive at the ultimate shaft friction.

Pile S1-1 may not have quite reached 100 % consolidation at the time of loading, whereas Pile S2-1 may be impacted by some ageing effect. The chosen value to represent 100 % consolidation was close to the average of the two test result, and is used in Appendix 3. It represents average values of $\alpha=0.60$ and $\beta=0.80$. It may be of interest to note that the normalised shaft friction values agree fairly well with the IC model pile tension tests at Cowden presented in Section 2.9.2, but is smaller than the compression results reported for the IC tests.

Table 3.7.1 – Summary of measured pile capacities, Cowden

Test No.	Time after inst (days)	Ultimate total load Q_{ut} (kN)	Estimated ultimate shaft load Q_{us} (kN)	Average shaft friction τ_{us} (kN)
Pile C1-1	48	1010	862	66.7
Pile C2-1	119	1030	882	68.3
Assumed for U=100%		1020	872	67.5

3.8 Femern

The Femern test site is located in the sea between Denmark and Germany. The water depth at the pile test site is about 12 m. The clay at this site is a rather uncommon deposit of very plastic and old Palaeogene clay (dating back about 20-60 million years).

The pile testing program is part of ongoing plans for a fixed link across the strait, either bridge or submerged tunnel. Femern A/S wanted to undertake a pile testing program at the site which is

essentially identical to the test program carried out at other sites as part of the "Time effects piles" project. Furthermore, the Femern project kindly made all soils and pile test results available to this project. NGI took part in the planning and execution of the tests and developed part of monitoring system. Per Aarslef A/S was contracted by Femern A/S to act as the general contractor with overall responsibility for execution of the tests.

The test piles used at Femern have a diameter of 508 mm and wall thickness of 22.5 mm. They were driven open-ended from a jack-up barge through a piling and loading frame pre-installed at the sea bottom. The piles were driven to a tip penetration of 25.0 m. During driving of the piles, the soil entering the piles was more or less continuously removed to avoid plugging, which could adversely affect (prolong) the pile set-up. For that reason the pile installation took several days. The loading frame was installed at the sea bottom and anchored with separate piles in the corners.

An extensive site investigation program has been carried out in several stages for the planned fixed link. The soils data presented in the following were mainly extracted from the summary report by Femern A/S (2011) which has been made fully open and can be downloaded from VWw.fehmarnlink.com. Focus is on soils data from within reasonable proximity of the pile test area.

At the pile test site there is an upper 2-3 m thick layer of sand followed by some more recent or re-worked clay. Below about 5 m there is folded and fissured Palaeogene clay of the so-called Røsnes formation. Figure 3.8.1 shows that the water content below the top part is typically 36 %. The average plasticity index increases from about 50 % at 5 m to 120 % at 20 m depth. Notice however, the upper and lower I_p ranges. The real I_p values actually vary within these ranges throughout the deposit, that is, on a very local level. The liquid limit is very close to, but typically 5% lower than the water content, giving a liquidity index that typically decrease fro 0.08 at 10 m to 0.05 at 30 m depth. The clay content is high and varies also locally from about 50 to 85 %.

A large number of CRS and IL type oedometer have been carried out on Femern clay. Figure 3.8.2 show the pre-consolidation pressures reported from the soil borings closest to the pile test site. Definition of the pre-consolidation pressure from oedometer tests on stiff clays can be difficult, considering also the possible impact of sample disturbance, ref. discussion related to Tilbrook data in Section 2.7. In the current case, samples were taken with the Geobore-S core drilling system. Even if great attention is given to the coring procedure, it is hard to eliminate any effect of sample disturbance. The individual oedometer tests have not been reviewed as part of this study. The pre-consolidation pressures and OCR values are assumed as they were reported by Femern AS (2011), knowing that highly qualified and experienced people undertook that work.
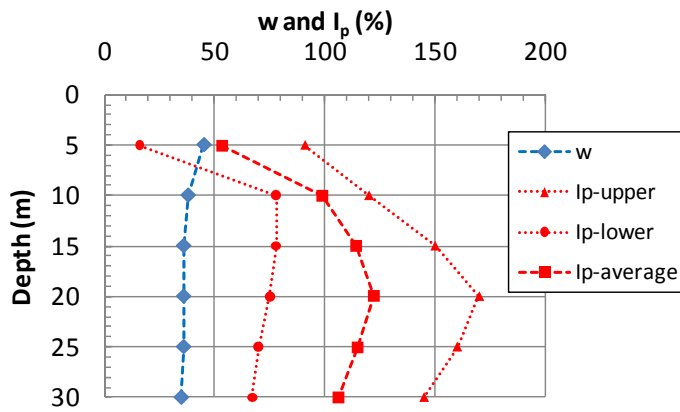
Figure 3.8.1 – Water content and plasticity index, Femern
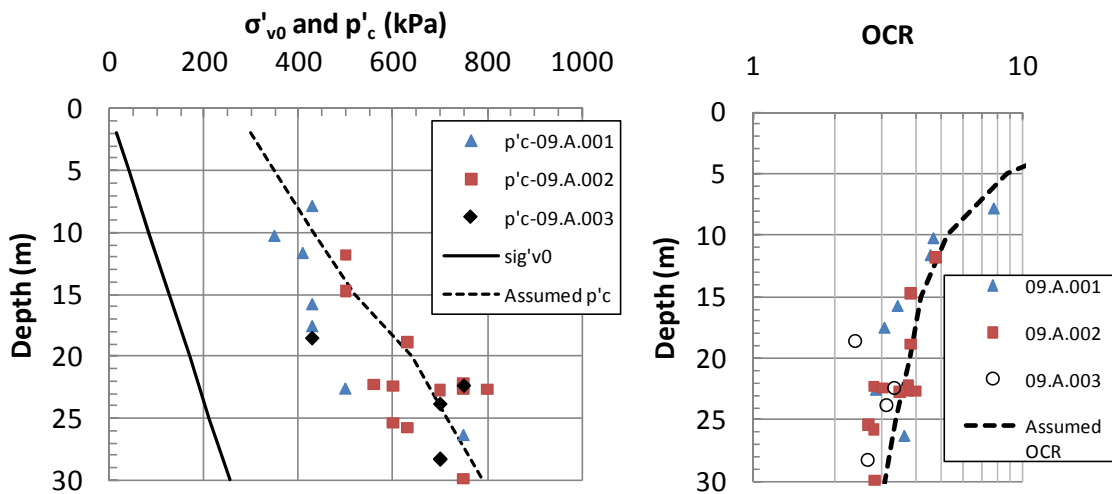
Figure 3.8.2 – Assumed in-situ stress conditions, Femern

The permeability of the clay is very low, measured values ranging from about $2 \cdot 10^{-12}$ to $2 \cdot 10^{-11}$ m/s.

The soil testing at Femern also included a series of DSS tests. Two test types were run:

1. The samples that were first consolidated up to but not above the assumed pre-consolidation pressure, and then un-loaded back to σ'_{v0} prior to undrained shearing. The purpose is to try to re-store the in-situ horizontal effective stress prior to shearing. This is also standard procedure used at NGI on OC clays, e.g.Lunne et al (2006).
2. The samples that were first consolidated to well beyond the pre-consolidation pressure and then un-loaded to various stress levels prior to undrained shearing. This is according to the SHANSEP procedure, Ladd et al (1977).

Figure 3.8.3 shows the results from the SHANSEP consolidated samples. They define average values of S= 0.23 and m=0.85. Figure 3.8.4 shows the results from samples consolidated with the p'_c- σ'_{v0} procedure. Herein is also shown the calculated strength using the SHANSEP procedure with the assumed OCR values from Figure 3.8.2. The two approaches led to quite similar s_{ud} values.
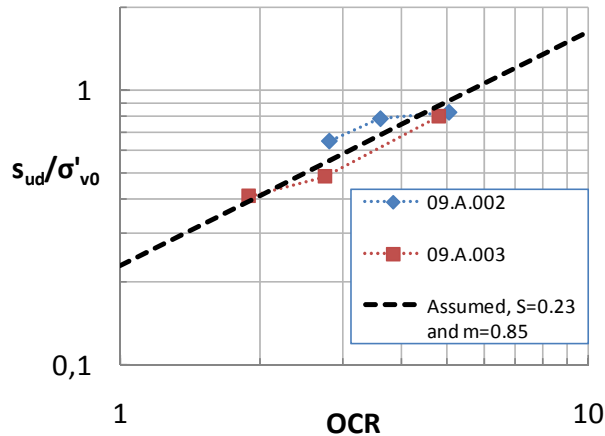
Figure 3.8.3 – Results of SHANSEP consolidated DSS tests, Femern
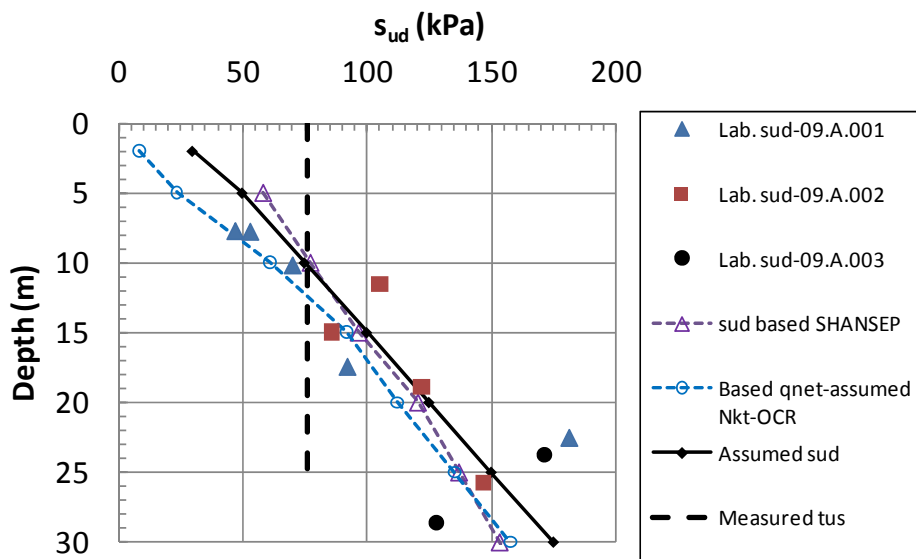
Figure 3.8.4- Summary of s_{ud} strengths, Femern

A number of CPTU tests have also been carried out at the Femern site. Figure 3.8.5 summarize the measured corrected tip resistance values, q_t. The tests 09.B001 and 09.B002 in the left diagram were carried out in an early phase, and were located somewhat up-slope and down-slope from the pile test site. These tests were of the stepwise downhole type. The tests in the right hand diagram were carried out in closer proximity of the test piles, and were based on direct push-in from the seabed. As seen in the left hand diagram, the average values from the two are in good agreement. The selected typically assumed profile is also shown herein.

In the Femern A/S (2011) report, the measured DSS strengths were presented in relation to the cone tip resistance. Figure 3.8.5 shows a correlation between $N_{kt} = (q_t - \sigma_{v0})/s_{ud}$ proposed by the author on that basis. Figure 3.8.4 shows the s_{ud}-profile established using this correlation and the typically assumed q_t profile in Figure 3.8.5. The CPTU deduced s_{ud} profile falls somewhat on the low side of the other values, especially in the top part. The s_{ud} profile proposed and used herein, and shown with black solid line in Figure 3.8.4, gives most weight to the s_{ud} strengths derived from the laboratory tests.
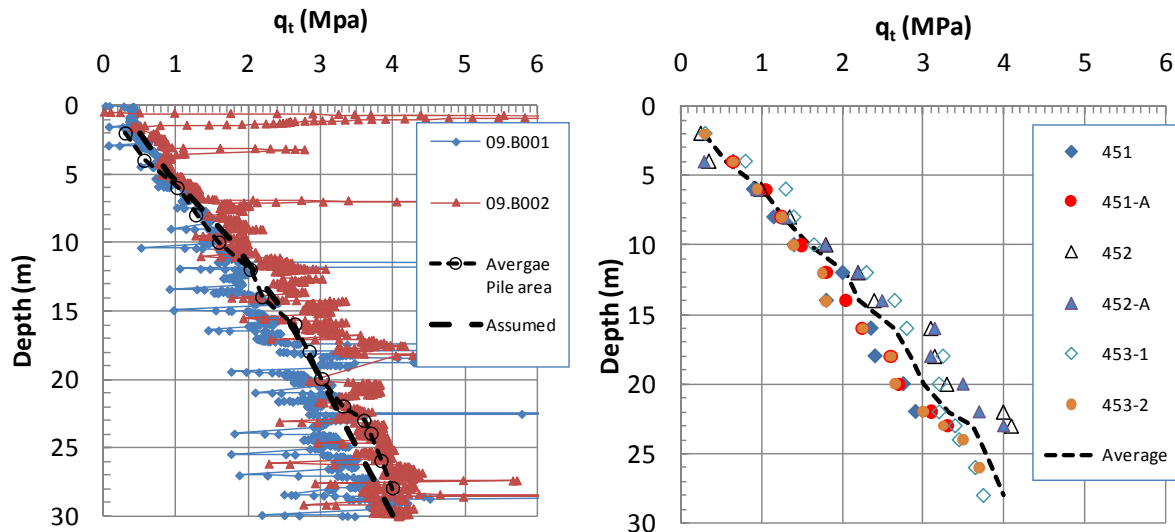
Figure 3.8.5 – Summary of corrected cone tip resistance values, Femern
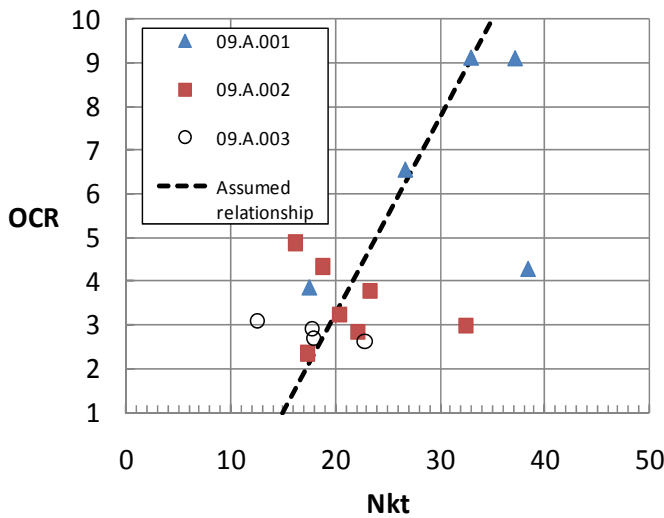
Figure 3.8.6 – Cone factor N_{kt} relating s_{ud} to OCR, Femern

The piles were loaded stepwise to failure in tension. Figure 3.8.7 shows the load displacement curve, and Table 3.8.1 presents the ultimate capacity from the first time testing of the first two test piles. As the piles were cored out to 5 m above the tip during driving (to avoid plugging), the net correction for weight of pile, plug and tip resistance is relatively speaking small in these cases, about 120 kN.

Table 3.8.1 – Summary of measured pile capacities, Femern

Test No.	Time after inst (days)	Ultimate total load Q_{ut} (kN)	Estimated ultimate shaft load Q_{us} (kN)	Average shaft friction τ_{us} (kN)
Pile F1-1	48	3150	3030	75.9
Pile F2-1	119	?3200	3080	77.2
Assumed for U=100%				77.2
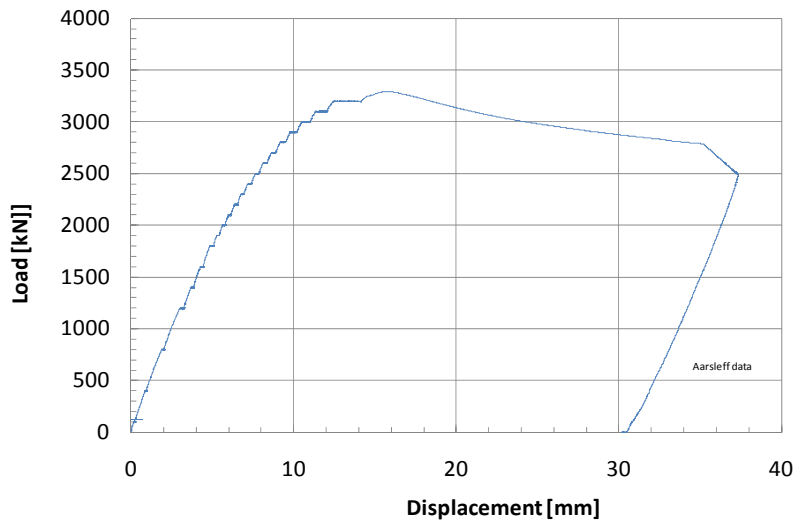
Figure 3.8 7- Load-displacement curves for pile test F1-1, Femern

A reference pile was installed at Femern which was identical to the others, but was instrumented with pore pressure sensors at two levels. Figure 3.8.8 shows that there was still significant excess pore pressure along this pile at the time of testing, about 1 and 3 months after the piles were installed. The measured pore pressures are also compared to end of installation pore pressures, calculated with the procedure recommended in Chapter 4. This suggests that the degree of consolidation at the time of testing had only reached 40-45 % at the upper level, and 75-80 % at the lower level. (The reason for using calculated and not measured installation pore pressures as a reference, is that the pore pressure sensors on this pile were not put in operation until sometime after installation, and needed time to equilibrate before reliable data could be obtained).
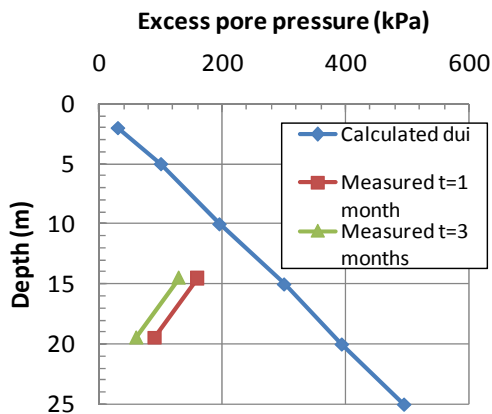
Figure 3.8.8 – Measured excess pore pressures against reference pile, Femern

In spite of diminishing excess pore pressure from test F1-1 to test F2-1, the capacities in Table 3.8.1 are essentially identical. This may suggest, that in this case the total earth pressures decreased by the same magnitude as the pore pressures during the later stages of the consolidation phase, giving no increase in capacity. Although it could be on the low side, the 3 month test has been assumed as the full set-up capacity for this case. As given in Appendix 3, this average shaft friction implies average values of $\alpha=0.91$ and $\beta=0.74$.

3.9 Oromieh

In connection with design of foundations for a bridge across the Oromieh lake in Iran, a steel pipe pile was installed and load tested. The case has been fully documented by Karlsrud and Mahan (2009). Therefore, only a short summary is given herein. The pile had a diameter $\Phi = 305$ mm and wall thickness t = 16 mm. It was driven open ended to 66.1 m depth below lakebed. The pile did not show any tendency for plugging during installation.

The clay deposit in the lake, located about 1000 m above sea level, is dated to be about 115,000-450,000 years old, increasing with depth. The water in the lake is essentially fully saturated with salt, i.e. it is a salt lake. The average unit weight of the pore water is 11.4 kN/m^3.

Figure 3.9.1 shows that the natural water content generally lies in the range 30-45% with a somewhat decreasing tendency with depth. The water content lies in between the plasticity and liquid limits, but closer to the latter as is typically of aged normally consolidated clay deposits. The plasticity index mostly lies in the range 15 to 30 %.

The undrained shear strength of the clay was determined from down-hole stepwise CPT. Figure 3.9.2 shows the interpreted s_{uc} strength profile based on the Karlsrud et al (2005) correlations. For this clay it was assumed $s_{ud} = 0.7 \cdot s_{uc} = 0.7 \cdot 0.38\sigma'_{v0} = 0.27\sigma'_{v0}$. The apparent over-consolidation ratio of the clay would for these normalised strengths correspond to about OCR=1.4.

The pile was loaded incrementally to failure in tension. Figure 3.9.3 shows the measured load-displacement response, which gave a failure load of 3000 kN. Total correction for weight of pile, soil plug and tip resistance amounts to 173 kN, giving an ultimate shaft load of Q_{us}=2827 kN. As presented in Appendix 3 this gives an average shaft friction of τ_{us} = 44.6 kPa, leading to average values of α=0.93 and β= 0.25.
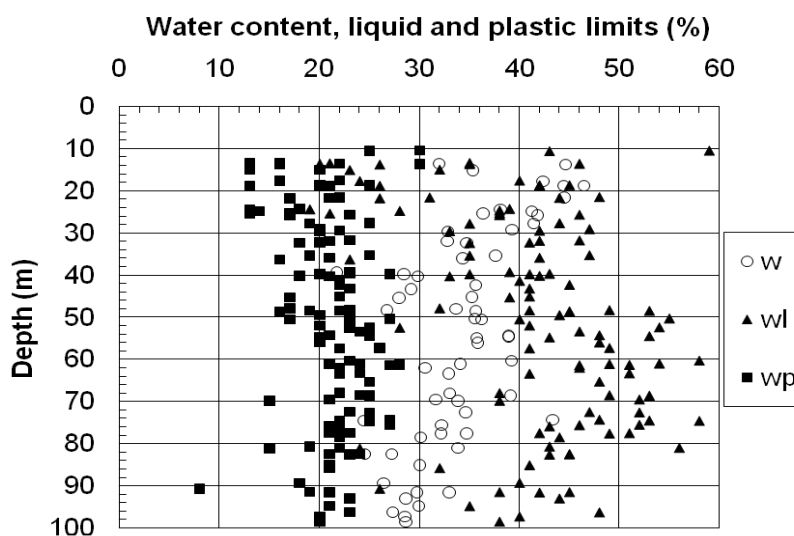
Figure 3.9.1- Water content and plastic limits, Oromieh (after Karlsrud and Mahan, 2009)
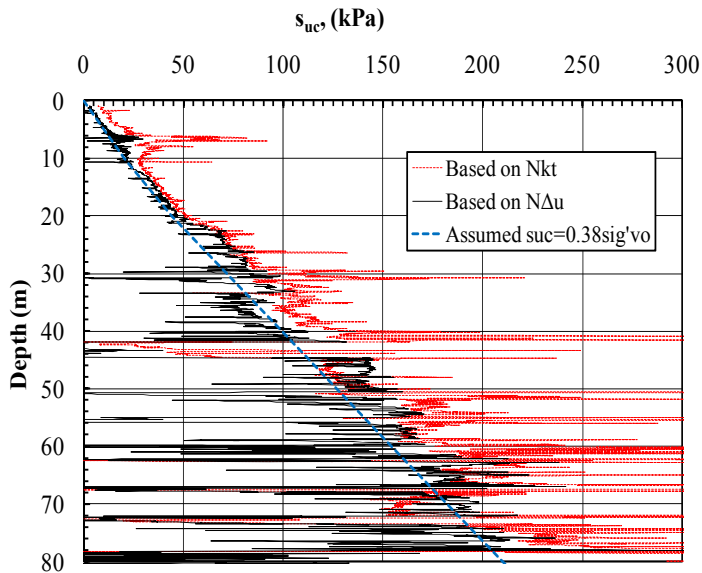
Figure 3.9.2- Undrained s_{uc} strength derived from CPTU, Oromieh (after Karlsrud and Mahan, 2009)
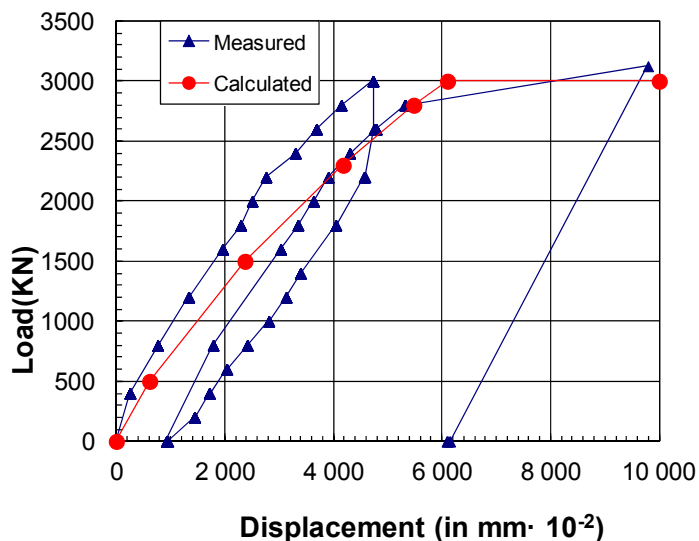
Figure 3.9.3 – Load-displacement response, Oromieh

3.10 Some overall observations

The non-instrumented pile tests cover a wide range of clay properties. The deduced normalised α- and β-values summarised in Appendix 3 also vary within a rather wide range, e.g α-values from 0.25 to 0.90. The lowest α-values are observed in the low plastic and low OCR deposits at Stjørdal and Børsa. This tends to confirm the low values also observed for some of the instrumented pile tests at Lierstranda and Pentre (ref. Appendix 2). The pile test in the very high plastic overconsolidated clay at Femern gave on the other hand an α-value that may be considered high compared its normalised undrained strength of $s_{ud}/\sigma'_{v0} = 0.79$ and oCR of about 4.3. This result tends, however, to support results of the instrumented IC-pile test in the high plastic and high OCR clay deposit at Cannons Park. Thus, the plasticity index also seems to be of some importance for high OCR clays. Chapter 6 discuss, compare and assess the ultimate shaft friction values in further detail.

4 THE PILE INSTALLATION PHASE

4.1 Models for predicting stresses and strains surrounding a pile

4.1.1 Methods considered

Stress changes caused by installation or driving of a pile into clay under undrained (no volume change) conditions can in its simplest way be determined by a de-coupled two-stage process. The displacements and strains in the soil around the pile after the pile tip has penetrated well beyond a point in the ground are determined first. The stress changes can then be calculated from generalised soil models that describe the relationship between stresses and strains in the soil. More rigorous analyses can be carried out by fully coupled FEM methods with linear or non-linear total or effective stress based soil models.

The most widely used methods for modelling stress and strain changes are based on the idealized Cavity Expansion Method (CEM), and the more elaborate Strain Path Method (SPM). The basics of these methods will only be briefly described in the following Sections 4.2 and 4.3, as they have been so rigorously described in past publications. Some examples of impact of soil model will be illustrated in Section 4.4, but there will be more specific comparisons to field observations in Section 4.5.

4.1.2 The Cavity Expansion Method (CEM)

The Cavity Expansion Methods (CEM) was developed quite early (e.g. Hill,1950; Gibson and Anderson,1961; Soderberg,1962; Ladanyi, 1963), but has later been widely used by other researchers in relation to piles (e.g. Vesic, 1972; Torstensson, 1977, Carter et al, 1978; Randolph et al, 1979; Randolph, 2003). The method assumes that the strains induced in a clay surrounding a pile only comes from ideal expansion of a long cylinder deeply embedded in the ground. Solutions have been developed for both closed- ended piles, i.e. for expansion from zero to full radius, r_0, of the pile, and for open- ended piles expanding from the inner to the outer radius. For an open-ended pile it may be assumed that the expansion corresponds to more than the pile wall thickness if the pile partially plugs, or less than the full wall thickness if the clay for some reason enters the pile more easily inwards into the pile than outwards. In the latter case this implies that the plug will end up above ground level at the end of pile installation.

The radial strain is for a general case given by the following approximate expression (neglecting 2nd order terms):

$$\varepsilon_r = -0{,}5\ln(1- (r_o^2-r_i^2)/r^2) \qquad \text{, where} \qquad (4.1.1)$$

r_o =outer radius at end of expansion (i.e. outer radius of the pile)

r_i = inner radius from which expansion starts

For an ideal open-ended pile that expands only outwards, the inner radius may be taken as $r_i = r_o-t$, where t= wall thickness. If the pile partially plugs, one may establish an equivalent internal radius,r_{ie}, through solving the following expression for the normalised displaced volume:

$$\Delta V/V_0 = (r_o^2-r_{ie}^2)/ r_{ie}^2 \qquad \text{, where} \qquad (4.1.2)$$

ΔV = Net displaced volume= Total volume of pile- Volume of plug inside the pile

r_{ie} = equivalent internal radius = $r_o -t_e$

t_e = equivalent wall thickness

If the length of the plug inside the pile at end of driving is known, the following expression can be developed for the average equivalent wall thickness:

$$t_e = r_o - (r_o - t) \cdot (l_p/L)^{1/2} \qquad , \text{ where} \qquad (4.1.3)$$

l_p = length of soil plug inside the pile

L= total length of the pile in the ground

t = actual wall thickness of the pile

Figure 4.1.1 shows examples of radial strains in relation to the normalised displaced volume for a closed-ended pile and an open-ended pile with D/t = 40, which is quite a typical ratio for driven open-ended tubular steel piles. The radial strain exceeds 100% close to the pile wall for the closed-ended pile, and decease to 1 % at a distance of 8 pile radii. For the open-ended pile the strains are just about 1/10 of that of the closed-ended pile.
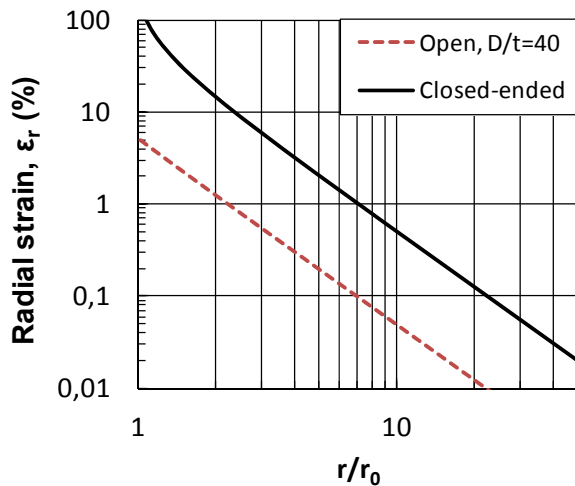
Figure 4.1.1- Examples of radial strains due to pile installation, CEM model

The CEM method has been coupled with various soil models to predict the stress changes in the clay as a result of the imposed strains. For perfectly undrained expansion the simplest solution is based on the assumption of an ideal isotropic linear -elastic-perfectly- plastic (EP) type soil model. The plasticized radius can then for a general case be determined from:

$$r_p = r_o \cdot (G/s_u)^{1/2} \cdot ((r_o^2 - r_{ie}^2)/r_0^2)^{1/2} \qquad , \text{ where} \qquad (4.1.4)$$

r_p = plasticized radius (distance to which shear stress exceeds s_u)

G = shear modulus up to failure

s_u = undrained shear strength

For this case the total stress changes against the pile wall are given by:

$$\Delta\sigma_r = s_u \cdot (1 + 2\ln(r_p/r_0)) \qquad (4.1.5)$$

$$\Delta\sigma_\theta = \Delta\sigma_r - 2s_u$$

$$\Delta\sigma_v = \Delta\sigma_r - s_u$$

Figure 4.1.2 shows an example of stress changes as function of pile radius predicted by the CEM-EP model for a case with $r_p \approx 8r_0$.
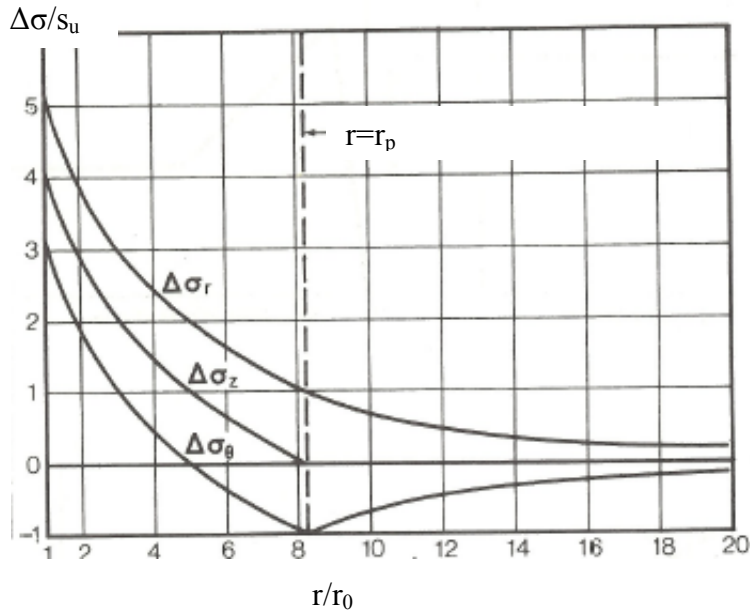
Figure 4.1.2 – Stress changes as function of radial distance for CEM-EP model (copied from Torstensson, 1977)

It has been commonly assumed (e.g. Torstensson, 1977; Randolph and Wroth, 1979) that the pore pressure change on the pile wall is equal to the octahedral total stress change, which becomes:

$$\Delta u = \Delta \sigma_{oct} = (\Delta\sigma_r + \Delta \sigma_\theta + \Delta \sigma_v)/3 = 2s_u \cdot \ln(r_p/ r_0) \qquad (4.1.6)$$

Outside the plasticized zone the stress changes are given by:

$$\Delta\sigma_r = s_u \cdot (r_p/ r)^2 \qquad (4.1.7)$$

$$\Delta \sigma_\theta = -\Delta\sigma_r$$

$$\Delta \sigma_v = 0$$

This then leads to $\Delta \sigma_{oct} = 0$.

For non-linear soil behaviour (without any strain softening), it may be reasonable to use the shear modulus at 50 % mobilization of the soil strength as an equivalent linear stiffness.

Figure 4.1.3 shows typical range of normalised shear modulus, G_{50}/s_{uc}, as observed from CAUC tests on high quality block samples. The figure is based on NGI data presented by Karlsrud and Hernandez (2011). The upper range for G_{50}/s_{uc} is observed for marine clays with water content mostly in the range 30-40%, which generally means clays with plasticity index in the range 12-20 %, and the lower range for more plastic clays with w = 60-70 %.

Figure 4.1.4 a) presents examples of computed values of normalised plasticized radius, $\lambda = r_p/r_0$ for a closed-ended pile, based on eq. (4.1.4) for the range of modulus values in Figure 4.1.3. Figure 4.1.4b) presents plasticized radius for open-ended piles for a range of diameter to wall thickness (D/t) ratios. Figure 4.1.5 a) and b) shows the corresponding calculated excess pore pressures $\Delta u_i/s_u$ against the pile shaft of closed-ended and open-ended piles. For this simple CEM-EP approach, it appears that an open mode of penetration can rather significantly reduce the excess pore pressure against the pile shaft as compared to a closed-ended pile.
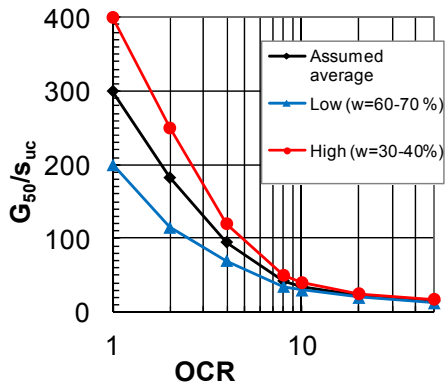
Figure 4.1.3 – Typical range of normalised G_{50}/s_{uc}- values obtained from CAUC triaxial tests on high quality block samples (based on Karlsrud and Hernandez, 2011)

b)

a)
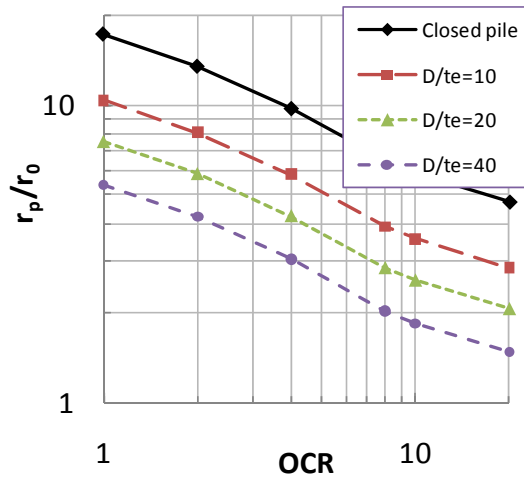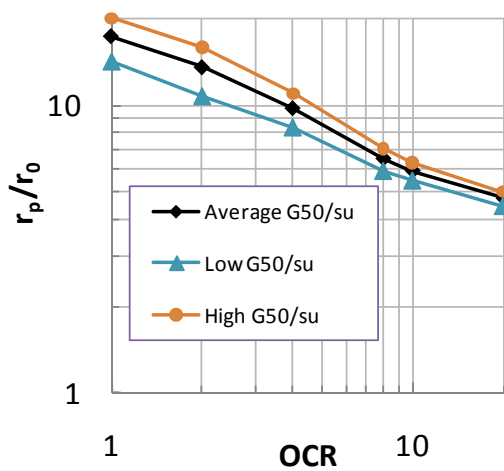
Figure 4.1.4 – Typical normalised installation plasticized radius based on CEM-EP model. a) For closed-ended piles for range of shear modulus values in Figure 4.1.3. b)Comparison closed- and open-ended piles for case with average shear modulus from Figure 4.1.3
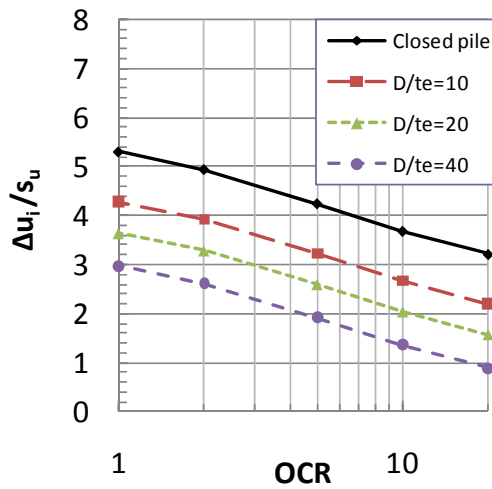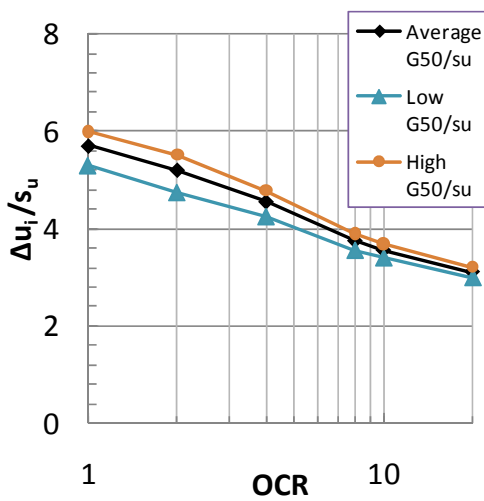
a)   b)

Figure 4.1.5 – Typical normalised installation excess pore pressures based on CEM-EP model. a) For closed-ended piles for range of shear modulus values in Figure 4.1.3. b) Comparison between closed- and open-ended piles for case with average shear modulus from Figure 4.1.3

It is in general an over-simplification to assume that excess pore pressures are equal to the octahedral stress change. This was also pointed out by Randolph et al (1979).The shear stresses induced will even for the idealized CEM expansion generate some additional pore pressures due to contraction and tendency for positive shear stress induced pore pressures in low and moderately over-consolidated clays. In heavily overconsolidated clays, negative pore pressure changes would be expected due to dilation.

Ladanyi (1963) presented calculated values of excess pore pressures for a strain softening soil. As illustrated by the example in Figure 4.1.6, the strain softening relationship was defined by a linear behaviour up to peak, defined by a Young's modulus, E_t, a peak shear stress τ_t, and a shear strain γ_t. This is followed by a linear decrease to a residual value defined as τ_f at a shear strain γ_f. The impact of such assumed strain softening is, as shown by the example in Figure 4.1.6, to decrease the pressures generated against the pile shaft.
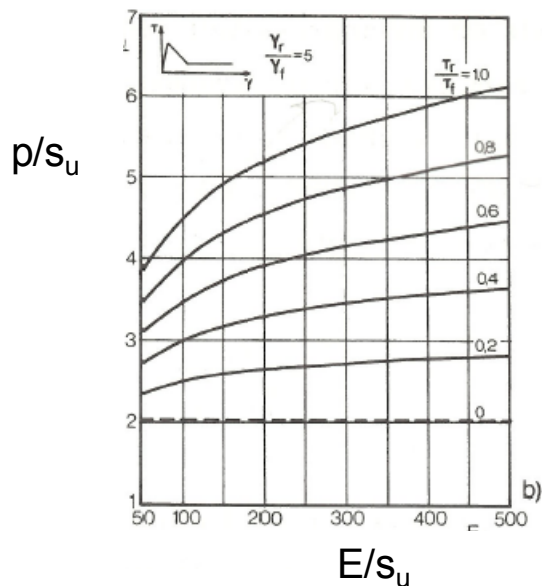
Figure 4.1.6 – Example of impact of strain softening on excess pore pressure against the pile shaft (from Ladanyi, 1963)

Numerous studies have been undertaken to combine the principles of CEM with more advanced soil models. Carter et al (1979) and Randolph et al (1979) presented for instance results of axi-symmetric FEM analyses using the strain-hardening effective stress based Modified Cam Clay (MCC) model (Roscoe and Burland, 1968). Randolph et al (1979) concluded that the predicted mean stress changes against the pile shaft agreed closely with what was predicted with the simple analytical CEM-EP model, provided that the shear modulus was taken as G_{50}.

One implication of the EP and MCC soil models is that they both predict a significant increase in radial effective stress at the pile surface as result of the pile installation. For the EP model that effective stress increase can be found from equations (4.1.5) and (4.1.6) to correspond to $\Delta\sigma'_r = s_u$.

The CEM approach has also been combined with anisotropic, non-linear and strain softening soil models. A series of such models were developed at MIT. Kavvadas (1982) presented results

based on a total stress model (called PCB) as well an effective stress based model (called MITE1). These soil models could reasonably well capture the behavior of lightly over-consolidated clays as observed in triaxial CAUC and CAUE tests and DSS tests. The effective stress based model was also developed to predict behavior during the re-consolidation phase, as dealt with in Chapter 5. This effective stress based model was further refined and modified by Baligh (1985), who made it fit better to over-consolidated clays (MITE2-model). The latest version, called MITE3, was developed and presented by Whittle (1987, 1992), and was shown to further enhance the agreement with CAUC and DSS laboratory test results, and the unloading-reloading stiffness in oedometer tests.

Figure 4.1.7 compares, as an example, predicted stresses at end of pile installation for the CEM model and the MITE1 model for normally consolidated clay. It clearly appears that the MITE1 model for this case predicts about 30 % lower excess pore pressures than the MCC model, but also significantly lower radial effective stress against the pile surface, more or less corresponding to the original effective stress. Both these effects of reduced stresses with the MITE1 model compared to the MCC and EP models, are probably mostly due to strain softening. This was also observed with the simpler strain-softening model of Ladanyi (1967).
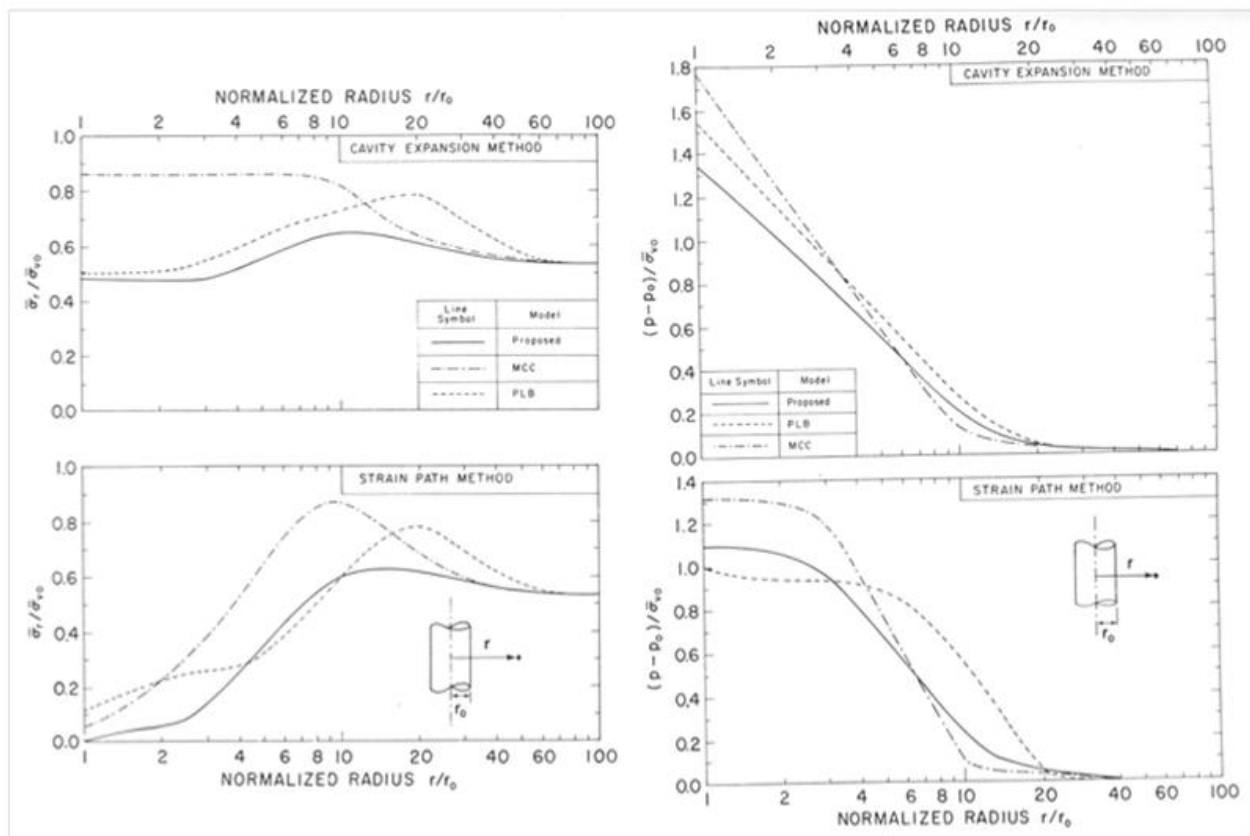
Figure 4.1.7 – Comparison of effects of soil model and installation model on radial stresses and pore pressures surrounding a closed-ended pile (after Kavvadas and Baligh, 1982)

4.1.3 The Strain Path Method (SPM)

The Strain Path Method was first developed by Baligh (1975) to predict soil deformations and stresses around a cone during steady penetration. The basic assumption is that the soil flow around a steadily penetrating cone or pile can be described as similar to the flow of a viscous liquid around the element. The theory was subsequently used to model both the penetration of

closed-ended piles (e.g. Kavvadas, 1982; Baligh, 1984 and 1985), and for open- ended piles (e.g. Chin, 1986; Whittle, 1987).

Figure 4.1.8 depicts the predicted soil deformations around a closed- and open-ended pile. The rounded nature of the pile point is necessary to ensure smooth laminar flow around the object and enabling a mathematical formulation of the displacements. Figure 4.1.9, taken from Whittle (1992), shows in more detail the predicted strain paths for closed and open penetration for some soil elements. It appears that close to the pile wall, the "vertical" simple shear strain is even larger than the cylindrical expansion strain close to the pile wall.
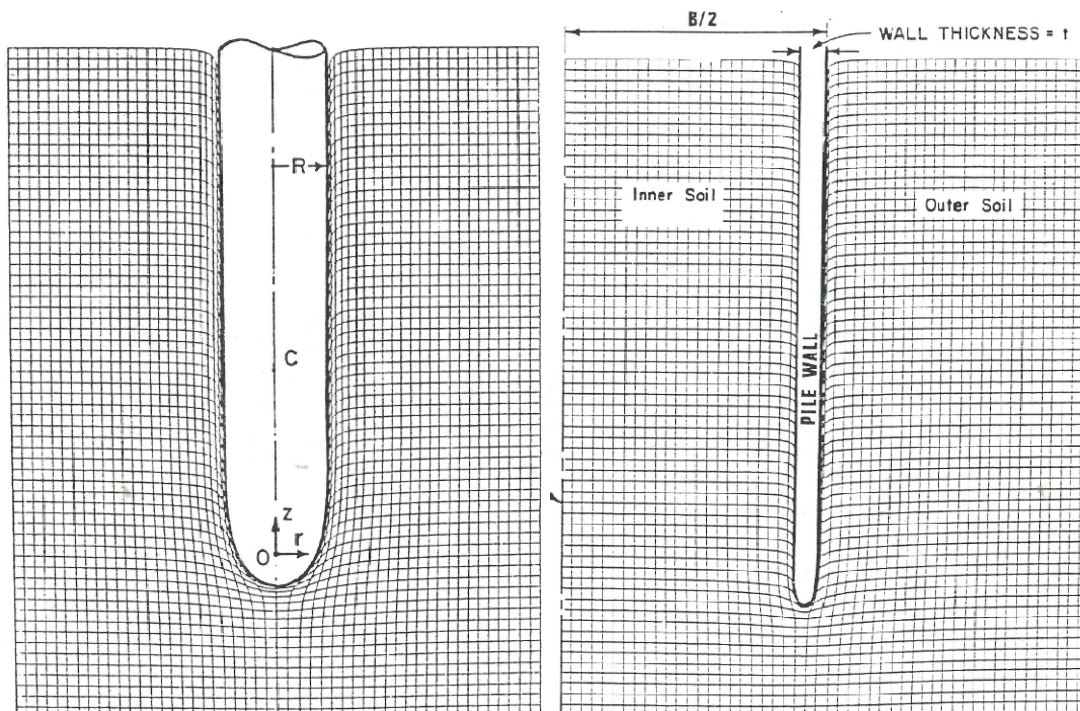
Figure 4.1.8 – Displacement pattern for open and closed-ended piles based on Strain Path method (Baligh, 1985)

Figure 4.1.10 shows an example of predicted stress changes for a normally consolidated BBC. The solid lines represent predictions with the SPM-MITE3 model, and the dashed lines with the CEM-MITE3 model. The difference in predictions is most significant when it comes to the effective stresses close to the pile wall, where SPM-MITE3 predicts much lower values than CEM-MITE3. At the pile wall, the excess pore pressures are also lower for SPM-MITE3. Both methods predict a radial extent of the initial excess pore pressure field that tapers off gradually and does not decrease completely to zero at a well defined radial distance from the pile wall, as predicted by the simple CEM-EP approach.

From the lower part of Figure 4.1.10 (where B means pile diameter D), it may be observed that for the open-ended pile the CEM approach predicts a fairly significant decrease in excess pore pressures against the pile shaft compared to the closed-ended pile, but much less so for the SPM model. Note that this figure uses an equivalent radius R_{eq} for normalizing the open pile result, defined as:

$$R_{eq} = (2r_0 \cdot t)^{1//2} \qquad\qquad\qquad (4.1.8)$$

The value of B/t = D/t = $2r_0/t$ =40 used in that analysis means R_{eq}/r_0= 0.316, which is why the normalised curve for the open-ended pile starts at r/ R_{eq}=1/0.316=3.16 in Figure 4.1.10.

a)   b)
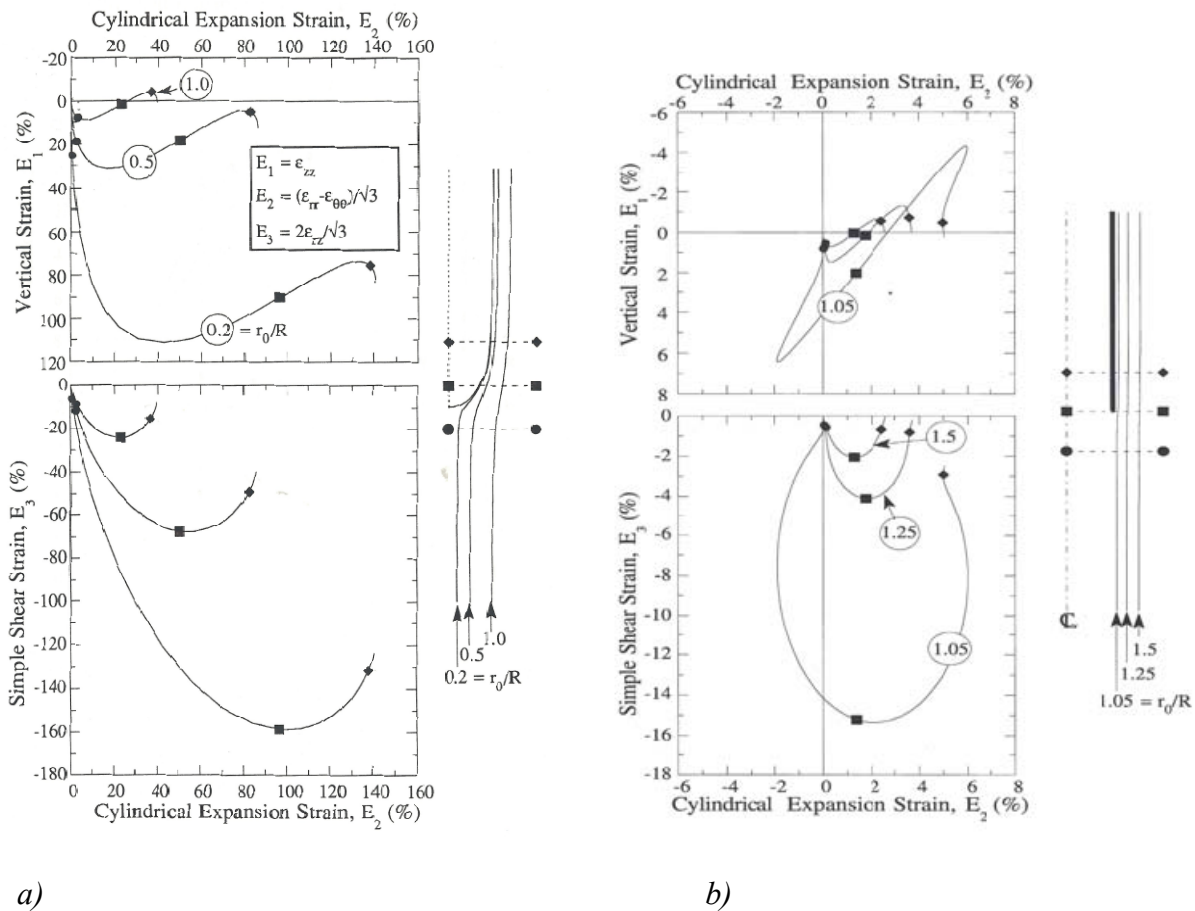
Figure 4.1.9 - Strain paths predicted around ideal piles according to SPM a) Closed-ended pile b) Open-ended pile (from Whittle, 1992)
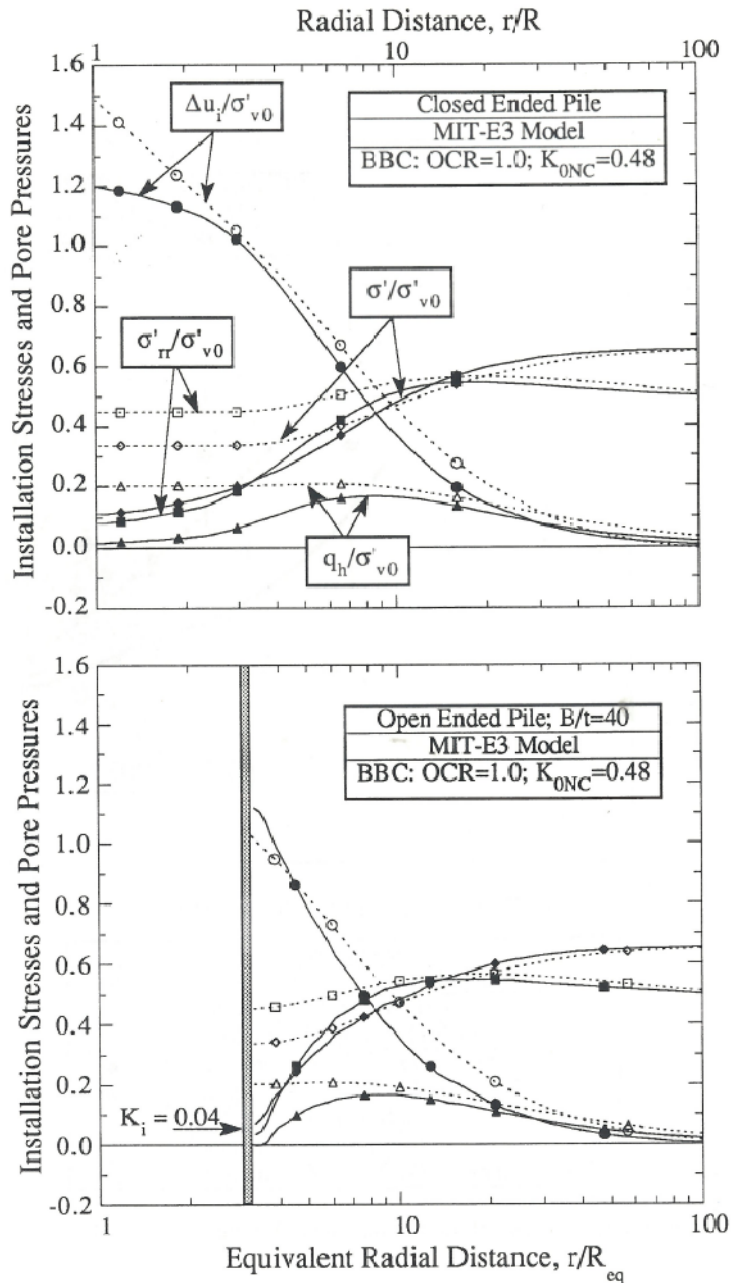
Figure 4.1.10- Comparison between stresses around closed and open-ended pile predicted with SPM-MITE3 model and the CEM-MCC model. Solid lines represent SPM and dashed lines CEM model   (from Whittle, 1992).

4.1.4 Impact of installation models and soil model on generated stresses

In order to further illustrate the impact of installation model and soil model on the predicted stresses, Table 4.1.1 compares some key results obtained with CEM and SPM installation models and the MCC and MITE type soil models, as found reported in the literature referred to above. The predicted values are also compared in Figures 4.1.11 and 4.1.12.

Table 4.1.1 – Comparison between normalized stresses against the shaft of a closed-ended pile predicted with different installation models and soil models

Clay type	OCR	Inst. model	Soil model	$\Delta u_i / \sigma'_{vo}$	K_i	K_c	Reference
BBC	1.0	CEM	MCC	1.77	0.86	1.54	Kavvadas (1982)
		CEM	MITE1	1.34	0.50	0.88	
		SPM	MCC	1.32	0.06	1.30	
		SPM	MITE1	1.1	0.00	0.40	
BBC	1.2	SPM	MITE1	1.19	0.02	0.56	
BBC	1.35	SPM	MITE1	1.32	0.04	0.80	
Empire	1.5	CEM	MCC	2.31	1.14	1.67	Baligh (1985b)
		SPM	MCC	1.31	0.34	1.34	
		SPM	MITE2	1.36	0.19	0.72	
Empire	2.0	CEM	MCC	2.76	1.43	2.11	
		SPM	MCC	1.56	0.44	1.79	
		SPM	MITE2	1.56	0.29	1.30	
BBC	1.0	CEM	MITE3	1.49	0.45	-	Whittle (1987)
	1.5	CEM	MITE3	2.08	0.70	-	
	2.0	CEM	MITE3	2.42	0.85	-	
	4.0	CEM	MITE3	3.65	1.44	-	
BBC	1.0	SPM	MITE3	1.20	0.08	0.40	
	1.5	SPM	MITE3	1.49	0.17	0.60	
	2.0	SPM	MITE3	1.68	0.20	0.70	
	4.0	SPM	MITE3	2.50	0.28	1.13	

Some observations that can be made from Table 4.1.1 and Figures 4.1.11 and 4.1.12 are as follows:

- The SPM installation model leads in all cases to lower pore pressures and effective stresses against the pile shaft than the CEM model.
- Use of the MITE1-2-3 models gives lower stresses than use of MCC for both the SPM and CEM installation model.
- As a consequence, the combination of SPM-MITE1-2-3 always leads to the lowest stresses.
- The MITE3 model tends to give somewhat higher stresses than the earlier MITE1-2 models.
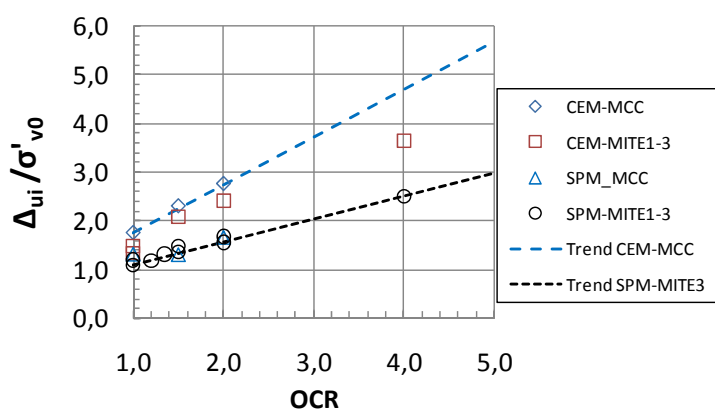
Figure 4.1.11 – Comparison between excess pore pressure at the pile shaft predicted by various

combinations of CEM and SPM installation models and MCC and MITE1-3 soil models (based on data in Table 4.4.1)
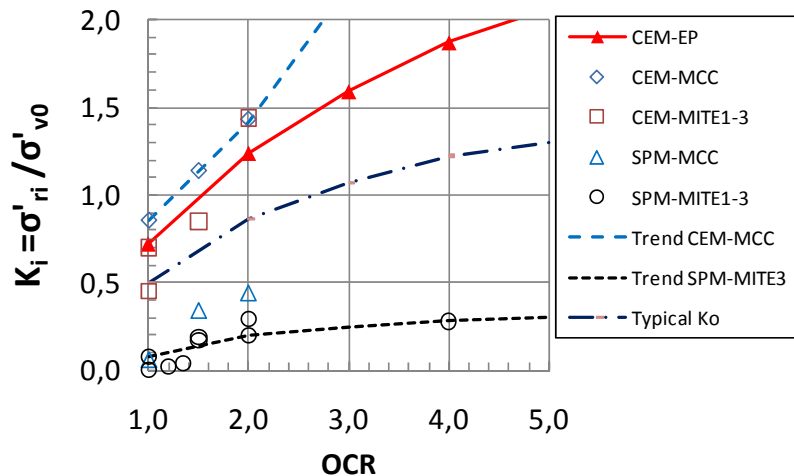
Figure 4.1.12 – Comparison between radial effective stresses at the pile shaft predicted by various combinations of CEM and SPM installation models and MCC and MITE1-3 soil models (based on data in Table 4.1.1)

The CEM and SPM methods also give notably different stresses and excess pore pressures as function of radial distance from the pile wall. This is illustrated by a typical example in Figure 4.1.13, comparing pore pressure distributions predicted with CEM and SPM models for BBC with OCR=1.5, and using the MITE3 soil model (based on results presented by Whittle, 1987). The figure shows the predicted excess pore pressures, Δu_i, normalised with respect to the predicted pore pressure at the pile wall, Δu_{i0}, as function of normalised radial distance r/r_0. In the left side of Figure 4.1.13 the radial distance is in a linear natural scale, and in the right hand side in a log scale. A log-linear distribution as predicted with CEM-EP is also shown for comparison. For the CEM-EP calculation a value of $G_{50}/s_u=220$ was selected. That value is what is implied by the non-linear MITE3 model prediction for BBC with OCR =1.5.

It appears from Figure 4.1.13 that both the CEM- and SPM-MITE3 predictions give excess pore pressures that have a long "tail" compared to the simple CEM-EP model. Furthermore, the CEM-MITE3 model shows, like CEM-EP, a log-linear decrease until the "tail" portion is reached, whereas the SPM-MITE3 more agrees with a true linear decrease until the "tail" is reached. The significance of these different excess pore pressure distributions on the time for pore pressure dissipation will be addressed in Chapter 5.
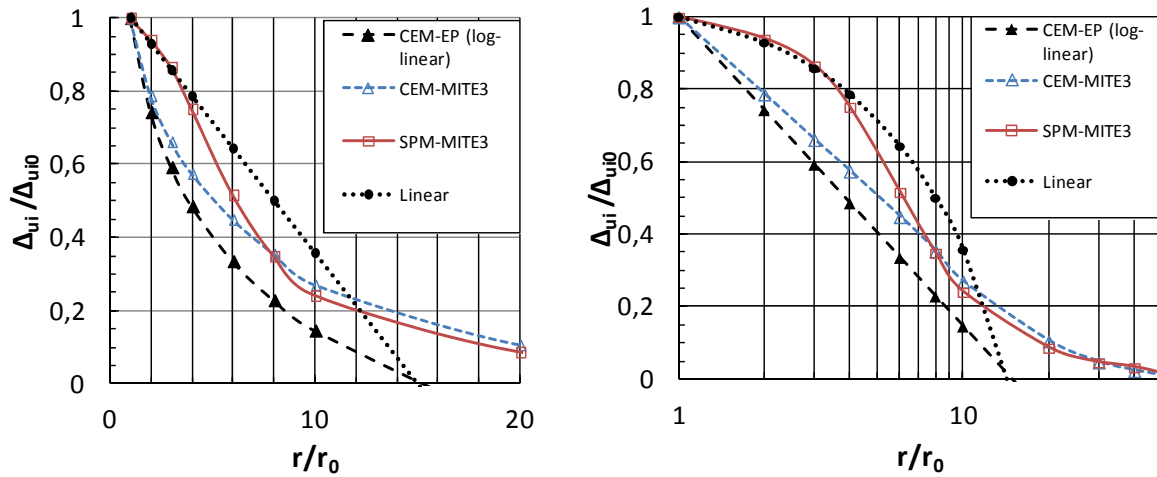
Figure 4.1.13 – Comparison of distributions of excess pore pressures as predicted by CEM and SPM with the MITE3 model for BBC with OCR=1.5 (based on results presented by Whittle, 1987)

4.2 Measured response and comparison to models

4.2.1 Soil displacements induced by pile installation

Figure 4.2.1 compares measured normalised vertical soil displacements of clay layers at Haga (ref. also Figure 2.2.18) to observations from some pin model tests in the laboratory presented by Steenfeldt et al (1981) and Francescon (1983). The pin model tests were carried out in Kaolin clay in a triaxial chamber. The pin model tests agree reasonably well with the Haga observations, but lie on the higher side. Also shown in Figure 4.2.1 are displacements predicted with the SPM approach (based on Baligh, 1975), which falls on the low side of all the actual data. In other words, the SPM seems to under predict the vertical displacements and associated shear strains.
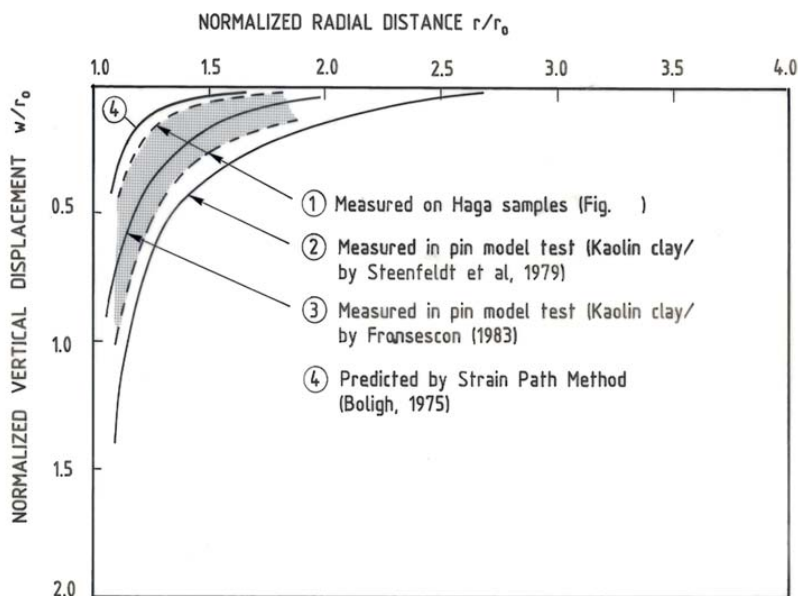
Figure 4.2.1 – Observed vertical soil displacements compared to SPM prediction for closed-ended piles (after Karlsrud, 1986)

As was shown in Figure 2.2.18, and also predicted with SPM (Figure 4.1.9), the vertical shear strains induced in the clay close to the pile wall exceed the shear strains due to cavity expansion, and are of the order more than 100 %.

As described in Section 2.2.2, and illustrated by Figure 2.2.18 and the photo in Figure 2.2.19, there is clear evidence of very "turbulent" soil displacements in the RR-zone close to the pile wall, leaving no trace of the original clay structure in that zone.

Based on trenching next to one of the IC test piles at Cannons Park, Bond and Jardine (1988) reported a similar but maybe not quite as distinct picture of the vertical soil displacements as for Haga, but described the inclination of shear surfaces observed in X-ray thin- sections as presented in Table 4.2.1. Qualitatively this seems to agree well with the data in Figure 4.2.1

Table 4.2.1 – Orientation of shear surfaces in thin-sections, Canons Park (based on Bond and Jardine, 1988)

Zone	Description	Inclination relative to vertical plane	Normalized extent of Zone, r/r_0	
			Driven pile	Jacked pile
1	Near vertical	$\leq 20^0$	1.24	1.21
2	Steeply inclined	$20-45^0$	1.49	1.45
3	Gently inclined	$45-70^0$	1.7	Not determined
4	Near horizontal	$>70^0$	>1.7	Not determined

These observed displacement patterns confirm that the vertical deformations, and associated shear strains, within a distance of say $r/r_0 < 2$ are very significant, reaching more than 100 % close to the pile wall. Such large vertical deformations and shear strains, in addition to the cylindrical cavity expansion strains, must cause significant changes in the basic stress-strain-and strength characteristics of the clay closest to the pile wall. The impact of that will be discussed further in Chapter 5 and 6.

4.2.2 Pore pressures against the pile shaft

Figure 4.2.2 shows the normalised excess pore pressures, $\Delta u_i /s_{ud}$, measured at end of pile installation in relation to OCR for all the instrumented piles presented in Chapter 2. To help understand this figure, solid symbols are used for closed-ended piles and open symbols for piles installed open-ended. The largest size symbols are used for the largest piles, and the smallest for the model piles. For all piles, data from measurements made closer than about 4 pile diameters from the pile tip or from the ground surface are excluded due to possible geometry effects. Also note that all excess pore pressure data from the Pentre site are excluded in Figure 4.2.2. The reason is the very high permeability of this special silt/clay deposit, which means that the pore pressure response during pile installation was far from undrained at this site, ref. Section 2.6.2.

The data in Figure 4.2.2 show a clear trend of decreasing $\Delta u_i /s_{ud}$ with OCR. It also appears that for OCR<3, the open-ended piles give typically 25 % smaller excess pore pressures than the closed-ended piles. There is no apparent difference between open- and closed-ended piles for the high OCR sites.

The scatter in the data in Figure 4.2.2 is rather large. The differences in pile size, and method and time used for pile installation, could have contributed to this scatter. Apart from the IC tests at

Cannons Park (CP), all the small model scale piles or probes seem to give larger excess pore pressures than the larger piles. This could have to do with the time used for installation, which generally was faster for the small model piles/probes than for the larger piles. The diameter effect on pore pressure dissipation (consolidation time proportional to r^2) should however, to some extent counteract such an effect. As an example, it took typically 6-8 hours to install the Onsøy and Lierstranda A-segment piles. Considering that they had a diameter of 219mm, 6 times the MIT-PLS probe (36mm), the dissipation would relatively speaking go 36 times more slowly for the On/Li piles than the MIT-PLS probe.

The data for the MIT probe in BBC were specifically collected during steady penetration of the probe into the ground (Morrison, 1984), whereas most other data represent values at the end of pile installation. This aspect may also explain the relatively high values of $\Delta u_i / s_{ud}$ reported for the MIT-PLS tests in BBC. At Empire, the PLS probe data reported by Azzouz and Baligh (1984) seem to be given for the end of the penetration phase, and fall more in line with the other pile data. At Empire the x-probe and 3" probe tests (e.g. Bogard, 2000, 2001) gave $\Delta u / s_{ud} \approx 10.5$, and higher than the PLS results of $\Delta u / s_{ud} \approx 7.5$ carried out in the same depth interval. This points to possible inaccuracy associated with the various sensor/instrumentation systems used, which could be an element in relation to all reported results.
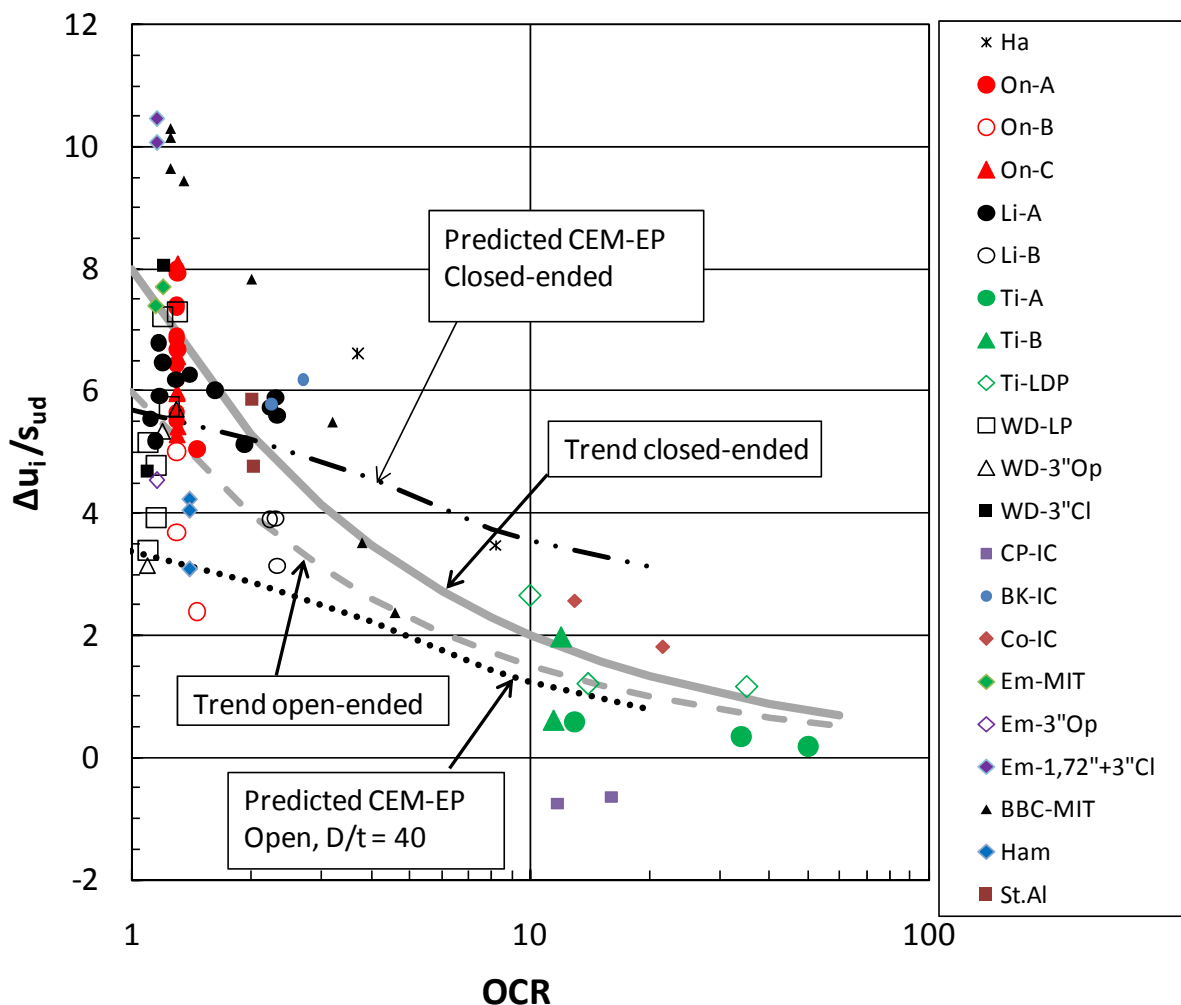
Figure 4.2.2 – Measured normalised excess pore pressure against the pile shaft, $\Delta u_i / s_{ud}$, versus OCR

Figure 4.2.3 compares $\Delta u_i / s_{ud}$ against I_p for the clays with OCR< 2,. The data suggest some tendency for increasing pore pressure with increasing I_p, both for the open- and closed-ended piles. An increase in $\Delta u_i / s_{ud}$ with I_p is however, contrary to what is anticipated from Figure 4.1.3 and 4.1.5, assuming that G_{50}/s_u decrease with increasing I_p.

The measurement of pore pressure during an installation process requires that the piezometer filters are carefully de-aired and fully saturated when they enter into the ground. This was very carefully controlled in the NGI tests at Onsøy and Lierstranda, and cannot explain the difference to the smaller pile/probe tests at similar OCR. Incomplete saturation could however, explain some of the other differences, especially in the high OCR clays, where negative pore pressures could be generated and cause cavitations and de-saturation even if the piezometer filters were reasonable well saturated when they first entered into the ground. Thus, the pore pressures measured shortly after pile installation could be too low.

The Hamilton piles seem to have given particularly low pore pressures considering both OCR and I_p values. As described in Section 2.7, at this site the pore pressures were increasing the first minutes after end of pile installation, which could be an indication of poor filter saturation.

At some of the stiff clay sites it was also observed that pore pressures increased during the first phase of the re-consolidation process. This was for instance the case at 20 m depth along the LDPTC-pile at Tilbrook, where it took 20 days for the pore pressure to build up to peak value (Figure 2.7.12) . At Cowden it was observed a much shorter delay of just a few minutes for the peak pore pressure to be reached (section 2.9.3).
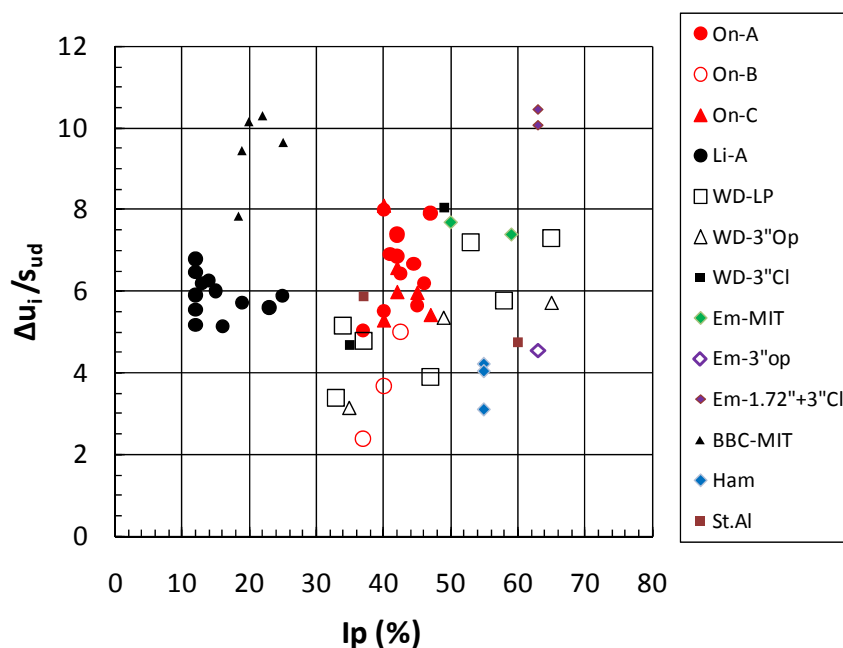
Figure 4.2.3 – Measured normalised excess pore pressure against the pile shaft, $\Delta u_i / s_{ud}$, versus I_p for OCR<2

The only tests that show a net negative pore pressure change at end of installation are for the IC tests at Cannons Park (CP). This clay has high plasticity and low permeability as compared to at Cowden, but has similar OCR. At Cowden significant positive excess pore pressures were measured (Figure 4.2.2 and 4.2.4). This large difference between the IC's data from Cowden and

CP may raise questions about the reliability of these data. It is the Cannons Park (CP) data that fall most out of line with the other data in Figure 4.2.2.

Figure 4.2.2 also shows, for direct comparison, excess pore pressures as typically predicted with the CEM-EP model (based on Figure 4.1.5). For both the closed-and open-ended case it appears that the excess pore pressures are under-predicted for low OCR clays and over-predicted for high OCR clays.

The trend lines suggested in Figure 4.2.2 are represented by the following expressions:

$$\Delta u_i / s_{ud} = 8 \cdot OCR^{-0.6} \text{ for closed-ended piles} \qquad (4.2.1)$$

$$\Delta u_i / s_{ud} = 6 \cdot OCR^{-0.6} \text{ for open-ended piles}$$

Figure 4.2.4 suggests more scatter in the data when the excess pore pressure is normalised with respect to the vertical effective stress, rather than the undrained strength, as in Figure 4.2.2. It is in Figure 4.2.4 difficult to draw or suggest a clear trend line for OCR >10. In reality, this is also the case in Figure 4.2.3, but the scatter becomes less obvious when the pore pressure is normalised with respect to the undrained strength.
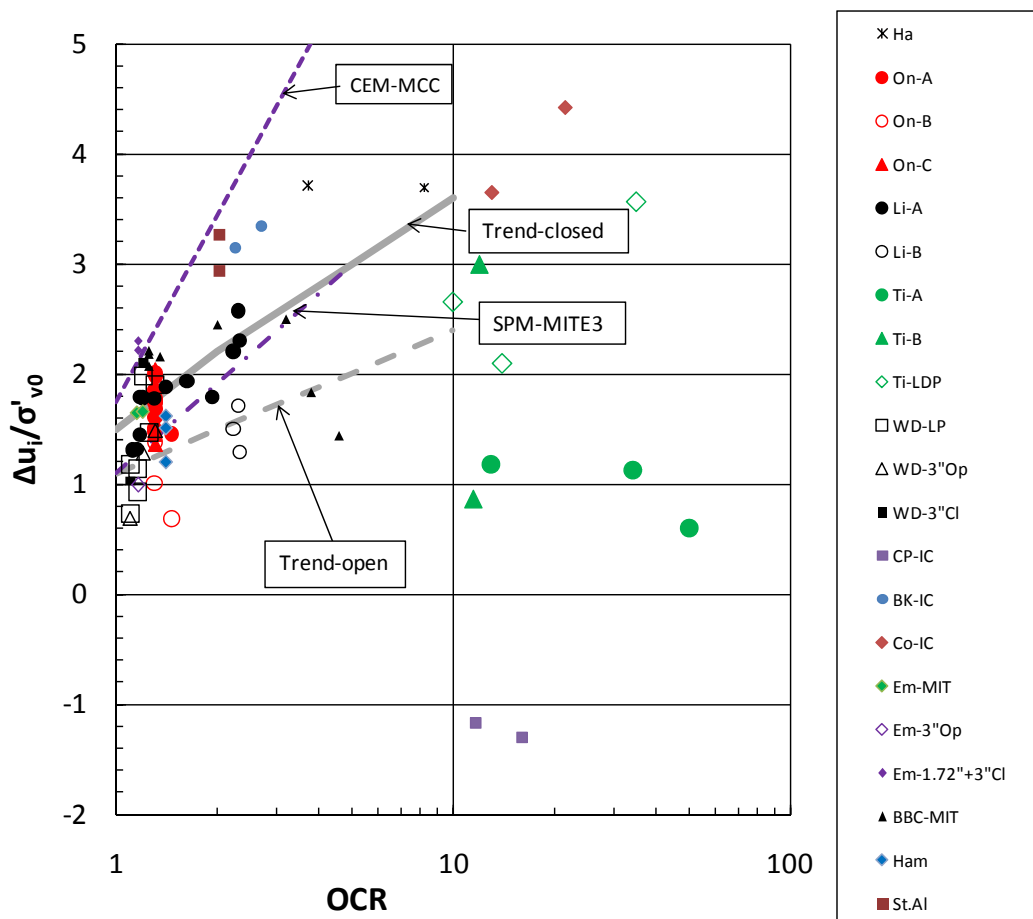
Figure 4.2.4 – Measured normalised excess pore pressure against the pile shaft, $\Delta u_i / \sigma'_{v0}$, versus OCR

The lines in Figure 4.2.4 representing $\Delta u_i / \sigma'_{v0}$ calculated with CEM-MCC and SPM-MITE3 models were taken from Figure 4.1.11. They are only valid for closed-ended piles, but seem to reasonably well bracket the observed data for OCR<6 to10. The CEM-MCC predicted values lie

on the high side of the observed data, and the SPM-MITE3 on the low side. Note that these predictions are made for idealized soil behaviour trying to match that of BBC. Use of site specific data may have slightly improved the comparison to observed response at some sites, but it is not likely to change the broad picture.

It is believed that very little of the scatter in the data in Figure 4.2.2 to 4.2.4 arise from uncertainties in the assessed values of s_{ud} and OCR. Such uncertainties are in the authors view in general less than about 10-15 % in the chosen s_{ud} values, and maybe 20-30 % in assumed OCR. Based on the discussion of soils data in Chapter 2, the uncertainties may be larger in relation to the Tilbrook Grange (Section 2.7.2), Cannons Park (Section 2.9.2) and Empire sites (Section 2.10.2).

As a check on consistency in soil data assumed for the different sites, Figure 4.2.5 presents the assumed normalised strength versus OCR for all the sites. This confirms that the data assumed are generally consistent and follow an average SHANSEP trend defined by S=0.21 and m= 0.78. The point that shows the highest strength for a given OCR lies between OCR 1.4 and about 2. They represent respectively the Hamilton site and the St.Alban site. The strengths at St.Alban are considered quite typical of the structured or cemented Champlain Sea clays, and there is no reason to doubt these values. The Hamilton site clay has relatively high plasticity and could also be somewhat structured or cemented.
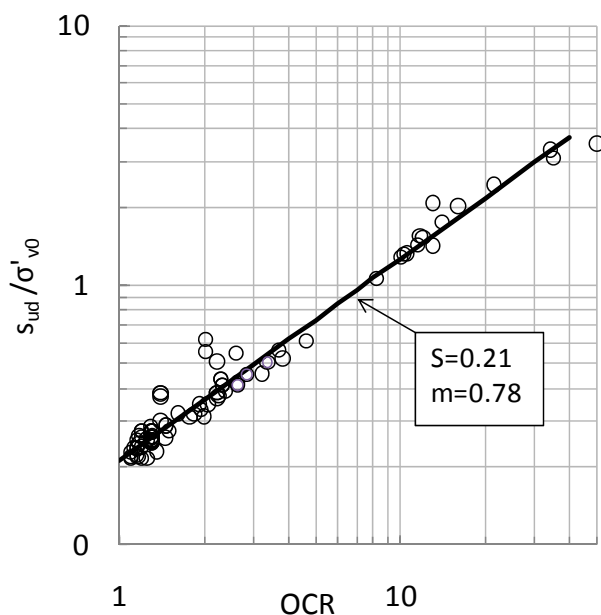
Figure 4.2.5 – Summary of actually assumed normalised s_{ud} /σ'_{vo} strength versus OCR for all sites

In conclusion the largest contribution to the scatter in the data in Figures 4.2.2 and 4.2.4 probably lies in the reliability of the measurements in themselves, and to some extent also details regarding method and time used for installation. Some of the scatter is probably also due to differences in stress-strain behaviour of the different clays, including post-peak large strain behaviour.

It is a bit discomforting that apparently no single numerical or analytical model seems to fully capture the trends in the data. The proposed trend curves may therefore presently represent the

most reliable approach to predicting the excess pore pressure against pile shafts. The uncertainty in this approach apparently becomes large for high OCR clays.

4.2.3 Horizontal (radial) effective stress against the shaft

The measurement of effective stress against a pile shaft during installation is in the outset a challenging task, considering that the generated total radial earth pressure and pore pressure are relatively large compared to in-situ stresses. It means that relatively small full scale errors in either total earth pressure or pore pressure could have a rather large impact on the relative effective stress level.

It may therefore be no surprise that the normalised radial effective stress values, $K_i = \sigma'_{ri} / \sigma'_{vo}$, in Figure 4.2.6 show large scatter for all OCR's. Negative values are of course in-correct, as measured for most of the Onsøy and Lierstranda piles, ref. the more detailed plot in the right hand side of Figure 4.2.6 and the discussion of this aspect in Section 2.4.3 and 2.5.3.

The data suggest a general trend of increasing K_i with increasing OCR. Even given the large scatter in these data, there seems to be no clear difference between open- and closed-ended piles.
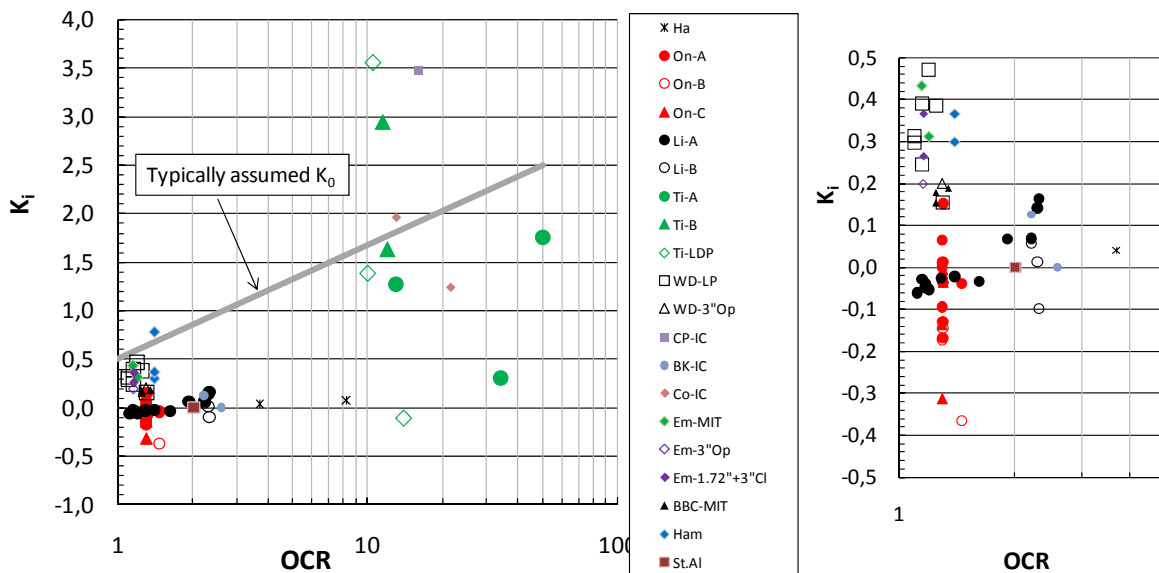
Figure 4.2.6 – Normalised effective stress ratio, K_i, at end of installation
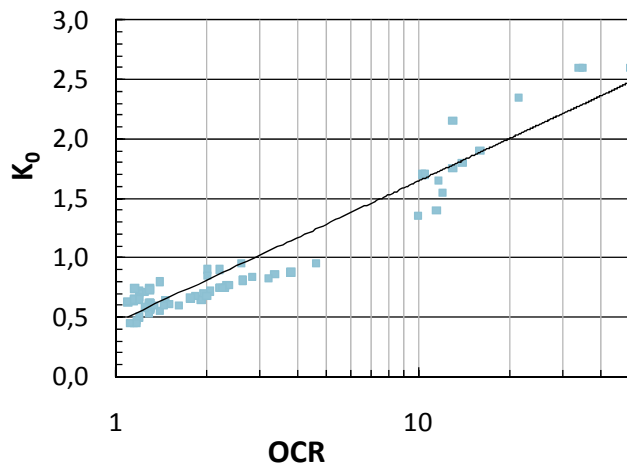
Figure 4.2.7 – Assumed in-situ K_0 in relation to OCR for all sites

The in-situ K_o as assumed for all sites is summarized in Figure 4.2.7. Also shown is a typical trend line for the assumed K_o values. The variation from this trend line mostly comes from the assumed impact of plasticity index on the assumed K_o.

When the trend line for K_o is compared to K_i in Figure 4.2.6, it appears that for most cases K_i is lower than the assumed K_o, especially for the clays with OCR< 10. The data indicate however, that for stiff clays with high OCR, like at Tilbrook, Cannons Park and Cowden, K_i is of the same order as K_o, and in some cases even larger.

The SPM-MITE3 approach seems to correctly reflect the low installation effective stresses in low OCR clays, whereas the CEM-EP or CEM-MCC model significantly overestimate K_i for such cases.

4.2.4 Free-field pore pressures

Free field pore pressures were measured at some of the sites included in this study, including the Haga site (Figure 2.2.27), and the St.Alban site (Figure 2.12.4). As can be seen from Figure 4.2.8, the decrease in Δu_i with radial distance at St. Alban shows a striking resemblance to what is predicted with the SPM-MITE3 model in Figure 4.1.13. The initial excess pore pressure at St. Alban approached zero at $r_p/r_o \approx 12$. At Haga the data are more uncertain and less conclusive due to apparent improper saturation of the piezometer filters. The Haga data may still suggest a shape with a more linear decrease in pore pressure with $\log (r_p/r_o)$.
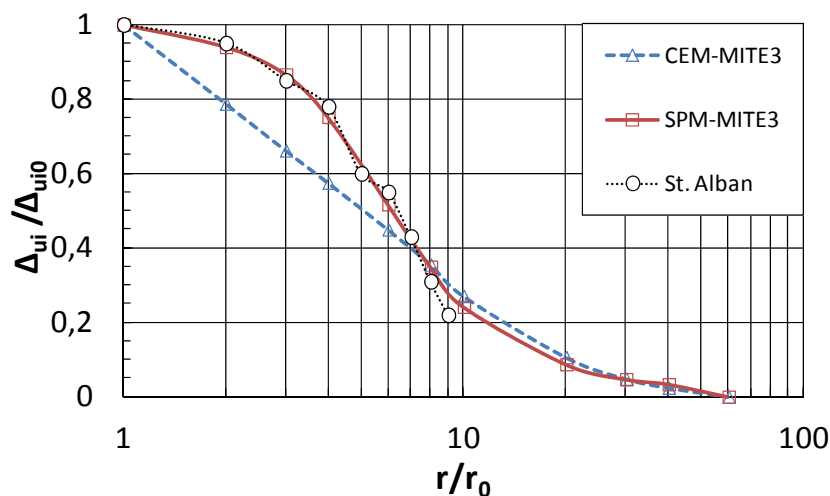
Figure 4.2.8 – Measured excess pore pressure field at St. Alban compared to CEM-and SPM-MITE3 predictions

In addition to the Haga and St. Alban data there are a number of other cases of excess pore pressures generated in the soil surrounding a pile in clay reported in the literature. No complete search for such data has been made as part of this study, but some data that were summarized by Randolph and Wroth (1979) are reproduced in Figure 4.2.9. These are all data from low OCR clays. The upper two cases suggest a linear decrease in Δu_i with $\log(r_p/r_o)$, agreeing with what is predicted with CEM, whereas the case in the lowest diagram may suggest more of the SPM type decrease. The radial extent of the excess pore pressure is $r_p/r_o \approx 12$ for the upper two cases and $r_p/r_o \approx 30$ for the lowest case.

It is concluded that the theoretical models seem to give a fair assessment of the radial extent of the excess pore pressure field, but the exact shape seem in some cases to agree with the SPM models, in others with the CEM models.
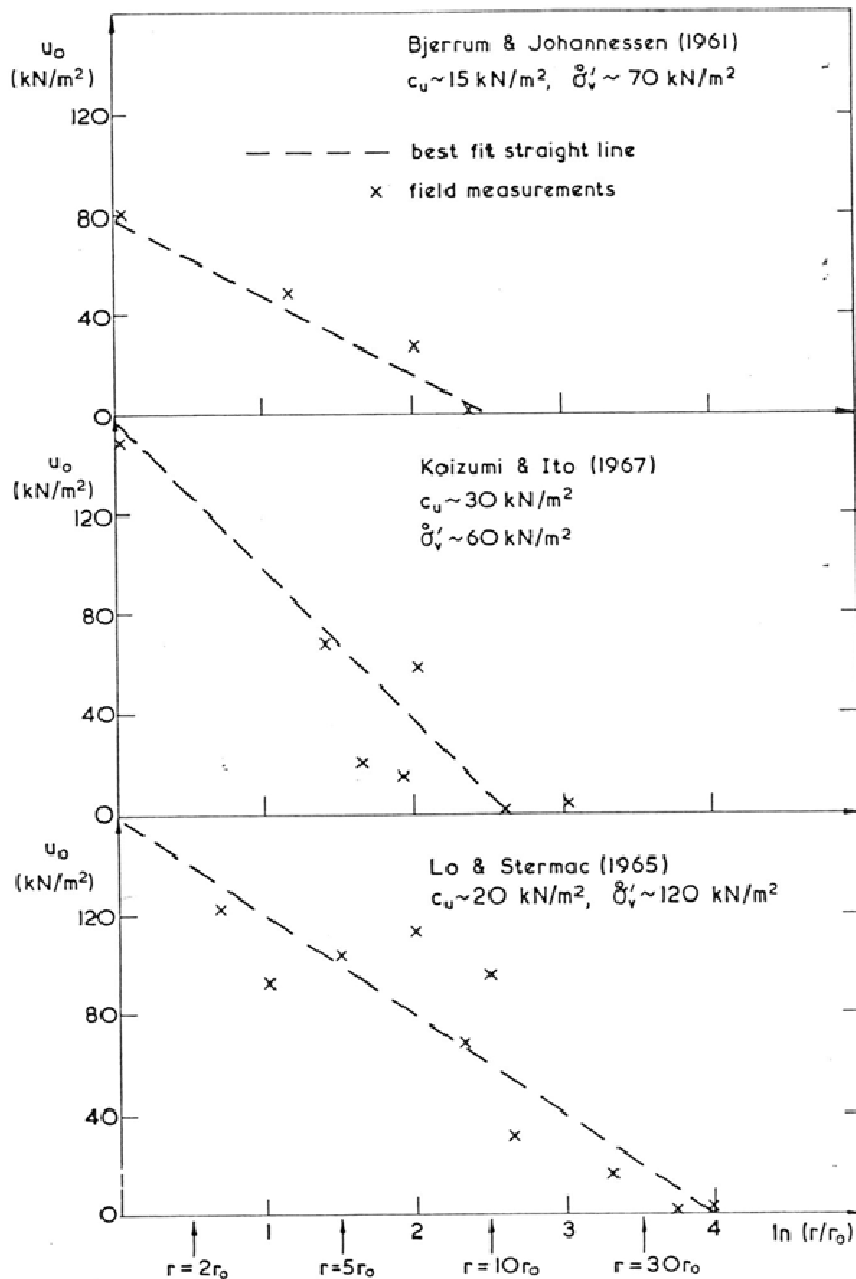
Figure 4.2.9 – Excess pore pressures induced by pile driving (from Randolph and Wroth, 1979)

4.2.5 Summary of main observations

The measured normalised excess pore pressures generated against the pile shaft follow a clear trend of decreasing values with increasing OCR, which also broadly agrees with theoretical models. The same applies to the radial extent of generated excess pore pressures.

There is also a clear trend that open-ended piles generate lower earth- and pore pressures than closed-ended piles, which relatively speaking also agree with what is predicted with the various theoretical models.

It is still a bit discomforting that no single numerical or analytical approach seems to fully capture the trends in the data. The empirical trend curves proposed by the author on basis of the available data may therefore presently represent the most reliable approach for predicting the excess pore pressure against the pile shaft. However, the uncertainty and variability in the data become rather large for high OCR clays.

The theoretical models also seem to give a fair assessment of the radial extent of the excess pore pressure field. The shape of the excess pore pressure field for closed-ended piles seem to agree best with the SPM type models.The impact and recommendation for choice of shape of the excess pore pressures distribution on the re-consolidation process, will be dealt with further in Chapter 5.

The radial effective stress after pile installation is generally much smaller than the in-situ K_o, especially for the soft low OCR clays, but these data show even more scatter than the excess pore pressures. This is most likely, primarily due to inaccuracies in measurements. At high OCR K_i seems to more approach K_o, but the data scatter is large. The SPM-MITE3 approach seems to correctly reflect the low installation effective stresses in low OCR clays, whereas the CEM-EP and CEM-MCC models significantly overestimate K_i for such cases.

It should again be noted that there is a fairly significant scatter in measured data, especially for stiff and high OCR clays. Part of that scatter is probably due to measurement errors and partly due to inherent variability in detailed stress-strain behaviour of the clays, especially at very large strains. Some of the scatter in the data is also likely to stem from variations in pile sizes, and method and time used for pile installation.

5 THE RE-CONSOLIDATION PHASE AROUND THE PILE SHAFT

5.1 Computational models for predicting rate of consolidation and stress changes

5.1.1 Models considered

The radial consolidation process following pile installation around a deeply embedded pile (i.e. neglecting surface and tip effects), depends on three main factors:

1. The radial extent of the excess pore pressure field as defined by $\lambda = r_p/r_0$
2. The shape or form of the excess pore pressure field
3. The operating coefficient of radial consolidation, c_h, and how it may vary with radial distance from the pile wall, and with effective stress changes that will occur during the re-consolidation process.

Modelling of the two first aspects were dealt with in Chapter 4, but it will in the following be given some examples of how the installation and soil models dealt with in Chapter 4 (the CEM and SPM installation models, and the EP, MCC and MITE1-3 soil models) will also impact the consolidation process. The main focus will be on the rate of pore pressures dissipation and the state of effective stresses against the pile shaft at the end of the re-consolidation process.

Modelling correctly the soil response during the re-consolidation process is in the outset a very complex task, primarily because the volumetric compressibility of the soil depends strongly on the effective stress level and effective stress changes that will occur during the re-consolidation process. This is further complicated by the fact that the large shear strains and severe remoulding that take place in the zone closest to the pile wall will also significantly impact the compressibility characteristics. Figure 2.2.22 and 2.4.12 showed for instance the very large effect of severe remoulding on the compressibility of Haga and Onsøy clay. The impact of the shear strains induced by the pile installation will taper off gradually from the pile surface. For imposed shear strains less than maybe 10 % or so, the impact may be relatively small.

Another aspect of the soil behaviour is that part of the soil will experience unloading and other parts re-loading at stresses that lie within the original yield surface of the undisturbed clay, (i.e. stresses below the pre-consolidation pressure). The un-loading and re-loading stiffness of clays are strongly non-linear and generally shows hysteretic type behaviour. Some years back the author had a series of oedometer tests made to study in detail the un-loading and re-loading stiffness of clay from Bjørvika in Oslo (typical w=45% and I_p= 25%). The test samples were pre-consolidated well beyond the in-situ pre-consolidation pressure, p'_c, and then unloaded and reloaded to a wide range of stress levels. The test results and interpretation can be found in a report from NGI (2003). The study showed that the tangent modulus in unloading could be well fitted to a relationship of the form:

$$M_{tu} = a \cdot \sigma' \cdot (\sigma' /(\sigma'_{max} - \sigma'))^b \qquad \text{where,} \qquad (5.1.1)$$

M_{tu} = tangent un-loading modulus

σ'_{max} = maximum effective stress the sample was subjected to at start of un-loading

σ' = effective stress during un-loading

a = constant = 250 for Bjørvika clay

b = power = 0.3 for Bjørvika clay

Figure 5.1.1 shows a typical example of how dramatically the tangent un-loading modulus reduces with effective stress for a sample pre-consolidated to 100 kPa. As an example, after unloading to 80 kPa, the un-loading modulus is 30 MPa, and reduces to about 1.5 MPa at a stress of 10 kPa.
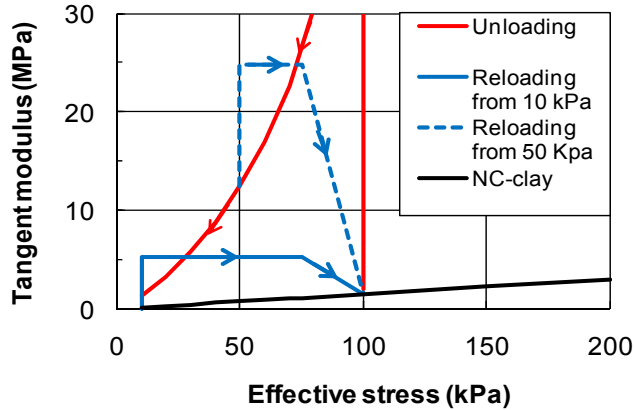
Figure 5.1.1 – Example of tangent un-loading and re-loading modulus for Bjørvika clay

The re-loading modulus depends strongly on the level at which un-loading stopped (i.e. on the apparent OCR). The modulus can be taken as approximately constant up until a stress level about 25% below the maximum past pressure, and then tend to decrease essentially linearly until it meets the modulus line for normally consolidated (NC) clay, Figure 5.1.1.

From the tests on Bjørvika clay, the more or less constant part for the re-loading modulus could be defined by a relationship of the form:

$$M_{tr} = m_0 \cdot \sigma'_{max} \cdot (c + d / (\sigma'_{max}/\sigma'_{min} - 1)^e) \qquad \text{where,} \qquad (5.1.2)$$

m_0 = modulus number for NC clay

σ'_{min} = minimum effective stress at start of re-loading

c = constant = 2.5 for Bjørvika clay

d = constant = 14 for Bjørvika clay

e = power = 1.2 for Bjørvika clay

Figure 5.1.1 shows examples for re-loading modulus when re-loading starts from a stress of respectively 10 kPa (representing OCR=10 at start of re-loading) and 50 kPa (representing OCR= 2). They are respectively M_{tr}= 5 MPa and 25 MPa, i.e. differ by a factor of 5. For comparison, the modulus is reduced to about 1.5 MPa when the stress reaches the virgin compression line.

5.1.2 Rate of excess pore pressure dissipation

The simplest solution to the pore pressure dissipation can be obtained by conventional linear radial consolidation theory, and assuming that the radial coefficient of consolidation is constant throughout the process. The only additional required input is then the distribution of excess pore pressure with radial distance from the pile surface.

The solution to this problem has been dealt with in numerous papers dealing with consolidation around piezocone as well as piles, e.g. Torstensson (1977), Randolph et al (1979),

Levadoux(1980), Kavvadas and Baligh (1982), Senneset et al (1982), Baligh and Levadoux (1986), Houlsby and Teh (1991). The book on Cone Penetration Testing by Lunne et al (1997), also discuss various methods developed for assessing dissipation following stop in piezocone penetration.

For linear radial consolidation solutions the degree of consolidation depends on the assumed radial extent of the excess pore pressure field, normally taken as the plasticized radius defined by eq. (4.1.4). Levadoux (1980) and Chin (1986) have presented solutions to this problem for two assumed initial excess pore pressure distributions:

1) Δu_i decrease linearly with $\log(r/r_0)$, as is actually predicted by the CEM-EP theory (ref. eq. 4.1.6)
2) Δu_i decrease linearly with the absolute value of (r/r_0)

In both cases $\Delta u_i=0$ at the distance of $\lambda = r_p/r_0$.

Figure 5.1.2 shows time factors, as defined by eq. (5.1.3), for these two cases as function of the degree of consolidation, U.

$$T = c_h \cdot t / r_0^2 \qquad (5.1.3)$$
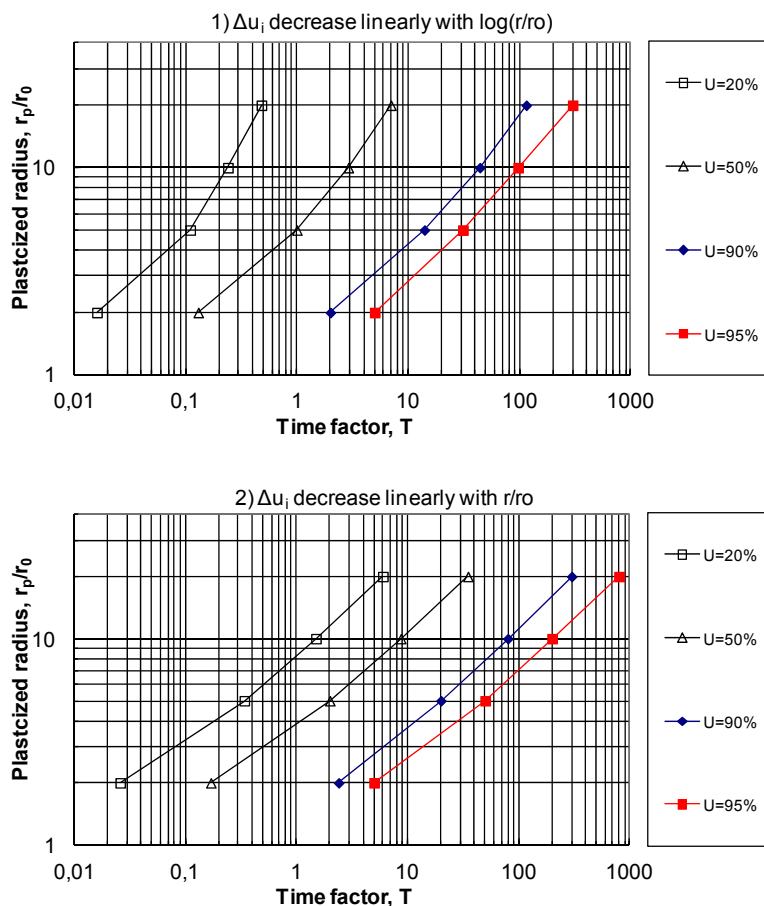
Figure 5.1.2 – Time factors versus degree of consolidation from linear radial consolidation theory for case of 1) Δu_i decrease linearly with $\log(r/r_0)$, 2) Δu_i decrease linearly with (r/r_0)(based on analytical results presented by Levadoux, 1982 and Chin, 1986)

Figure 5.1.3 compares more directly the equivalent time factors $T_{eq} = T \cdot \lambda^2$ for these two cases for a typical case of $\lambda = r_p/r_0 = 10$. The curves illustrate that the assumed shape of the excess pore pressure field has a significant impact on the consolidation times. As would be expected, the $\log(r/r_0)$ case gives the fastest consolidation.
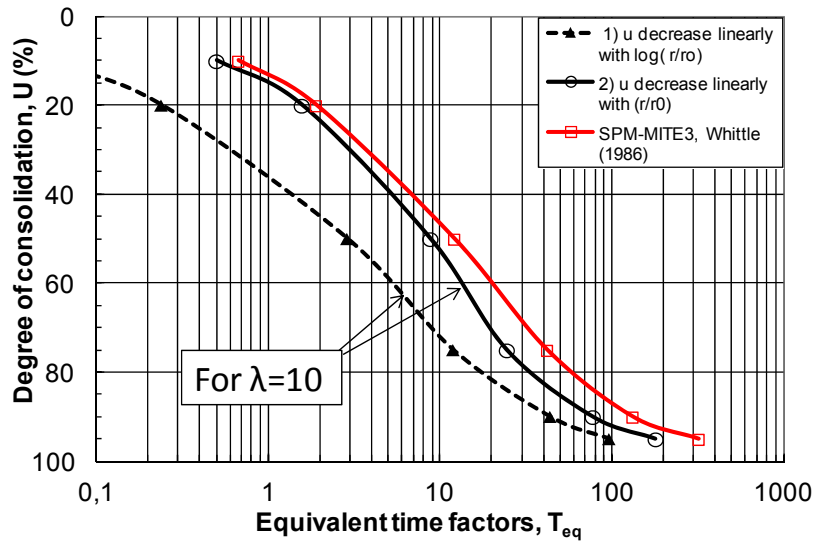
Figure 5.1.3 – Comparison between various calculated radial consolidation solutions

By introducing the displacement ratio, p, defined by the actual displaced volume normalized with respect to the displaced volume of a closed pile, Chin (1986) showed that equation (5.1.3) can be used for open-ended or partially plugging piles by introducing a modified λ^* defined as:

$$\lambda^* = p \cdot \lambda \quad \text{where,} \tag{5.1.4}$$

p = actual displaced volume/volume of closed-ended pile

The value of λ shall then be taken as for a closed-ended pile. This is may be an alternative approach (but with the same end result) as calculating the plasticized radius from eg. (4.1.4), and using Figure 5.1.2 for calculating the time factor T.

As for the installation phase, CEM and SPM installation models have been coupled with MCC and MITE1-3 soil models to numerically calculate the pore pressure dissipation as well as all relevant stress changes that will occur during the re-consolidation process. Examples of such analyses were for instance presented by Randolph et al (1979), Kavvadas and Baligh (1982), Chin (1986) and Whittle (1987, 1992). The following focuses on calculations with the SPM-MITE3 model, as presented in detail by Whittle (1987, 1992). Figure 5.1.4 and 5.1.5 show calculated pore pressure dissipation for respectively closed and open-ended piles assuming Boston Blue Clay properties with OCR in the range 1 to 4. Note that due to the strong non-linearity of the compressibility of the clay that is inherent in the MITE3 soil model, the time factor is defined without direct reference to the coefficient of consolidation. It is rather tied to the horizontal permeability, k_{h0} (which in the model is assumed constant and independent of volume change), as follows:

$$T = T^* = (1+2K_0/3) \cdot \sigma'_{v0} \cdot (k_{h0}/\gamma_w) \cdot (t/r_0^2) \tag{5.1.5}$$

Figures 5.1.4 and 5.1.5 show that the dissipation curves for the different OCR's are essentially parallel, and that the consolidation times decrease systematically with increasing OCR.
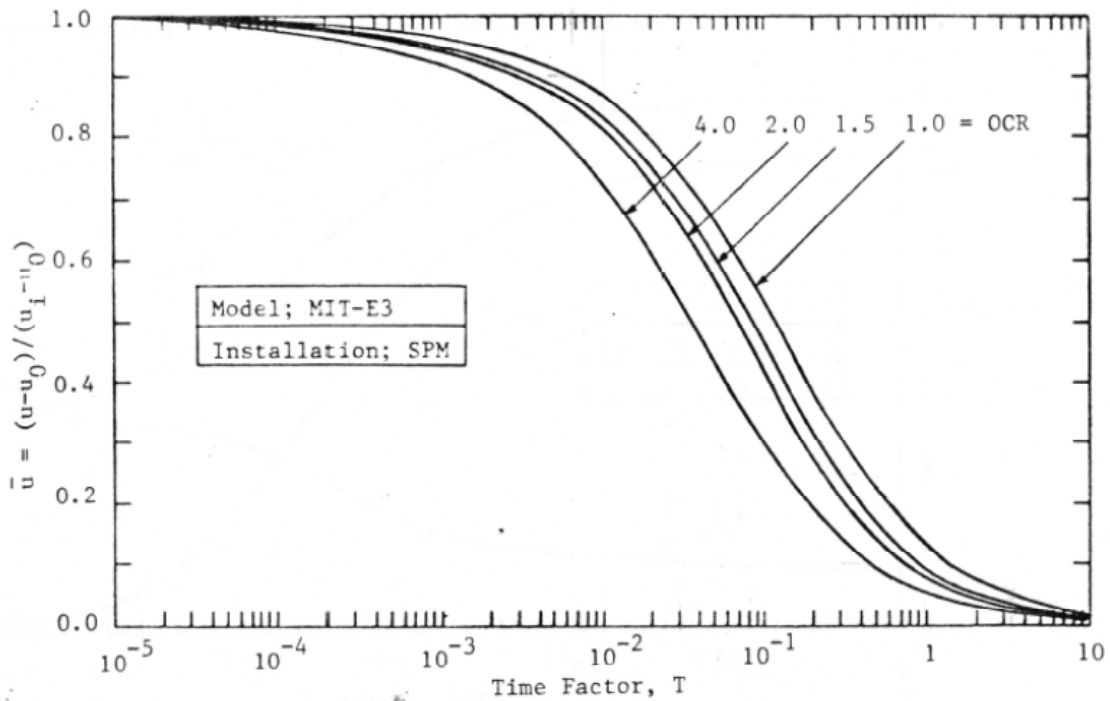
Figure 5.1.4 – Pore pressure dissipation for closed-ended pile in BBC based on the SPM-MITE3 model (from Whittle, 1987)
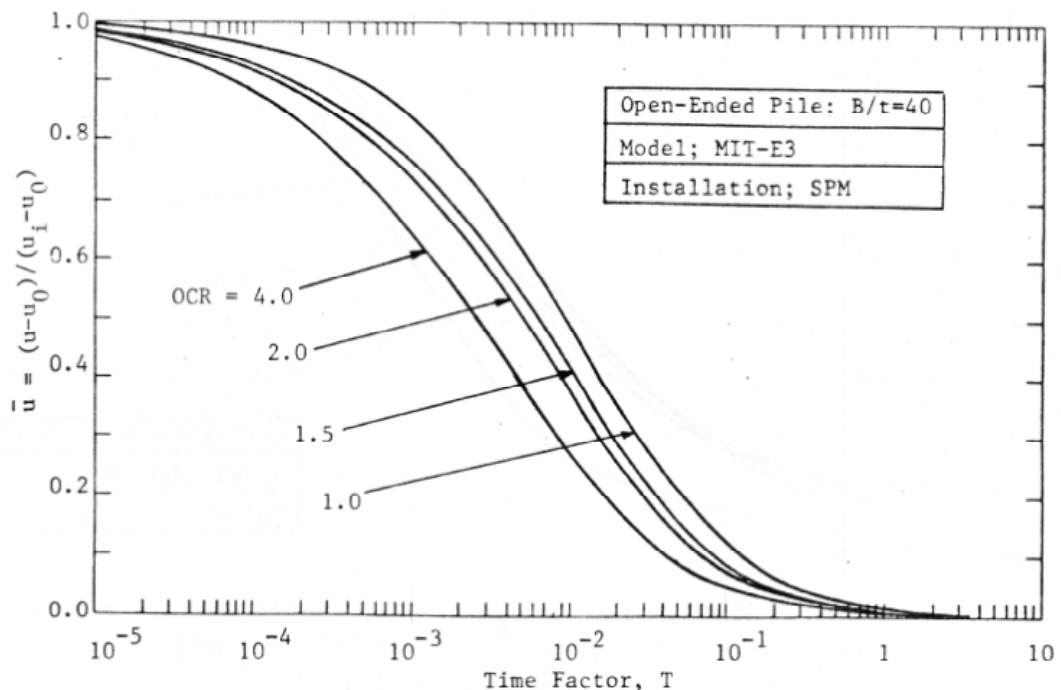
Figure 5.1.5 – Pore pressure dissipation for open-ended pile with D/t=40 in BBC based on the SPM-MITE3 model (from Whittle, 1987)

The SPM-MITE3 calculations show that the consolidation curves are also quite parallel for the case of open-ended piles. The consolidation times are also for open-ended piles decreasing relatively speaking by the same factor in relation to OCR as for the closed piles. Figure 5.1.6 compares directly the open-and closed-ended pile results for the case of OCR=1.0. The correction factor corresponding to the displacement ratio, p, has then been applied to the open-ended pile calculation. This makes the two curves match almost exactly.
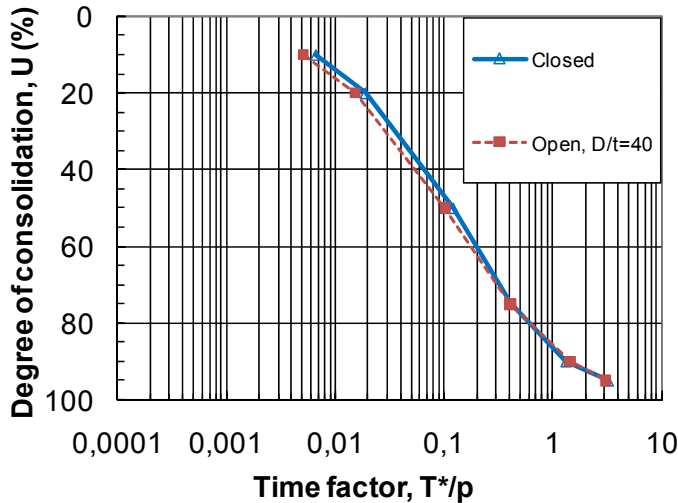
Figure 5.1.6 – Comparison between closed and open-ended (D/t=40) pore pressure dissipation based on SPM-MITE3. Open pile time factor is corrected for displacement ratio.

As a further comparison to the simpler models, the SPM-MITE3 calculation for the closed-ended pile is also shown in the earlier Figure 5.1.3. As the definition of time factors are not the same, the T* values from SPM-MITE3 were simply multiplied by a factor of 100. The interesting observation that can be made from this, as was also noted by Levadoux (1980), Chin (1986) and Whittle (1987), is that the SPM-MITE3 model follows the same dissipation pattern as the linear consolidation solution assuming the excess pore pressure decrease linearly with r/r_0. Thus, provided a representative value c_h and λ is selected to fit data, this simple linear consolidation model can give the same picture of relative rate of pore pressure dissipation as the far more advanced numerical SPM-MITE3 model. The implication of this observation will be discussed further in Section 5.2.

5.1.3 Effective stress changes
Linear consolidation theory based on CEM-EP installation models and a volumetric compressibility that is constant and the same at all distances from the pile surface, will give no change in total stresses in the soil during the re-consolidation phase. As a consequence, it can be shown that the effective stresses at end of consolidation are given by the following normalized effective stresses:

$$K_{rc} = \sigma'_{rc}/\sigma'_{v0} = K_0 + (s_u / \sigma'_{v0}) \cdot (\ln G/s_u + 1) \tag{5.1.6}$$

$$K_{\theta c} = \sigma'_{\theta c}/\sigma'_{v0} = K_0 + (s_u / \sigma'_{v0}) \cdot (\ln G/s_u - 1)$$

Assuming typical average values for G/s_u as proposed in Figure 4.1.3, leads to radial effective stress ratios, K_{rc}, as shown in Figure 5.1.7. The K_{rc} values for the CEM-EP case are as much as a factor of about 4 larger than the typically assumed K_0 for a given OCR.
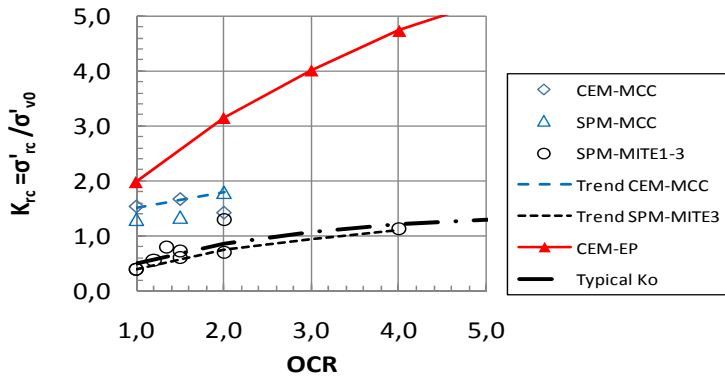
Figure 5.1.7 – Calculated radial effective stress ratio at end of re-consolidation according to different models for closed-ended piles.

The CEM-MCC approach has also been shown to give small total stress changes during the re-consolidation phase, e.g. Randolph et al (1979), Baligh and Kavvadas (1982). The SPM-MITE3 predicts on the other hand a considerable total stress reduction. This is illustrated by Figure 5.1.8 which shows calculated normalized total and effective radial stress during the consolidation process for a closed-ended pile in BBC clay with for OCR=1.0.

Figure 5.1.9 shows how the radial effective stress builds up with time for OCR values in the range 1.0 to 4.0. The radial effective stress first starts to increase significantly first after the time factor exceeds about $T = (0.4 \text{ to } 2)\cdot10^{-2}$. Introducing these values for T in Figure 5.1.3, implies that no significant increase in effective stress occurs before the degree of consolidation exceeds about U = 18-20 %.
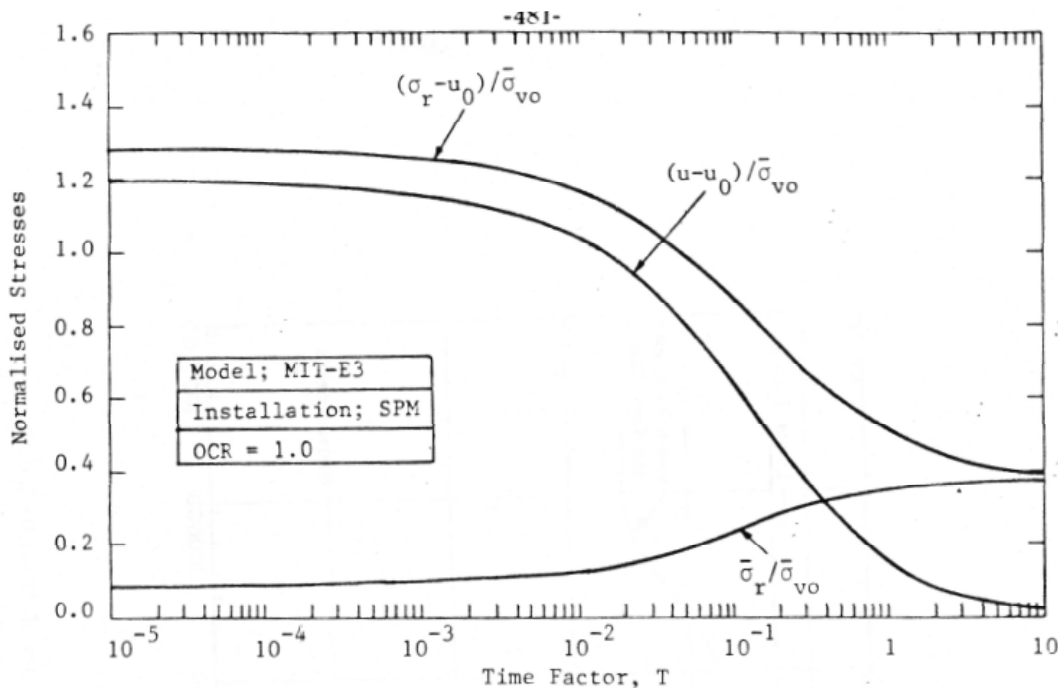
Figure 5.1.8- Example of normalized radial stress and pore pressure change calculated SPM-MITE3 for BBC with OCR =1.0 for closed-ended pile (from Whittle, 1987)
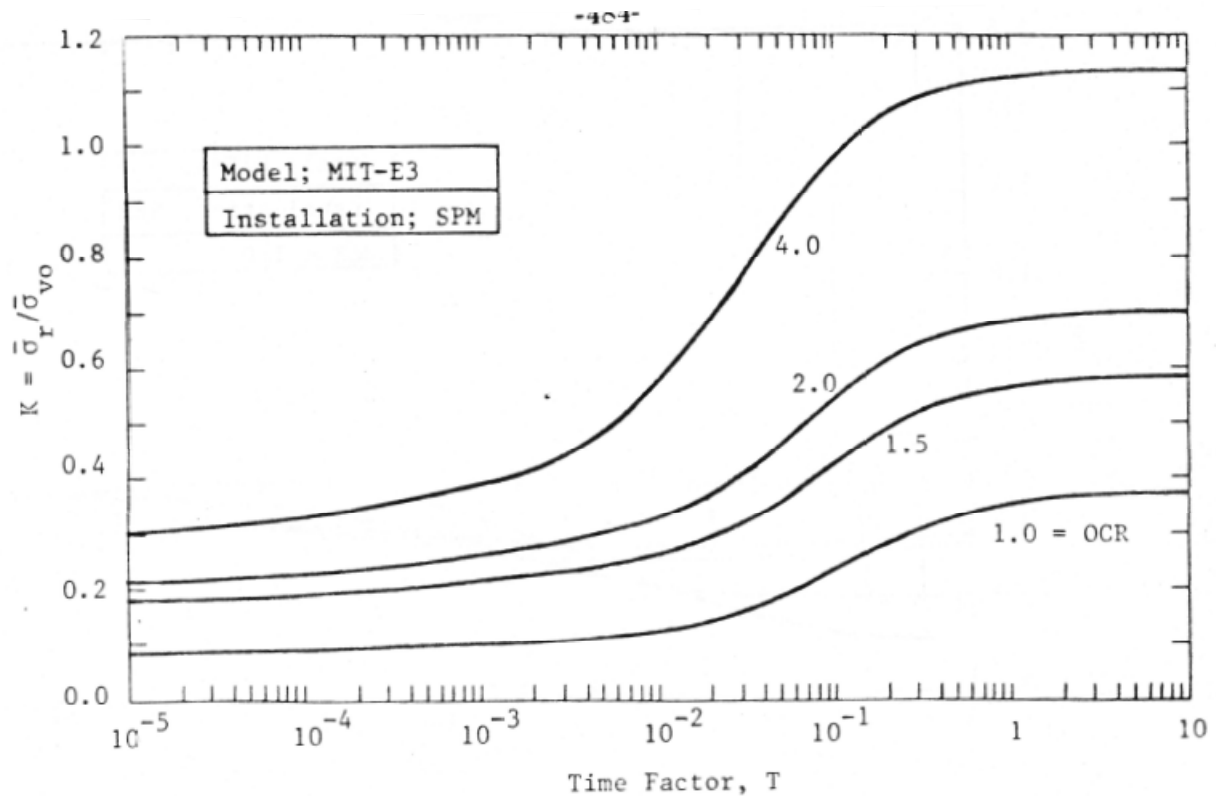
Figure 5.1.9 – Build-up of radial effective stress during the consolidation process as calculated with SPM-MITE3 model for BBC with OCR = 1 to 4 for closed-ended pile (after Whittle, 1987)

The final radial effective stress ratios calculated for closed-ended piles with all the different installation and soil models considered are compared in Figure 5.1.7 (based on results presented in table 4.1.1). It appears that the SPM-MITE3 approach typically predict values slightly on the low side of the assumed K_0 values, and a factor of about 4 times smaller than the CEM-EP case. The CEM-MCC and SPM-MCC approaches fall somewhere in between these two extreme cases.

Figure 5.1.10 and 5.1.11 show how the complete stress field looks like at end of re-consolidation for respectively OCR of 1.0 and 4.0 according to the SPM-MITE3 predictions. If this gives a correct picture of the real conditions, the differences between these two cases illustrate that OCR has a significant impact, not only on the near-field stresses, but also on stresses further away from the pile surface.
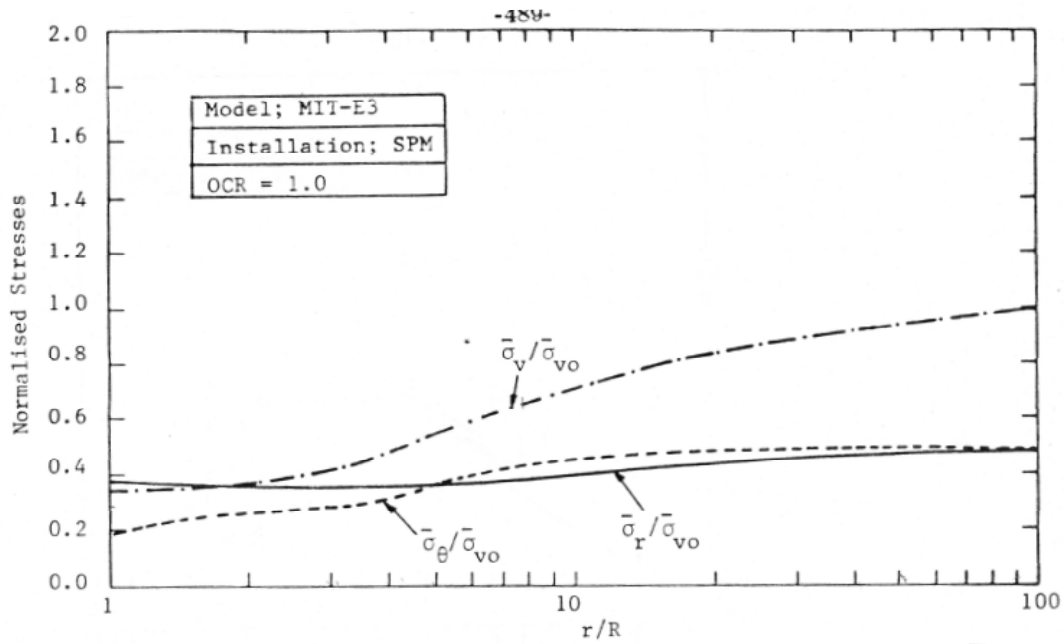
Figure 5.1.10 – Final equilibrium stresses calculated with SPM-MIT3 model for closed-ended pile in BBC with OCR =1.0 (after Whittle (1987)
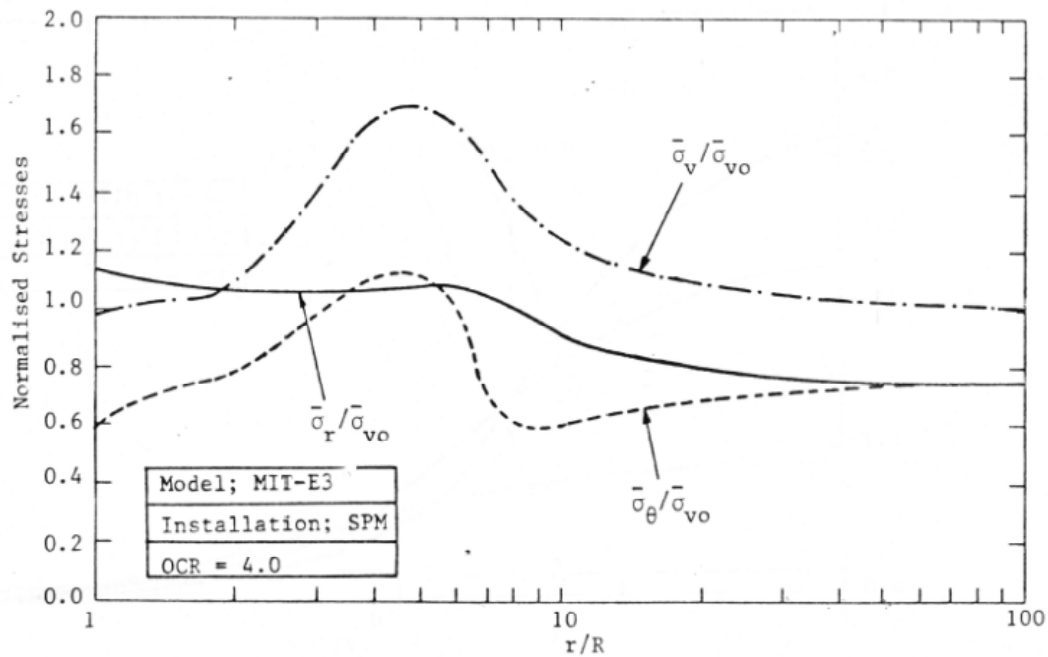
Figure

5.1.11 – Final equilibrium stresses calculated with SPM-MIT3 model for closed-ended pile in BBC with OCR =4.0 (after Whittle (1987)

The explanation for the large total stress reduction that are predicted with the SPM-MITE3 model lies in how the MITE3- soil model handles the volumetric compressibility of the clay. It is beyond the scope of this study to go into a detailed discussion of this model, but a simplistic way to describe its behaviour is that the yield surface shrinks as a result of the large shear strains that occurs in the zone closest to the pile wall, and that the re-consolidation path in this zone tends to follow a compression line more or less parallel to the virgin compression line for normally consolidated clay. This is illustrated by the numerical results presented in Figure 5.1.12.
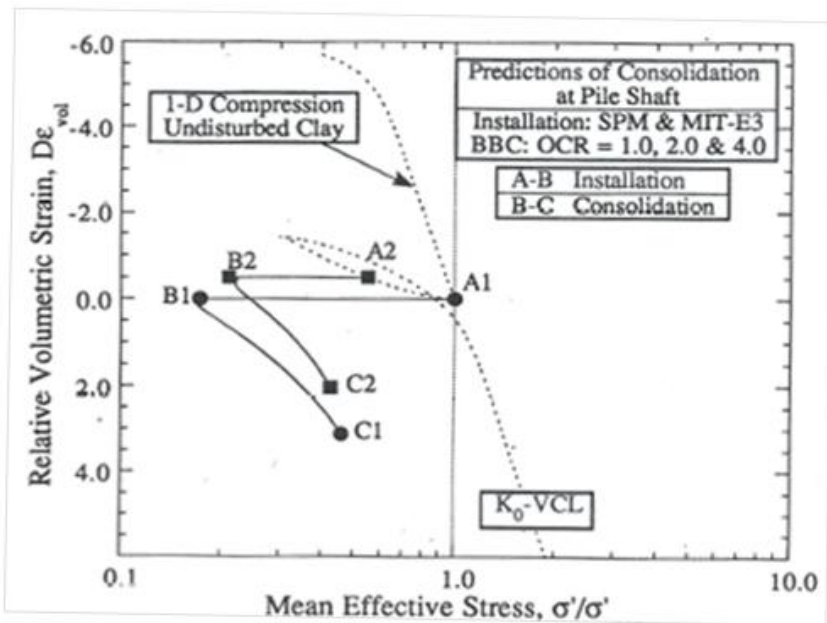
Figure 5.1.12 – Volumetric behaviour of soil element adjacent to the pile shaft during re-consolidation calculated for closed-ended pile in BBC with SPM-MITE3 model (after Whittle, 1992)

Figure 5.1.13 shows more directly the normalized radial and vertical effective stress changes that are predicted with the SPM-MITE3 models from pile installation to the end of re- consolidation. The stress changes are shown as function of normalized radial distance, r/r_0, from the pile surface. Note that the normalized values are defined as $\Delta K_r = (\sigma_{rc} - \sigma_{ri})/\sigma'_{v0}$ and $\Delta K_v = (\sigma_{vc} - \sigma_{vi})/\sigma'_{v0}$. Combined with Figures 5.1.8 to 5.1.12 above, the following may be worth noticing:

- For OCR=1 the effective radial stresses increase during the re-consolidation phase within a distance of $r/r_0 < 6$, and decrease beyond that. For OCR=4 this boundary between increase and decrease goes further out, at $r/r_0 \approx 10$.
- As stated earlier, the soil closest to the pile wall will experience large volume change as it compresses more or less along the shifted virgin compression line (Figure 5.1.11).
- Assuming that the soil beyond $r_p/r_0 > 2$ has essentially retained its in-situ compressibility characteristics, the stress changes in this outer zone will lie within the yield envelope of the clay. This is most obvious for the OCR=1 case, since the absolute final effective stresses are less than the in-situ effective stresses (e.g. Figure 5.1.9). But even for the OCR =4 case (Figure 5.1.10), the final effective stresses are considerably smaller than the pre-consolidation pressure and will also lie within the yield surface of the intact clay. Thus, the re-loading and un-loading type volumetric compression modulus will govern the consolidation process in the zone $r_p/r_0 > 2$ for both of these cases.
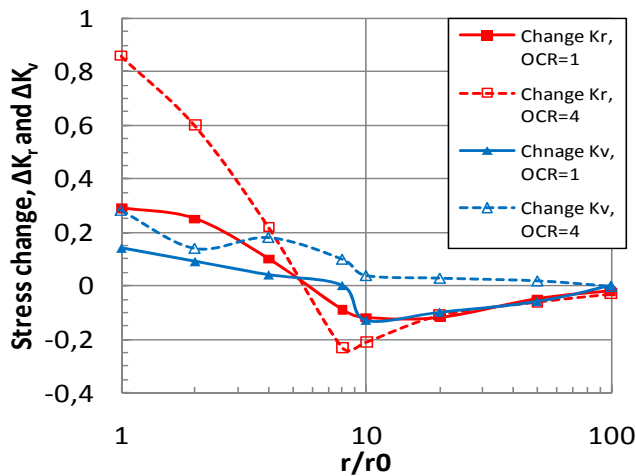
Figure 5.1.13 – Effective stress changes during the re-consolidation phase as predicted by SPM-MITE3 model for BBC with OCR = 1 and 4.

Andersen and Jostad (2002) presented some interesting FEM radial consolidation analyses of cylindrical suction anchors with very large radius and relatively small wall thickness. They clearly distinguished between volumetric compressibility of a thin remoulded zone experiencing virgin compression, as compared to the undisturbed zone further out experiencing unloading/reloading. The results confirmed, as would be expected, that the radial effective stress at end of reconsolidation decreased with increasing difference in volumetric compressibility in these two zones.

The installation and re-consolidation process has also been analysed by fully coupled finite element analyses. Liyanapathirana (2004) used for instance the general purpose finite element program ABAQUS coupled with the MCC model to analyse both the piezocone and PLS probe tests at the MIT Saugus test site, and the Imperial College model pile tests at Bothkennar. The results seem to have come out close to what would be expected from un-coupled CEM-MCC predictions, probably because much of the response is controlled by the soil model.

5.2 Comparison between model predictions and measured response

5.2.1 Pore pressure dissipation

As a first approach, a comparison has been made of measured times to reach respectively 50 and 90 % pore pressure dissipation, t_{50} and t_{90}, for all the piles against what is predicted with the simple linear consolidation theory. Two cases were considered, assuming respectively a linear decrease in initial excess pore pressure with $\log(r/r_0)$ as predicted with the CEM-EP approach, and a linear decrease with absolute value of (r/r_0). In both cases the plasticized radius was for each pile calculated with the CEM-EP method described in Section 4.1.2, and assuming values of G_{50}/s_u as represented by the assumed average curve in relation to OCR shown in Figure 4.1.3.

The assumed horizontal coefficient of consolidation was calculated from the classical expression $c_h = M \cdot k / \gamma_w$, but using the reported vertical permeability at zero volume change, k_0 (see Appendix 1), and an assumed average operating compression modulus corresponding to:

$$M = C_M \cdot m_o \cdot p'_c. \tag{5.2.1}$$

The factor C_M was after some trial and errors taken as $C_M = 4$, which means that M was chosen to be 4 times larger than what it is for NC-clay at a stress corresponding to p'_c. The reason for this choice was that un-loading re-loading conditions seem to govern in most of the stress field around a pile during consolidation. The permeability used should of course ideally have been the horizontal permeability, but due to lack of such data for most of these cases, the vertical permeability k_{v0} were used. This permeability, and the chosen values for G_{50}/s_u and M, should still be considered as semi-empirical factors that impact the consolidation process as calculated by this simple analytical approach.

Without initially distinguishing each pile site, Figure 5.2.1 shows the ratio of measured/calculated times plotted against OCR, and Figure 5.2.2 the same plotted against the plasticity index of the clay. Apart from the relatively large scatter, it appears that the log-linear excess pore pressure distribution gives a different and shifted match with respect to t_{50} as compared to t_{90}. The linear distribution is more balanced in that respect, i.e. matching t_{50} and t_{90} equally well. Both approaches suggest some dependency of the match on OCR, less on I_p.
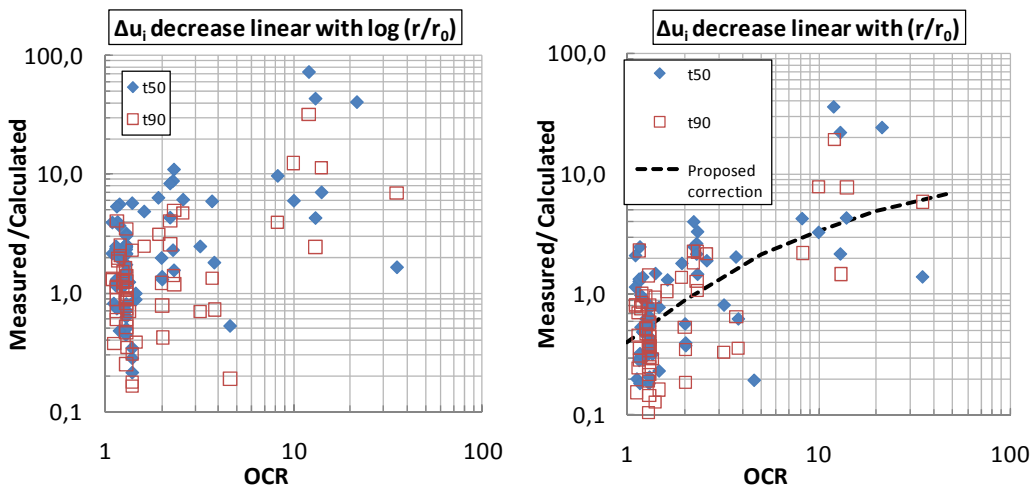
Figure 5.2.1 – Comparison between measured and calculated t_{50} and t_{90} values versus OCR based on CEM and linear consolidation theory
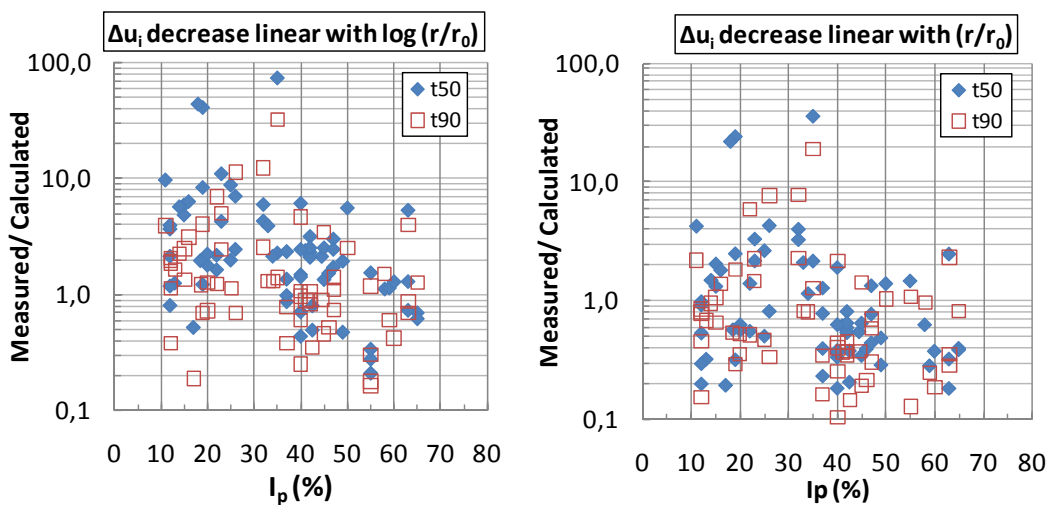
Figure 5.2.2 – Comparison between measured and calculated t_{50} and t_{90} values versus I_p based on CEM and linear consolidation theory

Based on Figures 5.2.1 and 5.2.2 it was concluded that the best merit in trying to improve the match between linear consolidation theory and measured data, was to pursue further the case of linear excess pore pressure distribution, which as shown in Figure 5.1.3, also tends to match the shape of the SPM-MITE3 dissipation curves reasonably well.

To get a better overall match, the main correction needed would be to decrease the calculated consolidation times (i.e. speed up consolidation) for low OCR, and increase for high OCR. This could be achieved in a number of alternative ways:

1. Correcting the assumed relationship between G_{50}/s_u and OCR in Figure 4.1.3, and thereby the radial extent of the initial excess pore pressure field (r_p/r_0)
2. Correcting directly (r_p/r_0) in relation to OCR
3. Correcting the assumed average modulus M, used to determine c_h, and for instance assume that the factor C_M in eq. (5.2.1) depends on OCR.
4. Correcting directly the calculated consolidation times in relation to OCR

As the first 3 approaches can give an impression of having some well founded basis in relation to real soil parameters, it was chosen to go directly for a correction of the consolidation times as per point 4.

After some trial and errors, and within the range of OCR's in question, the following correction was selected to be applied to the calculated consolidation times:

$$t_{corr} = C_t \cdot t_{cal} \tag{5.2.2}$$

$C_t = 0.6 + 4.5 \cdot (\log(OCR))^{1.5}$ for correcting t_{50}

$C_t = 0.32 + 6.4 \cdot (\log(OCR))^{1.5}$ for correcting t_{90}

Figure 5.2.3 shows that after application of these correction factors to the calculated times, the ratios of measured/calculated (M/C) consolidation times are reasonably well balanced, and they are on average close to 1.0 both in relation to OCR and I_p.
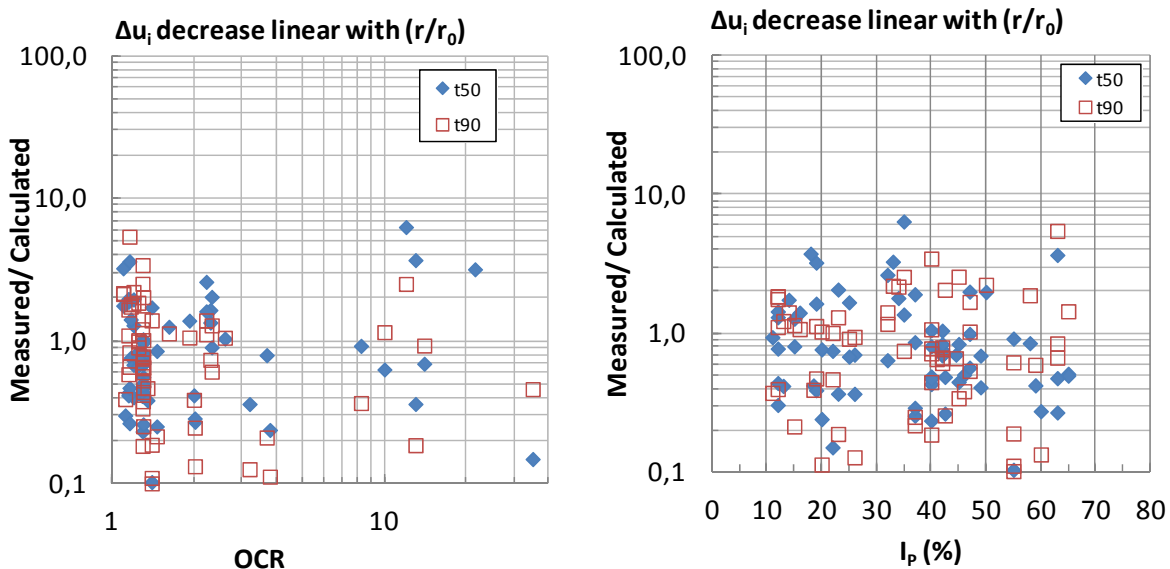
Figure 5.2.3 –Ratio of measured/calculated t_{50} and t_{90} values versus OCR and I_p, based on CEM and linear consolidation theory with proposed correction factor

Figure 5.2.4 and 5.2.5 present separately values for t_{50} and t_{90} based on the same data as Figure 5.2.3, but identifies also each individual pile and measurement made. The same data are plotted versus plasticity index in Figure 5.2.6 and versus depth in Figure 5.2.7.
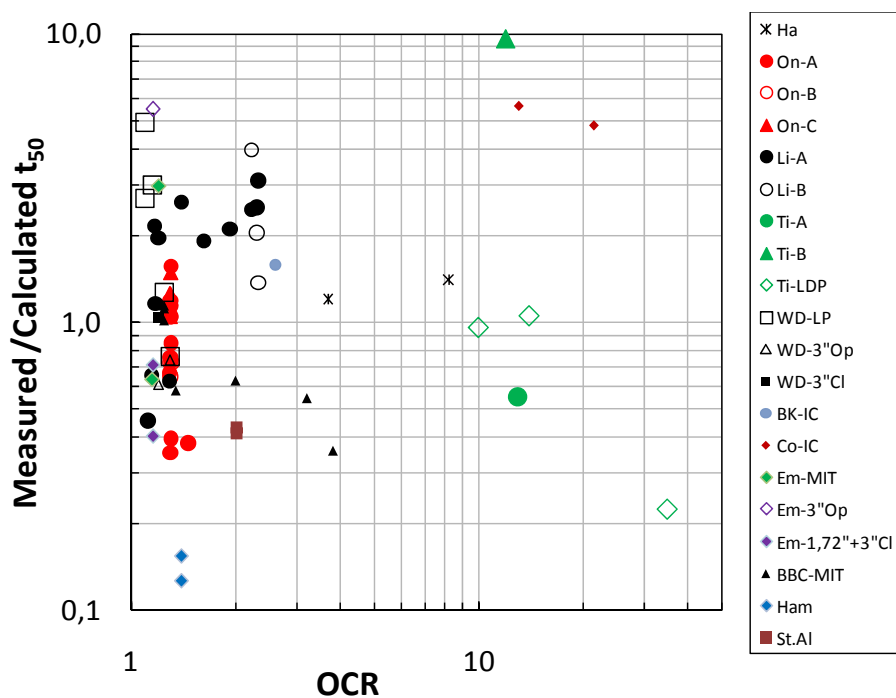
Figure 5.2.4 –Ratio of measured/calculated t_{50} values versus OCR for individual piles
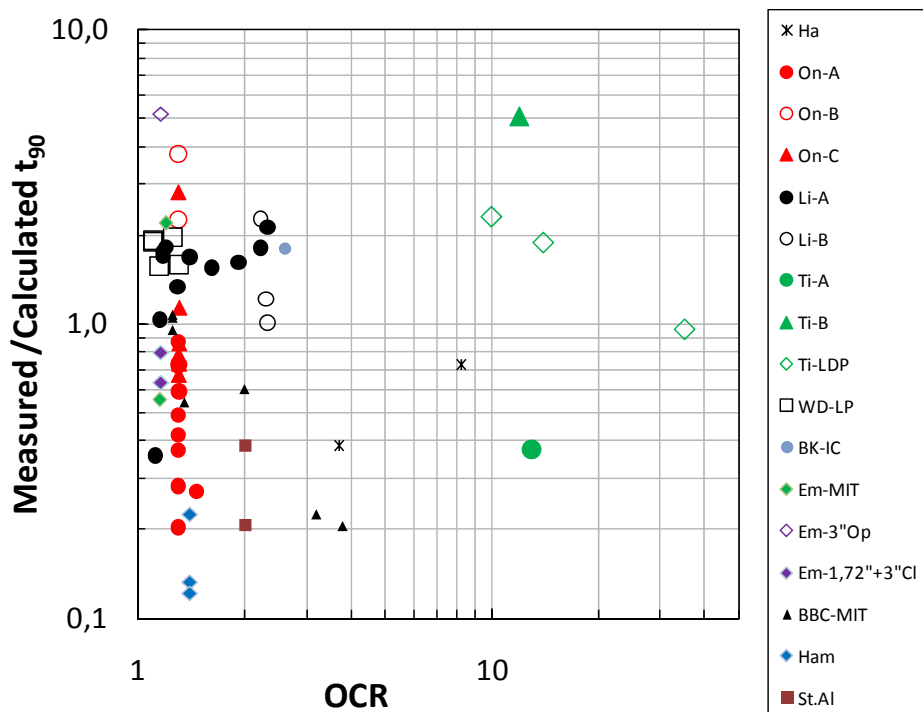
Figure 5.2.5–Ratio of measured/calculated t_{90} values versus OCR for individual piles
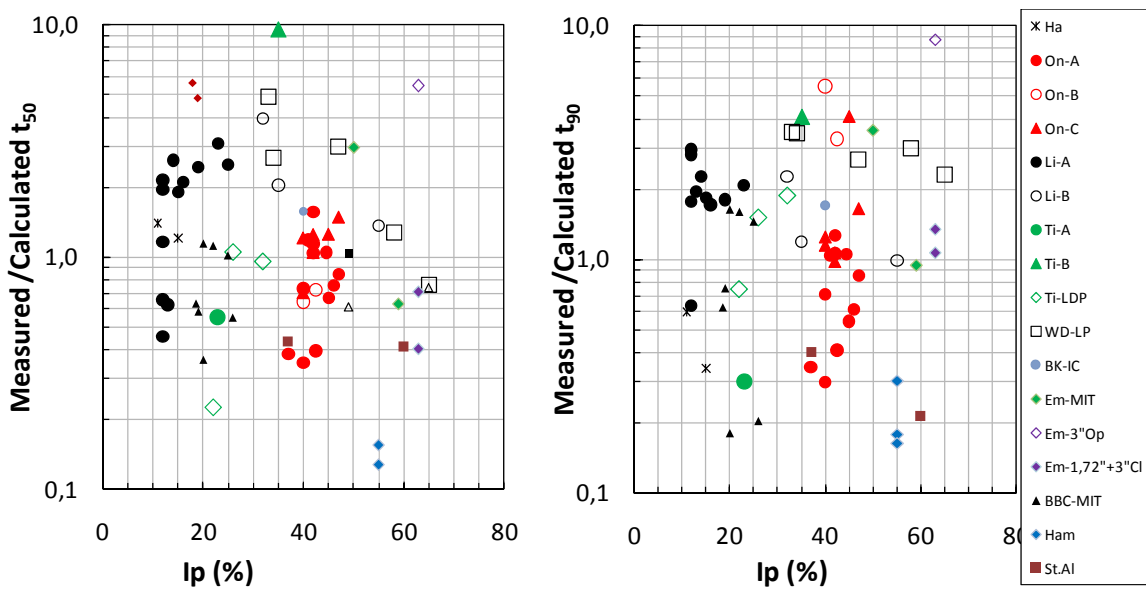
Figure 5.2.6–Ratio of measured/calculated t_{50} and t_{90} values versus I_p for individual piles
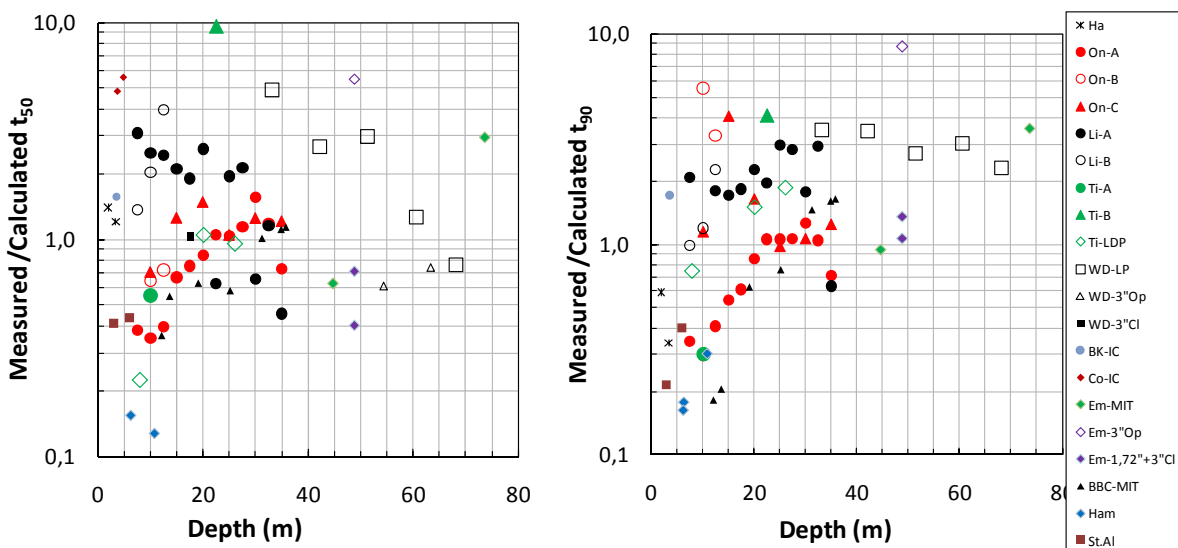
Figure 5.2.7–Ratio of measured/calculated t_{50} and t_{90} values versus depth for individual piles

The scatter in calculated/measured consolidation times is however, fairly large (see Figures 5.2.4 to 5.2.7), and shows a standard deviation of the calculated/measured ratio of 0.64. The main contribution to the scatter may lie in the assumed permeability values, which for a number of the sites was difficult to determine from available soils data. But weakness in the applicability of the idealized consolidation model and uncertainties in the other assumed soil parameters must also play a role.

Some observations that can be made from these data, and possible reasons for their scatter, are further discussed and summarized in the following.

At the West Delta, Onsøy and Lierstranda sites, where there are tests with different pile types, there seems to be no clear differences between open- and closed-ended piles, nor any apparent significant effect of pile diameter. The same observation applies when looking at all the data together. This suggests that the proposed semi-empirical approach captures well both scale effects and open-versus closed penetration.

Uncertainty in the selected permeability values is probably a major source of the spread in the measured/calculated consolidation times. This is most obvious for the Onsøy data. Referring to Figure 2.4.6, there is a significant variation in the measured permeability values, and the selection of the "trend line" could be made differently. A more balanced match between measured/calculated consolidation times with depth (figure 5.2.7) could be obtained for this site by increasing the selected permeability in the top part of the deposit towards the upper range of measured values, and lowering it towards the lower range in the lower part.

The BBC data show a similar trend as at Onsøy, in that the measured consolidation times are relatively speaking much smaller than calculated in the top part of the deposit than lower down, Figure 5.2.7. Based on the actual permeability data presented by Morrison (1984) and Baligh and Levadoux (1986), it would be more difficult to defend any significant upgrading of permeability in the upper part relative to the lower part of the deposit at this site. It may be of interest to note, however, that based on piezocone dissipation tests, Baligh and Levadoux (1986) observed a similar difficulty to match the permeability measured in the laboratory tests in the top part of the deposit.

The permeability values given in Appendix 1 were at several sites (WD, Til, Ham, St.Alb.) back-calculated from reported coefficients of consolidation, without the author having access to raw data to verify these values. At other sites (BK, CP, Co) the author used the reported permeability without knowing the specific basis for it (inferred from oedometer tests or by direct permeability tests in the field or in the laboratory).

An interesting point brought up in the report by Azzouz and Baligh (1984) relating to the Empire data, is that the permeability back-calculated from incremental oedometer tests (IL) tended to be a factor of 2-3 lower than what came out of CRS type oedometer test. Thus, there are significant uncertainties in the "measured" permeability. This uncertainty could in principal be further enhanced by possible anisotropy of the in-situ permeability. In homogeneous marine clays that are not varved and do not contain any distinct seams or layers of silt or sand, the ratio of horizontal to vertical permeability have commonly be reported to lie close to 1.0, e.g. Ladd and DeGroot (2003). For varved clays the ratio may approach 5-10 (e.g. Tavenas et al. 1983, Mesri and Feng 1994, DeGroot and Lutenegger 2003). Apart from the Pentre site, which is excluded from this part of the study due to its abnormally high permeability (Section 2.6.2), none of the clay deposits dealt with herein have been described or identified as distinctly varved or layered. This suggests that anisotropy of the permeability does not contribute significantly to the scatter in measured/calculated consolidation times.

As discussed earlier, some scatter in calculated values will inevitably also be associated with uncertainty and variations in soil stiffness during installation as well as reconsolidation. Use of site specific parameters rather than generalized stiffness relationships as assumed herein, therefore, would most likely also tend to reduce the scatter in measured/calculated consolidation times.

5.2.2 Final radial effective stress

Figure 5.2.8 presents all data for the radial effective stress ratio, $K_c = \sigma'_{rc}/\sigma'_{v0}$, as interpreted from the available data. Note that as described in Chapter 2, all data have been extrapolated to a degree of consolidation of U= 100 %, and that a correction have also been included for negative installation effective stresses as measured at some sites (mainly at Onsøy and Lierstranda).
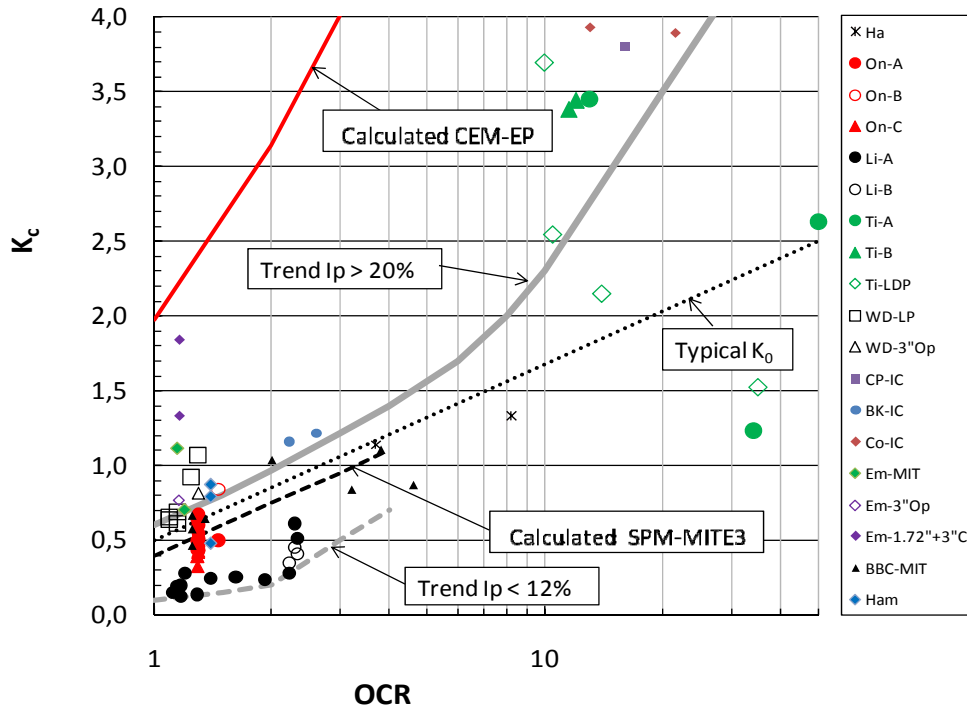
Figure 5.2.8 – Radial effective stress ratio, K_c, versus OCR – all tests

The data in Figure 5.2.8 generally show a clear trend of increasing K_c with increasing OCR, but the scatter in the data is rather significant at all OCR's. The values are much lower (factor of about 4) than predicted with the CEM-EP theory but the trend line suggested for clays with $I_p>$ 20 % agree fairly well with what is typically predicted for BBC with the SPM-MITE3 model. Reduction in total radial stresses in parallel with the pore pressure dissipation is the main explanation for the effective stresses ending up far below what is predicted by the CEM-EP approach, and is why the SPM-MITE3 model gives far better agreement with the measured data than the CEM-EP approach.

Figure 5.2.9 compares more directly the difference between measured K_c and the estimated K_0 values, expressed as the ratio K_c/K_0. For clays with $I_p>20$ the ratio tends to increase from around 1.2 when OCR exceeds about 6 and approach $K_c/K_0 = 2$ at OCR = 40, but there is significant scatter. For the clays with the lowest plasticity index, the ratio of K_c/K_0 can be as low as 0.2, but there is a lack of data for OCR beyond about 2.5 for low plastic clays.

Figure 5.2.10, presenting data for clays with OCR< 2 only, illustrates further the apparent significant effect the plasticity index has on the measured K_c values. The values are particularly low when I_p drops below 12-14 % as for the Lierstranda and partly the Pentre cases.
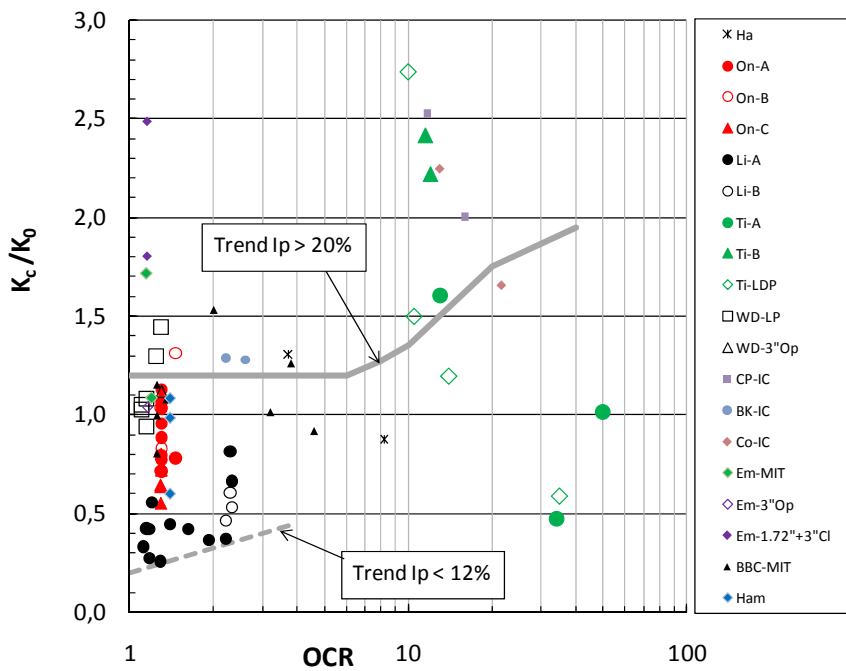
Figure 5.2.9 – Normalized radial effective stress ratio, K_c/K_0 , versus OCR – all tests
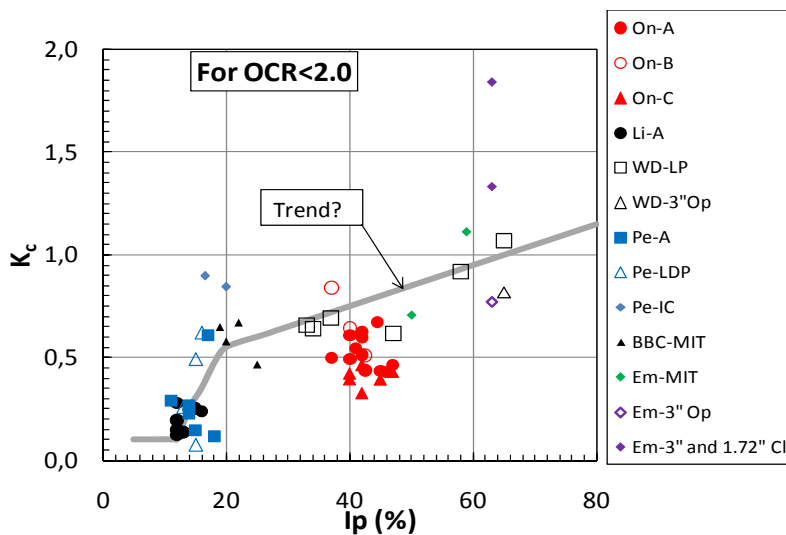
Figure 5.2.10 – Radial effective stress ratio, K_c, versus I_p for OCR <2

Some comments to the individual data and observed scatter are given in the following:

- In-spite of the correction applied to the Lierstranda and Onsøy A-segment tests to make the installation effective stress at least equal to zero (see Chapter 2 and 4), the measured K_c values from these tests could be on the low side of reality. It is quite apparent however, that the tests in low plastic clay at Lierstranda show much lower K_c values than in the more plastic Onsøy clay. Since the test piles and instrument units were the same, this difference gives clear evidence of the significant impact of I_p has on the K_c values.
- The open-ended pile B at Onsøy shows very good agreement with the West Delta LP test results. Pile B at Onsøy had a different size and detailed design of the earth pressure gage as compared to the A-segment piles (ref. Section 2.4), and may therefore have given more reliable results than the small gages used on the A-segment piles at both Lierstranda and Onsøy.

- The K_c values obtained with the closed 1.72" and 3" probes at Empire come out particularly high, considering that the results at West Delta with the same probe and in quite similar clay falls more along the trend line. The closed 1.72" and 3" probes at Empire also diverge significantly from the MIT's PLS tests at Empire. That is the reason for not giving much weight to the closed 1.72" and 3" probe results at Empire when drawing the trend lines in Figure 5.2.8 to 5.2.10.
- In the very stiff clay at Tilbrook the measurement of earth pressures in the top 5-10 m came out quite low compared to at larger depth (ref. Figure 2.7.20 and discussion in Section 2.7.3). These data points are the three with OCR>20 in Figures 5.2.8 and 5.2.9, and are also considered to be not representative.
- In relation to the IC model pile data it should be recalled that data from the "leading" sensors have been excluded from the data on account that they are located so close to the pile tip (typically 4 pile diameters behind the tip) that they are bound to be impacted by tip effects, and not be representative for a normal pile. This issue will be further discussed in Chapter 6.
- The available data suggest that there is no pronounced scale effect on the measured values of K_c, and that there is no obvious or clear difference between open- and closed-ended piles. Considering the large differences in strains caused by pile installation, that is really a rather surprising observation, but it tends to agree with what Whittle (1987) predicted with the SPM-MITE3 model.

5.3 Recommended predictive approach and needs for improvements

The author's proposed semi-empirical approach for predicting pore pressure dissipation includes the following steps:

1) Use an initial excess pore pressure distribution that decreases linearly with the normalized radial distance, r/r_0, from the pile wall.
2) The plasticized radius, r_p, shall be computed according to the simple CEM-EP approach for both open-ended and closed ended piles as given by eq. (4.1.4), and assuming a value for the normalized shear modulus G_{50}/s_{ud} as proposed in Figure 4.1.3.
3) Use of linear radial consolidation theory assuming that the coefficient of consolidation is constant in time and as function of radial distance from the pile shaft. This gives degree of consolidation in relation to time factor as presented in Figure 5.1.3. The consolidation time is then found from the expression:
   $t = T \cdot r_0^2 / c_h$
4) The horizontal coefficient of consolidation shall be computed from:
   $c_h = M \cdot k_0 / \gamma$, where the empirically derived oedometer modulus M, shall be taken as:
   $M = 4 \cdot m_0 \cdot p'_c$

   Note that it is the **vertical** in-situ permeability, k_0, which shall be used in the expression above. The empirical correlations cater for possible difference between the horizontal and vertical permeability in homogenous non-layered clays.

For layered or stratified clays, the ratio of horizontal to vertical permeability can be much larger than for the generally homogenous clays dealt with in this study. For such stratified clays it is recommended to use the best estimate of average horizontal permeability divided by a factor of 1.5 to calculate the coefficient of consolidation to be applied.

5) To get good match to measured consolidation times the calculated consolidation times shall finally be corrected according to eq. (5.2.2)

One of the major uncertainties actually in the proposed method seems to lie in determining the in-situ permeability of the clay with sufficient accuracy. It would in this connection be valuable to make further detailed studies and comparisons of permeability of clays as determined indirectly from IL or CRS oedometer tests, or from direct hydraulic conductivity tests in the field or in the laboratory.

For moderately over-consolidated medium plastic clays, the SPM-MITE3 approach has been shown to give good predictions of the pore pressure dissipation as well as the final effective radial stress.

It is likely that further improvement could be made to the SPM-MITE3 model to better capture the full impact of large shear strains on the volumetric- and shear related stress- strain characteristics of the clay closest to the pile wall. With appropriate selection of relevant parameters, the SPM-MITE3 approach could possibly also capture the particularly low effective stresses observed for piles in low plastic clays.

Such an improvement of the SPM-MITE3 model would in the author's view require more systematic studies of the compressibility characteristics of clay subjected to different levels of "disturbance" or shear strains prior to re-consolidation. Rather than trying to capture that effect in a single soil model, it may be a better approach to develop a separate model for predicting the behaviour of clays subjected to various degrees of shear straining. This may, for instance, be achieved by grouping the clay behaviour into three main categories; completely remoulded (shear strain above 100 %), severely strained (strains within say 20-100 %) and moderately strained (less than 20 %).

For the time being, the empirical K_c data presented herein may give the best guidance to assessing the radial effective stress level at full set-up. This effective stress ratio may not however, be the key to predicting the ultimate shaft friction. This issue will be discussed further in Chapter 6.

6 ANALYSIS AND PREDICTION OF ULTIMATE SHAFT FRICTION

6.1 Introductory remarks

This chapter first gives an overview of the design methods that were developed for predicting the ultimate shaft friction along piles in clays over the time period up until 1983. This also includes a review of some old pile load test experiences, starting as early as 1900.

The results of the pile load tests which this study focuses on are then summarized and compared against basic soil parameters. On that basis, new semi-empirical design methods are proposed.

The pile load test results are also discussed in relation to more recent design methods that have been proposed in the period after 1983, many of which are presently being used in the profession.

The time for "set-up", and how the shaft friction increases during the reconsolidation phase, is discussed as a separate item at the end of this Chapter. The aspect of ageing effects, or possible further increase in shaft friction with time after 100 % reconsolidation is reached, is also briefly discussed.

6.2 Overview of past work and design approaches, period 1900 to 1984

Period 1900-1973

The following highlights efforts made in the period from around 1900 to 1973 to establish understanding of the axial bearing capacity of piles in clay. It is to a large extent based on the rather comprehensive historic reviews presented by Flaate (1968) and Torstensson (1973).

Probably the first systematic study of the bearing capacity of friction piles in clay was reported by Wendel (1900). The study included testing of 17 wooden piles installed in Gothenburg clay. Various types of wooden piles with different pile dimensions were tested. The piles were also tested at different times after installation. At the time, the concept of undrained strength of clays was not known, but Wendel showed interestingly enough that there was a clear increase in bearing capacity with time, and that the maximum was reached after typically 2-3 weeks. Keeping in mind that the Gothenburg clay is highly plastic with water content around 80%, this time effect is an interesting observation which will be discussed in a broader context in Section 6.4.

Hultin (1928) studied a larger number of load tests on wooden piles of length up to 27 m carried out in Gothenburg in the period 1900-1928, and concluded that the shaft friction increased linearly with depth. This observation is consistent with what would presently be expected for a normally consolidated highly plastic clay deposit such as the Gothenburg clay.

When the fall cone test later was introduced in Scandinavia, Hultin (1937) concluded that the observed shaft friction generally agreed closely with the fall cone strength determined on tube samples.

On basis of 33 pile load tests collected from Norway, Sweden and Finland, Skaven-Haug (1940) proposed that both the undisturbed and remoulded fall cone strength affected the shaft friction.

As illustrated by figure 6.2.1, Bjerrum (1953) came to the same conclusion as Hultin (1937) that the ultimate shaft friction could be taken as the fall cone strength on undisturbed samples.
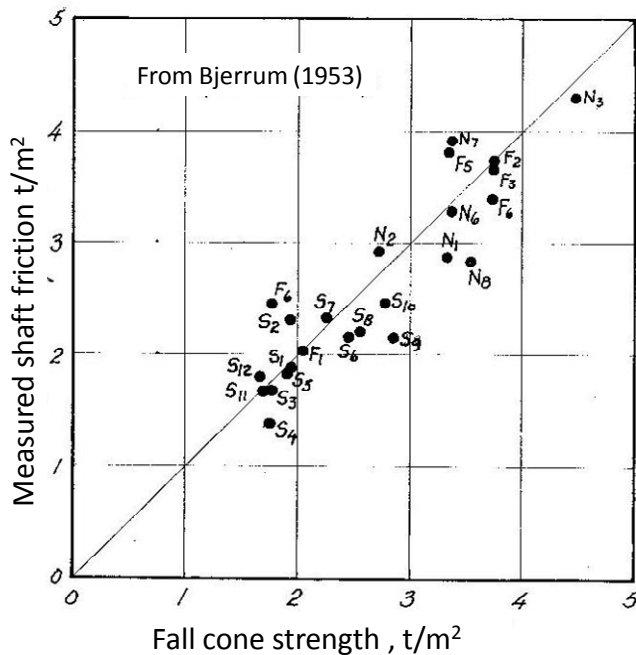
Figure 6.2.1- Measured shaft friction in relation to fall cone strength (after Bjerrum, 1953)

The field vane test was developed in Sweden in the early 1950's (Cadling & Odenstad, 1950). Fellenius (1955) showed on basis of a number of new pile load tests that the average shaft friction was typically 15 % smaller than the in-situ vane strength, but 30 % higher than the fall cone strength. This view was not shared by Bergfelt (1957), who based on 72 pile load tests collected at the time, suggested as Hultin (1937) and Bjerrum (1953), that the shaft friction was best calculated by the fall cone strength.

Tomlinson (1957) suggested in contrast to the aforementioned studies that the ultimate shaft friction was given by an adhesion factor (later and herein called α-value) times the undrained strength, i.e.

$$\tau_{us} = \alpha \cdot s_u \qquad\qquad (6.2.1)$$

Figure 6.2.2 shows that Tomlinson's adhesion factor decreases considerably with the undrained strength, from a value of 1.25 for very soft clay, to 0.25 for stiff clays with $s_u > 100$ kPa. Tomlinson also suggested somewhat higher α-values for tapered wooden piles than for concrete piles.

Going back to Bjerrum's figure 6.2.1, there is a scatter in the data, and apparent α-values would range from about 0.75 to 1.32. Notice that Bjerrum's figure 6.2.1 covers average shaft friction values typically between 15 and 40 kPa. For such strengths, Tomlinson's data in figure 6.2.2 show apparent α-values ranging from 0.75 to 1.5, which is close to the scatter in Bjerrum's figure 6.2.1. Thus, these data are not so much in conflict with each other.

Broms (1965) suggested that for clays with s_u less than 50 kPa, the α-value depended strongly on the pile material, and should be taken as 0.5 for steel, 0.8 for concrete and 1.0 for wooden piles.
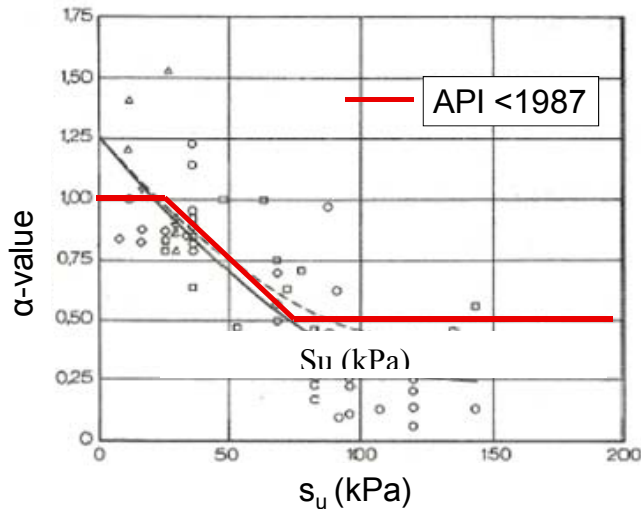
Figure 6.2.2- Adhesion factor or α-value versus s_u proposed by Tomlinson (1957), and API (1987)

Flaate (1968), using some of the same data as the previously referred studies, but supplemented by some newer load tests carried out in Norway and abroad, suggested as Tomlinson (1957) that the α-value decreased with undrained strength. Furthermore, for soft clays Flaate concluded that the α-value was much smaller for highly plastic clays than for low plastic silty clays, figure 6.2.3. As will be shown in Section 6.3, that conclusion is in direct conflict with conclusions drawn by Karlsrud (1992[a]) and Karlsrud et al (2005).
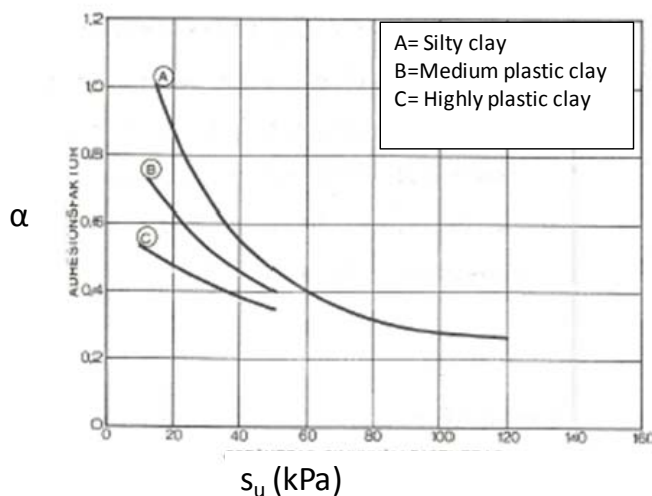
Figure 6.2.3- Adhesion factor or α-value versus s_u proposed by Flaate (1968)

Many of the 84 test piles included in Flaate's database were load tested several times after installation, se for instance Figure 6. 2.4. Flaate used the tests carried out after typically 90 days as his reference. His basis for selecting 90 days was that the increase in capacity after 90 days was relatively speaking small as compared to the increase that occurred prior to that. Flaate recognized that when the same pile was loaded to failure several times after its installation that could, in addition to the pure time element, contribute to an apparent increase in capacity with time. But Flaate, due to lack of specific evidence, neglected that in his interpretation of results. As will also be discussed later in section 6.3, loading the same pile to failure can have an important impact on the way pile load test data have been interpreted in the past.
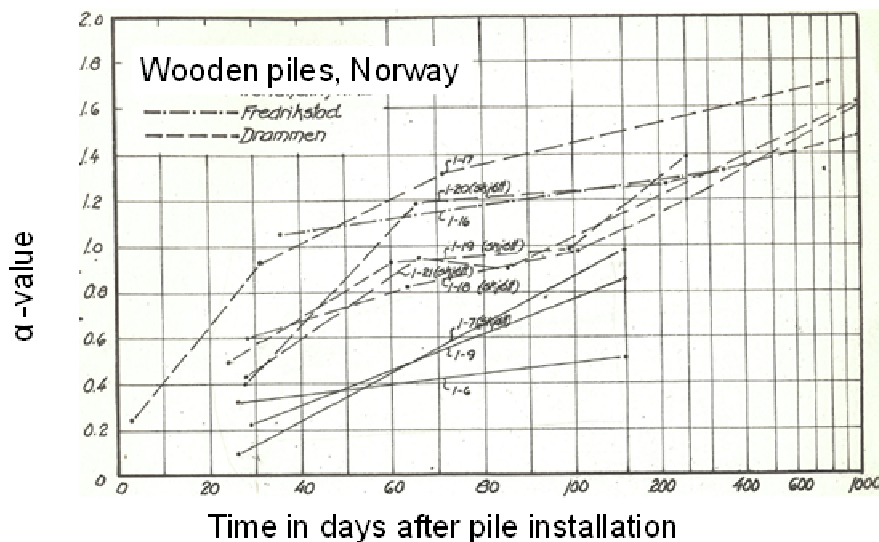
Figure 6.2.4 – Example of repeated load test results on the same pile, from Flaate (1968).

Flaate (1968) and Torstensson (1973) both fully appreciated that pile installation and the subsequent re-consolidation could significantly alter the undrained strength of the clay surrounding a pile, and that the shear strength could vary considerably with distance from the pile surface. Thus, they also recognised that failure is not necessarily taking place at the pile surface. That is in accordance with the common observation that a layer of clay often adheres to a pile when it is pulled out after having been in the ground for some time. This was actually already suggested by Taylor (1948), ref. his illustration in figure 6.2.5. Zeevaert (1950) also discussed the important impact of pile driving on the properties of the surrounding clay.

Flaate (1968 and 1971) showed results of trenching or sampling close to driven piles in soft to medium clays, which documented that the most severely remoulded clay closest to the pile surface had a significantly lower water content and higher undrained strength than the clay at larger distance from the pile. In one case this zone was of thickness of about 10 cm, corresponding to half a pile diameter.

Flaate (1968) recognized that how the undrained shear strength of the clay was determined introduced a significant element of uncertainty into the interpretations. Based on his previous studies (Flaate, 1965) he had for instance found that the undrained shear strength from unconfined compression tests carried out on 54 mm piston samples gave s_u- values that were on average 10 % larger than according to in-situ field vane tests, but it could vary from about 0.65 to 1.65 times the vane strength. The significance of this important issue was the basis for the

author's choice of using the s_{ud} strength determined in a consistent manner as basis for the present study, ref. discussion in Section 2.1.
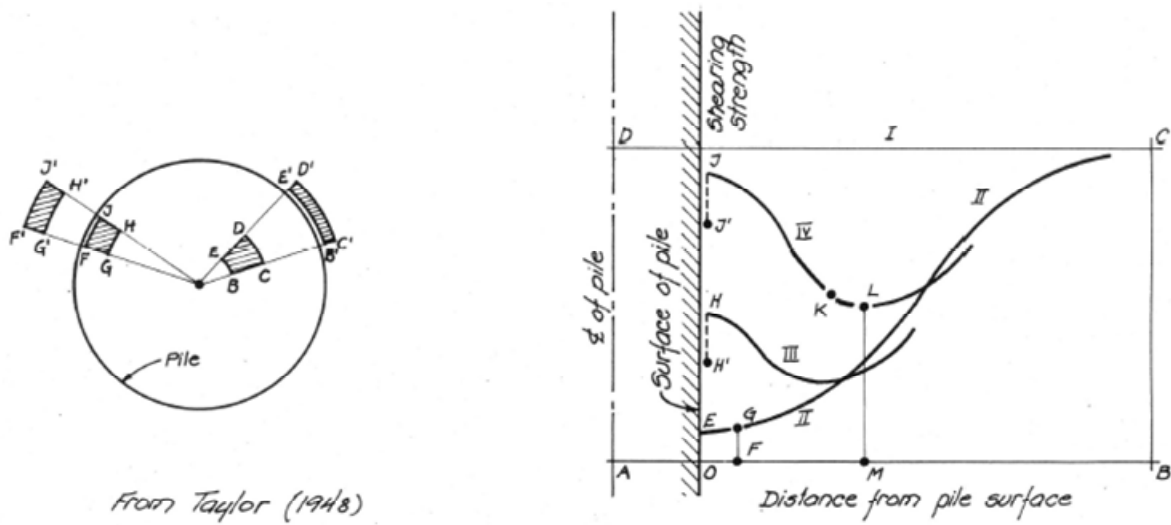
Figure 6.2.5- Illustration of impact of pile installation on shear strength of clay surrounding a pile presented by Taylor (1948).

Effective stress based approaches of the form given by equation (6.2.2) were proposed quite early by for instance Zeevaert (1959), Eide et al (1961) (primarily for drained long-term loading cases), Bjerrum (1965), Chandler (1966 and 1968), and Burland (1973).

$$\tau_s = K \cdot \sigma'_{v0} \cdot \tan\delta \tag{6.2.2}$$

Note that $\tan\delta$ defines the mobilised soil/pile interface friction angle, which may differ from the maximum true effective friction angle.

By defining $\beta = K \cdot \tan\delta$ equation (6.2.2) becomes the classical expression:

$$\tau_s = \beta \cdot \sigma'_{v0} \tag{6.2.3}$$

Burland (1973) discussed how various factors may impact the parameters in equation (6.2.2) for soft and stiff clays. Based on a limited review of published load tests, Burland proposed typical ranges of $\beta = 0.25$ to 0.40 for soft clays. For stiff clays he proposed conservatively to assume $K = K_0$, but does not give clear recommendations for $\tan\delta$ other than stating that it is the drained interface friction angle.

Janbu (1976) proposed an effective stress based approach applicable to long-term drained loading situations. In that connection he introduced the possible impact of the direction of applied load on the effective stress state for soil elements close to the pile wall. His general formulation was of the form.

$$\tau_s = S_v \cdot (\sigma'_{vo} + a) \qquad \text{, where} \tag{6.2.4}$$

S_v = shaft friction number

a = soil attraction = $c \cdot \cot\varphi$

 The shaft friction number depends on the coefficient of active lateral earth pressure, the friction angle and the assumed interface roughness. The active earth pressure coefficient used corresponds to plane strain conditions, which depend on the direction of applied shear stress along the pile. A consequence of this theory is that for a clay with a friction angle of 30^0, and assuming a roughness number of 0.8, the shaft friction in compression will correspond to $\beta = 0.19$, whereas it drops to $\beta=0.12$ for tension loading.

Vijayvergiya and Focht (1972) proposed that the ultimate shaft friction was best determined by an empirical combination of undrained strength and effective strength parameters, the so-called λ-approach. The method also includes a reduction factor for length of pile driven into the ground. The proposed expression for the ultimate limit shaft friction was:

$$\tau_s = \lambda \cdot (\sigma'_{v0m} + 2s_{um}) \qquad\qquad\qquad (6.2.5)$$

The suffix "m" in equation (6.2.5) means that the values are to be taken as average over the entire embedded pile length. The factor λ is a function of pile length, starting at $\lambda = 0.5$ for L=0, and decreasing to $\lambda = 0.2$ for L=15 m, $\lambda = 0.165$ for L=30 m, and $\lambda = 0.120$ for L=60 m.

Period 1974-1983

In 1975 the American Petroleum Institute adopted a pure α-method for design of pile foundations for offshore structures, API-RP2A (1975). The method is herein referred to as API1 and separates between highly plastic clays as found in the Gulf of Mexico (GOM) and "other" clays as follows:

For highly plastic clays like in GOM

| Under-or normally consolidated | $\alpha= 1.0$ | (6.2.6a) |
| Overconsolidated clays | $\tau_s = 0.25\ \sigma'_{v0}$ | |

For "other" clays:

$$\alpha= 1.25 - s_u/96 \quad (s_u \text{ in kPa}) \qquad\qquad (6.2.6b)$$
but
$$0.5 < \alpha < 1.0$$

Figure 6.2.2 shows that the α-value proposed for "other clays" is very similar to what Tomlinson (1957) had proposed earlier.

Meyerhof (1976) also proposed to use the effective stress equation (6.2.2) as basis. For soft to medium stiff clays he suggested to use $K = K_0$ as a typical value (as did Burland, 1973). Meyerhof's comparison against load test data showed that for soft to medium stiff clays β tended to decrease with pile length from typically 0.3 to 0.5 at depths less than about 15 m to 0.1 to 0.25 at a depth of 60 m. Soft clays with low to medium high plasticity typically have an effective friction angle in the range 28^0 to 35^0 (e.g. Karlsrud and Hernandez, 2011), and K_0 in the range 0.5 to 0.6. That would according to equations (6.2.2) and (6.2.3) give β in the range 0.27 to 0.35, which for long piles lies on the non-conservative side of the data Meyerhof used as basis.

Meyerhof made a clear distinction for stiff clays, and suggested for this case to typically use K_s= 1.5 K_0. The value of K_0 was assumed to increase with OCR according to common correlations (he actually proposed K_0= (1-sinφ)·(OCR)$^{0.5}$) . The load test data he presented showed however, considerable scatter compared to this proposal.

Flaate and Selnes (1977) proposed a semi-empirical and mainly effective stress based approach based on the following expression, which also introduced OCR, pile length and the plasticity index as main parameters affecting the ultimate shaft friction:

$$\tau_s = \mu_L \cdot ((0.3-0.001 I_p) \cdot OCR^{0.5} \cdot \sigma'_{v0} +0.008 \cdot I_p \cdot s_u) \quad , where \qquad (6.2.7)$$

$$\mu_L = Length\ factor =(L+20)/(2L+20)$$

They also suggested that (6.2.7) could be approximately simplified to:

$$\tau_s = \mu_L \cdot (0.3\ to\ 0.5) \cdot \sigma'_{v0} \cdot \sqrt{OCR} \qquad (6.2.8)$$

Flaate and Selnes (1977) compared their method against what they felt were the 42 best load tests previously presented by Flaate (1968), and found it superior to use of the approaches of Tomlinson (1957), Vijayvergiya and Focht (1972) and Burland (1973). 35 of the 42 load tests had been carried out on wooden piles, 4 on concrete piles and 3 on steel piles. No distinct effect of pile material was observed.

In the late 1970's the offshore piling industry, together with a number of consultants and University researchers, joined forces to try to develop a sound theoretical approach for calculating the bearing capacity of piles. This multi-industry project was headed by Amoco and called the Effective Stress Axial Capacity Cooperative (ESACC) program. As summarised by Kraft et al (1980), this research program focused on five main elements:

- Use of a soil model for clay based on the concepts of Critical State Soil Mechanics (CSSM) as developed by researchers at Cambridge University,(also called the Cam Clay Model (CCM), e.g. Schofield and Wroth, (1968). The use and potential application of CSSM for this purpose was actually proposed by Kirby and Wroth (1977) who both played a very active role in the ESACC project.
- Predicting the stresses around the pile during the installation and re-consolidation phase using FEM coupled with use of the CCM model.
- A series of pin-model tests carried at Cambridge University in a 250 mm diameter special triaxial cell to study stress changes during pile insertion and shaft friction in relation to effective stress conditions after re-consolidation. The 19 mm diameter and 600 mm long pin model pile was instrumented with axial load cells and radial stress cells at 4 levels. In addition, there were pore pressures transducers placed within the clay sample at various positions. Tracers within the clay allowed assessment of displacements during penetration of the pile into the sample. The clay used in the tests was artificially prepared samples of Speswhite kaolin. The clay has a plasticity index of I_p =31 %. Tests were carried out on samples prepared with OCR=1, 2 and 8. The valuable outcome of the pin model tests with respect to effects of pile installation was included in Chapter 4, and is not dealt with any further herein.

- In-situ load tests carried out on 4 model piles with diameter 114 mm driven or jacked to 12.2 m depth into an essentially normally consolidated highly plastic San Francisco Bay mud Theses are the tests at Hamilton Air force base already dealt with in Section 2.8.
- Assessment of results from a pile load testing program carried out in 1975 at Empire, Louisiana, as dealt with in Section 2.10.2 and 3.2.

In terms of methods for predicting ultimate shaft friction, a series of 3 different effective stress methods (ESM) were proposed during the course of the ESACC project , but a fourth method was later added by Kraft (1982).

These four different semi-theoretical approaches each contained an "Installation module", describing the mean effective stress against the pile surface after the installation and re-consolidation phase, and a "Loading module ", describing both possible effective stress changes during the loading phase and different failure criteria in terms of the state of effective stress and critical shear plane at failure. In this context it was recognised that the effective shear strength characteristics of the severely remoulded clay close to the pile surface could differ from that of intact clay, and that failure could be governed by the maximum pile/clay interface friction angle rather than the peak friction angle of the clay.

The following equation (6.2.9) coupled with figure 6.2.6 presents as an example the so-called ESM4 model finally proposed by Kraft (1982).

$$\tau_{us} = (\eta p'_{rIi} + \xi u_e)(p'_r / p'_k) \cdot \sin\Phi_r \qquad \text{where} \qquad (6.2.9)$$

η = Parameter to account for that mean effective stress after installation being less than p'_r

p'_{rIi} = Mean effective stress at the pile surface after installation

ξ = Parameter to account for change in mean effective stress, as related to u_e

u_e = Excess pore pressure generated at the pile surface at the end of pile installation

p'_r = Mean effective stress at critical state line for remoulded clay

p'_k = p' on virgin k_o compression line for remoulded clay

φ_r = Effective friction angle of remoulded clay
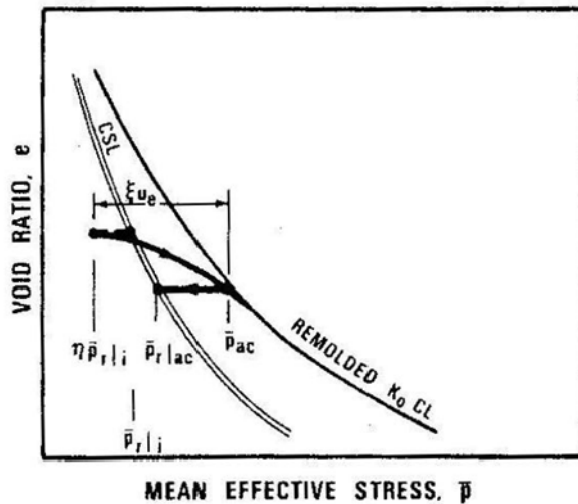
Figure 6.2.6 – Illustration of parameters included in the ESM-4 model (after Kraft, 1982)

Kraft (1982) used the four ESM based approaches, as well as the API- and the λ- methods, to predict the pin model tests carried out at Cambridge University and the model- and full scale-load tests at Hamilton and Empire. Compared against these tests, the ESM approaches did not do any better than the pure empirical methods. Kraft (1982) concluded therefore, that although the ESM approaches did provide further insight, they should not be adopted as a standard or only design tool. For such models to become applicable he saw a great need for further research efforts to:

1. Establish a more accurate stress-strain and strength model for the soil (It is assumed that he then meant both for intact and remoulded clay).
2. An improved understanding of the influences of installation details on the effective mean stress after installation.
3. An improved understanding of pile loading, especially after the peak resistance is developed.

On contract from API, Olson &Winter (1981) compiled a large data base on published load test results worldwide, which for clay included about 180 piles of various types and materials. Using this data base, Dennis and Olson (1983) suggested a modified α-method which included a length factor. The recommended α-values and length factor, F_L, are presented in Figure 6.2.7. Note that the length factor F_L in Figure 6.2.8 is a multiplication factor, i.e. $\tau_{us} = \alpha_p \cdot F_L \cdot s_u$, and that F_L actually increases with penetration depth. That is not very logical, but is comes out of their statistical correlation study. It may reflect that deep samples tend to be more disturbed and show lower undrained strength than they should relative to shallow samples.
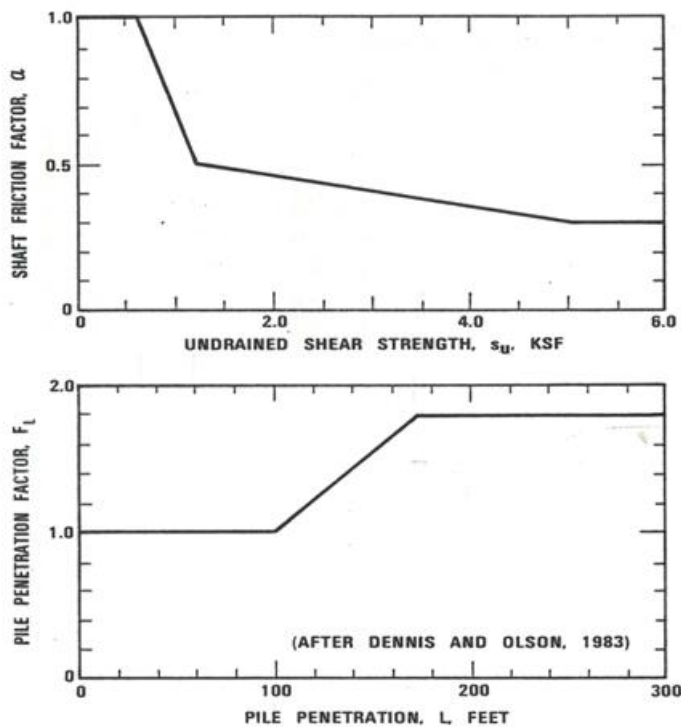
Figure 6.2.7- α-values and length factor, F_L, proposed by Dennis and Olson (1983)

Semple and Rigden (1984) focused on driven steel pipe piles and selected what they thought were the 33 best case records at the time. Based on these data they proposed a new α-approach where the α-value is correlated to the normalised strength ratio, s_u/σ'_{v0}, combined with a length reduction factor related to the aspect ratio L/D, figure 6.2.8. Note that also the length factor F_L in figure 6.2.8 is a multiplication factor, but that it decreases rather than increases with pile length as proposed by Dennis and Olsson (1983).

Semple and Rigden recognised that the s_u/σ'_{v0} ratio is closely related to OCR as in the SHANSHEP approach (eq. 2.5.1, Ladd and Foott, 1974). The introduction of s_u/σ'_{v0} or OCR as an important parameter was in general agreement with previous suggestions by for instance Wroth (1972), McClelland (1974) and Meyerhof (1977). Note that Semple and Rigden used the average strength and vertical effective stress along the pile as basis for their proposed method.

The undrained strength used as reference by Semple and Rigden was generally the UC strength determined on samples taken with thin- walled samplers, but for soft clays with poor sample quality the in-situ vane or laboratory vane strengths were used as basis.

Randolph and Murphy (1985) proposed what formed the basis for the present API-RP2A design guideline (API, 1987, 2007), which also relates α to the s_u/σ'_{v0} value as follows:

$$\text{For } s_u/\sigma'_{v0} <1.0, \ \alpha= 0.5(s_u/\sigma'_{v0})^{-0.5} \tag{6.2.10}$$

$$\text{For } s_u/\sigma'_{v0} >1.0, \ \alpha= 0.5(s_u/\sigma'_{v0})^{-0.25}$$

This α-relationship is shown in figure 6.2.9. It does not, like Semple and Rigden (1984), include any specific length factor. In API (2007) the length does come indirectly into the calculation of the ultimate pile capacity through the softening post-peak t-z relation in figure 6.2.10. This means that the capacity also will depend on the pile length and stiffness.
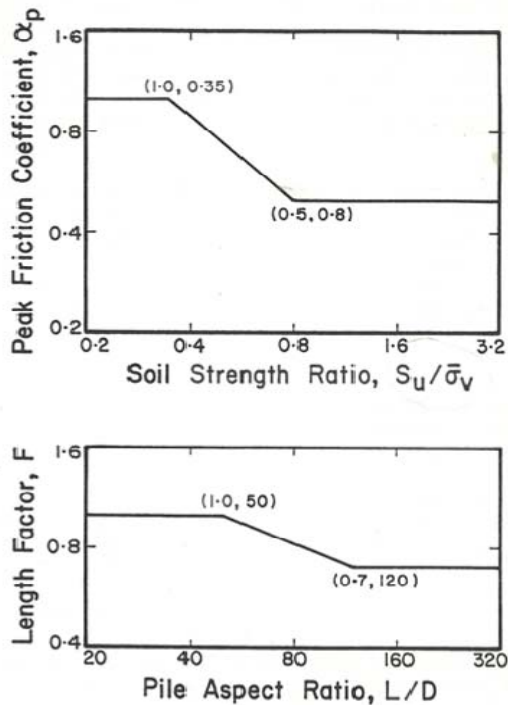
Figure 6.2.8 - α-values and length factor, F, proposed by Semple and Rigden (1984)
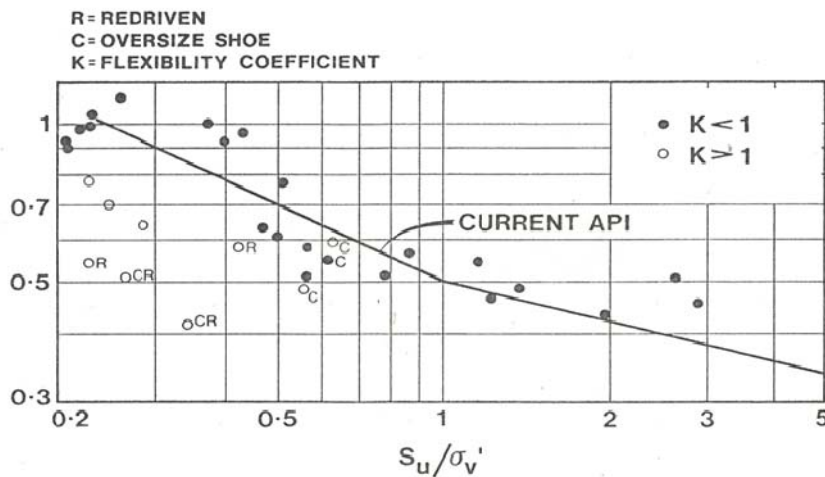

Figure 6.2.9 - α-values according to API method (1987-to present). (The data points are those included in the original paper by Randolph and Murphy, 1985)
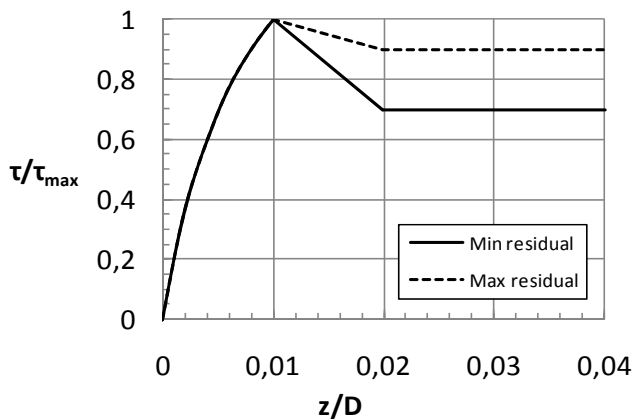

Figure 6.2.10 – Strain softening t-z curves to be applied with the current API (2007) α-method.

In the commentary to the API-RP2A (1987) code it is also stated that *"Unconsolidated – undrained (UU) triaxial compression tests on high quality samples , preferable taken by pushing a thin-walled sampler with a diameter of 3.0 inches or more, are recommended for establishing strength profile variation because of their consistency and repeatability."* To what extent the UU strength can be assumed representative for the in-situ strength was discussed in Section 2.1. It is however clear that such UU tests only had been carried out at a limited number of the pile load test sites which formed the basis for the development of this design guideline.

For a more detailed discussion on the development of the API design guidelines and relevant papers that they are based upon, it is referred to a comprehensive review made by Pelletier et al (1993). They bring up some valuable points and observations in relation to past load test data that empirical methods have been based upon:

- Many of the load tests included in past data bases (e.g. the API data base, Dennis Olson, 1983), were carried out on piles that apparently had not reached full set-up, or piles that had been subjected to re-striking. That means many capacities would be expected to lie on the low side.
- They recognised the uncertainties related to the undrained strength that had been used as basis for the back-calculated α-values. These uncertainties could arise from questionable and variable sample quality, and the range of different types of undrained strength tests that lie behind the interpretations. In that respect they regarded the recommendation in API (1987), as described above, to consistently use the UU-strength as a significant improvement compared to past practice.
- They rightly point out that relating the α-value to the s_u/σ'_{v0} ratio rather than the undrained strength as in the earlier API versions, dampens some of the uncertainty associated with the undrained strength, as it also brings in some impact of the state of vertical effective stress.

As a comment to the last issue, the sensitivity of the calculated shaft friction to an uncertainty in undrained strength is primarily reduced when $s_u/\sigma'_{v0}<1$. In such cases, an uncertainty in undrained strength of 20 % will reduce to about 10% uncertainty in the calculated shaft friction. For $s_u/\sigma'_{v0}>1$ the effect of uncertainty in s_u is, much smaller.

It can certainly be questioned why these early past studies conclude so differently with respect to how the ultimate shaft friction should be determined, as they are based on at least to some extent the same load test data. That is an issue which will be discussed further in subsequent sections.

6.3 Results from pile load tests

6.3.1 Measured ultimate shaft friction related to in-situ undrained shear strength
This section addresses the measured ultimate shaft friction values as summarized in Appendix 2 in relation to the assumed undrained strength of the clay. It may be recalled that the mobilized ultimate shaft friction values are normalized to the undrained direct simple shear strength, i.e. $\alpha = \tau_{us}/s_{ud}$. The mobilized α –values are in the following seen in relation to the normalized undrained strength value, s_{ud}/σ'_{v0}. This is a similar approach to that in the current API (2007) procedure (Figure 6.2.8), apart from the use of s_{ud} herein, rather than the UU-strength as with the

API procedure. In addition, the impact of the plasticity index of the clays is considered in this study.

Karlsrud et al (1992) were the first to bring in the potential significant impact of clay plasticity on the ultimate shaft friction in clay. That was partly based on the Lierstranda tests, and partly on a review of some old tests on wooden piles taken from the data collected by Flaate (1968). As shown in Figure 6.3.1, these old tests suggested a very significant impact of the plasticity index. Note that the undrained strength used as basis for the data in Figure 6.3.1 was determined from a variety of test types, mainly field vane tests, UC tests and fall cone tests carried out on 54 mm piston samples.

Based on some newer pile tests, including some of those included herein, Karlsrud et al (2005) proposed a new correlation between α, OCR and I_p as shown in Figure 6.3.2. That was, as in API (1987), also based on using the UU strength as reference strength. When UU strengths were not available it was estimated on basis of approximate correlations to other undrained strength values.
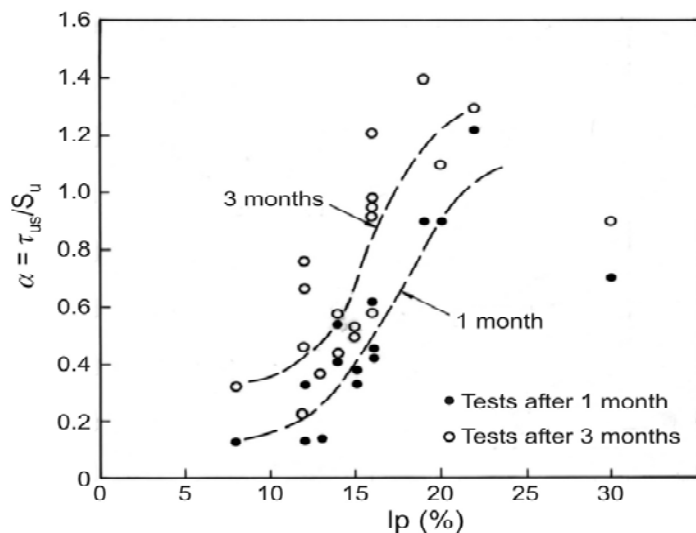
Figure 6.3.1 – Relationship between α-value and plasticity index from load tests on wooden piles in Norway (from Karlsrud et al, 1992)

With the above correlations as a background carpet, Figure 6.3.3 presents mobilized values of α versus s_{ud}/σ'_{v0} for all sites and piles included in this study. The scatter in the data must at a first glance be characterized as very large. But following the suggestion of Karlsrud et al (1992) and Karlsrud et al (2005), further studies of the data verified that the plasticity index has a large impact on the mobilized ultimate shaft friction and corresponding α-values. To substantiate that, Figure 6.3.4 presents the α-values versus plasticity index I_p for the different piles grouped into three ranges of s_{ud}/σ'_{v0}, respectively of $s_{ud}/\sigma'_{v0} \leq 0.4$, $s_{ud}/\sigma'_{v0} = 0.4$ to 0.8, and $s_{ud}/\sigma'_{v0} = 1.4$ to 3.0.

By combining the impact of s_{ud}/σ'_{v0} and I_p, a coupled α- correlation was developed as presented by the trend lines shown in Figure 6.3.3 and 6.3.4. This was a trial and error process, in which large scale tests were given more weight than small scale tests, and data that were considered particularly uncertain were also given less weight than data considered most reliable. This new correlation represents some changes from the NGI-05 method in Figure 6.3.2, mainly because:

new data are included herein; all previous data have been re-interpreted; and the estimated s_{ud} strength is consistently determined and used as reference strength.
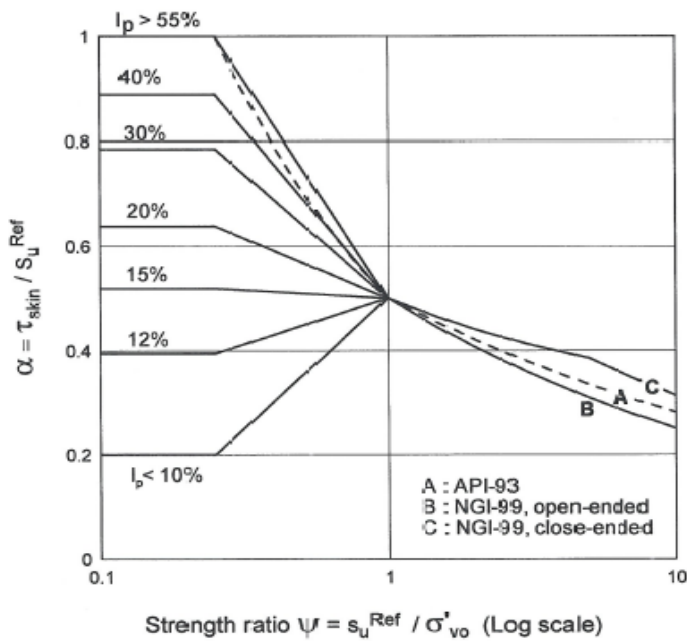
Figure 6.3.2 – Basis for selection of α-values according to the NGI-05 procedure (from Karlsrud et al, 2005)
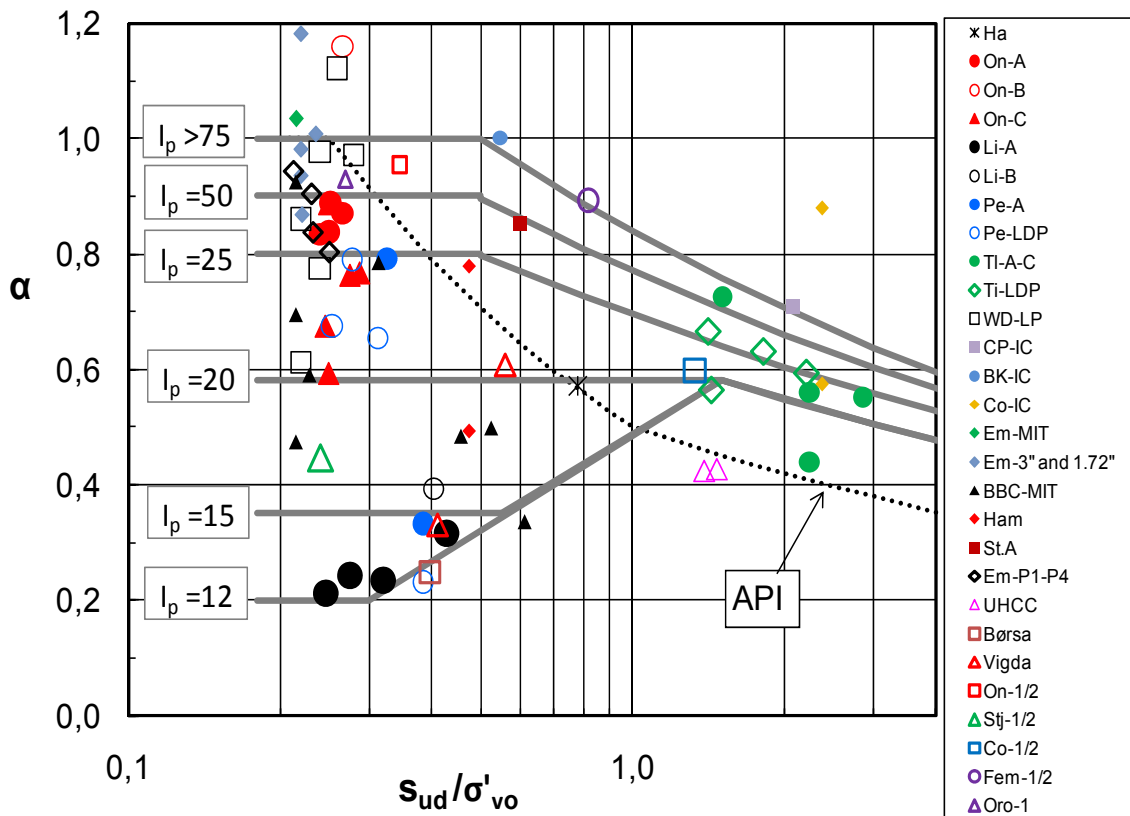
Figure 6.3.3 – Measured values of α in relation to normalized strength, all piles
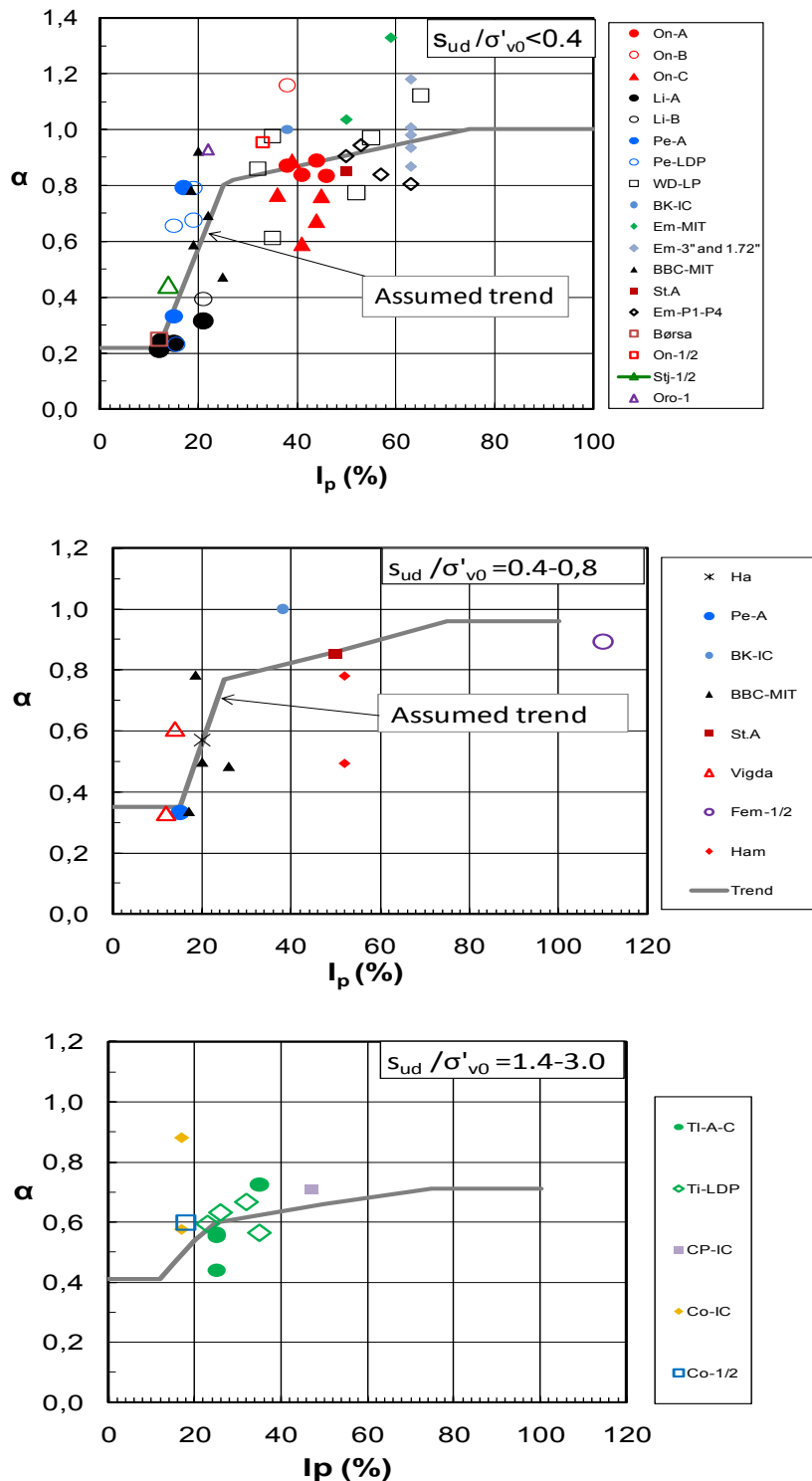
Figure 6.3.4 – Measured values of α in relation to plasticity index fro various ranges of s_{ud}/σ'_{v0}

To test out that the proposed trend lines were reasonably balanced, Figures 6.3.5 and 6.3.6 shows the ratio of Calculated/Measured values of α (hereafter called C/M ratio) in relation to s_{ud}/σ'_{v0} and I_p. As shown, there is reasonable balance of the C/M ratio in relation to both factors. It is apparent that the scatter in the data becomes larger when the plasticity index drops below about 20 %. This can also be seen from Figure 6.3.4. It implicitly means that low plastic clays in their nature are more variable in their basic behaviour than more plastic clays, and that the plasticity index can not capture all aspects that are important. Uncertainties in determination of plastic and liquid limits will also affect this scatter. As this is really "handwork", and depends to some

extent on judgement by the persons running the tests, an error of say 2 % could easily be made. For NC clays with $I_p < 25$ % it is an unfortunate fact of the data presented that only 2 % change in I_p will have a large impact on the ultimate shaft friction. For instance changing I_p from 12 to 14 % changes the α-value from 0.2 to 0.4, i.e. a doubling of the shaft friction.

As a further check on the scatter implied by the proposed correlations, the actual shaft friction was calculated for each pile with the proposed correlations and compared to the measured values. The outcome gave an overall mean C/M ratio of 1.04, and a standard deviation of 0.22, Table 6.3.1. A special note is made in relation to such determination of statistical averages. As shown in Table 6.3.1, when the ratio Measured/Calculated (M/C) is used in stead of the C/M ratio, the statistical average for that comes out at 1.035. Thus, the average M/C ratio is not just equal to the inverse of the average C/M ratio.
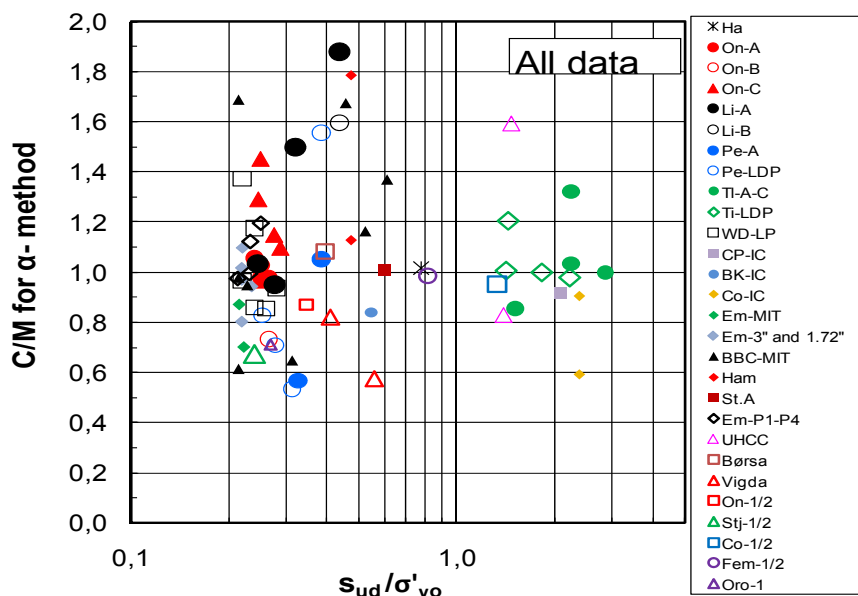
Figure 6.3.5 – Ratio of Calculated/Measured ultimate shaft friction versus s_{ud}/σ'_{v0} for proposed α-method
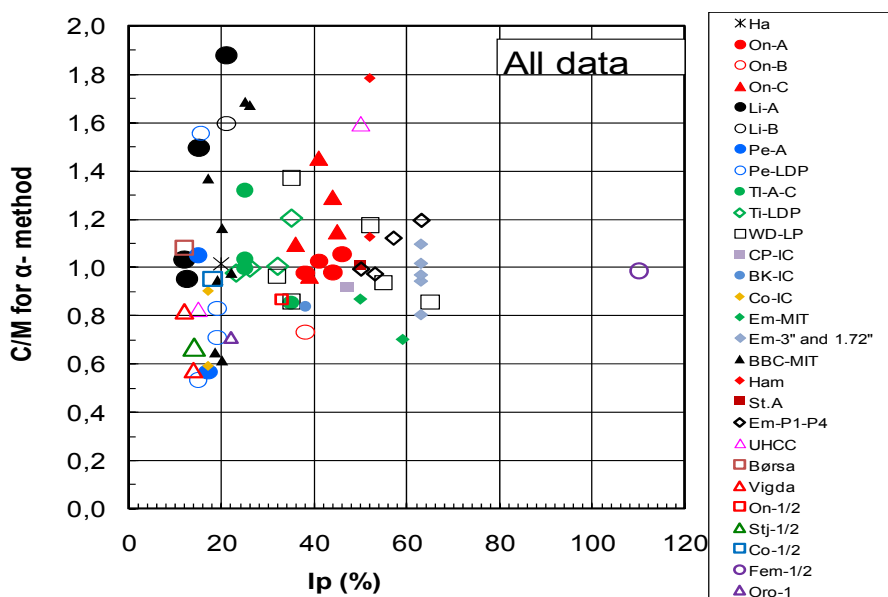
Figure 6.3.6 – Ratio of Calculated/Measured ultimate shaft friction versus I_p for proposed α-method

Table 6.3.1- Statistical average and standard deviation for C/M and M/C ratios for proposed α- and β-methods

	Calculated /Measured (C/M ratio)		Measured/Calculated (M/C ratio)	
	Average	Std. deviation	Average	Std. deviation
α-method	1.035	0.211	1.041	0.206
β-method	1.081	0.244	1.003	0.220

There is no clear evidence in the data in Figure 6.3.3 to 6.3.6 that open- versus closed-ended pile has any clear impact on the ultimate shaft friction. Where there are directly comparable data, like at Lierstranda, Onsøy, Tilbrook, Empire and Pentre, open piles sometimes show somewhat lower shaft friction than closed, in other cases it is the other way around. That there seems to be no clear difference between open- and closed-ended piles has also been concluded from several studies in the past, and is also reflected in essentially all current design procedures, ref. for instance the review in Section 6.2 and later discussion of other design methods.

Pile length, diameter, or stiffness of a pile has commonly been assumed to have some impact on the ultimate shaft friction, see for instance design methods reviewed in Section 6.2 and other methods reviewed subsequently. Length effects have been attributed to the following three factors:

1) Effects of pile flexibility and strain- softening (progressive failure) along the pile shaft
2) Effect of length of pile driven beyond a point in the ground. That may partly be considered as a "friction fatigue" aspect related to variations along the pile in soil and interface displacements and shear strains, as imposed by the pile installation. Such an effect should in principal be independent of the pile stiffness.
3) Pile "whipping" effects, i.e. lateral movements of the pile during the pile driving, which may tend to cause a permanent reduction of lateral stresses against the pile. "Whipping" effects may be most dominant near the ground surface where a pile normally is the least restrained laterally, but will also depend on the moment stiffness of the pile relative to the strength and lateral resistance of the surrounding clay.

The possible direct impact of pile flexibility and strain-softening on the total ultimate capacity will be discussed in Chapter 7 dealing with load-displacement response.

To try to see if any length effects were apparent from the data included in this study, Figure 6.3.7 presents the C/M ratio as function of normalized pile length L/D. This comes out balanced with no specific trend.

In Figure 6.3.8 the data have also been seen in relation to the normalized distance, h/r_0, from the pile tip, where h is the distance from the tip to where shaft friction is measured. The h/r_0 ratio is a direct element of the IC-96 and FBV-96 methods described later. For most piles the shaft friction was averaged over the full embedded pile length. In Figure 6.3.8 it is therefore only the WD-LP, On- C1 and Til-LDP piles that can give direct evidence of any such effect.

In Figure 6.3.8, the On-C1 pile can give an impression of some h/r_0 effect. But as discussed in Section 2.4 in relation to the Figure 2.4.23 showing the detailed Onsøy results, the relative low shaft friction along the middle part of On-C1 pile is believed to be mainly an effect of "whipping". The many threaded joints in pile C1 is believed to have significantly reduced its

lateral stiffness as compared to a pile without such joints. The fact that the non-instrumented On-C2 pile, of identical dimensions but without joints, showed the same average α-value as the On-A segment type piles, lends support to this argument. For this reason, the On-C1 pile was also given little weight when drawing the trend lines in Figures 6.3.3 and 6.3.4.
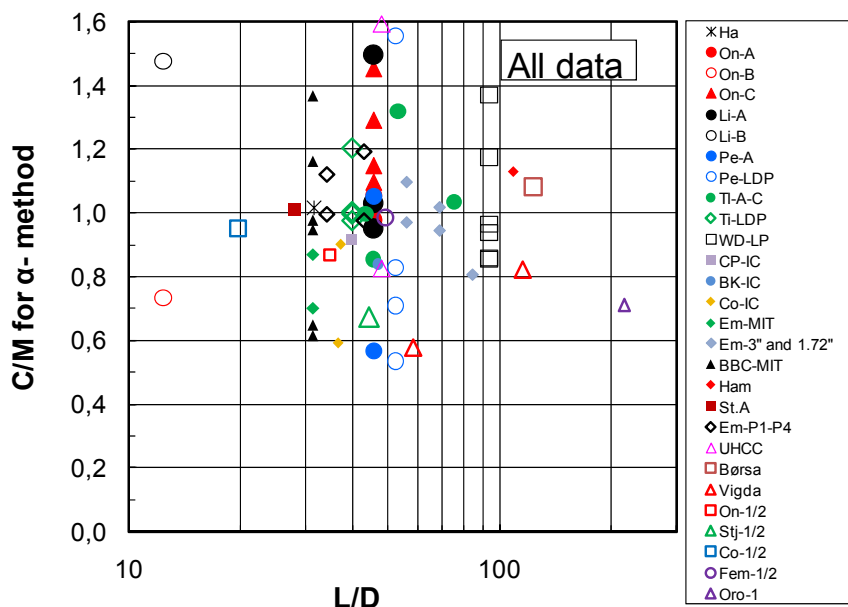
Figure 6.3.7 – Ratio of Calculated/Measured ultimate shaft friction versus L/D for proposed α-method
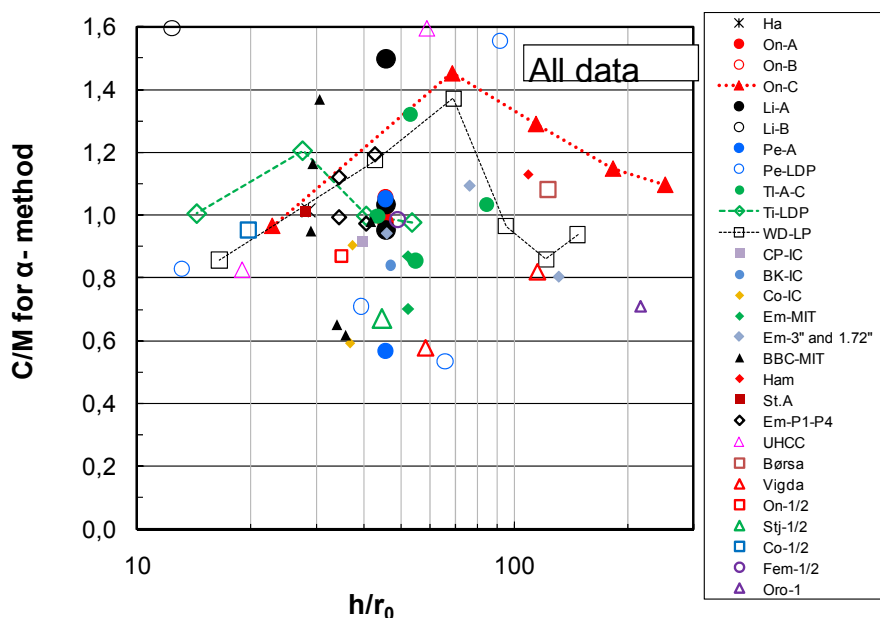
Figure 6.3.8 – Ratio of Calculated/Measured ultimate shaft friction versus h/r₀ for proposed α-method

Figure 2.3.24 showed that also for the WD-LP pile there is a minimum α-value near the middle part of the pile. In this case, that coincides with the level of minimum I_p. With the proposed α-correlations, Figure 6.3.8 shows that the variation in C/M ratio becomes less than the variation in α-values shown in Figure 2.3.24 for this pile. There still remains a clear tendency for relatively speaking lower shaft friction along the middle part of this pile. The WD-LP pile does not suggest

however, any clear h/r_0- effect, in which it would be expected that the shaft friction relatively speaking would decrease continuously with distance from the pile tip.

The Til-LDP pile data that were discussed in Section 2.7.3 and summarized in Figure 2.7.26-28, showed on a local level fairly large variation in measured ultimate shaft friction. That is most likely due to unreliable measurements. Figure 6.3.8 does not however, suggest any significant or clear h/r_0- effect for these piles.

Length effects are directly included in the design methods of Flaate and Selnes (1977) and Semple and Rigden (1984) reviewed in Section 6.1, and in the more recent methods proposed by Nowacki et al (1992), Kolk and van der Velde (1996) and Jardine et al (2005).

The Kolk and van der Velde (1996) method, here called FBV-96, is an α-approach similar to API-87, in which the α-value shall be calculated as:

$$\tau_{us} = \alpha \cdot s_u \qquad\qquad (6.3.1)$$
$$\alpha = 0.9 \cdot F_L \cdot (s_u / \sigma'_{v0})^{-0.3}$$
$$\alpha < 1.0$$
where
s_u = undrained shear strength from UU triaxial tests
σ'_{v0} = Vertical effective stress at depth z

$F_L = [(L - z) / D]^{-0.2}$ = length term

L = depth from the surface to the pile tip
z = depth from the surface to the point considered
D = outside diameter of pile

Jardine and Chow (1996) and Jardine et al (2005) have proposed an effective stress based method called IC-96, as follows:

$$\tau_{skin} = \sigma'_{rf} \cdot \tan \delta_f \qquad\qquad (6.3.2)$$

$$\sigma'_{rf} = 0.8 \cdot \sigma'_{rc}$$

$$\sigma'_{rc} = K_c \cdot \sigma'_{vo}$$

$$K_c = \{ 2.2 + 0.016 \cdot OCR - 0.87 \cdot \log_{10}(S_t) \} \cdot OCR^{0.42} \cdot F_L$$

σ'_{rf} = Radial effective stress against the pile wall at failure

δ_f = Pile/soil friction angle, depends upon I_p

σ'_{rc} = Radial effective stress against the pile wall after full consolidation

K_c = Radial effective earth pressure coefficient after full set-up

σ'_{vo} = In situ vertical stress

OCR= Apparent over-consolidation ratio (called YSR by the authors)

S_t = Clay sensitivity

$F_L = (h/r_0)^{-0.2}$, but with h/r_0 not lower than 8.0.

h = Distance from the layer considered to the pile tip= L-z

r_0 = Outer radius of the pile

Note that Jardine & Chow (1996) includes alternative expressions for K_c, based upon parameters to be determined from oedometer tests on re-constituted and intact clay, rather than direct use of the sensitivity S_t.

The above expressions (eq. 6.3.2), apply for piles driven closed-ended in clay. For open-ended piles, the radius r_o shall be replaced by R^*, calculated from:

$$R^* = (r_o^2 - r_i^2)^{0.5} \qquad\qquad (6.3.3)$$

Nowacki et al (1992) used some of the same data included herein, and concluded likewise that it was difficult to find strong evidence of length effects and what factors that may govern it. In their proposed slight modification (increase) to the API α-values, here called NGI-92 method, they suggested that some length effect may cautiously, and pragmatically, be accounted for by reducing local α-values by a length factor $F_L=0.5$ acting from the pile top to $z=15 \cdot D$ or $z = 0.25 \cdot L$, whichever is smallest. At large depths they suggested to use $F_L=1.0$.

A comparison has been made of the relative impact of length factors proposed by the methods discussed above. For this purpose it was assumed a pile with a diameter of 1.0 m and wall thickness of 20 mm, with pile length varying from 10 to 100 m. Figure 6.3.9 shows a direct comparison between how the length reduction factors vary locally along a 10 m and 100 m long pile according to the FBV-96 and IC-96 methods. Note that the absolute values are not directly comparable because the two methods also differ in other factors used for calculating the local shaft friction. A main difference between these two methods is the cut-off in F_L at h/r_o and $h/R^*= 8$ with the IC-96 method.
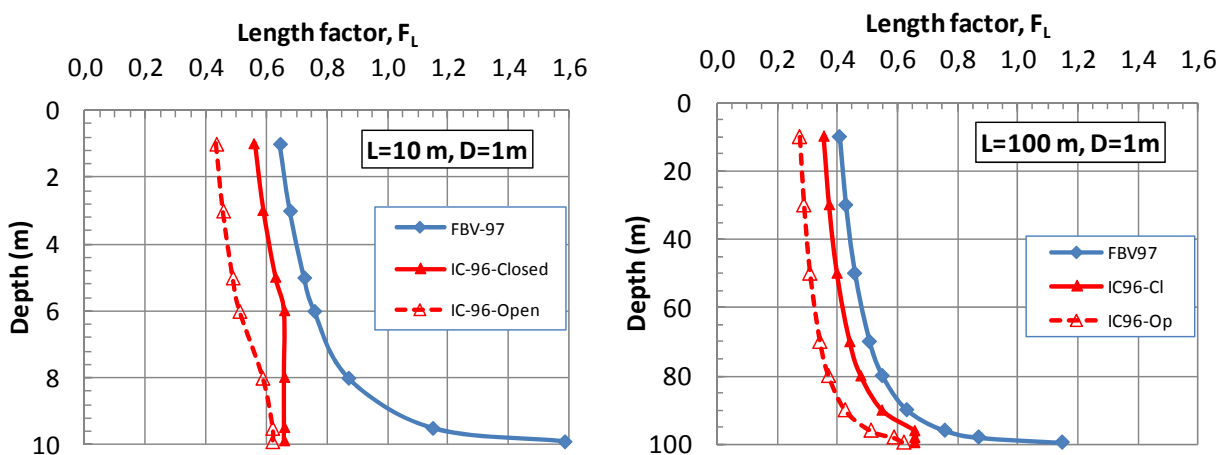
Figure 6.3.9 – Variation in local length factor with depth for piles of length 10m and 100 m according to the FBV-96 and IC-96 methods

To enable a more direct comparison between relative length effects, it is of more interest to compare the average operating length factor, F_{Lav}, along the entire length of a pile, and normalize that with respect to the average length factor computed for a 10 m long pile. The outcome of that is presented in Figure 6.3.10. It shows that for long piles, the length factor is quite significant, giving from 25 to 35 % reduction for a pile length of 100 m (except for the NGI-92 method which gives less).

It is difficult from the pile data Figure 6.3.7 and 6.3.8 to see any significant length effect. Karlsrud et al (2005) made the same observation when developing the NGI-05 method. It is on this basis concluded that length effects arising from length of pile driven is a secondary factor

compared to other prime factors (s_{ud}/σ'_{v0}, I_p) that impact on the local ultimate shaft friction. Thus, when using the α-correlation proposed in Figure 6.3.3 for computing the local ultimate shaft friction along a pile, length effects shall generally be disregarded. Possible effects of strain softening and pile flexibility when computing the total ultimate capacity of a pile may still have to be accounted for, as will be discussed in Chapter 7.
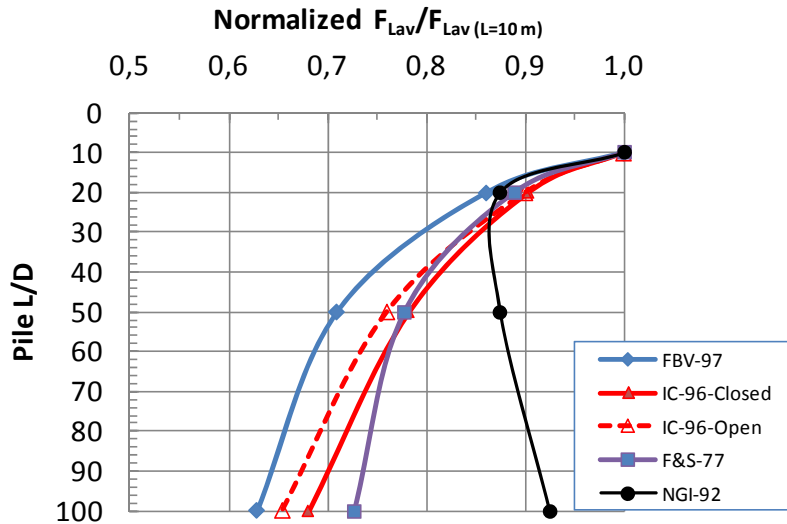
Figure 6.3.10 – Variation in normalized average length factors with depth according to different proposed design methods

Some comments may be given to possible reasons for the scatter in the measured α-values presented in Figure 6.3.3:

1. To some extent there will always be an element of variability and dependency of the ultimate shaft friction on the exact procedure for pile installation and testing that was followed in each case. Evidence of this has for instance been seen in some of the IC-model pile tests, where effect of jacking at different rates as well as driving was studied (e.g. Cannons Park tests described in Section 2.9.2; Bond and Jardine, 1995).
2. The behaviour of natural clays will always to some extent depend on its origin, depositional environment, mineralogy, fabric, geochemical characteristics etc. Thus, it can hardly be expected that the ultimate shaft friction will depend solely on three single parameters like undrained strength, vertical effective stress and plasticity index. This point can be illustrated by the fairly significant variability in normalized undrained strength determined by CAUC tests on very high quality block samples that was presented in Figure 2.5.6. Karlsrud and Hernandez (2011) have also shown that compressibility and stiffness parameters show similar variability.
3. There is, for some of the test sites included herein, fairly significant uncertainty in the actual selected values of undrained strength and in-situ vertical effective stress, OCR, and in some cases also in plasticity index. Given the very large impact of the plasticity index when it falls below about 25 %, small errors in measured I_p can, as was shown above, have a rather significant impact. There is also in some cases fairly large uncertainty in the actual measured ultimate shaft friction values.

6.3.2 Measured ultimate shaft friction related to in-situ vertical effective stress

The measured ultimate shaft friction has for all tests also been normalized with respect to the in-situ vertical effective stress as defined by $\beta = \tau_{us}/\sigma'_{v0}$. Mobilized β-values were first looked at in relation to the overconsolidation ratio and plasticity index of the clay, in the same manner as done in relation to α–values in the preceding section. Due to the inherent correlation between OCR and normalized undrained strength ratio as assumed herein (e.g. Figure 4.2.5), the β-values are indirectly influenced by the undrained strength, but not to the same extent as the α–values. Figure 6.3.11 presents all the data as log(β) versus log(OCR). The same data are shown in a semi-log plot in Figure 6.3.12. It should be no surprise that the plasticity index also in this case has an important impact on the mobilized β-values. Some trial and errors were made to arrive at a reasonably balanced fit of β in relation to both OCR and I_p. The end result is shown in Figures 6.3.11 and 6.3.12, and by the plots of C/M ratios in Figures 6.3.13 and 6.3.14.

As can be seen from the previous Table 6.3.1, the statistical average and standard deviation for the proposed β-correlations are slightly poorer than for the α-correlations. It is possible that further trial and errors could have narrowed the gap.

To see if, or to what extent-, there is any systematic bias between the two methods, the ratio of shaft friction values predicted with these proposed α- and β- methods was calculated. The results, presented in Figure 6.3.15, suggest no such systematic bias, neither in relation to OCR nor I_p.

As for the back-calculated α-values, there is no clear indication that the β-values depend on pile length and diameter, or that there is any difference between open-and closed-ended piles.
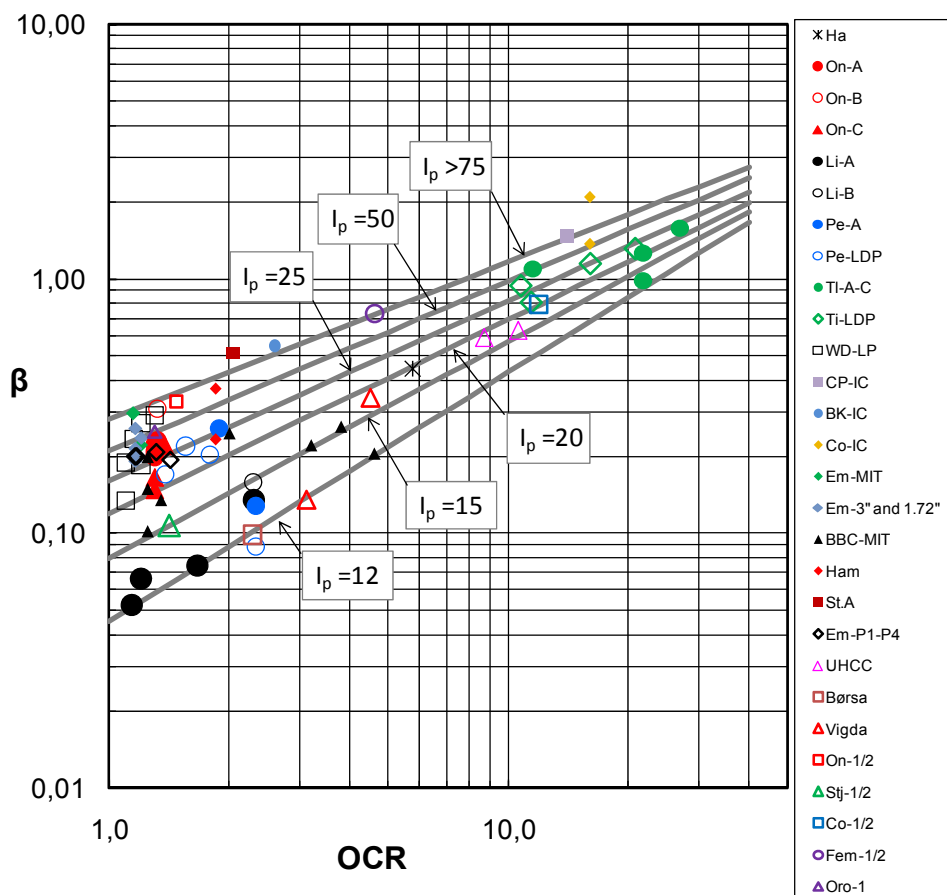
Figure 6.3.11 – Measured values of β in relation to OCR, double- log plot, all tests
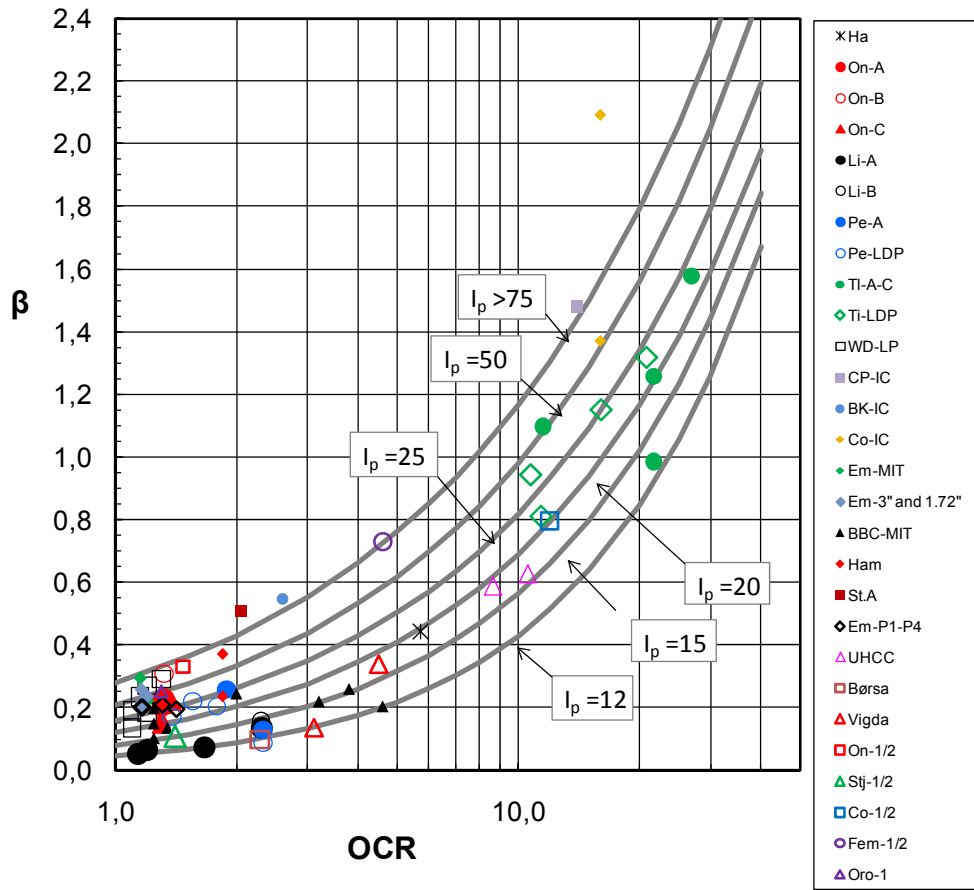
Figure 6.3.12 – Measured values of β in relation to OCR, semi- log plot, all tests
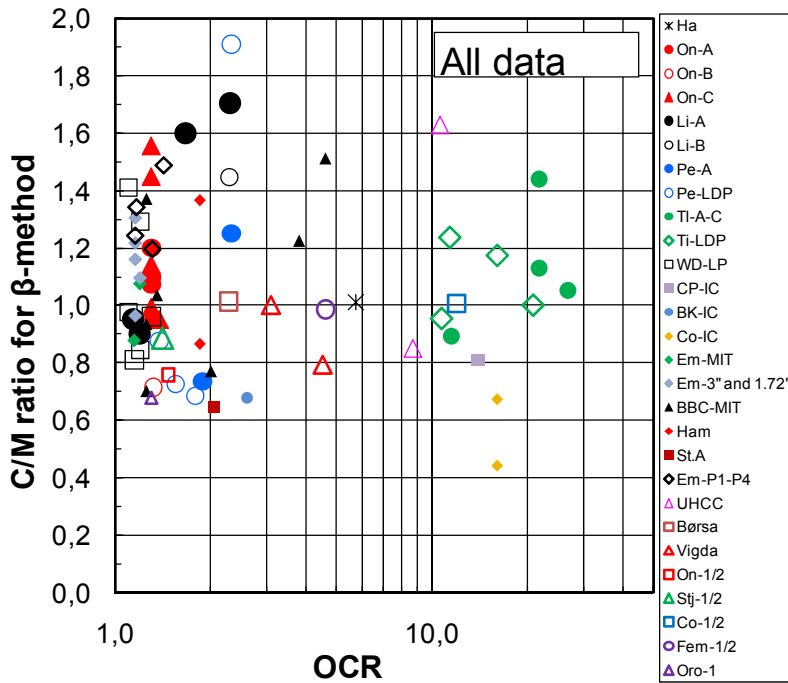
Figure 6.3.13 – Ratio of Calculated/Measured ultimate shaft friction versus OCR for proposed β-method
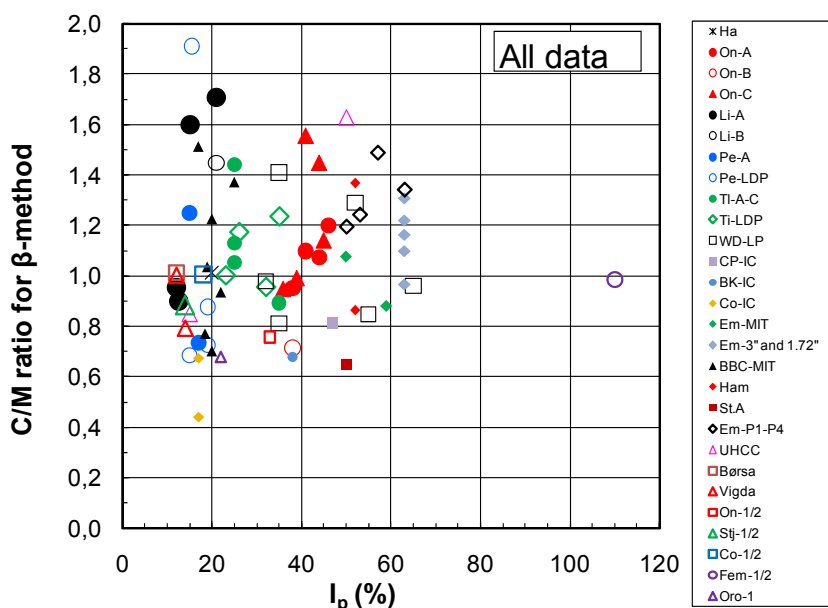
Figure 6.3.14 – Ratio of Calculated/Measured ultimate shaft friction versus I_p for proposed β-method
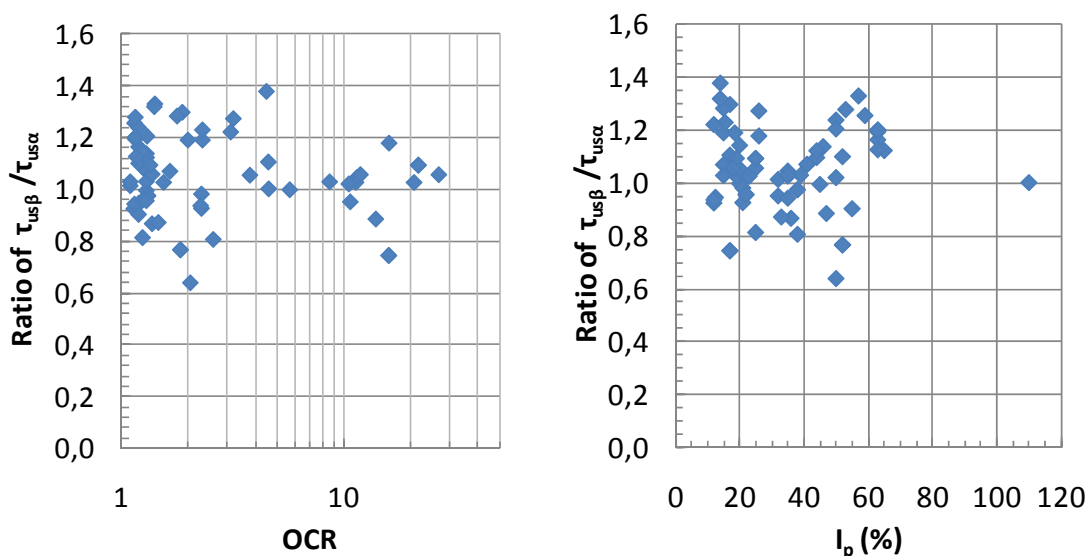
Figure 6.3.15 – Ratio of shaft friction calculated with proposed β- and α-methods in relation to OCR and I_p

As for the α-values, no previously proposed design method captures the observed low β-values for low plastic clays. Some examples of what earlier β-methods would lead to are still given in the following.

The Janbu (1976) approach gives β -values that in general are far too low and do not capture the impact of OCR.

For normally consolidated clays Burland (1973) suggest β-values, in the range 0.25 to 0.4. That covers the range of β-values in Figure 6.3.11 for clays with $I_p> 25$ %, but as stated earlier miss the lower values. At OCR = 10 the Burland approach, assuming $K=K_0$ and interface friction angle in the range 20 to 30^0, would typically lead to about β = 0.6 to 1.0, which would bracket data for $I_P= 15$ to 50 % in Figure 6.3.11.

The Flaate and Selnes (1977) method (eq. 6.2.7 and 6.2.8), starts off at β= 0.3 to 0.5 for OCR =1, but also include a length reduction factor. Figure 6.3.16 shows how this empirical method typically comes out for pile lengths in the range 20 to 80 m. As compared to the method proposed herein it appears to give a reasonable agreement for clays with plasticity index above 15- 20 %.
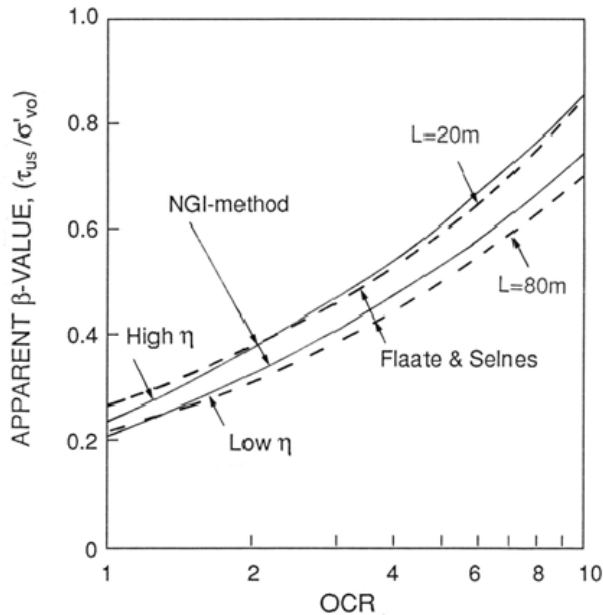
Figure 6.3.16 – Values of β vs OCR predicted with the Flaate and Selnes and NGI-90 methods (after Karlsrud and Nadim, 1990).

6.3.3 Measured ultimate shaft friction related to horizontal effective stress against pile shaft

Figure 6.3.17 presents measured ultimate shaft friction, τ_{us}, in relation to the measured horizontal (radial) effective stress, σ'_{hc}, at onset of pile loading. This is also based on the data presented in Appendix 2. Recall in this respect that for the shortest piles it is typical averaged values over the entire pile length that is given. For the longer piles values are averaged over lengths of 10-20 m. To facilitate identification of individual results the left side of diagram shows all tests over the full range of stresses, and the right side a blown-up view of the results that lie in the lower stress range.

The data shows, as one would expect, a clear correlation between ultimate shaft friction and measured horizontal effective stress against the pile surface, with most of the results falling in the range $\tau_{us}= (0.2-0.4)\cdot\sigma'_{hc}$. The data points that lie particularly high are those for the Pentre test site. This may partly be due to the high permeability and drained loading conditions in these tests, and partly due to too low measured effective stresses, ref. discussion in Section 2.6.3.

As stated in Chapter 4 and 5, as well as in Sections 2.4, 2.5 and 2.6, it is possible that the earth pressure gauges on the NGI-A type piles have generally given too low values. That may consequently explain why the data for the Onsøy and Lierstranda piles tend to lie on the high side in Figure 6.3.17.
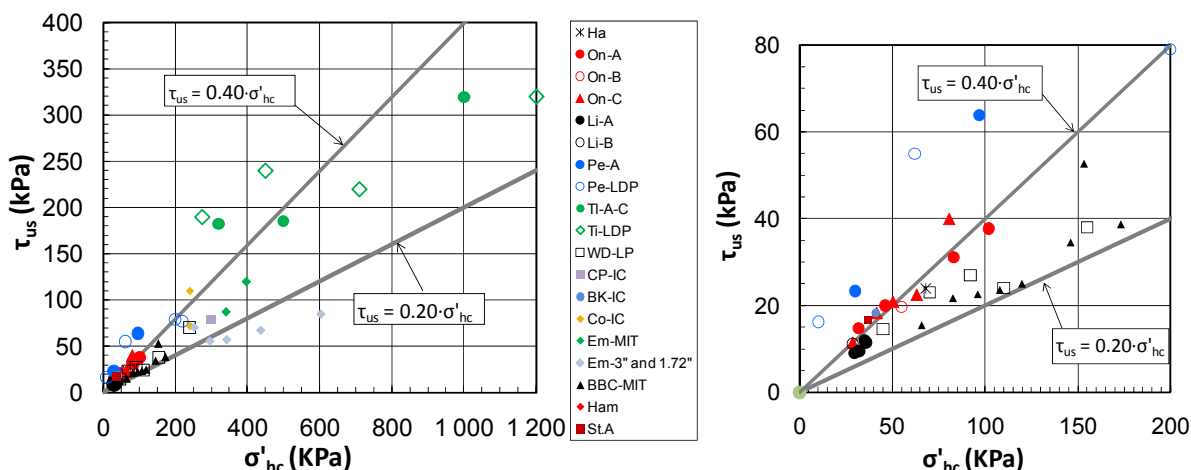
Figure 6.3.17 – Measured ultimate shaft friction versus measured radial effective stress at onset of pile loading- instrumented tests

To explore further possible correlations, Figure 6.3.18 presents the normalized ratio of τ_{us}/σ'_{hc} against OCR and I_p. It seems in this case that OCR and I_p has little impact, which is in strong contrast to the large impact on the α- and β-values (ref. Sections 6.3.1 and 6.3.2). This suggests that the impact of OCR and I_p on the ultimate shaft friction is mainly coming through its impact on the horizontal effective stress, σ'_{hc}, which as was shown in Figures 5.2.8 to 5.2.10 is quite significant.

It can in principle be a viable alternative approach for predicting the ultimate shaft friction by combining the K_c data in Figures 5.2.8 to 5.2.10 with the normalized shaft friction values in Figure 6.3.18. The measured K_c values are however, associated with rather significant uncertainties. It would therefore, be difficult to establish a sufficiently reliable correlation between for instance K_c, OCR and I_p. Considering also the spread in the normalized ultimate shaft friction values in Figure 6.3.18, such an approach would no doubt lead to much more uncertainty (larger standard deviation) than for the more direct α- and β-methods proposed by the author in Section 6.3.1 and 6.3.2.
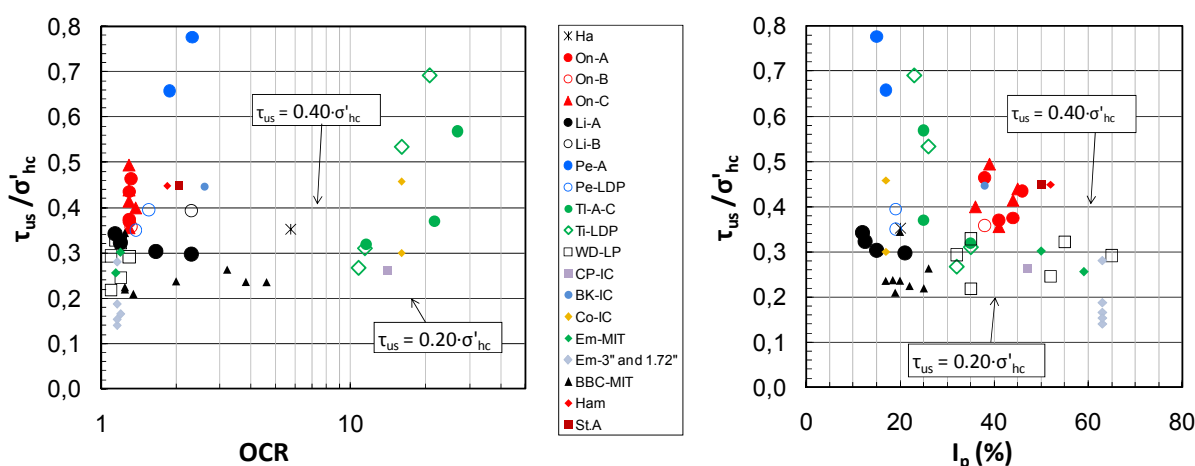
Figure 6.3.18 – Measured ultimate shaft friction normalized with respect to measured horizontal effective stress at onset of pile loading seen in relation to OCR and I_p

A further complicating factor is that from a theoretical point of view the undrained failure of a soil element close to the pile wall should depend on the complete state of effective stress at onset of pile loading, and not only the horizontal effective stress. In addition, the large shear strains

and subsequent volume changes caused by the pile installation will in general have a significant impact on the undrained stress-strain response of a clay, reference for instance earlier discussion in Section 2.2 dealing with the Haga results.

Karlsrud (1986) developed a tentative method for predicting the ultimate shaft friction which tries to tie the complete state of effective stress against the pile surface at onset of pile loading to the undrained strength determined in DSS tests on completely remoulded and re-consolidated clay. The method, later called the NGI-90 method, has also been presented by Karlsrud and Nadim (1990) and Karlsrud et al (1992). Just a brief description and some implications of the method are presented in the following.

The NGI-90 method assumes that the ultimate shaft friction is partly governed by the undrained DSS type strength of the completely remoulded and re-consolidated (RR) clay, and that is proportional to the horizontal effective stress, σ'_{hc}, at onset of pile loading through the expression:

$$\tau_{us} = \xi \cdot (\tau_f^{RR}/ \sigma'_{ac}) \cdot \sigma'_{hc} \qquad \text{, where} \qquad (6.3.4)$$

τ_f^{RR} = undrained DSS strength of the remoulded-reconsolidated (RR) clay

σ'_{ac} = axial consolidation stress applied to the RR clay in the DSS test

ξ = factor that corrects for differences in the complete state of effective stress for a soil element next to the pile wall, and a soil element in the DSS apparatus.

σ'_{hc} = horizontal (radial) effective stress against the pile surface at onset of pile loading

A fairly large number of DSS tests have been carried out at NGI on RR clay on a variety of different clays, including the Haga, West Delta, Onsøy, Lierstranda and Pentre clays, as well as a number of clays from different offshore areas. Even for rather stiff and high OCR clays, the strength was found to be essentially proportional to the axial consolidation stress, σ'_{ac}, that the samples were consolidated under in the DSS apparatus. Figure 6.3.19 summarizes the normalized strength data for the different clays tested. Some clays, (low-plastic in particular), showed a fairly strong tendency for dilation at large strain. Figure 6.3.19 therefore shows for all tests two points:

a) The filled black symbol, representing what was defined as failure, τ_f, when the effective stress paths really started to show strong dilation, climbing up the Mohr-Coulomb failure line. This was as a minimum taken as 6 % shear strain.
b) The open red symbols representing the shear stress τ_{max}, which was either taken as when a peak was reached or when the shear strain reached 15 %.

The data shows some tendency for the normalized strengths to increase with OCR of the intact clay. Apart from the τ_{max} values for low plastic clays, the plasticity index seems not to have any significant impact on the normalized srengths.
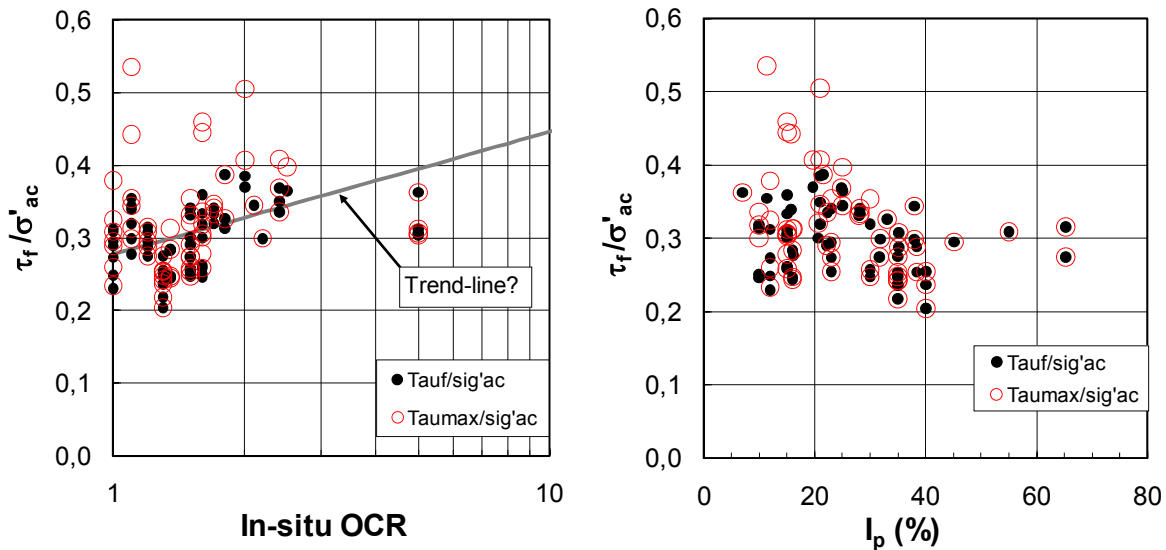
Figure 6.3.19 – Normalized undrained DSS strength of completely remoulded and re-consolidated (RR) clay (based on Karlsrud and Nadim, 1990 and NGI files)

To explain further the background for the factor ξ in eq. (6.3.4), it is a main assumption that the undrained simple shear strength of completely remoulded and re-consolidated (RR) clay is proportional to the mean effective stress under which it is consolidated. This was shown by Karlsrud (1986) to be the case for the general soil model proposed by Matsuoka et al (1986), and is also the case for the MIT-E1-E3 clay models, e.g. Whittle (1987). In the DSS apparatus this mean effective stress is given by:

$$\sigma'_{mcDSS} = (1+2K_{rc}) \cdot \sigma'_{ac} / 3 \qquad \text{, where} \qquad (6.3.5)$$

K_{rc} = radial effective stress ratio achieved in the DSS test, assumed to correspond to K_0 for normally consolidated clay, here called K_{0NC}

Referring to Figure 6.3.20, for a soil element along the pile surface, the mean effective stress is given by:

$$\sigma'_{mcPile} = (\sigma'_{vc} + \cdot\sigma'_{hc} + \sigma'_{\theta c}) / 3 \qquad (6.3.6)$$

Thus the factor ξ is given by the ratio:

$$\xi = \sigma'_{mcPile} / \sigma'_{mcDSS} = (\sigma'_{vc} + \sigma'_{hc} + \sigma'_{\theta c}) / (1+2K_{oNC}) \cdot \sigma'_{ac}$$

Only σ'_{hc} is established from the pile tests, the other stresses are not fully known. Karlsrud (1986) suggested originally that it may be reasonable to assume that σ'_{vc} is approximately equal to σ'_{v0}, and that $\sigma'_{\theta c}$ may be estimated to be close to $K_{0NC}\cdot\sigma'_{hc}$. Based on that assumption the factor ξ becomes:

$$\xi = (1+1/K_c+K_{0NC})/(1+2 K_{0NC}) \qquad (6.3.7)$$
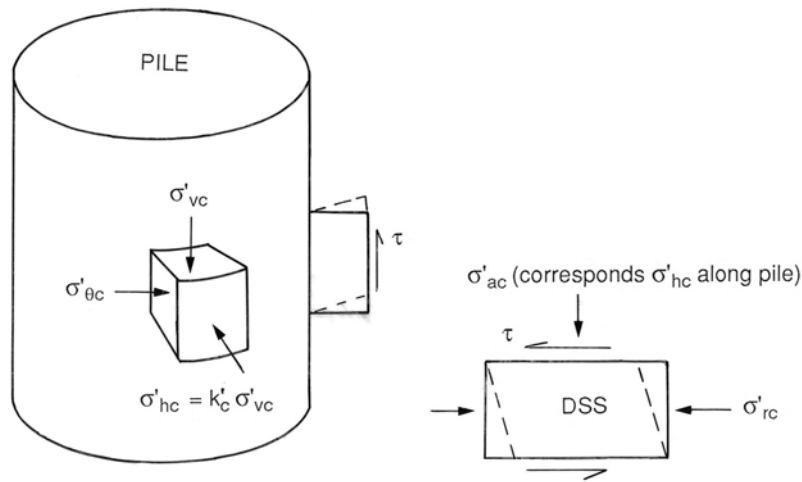
Figure 6.3.20 – Stress conditions around a pile compared to that in DSS test (after Karlsrud and Nadim, 1990)

The above assumes that failure takes place at the pile/soil surface. It is therefore, necessary to check if failure could occur in the clay at some distance outside the pile surface, and lead to lower capacity. Assessments and example analyses presented in a report by NGI (1989) concluded that assuming failure to occur within the RR zone would maximum over predict the shaft friction by 10-20 %. That was based on a fairly simple assumption on how the strength may vary from the RR-zone, through the "Disturbed zone" to Intact clay (ref. Illustration in Figure 2.2.20). Based on the assumed strength variation it was also shown that failure was likely to take place within the RR-zone very close to the pile wall if OCR<4, and in the "Disturbed zone" if OCR>4. That was found to agree with the observations made when trenching next to one of the Haga test piles (ref. Section 2.2 and Figure 2.2.17). It is also a general observation at all sites with low OCR clays where piles have been pulled out after testing, that a layer of clay that may be up to a few cm thick sticks to the pile surface. This was for instance the case at Lierstranda, Onsøy, Wets Delta, BBC and Empire test sites.

Maybe the weakest element of the NGI-90 method is that it depends on empirical data on measured Kc-values. As was shown in Chapter 5 (Figure 5.2.9) the available data shows considerable scatter, partly due to questionable reliability of some of the data. Furthermore, there could also be significant uncertainties in relation to actual values of σ'_{vc} and $\sigma'_{\theta c}$. In this respect, the results of analyses with the SPM-MITE3 model presented in Figure 5.1.19 and 5.1.11 suggest that it may be reasonable to assume that $\sigma'_{\theta c} \approx 0.5 \cdot \sigma'_{hc}$. Especially for low OCR clay it seems however, like σ'_{vc} can become considerably smaller than σ'_{v0}. In the example for OCR=1.0 in Figure 5.1.9, the vertical effective stress is as low as $\sigma'_{vc} = 0.4 \cdot \sigma'_{v0}$. All other factors being the same, this would reduce the shaft friction by about 30 % according to the NGI-90 method.

The NGI-90 method has been attempted applied to the rather extreme case of the Lierstranda A9 pile. By using the DSS strength of RR clay of $\tau_f^{RR}/\sigma'_{ac} = 0.26$ as measured for this clay, using the measured $\sigma'_{hc} = 0.2 \cdot \sigma'_{v0}$, assuming $\sigma'_{\theta c} = 0.5 \cdot \sigma'_{hc}$ and $\sigma'_{vc} = 0.4 \cdot \sigma'_{v0}$ (as per MIT-E3 prediction), and finally taking $K_{0NC} = 0.5$, the ultimate shaft friction becomes:

$$\tau_{us} = 0.26 \cdot \sigma'_{v0} \cdot (0.2+0.1+0.4)/(1+2 \cdot 0.5) = 0.09 \cdot \sigma'_{v0}$$

For comparison, the measured value was $\tau_{us} = 0.07 \cdot \sigma'_{v0}$. Thus, the NGI-90 method seems to give a very plausible explanation for the extremely low shaft friction observed for the deepest Lierstranda piles located within the very silty clay layer. For the low-plastic clays, both the "cylindrical arching" effect as well as "vertical silo-like" effects set up during the re-consolidation phase could probably make the vertical effective stress even somewhat lower than predicted with the MIT-E3 model.

A similar calculation for a typical Onsøy pile (A3), gives:

$$\tau_{us} = 0.24 \cdot \sigma'_{v0} \cdot (0.62+0.31+0.4)/(1+2 \cdot 0.5) = 0.16 \cdot \sigma'_{v0}$$

In that case the measured value was somewhat higher and given by $\tau_{us} = 0.21 \cdot \sigma'_{v0}$. That could be explained by slightly larger vertical or circumferential effective stress than assumed with the NGI-90 method.

The NGI-90 method, as outlined above, probably captures some of the main elements impacting the ultimate shaft friction for undrained loading conditions. Given its dependency on the complete state of effective stress surrounding a pile, which is still considered associated with significant uncertainties, the author is reluctant to recommend NGI-90 as a primary approach. It is still considered a useful method to check against the new α- and β-methods proposed in Section 6.3.1 and 6.3.2.

The IC-96 method presented in Section 6.3.3 (eq. 6.3.2), makes the basic assumption that the ultimate shaft friction is mainly governed by the interface friction angle of re-constituted clay as determined by ring shear tests, and the horizontal (radial) effective stress acting against the pile surface at failure. As seen from eq. (6.3.2), it is further assumed that the horizontal effective stress at failure is 20 % lower than the effective stress at onset of pile loading. This is due to possible generation of excess pore pressures, or reduction in total horizontal stress, during pile loading.

It is very plausible that for some high-plastic and over-consolidated clays, the pile installation may cause formation of slickensides and a reduced effective friction angle compared to the peak value determined by for instance CAUC traxial tests on undisturbed intact clay. Figure 6.3.21 and 6.3.22 show data on peak and ultimate friction angle from ring shear tests presented by Jardine et al (2005). The data show large scatter, and the authors therefore also state that application of the method strictly requires site specific ring-shear tests.

No attempt has been made herein to try to apply the IC-96 method to the pile data base included in this study. The author would still like to express some views regarding the general applicability and reliability of the IC-96 method, as seen in the light of the results of the pile tests included in this study:

1. The IC-96 method relies on a semi- empirical correlation between radial effective stress against the pile shaft at failure and the peak and residual interface friction angle. Whereas this may appear conceptually correct and reasonable, the assumption that only the radial effective stress, and not the complete state of effective stress against the pile shaft is accounted for, is questioned.

2. The method relies on a purely empirical procedure to establish the radial effective stress at failure. The data included in this study suggests that such correlations are presently associated with significant uncertainty.

3. In the guidelines for the method (Jardine et al, 2005) it is stated that the interface friction angle should be taken somewhere *between* peak and ultimate value from ring shear tests, but these can vary within wide limits, and criteria for what *between* shall imply are not given.

4. The method is not at all able to capture the low ultimate shaft friction observed for low-plastic clays. In this connection it can be mentioned that Ridgeway and Jardine (2007) presented results of ring-shear tests on the Lierstranda clay undertaken at Imperial College. Those tests showed a peak and residual interface effective friction angle that was quite compareable to what comes out of triaxial tests (typically $\varphi = 30^0$). Thus, Ridgeway and Jardine (2007) also concluded that the very low shaft friction observed at Lierstranda could not be explained by low interface friction. They speculated on the other hand, that for some unknown reasons, the pile installation method could have had a special impact on the Lierstranda results. The Lierstarnda piles were however, driven into the ground in a normal manner. Ridgeway and Jardine (2007) also questioned if installation and emptying of the casings at Lierstranda could have adversely affected the shaft capacity. This can hardly be the case as emptying was done in a slurry-filled casing. In any case the effect cannot extend deep below the casing. Furthermore, the Lierstranda case is not a stand- alone case. Similar low shaft friction has been observed in several other cases included in this study (i.e. Stjørdal, Vigda, Børsa and Pentre).

5. The method includes a significant length effect (e.g. Figure 6.3.9-10) which is not found to be supported by the data included in this study.
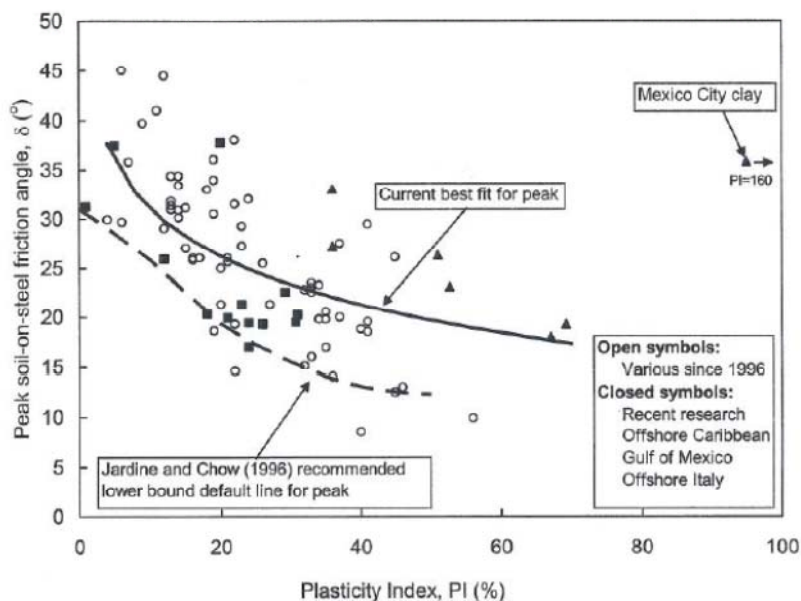

Figure 6.3.21 – Peak interface friction angle from ring-shear test (after Jardine et al, 2005)
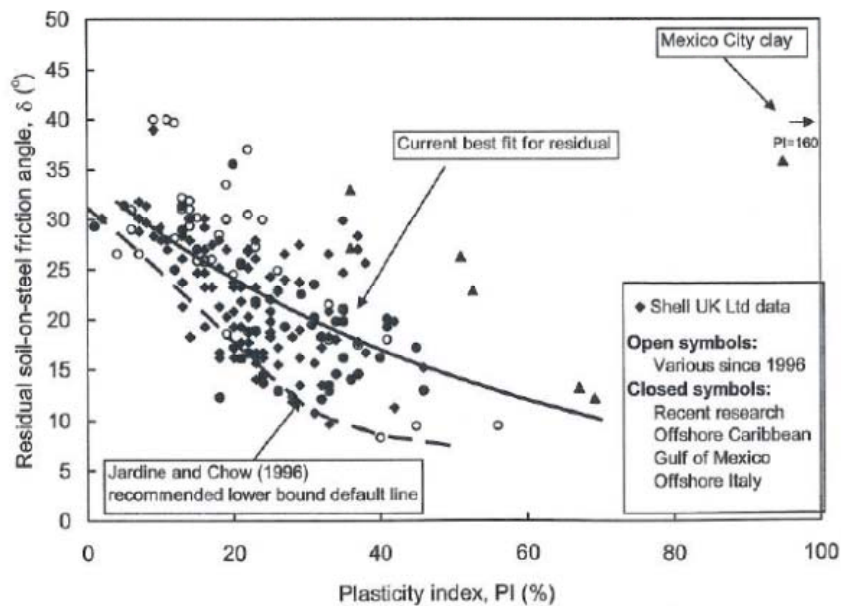
Figure 6.3.22 – Ultimate (residual) interface friction angle from ring-shear test (after Jardine et al, 2005)

The SPM-MITE3 numerical FEM approach has been shown to give a fair picture of the effective stress against the pile surface and also gives a reasonable picture of the ultimate shaft friction for moderately over-consolidated plastic clays. The actual β-values predicted for BBC clay increase from about 0.20 for OCR=1 to 0.40 for OCR=4.0 (e.g. Whittle, 1987, 1990). That lies reasonably well within the range of what is measured for medium plastic clays, Figure 6.3.12.

So far the SPM-MITE3 model has not been shown to enable prediction of such low shaft friction that has been observed in low-plastic clays. The general approach is considered sound, but the soil model needs to be improved to fully capture the true impact of the large shear strains, volume changes and stress changes caused by the pile installation and re-consolidation phase on the stress- strain-and strength characteristics of clays. As discussed in Chapter 5, it may for that purpose be a more convenient approach to establish different soil models for the different zones around the pile. It should also be considered to use true 3-D axis-symmetric models to capture possible "silo type" effects on the vertical stress conditions close to the pile shaft. This may, in addition to the "circumferential" arching effect that is so apparent for low-plastic clays, contribute to very low mean effective stress level close to the pile shaft in such cases.

6.4 Effect of time on the ultimate shaft friction

6.4.1 Factors contributing to gain in shaft friction with time
The shaft friction along a pile can after pile installation be influenced by time through the following processes:

1. A gain in strength due to thixotropy, which means a strength increase under constant volume and effective stress. This can be considered as a pure geochemical effect. Andresen and Jostad (2002) summarized some data from normally consolidated clays. Compared to the strength immediately after remoulding, the strength increased to 1.5 to 2.5 times the remoulded strength in about 100 days. Most of this increase occurred within the first few days after remoulding. The increase was most pronounced for clays with

plasticity index above 35-40 %. Little seems to be known about stiff overconsolidated clays in relation to thixotropy effects.

2. A gain in strength as a result of dissipation of excess pore pressures and gain in effective stress. This issue will be dealt with further in the following Section 6.4.2.

3. After all excess pore pressures set up during pile installation are dissipated, there is ample evidence that the ultimate shaft friction can continue to increase with time. An example of this was shown by the Haga pile tests in Section 2.2.3 (Figure 2.2.35). This is often referred to as ageing effects, and will be discussed further in Section 6.4.3.

4. Subjecting a pile to multiple loading to failure at different time intervals following pile installation, will often further enhance the ultimate shaft friction. This was also clearly demonstrated by the Haga tests in Figure 2.2.35. As time effects have often been inferred from repeated testing of the same pile, such testing can therefore lead to quite erroneous conclusions as to time effects. This issue will not be dealt with further herein, because a pile in real situations would never intentionally be loaded repeatedly to failure.

6.4.2 Set-up during the re-consolidation phase

For low to moderately overconsolidated clays it may be a reasonable assumption to assume that the ultimate shaft friction builds up in relation to the build up of horizontal (radial) effective stress against the pile shaft. The thixotropy effect may run more or less in parallel with that process, but is difficult to distinguish from it.

Most data for low OCR sites presented in Chapter 2 suggest that the horizontal effective stress against the pile wall first starts to increase after the degree of consolidation (pore pressure dissipation) has surpassed 30-50 %. The main exception is the data from PLS measurements in BBC (Section 2.10.3), where the effective stress build-up started at U=17 %.

The West Delta data in Figure 2.3.16, and other results of 3"- and x-probe tests summarized by Bogard and Matlock (2011), confirms that the increase in shaft friction with time after pile installation closely follows the degree of consolidation and relative build-up of horizontal effective stress against the pile surface. For normally and moderately overconsolidated clays the author proposes on this basis that the ultimate shaft friction develops with degree of consolidation as shown in Figure 6.4.1. It starts off with a shaft friction corresponding to the fully remoulded strength of the clay (just assumed to correspond to 30 % of the final value in Figure 6.4.1), and is constant until the degree of consolidation typically exceeds 40 %. From that point on, the shaft friction is assumed to increase linearly with the degree of consolidation until U= 100%.

This may be considered as a conservative approach, as thixotropy may also contribute to some increase during early stages of the re-consolidation process. It is however, hard to see from the limited available data (e.g. Figure 2.3.16 from West Delta tests) that there is any clear gain in shaft friction during the early phases of the re-consolidation process.

For very stiff and high OCR clays there exists little direct evidence on how the capacity depends on the degree of consolidation. For high OCR clays with water content close to or below the plastic limit, it is also difficult to define and determine a remoulded strength of the material. There have been suggestions in the literature that the capacity in high OCR clays can decrease during the initial phases of the reconsolidation process due to negative or very low excess pore

pressures at the pile surface at the end of installation, followed by first increase then decrease in pore pressure. This was for instance suggested by Lehane and Jardine (1993) on basis of the IC pile tests at Cowden. It is therefore for stiff and high OCR clays difficult to give very precise and well founded recommendations. A tentative approach is to assume that the shaft friction may typically be 80 % of the final capacity immediately after installation (U=0), and increase linearly from that point with the degree of consolidation as illustrated in Figure 6.4.1. But more data from testing different piles at different times after pile installation are really needed to get a better handle on hoe the capacity build up with time in very stiff and high OCR clays.
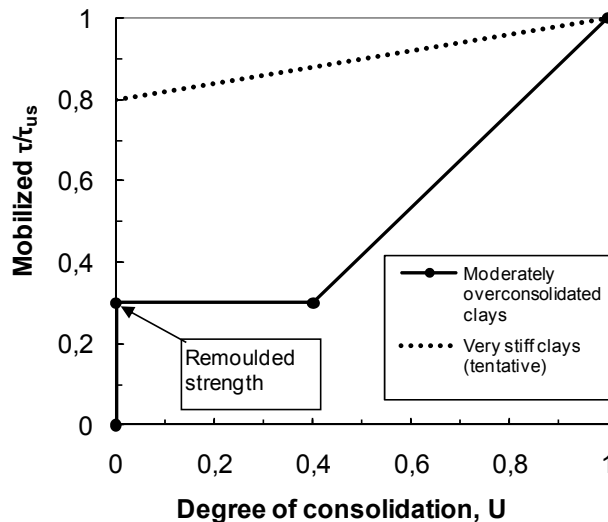
Figure 6.4.1 – Proposed build-up of shaft friction during the re-consolidation phase

A very important effect of the proposed procedure for predicting the degree of consolidation and set-up of the pile capacity is that it gives very much larger times for full set-up for a closed-ended pile than for an open-ended pile. Furthermore, it is worth noticing that the time for re-consolidation and set-up is proportional to the square of the pile diameter. This can have very important implications for design of pile foundation for offshore structures, which commonly makes use of piles with diameter around 2-2.5 m.

As an illustration, Table 6.4.1 presents the times to reach 50 and 90 % consolidation for a 2 m diameter pile with wall thickness of 50 mm installed in lightly overconsolidated medium plastic clay. The clay is assumed to have a permeability $k_0 = 0.5 \cdot 10^{-9}$ m/s, modulus $G_{50}/s_{ud} = 250$, modulus number $m_0 = 10$ and preconsolidation pressure $p'_c = 500$ kPa. The results show that it takes about 10 times longer time to reach t_{50} and t_{90} for a pile that is closed-ended or plugs during installation than for a pile that penetrates open-ended. For the plugged pile it takes more than 4 years for t_{90} to be reached. It will therefore have important design and safety implications if such a pile should unintentionally plug during driving. For all piles that are designed to penetrate without plugging it is therefore very important to verify that such is the case in reality.

Table 6.4.1 – Example of calculated consolidation times for open-and closed ended pile with diameter of 2 m and wall thickness of 50 mm installed in a medium plastic clay deposit

Pile	$\lambda = r_p/r_0$	T_{50}	T_{90}	t_{50} (days)	t_{90} (days)
Open-ended	15.8	1.77	20.5	18	169
Closed-ended	4.9	21.8	195	221	1600 (4.4 yrs)

6.4.3 Effect of ageing and previous loading history

The increase in pile capacity after the end of the re-consolidation phase may be due to enhanced chemical bonding between clay platelets (i.e. a geochemical effect) and/or further increase in total and effective stresses due to creep effects. The latter explanation may be most relevant for low plastic and low OCR clays, where the radial effective stresses have been found to be considerably lower than the in-situ effective stresses (e.g. Figure 5.2.9). Partly based on the work by Augustesen (2006), Clausen and Aas (2000) proposed that this time effect could tentatively be accounted for by use of the following expression:

$$Q(t) = Q(100) \cdot [1 + \Delta10 \cdot \log_{10}(t/100)] \qquad \text{, where} \qquad (6.4.1)$$

$$\Delta10 = 0.1 + 0.4 \cdot (1 - I_p / 50) \cdot OCR^{-0.8}$$

t= time in days after pile installation in days

Q(100)= capacity of the pile after 100 days or complete re-consolidation

Q(t) = capacity at a later time

This procedure is also considered to be a part of the NGI-05 method proposed by Karlsrud et al (2005). Figure 6.4.2 shows examples of how the pile capacity will increase relative to end of re-consolidation (assumed 3 months) for piles installed in a caly with oCR01.3.. It illustrates that an important implication of this proposed ageing factor is that the capacity will increase much more with time in low-plastic clays than in clays with high plasticity.

Confirmation of such ageing effects was a main motivation for the ongoing field testing program at NGI "Time effects piles" referred to in Chapters 1 and 3. Although the test results are still confidential, it can be disclosed that the plasticity index indeed has been confirmed to have a major impact on the ageing factor. Thus, after some years, the extremely low shaft friction observed in low-plastic clays will to some extent heal itself.
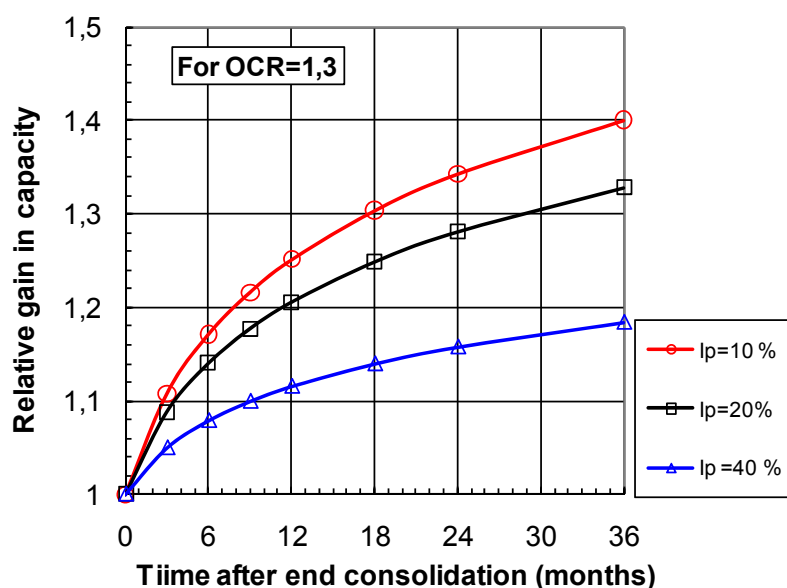

Figure 6.4.2 – Example of calculated increase in pile capacity following end of consolidation (here assumed 3 months) based on the procedure in Karlsrud et al (2005)

6.5 Recommended design approach and needs for improvement

Based on the load test results collected, reviewed and assessed as part of this study, the author has proposed a new α-method. The α-values are to be determined on the basis of the normalized undrained undisturbed strength, s_{ud}/σ'_{vo}, derived from DSS-CCV tests, and the plasticity index, I_p, of the clay. The proposed procedure may be regarded as a modified and improved version of the NGI-05 method proposed by Karlsrud et al (2005). Through the use of a normalized undrained strength it also partly follows the ideas behind the current API (2007) procedure.

The undisturbed s_{ud} strength was chosen as reference strength because it is the most relevant mode of shearing for a soil element close to the pile surface. It should ideally be determined from DSS-CCV tests on high quality piston samples, but can also be reasonable well assessed on the basis of CAUC triaxial tests and empirical correlations between the s_{ud} and s_{uc} strengths based on data presented by Karlsrud and Hernandez (2011). The s_{uc} strength can also with reasonable confidence be determined from CPTU tests using the correlations proposed by Karlsrud et al (2005) and which has also been used to assess the strength at several of the test sites dealt with in this study.

The choice of a "true" in-situ undisturbed s_{ud} strength as reference strength is also considered to represent an improvement over earlier α-methods , as it limits the impact of sample disturbance, and better reflects the impact of in-situ stresses and stress history on the undrained strength than simpler tests like UU, UC and fallcone tests.

A new and alternative β-method is also proposed by the author, where β is correlated against OCR and I_p. This approach is found to give nearly as good correlations to observed ultimate shaft friction as the proposed α-method. As OCR and the s_{ud}/σ'_{vo} ratio are closely correlated, this method also can be regarded as being tied to the undrained strength. Thus, unlike some earlier proposed β-methods, the effective friction angle of the clay is not an element in this method.

As this study documents, the plasticity index of the clay has a very significant impact on the α- and β-values. This aspect is not accounted for in other design methods (except the NGI-05 method). For that reason, it has not been found of relevance to make any direct attempt to compare other methods to the pile test results included in this study, but most methods developed in the past have been reviewed and assessed.

The reason for why the ultimate shaft friction is lower than the in-situ undrained strength is the impact of the severe disturbance caused by the pile installation on the stress-strain and strength properties of the clay closest to the pile wall. This aspect has been appreciated for a great many years. Many attempts have been made in the past to account for this through use of analytical and numerical methods as reviewed in this Chapter, as well as in Chapters 4 and 5 dealing with the installation and re-consolidation phases.

FEM type analyses based on the SPM, coupled with the MIT-E3 model (e.g. Whittle, 1987), have shown a definite potential for capturing most of the impact of pile installation and re-consolidation on the ultimate shaft friction, but so far limited to clays with OCR up to about 4. As also discussed in Chapter 5, the key to improve this approach is, through laboratory tests and further development of soil models, to get a better and more complete picture of how various

degrees of shear straining or disturbance will impact the compressibility and strength of the clay surrounding a pile.

The data presented herein show, as one would expect, a clear tendency for the ultimate shaft friction to increase with horizontal effective stresses as measured against the pile surface. The scatter in the data is however, large. The scatter must partly be contributed to inaccuracies in measured effective stresses. An additional issue is that for a general case, the undrained strength and ultimate shaft friction depends on the complete state of effective stresses surrounding a pile, and not only on the horizontal (radial) effective stress. Furthermore, for clays with OCR less than approximately 4, the critical shear plane is not likely to be at or near the pile surface where the effective stresses have been measured, but at some distance from the surface. It has been well documented from excavation around piles, as well as from the observations when piles are pulled out of the ground after testing, that a layer of clay normally sticks to the pile in low OCR clays.

For these reasons, the author has concluded that design approaches based on empirical correlations between measured ultimate shaft friction and measured horizontal effective stresses, are presently not viable. Such an approach may still be used for checking against the proposed α- and β-methods. It is also encouraged in the future to pursue further large scale fully instrumented pile testing to try to improve such correlations and calibrate new and improved numerical models. Such testing requires great attention to instrumentation details, and specially for measuring total horizontal stresses.

7 ANALYSES AND PREDICTION OF LOAD-DISPLACEMENT RESPONSE

7.1 Overview and discussion of existing methods

Load-displacement response of axially loaded piles is most commonly analysed by modelling the pile with its real axial elastic stiffness and the mobilization of shaft friction as a set of linear or non-linear springs distributed down along the shaft, ref. principal sketch in Figure 7.1.1. Springs are also used to represent the mobilization of tip resistance. Such spring concepts were probably first developed by Seed and Reese (1957), but has been addressed in numerous other papers, for instance early papers by Coyle and Reese (1966), Holmquist and Matlock (1976), Randolph and Wroth (1978) and Kraft et al (1981).
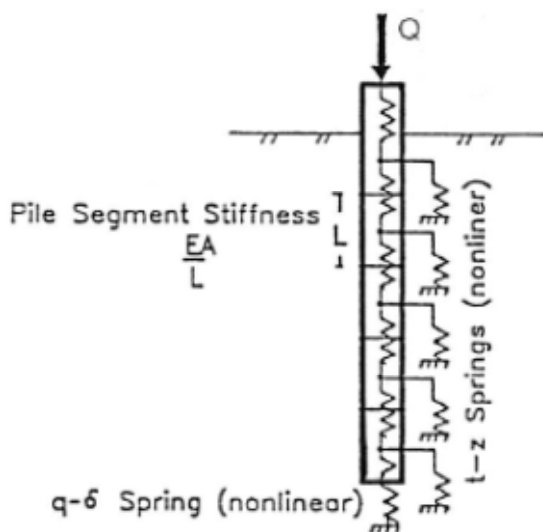

Figure 7.1.1 – Illustration of spring model for axial pile-soil interaction (from Karlsrud and Nadim, 1990)

Such spring models have been in common use for several decades and are incorporated into many computer programs. Early examples were programs like SPLICE (Clausen, 1980), PILGIP (O'Neill, 1980), and GROUP (SINTEF, 1999). These programs can also handle interactions between a pile group and a foundation element. A large variety of such programs are presently on the market, but it is outside the scope of this work to go into the merits and details of such programs.

The t-z springs were traditionally established from back-calculation of pile load test results. The most commonly applied "t-z" springs for application to piles in clay, are those recommended in API (2007). They were empirically derived and shown in Figure 6.2.10. It includes a non-linear part up to a peak, and then some reduction to a residual value 10 to 30 % lower than the peak.

An alternative approach to use empirically derived "t-z" springs is to derive them from the stress-strain behaviour of the clay as determined from relevant laboratory tests, coupled with the distribution of imposed shear stress as function of radial distance from the pile surface. A procedure along these lines was for instance outlined by Kraft et al (1981). Such an approach was also incorporated into the PAX2 computer program developed and documented by Nadim in a report issued by NGI (1994). With reference to the illustration in Figure 7.1.2 the following highlights how PAX2 handles this aspect.

1) The distribution of the shear stress imposed by the pile in the surrounding soil is simply given by the expression:

$$\tau = \tau_0 \cdot r_0/r \qquad\qquad (7.1.1)$$

2) For an assumed shear stress level at the pile wall, the degree of mobilization, as defined by the ratio τ/s_u, is first calculated as function of radial distance. In this connection, the distribution of the strength of the clay as function of radial distance from the pile wall may be assumed to vary (i.e. different strength in RR zone, disturbed zone and intact zone as illustrated in Figure 7.1.2).

3) From the assumed normalized stress-strain curve of the clay, which also may be assumed different in different zones around the pile, the shear strain as function of radial distance is then determined.

4) The displacement at the pile wall is found by integration of these shear strains as function of radial distance. A cut-off is required on stiffness and/or radial distance from the pile surface to avoid going to infinite values.

5) By going through an incremental increase in imposed shear stress at the pile wall, the complete t-z curve is developed.
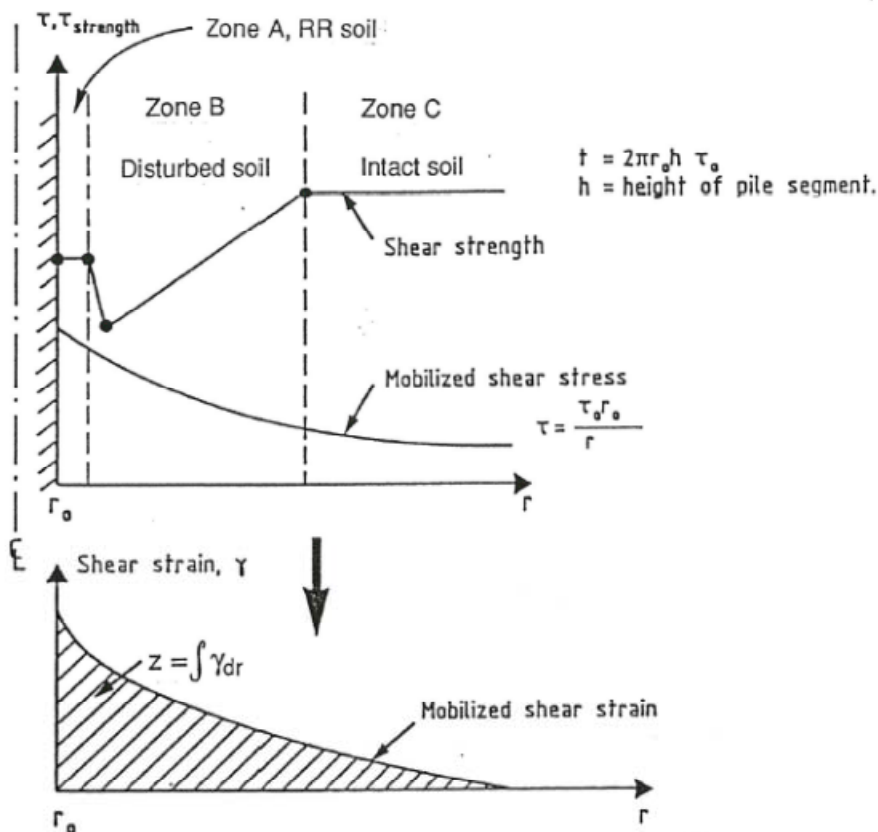

Figure 7.1.2 – Illustration of method for calculating t-z response based on stress-strain behaviour and strength of clay surrounding a pile (from NGI, 1994)

Figure 2.4.20 b) in section 2.4.3 showed the results of application of this procedure to the Onsøy C1- and C2- piles. The agreement between measured and predicted response was very good for both piles. The reason for the difference in response between the C1 and C2 piles is the assumed reduced axial stiffness of the C1 pile due to the threaded joints, as described earlier in Section 2.4.3.

The effect of strain-softening under axial loading beyond peak can in principal also be dealt with in such an incremental procedure. The same applies to cyclic degradation effects, which actually is a main element incorporated into the PAX2 computer program, as will be further discussed in Chapter8.

7.2 Observed t-z response

For all the instrumented pile tests described in Chapter 2 where sufficiently reliable data on t-z response are available, the displacement at maximum mobilized shear stress, z_p, have been normalized with respect to the pile diameter, D. Figure 7.2.1 and 7.2.2 shows these normalized values of z_p/D for all the piles plotted against OCR and I_p of the clays. It is hard from these data to see very specific trends in relation to impact of OCR and I_p. There seems however, to be a trend that the open piles show smaller displacements than the closed ones. Most open piles suggest values in the range z_p/D=0.01 to 0.02, and most closed piles suggest values in the range z_p/D=0.02 to 0.04.
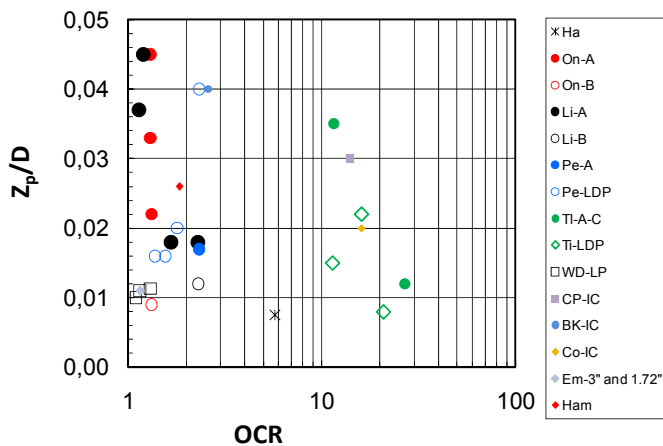

*Figure 7.2.1 – Normalized local peak displacement z_p/D versus OCR, all sites*
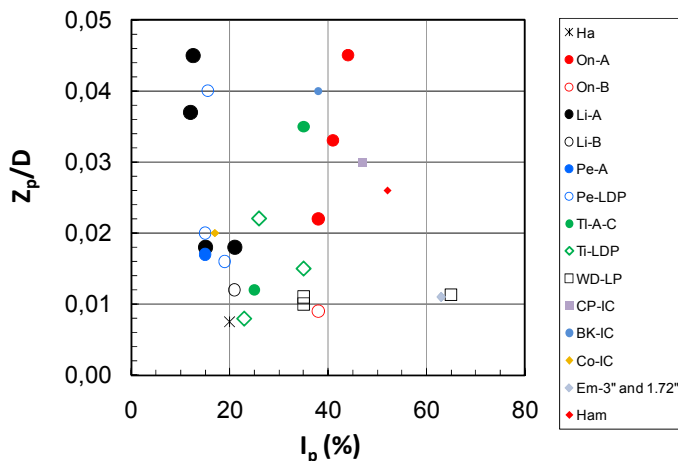
Figure 7.2.2 – Normalized local peak displacement z_p/D versus I_p, all sites

Compared to the API (87) procedure suggesting $z_p/D = 0.01$, it is rather surprising that most data herein gives values that are significantly larger than that. On basis of these results, and a view to typical non-linear response up to peak that have been observed in these pile tests, Figure 7.2.3 presents tentative new and revised t-z curves as compared to API(1987).
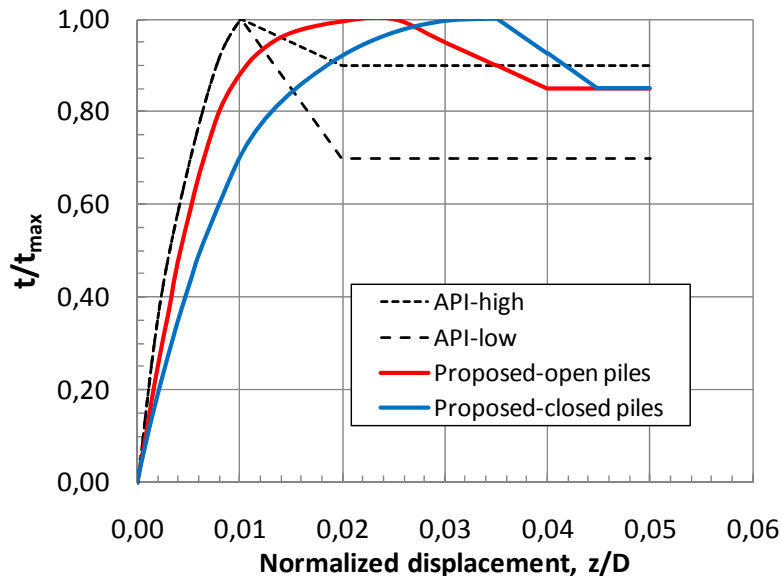

Figure 7.2.3 – Proposed new t-z curves compared to API (2007)

An important issue in relation to load-displacement response at the pile head is if, or to what extent, strain softening beyond peak should be accounted for. In most displacement-controlled tests incorporated in this study, the data suggests some post-peak reduction in shaft friction, mostly in the range 10 to 20 %, but there are also cases with no reduction. Where data are available, the minimum post-peak strength seems to be developed at a displacement of about 1.5-2 times the displacement at peak.

In load-controlled tests, as in all NGI's load tests, post-peak reduction is difficult to observe because such softening will rather be reflected in a rapid increase in the rate of displacement as failure emerges. Accounting for strain softening can actually be seen in the same light as accounting for the impact of rate of straining, rate of loading or time to failure on the undrained strength. These are in many respects synonymous effects.

Another point worth noticing, is that for the non-instrumented piles, some element of strain softening (if real) will already be incorporated in the deduced average ultimate shaft friction values, as the average ultimate shaft friction is taken as when the peak load was reached at the pile head. For the displacements in question, the upper part of these piles could have experienced some strain softening effects (if there is one), but it is difficult to deduce from the results.

From the discussion above, and under the assumption that the method proposed herein is used to calculate the ultimate (peak) shaft friction, it is recommended to only account for a nominal strain softening effect of up to maybe 15% for design purposes. This is indicated in the proposed t-z curves in Figure 7.2.3. Post-peak softening is probably most relevant to account for in stiff OC plastic clays where well defined localized shear planes are most likely to develop, or in clays where DSS tests show very distinct softening beyond peak.

As a final comment to the importance of strain softening, the ultimate shaft friction will in almost every real case increase with depth. This is most obvious for NC clays, but even in OC clays with su constant with depth the ultimate shaft friction will be much larger than in the top due to the impact of s_{ud}/σ'_{vo} and OCR on the α and β values. As relative soil/pile displacements inevitably will decrease with depth, it means that potential strain softening effects will be largest along the pile that carries the smallest proportion of the load. This will therefore, dampen the net effect of strain softening on the ultimate peak pile capacity.

7.3 Recommended approach and needs for improvements

The author has on basis of the data presented above proposed new t-z curves that are softer than what is recommended by the commonly applied API (2007) design rules. The proposed t-z curves (figure 7.2.3) are somewhat stiffer for open-ended non-plugging piles than for closed-ended piles.

For specific cases, t-z curves may also be developed from the stress-strain and strength characteristics of the clay as determined by DSS tests, and also accounting for how the strength and stiffness may vary with distance from the pile surface (Figure 7.1.2). Such t-z curves can then be directly incorporated in the commonly applied spring models (Figure 7.1.1).

The author considers that the effect of strain softening or post-peak reduction on the peak ultimate capacity of a pile is an unresolved issue. When the t-z approach is combined with the procedure for calculating the peak ultimate shaft friction as proposed in this study, it is suggested that such strain softening is limited to 15 % post-peak reduction at a displacement corresponding to about 1.5-2 times the displacement at peak (Figure 7.2.3)

For real situations and designs, flexibility of the pile itself will often contribute significantly to the displacement at the pile top, and can have a larger impact on the interaction between a pile foundation and the superstructure it shall carry, than the t-z curves themselves.

Some elements that may be considered for further improvements of the prediction of load-displacement response of piles in clay are as follows:

- The whole issue of strain softening requires further studies and understanding: For instance, of how softening may depend on the basic clay characteristics, type of loading applied to a pile, (i.e. rate of loading or rate of displacement), and how this also ties in with strain softening, rate effects and undrained creep effects as observed in undrained laboratory tests.
- Under what conditions strain localization and formation of well defined slip planes may occur, which may impact the potential for strain-softening effects.
- How the basic stress-strain behaviour and undrained shear strength of the clay varies with the distance from the pile surface, considering the effects of pile installation and re-consolidation on these properties, and consequently how this impacts the t-z behaviour.

8 ANALYSES AND PREDICTION OF AXIAL CYCLIC RESPONSE

8.1 Definitions and brief review of past work

This chapter is primarily included to give some understanding as to how cyclic loading may affect axial pile performance and how it can be rationally accounted for in design. In research and design practice the static capacity is used as key reference capacity when addressing the cyclic capacity.

It is beyond the scope of this study to present a detailed review of cyclic pile load tests that have been carried out, but some results are included for illustration. The review of numerical or analytical approaches that have been developed for handling cyclic loading effects focuses on a method proposed and developed by NGI, partly based on the authors input and suggestions.

Figure 8.1 shows how cyclic loads on a pile are normally defined by the average load, Q_{ave}, and the cyclic load amplitude, Q_c. The loading is designated as "one-way" when there is no load reversal, e.g. Q_{min} and Q_{max} act in the same direction, and "two-way" if there is such reversal and they act in opposite directions. Cyclic displacements are defined by the average displacement that has accumulated during the duration of cyclic loading, δ_{acc}, (i.e. in addition to the displacement caused by the first application of the average load), and the cyclic displacement amplitude, δ_c. On a local level, the cyclic shear stresses and shear strains are defined in a similar manner as the loads.
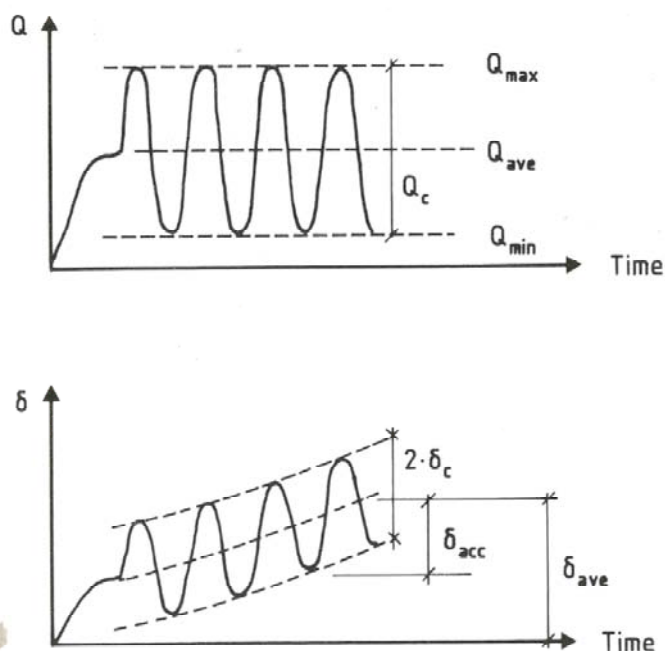
Figure 8.1 – Definition cyclic pile loads and displacements

The potential effects of cyclic loading on the response and bearing capacity of structures were given increased attention from the early 1970's, as the petroleum developments moved into deeper waters and wave loading became an increasingly important design factor. Design procedures accounting for the effect of cyclic wave loads came first in relation to gravity based structures, (e.g. Andersen, 1976 and Andersen et al 1978).

Most of the early studies of effects of cyclic loading on pile performance was based on two-way cyclic displacement controlled "pin-model" tests in test drums or triaxial chambers, e.g. Matlock and Holmquist (1976), Grosch and Reese (1980), Kraft et al (1981), Poulos (1982) and Matlock et al (1982). These studies focused on degradation of the shear transfer related to the cyclic displacement amplitude and number of displacement cycles applied. The study by Poulos (1982) also included load-controlled tests and study of post- cyclic static capacity.

A very comprehensive cyclic load testing program was carried out on the Haga piles (Section 2.2), described by Karlsrud and Haugen (1983, 1984), Karlsrud et al (1986) and Karlsrud (1986). The tests were all load controlled and covered a wide range of cyclic load levels, from one-way to symmetric two-way loading. Figure 8.2 shows key results in an interaction diagram presenting the number of load cycles to failure in relation to the cyclic load levels applied. All loads are normalized with respect to the measured static capacity. The figure shows that the cyclic degradation effect becomes increasingly important when the cyclic loads move into the two-way region, and the cyclic capacity is as low as 42 % of the static capacity for symmetric two-way loading with N_f=100 cycles to failure. In the one-way region, the cyclic capacity can actually be higher than the reference static capacity if only a few load cycles are applied. That is due to the effects of rate or duration of loading.
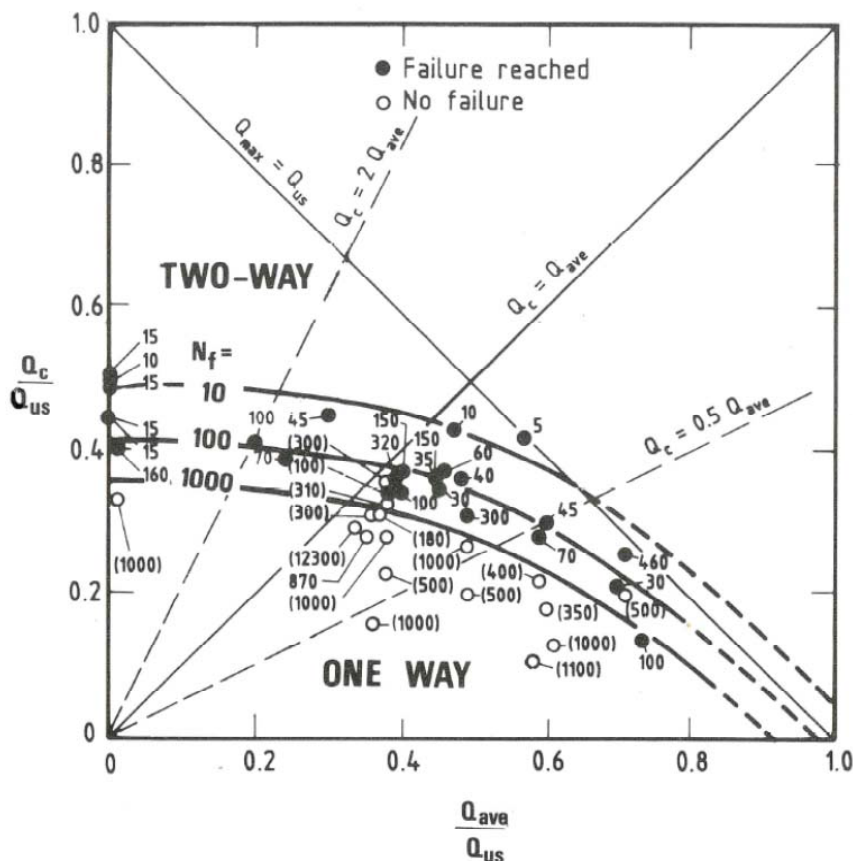
Figure 8.2 – Interaction diagram with number of cycles to failure as function of cyclic load levels applied for pile test at Haga (after Karlsrud et al, 1986)

An important observation in relation to the mode of failure in the Haga tests was that during symmetric two-way cyclic loading, failure was primarily associated with rapidly increasing cyclic displacement amplitude. In one-way loading on the other hand, failure was associated with rapidly increasing accumulated displacement, and little increase in the cyclic displacement

amplitude. Furthermore, Karlsrud et al (1986) showed that the accumulated displacement during one-way cyclic loading was very much an effect of creep that occurred during the short time period the peak load was acting under each load cycle.

The Haga project showed that there was a great similarity between the cyclic degradation that was observed for the piles and what was observed from a series of cyclic DSS tests that were carried out on both intact and RR clay. Karlsrud et al (1986), Karlsrud (1986) and Karlsrud and Nadim (1990) briefly reviewed some other early studies of cyclic loading effects and concluded that they showed very similar results as were observed in the Haga tests. Figure 8.3 compares one-way cyclic capacities measured in cyclic tests at Onsøy and Lierstranda to the Haga results. Note that in this interaction diagram Q_{max}/Q_{us} rather than Q_c/Q_{us} is used on the vertical axis, which gives a more direct impression of the effect of cyclic loading on the capacity. The Onsøy and Lierstranda tests suggest even stronger effect of cyclic loading than the Haga tests, especially in the two-way region.
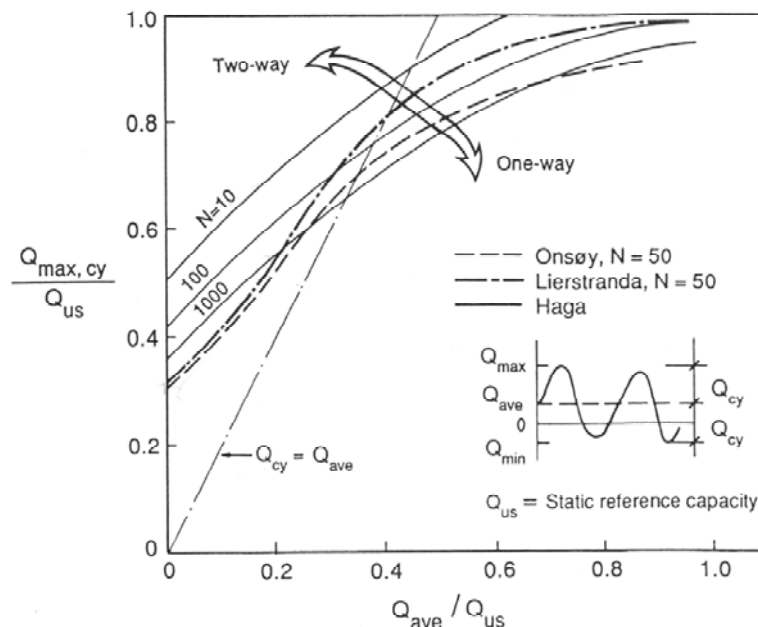

Figure 8.3 – Comparison between cyclic pile capacities at Haga, Onsøy and Lierstranda (fraom Karlsrud et al, 1992)

8.2 Prediction of pile response to cyclic loads

For short or stiff piles a first and reasonably reliable design approach is to directly use interaction diagrams like those presented in Figures 8.2 and 8.3. This should preferably be based on site specific DSS tests on RR and/or intact clay, and with cyclic load periods typical for the case at hand.

For long and flexible piles it becomes increasingly important to properly account for cyclic loading effects on the local shaft friction and displacements, and use programs that satisfy compatibility in terms of local and global stresses, loads and displacements.

Goulois (1982) was one of the first to develop a numerical procedure for handling cyclic loading effects, and he implemented that into a computer program "TLPILE". It had focus on capacity of piles supporting Tension Leg Platforms, which came into the deepwater platform market in that

period. At the time, the industry was quite concerned that such piles could experience "un-zipping" effects as a result of sustained cyclic tension loading.

The numerical approach used by Goulois (1982) is similar to a "t-z" approach for static loads, in that it handles both pile flexibility and soil stiffness. In addition it accounts for effects of cyclic degradation on the local ultimate shaft friction and soil stiffness. It is a decoupled approach. The local cyclic shear stresses induced by the first load cycle are calculated first. On that basis, the strength and stiffness are modified to account for the effect of the calculated local cyclic shear stresses along the pile and the given number of load cycles to be applied. Iterations are made to achieve compatibility between applied shear stresses and computed shear stresses, and cyclic and accumulated displacements. DSS tests are used as basis for assessing stiffness and degradation effects. The TLPILE program predicts both accumulated and cyclic displacements as well as the distribution of cyclic and average shear stresses down along the pile.

How cyclic loading effects on long flexible piles could be handled in design was also proposed and discussed by Karlsrud et al (1986), Karlsrud (1986) and Karlsrud and Nadim (1990). At NGI a numerical procedure and computer program called PAXCY (Nadim et al, 1989) was developed, that later was modified into the PAX2 program (NGI, 1994), referred to in Chapter 7. PAXCY and PAX2 represent a further development of the TLPILE program by Goulois (1982). It makes use of "cyclic strain-contour-networks" that are determined from DSS tests that cover an appropriate range of cyclic load levels and number of load cycles. An example of this is shown in Figure 8.4. This use of "cyclic strain-contour-networks" was first developed for design of offshore gravity platforms by Andersen (1976) and Andersen et al (1978). The PAX2 program can handle variation in cyclic load levels with time and, as for the static case (Chapter 7), possible variations in cyclic strength and stiffness as function of distance from the pile wall (i.e. from the RR zone to the intact zone around a pile).
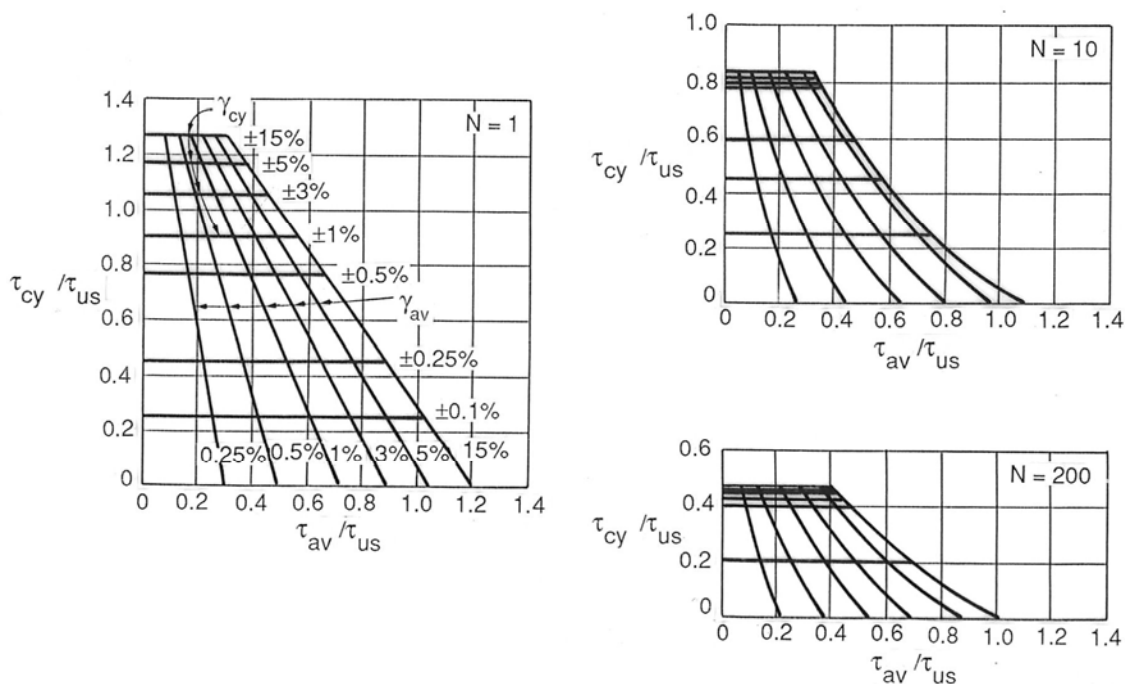

Figure 8.4 – Example of strain contour networks (from Karlsrud and Nadim, 1990)

Figure 8.5 shows examples of cyclic failure loads calculated for a 100 m long pile installed in NC plastic clay, as presented by Karlsrud and Nadim (1990). The pile diameter was 2.032 m and wall thickness 63.5 mm. It was subjected to a typical North Sea design "wave train", starting with 200 cycles with a peak cyclic load, Q_{max}, corresponding to 64 % of the maximum wave load, then with the number of load cycles decreasing and the cyclic maximum load increasing stepwise, until at the end, 1 cycle at the maximum load was applied. Five cases with different level of average and cyclic load amplitude were analysed. The relative load levels were in each case adjusted to find the level that caused failure.
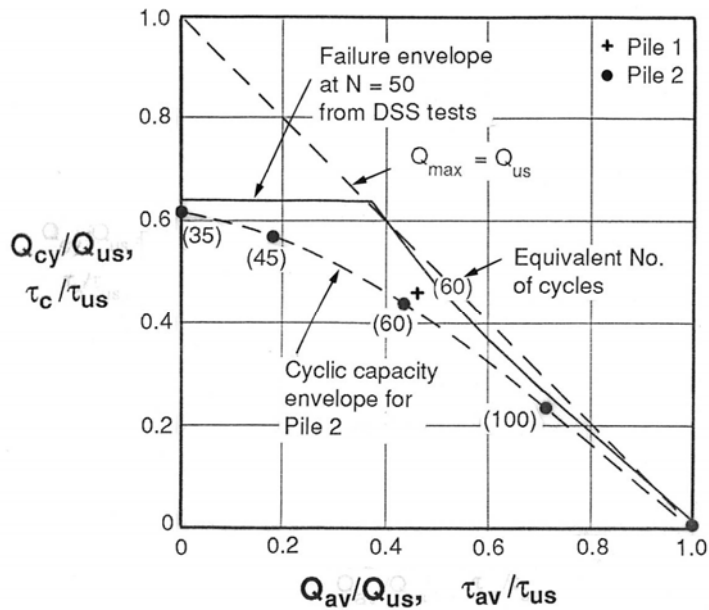

Figure 8.5 – Examples of calculated cyclic capacity of 100 m long pile in NC clay subjected to wave storm loading (from Karlsrud and Nadim, 1990)
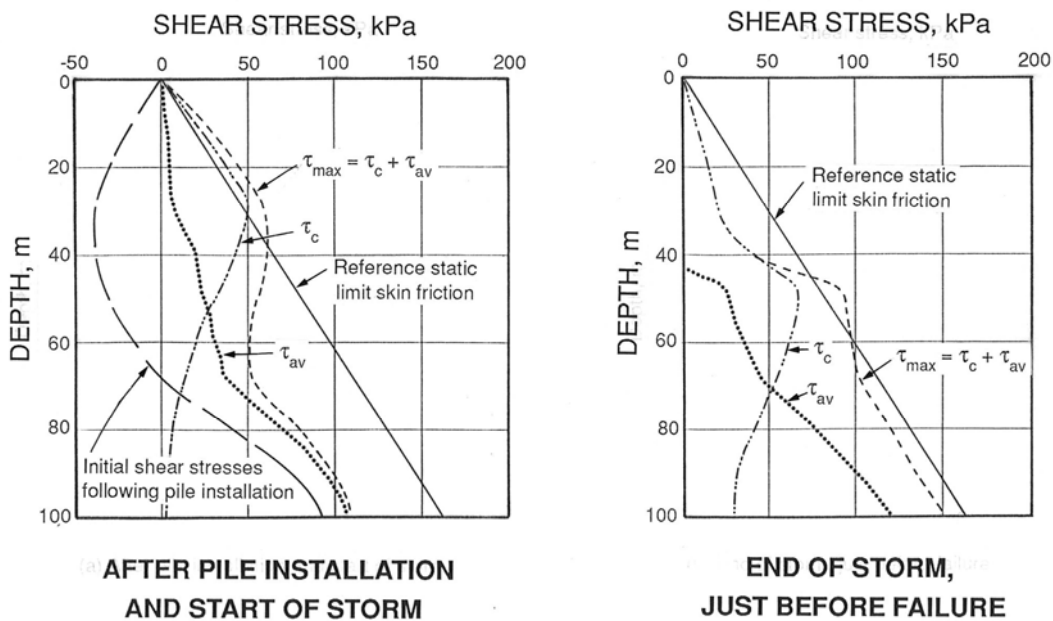

Figure 8.6 – Example of distribution of shear stresses along 100 m long pile calculated with PAXCY at start and end of storm loading (from Karlsrud and Nadim (1990)

Some important observations that can be made from this example study are:

- When compared to the clay degradation observed in the DSS tests that formed the basis for the analyses, the cyclic pile capacity is lower. This is mostly a direct effect of the pile flexibility.
- Even with only pure one-way cyclic loading applied at the pile top, some elements of the soil along the pile will still experience two-way cyclic loading. This can be seen from Figure 8.6 presenting calculated local shear stresses along the pile. The upper 40 m of the pile experience two-way cyclic loading and the shaft friction here degrades to about 40 % of the static strength. This may be considered as a sort of "un-zipping" effect, with the degradation progressively going deeper. However, the process does not continue if the lower part of the pile can take the load that is shed down from the top part.
- For direct comparison against the stepwise increasing "wave train" type loading, analyses have also been carried out with constant amplitude cyclic loading at a load level equal to the maximum wave load. Figure 8.5 shows that in the constant load amplitude analyses cyclic failure occurred after application 35 load cycles for symmetric two-way loading, increasing to about 100 load cycles for one-way loading.

8.3 Recommended work to improve design practice

To the author's knowledge, no single method has been recommended in any current design codes for how to account directly or indirectly for the effects of cyclic loading on the axial pile capacity, whether they are installed in clays or sands. In Section 6.6.2 of the current API (2007) the following is stated in relation to cyclic response: *"Unusual pile loading conditions or limitations on design pile penetration may warrant detailed consideration of cyclic loading effects"*. It also states: *"The design of pile penetration can be confirmed by performing pile response analyses of the pile-soil system subjected to static and cyclic loading. Analytical methods to perform such analyses are described in the commentary to this section"*. In the commentary Section C6.6.2 it is stated that: *"For most fixed platforms supported on piles, experience has proven that pile penetration based on static capacity evaluations, and static ultimate design loads and commonly accepted factors-of-safety that, in part, account for cyclic loading effects. For some novel platform concepts (e.g., Compliant Tower and Tension Leg Platforms), soils, and loading conditions, or when there are unusual limitations on pile penetration, detailed considerations of cyclic loading effects may be warranted"*. For specific analyses of cyclic loading effects, API (2007) only gives some very general recommendations and refers to some published papers on the subject.

One challenge in relation to accounting for cyclic loading effects in current design practice is that numerical methods/computer programs that can appropriately handle this, are not commercially available, and/ or that they require fairly advanced and extensive cyclic soil testing to arrive at required input parameters. However, in relation to input parameters, Andersen (2004) has published cyclic DSS interaction diagrams for a range of different clays. With such data as a background basis, the need for site specific cyclic DSS tests may be greatly reduced.

In the author's view, the design of offshore pile foundation should as a rule, not an option for special cases, consider possible cyclic loading effects. The same applies to other structures that may experience significant cyclic loads, for instance due to wind or earthquakes. In relation to

earthquakes the author would expect that cyclic loads will not govern the design for piles in clay that only will experience one-way cyclic loads. The reason is the positive effect of strain rate or time effects on the shear strength of clays associated with the high loading frequency and the limited number of load cycles involved in an earthquake as compared to wave loading.

The author recommends parametric studies with programs like PAX2 to look more into the relative effects of cyclic loading for a range of cyclic load levels, clay conditions and pile dimensions. Such parametric studies could well end up in simpler design approaches, relating the relative cyclic design capacity directly to basic soil parameters, relative cyclic load levels and pile stiffness. In this process, it would also be worthwhile to do more verification of programs and design approaches by back-analysis of published cyclic load tests.

9 SUMMARY, CONCLUSIONS AND RECOMMENDATIONS

9.1 Summary of work done

This study deals with the axial capacity and response of piles installed in clay deposits. The study is mainly founded on the collection and critical review and analysis of the data from a number of well instrumented pile load tests. The pile instrumentation allows measurement of the distribution of loads or shaft friction, pore pressure and earth pressure along the pile shafts. The soil conditions range from soft NC clays with undrained shear strength down to about 15 kPa, to very stiff and high OCR clays with undrained shear strength up to about 500 kPa. The plasticity index of the clays lies in range 10 to 60 % at most sites, but up to 120 % at one site. The test piles range from small scale model piles with diameter down to 36 mm and length down to about 1- 2 m, to large scale piles with diameter up to 800 mm and length up 71 m. In addition to these fully instrumented pile tests, some recent large scale tests on non-instrumented piles are also reviewed and included as basis for developing the new design procedures. The author has been responsible for, or involved with, planning and interpretation of several of these load tests, but has herein made a fresh and new assessment of all test results.

The study includes a brief historic review, going back to the beginning of the 1900's, of ideas concerning what governs the ultimate shaft friction in clays. A critical review is given of existing empirical design methods, as well as relevant analytical and numerical methods that have been developed in the past for analyzing the pile performance through the installation phase, the re-consolidation phase and the pile loading phase.

Special attention has been given to define key soil parameters in a consistent and coherent manner. In terms of ultimate shaft friction, key soil parameters are the plasticity index, in-situ effective stress, the "true" in-situ undrained strength for a simple shear mode of loading, and the preconsolidation pressure or overconsolidation ratio. In terms of pile "set-up", the undrained shear stiffness, the permeability of the clay and the virgin compressibility are three key parameters considered.

The ultimate static shaft friction after full "set-up", and how it varies with depth, is determined for each pile test. All ultimate shaft friction data are then compared and tried correlated to the key soil parameters.

The author has related the time for pile "set-up" to the time for dissipation of excess pore pressures induced by the pile installation, and as can be predicted from simple analytical linear radial consolidation analyses. Empirical correction factors are introduced to give the best match between calculated and measured times for re-consolidation.

The effects of "ageing" or possible increase in pile capacity after full re-consolidation is reached are also briefly discussed.

This study also deals with- , and gives recommendations for, how to analyze the load-displacement response of piles and determine the total ultimate peak pile capacity, including the effect of cyclic loading.

9.2 Overall conclusions

The following summarizes the main findings from this study. Further details regarding recommended design methods and needs for improvements are given in the subsequent sections.

- The pile shaft resistance in clay is best simulated by relating it to the shear resistance determined in a direct simple shear (DSS) mode of failure.
- Based on the load test data included in this study, the author proposes two new empirical approaches for calculating the ultimate shaft friction:
  - The primary method is an α-method. The ultimate shaft friction is then given by $\tau_{us} = \alpha \cdot s_{ud}$, where s_{ud} is the in-situ undisturbed strength determined from DSS tests. The α-value is a function of the normalized strength ratio, s_{ud}/σ'_{v0}, and the plasticity index of the clay.
  - An alternative method is a β- method, where $\tau_{us} = \beta \cdot \sigma'_{v0}$. The β - value depends on the overconsolidation ratio of the clay and the plasticity index.
- Although considered as separate, the two methods are to some extent correlated through the classical relationship between normalized undrained strength and the overconsolidation ratio. The significant dependency of the ultimate shaft friction on the plasticity index should be noted. For NC low-plastic clays the minimum recommended α-value is actually as low as α= 0.2. The main explanation for the low shaft resistance in low-plastic clays is that the horizontal (radial) effective stress is found to be extremely low in such clays.
- There is no clear evidence that the ultimate shaft friction is any different for closed-and open-ended piles, or that there is any difference between piles loaded in compression or tension. This is in agreement with most other methods that have been proposed in the past.
- The pile dimensions, including pile length or flexibility, do not seem to affect the local ultimate shaft friction. This actually contradicts the fairly significant length or pile flexibility effect that is included in several design methods proposed over the past 20 years or so.
- The data presented herein show a clear tendency for the ultimate shaft friction to increase with horizontal effective stresses as measured against the pile surface. However, as discussed in Section 6.3, design approaches based on semi-empirical correlations between measured ultimate shaft friction and measured horizontal effective stresses, are presently not considered viable.
- When analyzing the load-displacement response and ultimate capacity of the piles, some post-peak softening of the local shaft friction should be accounted for, but this will normally reduce the predicted peak pile capacity by less than 5 %.
- Cyclic loading can have a significant effect on the ultimate capacity of piles, depending on the relative level of the cyclic load amplitude as compared to the average load, and on the number of load cycles applied. For the extreme case of symmetric two-way cyclic loading the capacity can be as low as 35-45 % of the static capacity if the pile is subjected to 50 uniform load cycles.

- The author proposes a semi-empirical procedure for predicting the time for full re-consolidation and set-up of the ultimate shaft friction. The method is based on linear radial consolidation theory and assumes that the initial excess pore pressures decrease linearly with the normalized radial distance from the pile surface. The Cavity Expansion Method (CEM), with a linearly elastic- perfectly plastic soil model, is used for calculating the radial extent of the excess pore pressure. The key soil parameters are undrained strength and shear modulus for predicting the initial excess pore pressure field, the in-situ permeability, and an empirically derived un-loading re-loading volumetric compressibility. Some correction factors are also introduced to give a good match to measured consolidation times.

- It can be important in design practice to account for possible further increase in pile capacity due to "ageing" after full re-consolidation is reached.

9.3 Recommended procedure for predicting ultimate shaft friction and load- displacement response

9.3.1 Ultimate shaft friction

Based on the data presented herein, the author proposes two new semi-empirical design methods for the determination of ultimate shaft friction along piles in clay.

The primary α- method ties the ultimate shaft friction to the best possible estimate of the in-situ undrained strength, s_{ud}, corresponding to a direct simple shear mode of shearing, the in-situ vertical effective stress and the plasticity index of the clay, Figure 9.1. The undrained strength can be determined directly from DSS tests on good quality undisturbed samples. Alternatively, it can be determined from empirical correlations to the undrained triaxial compression strength, s_{uc} (Karlsrud et al, 2005 and Karlsrud and Hernandez, 2011). A reasonably reliable determination of s_{uc} can, in lack of laboratory tests on good quality samples, be determined from CPTU tests using the correlations presented by Karlsrud et al (2005).
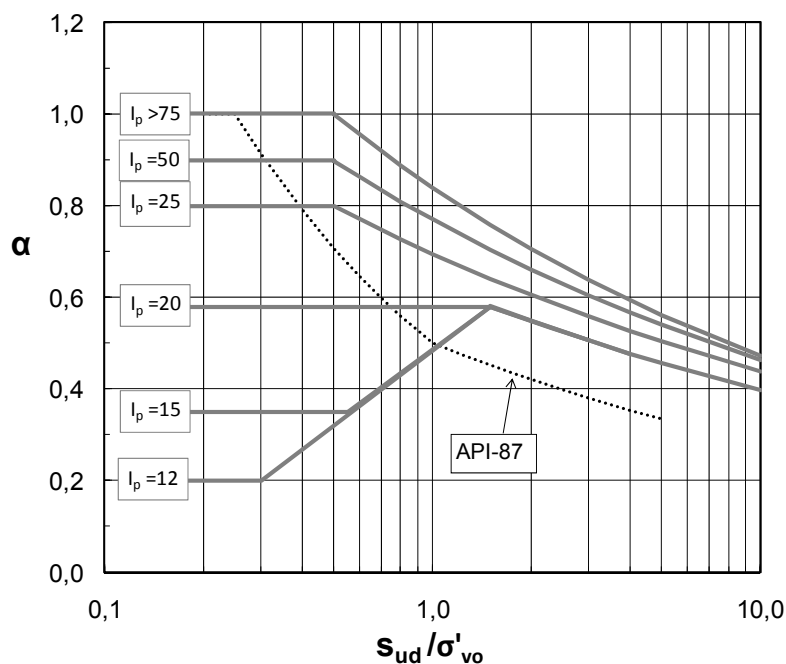

Figure 9.1- Proposed chart for determination of α-values

The proposed α- method can be seen as a modification to the NGI-05 method proposed by Karlsrud et al (2005) and has also some resemblance to the API (1987) method. However, the two latter methods use the UU strength as a reference. In the author's view it is important to get away from use of the UU strength as reference strength. The reason is that the UU strength is far more affected by sample quality and disturbance, than the s_{ud} strength. In present engineering practice, it is time to move away from the rather rudimentary soil investigations and soil parameters that many semi-empirical design methods have been based upon.

Figure 9.1 shows that the clay plasticity index has a very significant effect on the ultimate shaft friction, and is as important a parameter as the normalized undrained strength for determination of the appropriate α-value. This is further demonstrated by Figure 9.2, showing α-values from the actual pile tests for moderately overconsolidated clays with $s_{ud}/\sigma'_{v0}<0.4$.

The effects of the large shear strains caused by the pile installation on the stress-strain and strength properties of the clay closest to the pile wall, is the main reason why the ultimate shaft friction comes out lower than the in-situ undrained strength.
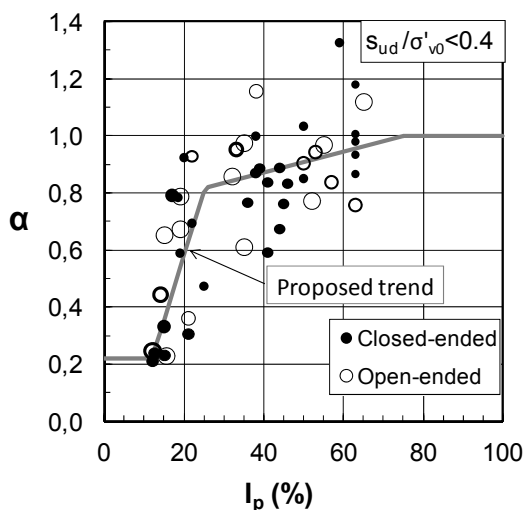

Figure 9.2 – Effect of plasticity index on α-value for pile tests in clays with $s_{ud}/\sigma'_{v0}<0.4$

Figure 9.3 shows the alternative β- method proposed by the author. Notice the log-scale in this diagram, and that β- values can go from as low as 0.045 for low-plastic NC clays to about 2.0 to very stiff clays with OCR of 40, which is the upper range of available pile data.

The recommended α- and β- methods have been applied to the pile data base established in this study. A comparison between calculated and measured values confirms that both methods are well balanced in relation to dependency on the key soil parameters used. The ratio of Calculated to Measured capacities show a standard deviation of 0.21 for the α- method and 0.24 for the β- method.
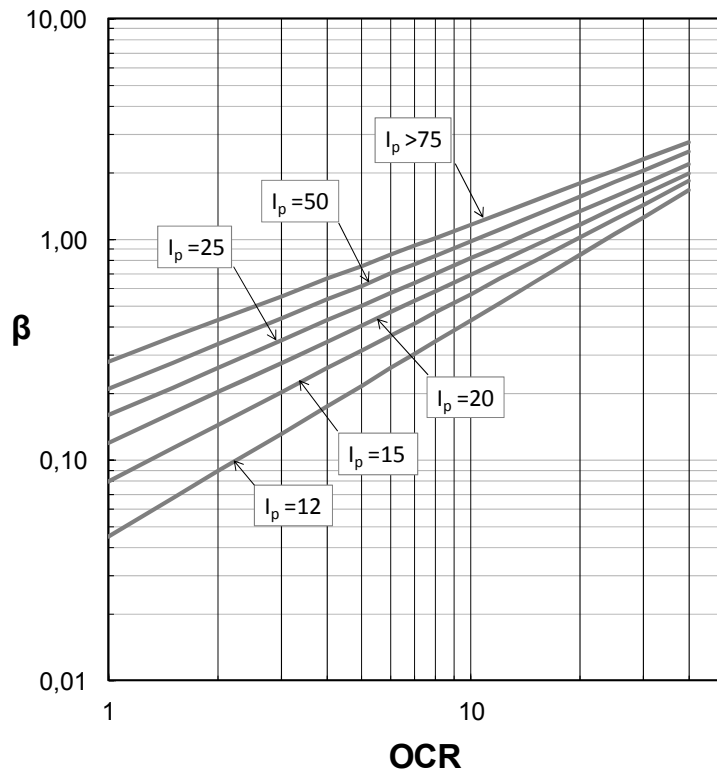
Figure 9.3 - Proposed chart for determination of β –values

Many attempts have been made in the past to account for the effect of the large shear strains caused by the pile installation on the properties of the surrounding clay and the ultimate shaft friction. This has partly been based on analytical and numerical methods as reviewed in Chapter 6, as well as in Chapters 4 and 5 dealing with the installation and re-consolidation phases.

FEM type analyses based on the Strain Path Method (SPM), coupled with the MIT-E3 model (Whittle, 1987), have shown a definite potential for capturing most of the effect of pile installation and re-consolidation on the ultimate shaft friction, but the analyses have so far been limited to clays with OCR up to about 4. The SPM-MITE3 approach has however, so far failed to predict the extremely low ultimate shaft friction values as have been observed in low-plastic clays. The main reason is believed to lie in underestimation of the compressibility of the severely strained clay closest to the pile wall as compared to the compressibility of the clay at larger distance from the pile surface, which to a large extent will experience un-loading/re-loading type stress changes and therefore, behave much stiffer.

The simplest CEM-EP model, as well as the CEM-MCC model, grossly over predicts the measured horizontal effective stresses, especially for clays that are up to moderately overconsolidated. Such numerical methods will therefore also grossly over predict the ultimate shaft friction.

9.3.2 Load-displacement response - monotonic loading
The load-displacement response of axially loaded piles is most commonly analysed by modelling the pile with its real axial elastic stiffness, and modelling mobilization of shaft friction by a set of linear or non-linear springs distributed down along the shaft. This is also the approach recommended by the author for general use.

Figure 9.4 presents "t-z" shear transfer curves proposed by the author for predicting the load-displacement response and ultimate peak pile capacity of open-ended and closed-ended piles. The curves indicate softer behaviour up to peak than what is recommended in the current API (2007), but suggest that post-peak softening is limited to 15 %.
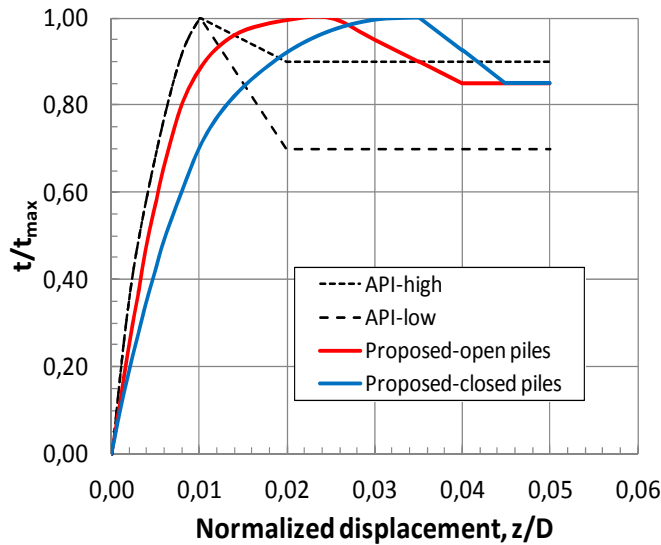

Figure 9.4 – Proposed t-z curves

A consequence of the proposed t-z curves is that pile length or flexibility will have a very limited effect on the ultimate peak pile capacity, maximum about 5 %.

It is also possible to develop t-z curves from the stress-strain and strength characteristics of the clay as determined by DSS tests (Karlsrud and Nadim,1990). Their proposed procedure accounts for how the clay strength and stiffness may vary with distance from the pile surface, as illustrated by Figure 9.5. Such numerically derived t-z curves can then be directly incorporated in the commonly applied spring models.
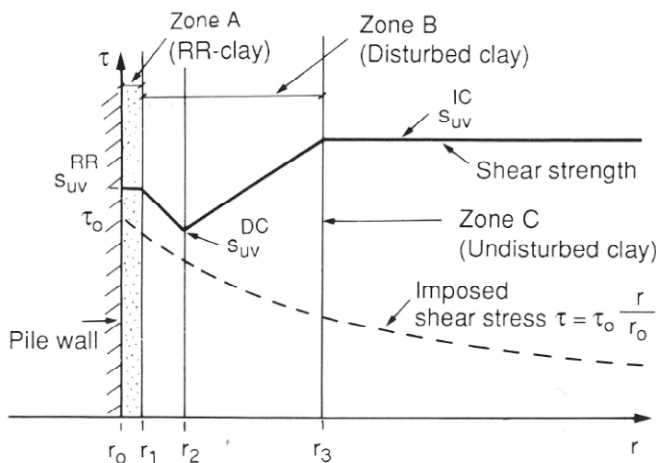

Figure 9.5 – Illustration of possible variation in strength as function of distance from the pile surface (from Karlsrud and Nadim, 1990)

It is also possible to use axi-symmetric continuum FEM models for predicting the load – displacement response. That requires that the input soil parameters reflect the correct ultimate shaft friction, and that it is also accounted for the possible variation in strength and stiffness with distance from the pile surface.

9.3.3 Load-displacement response - cyclic loading

Cyclic loading, and in particular as induced by wave loading, can significantly affect pile displacements and the ultimate pile capacity. The author recommends that for offshore piled structures the cyclic capacity should always be determined. As this has not been a standard design procedure up until now, it will be necessary also to address how load and material factors shall be introduced in practical design.

For relatively stiff piles, Figure 9.6 may give some guidance, as to the possible effect of cyclic loading on the pile capacity relative to the static capacity. Note that the ultimate static shaft friction and pile capacity form a reference value for the cyclic capacity, and must always be determined.

As seen from Figure 9.6, the reduction in capacity is largest for piles that experience symmetric two-way cyclic loading.

Cyclic DSS tests on RR and intact clay are recommended to assess and verify the effects of cyclic loading on the ultimate shaft friction. To simplify the cyclic lab testing program, it is recommended to make use of the cyclic strength data presented by Andersen (2004) for a range of different clays. Furthermore, analyses presented by Karlsrud and Nadim (1990) suggest that a typical design storm with varying load levels can be approximated by a constant amplitude loading with 35 to 100 load cycles at the final peak wave load level.

For long and flexible piles, numerical analyses are in general needed. To the author's knowledge, the most rigorous method developed so far is the one described by Nadim et al (1989). This procedure has been shown by Karlsrud and Nadim (1990) to reproduce quite well the measured response of test piles subjected to cyclic loading.
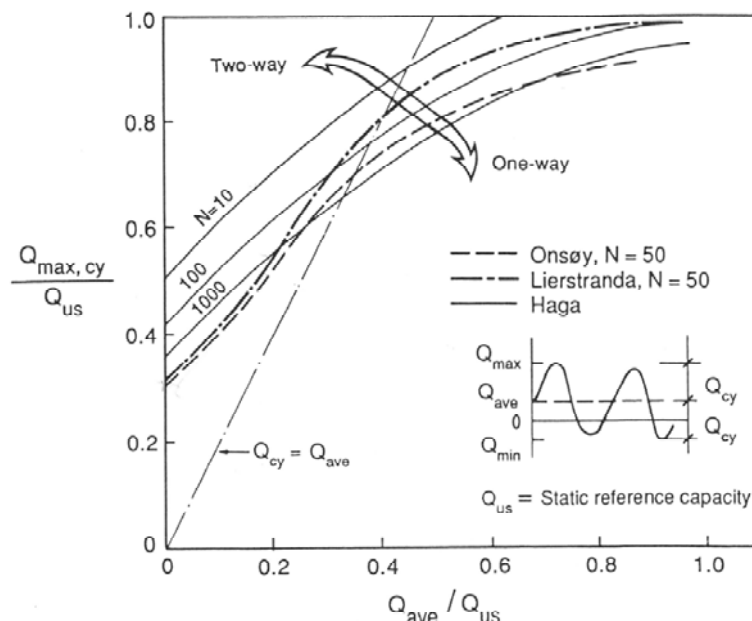

Figure 9.6 – Cyclic capacity interaction diagram from cyclic pile tests at Haga, Onsøy and Lierstranda

9.4 Recommended approach for predicting earth and pore pressures against the pile shaft and time for pile set-up

9.4.1 Stresses induced by pile installation

When a pile penetrates into a clay deposit it will cause very large shear strains in the surrounding clay, and as a consequence induce large changes in total stress and pore pressures in the clay. The radial cylindrical expansion strains are typically of the order 100 % near the pile wall for closed-ended piles, but less that 1/10 of that for a typical un-plugging open-ended pile. In addition to the cylindrical strains, very large vertical shear strains will be induced by the "downdrag" action caused by the pile penetration. These shear strains can close to the pile wall be much larger than the radial strains due to cylindrical expansion.

Measured earth and pore pressures have been compared to predictions based on Cavity Expansion Theory (CEM) and the Strain Path method (SPM), coupled with various soil models (Elasto-Plastic, Modified Cam Clay and MITE1-E3). No single numerical approach has been found to give a complete and correct picture of the measured earth- and pore- pressures set up by the pile installation. The author therefore recommends that the excess pore pressure set up against the pile shaft is determined from the empirical data based on reported load tests, as presented in Figure 9.7.Some data on how the measured excess pore pressure towards the end of installation decays with distance from the pile surface are included in this study. They show reasonable agreement with that predicted with the CEM and SPM type models. How the assumed excess pore pressure distribution affects the prediction of time for re-consolidation and pile "set-up", is dealt with in Section 9.4.3.

The measured horizontal (radial) effective earth pressures at end of pile installation increase with OCR, but shows considerable scatter. Possible reasons for such scatter were summarized in Section 5.2.2. Essentially all data show values of $K_i = \sigma'_{hi}/\sigma'_{v0}$ that are considerably lower than the estimated in- situ K_0 values. This is in strong contrast to that predicted with the CEM- based models, which predict K_i well above K_0. The SPM-MITE3 approach seems to capture reasonably well the trend in the data, but such analyses have so far been limited to clays with OCR<4. Due to the large scatter in the data, the author has not found it appropriate to recommend any empirical approach for predicting K_i.
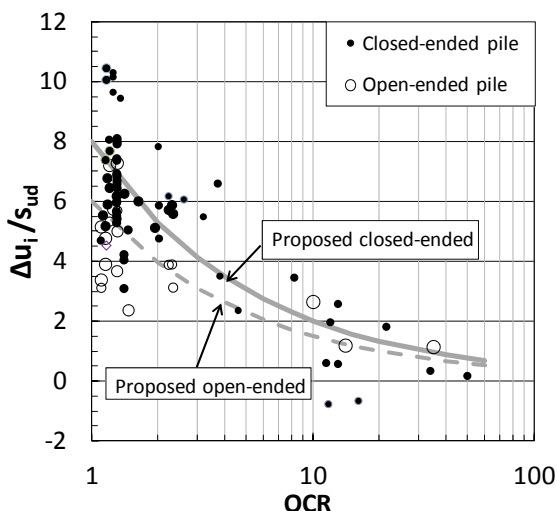

Figure 9.7 –Proposed empirical correlation for predicting excess pore pressure against the pile shaft at end of pile installation

9.4.2 Effective stress at the end of re-consolidation

During the re-consolidation phase the instrumented piles showed that the total earth pressures against the pile in general decreased significantly, but most so for piles in low to moderately OC clays. Figure 9.8 summarizes the measured values of normalized horizontal effective stress after all excess pore pressures set up by the pile installation have dissipated.

The data show large scatter, but with a clear trend for K_c to increase with OCR. There is also a clear trend that measured K_c- values are particularly low for low-plastic clays, and well below in-situ K_0-values. The author has concluded however, that the scatter in measured values of K_c is too large to define any unique correlations to OCR and plasticity index of the clay. That is, as described in Section 9.3.1, one of the reasons for not recommending any method for predicting the ultimate shaft friction that is tied to measured values of K_c.
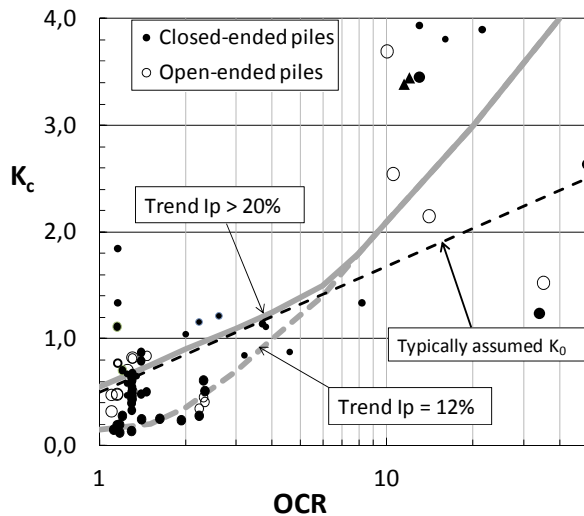

Figure 9.8 – Summary of measured values of horizontal effective stress ratio, K_c, at the end of re-consolidation (at U=100%)

9.4.3 Time for re-consolidation and set-up

The semi-empirical method proposed by the author in Chapter 5 for predicting the time for pore pressure dissipation following pile installation includes the following steps:

1. Use an initial excess pore pressure distribution that decrease linearly with the normalized radial distance, r/r_0.
2. The plasticized radius, r_p, shall be computed according the simple CEM-EP approach and the recommended shear modulus in relation to OCR.
3. Use linear radial consolidation theory assuming that the coefficient of consolidation is constant in time and as function of radial distance from the pile shaft (Figure 5.1.3).
4. Compute the horizontal coefficient of consolidation from the in-situ permeability and an empirically derived oedometer modulus M.
5. To get good match to measured consolidation times the calculated consolidation times shall finally be corrected according to eq. (5.2.2).

This recommended semi-empirical method for predicting consolidation times is found to be reasonably balanced with respect to the effect of OCR and plasticity index of the clay. The same applies to effect of closed-ended versus open-ended piles. The scatter in calculated/measured

consolidation times is however, fairly large (see Figures 5.2.4 to 5.2.7), and shows a standard deviation of the Calculated/Measured ratio of 0.64.

For moderately over-consolidated medium plastic clays, the SPM-MITE3 approach has been shown to give good predictions of the pore pressure dissipation as well as the final effective radial stress.

Immediately after pile installation the pile capacity will correspond to the remoulded undrained strength of the clay. The measurements herein show that in moderately overconsolidated clays the degree of consolidation must exceed 20 to 50 % before the shaft friction increase beyond the remoulded strength. This observation coincides with no measured increase in horizontal effective stresses up to that stage. Through the later stages, the increase in shaft friction can be taken as linear with the degree of consolidation as shown (Figure 6.4.1).

For very stiff and high OCR clays there exists little and conflicting evidence on how the capacity depends on the degree of consolidation. It is therefore for very stiff and high OCR clays difficult to give a very precise and well founded recommendation.

As discussed in Section 6.4.3, there is strong evidence that the pile capacity will continue to increase with time after 100 % re-consolidation is reached, referred to as "ageing" effects. Recent, but still confidential, data generated in NGI's on-going "Time effect piles" project, have fully confirmed that the ageing effect is particularly large for NC low-plastic clays, which in the outset show extremely low shaft friction at the end of the re-consolidation process. In high OCR plastic clays the aging effect is much smaller. These observations broadly agree with the effect of ageing proposed with the NGI-05 method (Karlsrud et al, 2005) as summarized in Section 6.4.3.

9.5 Needs for further improvement sin predictive methods

The author recommends further large scale fully instrumented pile testing to try to improve semi-empirical design methods, as well as to calibrate, verify and improve upon numerical models. Such testing requires great attention to instrumentation details, and especially for measuring total horizontal stresses. New well documented tests on non-instrumented piles will also be of benefit.

It is vital that such new pile tests are accompanied by appropriate laboratory tests to define, in the best possible way, the "true" behaviour of the clay as it is in-situ. This requires high quality sampling, "advanced" laboratory testing like triaxial, DSS and oedometer tests, and coupled with high quality CPTU testing. Ring shear tests may also be useful for stiff high OCR plastic clays.

To promote further understanding, and enable improvement of numerical methods, relevant laboratory tests are needed on clays subjected to various degrees of shear straining and stress changes resulting from the pile installation and re-consolidation phases. One way of inducing, and study effects of, various levels of pre-straining, may be to extrude samples through a tapered cylinder. The extruded sample can then be consolidated to relevant stress levels, and be further built into the triaxial or DSS apparatus for undrained shearing.

The SPM-MITE3 numerical approach (Whittle, 1987) seems so far to be best suited for capturing the complete pile response during installation, re-consolidation and pile loading. The

author still sees a need for further improvements to the MITE3 soil model to ensure that it can properly handle the effect of pile installation on the stress-strain- strength and compressibility characteristics of the clay, and how they vary with radial distance from the pile surface. Rather than trying to capture the effects of large shear strains induced by the pile installation in a single soil model, it may be a better approach to develop a separate model for predicting the behaviour of clays subjected to various degrees of shear straining. This may, for instance, be achieved by grouping the clay behaviour into three main categories; completely remoulded (shear strain above 100 %), severely strained (strains within say 20-100 %) and moderately strained (less than 20 %).

One of the major uncertainties in predicting the time for re-consolidation or set-up seems to lie in determining the in-situ permeability of the clay with sufficient accuracy. It would in this connection be valuable to make further detailed studies and comparisons of permeability of clays as determined indirectly from IL or CRS oedometer tests, or from direct hydraulic conductivity tests in the laboratory and in the field.

Ageing effects can lead to significant further gain in the ultimate shaft friction and pile capacity after the re-consolidation phase is over (i.e. after 100% degree of consolidation is reached), especially in low to moderately plastic clays, and is an aspect that should be accounted for in design. This aspect is being systematically studied through an on-going pile testing program "Time effect piles" as initiated by the author. It is still recommended to carry out further tests to determine ageing effects in a wider range of clay deposits than the four sites covered in this on-going project. It is vital that such testing is carried on an identical set of piles loaded first time to failure at different times after the piles were installed, and not as repeated load testing on the same pile, which can lead to quite misleading results.

Some elements that may be considered for further improvements of the prediction of the load-displacement response of piles in clay are as follows:

- The whole issue of strain softening requires further studies and understanding of how softening may depend on the basic clay characteristics, type of loading applied to a pile, (e.g. rate of loading or rate of displacement), and how this also ties in with strain softening, rate effects and undrained creep effects as observed in undrained laboratory tests.
- Under what conditions strain localization and formation of well defined slip planes may occur, which may affect the potential for strain-softening effects.
- How the basic stress-strain behaviour and undrained shear strength of the clay varies with the distance from the pile surface, considering the effects of pile installation and re-consolidation on these properties, and consequently how this affects the t-z behaviour.

The author recommends parametric studies with programs like PAX2 to look more into the relative effects of cyclic loading for a range of cyclic load levels, clay conditions and pile dimensions. Such parametric studies could well end up in simpler design approaches, relating the relative cyclic design capacity directly to basic soil parameters, relative cyclic load levels and pile stiffness. In this process, it would also be worthwhile to do more verification of programs and design approaches by back-analysis of published cyclic load tests.

References

Aas, G., Lacasse, S., Lunne, T. and Høeg, K. (1986). "Use of In Situ Tests for Foundation Design on Clay." ASCE Conf. in Situ '86, Blacksburg, Virginia, USA, 1968, pp. 1-30.

Aas-Jakobsen, AS (2003[a]). "Bru over Børselva. Vurdering av resultater fra prøvebelastning av peler." Prosjekt nr. 7618. Dok. nr. KK030-G-005, datert 7. desember 2003.

Aas-Jakobsen, AS (2003[b]). "Bru over Vigda. Vurdering av resultater fra prøvebelastning, PDA-målinger og CAPWAP analyse av stålrørspeler." Prosjekt nr. 7616. Dok. nr. KK030-G-006, datert 26. august 2003.

American Petroleum Institute (1978). "Planning, designing and constructing fixed offshore platforms." Recommended practice, API-RP2A, 5th edition.

American Petroleum Institute (1987). "Planning, designing and constructing fixed offshore platforms." Recommended practice, API-RP2A, 17th edition.

American Petroleum Institute (2000 – 2007). Recommended practice for planning, designing and constructing fixed offshore platforms – Working stress design. API RP 2A-WSD 21st ed. 2000, including Errata and Supplement Nos. 1 – 3, 2002-2007.

Andersen, K.H. (1976). "Behaviour of Clay Subjected to Undrained Cyclic Loading". Int. Conf. on the Behaviour of Off-shore Structures. 1. BOSS' 76. Trondheim, 1976, Proc., Vol. 1, pp. 392-403. Also publ. in NGO publ. 114.

Andersen, K.H. (2004). "Cyclic Clay Data for Foundation Design of Structures Subjected to Wave Loading." Invited Keynote Lecture: Int. Conf. on Cyclic Behaviour of Soils and Liquefaction Phenomenon. CBS04, Bochum, Germany. Proc. pp. 371-387. Balkema Publishers.

Andersen, K.H., Hansteen, O.E., Høeg, K. and Prévost, J.H. (1978). "Soil deformations due to cyclic loads on offshore structures." Numerical methods in offshore engineering. Ed. By O.C. Zienkiewicz, R.W. Lewis and K.G. Stagg. Chichester, Wiley, pp. 413-452.

Andersen, K. H. and Stenhamar, P. (1982). "Static plate loading tests on overconsolidated clay." ASCE, Proc. Vol. 108, No. GT 7, pp. 918-934.

Andersen, K.H. and Jostad, H.P. (2002). "Shear Strength Along Outside Wall of Suction Anchors in Clay After Installation." Proc. of the 12th (2002) International Offshore and Polar Engineering Conference (ISOPE), Kyushu, Japan.

Audibert, J.M. E. and Hamilton, T. K. (1998). "West Delta 58A Site Selection Characterization." Proc., Offshore Technol. Conf., Houston 1982, Vol. 1, pp. 415-431.

Augustesen, A.H. (2006). "The effects of time on soil behaviour and pile capacity." DCE Thesis (Ph.D thesis) no 4. Aalborg University, Dept. of Civil Engineering, Aalborg, Denmark, ISSN 1901.

Azzouz, A.S. and Baligh, M.M. (1984). "Behaviour of friction piles in plastic Empire clays." Volume 1. MIT, Dep. og Civ. Eng., Research Report No. R84-14, September 1984.

Azzouz, A.S. and Lutz, D.G. (1986). "Shaft behaviour of a model pile in plastic Empire clays." ASCE. Journal of Geotechnical Engineering, Vol. 112, No. 4, pp. 389-406.

Azzouz, A.S. and Morrison, M.J. (1988). "Field Measurements on Model Pile in Two Clay Deposits," ASCE. Journal of Geotechnical Engineering, Vol. 114, No. 1, pp. 104-121.

Azzouz, A.S., Baligh, M.M. and Whittle, A.J. (1990). "Shaft resistance of piles in clay" J. Geotech. Engng Div., ASCE 116(2), pp. 205-221.

Baligh, M.M. (1975). "Theory of deep static cone penetration resistance". Publication No. R75-56. Dept. of Civil Engineering, MIT, Cambridge, MA.

Baligh, M.M. (1984). "The Simple-pile Approach to Pile Installation in Clays". Analysis and Design of Pile Foundations. Proc. Symp. On Codes and Standards, ASCE National Conv., San Francisco, pp. 310-330.

Baligh, M.M. (1985). "Strain Path Method." J. Geotech. Engng, ASCE 111(9), pp. 1108-1136.

Baligh, M.M., Azzouz, A.S. and Chin, C.T. (1987). "Pore pressure dissipation after cone penetration." Research Report R80-11, Dept. of Civil Engineering, MIT, Cambridge, MA.

Baligh, M.M. and Levadoux, J-N. (1986). "Consolidation after undrained piezocone penetration.
II: Interpretation." ASCE. JGED, Vol. 112, No. 7, pp. 727-744.

Bergfelt, A. (1957). "The axial and Lateral Load Bearing Capacity and Failure by Buckling of Piles in Soft Clay." 4. ICSMFE, Vol. 2, pp. 8-13. London.

Berre, T. (1981). "Triaxial testing at the Norwegian Geotechnical Institute." Norwegian Geotechnical Institute, Oslo. Publication, 134, pp. 7-23. Rev.ed. publ. in: Geotechnical Testing Journal, Vol. 5, 1982, No. ½, pp. 3-17.

Bjerrum, L. (1953). "Les pieux de fondation en Norvege." Institut technique du batiment et des travaux publics. Annales, Vol. 6, No. 63/64, pp. 375-376. Also publ. in: NGI Publ. No. 3.

Bjerrum, L. (1973). "Problems of Soil Mechanics and Construction on Soft Clays". State-of-the-Art Report, Session IV, Proc. 8th Int. Conf. SMFE, Moscow 1973. Also in NGI Publ. 100

Bogard, B. (2001). "Effective Stress Axial Pile Capacity: Lessons from Empire." Proc. Offshore Technol. Conf., Houston 2001. Paper 13059-MS. 12p.

Bogard, D. Matlock, H. (1998[a]). "Static and Cyclic Load Testing of a 30-inch-diameter Pile over a 2.5-year period." Proc., Offshore Technol. Conf. Houston 1998, Vol. 1, pp. 455-468.

Bogard, D. Matlock, H. (1998[b]). "Lateral Pressure Measurements During 2.5 Years of Consolidation Setup." Proc., Offshore Technol. Conf., Houston 1998, Vol. 1, pp. 433-444.

Bogard, J.D. and Matlock, H. (1990). "In-situ Segment Model Experiments at Empire, Louisiana." Proc. Offshore Technol. Conf., Houston 1990, Vol. 2, pp. 459-467.

Bogard, J.D. Matlock, H. (1990). "Application of Model Pile Tests to Axial Pile Design." Proc. 22nd Offshore Technol. Conf., Houston 1990, Vol. 3, OTC Paper 6376, pp. 271-278.

Bogard, J.D., Matlock, H. Chan, H.C. (2000). "Comparison of probe pile tests." ASCE Geot. Special Publ. No.100. Proc. Geo-Denver 2000, pp. 284-296.

Bond, A.J. (1989). "Behaviour of displacement piles in overconsolidated clays." Ph.D. Thesis, Univ. Of London (Imperial College).

Bond, A.J. and Jardine R.J. (1990). "Research on the behaviour of Displacement piles in overconsolidated clay." UK Dept. of Energy. OTH Report, OTH-89 296, HMSO, London.

Bond, A.J. and Jardine R.J. (1995). "Shaft capacity of displacement piles in high OCR clay." Géotechnique, Volume 45, No .1, pp. 3-23.

Broms, B. (1965). "Beräkning av vertikala pålars bärförmåga." Statens Geotekniska Institut, Stockholm. Särtryck och Prelim. Rapp. No. 9. 26p.

Brooker, E.W. and Ireland, H.O. (1965). "Earth pressures at rest related to stress history." Canadian Geotechnical Journal, Vol. 2, No. 1, pp. 1-15.

Burland, J.F., (1973). "Shaft friction of piles in clay; A simple fundamental approach." Ground Engineering, Vol. 6, No. 3, pp. 30-32, 37-42.

Carter, J.P., Randolph, M.F. and Wroth, C.P. (1979). "Driven piles in clay – the effects of installation subsequent consolidation." Géotechnique, Vol. 29, No. 4, pp. 361-393.

Chan, J.H.C. and Birrell, N.D. (1998). "Project Overview Organization - Tension Pile Study."Offshore Technol. Conf. Houston 1998.

Chandler, R.J. (1968). "The shaft friction of piles in cohesive soils in terms of effective stresses." Civ. Eng. Publ. Works Rev. Vol. 63, No. 738, pp. 48-51.

Chaw, F. (1996). "Investigation into the behaviour of displacement piles for offshore structures." Ph.D. Theses submitted to Imprial College, London.

Chen, Y.-J. and Kulhawy, F.H. (1993). "Undrained Strength Interrelationships Among CIUC, UU and UC Tests." ASCE. J. Geot. Eng, Vol. 119, No. 11, pp. 1732-1750.

Chin, C.T. (1986). "Open-ended pile penetration in saturated clays." Ph.D. Thesis, Massachusetts Institute of Technology.

Chow, F.C. (1996), "Data reduction programs for analysis of instrumented pile readings." Imperial College Internal Report, August 1996.

Clarke, J., Long, M.M. and Hamilton, J. (1993). "The Axial Tension Test of an Instrumented Pile in Overconsolidated Clay at Tilbrook Grange." Proc. Conf. Large-Scale Pile Tests in Clay, London 1992, Thomas Telford (publ.), pp. 362-380.

Clausen, C.J.F. (1980). "Documentation of computer program package for structure-pile-soil interaction analysis." Rev. 3 1994. Report No. 8407 (1-10). (Splice a computer program for structure-pile-soil interaction analysis. Report No.8407-2, -6 and -9. 1004-07-01).

Cox, W.R., Cameron, K. and Clarke, J. (1992). "Static and Cyclic Axial Load Tests on Two 762 mm Diameter Pipe Piles in Clays." Proc. Conf. Large-Scale Pile Tests in Clay, London 1992. Publ. by Thomas Telford, pp. 268-284.

Cox, W.R., Kraft, L.M. and Verner, E.A. (1979), "Axial Load Tests on 14-inch Pipe Piles in Clay." Proc., 11th Offshore Technol. Conf., Houston 1979, Vol. 2, pp. 1147-1158.

Coyle, H.M., and Reese, L.C., (1966). "Load transfer for steel piles in clay." Journal of the Soil Mechanics and Foundations Division, ASCE, Vol. 92, No. SM2, pp 1- 26.

Dennis, N.D. and Olson, R.E. (1983). "Axial Capacity of Steel Pipe Piles in Clay." Proc. Geotechnical Practice in Offshore Engineering, Austin, Texas, 1983. Pp. 389-402.

Eide, O., Hutchinson, J.N. and Landva, A. (1961). "Short and Long-term Test Loading of a Friction Pile in Clay." Proc. 5th Int. Conf. Soil Mech. Found. Eng, Paris 1961, pp. 45-53. Also in NGI Publ. no. 45.

Ertec Inc. (1982). Tension pile study. Volume 1. "Site investigation soil characterization study at Block 58." West Delta Area. Gulf of Mexico. 82-200-1, April 1982.

Ertec Inc. (1985). Tension pile study. Volume IV. "Testing of a 30-inch diameter instrumented pile in soil clay." 82-200-4, June 1985.

Ertec Inc. (1986[a]). Tension pile study. Volume V. "In situ model pile experiments in soft clay." 82-200-6, February 1986.

Ertec Inc. (1986[b]). Tension pile study. Volume VII. "Long-term retesting of a 30-inch diameter instrumented pile in soft clay." 82-009-01, (draft), January 1986.

Ertec Inc. (1986[c]). Tension pile study. Vol. VII. "Proposed methods for design of axially loaded piles in normally consolidated clays." 82-200-7, February 1986.

Fellenius, Bror (1955). "Resultat från pålprovningar vid Göteborg C." Kungl. Järnvägsstyrelsen, Stockholm. Geotekniska avdelning. Meddelande, 5. 22p.

Femern A/S (2011). "Ground Investigation Report." Rep. GDR 00.1-001. Prepared by Ramböll Arup Joint Venture

Flaate, K. (1965). "A statistical analysis of some methods for shear strength determination in soil mechanics." Norwegian Geotechnical Institute, Oslo. Publ. No. 62. 8p.

Flaate, K. (1968). "Bearing capacity of friction piles in clay."(In Norwegian), NGF Stipend 1967-1968, Veglaboratoriet, Oslo, 1968. 60p

Flaate, K. (1971). "Effects of pile driving in clays". Canadian Geotechnical Journal, Vol. 9, No. 1, pp. 81-88.

Flaate, K. and Selnes, P. (1977). "Side Friction of Piles in Clay." Proc. 9th Int. Conf. Soil

Mech. Found. Eng, Tokyo 1977. Vol. 1, pp. 517-522. Also in NGI Publ. No. 118.

Francescon, M. (1982). "Model pile tests in clay. Stresses displacements due to installation axial loading." Ph.D. Tesis, Univ. of Cambridge.

Gibbs, C.E., McCauley, J., Mirza, U.A. and Cox, W.R. (1993). "Reduction of Field Data Interpretation of Results for Axial Load Tests of Two 762mm diameter Pipe Piles in Clay." Proc. Conf. Large-Scale Pile Tests in Clay, London, 1992, Thomas Telford (publ.), pp. 285-345.

Gibson, R.E. and Anderson, W.F. (1961). "Insitu measurement of soil properties with the pressure meter." Civ. Eng. Public Works Rev. Vol. 56, pp. 615-618.

Goulois, A.M. (1982). "Contribution to the study of tension piles under cyclic loading." Ph.D. Thesis. Mass Inst. of Techn., Cambridge, Mass.

Goulois, A.M., Whitman, R.W. and Høeg, K. (1985). "Effects of sustained shear stresses on the cyclic degradation of clay." ASTM Special technical publication, 883, pp. 330-351.

Grosch, J.J. and Reese, L.C. (1980). "Field Tests of Small Scale Pile Segments in a Soft Clay Deposit under Repeated Axial Loading." Offshore Techn. Conf., 12. Houston, Texas 1980. Proc., Vol. 4, pp 143-151.

Heydinger, A.G. and O'Neill, M.W. (1986). "Analysis of axial pile-soil interaction in clay."
Int. J. Num. Meth. in Geomech., Vol. 10, No. 4, pp. 367-381.

Hight, D.W., Böese, R., Butcher, A.P., Clayton, C.R.I. and Smith, P.R. (1992). "Disturbance of the Bothkennar clay prior to laboratory testing." Géotechnique, Vol. 42, No. 2, pp. 199-217.

Hight, D.W., Bond, A.J., and Legge, J.D. (1992). "Characterization of the Bothkennar clay: an overview." Géotechnique, Vol. 42, No. 2, pp. 303-347.

Hill, R. (1950). "The mathematical theory of plasticity." Oxford University Press, London. 356p.

Holmquist, D.V., and Matlock, H., (1976). "Resistance-displacement Relationships for Axially-loaded Piles in Soft Clay." Proc., 8th Offshore Technol. Conf., Houston, 1976, Vol. 1, pp 553-569.

Houlsby, G.T. and The, C.I. (1988). "Analysis of the Piezocone in Clay." Proceedings of the International Symposium on Penetration Testing, ISOPT-1, Orlando, Vol. 2, pp 777-83, Balkema Pub., Rotterdam.

Hultin, Torsten, (1928). "Bidrag til kännedomen om friktionspålars bärighet."
Svenska kommunal-tekniska föreningen, Stockholm. Festskrift, pp. 121-144.

Jakobs, P.A. and Coutts, J.S. (1992). "A comparison of electric piezocone tips at the Bothkennar test site." Géotechnique, Vol. 42, No. 2, pp. 369-375.

Janbu, N. (1963). "Soil Compressibility as Determined by Oedometer and Triaxial Tests." Proc. European Conf on Soil Mech. Found. Eng., Wiesbaden 1963. Vol. 1, pp. 19-25.

Janbu, N. (1976). "Static Bearing Capacity of Friction Piles." Proc. ECSMFE, Vol. 1.2, pp 479-488.

Jardine, R.J. (1985). "Investigations of pile-soil behaviour, with special reference to the foundations of offshore structures." Ph.D. Thesis, Univ. Of London (Imperial College).

Jardine, R.J. and Lehane B.M. (1993). "Research into the behaviour of offshore piles: Field experiments in soft clay." Health Safety Executive UK, Offshore Technology Report, 1993.

Jardine, R.J. and Lehane B.M. (1994). "Displacement pile behavior in glacial clay". Canadian Geotechnical Journal, Vol. 31, No. 1, pp. 79-90.

Jardine, R.J. and Chow, F.C. (1996). "New design methods for offshore piles." Marine Technology Directorate Ltd. Publication MTD 96/103, London 1996.

Karlsrud, K. (1986). "Analysis of fundamental aspects of pile-clay interaction under static cyclic axial loading based on field model tests." Norwegian Geotechnical Institute, Oslo. Report 40018-12.

Karlsrud, K. and Haugen, T. (1983). "Cyclic loading of piles and pile anchors – field model tests." Final report. Summary evaluation of test results. Norwegian Geotechnical Institute, Oslo. Report 40010-28.

Karlsrud, K. and Haugen, T. (1984), "Cyclic loading of piles and pile anchors – field model tests – Phase II." Final report. Summary evaluation of test results computational models. Norwegian Geotechnical Institute, Oslo. Report 40018-11.

Karlsrud, K. and Haugen, T. (1985[a]). "Axial static capacity of steel model piles in over-consolidated clay." Proc. 11th Int. Conf. Soil Mech. Found. Eng. San Francisco 1985. Vol. 3, pp. 1401-1406. Also in NGI Publ. No. 163.

Karlsrud, K. and Haugen, T. (1985[b]). "Behaviour of Piles in Clay under Cyclic Axial Loading - results of field model tests." Proc. Int. Conf. on Behaviour of Offshore Structures, 4. BOSS'85. Delft 1985. pp. 589–600.

Karlsrud, K., Nadim, F. and Haugen, T. (1986). "Piles in Clay under Cyclic Axial Loading - Field Tests and Computational Modelling." International Conference on Numerical Methods in Offshore Piling, 3. Nantes 1986. Proc., pp. 165-190. Paris, Editions Technip, 1986. Also publ in: NGI Publ.No.169, 1987.

Karlsrud, K. and Nadim, F. (1990). "Axial Capacity of Offshore Piles in Clay." Proc. Offshore Techn. Conf. Houston 1990. Paper No. 6245. Also in NGI Publ. No.188.

Karlsrud, K., Hansen, S.B., Dyvik, R. and Kalsnes, B. (1993). "NGI's Pile Tests at Tilbrook and Pentre - Review of Testing Procedures and Results." Proc. Conf. on Recent Large Scale Fully Instrumented Pile Tests in Clay. Thomas Telford Ltd., pp. 405-429. Also in NGI Publ. No. 188.

Karlsrud, K., Kalsnes, B. and Nowacki, F. (1993). "Response of Piles on Soft Clay Silt Deposits to Static Cyclic Loading Based on Recent Instrumented Pile Load Tests". Proc., Conference on Offshore Site Investigation Foundation Behavior, London 1992. Society for Underwater Technology, pp. 515-537.

Karlsrud, K., Lunne, T., Kort, D.A. and Strandvik, S. (2005). "CPTU Correlations for Clays." Proc. Int. Conf. on Soil Mech. Found. Eng., 16. Osaka 2005. Vol. 2, pp. 683-702.

Karlsrud, K., Clausen, C.J.F. and Aas, P.M. (2005). "Bearing Capacity of Driven Piles in Clay, the NGI Approach." Proc. Int. Symp. on Frontiers in Offshore Geotechnics, 1. Perth 2005. pp. 775-782.

Karlsrud, K. and Hernandez-Martinez, F.G. (2012). "Stress-strain-and strength characteristics of clays from high quality block samples". To be published.

Kavvadas, M. (1982). "Non-linear consolidation around driven piles in clays." ScD Thesis, Dept. of Civil Engineering, MIT, Cambridge, MA.

Kirby, R.C. and Wroth, C.P. (1977). "Application of Critical State Soil Mechanics to the Prediction of Axial Capacity for Driven Piles in Clay." Offshore Technol. Conf. 9. Houston 1977. Proc., Vol. 3, pp. 483-494.

Kolk, H.J. and Velde, E.v.d. (1996). "A Reliable Method to Determine Friction Capacity of Piles driven into Clays." Proc. Offshore Technol. Conf. Houston 1996. Paper No. 7993.

Konrad, J.-M. and Roy, M. (1987). "Bearing capacity of friction piles in marine clay." Geotechnique, Vol. 37, No. 2, pp. 163-175.

Kraft, L.M. (1982). "Effective stress capacity model for piles in clay." ASCE Journal of Geotechnical Engineering, Vol. 108, No. 11, pp. 1387-1404.

Kraft, L.M., Esrig, M.I. and Murphy, B.S. (1980). "Amoco effective stress axial capacity cooperative program." ESAAC project summary report. Prepared for Amoco Production Co.

Kraft, L.M., Ray, R.P. and Kagawa, T. (1981). "Theoretical t-z curves." ASCE. Proc., Vol. 107, No. GT. 11, pp. 1543-1561.

Kraft L.M., W.R. Cox & E.A. Verner (1981)." Pile Load Tests: Cyclic Loads and Varying Load Rates." ASCE, JGED, Vol. 107, No. GT1, pp 1-19.

Lacasse, S. (1979). "Gravity platforms – evaluation of plate loading tests. Undrained behavior of Haga clay from static simple shear and trivial tests." NGI Internal Rep. 51507-14, September 1979.

Lacasse, L., Berre, T. and Lefebvre,G. (1985). "Block Sampling of Sensitive Clays." Proc. Int. Conf. on Soil Mech. Found. Eng. 11. San Francisco 1985. Vol. 2, pp. 887- 892. Also publ. in: NGI Publ.No163

Ladanyi, B. (1963). "Expansion of a cavity in a saturated clay medium." ASCE. Proc., Vol. 89, No. SM 4, pp. 127-161.

Ladanyi, B., (1967). "Deep Punching of Sensitive Clays".
Presented at the 3. Panamerican Conf. on Soil Mech. and Found. Eng. Caracas 1967.

Ladd, C.C. and Edgers, L. (1972). "Consolidated-undrained direct-simple shear tests on saturated clays." Massachusetts Institute of Technology, Cambridge, Mass. Department of Civil Eng. Research report, R72-82 – Soils publication, 248.

Ladd, C.C. and Foott, R. (1974). "New design procedure for stability of soft clays." ASCE Journal of Geotechnical Engineering, Vol. 100, No. 7, pp 763-786.

Ladd, C. C., Foott, R., Ishihara, K., Schlosser, F. and Poulos, H.G. (1977). "Stress-Deformation and Strength Characteristics." State-of-the-Art Report. Proc. Int. Conf. Soil Mech. Found Eng. 9. Tokyo 1977. Vol. 2, pp. 429-494.

Ladd, C.C. and DeGroot, D.J. (2003). "Recommended Practice for Soft Ground Site Characterization": Arthur Casagrande lecture. Proc. Panamerican Conf. on Soil Mech. Geotechn. Eng, 12. MIT, Cambridge Mass., 2003. Vol. 1, pp. 3-57.

Lambson, M.D., Clare, D.G. and Semple, R.M. (1993). "Investigation Interpretation of Pentre and Tilbrook Grange Soil Conditions." Proc. Conf. Large-scale Pile Tests in Clay, London 1992, Thomas Telford (publ), pp. 134-196.

Lehane, B.M. (1992). "The behaviour of a displacement using instrumented field piles." Ph.D. Thesis, Univ. of London (Imperial College).

Lehane, B.M. and Jardine, R.J. (1992)."The Behaviour of Displacement Piles in Glacial Till." Behaviour of Offshore Structures, BOSS'92, Proc., BPP Technical Services, Vol. 1, p. 555.

Lehane, B.M. and Jardine, R.J. (1994). "Displacement-pile behaviour in soft marine clay." Canadian Geotechnical Journal, Vol. 31, No. 2, pp. 181-191.

Leroueil, S., Samson, L. and Bozozuk (1983). "Laboratory and field determination of preconsolidation pressures at Gloucester." Canadian Geotechnical Journal, Vol. 20, No. 3, 1983.

Levadoux, J-N. (1980). "Pore pressures in clays due to cone penetration." Ph.D. Thesis, Dept. of Civil Engineering, MIT, Cambridge, MA, 752 p.

Liyanapathirana, D.S. (2004). "A Numerical Model for Predicting Pile Set-Up in Clay." Proc. GeoCongress, New Orleans 2008. ASCE. Geotechnical Special Publication No. 179, pp. 710-717.

Lunne, T., Lacasse. S Rad N.S. (1989). "SPT, CPT, Pressure Meter Testing and Recent Developments on In Situ Testing of Soils." General Report. Proc. Int. Conf. on Soil Mech. Found. Eng., 12. Rio de Janeiro 1989, Vol. 4, pp. 2339-2448.

Lunne, T., Robertson, P.K. and Powell, J.J.M. (1997). "Cone Penetration Testing." Blackie Academic & Professional – an imprint of Chapman & Hall. 1997.

Lunne, T. Berre, T. and Strandvik, S. (1997). "Sample Disturbance Effects in Soft Low Plastic Norwegian Clay." Proc. Conf. on Recent Developments in Soil Pavement

Mechanics, Rio de Janeiro 1997, pp. 81-102.

Lunne, T., Berre, T., Andersen, K.H., Strandvik, S. and Sjursen, M. (2006). "Effects of sample disturbance and consolidation procedures on measured shear strength of soft marine Norwegian clays." Canadian Geotechnical Journal, Vol. 43, No. 7, pp. 726-750.

Lunne, T. and Andersen, K.H. (2007). "Soft Clay Shear Strength Parameters for Deepwater Geotechnical Design." Proceedings of the 6th Int. Offshore Site Investigation and Geotechnics Conference: Confronting New Challenges and Sharing Knowledge, 2007, London, UK

Lunne,T., Berre, T.,Andersen, K.H., Sjursen and M. Mortensen, N. (2008). "Effects of Sample Disturbance on Consolidation Behavior of Soft Marine Norwegian Clays." Geotechnical and Geophysical Site Characterization: Proc. of the Third International Conference on Site Characterization ISC'3, Taipei, Taiwan 2008. CD, pp. 1471-1479.

Matlock, H. and Holmquist, D.V. (1976). "A model study of axially loaded piles in soft clay." University of Texas at Austin. Report to API.

Matlock, H., Lam, I. and Cheang, L. (1982). "Analytical Interpretation of Pile Installation and Axial Performance." Int. conf. on Numerical Methods in Piling, 2. Austin, Texas 1982. Proc., pp. 133-162.

Matsuoka, H., Iwata, Y. and Sakaibara, K. (1986). "A Constitutive Model of Sands and Clays for Evaluating the Influence of Rotation of Principal Stress Axis." Proc. Int. Symp. on Num. Models in Geomech., 2. Ghent, Belgium 1986.

Mayne, P.W. and Kulhawy, F.H. (1982). "K0-OCR relationships in soil." American Society of Civil Engineers. Proceedings, Vol. 108, No. GT 6, pp. 851-872.

McClelland Ltd. (1988[a]). "Large diameter pile testing program." Soil and foundation investigation Tilbrook site – Final report to BP Int., June 1988.

McClelland Ltd. (1988[b]). "Large diameter pile tests program. Tilbrook pile tests, results, analyses and interpretations." Report to BP Int., December 1988.

Mesri, G., Feng, T.W., (1992). "Constant rate of strain consolidation testing of soft clays." Invited lecture. Marsal Volume, Mexico City, pp. 49-59.

Meyerhof, G.G. (1976). "Bearing capacity and settlement of pile foundations." ASCE. JGED. Vol. 102, No. 3, pp. 197-228.

Morrison, M.J. (1984). "In situ measurements on model piles." Ph.D. Thesis. Massachusetts Institute of Technology, Cambridge, Mass. Department of Civil Engineering.

Mullis, C.R. (1993). "Large Diameter Pile Test Project – Overview."Proc. Int. Conf. on Recent Large Scale Fully Instrumented Pile Tests in Clay, London, Instn. Civ. Engrs./Thomas Telford Ltd.

Nadim, F., Gabr, M. and Hansen, B. "Sensitivity study of the cyclic axial capacity of a single pile." Proc. ASCE Found. Eng. Cong., Evanson, Illinois, 1989.

Nash, D.F.T., Powell, J.J.M. and Lloyd, I.M. (1992), "Initial investigations of the soft clay test site at Bothkennar." Géotechnique, Vol. 42, No. 2, pp. 163-181.

Nordal, S. (1985). PIA2 – Versjon 02. Users Manual. A program for pile soil interaction, Part 1, Horizontal load. SINTEF Report STF69 F85004.

Norwegian Geotechnical Institute (1973[a]). "Grunnundersøkelser i forbindelse med prøvefyllingen i Onsøy." NGI Internal Report 50322-1, april 1973.

Norwegian Geotechnical Institute (1973[b]). "Simple shear tests (CCV) on plastic clay from Onsøy". NGI Internal Report 50322-3, September 1973.

Norwegian Geotechnical Institute (1973[c]). "Standard undrained triaxial tests on plastic clay from Onsøy." NGI Internal Report 50322-2, November 1973.

Norwegian Geotechnical Institute (1973[d]). "Oedometer tests on plastic clay from Onsøy." NGI Internal Report 50322-4, November 1973.

Norwegian Geotechnical Institute (1985[a]). "Oedometer testing at the Norwegian Geotechnical Institute." NGI Report 56300-9. Rev. April 1985.

Norwegian Geotechnical Institute (1985[b]). "In situ site investigation techniques and interpretation for offshore practice. Interpretation of piezocone tests in Onsøy and Haga sites." NGI Report 40019-23, December 1985.

Norwegian Geotechnical Institute (1985[c]). "In situ site investigation techniques and interpretation. Laboratory tests on Onsøy clay." NGI Report 40019-17, December 1985.

Norwegian Geotechnical Institute (1986[a]). "Design of offshore piles in clay – Field tests and computational modelling." Results of laboratory tests. NGI Report 52523-3, April 1986.

Norwegian Geotechnical Institute (1987). "Design of offshore piles in clay – Field tests and computational modelling. " Summary, interpretation and analyses of the pile load tests at the Onsøy test site. NGI Report 52523-23, December 3rd 1987, Revised March 1988.

Norwegian Geotechnical Institute (1988). "Design of offshore piles in clay – Field tests and computational modelling." Summary, interpretation and analyses of the pile load tests at the Lierstranda test site. NGI Report 52523-26, March 25th 1988, Revised 1988.

Norwegian Geotechnical Institute (1988). "Design of offshore piles in clay – Field tests and computational modelling." Summary, interpretation and analyses of the pile load tests at the Pentre test site. NGI Report 52523-27, April 29th 1988, Revised August 1988.

Norwegian Geotechnical Institute (1988). "Design of offshore piles in clay – Field tests and computational modelling. " Final report. Summary and recommendations. NGI Report

52523-28, April1988, Revised September 1988.

Norwegian Geotechnical Institute (1989[a]). "Pile load tests West Delta – Review and assessment of reliability of test data." NGI Report 882016-1, Revision 1, 1989.

Norwegian Geotechnical Institute (1989[b]). "Pile load tests West Delta – Review of analytical models." NGI Report 882016-2, 1989.

Norwegian Geotechnical Institute (1989[c]). "Pile load tests West Delta – Supplementary laboratory tests and interpretation of soil data." NGI Report 882016-3, 1989.

Norwegian Geotechnical Institute (1989[d]). "Pile load tests West Delta – Analyses and comparisons to other test results." NGI Report 882016-4, 1989.

Norwegian Geotechnical Institute (1989). "Pile load tests in stiff clay – Presentation of data from tests at Tilbrook Grange." NGI Report 885032-1, 1989.

Norwegian Geotechnical Institute (1991). "Pile load tests in stiff clay – phase II." Summary and evaluation of NGI's pile tests at Tilbrook Grange. NGI Report 885032-2, 1989. Revised 1991.

Norwegian Geotechnical Institute (1996). "The development of semi empirical design procedures for foundations". Factual report on in situ testing at Lierstranda. For EU; Report T3-07. NGI Internal Report 521551- 09, 1996.

Norwegian Geotechnical Institute (1996). "Optimal use of soil data from deep water sites." NGI Internal Report 521676-4, 1996.

Norwegian Geotechnical Institute (1996). "Optimal use of soil data from deep water sites." Analyses and Recommendation Report. NGI Internal Report 521676-5, 1996.

Norwegian Geotechnical Institute (2002). "Quality of CPTU". Statistical analyses of CPTU data from Onsøy. NGI Report No. 20001099-2, 2002.

Norwegian Geotechnical Institute (2003). "Deformasjonsparametere for bruk i geotekniske beregninger." Prosjekt 20011284: E18 Bjørvika – Revidert reguleringsplan. Teknisk Notat 2-G-201.

Norwegian Geotechnical Institute (2011). "Data base for tests on high quality block samples on clay. Summary of compressibility, strength and deformation parameters in relation to index properties". Report 20051014-1, 2011.

Olson, R.E. and Dennis, N.D. (1982). "Review and compilation of Pile Test Results, Axial Pile Capacity." Final Report to API on Project PRAC 81-29, Univ. Texas at Austin.

O'Neill, M.W. "Program PILGPI User's Guide", Univ. of Houston, Civ. Engrg. Dept., Houston, Texas 1980.

O'Neill, M.N., Hawkins R.A. and Audibert, J.M. (1982). "Installation of pile group in overconsolidated clay." ASCE. Journal of the Geotechnical Engineering, Vol. 108, no. GT 11, pp. 1369-1386.

O'Neill, M.W., Hawkins, R.A. and Mahar, L.J. (1982). "Load Transfer Mechanisms in Piles and Pile Groups." ASCE, JGED, Vol. 108, No. GT12, 1982, pp 1605-1623.

Ove Arup and Partners (1988). "Tension and lateral pile tests at Tilbrook Grange." Report prepared for BP-International, dated November 1988.

Pelletier, J.H., Murf, J.D. and Young, A.C. (1993). "Historical Development and Assessment of the Current API Design Method for Axially Loaded Pipes." Proc. Offshore Technol. Conf. Houston 1993. pp. 253-282.

Poskitt, T., Yip-Wong, K. and Cox, W. (1993), "Measurement of Axial Strain Pile Wall Displacement, Determination of Skin Friction During the Driving of Instrumented Piles." Proc. Conf. Large-scale Pile Test in Clay, London 1992, Thomas Telford (publ.), pp. 250-267.

Poulos, H.G. (1982). "Influence of Cyclic Loading on Axial Pile Response." Int. Conf. on Numerical Methods in Offshore Piling, 2. Austin, Texas 1982. Proc., pp. 419-440.

Puech, A.A. (1982). "Basic Data for the Design of Tension Pile in Salty Soils." Int. Conf. on the behaviour of off-shore structures, 3. BOSS'82. Cambridge, Mass. 1982. Proc., Vol. 1, pp. 141-157.

Randolph, M.F. (2003). "Science and empiricism in pile foundation design." Géotechnique Vol. 53, No. 10, pp. 847-875.

Randolph, M.F., Carter, J.P. and Wroth, C.P. (1979), "Driven piles in clay: Effects of installation subsequent consolidation." Géotechnique Vol. 29, No. 4, pp. 361-393.

Randolph, M.F. and Wroth, C.P. (1978). "Analysis of deformation of vertically loaded piles." ASCE. JGED, Vol. 104, No. GT12, 1978, pp 1465-1488.

Randolph, M.F. and Wroth, C.P. (1979). "An analytic solution for the consolidation around a driven pile." Int. J. for Numerical and Analytic Methods in Geomechanics, Vol. 3, No. 3, pp. 217-229.

Randolph, M.F. and Wroth, C.P. (1981). "Application of the failure state in undrained simple shear to the shaft capacity of driven piles." Geotecnique, Vol. 31, No. 1, pp. 143-157.

Randolph, M.F. and Murphy, B.S. (1985). "Shaft Capacity of Driven Piles in Clay." OTC Paper 4883, Houston, 1985.

Roscoe, K.H. and Barland, J.B. (1968). "On the Generalized Behaviour of Wet Clays." Engineering Plasticity, Eds. J. Heymann and F.A. Leckie, Cambridge University Press, pp. 535-609.

Roy, M., Blanchet, R., Tavenas, F. and LaRochelle, P. (1981). "Behaviour of sensitive clay during pile driving." Canadian Geotechnical Journal, Vol. 18, No. 1, pp. 67-85.

Roy, M. and Lemieux, M. (1985). "Long-term behaviour of reconsolidated clay around a driven pile." Canadian Geotechnical Journal, Vol. 23, No. 1, pp. 23-29.

Sandbækken, G., Berre, T. and Lacasse, S. (1985). "Oedometer testing at the Norwegian Geotechnical Institute." Consolidation of soils: Testing and Evaluation. A symposium, Fort Launderdale, Florida 1985. ASTM STP 892, pp. 329-353.

Sällfors, G. (1975). "The Preconsolidation Pressure of a High Plastic Clay – a comparison between field and laboratory test." Proc. Nordic Geotech. Meeting, Copenhagen 1975, pp. 143-154.

Schofield, A.N. and Wroth, C.P. (1968). "Critical state soil mechanics." McGraw-Hill, London. 310p.

Semple, R.M. and W.J. Rigden (1984). "Shaft Capacity of Driven Pipe Piles in Clay." Proc. Symp. on Analysis and Design of Pile Foundations, ASCE, San Francisco 1984. Pp. 59-79.

Senneset, K., Janbu, N. and Svanø, G. (1982). "Strength and Deformation Parameters from Cone Penetration Tests." Proceedings of the 2nd European Symposium on Penetration Testing, ESOPT, Amsterdam, Vol. 2, pp. 863-70, Balkema Pub., Rotterdam.

SINTEF (1999). GROUP/PSI – A pile group analysis program. User's Manual. Report STF22 F99617.

Skaven-Haug, S. (1940). "Svevende trepelers bæreevne i leire." NSB, Oslo. Meddelelser, Vol. 15, No. 2. 7p.

Soderberg, L.O. (1962). "Consolidation theory applied to foundation pile time effects." Géotechnique, Vol. 12, No. 3, pp. 217-225.

Solomon, I.J., Cox, W.R., Clarke, J. and Poskitt, T.J. (1993). "The Development of Instrumentation for Drivability Testing Load Testing of Large Diameters Piles." Proc. Conf. on Recent Large Scale Fully Instrumented Pile Test in Clay, London 1992, Thomas Telford (publ.), pp. 197-216.

Steenfelt, J.S., Randolph, M.F. and Wroth, C.P. (1981). "Instrumented Model Piles Jacked into Clay". Proc. Int. Conf. on Soil Mech. Found. Eng., Stockholm 1981, Vol. 2, pp. 857-864.

Tavenas, R., Jean, P., Leblond, P. and Leroueil, S., (1983). "The permeability of natural soft clays. Part II: Permeability characteristics." Canadian Geotechnical Journal, Vol. 20, No. 4, pp. 645-660.

Taylor, D.W. (1948). "Soil Mechanics." John Wiley and Sons, Inc. New York, pp. 648-654.

Tomlinson, M.J., (1957). "The Adhesion of Piles Driven in Clay Soils."
Proc. Int. Conf. on Soil Mech. Found. Eng. 4, London 1957.Vol. 2, pp. 66-71.

Torstensson, B-A., (1973). "The Behaviour of a Cohesion Pile Group in Soft Clay."
Proc. Int. Conf. on Soil Mech. Found. Eng. 8. Moskva 1973. Vol. 2.1, pp. 237-242.

Torstensson, B-A. (1977). "The pore pressure probe." Norsk jord- og fjellteknisk forbund. Fjellsprengningsteknikk – bergmekanikk – geoteknikk 1977. Foredrag, pp. 34.1-34.15.

Trondheim, Tapir.

Veritec (1984). Tension pile study CNRD 13-2. Final report with Appendices A-E F-L. 84-3861, Revised 1985.

Vesić, A.S. (1972). "Expansion of cavities in infinite soil mass."
J. Soil Mech. and Found. Div., ASCE. Vol. 98, No. SM3, pp. 265-290.

Vijayvergiya, V.N. and Focht Jr, J.A. (1972). "A New Way to Predict Capacity of Piles in Clay." Proc. Offshore Technol. Conf., Houston 1972. Paper OTC 1718.

Wendel, E. (1900). "Om profbelastning på pålar med tillämpning deraf på grundläggningsförhållena i Göteborg." Tekniska samfundet i Göteborg. Handlingar. Göteborg.

Whittle, A.J. (1987). "A constitutive model for overconsolidated clays with application to the cyclic loading of friction piles." Ph.D Thesis, Massachusetts Institute of Technology.

Whittle, A.J. (1992). "Assessment of an effective stress analysis for predicting the performance of driven piles in soft clay." Proc. Conf. on Offshore Site Investigation and Foundation Behaviour, London 1992: Society for Underwater Technology, Kluwer Academic Publishers, pp. 607-644.

Woodward-Clyde Consultants (1979). "ESSAC project. Evaluation of prediction methods. Field model pile load tests Hamilton Airforce Base, Novato California." Report prepared for Amoco Production Company, Nov. 1979.

Wroth, C.P., Carter, J.P. and Randolph, M.F. (1979). "Stress Changes around a Pile Driven into Cohesive Soil." Proc., Conf. on Recent Developments in the Designs and Construction of Piles, Inst. of Civil Engineering, London, pp. 345-354.

Zeevaert, L. (1950). Discussion on "Effect of driving piles into soft clay."
ASCE. Transactions, vol. 115, pp. 286-292, New York.

SYMBOLES

ENGLISH

a	=	Attraction (=c' cot Φ', in terms of effective stress).
c	=	Cohesion
c	=	Coefficient of consolidation
c_v	=	Vertical coefficient of consolidation
c_h	=	Horizontal coefficient of consolidation
c_c	=	Compression index
e	=	Void ratio
e_o	=	Initial void ratio
E	=	Young's modulus
E_{50}	=	Secant modulus at 50% of maximum stress
G	=	Shear modulus
G	=	Specific weight
I_p	=	Plasticity index
k	=	Coefficient of permeability, hydraulic conductivity
k_0	=	Coeficient of peremeability at zero volume change
K_o	=	Coefficient of earth pressure at rest = $\sigma`_{ho}/ \sigma`_{vo}$
K_c	=	Horisontal (radial) effective stress ratio after full re-conmsolidation
K_i	=	Horisontal (radial) effective stress ratio at end of pile installation
L	=	Length
L/D		Pile length/pile diameter
LI	=	Liquidity index =$(w - w_p)(w_L - w_p)$
m	=	Power in SHANSEP equation
m	=	Dimensionless deformation modulus number
m_0	=	Valume of m when p'_r is assumed zero
M	=	Oedometer modulus
N_{kt}	=	Cone factor tip resistance
$N_{\Delta u}$	=	Cone factor pore pressure
p'_r	=	reference pressure for modulus number concept
P'_{cv}	=	Vertical effective preconsolidation stress
P'_{ch}	=	Horizontal effective preconsolidation stress
Q	=	Axial load at pile capacity
Q_{ave}	=	Average axial load at pile top during a cyclic lest
Q_{max}	=	Maximum axial load at pile top during a cyclic lest
Q_{min}	=	Minimum axial load at pile top during a cyclic lest
Q_{us}	=	Ultimate pile shaft friction capacity
Q_{ult}	=	Ultimate total pile axial capacity
q_c	=	Measured cone resistance
q_t	=	Corrected cone resistance = $q_c + (1 - a)u_2$
r	=	Radial distance from center of pile
r_i	=	Inner pile radius
r_o	=	Outer pile radius
r_p	=	Radius of plastic zone
s_u	=	Undrained shear strength

s_{ur}	=	Remoulded undrained shear strength
s_{uc}	=	Undrained shear strength from triaxial compression test
s_{ue}	=	Undrained shear strength from triaxial extension test
s_{ud}	=	s_u from direct simple shear test
s_{ue}	=	s_u from triaxial extension test
s_{uv}	=	s_u from vane boringt
S	=	Normalized undrained strength for OCR=1 (SHANSEP)
S_t	=	Sensitivity
T	=	Time factor
T^*	=	Modified time factor
t	=	Time
t_{50}	=	Time for 50 % dissipation of excess pore water
t_{90}	=	Time for 90 % dissipation of excess pore water
t_f	=	Time to failure
u	=	Pore water pressure
u_o	=	*In situ* pore pressure
u_i	=	Pore pressure at time $t = 0$
Δu	=	Excess
U	=	Normalized excess pore pressure (degree of dissipation)
w	=	Water content
w_L	=	Liquid limit
w_p	=	Plastic limit
x	=	Depth below pile top
z	=	Depth
Δz	=	Thickness of sublayer

GREEK

α	=	Ultimate shaft friction normalized to undrained strength
β	=	Ultimate shaft friction normalized to vertical effective stress
γ	=	Shear strain
γ'	=	Effective unit weight
$\dot{\gamma}$	=	Rate of shear strain
γ_t	=	Total unit weight
γ_w	=	Unit weight of water
γ_{ave}	=	Average shear strain in cyclic DSS test
γ_{cy}	=	Cyclic shear strain in cyclic DSS test
γ_{rz}	=	Shear strain in the r-z plane
δ	=	Axial pile top displacement
δ_{acc}	=	Accumulated axial pile top displacement during cyclic part of load test
δ_{ave}	=	Total accumulated axial pile top displacement during cyclic load test
δ_c	=	Cyclic axial pile top displacement amplitude during cyclic load test
$\dot{\delta}$	=	Axial pile top displacement, rate of displacement (sustained static loading)
φ	=	Effective friction angle
ε	=	Strain
ε_c	=	Axial strain during consolidation

ε_v	=	Volumetric strain
ρ_H	=	Mobilized friction angle on the horizontal plane in a DSS-test
ρ	=	Mobilized friction angle on the pile/clay interface
σ'_a	=	Axial effective stress in a DSS-test
σ'_c	=	Effective consolidation stress in a DSS- or SB-test
σ'_r	=	Effective radial (horizontal) stress on the pile surface during testing
σ'_{ri}	=	Effective radial (horizontal) stress on the pile surface at end of installation
σ'_{re}	=	Effective radio (horizontal) stress on the pile surface at start of pile loading
σ'_{ho}	=	In-situ effective horizontal stress
σ'_{vc}	=	Vertical consolidation stress
σ'_{vo}	=	In-situ effective vertical stress
σ_1, σ'_1	=	Major principal stress (total, effective)
σ_2, σ'_2	=	Intermediate principal stress (total, effective)
σ_3, σ'_3	=	Minor principal stress (total, effective)
σ_h, σ'_h	=	Horizontal stress (total, effective)
$\sigma_{ho}, \sigma'_{ho}$	=	Initial horizontal stress (total, effective)
σ_v, σ'_v	=	Vertical stress (total, effective)
$\sigma_{vo}, \sigma'_{vo}$	=	Overburden stress (total, effective)
τ	=	Shear stress
τ_0	=	Initial shear stress a sample is consolidated under
τ_{av}	=	Average shear stress in cyclic DSS test
τ_{cy}	=	Cyclic shear stressamplitude in cyclic DSS test
τ_f	=	Horizontal shear stress at failure in a DSS- or SB-test
τ_h	=	Horizontal shear stress in a DSS- or SB-test
τ_s	=	Shear stress on pile surface (shaft friction)
τ_{us}	=	Ultimate shaft friction on pile surface at failure
$\bar{\tau}_{us}$	=	Overall average ultimate shaft friction over length of pile

ABBREVIATIONS

ASCE	=	American Society of Civil Engineers
BRE	=	Building Research Establishment
CAUC	=	Anisotropic Consolidated Undrained Triaxial Test Sheared in Compression
CAUE	=	Anisotropic Consolidated Undrained Triaxial Test Sheared in Exetension
CEM	=	Cavity Expansion Method
CPTU	=	Cone Penetration Test with Pore Pressure Measurement (Piezocone test)
CRS	=	Constant Rate of Strain oedometer test
CSSM	=	Critical State Soil Mechanics
DSS	=	Direct Simple Shear
EP	=	Linear Elastic perfectly Plastic soil model
ESM	=	Efective Stress Method
GWT	=	Ground Water Table
IC	=	Imperial College
MCC	=	Modified Cambridge Clay model
MIT	=	Massachusetts Institute of Technology
MITE1-3	=	Effective stress based clay models developed at MIT
NC	=	Normally Consolidated
NGI	=	Norwegian Geotechnical Institute
OCR	=	Overconsolidation ratio
SB	=	Shear Box
SPM	=	Strain Path Method
UU	=	Undrained, unconsolidated triaxial test

Appendix 1

Summary tables with measured data from installation

and re-consolidation phase-

Instrumented pile tests

Test Site	Pile Name	D (mm)	t (mm)	R_{eq} (mm)	Depth (m)	w (%)	I_p (%)	u_0 (kPa)	σ'_{v0} (kPa)	p'_c (kPa)	OCR	K_0	s_{ud} (kPa)	s_{ud}/σ'_{v0}	Perm. k_0 (m/s)	Mod. no. m_0	Δu_i (kPa)	$\Delta u_i/s_{ud}$	$\Delta u_i/\sigma'_{v0}$	σ'_{ri} (kPa)	K_i
Haga	B-piles	154	4.5	76.5	1.9	35	11		39	320	8.21	1.52	41.5	1.064	7.00E-10	16	144	3.47	3.69	3	0.08
		154	4.5	76.5	3.4	40	15		73	270	3.70	0.87	41	0.562	9.00E-10	16	271	6.61	3.71	3	0.04
Onsøy	A1	219	8.2	109.5	7.5	64	37	73.3	52	76	1.46	0.64	15	0.288	2.00E-09	7	76	5.05	1.46	-2	-0.04
		219	8.2	109.5	10	68	40	101.5	64	83	1.30	0.62	17.5	0.273	1.00E-09	6.3	96	5.51	1.51	-6	-0.09
Onsøy	A2	219	8.2	109.5	12.5	65.5	42.5	129.7	76	99	1.30	0.615	21	0.276	9.00E-10	6.6	135	6.44	1.78	1	0.01
		219	8.2	109.5	15	63	45	157.9	88	114	1.30	0.61	23	0.261	8.00E-10	6.8	130	5.66	1.48	1	0.01
		219	8.2	109.5	17.5	62.5	46	186.1	100	130	1.30	0.6	26	0.260	7.70E-10	7	161	6.19	1.61	0	0.00
Onsøy	A3	219	8.2	109.5	20	62	47	214.3	112	146	1.30	0.6	28	0.250	8.00E-10	7.2	222	7.92	1.98	-4	-0.04
		219	8.2	109.5	22.5	58	44.5	242.5	125	163	1.30	0.595	31.5	0.252	7.20E-10	7.4	210	6.68	1.68	19	0.15
		219	8.2	109.5	25	54	42	270.7	139	180.5	1.30	0.59	34.5	0.248	7.00E-10	7.65	254	7.37	1.83	9	0.06
Onsøy	A4	219	8.2	109.5	27.5	53.5	42	298.9	152	197.5	1.30	0.58	38	0.250	6.80E-10	7.9	282	7.42	1.86	-5	-0.03
		219	8.2	109.5	30	53	42	327.1	166	216	1.30	0.58	42	0.253	6.60E-10	8.15	288	6.85	1.73	-28	-0.17
		219	8.2	109.5	32.5	52.2	41	355.3	180	234	1.30	0.57	45.5	0.253	6.40E-10	8.4	315	6.92	1.75	-6	-0.03
		219	8.2	109.5	35	52	40	383.5	195	254	1.30	0.57	49	0.251	6.20E-10	8.65	391	7.99	2.01	-25	-0.13
Onsøy	B1(open)	809	9.5	87.2	7.5	64	37	73.3	52	76	1.46	0.64	15	0.288	2.00E-09	7	36	2.38	0.69	-19	-0.37
		809	9.5	87.2	10	68	40	101.5	64	83	1.30	0.62	17.5	0.273	1.00E-09	6.3	64	3.68	1.01	-11	-0.17
		809	9.5	87.2	12.5	65.5	42.5	129.7	76	99	1.30	0.615	21	0.276	9.00E-10	6.6	105	5.01	1.39	-11	-0.14
Onsøy	CI	219	8.2	109.5	10	68	40	101.5	64	83	1.30	0.62	17.5	0.273	1.00E-09	6.3	92	5.28	1.45	-20	-0.31
	CI	219	8.2	109.5	15	63	45	157.9	88	114	1.30	0.61	23	0.261	8.00E-10	6.8	137	5.96	1.56	-12	-0.14
	CI	219	8.2	109.5	20	62	47	214.3	112	146	1.30	0.6	28	0.250	7.50E-10	7.2	152	5.42	1.35	-4	-0.04
	CI	219	8.2	109.5	25	54	42	270.7	139	180.5	1.30	0.59	34.5	0.248	6.60E-10	8.15	206	5.98	1.48	-2	-0.01
	CI	219	8.2	109.5	30	53	42	327.1	166	216	1.30	0.58	42	0.253	6.60E-10	8.15	276	6.57	1.66	-1	-0.01
	CI	219	8.2	109.5	35	52	40	383.5	195	254	1.30	0.57	49	0.251	6.20E-10	8.65	396	8.09	2.03	-5	-0.03
Lierstranda	A7	219	8.2	109.5	7.5	42	23	83.0	61.1	142	2.32	0.77	25.2	0.412	2.00E-09	11.5	141	5.60	2.31	10	0.16
		219	8.2	109.5	10	43	25	112.6	70.5	162	2.30	0.75	30.8	0.437	1.80E-09	10.5	181	5.89	2.57	10	0.14
		219	8.2	109.5	12.5	39	19	142.2	86.5	192	2.22	0.75	33.3	0.385	1.60E-09	11.2	191	5.73	2.21	6	0.07
Lierstranda	A8	219	8.2	109.5	15	34	16	171.8	102.4	197	1.92	0.65	35.7	0.349	1.40E-09	11.8	183	5.13	1.79	7	0.07
		219	8.2	109.5	17.5	33.5	15	201.5	119.8	194	1.62	0.6	38.5	0.321	1.40E-09	13	232	6.01	1.93	-4	-0.03
		219	8.2	109.5	20	33	14	231.1	137.2	192	1.40	0.555	41.3	0.301	1.55E-09	14	259	6.27	1.89	-3	-0.02
Lierstranda	A9	219	8.2	109.5	22.5	32.5	13	260.7	154.9	200	1.29	0.53	44.5	0.287	1.70E-09	14.5	275	6.19	1.78	-4	-0.03
		219	8.2	109.5	25	32	12	290.3	172.5	207	1.20	0.5	47.6	0.276	1.90E-09	15	308	6.46	1.78	-9	-0.05
Lierstranda	A10	219	8.2	109.5	27.5	30	12	320.0	191	224	1.17	0.47	50.4	0.264	2.30E-09	15	342	6.79	1.79	-9	-0.05
		219	8.2	109.5	30	28	12	349.6	209.6	241	1.15	0.45	53.3	0.254	2.60E-09	15	276	5.19	1.32	-6	-0.03
		219	8.2	109.5	32.5	27.5	12	379.2	229	269	1.17	0.45	56.3	0.246	2.80E-09	15	333	5.91	1.45	-9	-0.04
		219	8.2	109.5	35	27	12	408.8	248.4	278	1.12	0.45	58.8	0.237	3.00E-09	15	326	5.55	1.31	-15	-0.06
Lierstranda	B2(open)	809	9.5	87.2	7.5	42	23	83.0	61.1	142	2.32	0.77	25.2	0.412	2.00E-09	11.5	79	3.14	1.29	-6	-0.10
		809	9.5	87.2	10	43	25	112.6	70.5	162	2.30	0.75	30.8	0.437	1.80E-09	10.5	120	3.91	1.71	1	0.01
		809	9.5	87.2	12.5	39	19	142.2	86.5	192	2.22	0.75	33.3	0.385	1.60E-09	11.2	130	3.90	1.50	5	0.06
Pentre	A5	219	8.2	109.5	17.5	32	15	185	158	417	2.64	0.81	66.5	0.421	Very high	NA	NA	NA	NA	NA	NA
	A5	219	8.2	109.5	20.0	30	18	212	179	426	2.38	0.77	70	0.391	Very high	NA	NA	NA	NA	NA	NA
	A5	219	8.2	109.5	22.5	27	14	238	200	444	2.22	0.75	73.5	0.368	Very high	NA	NA	NA	NA	NA	NA
Pentre	A6	219	8.2	109.5	25.0	28	11	265	221	455	2.06	0.72	77	0.348	Very high	NA	NA	NA	NA	NA	NA
	A6	219	8.2	109.5	27.5	25	14	291	242	472	1.95	0.70	80.5	0.333	Very high	NA	NA	NA	NA	NA	NA
	A6	219	8.2	109.5	30.0	26	17	318	263	484	1.84	0.68	84	0.319	Very high	NA	NA	NA	NA	NA	NA
Pentre	LDP(open)	762	15	105.9	21.5	28	15	215	191.3	430	2.25	0.75	72	0.376	Very high	Ass. 20	NA	NA	NA	NA	NA
	LDP(open)	762	15	105.9	32.1	26.5	13	327	280.4	496	1.77	0.66	87.5	0.312	Very high	Ass. 20	NA	NA	NA	NA	NA
	LDP(open)	762	15	105.9	42.3	24	16	435	372.8	559	1.5	0.61	103	0.276	Very high	Ass. 20	NA	NA	NA	NA	NA
	LDP(open)	762	15	105.9	51.3	25	15	531	451.3	654	1.45	0.60	117	0.259	Very high	Ass. 20	NA	NA	NA	NA	NA
Pentre	IC	101	?	50.53	12.5	28	20	132	118	396	3.36	0.86	59.5	0.504	NA	NA	NA	NA	NA	NA	NA
	IC	101	?	50.53	15	30	16.5	159	139	395	2.84	0.84	63	0.453	NA	NA	NA	NA	NA	NA	NA
	IC	101	?	50.53	17.5	31	14	185	161	425	2.64	0.81	66.5	0.413	NA	NA	NA	NA	NA	NA	NA

TEST SITE	PILE NAME	D (mm)	t (mm)	R_eq (mm)	Depth (m)	w (%)	I_p (%)	u_0 (kPa)	σ'_v0 (kPa)	p'_c (kPa)	OCR	K_0	s_ud (kPa)	s_ud/σ'_v0	Perm. k_0 (m/s)	Mod. no. m_0	Δu_i (kPa)	Δu_i/s_ud	Δu_i/σ'_v0	σ'_ri (kPa)	K_i
Tilbrooke	NGI-A	219	16	109,5	5,11	15	22	28	81	2754	34,00	2,60	270	3,333	2,50E-11	36	92	0,34	1,13	25	0,31
	NGI-A	219	16	109,5	7,61	15	22	51	114	5700	50,00	2,60	400	3,509	2,50E-11	31,5	69	0,17	0,60	200	1,75
	NGI-A	219	20	109,5	10,1	15	23	74	145	1885	13,00	2,15	300	2,069	2,50E-11	29	171	0,57	1,18	185	1,28
Tilbrooke	NGI-B	219	16	109,5	20	17	35	164	272	2802	10,30	1,70	360	1,324	1,50E-11	30	NA	NA	NA	670	2,46
	NGI-B	219	16	109,5	22,5	17	35	187	305	3660	12,00	1,55	465	1,525	1,40E-11	28,5	913	1,96	2,99	500	1,64
	NGI-B	219	16	109,5	25	17	35	203	340	3910	11,50	1,40	485	1,426	1,30E-11	27	292	0,60	0,86	1000	2,94
Tilbrooke	LDP (open)	762	36	305,2	7,99	15	22	55	118	4130	35,00	2,60	365	3,093	2,50E-11	32,5	420	1,15	3,56	-153	-1,30
	LDP (open)	762	36	305,2	14,26	15	26	112	200	2800	14,00	1,80	350	1,750	2,50E-11	24	420	1,20	2,10	-21	-0,11
	LDP (open)	762	36	305,2	20,18	17	35	166	275	2888	10,50	1,70	365	1,327	1,50E-11	29,5	NA	NA	NA	978	3,56
	LDP (open)	762	36	305,2	26,18	18	32	210	360	3600	10,00	1,35	460	1,278	1,40E-11	28	1222	2,66	3,39	499	1,39
West Delta	LP (open)	762	19,1	119,1	14	70	53	330	51	61	1,20	0,72	14	0,275	5,00E-10	8,8	101	7,21	1,98	24	0,47
	LP (open)	762	19,1	119,1	23,9	50	37	450	97	112	1,15	0,64	23	0,237	4,00E-10	12	110	4,78	1,13	38	0,39
	LP (open)	762	19,1	119,1	33,1	42	33	575	137	151	1,10	0,63	29,5	0,215	2,00E-10	14,5	100	3,39	0,73	43	0,31
	LP (open)	762	19,1	119,1	42,2	39,5	34	700	162	178	1,10	0,63	37	0,228	2,00E-10	14,5	191	5,16	1,18	48	0,30
	LP (open)	762	19,1	119,1	51,4	48	47	830	195	224	1,15	0,66	46	0,236	1,90E-10	10,4	180	3,91	0,92	48	0,25
	LP (open)	762	19,1	119,1	60,5	55,5	58	970	223	279	1,25	0,71	57	0,256	1,30E-10	8,7	328	5,75	1,47	86	0,39
	LP (open)	762	19,1	119,1	68,1	56	65	1070	252	328	1,30	0,74	66	0,262	1,10E-10	7	481	7,29	1,91	39	0,15
West Delta	3"-Closed	76	Ass. 3	76	17,7	65	49	380	67	80	1,20	0,70	17,5	0,261	5,00E-10	9,5	141	8,06	2,10	38	0,57
	3"-Closed	76	Ass. 3	76	45,1	39	35	750	178	196	1,10	0,63	39	0,219	2,00E-10	12,7	183	4,69	1,03	40	0,22
West Delta	3"-p-Open	76	Ass. 3	21,1	45,1	39	35	750	178	196	1,10	0,63	39	0,219	2,00E-10	12,7	122	3,13	0,69	11	0,06
	3"-p-Open	76	Ass. 3	21,1	54,3	52	49	885	203	244	1,20	0,67	48,5	0,239	1,80E-10	10	259	5,34	1,28	34	0,17
	3"-p-Open	76	Ass. 3	21,1	63,4	57	65	1015	235	306	1,30	0,73	61	0,260	1,20E-10	8,5	348	5,70	1,48	47	0,20
Bothkennar	IC-pile	101	?	50,53	3,5	61	40	27	32,9	86	2,60	0,95	18,1	0,550	1,60E-09	18	110	6,08	3,34	0	0,00
	IC-pile	101	?	50,53	4,65	68	52	38,5	39,7	88	2,22	0,9	20,2	0,509	1,40E-09	18	125	6,19	3,15	5	0,13
Cowden	IC-pile	101	?	50,53	3,78	17	19	25,2	56,5	1215	21,5	2,35	138	2,442	Ass.1E-10	Ass. 30	250	1,81	4,42	70	1,24
	IC-pile	101	?	50,53	4,9	16	18	38,6	71,2	926	13	1,75	101	1,419	Ass.1E-10	Ass. 30	260	2,57	3,65	140	1,97
Cannons P.	IC-pile	101	?	50,53	2,84	28	54	25	46	1840	16	1,9	93	2,022	NA	NA	-60	-0,65	-1,30	160	3,48
	IC-pile	101	?	50,53	3,98	30	40	40	60	1800	11,7	1,65	93	1,550	NA	NA	-70	-0,75	-1,17	280	4,67
Empire	PLS	38	?	19,0	44,7	46	59	475	296	340	1,15	0,65	66	0,223	2,00E-10	8	488	7,39	1,65	128	0,43
MIT	PLS	38	?	19,0	73,6	38	50	775	538	646	1,2	0,65	116	0,216	2,00E-10	8	893	7,70	1,66	168	0,31
Empire	3"-open	76	Ass. 3	14,8	48,8	47	63	526	328	380	1,16	0,74	72	0,220	2,00E-10	8	327	4,54	1,00	65	0,20
Mccll	3"-closed	76	Ass. 3	38	48,8	47	63	526	328	380	1,16	0,74	72	0,220	2,00E-10	8	753	10,46	2,30	120	0,37
	x-probe	43,6	?	21,8	48,8	47	63	526	328	380	1,16	0,74	72	0,220	2,00E-10	8	725	10,07	2,21	87	0,27
BBC	PLS	38	?	19,0	10,5	33	17	90,0	75,1	346	4,6	0,95	45,9	0,610	1,00E-09	16,4	108,0	2,36	1,44	NA	NA
MIT	PLS	38	?	19,0	12,0	43	20	105,3	86,5	329	3,8	0,88	45,3	0,524	9,00E-10	14,8	158,7	3,50	1,83	NA	NA
	PLS	38	?	19,0	13,6	42	26	120,7	98,0	314	3,2	0,83	44,7	0,456	7,50E-10	13,5	245,3	5,48	2,50	NA	NA
	PLS	38	?	19,0	19,1	40	18,5	175,4	140,5	281	2	0,68	44,0	0,313	4,00E-10	12,1	344,6	7,83	2,45	NA	NA
	PLS	38	?	19,0	25,1	45	19	237,1	185,1	250	1,35	0,6	42,4	0,229	4,00E-10	9,6	399,9	9,44	2,16	35,17	0,19
	PLS	38	?	19,0	31,2	43	25	296,9	230,9	289	1,25	0,58	49,7	0,215	6,00E-10	9,4	479,1	9,64	2,07	41,57	0,18
	PLS	38	?	19,0	34,9	41	22	333,5	259,3	324	1,25	0,58	55,8	0,215	6,00E-10	9,2	574,5	10,30	2,22	40,19	0,16
	PLS	38	?	19	35,8	41	20	342,7	265,3	332	1,25	0,58	57,1	0,215	6,00E-10	9,2	579,3	10,15	2,18	41,12	0,16
Hamilton	TP1-JC	112	?	55,95	6,3	97	55	51	47	65,8	1,4	0,8	18	0,383	7,00E-10	5	76	4,22	1,62	14	0,30
	TP3-DC	112	?	55,95	6,2	97	55	50	46	64,4	1,4	0,8	17,8	0,387	7,00E-10	5	55	3,09	1,20	36	0,78
St.Alban	Pile B	219	8	109,5	3	80	60	25,5	23,3	47	2,02	0,9	14,4	0,618	3,20E-09	6	68,5	4,76	2,94	NA	NA
	Pile B	219	8	109,5	6	60	37	55	41,7	84	2,01	0,85	23,2	0,556	2,40E-09	7	136	5,86	3,26	NA	NA

Column groupings: PILE DATA (D, t, R_eq); TYPICAL SOIL DATA (Depth, w, I_p, u_0, σ'_v0, p'_c, OCR, K_0, s_ud, s_ud/σ'_v0, Perm. k_0, Mod. no. m_0); INSTALLATION STRESSES (Δu_i, Δu_i/s_ud, Δu_i/σ'_v0, σ'_ri, K_i).

TEST SITE	PILE NAME	PILE DATA			TYPICAL SOIL DATA											CONS. TIMES			AT TEST		EST. AT U=100%		
		D (mm)	t (mm)	R_{eq} (mm)	Depth (m)	w (%)	I_p (%)	σ'_{vo} (kPa)	p'_c (kPa)	OCR	K_o	s_{ud} (kPa)	s_{ud}/σ'_{vo}	Perm. k_o (m/s)	Mod. no. m_o	t_{50} (days)	t_{90} (days)	Deg. cons U	σ'_{rc} (kPa)	K_c	σ'_{rc} (kPa)	K_c	K_c/K_o
Haga	B-piles	154	4,5	76,5	1,9	35	11	39	320	8,21	1,52	41,5	1,064	7,00E-10	16	0,75	4,17	1,000	52	1,33	52	1,33	0,88
		154	4,5	76,5	3,4	40	15	73	270	3,70	0,87	41	0,562	9,00E-10	16	0,708	2,25	1,000	83	1,14	83	1,14	1,31
Onsøy	A1	219	8,2	109,5	7,5	64	37	52	76	1,46	0,64	15	0,288	2,00E-09	7	1,40	9	0,974	25,3	0,49	26,0	0,50	0,78
		219	8,2	109,5	10	68	40	64	83	1,30	0,62	17,5	0,273	1,00E-09	6,3	2,50	13	0,979	31,0	0,48	31,7	0,49	0,80
		219	8,2	109,5	12,5	65,5	42,5	76	99	1,30	0,615	21	0,276	9,00E-10	6,6	2,50	16	0,926	31,0	0,41	33,3	0,44	0,71
Onsøy	A2	219	8,2	109,5	15	63	45	88	114	1,30	0,61	23	0,261	8,00E-10	6,8	4,00	20	0,962	37,0	0,42	38,4	0,44	0,72
		219	8,2	109,5	17,5	62,5	46	100	130	1,30	0,6	26	0,260	7,70E-10	7	4,00	20	0,950	41,0	0,41	43,0	0,43	0,72
		219	8,2	109,5	20	62	47	112	146	1,30	0,6	28	0,250	7,50E-10	7,2	4,00	25	0,914	47,7	0,43	51,8	0,46	0,77
Onsøy	A3	219	8,2	109,5	22,5	58	44,5	125	163	1,30	0,595	31,5	0,252	7,20E-10	7,4	4,50	28	0,976	82,0	0,66	83,9	0,67	1,13
		219	8,2	109,5	25	54	42	139	180,5	1,30	0,59	34,5	0,248	7,00E-10	7,65	4,00	25	0,988	86,0	0,62	87,0	0,63	1,06
		219	8,2	109,5	27,5	53,5	42	152	197,5	1,30	0,58	38	0,250	6,80E-10	7,9	4,00	23	0,993	90,4	0,59	91,0	0,60	1,03
Onsøy	A4	219	8,2	109,5	30	53	42	166	216	1,30	0,58	42	0,253	6,60E-10	8,15	5,00	25	0,944	80,8	0,49	85,2	0,51	0,89
		219	8,2	109,5	32,5	52,2	41	180	234	1,30	0,57	45,5	0,253	6,40E-10	8,4	3,50	19	0,978	96,0	0,53	98,2	0,55	0,96
		219	8,2	109,5	35	52	40	195	254	1,30	0,57	49	0,251	6,20E-10	8,65	2,00	12	0,982	116,8	0,60	118,8	0,61	1,07
Onsøy	B1(open)	809	9,5	87,2	7,5	64	37	52	76	1,46	0,64	15	0,288	2,00E-09	7	2,00	NA	0,776	35,7	0,69	43,7	0,84	1,31
		809	9,5	87,2	10	68	40	64	83	1,30	0,62	17,5	0,273	1,00E-09	6,3	2,00	150	0,690	31,4	0,49	41,1	0,64	1,04
		809	9,5	87,2	12,5	65,5	42,5	76	99	1,30	0,615	21	0,276	9,00E-10	6,6	2,00	80	0,763	31,4	0,41	38,8	0,51	0,83
Onsøy	C1	219	8,2	109,5	10	68	45	64	83	1,30	0,62	17,5	0,273	1,00E-09	6,3	5,00	50	0,762	20,4	0,32	25,3	0,39	0,64
	C1	219	8,2	109,5	15	63	47	88	114	1,30	0,61	23	0,261	8,00E-10	6,8	7,50	150	0,847	30,0	0,34	34,6	0,39	0,65
	C1	219	8,2	109,5	20	62	42	112	146	1,30	0,6	28	0,250	7,50E-10	7,2	7,00	48	0,895	43,7	0,39	48,3	0,43	0,72
	C1	219	8,2	109,5	25	54	42	139	180,5	1,30	0,59	34,5	0,248	6,60E-10	8,15	4,00	23	0,976	44,3	0,32	45,4	0,33	0,55
	C1	219	8,2	109,5	30	53	42	166	216	1,30	0,58	42	0,253	6,60E-10	8,15	4,00	21	0,996	76,7	0,46	76,9	0,46	0,80
	C1	219	8,2	109,5	35	52	40	195	254	1,30	0,57	49	0,251	6,20E-10	8,65	3,30	21	0,987	81,4	0,42	82,4	0,42	0,74
Lierstranda	A7	219	8,2	109,5	7,5	42	23	61,1	142	2,32	0,77	25,2	0,412	2,00E-09	11,5	4,30	28	0,957	30,0	0,49	31,3	0,51	0,66
		219	8,2	109,5	10	43	25	70,5	162	2,30	0,75	30,8	0,437	1,80E-09	10,5	3,70	NA	0,923	40,0	0,57	43,1	0,61	0,81
		219	8,2	109,5	12,5	39	19	86,5	192	2,22	0,75	33,3	0,385	1,60E-09	11,2	3,20	22,3	0,948	23,0	0,27	24,2	0,28	0,37
Lierstranda	A8	219	8,2	109,5	15	34	16	102,4	197	1,92	0,65	35,7	0,349	1,40E-09	11,8	2,80	20	0,984	24,0	0,23	24,4	0,24	0,37
		219	8,2	109,5	17,5	33,5	15	119,8	194	1,62	0,6	38,5	0,321	1,40E-09	13	2,20	16,4	0,983	29,7	0,25	30,2	0,25	0,42
		219	8,2	109,5	20	33	14	137,2	192	1,40	0,555	41,3	0,301	1,55E-09	14	2,40	14	0,973	33,0	0,24	33,9	0,25	0,45
Lierstranda	A9	219	8,2	109,5	22,5	32,5	13	154,9	200	1,29	0,53	44,5	0,287	1,70E-09	14,5	0,47	9	0,975	20,7	0,13	21,2	0,14	0,26
		219	8,2	109,5	25	32	12	172,5	207	1,20	0,5	47,6	0,276	1,90E-09	15	1,20	10	0,977	47,0	0,27	48,1	0,28	0,56
Lierstranda	A10	219	8,2	109,5	27,5	30	12	191	224	1,17	0,47	50,4	0,264	2,30E-09	15	1,00	7	0,980	37,0	0,19	37,8	0,20	0,42
		219	8,2	109,5	30	28	12	209,6	241	1,15	0,45	53,3	0,254	2,60E-09	15	0,25	3,5	1,000	40,0	0,19	40,0	0,19	0,42
		219	8,2	109,5	32,5	27,5	12	229	269	1,17	0,45	56,3	0,246	2,80E-09	15	0,37	5	1,000	28,0	0,12	28,0	0,12	0,27
		219	8,2	109,5	35	27	12	248,4	278	1,12	0,45	58,8	0,237	3,00E-09	15	0,13	0,9	1,000	37,1	0,15	37,1	0,15	0,33
Lierstranda	B2(open)	809	9,5	87,2	7,5	42	23	61,1	142	2,32	0,77	25,2	0,412	2,00E-09	11,5	0,69	7,00	1,000	25,0	0,41	25,0	0,41	0,53
		809	9,5	87,2	10	43	25	70,5	162	2,30	0,75	30,8	0,437	1,80E-09	10,5	1,10	9,00	1,000	32,0	0,45	32,0	0,45	0,61
		809	9,5	87,2	12,5	39	19	86,5	192	2,22	0,75	33,3	0,385	1,60E-09	11,2	1,90	15,00	1,000	30,0	0,35	30,0	0,35	0,46
Pentre	A5	219	8,2	109,5	7,5	32	15	158	417	2,64	0,81	66,5	0,421	Very high	NA	NA	NA	1,000	23	0,15	23,0	0,15	0,18
	A5	219	8,2	109,5	10	30	18	179	426	2,38	0,77	70	0,391	Very high	NA	NA	NA	1,000	21	0,12	21,0	0,12	0,15
	A5	219	8,2	109,5	12,5	27	14	200	444	2,22	0,75	73,5	0,368	Very high	NA	0,0196	0,179	1,000	46	0,23	46,0	0,23	0,31
Pentre	A6	219	8,2	109,5	20,0	28	11	221	455	2,06	0,72	77	0,348	Very high	NA	NA	NA	1,000	64	0,29	64,0	0,29	0,40
	A6	219	8,2	109,5	22,5	25	14	242	472	1,95	0,70	80,5	0,333	Very high	NA	NA	NA	1,000	65	0,27	65,0	0,27	0,38
	A6	219	8,2	109,5	25,0	28	17	263	484	1,84	0,68	84	0,319	Very high	NA	0,0083	0,027	1,000	160	0,61	160,0	0,61	0,89
Pentre	LDP(open)	762	15	105,9	27,5	28	15	191,3	430	2,25	0,75	72	0,376	Very high	Ass. 20	NA	NA	1,000	14,2	0,07	14,2	0,07	0,10
	LDP(open)	762	15	105,9	21,5	26,5	13	280,4	496	1,77	0,66	87,5	0,312	Very high	Ass. 20	NA	0,083	1,000	72,3	0,26	72,3	0,26	0,39
	LDP(open)	762	15	105,9	32,1	24	16	372,8	559	1,5	0,61	103	0,276	Very high	Ass. 20	NA	1,04	1,000	231,2	0,62	231,2	0,62	1,02
	LDP(open)	762	15	105,9	42,3	25	15	451,3	654	1,45	0,60	117	0,259	Very high	Ass. 20	NA	0,625	1,000	221,6	0,49	221,6	0,49	0,82
Pentre	IC	101	?	50,53	51,3	28	20	118	396	3,36	0,86	59,5	0,504	NA	NA	NA	NA	1,000	100,0	0,85	100,0	0,85	0,99
	IC	101	?	50,53	12,5	30	16,5	139	395	2,84	0,84	63	0,453	NA	NA	NA	NA	1,000	125,0	0,90	125,0	0,90	1,07
	IC	101	?	50,53	15	31	14	161	425	2,64	0,81	66,5	0,413	NA	NA	NA	NA	1,000	165,0	1,02	165,0	1,02	1,27

TEST		PILE DATA				TYPICAL SOIL DATA									Mod. no.	CONS. TIMES		Deg. cons	AT TEST		EST. AT U=100%		
SITE	NAME	D	t	Req	Depth	w	Ip	σ'vo	p'c	OCR	Ko	sud	sud/σ'v0	Perm.ko	mo	t50	t90	U	σ'rc	Kc	σ'rc	Kc	Kc/Ko
		(mm)	(mm)	(mm)	(m)	(%)	(%)	(kPa)	(kPa)			(kPa)		(m/s)		(days)	(days)		(kPa)		(kPa)		
Tilbrooke	NGI-A	219	16	109,5	5,11	15	22	81	2754	34,00	2,60	270	3,333	2,50E-11	36	NA	NA	NA	50,0	0,62	100,0	1,23	0,47
	NGI-A	219	16	109,5	7,61	15	22	114	5700	50,00	2,60	400	3,509	2,50E-11	31,5	NA	NA	NA	250,0	2,19	300,0	2,63	1,01
	NGI-A	219	20	109,5	10,1	15	23	145	1885	13,00	2,15	300	2,069	2,50E-11	29	1,3	10	0,96	500,0	3,45	500,0	3,45	1,60
Tilbrooke	NGI-B	219	16	109,5	20	17	35	272	2802	10,30	1,70	360	1,324	1,50E-11	30	NA	NA	NA	820,0	3,01	950,0	3,49	2,05
	NGI-B	219	16	109,5	22,5	17	35	305	3660	12,00	1,55	465	1,525	1,40E-11	28,5	22,0	130	0,84	900,0	2,95	1050,0	3,44	2,22
	NGI-B	219	16	109,5	25	17	35	340	3910	11,50	1,40	485	1,426	1,30E-11	27	NA	NA	0,51	970,0	2,85	1150,0	3,38	2,42
Tilbrooke	LDP (open)	762	36	305,2	7,99	15	22	118	4130	35,00	2,60	365	3,093	2,50E-11	32,5	0,8	45	0,96	160,0	1,36	180,0	1,53	0,59
	LDP (open)	762	36	305,2	14,26	15	26	200	2800	14,00	1,80	350	1,750	2,50E-11	24	14,0	300	0,83	350,0	1,75	430,0	2,15	1,19
	LDP (open)	762	36	305,2	20,18	17	35	275	2888	10,50	1,70	365	1,327	1,50E-11	29,5	NA	NA	NA	500,0	1,82	700,0	2,55	1,50
	LDP (open)	762	36	305,2	26,18	18	32	360	3600	10,00	1,35	460	1,278	1,40E-11	28	18,0	500	0,81	1080,0	3,00	1330,0	3,69	2,74
West Delta	LP (open)	762	19,1	119,1	14	70	53	51	61	1,20	0,72	14	0,275	5,00E-10	8,8	NA	NA	NA	NA	NA	NA	NA	NA
	LP (open)	762	19,1	119,1	23,9	50	37	97	112	1,15	0,64	23	0,237	4,00E-10	12	19	NA	0,74	47,0	0,48	67	0,69	1,08
	LP (open)	762	19,1	119,1	33,1	42	33	137	151	1,10	0,63	29,5	0,215	2,00E-10	14,5	40	180	0,74	44,0	0,32	90	0,66	1,05
	LP (open)	762	19,1	119,1	42,2	39,5	34	162	178	1,10	0,63	37	0,228	2,00E-10	14,5	18,5	150	0,86	77,0	0,48	104	0,64	1,03
	LP (open)	762	19,1	119,1	51,4	48	47	195	224	1,15	0,66	46	0,236	1,90E-10	10,4	24	145	0,80	93,0	0,48	120	0,62	0,94
	LP (open)	762	19,1	119,1	60,5	55,5	58	223	279	1,25	0,71	57	0,256	1,30E-10	8,7	14,5	260	0,83	158	0,71	205	0,92	1,29
	LP (open)	762	19,1	119,1	68,1	56	65	252	328	1,30	0,74	66	0,262	1,10E-10	7	11	265	0,83	208	0,83	270	1,07	1,45
West Delta	3"-p-Closed	76	Ass. 3	76	17,7	65	49	67	80	1,20	0,70	17,5	0,261	5,00E-10	9,5	1,18	NA	NA	NA	NA	NA	NA	NA
	3"-p-Closed	76	Ass. 3	76	45,1	39	35	178	196	1,10	0,63	39	0,219	2,00E-10	12,7	NA	NA	NA	NA	NA	NA	NA	NA
West Delta	3"-p-Open	76	Ass. 3	21,1	45,1	39	35	178	196	1,10	0,63	39	0,219	2,00E-10	12,7	0,15	NA	NA	NA	NA	NA	NA	NA
	3"-p-Open	76	Ass. 3	21,1	54,3	52	49	203	244	1,20	0,67	48,5	0,239	1,80E-10	10	0,26	NA	NA	NA	NA	NA	NA	NA
	3"-p-Open	76	Ass. 3	21,1	63,4	57	65	235	306	1,30	0,73	61	0,260	1,20E-10	8,5	NA	NA	NA	175	0,74	192	0,82	1,12
Bothkennar	IC-pile	101	?	50,53	3,5	61	40	32,9	86	2,60	0,95	18,1	0,550	1,60E-09	18	0,63	6,9	0,85	37	1,12	40	1,22	1,28
	IC-pile	101	?	50,53	4,65	68	52	39,7	88	2,22	0,9	20,2	0,509	1,40E-09	18	NA	NA	0,85	42	1,06	46	1,16	1,29
Cowden	IC-pile	101	?	50,53	3,78	17	19	56,5	1215	21,5	2,35	138	2,442	Ass.1E-10	Ass. 30	0,694	NA	NA	220	3,89	220	3,89	1,66
	IC-pile	101	?	50,53	4,9	16	18	71,2	926	13	1,75	101	1,419	Ass.1E-10	Ass. 30	1,39	NA	NA	280	3,93	280	3,93	2,25
Cannons P.	IC-pile	101	?	50,53	2,84	28	54	46	1840	16	1,9	93	2,022	NA	NA	NA	NA	NA	175	3,80	175	3,80	2,00
	IC-pile	101	?	50,53	3,98	30	40	60	1800	11,7	1,65	93	1,550	NA	NA	NA	NA	NA	250	4,17	250	4,17	2,53
Empire	PLS	38	?	19,0	44,7	46	59	296	340	1,15	0,65	66	0,223	2,00E-10	8	0,125	0,972	1	330	1,11	330	1,11	1,72
MIT	PLS	38	?	19,0	73,6	38	50	538	646	1,2	0,65	116	0,216	2,00E-10	8	0,313	2,08	1	380	0,71	380	0,71	1,09
Empire	3"-open	76	Ass. 3	14,8	48,8	47	63	328	380	1,16	0,74	72	0,220	2,00E-10	8	0,528	5,42	0,924	233	0,71	252,2	0,77	1,04
McII	3"-closed	76	Ass. 3	38	48,8	47	63	328	380	1,16	0,74	72	0,220	2,00E-10	8	0,505	5,03	0,824	498	1,52	604,4	1,84	2,49
	x-probe	43,6	?	21,8	48,8	47	63	328	380	1,16	0,74	72	0,220	2,00E-10	8	0,094	1,31	0,839	367	1,12	437,4	1,33	1,80
BBC	PLS	38	?	19,0	10,5	33	17	75,1	346	4,6	0,95	45,9	0,610	1,00E-09	16,4	0,0023	0,0116	1	65,6	0,87	65,6	0,87	0,92
MIT	PLS	38	?	19,0	12,0	43	20	86,5	329	3,8	0,88	45,3	0,524	9,00E-10	14,8	0,0116	0,066	1	95,9	1,11	95,9	1,11	1,26
	PLS	38	?	19,0	13,6	42	26	98,0	314	3,2	0,83	44,7	0,456	7,50E-10	13,5	0,0243	0,098	1	82,5	0,84	82,5	0,84	1,01
	PLS	38	?	19,0	19,1	40	18,5	140,5	281	2	0,68	44,0	0,313	4,00E-10	12,1	0,061	0,544	1	146,1	1,04	146,1	1,04	1,53
	PLS	38	?	19,0	25,1	45	19	185,1	250	1,35	0,6	42,4	0,229	4,00E-10	9,6	0,069	0,579	0,97	116,2	0,63	119,8	0,65	1,08
	PLS	38	?	19,0	31,2	43	25	230,9	289	1,25	0,58	49,7	0,215	6,00E-10	9,4	0,069	0,579	0,97	104,7	0,45	107,9	0,47	0,81
	PLS	38	?	19,0	34,9	41	22	259,3	324	1,25	0,58	55,8	0,215	6,00E-10	9,2	0,069	0,579	0,97	168,1	0,65	173,3	0,67	1,15
	PLS	38	?	19	35,8	41	20	265,3	332	1,25	0,58	57,1	0,215	6,00E-10	9,2	0,069	0,579	0,97	148,8	0,56	153,4	0,58	1,00
Hamilton	TP1-JC	112	?	55,95	6,3	97	55	47	65,8	1,4	0,8	18	0,383	7,00E-10	5	0,42	5,2	1	32,9	0,79	37,1	0,79	0,99
	TP3-DC	112	?	55,95	6,2	97	55	46	64,4	1,4	0,8	17,8	0,387	7,00E-10	5	0,69	4,86	1	40	0,87	40,0	0,87	1,09
St.Alban	Pile B	219	8	109,5	3	80	60	23,3	47	2,02	0,9	14,4	0,618	3,20E-09	6	2	9,4	NA	NA	NA	NA	NA	NA
	Pile B	219	8	109,5	6	60	37	41,7	84	2,01	0,85	23,2	0,556	2,40E-09	7	1,35	11,2	NA	NA	NA	NA	NA	NA

Appendix 2

Summary table with measured shaft friction-

Instrumented pile tests

TEST SITE	PILE NAME	D (mm)	t (mm)	Emb. L (m)	z_{tip} (m)	z_{av} (m)	w (%)	Ip (%)	σ'_{vo} (kPa)	p'_c (kPa)	OCR	K_0	s_{ud} (kPa)	s_{ud}/σ'_{vo}	σ'_{hc} (kPa)	K_c	K_c/K_0	τ_{us} (kPa)	$\beta=\tau_{us}/\sigma'_{vo}$	$\alpha=\tau_{us}/s_{ud}$	τ_{us}/σ'_{hc}
Haga	B-piles	154	4.5	4.85	4.85	2.65	38	20	54	310	5.74	1.1	42	0.78	68	1.26	1.14	24	0.44	0.57	0.35
Onsøy	A1	219	8.2	10	15.00	10.00	64	38	64	84	1.32	0.62	17	0.27	31.9	0.50	0.80	14.8	0.23	0.87	0.46
	A2	219	8.2	10	22.50	17.50	62	46	100	130	1.30	0.605	24	0.24	46	0.46	0.76	20	0.20	0.83	0.43
	A3	219	8.2	10	30.00	25.00	56	44	139	181	1.30	0.59	35	0.25	83	0.60	1.01	31.1	0.22	0.89	0.37
	A4	219	8.2	10	37.50	32.50	52	41	180	234	1.30	0.575	45	0.25	102	0.57	0.99	37.7	0.21	0.84	0.37
Onsøy	C1	219	8.2	10	35.00	7.50	63	36	52	72	1.38	0.64	15	0.29	28.8	0.55	0.87	11.5	0.22	0.77	0.40
	C1	219	8.2	10	35.00	15.00	63	45	87	113	1.30	0.61	24	0.28	41.7	0.48	0.79	18.3	0.21	0.76	0.44
	C1	219	8.2	10	35.00	22.50	58	44	126	164	1.30	0.595	31	0.25	50.5	0.40	0.67	20.9	0.17	0.67	0.41
	C1	219	8.2	10	35.00	27.50	53.5	41	152	198	1.30	0.585	38	0.25	63.3	0.42	0.71	22.5	0.15	0.59	0.36
	C1	219	8.2	10	35.00	32.50	51	39	180	234	1.30	0.575	45	0.25	80.8	0.45	0.78	39.9	0.22	0.89	0.49
Onsøy	B1(open)	809	9.5	10	15.00	10.00	64	38	64	84	1.32	0.62	17	0.27	55	0.86	1.39	19.7	0.31	1.16	0.36
	A7	219	8.2	10	15.00	10.00	40	21	70.5	162	2.30	0.75	30.8	0.44	32	0.45	0.61	9.5	0.13	0.31	0.30
Lierstranda	A8	219	8.2	10	22.50	17.50	34	15	120	199	1.66	0.6	38.5	0.32	29.6	0.25	0.41	9	0.08	0.23	0.30
	A9	219	8.2	10	30.00	25.00	31	12.5	172.5	207	1.20	0.5	47.6	0.28	35.7	0.21	0.41	11.5	0.07	0.24	0.32
	A10	219	8.2	10	37.50	32.50	29.00	12	229	261	1.14	0.45	56.3	0.25	35	0.15	0.34	12	0.05	0.21	0.34
Onsøy	B2(open)	809	9.5	10	15.00	10.00	40	21	70.5	162	2.30	0.75	30.8	0.44	28.5	0.40	0.54	11.2	0.16	0.36	0.39
Pentre	A5	219	8.2	10	25.00	20.00	29	15	182	423	2.32	0.76	70	0.38	30	0.16	0.22	23.3	0.13	0.33	0.78
NGI-tests	A6	219	8.2	10	32.50	27.50	27	17	247	466	1.89	0.69	80.5	0.33	97	0.39	0.57	63.8	0.26	0.79	0.66
Pentre	LDP (open)	762	15	40	55.00	20.00	30	15.5	182	423	2.32	0.76	70	0.38	10	0.05	0.07	16.2	0.09	0.23	1.62
McClelland-test	LDP (open)	762	15	40	55.00	30.00	27	15	269	481	1.79	0.67	84	0.31	62	0.23	0.34	55	0.20	0.65	0.89
	LDP (open)	762	15	40	55.00	40.00	26	19	359	558	1.55	9.62	100	0.28	200	0.56	0.06	79	0.22	0.79	0.40
	LDP (open)	762	15	40	55.00	50.00	27	19	450	621	1.38	0.57	114	0.25	220	0.49	0.86	77	0.17	0.68	0.35
Tilbrooke	A	219	16	9.5	12.50	7.75	15.2	25	115.4	3100	26.86	2.45	330	2.86	320	2.77	1.13	182	1.58	0.55	0.57
NGI-tests	B	219	16	10	27.50	21.50	16.8	35	290.8	3350	11.52	1.6	440	1.51	1000	3.44	2.15	319	1.10	0.73	0.32
	C	219	20	16.5	19.50	10.25	15.1	25	147.2	3200	21.74	2	330	2.24	500	3.40	1.70	185	1.26	0.56	0.37
	D-open	273	16	14.5	17.50	10.25	15.1	25	147.2	3200	21.74	2	330	2.24	NA	NA	NA	145	0.99	0.44	NA
Tibrooke	LDP (open)	762	40	30.5	30.50	10.00	15	23	144.2	3000	20.80	2.2	320	2.22	275	1.91	0.87	190	1.32	0.59	0.69
Mclelland-tests	LDP (open)	762	40	30.5	30.50	15.00	15.5	26	208.7	3350	16.05	1.7	380	1.82	450	3.12	1.42	240	1.15	0.63	0.53
(Atrup)	LDP (open)	762	32	30.5	30.50	20	17	35	272	3100	11.40	1.65	390	1.43	710	3.40	2.00	220	0.81	0.56	0.31
	LDP (open)	762	32	30.5	30.50	25.00	17	32	339.8	3650	10.74	1.38	480	1.41	1200	4.41	2.67	320	0.94	0.67	0.27
West Delta	LP	762	19.1	71.3	71.30	15	70	55	53.3	64	1.20	0.72	14.9	0.28	45	0.84	1.17	14.5	0.27	0.97	0.32
	LP	762	19.1	71.3	71.30	25	50	35	98.1	113	1.15	0.63	23.5	0.24	70	0.71	1.13	23	0.23	0.98	0.33
	LP	762	19.1	71.3	71.30	35	40	32	142.7	157	1.10	0.61	31.4	0.22	92	0.64	1.06	27	0.19	0.86	0.29
	LP	762	19.1	71.3	71.30	45	40	35	178.0	196	1.10	0.63	39.2	0.22	110	0.62	0.98	24	0.13	0.61	0.22
	LP	762	19.1	71.3	71.30	55	5	52	204.4	245	1.20	0.67	49.1	0.24	155	0.76	1.13	38	0.19	0.77	0.25
	LP	762	19.1	71.3	71.30	65	57	65	240.1	312	1.30	0.74	62.4	0.26	240	1.00	1.35	70	0.29	1.12	0.29
Bothkennar	IC-pile	102	?	4.8	6.00	3.6	63	38	33.5	87	2.60	0.92	18.3	0.55	41	1.22	1.33	18.3	0.55	1.00	0.45
Cowden	IC-pile-C	102	?	3.74	6.24	4.37	19	17	52.6	842	16.00	2	125	2.38	240	4.56	2.28	110	2.09	0.88	0.46
	IC-pile-T	102	?	3.8	6.30	4.4	19	17	52.6	842	16.00	2	125	2.38	240	4.56	2.28	72	1.37	0.58	0.30
Cannons P.	IC-pile	102	?	4.06	6.06	4.03	29	47	53.2	745	14.00	1.8	111	2.09	300	5.64	3.13	78.7	1.48	0.71	0.26
UHC	UHCC-top	273	9.2	13.1	13.10	5.1	27	50	85	900	10.59	1.65	125	1.47	NA	NA	NA	53.3	0.63	0.43	NA
	UHCC-bot	273	9.2	13.1	13.10	10.5	17	15	136	1180	8.68	1.3	189	1.39	NA	NA	NA	80	0.59	0.42	NA
Empire	PLS	38.3	?	1.2	45.70	44.7	46	59	296	340	1.15	0.65	66	0.22	342.0	1.16	1.78	87.6	0.30	1.33	0.26
MIT	PLS	38.3	?	1.2	74.60	73.6	38	50	538	646	1.20	0.65	116	0.22	398.0	0.74	1.14	120	0.22	1.03	0.30
Empire	x-probe	43.6	?	3	37.60	36.6	45	63	240	288	1.20	0.76	56.5	0.24	343.0	1.48	1.95	56.9	0.24	1.01	0.17
McClelland	3"open	76.2	?	4.28	45.90	43	45	63	290	336	1.16	0.74	64	0.22	296.0	1.02	1.38	55.5	0.19	0.87	0.19
	3"-open	76.2	?	4.28	61.70	48.8	47	63	328	380	1.16	0.74	72	0.22	252.2	0.77	1.04	70.6	0.22	0.98	0.28
	3"-closed	76.2	?	6.42	53.80	48.8	47	63	328	380	1.16	0.74	72	0.22	604.4	1.84	2.49	85	0.26	1.18	0.14
	x-probe	43.6	?	3	37.60	48.8	47	63	328	380	1.16	0.74	72	0.22	437.4	1.33	1.80	67.3	0.21	0.93	0.15
BBC	PLS	38.3	?	1.2	11.10	10.5	33	17	75	346	4.6	0.95	45.9	0.61	65.6	0.87	0.92	15.4	0.21	0.34	0.23
MIT	PLS	38.3	?	1.2	12.60	12.0	43	20	87	329	3.8	0.88	45.3	0.52	95.9	1.11	1.26	22.6	0.26	0.50	0.24
	PLS	38.3	?	1.2	14.20	13.6	42	26	98	314	3.2	0.83	44.7	0.46	82.5	0.84	1.01	21.7	0.22	0.48	0.26
	PLS	38.3	?	1.2	19.70	19.1	40	18.5	140	281	2	0.68	44.0	0.31	146.1	1.04	1.53	34.6	0.25	0.78	0.24
	PLS	38.3	?	1.2	25.70	25.1	45	19	185	250	1.35	0.6	42.4	0.23	119.8	0.65	1.08	25.0	0.14	0.59	0.21
	PLS	38.3	?	1.2	31.80	31.2	43	25	231	289	1.25	0.58	49.7	0.22	107.9	0.47	0.81	23.6	0.10	0.47	0.22
	PLS	38.3	?	1.2	35.70	34.9	41	22	259	324	1.25	0.58	55.8	0.22	173.3	0.67	1.15	38.8	0.15	0.69	0.22
	PLS	38.3	?	1.2	36.50	35.8	41	20	265	332	1.25	0.58	57.1	0.22	153.4	0.58	1.00	52.8	0.20	0.92	0.34
Hamilton	TP1-JC	112	?	12.2	12.20	6.1	87	52	44.9	83	1.85	0.8	21.3	0.47	37.0	0.82	1.03	16.6	0.37	0.78	0.45
Hamilton	TP3-DC	112	?	12.2	12.20	6.1	87	52	44.9	83	1.85	0.8	21.3	0.47	NA	NA	NA	10.5	0.23	0.49	NA
St.Alban	Pile B	219	8	6.1	7.60	4.55	65	50	33	66	2.05	0.85	19.5	0.60	37.0	1.14	1.34	16.6	0.51	0.85	0.45

Appendix 3

Summary table with measured shaft friction-

Non-instrumented pile tests

TEST	PILE	Pile data					TYPICAL SOIL DATA								MEASURED RESULTS (extrap. to 100%dissipation)		
		D	t	Emb. L	z_{tip}	z_{av}	w	Ip	σ'_{v0}	p'_c	OCR	K_0	s_{ud}	s_{ud}/σ'_{v0}	τ_{us}	$\beta=$ τ_{us}/σ'_{v0}	$\alpha=$ τ_{us}/s_{ud}
SITE	NAME	(mm)	(mm)	(m)	(m)	(m)	(%)	(%)	(kPa)	(kPa)			(kPa)		(kPa)		
Empire	Em1 (open)	356	?	15,3	50,30	42,7	46	63	280	328	1,17	0,8	70	0,25	56,3	0,20	0,80
	Em2 (open)	356	?	15,3	77,80	70,6	36	53	512	594	1,16	0,74	109	0,21	102,9	0,20	0,94
	Em3 (open)	356	?	12,2	94,50	88,4	36	50	665	871	1,31	0,82	153,5	0,23	138,9	0,21	0,90
	Em4 (open)	356	?	12,2	109,40	103,3	38	57	794	1127	1,42	0,85	184,5	0,23	154,7	0,19	0,84
Børsa	Bø1/2 (open)	406	12,5	50	50,00	25,00	30	12	230	525	2,28	0,67	91	0,40	22,7	0,10	0,25
Vigda	ViA (open)	457	12,5	26,7	26,70	13,35	29	14	112	505	4,51	0,90	62,8	0,56	38,1	0,34	0,61
	ViB (open)	457	12,5	52,9	52,90	26,45	27	12	212	660	3,11	0,74	86,9	0,41	28,6	0,13	0,33
Onsøy2	On1/2 (open)	508	6,3	17,7	19,10	10,25	60	33	68	100	1,47	0,60	23,5	0,35	22,44	0,33	0,95
Stjørdal	S1/2 (open)	508	6,3	22,6	23,60	12,30	29	14	136	192	1,41	0,60	32,7	0,24	14,6	0,11	0,45
Cowden	Col/2 (open)	457	12,5	9	10,00	5,50	16	18	85	1014	11,93	1,80	113	1,33	67,6	0,80	0,60
Femern	F1/2 (open)	508	22,5	25	25,00	12,50	37	110	104	480	4,62	1,50	85	0,82	75,9	0,73	0,89
Oromieh	O1 (open)	305	16	66,1	66,10	33,05	36	22	178	231	1,3	0,59	48	0,27	44,6	0,25	0,93